

**FINAL REPORT**  
**LONG-TERM MONITORING GROUNDWATER OPTIMIZATION**  
**AT SITE 49 PEASE AFB, NEW HAMPSHIRE USING THE**  
**GEOSTATISTICAL TEMPORAL/SPATIAL (GTS) ALGORITHM**

CONTRACT NUMBER: F41624-00-D-8030  
TASK ORDER 0062  
TASK 3

May 2004

Submitted to:

HQ AFCEE/BCE  
3300 Sidney Brooks Road  
Brooks AFB TX 78235

Submitted by:

Science Applications International Corporation  
11251 Roger Bacon Drive  
Reston, VA 20190

SAIC Project No. 06-6312-04-4567-003

This page left intentionally blank for duplicating purposes.

## Table of Contents

<b>Introduction.....</b>	<b>1</b>
<b>Section 1. Executive Summary.....</b>	<b>2</b>
<b>Section 2. Description of Site 49, Pease AFB.....</b>	<b>3</b>
Section 2.1. Site Hydrogeology and Contaminant Sources .....	3
Section 2.2. Monitoring Network .....	4
<b>Section 3. Temporal Optimization at Site 49.....</b>	<b>5</b>
Section 3.1. Data Preparation.....	5
Section 3.2. Temporal Methodology .....	8
Section 3.2.1. Temporal Variograms .....	8
Section 3.2.2. Iterative Thinning.....	11
Section 3.3. Trend Mapping.....	16
Section 3.4. Temporal Optimization Results .....	17
Section 3.4.1. Temporal Variograms .....	18
Section 3.4.2. Iterative Thinning.....	18
Section 3.4.3. Trend Maps .....	21
<b>Section 4. Spatial Optimization .....</b>	<b>26</b>
Section 4.1. Data Preparation.....	26
Section 4.2. Methodology.....	27
Section 4.2.1. Declustered CDF.....	28
Section 4.2.2. Spatial Bandwidth and Search Radius .....	30
Section 4.2.3. Creating Base Maps with LWQR .....	31
Section 4.2.4. Constructing the Base Map.....	33
Section 4.2.5. Global Regression Weights.....	35
Section 4.2.6. Local and Global Variance Measures .....	36
Section 4.2.7. Iterative Elimination of Wells.....	37
Section 4.3. Spatial Optimization Results.....	37
Section 4.3.1. Global Measures of Redundancy .....	38
Section 4.3.2. Local Indications of Redundancy .....	40
Section 4.3.3. Base Map Accuracy .....	41
<b>Section 5. Recommendations for Pease AFB, Site 49 .....</b>	<b>42</b>
Section 5.1 Recommendations Regarding Sampling Frequency .....	42
Section 5.2 Recommendations Regarding Spatial Redundancy .....	45
Section 5.3 Recommendations Regarding Siting of New Wells .....	48
Section 5.4. Cost Analysis and Summary .....	50
Section 5.4.1. Initial Monitoring and Cost Information.....	50
Section 5.4.2. Scenario Cost Estimates.....	51
Section 5.4.3 Resulting Cost Savings .....	52
<b>Section 6. References .....</b>	<b>53</b>

## Appendixes

- Appendix 3-1 Temporal Optimization: Temporal Variograms
- Appendix 3-2 Temporal Optimization: Iterative Fitting Trend Overlays
- Appendix 3-3 Temporal Optimization: Iterative Fitting Result Graphs
- Appendix 3-4 Temporal Optimization: Trend Maps
- Appendix 4-1 Spatial Optimization: Global Redundancy Measures
- Appendix 4-2 Spatial Optimization: DCA11 Indicator Difference Maps,  
Time Slice 1 — 2001
- Appendix 4-2 Spatial Optimization: DCA11 Indicator Difference Maps,  
Time Slice 2 — 2002
- Appendix 4-2 Spatial Optimization: DCE12C Indicator Difference Maps,  
Time Slice 1 — 2001
- Appendix 4-2 Spatial Optimization: DCE12C Indicator Difference Maps,  
Time Slice 2 — 2002
- Appendix 4-2 Spatial Optimization: TCE Indicator Difference Maps,  
Time Slice 1 — 2001
- Appendix 4-2 Spatial Optimization: TCE Indicator Difference Maps,  
Time Slice 2 — 2002
- Appendix 4-3 Spatial Optimization: DCA11 Local Variance Maps, Time Slice 1 — 2001
- Appendix 4-3 Spatial Optimization: DCA11 Local Variance Maps, Time Slice 2 — 2002
- Appendix 4-3 Spatial Optimization: DCE12C Local Variance Maps,  
Time Slice 1 — 2001
- Appendix 4-3 Spatial Optimization: DCE12C Local Variance Maps,  
Time Slice 2 — 2002
- Appendix 4-3 Spatial Optimization: TCE Local Variance Maps, Time Slice 1 — 2001
- Appendix 4-3 Spatial Optimization: TCE Local Variance Maps, Time Slice 2 — 2002
- Appendix 4-4 Spatial Optimization: DCA11 Base Concentration Maps
- Appendix 4-4 Spatial Optimization: DCE12C Base Concentration Maps
- Appendix 4-4 Spatial Optimization: TCE Base Concentration Maps
- Appendix 5-1 Estimate of Cost Savings (MS Excel file)

**Figures**

Figure 5-1. Approximate Locations of Greatest Local Uncertainty ..... 50

**Tables**

Table 2-1. Existing Site 49 Baseline LTM Network (All measurements in feet)..... 4

Table 3-1. COC Detection Frequencies ..... 6

Table 3-2. Well Detection Rates for Selected COCs ..... 7

Table 3-3. Temporal Variogram Ranges and Recommended Sampling Interval ..... 18

Table 3-4. Summary of Iterative Thinning Results, By COC and Well Location..... 20

Table 3-5. Optimal Sampling Intervals and Frequencies Measured Across All COCs.... 21

Table 3-6. Estimated Trend Magnitudes and Confidence Intervals by COC and Well Location ..... 23

Table 4-1. Parameters of Final Spatial Correlation Models ..... 29

Table 4-2. Reference Concentrations and Corresponding Percentiles of Declustered CDF for Each COC..... 32

Table 4-3. Boundaries of Optimization Box..... 34

Table 4-4. Hypothetical LWQR Results for TCE..... 34

Table 5-1. Example Sampling Plan for the First Two-Year Sampling Interval of the Optimized LTM Sampling Program ..... 44

Table 5-2. Essential Monitoring Network Based on Analysis of All COCs (All measurements in feet) ..... 46

Table 5-3. Redundant Monitoring Wells Based on Analysis of All COCs (All measurements in ft)..... 47

Table 5-4. Essential Monitoring Network Based on Analysis of TCE in 2002 (All measurements in feet) ..... 47

Table 5-5. Redundant Monitoring Wells Based on Analysis of TCE in 2002 (All measurements in ft)..... 48

Table 5-6. Approximate Locations of Greatest Local Relative Uncertainty ..... 49

Table 5-7. Estimate of Cost Savings..... 53

This page left intentionally blank for duplicating purposes.

# **Long-Term Monitoring Groundwater Optimization at Site 49 Pease AFB, New Hampshire Using the Geostatistical Temporal/Spatial (GTS) Algorithm**

*Prepared by SAIC and MacStat Consulting, Ltd., May 2004*

## **Introduction**

This report summarizes the effort to optimize the existing long-term groundwater monitoring (LTM) network at site 49 on Pease Air Force Base in New Hampshire. The optimization analysis is based on an application of the Geostatistical Temporal/Spatial (GTS) algorithm, which was designed for the Air Force Center for Environmental Excellence (AFCEE) by MacStat Consulting, Ltd. The analysis and the algorithm consist of two basic parts: a temporal optimization component and a spatial optimization component. The twin goals of the study are to determine, based on the existing sampling data and sampling network, 1) to what extent sampling frequencies at the site can be optimized so as to pare sampling and analysis budgets efficiently, and 2) to what extent locations within the sampling network can be optimized so that sampling information is not being collected at statistically redundant groundwater wells. Set against these goals is the overriding mandate that information critical to the success of the LTM program at site 49 should not be sacrificed.

It should be noted that GTS is not designed around a traditional hypothesis testing framework. As an example, considering the spatial analysis, rather than deciding whether or not the mean concentration level at the site is above or below a fixed concentration limit, and then designing the monitoring network with the goal of balancing the risks of false positive and false negative decision errors, GTS is fundamentally aimed at balancing a different kind of trade-off. In particular, GTS assumes that the existing network of sampling locations is the 'most informative' available, and that a map of the spatial distribution of concentration levels based on all the existing sampling information is the most accurate map that can be estimated barring significant numbers of additional well locations. Under this presumption, GTS then balances the information lost in map accuracy against the savings in sampling and monitoring resources that otherwise would be spent maintaining the current network. Optimization is thus defined with respect to this accuracy-cost trade-off and not with respect to the false negative-false positive trade-off common to hypothesis testing.

The report is organized into six major sections. The first section is the executive summary of the optimization results and recommendations. The second section provides a brief description of the site and its existing groundwater monitoring scheme. The next two sections correspond to the temporal and spatial analyses respectively. As explained below, the temporal component is further divided into three parts: temporal variogram analysis, iterative fitting of individual wells, and trend mapping. The spatial analysis consists of a series of iterative steps. The site maps corresponding to these iterations are collected in appendices to the report. The fifth section of the report summarizes the

conclusions of the optimization effort, offers a number of recommendations, and provides a cost analysis at the site based on the optimization results. The final section provides relevant technical references.

## Section 1. Executive Summary

After using the Geostatistical Temporal/Spatial (GTS) algorithm to optimize the long-term monitoring network at Site 49 on Pease AFB, the following key results were found:

- GTS exploratory analyses were used to determine 2 to 3 ‘best’ candidates for the optimization routine. The COCs were not chosen *primarily* on the basis of regulatory concern or health risk-exposure (although these factors were considered), but rather with the intent to include those parameters in the optimization routine that offered *the most statistical information* concerning temporal and spatial redundancy. The best such parameters typically exhibit larger detection rates and more widespread spatial occurrence. At Site 49, based on detection frequencies, per-well ‘hit’ rates, and spatial plotting of the maximum per-well concentration values, the most promising candidates appeared to be trichloroethylene (TCE), 1,1-dichloroethane (DCA11), and cis-1,2-dichloroethene (DCE12C).
- The *common* sampling schedule for Site 49 as a whole ought to be adjusted. Temporal variograms generated by combining all the available sampling information indicate that the common sampling interval could be set to one sampling event every 2 years with little loss of statistical information, compared to the current annual or semi-annual sampling regimen.
- If the results of the GTS optimization analysis are implemented at Site 49, there ought to be a similar follow-up analysis conducted after 3 to 5 years in order to assess whether or not the same recommendations would still hold. However, any new sampling schedules should be implemented with care. The Temporal Variograms, for instance, depend significantly on having pairs of measurements from any given well with a variety of inter-event time intervals. If all wells are sampled at the same time every two years after implementation, the range of between-sample intervals will be reduced, and consequently it will be much harder to construct a future Temporal Variogram to test the original recommendation. Instead, it is recommended the overall set of wells be divided in half, and that one year of each subsequent pair of years be selected at random for the sampling of each half-group. Thus, during a given two-year span, one half the wells might be sampled during Year 1, while the other half is sampled the following year (during Year 2), and the entire process repeated (including the random selection of half the wells) for the next pair of years. This approach will allow some inter-event times to be as short as the recent change of schedule to annual sampling, even though each well would only be sampled once every two years.

It would also help — even if more operationally cumbersome — to further subdivide each half-group into fourths and to randomly pick the quarter during which each one-fourth of the wells would be sampled. This approach will allow some inter-event times to be even shorter than annually, even though again each well would only be sampled once every 2 years. **Table 5-1** in **Section 5.1** illustrates a possible schedule for the first five years after.

- The spatial optimization analysis at Site 49 revealed varying levels of spatial redundancy. For the 2001 data, a ‘safe’ level of redundancy appeared to be about 20% of the total well network. For the most recent TCE data, this safe level increased to approximately 40%.
- Seven wells were listed as potentially redundant across the COCs, amounting to 10 percent of the total baseline well set. However, when considering the most recent TCE data — TCE being the highest priority contaminant at the site — 24 wells might be considered redundant or 36% of the baseline LTM network.
- The GTS optimization algorithm can offer potentially significant cost savings over the existing LTM program at Site 49. Accurate estimates of plume magnitude and extent can be made using fewer wells than the current network and sampling at a lower frequency than presently in place. Estimates of specific potential cost savings off the total annual project budget range from 49-52%, amounting to between roughly \$85,000 and \$89,000 per year.

## **Section 2. Description of Site 49, Pease AFB**

### **Section 2.1. Site Hydrogeology and Contaminant Sources**

Site 49 at Pease Air Force Base consists of an area of approximately five acres around the former communications building (Building 22). Building 22 is located near the intersection of Pease Boulevard and International Drive. During an Environmental Site Assessment (ESA) conducted in 1997 as part of site redevelopment, groundwater contamination was discovered at the site. The source of the groundwater contamination plume was an underground storage tank located adjacent to the building. The plume was determined to extend southeastward from the south side of the building, with contamination extending more than 500 feet in a southwestward direction from the site as well.

The subsurface geology at Site 49 is characterized as fractured gray phyllite bedrock overlain by variable glacial till, clayey and/or gravelly silts, and fine sand or sandy silt. There is a difference in the overlying geology between the area of the source near Building 22, and further downgradient in the area of the plume. Near the building, fill material covers approximately 5 to 8 feet of clayey silt containing sand, gravel, cobble, and stones. In the area of the plume, the overlying geology consists of fine sand and silt. Groundwater at the site occurs at depths of five to ten feet below ground surface across

the entire site. The groundwater flow direction in both the overburden and fractured bedrock layers is to the west/southwest.

## Section 2.2. Monitoring Network

For the ESA, approximately 20 monitoring wells were screened in the overburden materials, and four wells were screened in the fractured bedrock. In addition, samples were obtained from eight hydropunch/boreholes and six temporary sampling points. The existing monitoring network used as a baseline for the optimization analyses at Site 49 includes 67 wells as listed in **Table 2-1**. The depths of screened intervals range from approximately 6 feet to 78 feet below ground surface (bgs). The ground surface itself varies across well locations by approximately 15 feet. The deepest overburden well is located about 35 feet bgs, while the shallowest bedrock wells are located approximately 13 feet bgs. Because there were only a handful of bedrock wells at Site 49, the spatial optimization analysis was carried out on the data set as a whole, considered as three-dimensional site volume, rather than as separate two-dimensional (areal) horizons.

The primary constituents of concern for the ESA included 1,1-Dichloroethene, tetrachloroethene (PCE), and trichloroethene (TCE). The constituents of concern for the optimization analysis are listed in **Section 3.1, Data Preparation**, and included both the ESA COCs along with other organic constituents. Available data for this analysis covered the period from mid-1997 through 2002. Wells in the network were sampled at least once per year except for 2000, when no sampling data was collected, quarterly in 2001, and semi-annually in 2002. More recently, after the period covered by this analysis, the general sampling frequency was reduced to annually.

**Table 2-1. Existing Site 49 Baseline LTM Network (All measurements in feet)**

**Note:** Screen Elevation is recorded as the midpoint depth of a screen typically 10 feet in length

WELL_ID	EASTING	NORTHING	DEPTH	SCREEN ELEVATION
49-5562(D)	1212854	215270	21.5	55.28
49-5563(S)	1213011	215306	9.5	64.625
49-5564(D)	1212930	215180	20.5	53.11
49-5565(S)	1212924	215184	10	63.74
49-5566(S)	1212855	215266	8	67.2
49-5567(D)	1213430	215244	19	49.6
49-5568(D)	1213344	215122	13	55.455
49-5573(D)	1213180	215177	15.5	53.65
49-5574(S)	1213181	215174	8.5	60.665
49-5577(D)	1212915	215277	19.5	56.51
49-5578(S)	1212919	215278	11.5	64.33
49-5967(D)	1213634.39	215132.89	25.5	44.34
49-5969(S)	1213634.39	215132.58	8.05	58.505
49-5970(D)	1213403.93	215426.31	29.5	39.515
49-5971(D)	1213003.18	215303.58	9.7	63.525
49-5973(D)	1213015	215231.3	12.8	59.065
49-5980(D)	1213087.06	215385.48	11.5	59.715
49-5981(D)	1212903.02	215321.5	19.5	55.5955
49-5982(D)	1213283.75	215067.61	16.5	53.135
49-6515(S)	1212858	215262	39.3	35.7
49-6516(S)	1213093	215386	21.6	50

WELL_ID	EASTING	NORTHING	DEPTH	SCREEN ELEVATION
49-6517(S)	1213338	215120	23	45.67
49-6663(S)	1213456.96	215130.93	31.5	38.55
49-6664(S)	1213628.7	215131.26	17	49.52
49-6665(S)	1213183.89	215178.03	18.3	52.425
49-6666(DBR)	1213017	215220.6	78	-6.41
49-6667(S)	1213015	215226.2	18	53.71
49-6668(S)	1213408	215433.3	35.8	32.7
49-6669(S)	1212908	215266.5	28	47.515
49-6670(DBR)	1213640	215134.9	70	-3.425
49-6700	1213536.408	215817.0246	20.5	46.27
49-6701	1214189.944	215982.6607	14.5	48.64
49-MW002(SBR)	1213145.92	215153	34.5	34.94
49-MW003(SBR)	1213141.15	215116.65	29.5	40.58
49-MW006(DOB)	1212997.33	215233	17	54.63
49-MW006(SBR)	1212999.33	215230.7	29.5	42.265
49-MW006(SOB)	1212996	215237	6.5	65.4
49-MW008(DOB)	1213211	214999	22.5	51.055
49-MW008(SBR)	1213210	215002	30	43.425
49-MW009(DOB)	1213509	215013	15	54.71
49-MW009(SBR)	1213510	215017	22.5	47.015
49-MW01	1213408	215440	12	56.62
49-MW010(DOB)	1213103	215352	7.5	63.26
49-MW010(SBR)	1213107	215353	15.5	55.21
49-MW011(DOB)	1213592	215429	12.5	54.075
49-MW011(SBR)	1213590	215433	20.5	46.16
49-MW012(SBR)	1213464	215197	28	41.2
49-MW013(DOB)	1213865	215081	14.5	51.285
49-MW013(SBR)	1213860	215081	19	47.78
49-MW013A(SBR)	1213804	215076	14.5	50.385
49-MW014(DOB)	1213530	215668	22.5	42.815
49-MW014(SBR)	1213526	215666	32	34.185
49-MW02	1212932	215409	11.5	64.61
49-MW03	1213431	215248	12	57.1
49-MW04	1213047	215134	10.5	60.63
49-PZ001(SBR)	1213007	215303	17.2	55.945
49-PZ002(DOB)	1213031	215223	12	60.15
49-PZ002(SBR)	1213030	215225	19	53.205
49-PZ002(SOB)	1213029	215228	6.5	65.585
49-PZ003(DOB)	1213045	215173	12.7	59.75
49-PZ003(SBR)	1213044	215176	21.5	50.935
49-PZ003(SOB)	1213044	215178	6.5	65.84
49-PZ004(DOB)	1213023	215184	14	57.92
49-PZ004(SBR)	1213024	215182	22	49.835
49-PZ004(SOB)	1213022	215183	7.5	64.275
49-PZ005(DOB)	1213051	215133	14	57.17
49-PZ005(SBR)	1213052	215130	21.7	49.495

## Section 3. Temporal Optimization at Site 49

### Section 3.1. Data Preparation

Data queries were made by AFCEE and Montgomery Watson of all available electronic sampling records from Site 49. Data covered the period from mid-year 1997 until late 2002. In order to better gauge sources of variability — especially spatial variation — among the chemical data, data queries specifically asked for field duplicates as well as normal environmental samples.

Included in the database were a number of sets of multiple records associated with the same sampling date and sample type. Each set apparently represented multiple laboratory

runs on the same sample. To ensure that only one sample result of a given type (field duplicate or normal) was kept per sampling date (at a given location and depth), all of the sets of multiples were screened by manual inspection. Although this screening process was somewhat subjective and imperfect, a list of rules and priorities was developed to make the screening as consistent as possible. These rules included giving priority to sampling records with lower dilution factors (when dilution information was available) or lower reporting limits (“RLs”); and quantified concentrations (“hits”) over estimated concentrations (“J” values) or non-detects (NDs). In addition, even when dilution factors were present, priority was given to hits with higher dilution over either J values or NDs with lower dilution, and J values with higher dilution over NDs with lower dilution.

Another issue corrected within the database was the presence of unique sampling locations that were labeled with multiple well identifiers. These, and any missing easting and northing coordinates, were corrected with the help of Montgomery Watson.

Overall, the database included 6,842 records covering the following twelve constituents of concern (COC): benzene (BZ), toluene (BZME), (CDS), 1,1-dichloroethane (DCA11), 1,1-dichloroethene (DCE11), 1,2-c-dichloroethene (DCE12C), ethylbenzene (EBZ), methyl ethyl ketone (MEK), naphthalene (NAPH), perchloroethene (PCE), trichloroethene (TCE), and vinyl chloride (VC). These COCs were noted in site documents and reports as chemicals being monitored at Site 49 and that had been detected in laboratory analyses of sampling data. Initial detection rates by sample record for these COCs are given in **Table 3-1**:

**Table 3-1. COC Detection Frequencies**

<b>COC</b>	<b>Rate of Detection (%)</b>
TCE	57.6
DCE12C	56.1
DCA11	54.8
DCE11	34.9
PCE	21.4
VC	18.7
CDS	6.3
BZ	5.2
MEK	4.8
BZME	4.4
NAPH	2.2
EBZ	0.5

Based on these detection rates, six COCs were quickly eliminated from consideration as not exhibiting enough statistical variation for meaningful analysis: BZ, BZME, CDS, EBZ, MEK, and NAPH. It was also observed that these same six parameters were likely to exhibit what could be termed ‘dilution outliers.’ By this is meant the presence of non-detect samples with unusually high dilution factors and/or reporting limits, leading to reported values typically much greater than either other non-detects or results of the same

compound that were detected.

Among the remaining constituents, TCE, DCE12C, and DCA11 had the highest detection frequencies, all with rates greater than fifty percent. Another useful exploratory statistic is per-well detection rates, the fraction of wells for a given compound with at least one detection. In addition, it is helpful to consider per-well detection rates above specific concentration levels of interest (usually a primary or secondary MCL). Summaries of these statistics are given in **Table 3-2** below:

**Table 3-2. Well Detection Rates for Selected COCs**

COC	Well Hit Rate (%)	MCL (ppb)	Hits > MCL (%)
DCA11	73.9	5	56.4
DCE11	62.5	6	23.1
DCE12C	73.9	7	52.6
PCE	38.6	5	32.0
TCE	76.1	5	65.4
VC	38.6	2	33.3

Based on these summaries and initial time series plots of all the COCs (not shown), the most promising candidates for the GTS optimization routine appeared to be TCE, DCA11, DCE12C. Spatial plotting of the maximum per-well concentration values were then conducted to determine the crude spatial distribution of the hits for each parameter. These plots generally confirmed that the most frequently detected COCs also had the most widespread spatial distribution at Site 49. So these three candidates were chosen for the optimization analysis.

Note in this regard that one of the purposes of the initial exploratory analysis was to determine 2 to 3 ‘best’ candidates for the optimization routine. Including a larger number of COCs significantly increases the amount of work required to run the GTS algorithm without typically improving the results. The aim is *not* to determine which COCs to monitor, but rather to include only those parameters in the optimization routine that offer *the most statistical information* concerning temporal and spatial redundancy. The best such parameters typically exhibit larger detection rates and more widespread spatial occurrence.

Another preparation step that was taken to prepare the remaining data for temporal optimization was to average values for a given sampling date by duplicate status and across multiple depths (when they existed). That is, if a given well on a given date had both normal samples and field duplicates and/or had multiple samples collected at different depths, all of these values were averaged in order to create a single analysis value for that well and sampling event. The major reason for doing this was to ensure that estimates of the typical interval between samples were not biased downward by the presence of multiple samples on a given date. Most of the wells and sampling dates only included a single sample at depth, so to include all the sample records without this

averaging step would tend to skew the results.

As a final note, non-detects were handled prior to analysis by converting them to half the listed reporting limit (RL). In addition, part of the temporal analysis required keeping track of which samples were non-detects and which were detections. For single, non-averaged samples this posed no difficulty. But for values that were averaged across duplicate status and/or depth, if any of the samples to be averaged were ‘hits,’ the average value was also considered a hit. If all were non-detects, the average value was also labeled a non-detect.

## **Section 3.2. Temporal Methodology**

The temporal optimization analysis in GTS consists of three basic components: 1) temporal variograms applied to groups of wells, 2) iterative thinning of individual wells, and 3) trend mapping over specific time periods. Each of these components is explained below. Note again that the temporal analysis is *not* designed to determine which well locations might be redundant and perhaps unnecessary to the LTM program. Rather, the major goal of the temporal portion of GTS is to examine and optimize well sampling frequencies for *currently existing* locations.

### **Section 3.2.1. Temporal Variograms**

The first piece of the GTS temporal puzzle is the Temporal Variogram. The Temporal Variogram technique is designed to optimize sampling frequencies simultaneously over a *group* of well locations. These locations might represent all wells at a given site, those connected with a particular regulatory unit, or even selected wells that are part of a treatment system network. Whatever the grouping, the Temporal Variogram aims to provide a single optimal sampling interval that can be applied to every well within the group. Thus, this technique can be particularly helpful when a site manager wants to establish uniform operational sampling schedules at the site, and the optimization of individual well frequencies is not deemed as high a priority.

Results from the Temporal Variogram should not be viewed as optimal for any *single* well. The Temporal Variogram in GTS combines data from all wells in the group in its construction. Consequently, it attempts to find an optimal sampling interval, *on average*, for the group. Some individual wells might be better optimized with shorter or longer sampling intervals. Nevertheless, when a uniform sampling frequency is desired, the Temporal Variogram can provide a reasonable way to estimate it for the well group simultaneously.

Another advantage of the Temporal Variogram as employed in GTS is that even wells with very little sampling data can be included in its construction. The trend fitting methods for individual wells explained in **Section 3.2.2** generally require at least 8 or more distinct sampling events to provide a reasonable fit. With the temporal variogram, any well with at least two distinct sampling events can be included.

The Temporal Variogram is constructed using nested pairs of concentration measurements from each well in the group. By nested what is meant is that given a particular location, all pairs of measurements are formed for that well and one-half the

squared difference is then computed for each pair. Pairs are never formed *across* distinct wells, which would introduce unwanted spatial variability, but rather are *nested within* wells. This allows an independent estimate of temporal variability from each well. Then, to allow the inclusion of wells with only minimal amounts of sampling data, and to gauge average temporal variation for the group as a whole, the squared differences are amalgamated together into a single set of *pair differences* for the entire group.

In previous versions of GTS, a Temporal Variogram was actually constructed for each well, but then a weighted average of the individual variograms was formed to get the final overall Temporal Variogram. In the current version of GTS, this process is streamlined by simply estimating the final variogram from the entire unweighted set of half-squared pair differences. In this fashion, wells with more data are naturally given greater weight in the final Temporal Variogram (since they contribute more pairs), while well locations with less data are given some, but lesser weight.

The Temporal Variogram itself is simply a graph of a unitless variogram measure plotted against time, or more specifically, against the time lag between successive sampling events. It is estimated using locally-weighted quadratic regression (LWQR), taking the half-squared difference pairs as the *y*-variable and the time lag or time difference between sampling event pairs as the *x*-variable. All sampling dates at Site 49 were converted into number of weeks since a reference date prior to any actual historical sampling. The time lag differences were thus expressed in number of *weeks* between sampling events.

As explained in more detail in **Section 3.2.2** on the use of LWQR in Iterative Fitting, the GTS analyst must choose an appropriate bandwidth parameter prior to estimating the Temporal Variogram. However, testing of various data sets has shown that smaller bandwidths do not do a good job of capturing the most important features of the variogram. Instead larger bandwidths provide better and more interpretable results.

For this reason, all the Site 49 Temporal Variograms were computed at two larger bandwidths: 50% and 70%. Both of these estimated fits are graphed for each constituent in **Appendix 3-1**. The use of LWQR also allowed the estimation of confidence bands around the fit, in order to better gauge possible variation in the estimate. Confidence bands were constructed for both bandwidths; however, for visual clarity only the 50% bandwidth confidence bands are actually plotted on the graphs in **Appendix 3-1**. Sometimes the LWQR fit at the 70% bandwidth is different enough from the 50% bandwidth fit as to make the former estimate fall outside the confidence bands. Nonetheless, as described below, the key to comparing results at different bandwidths is not whether the *magnitude* of the Temporal Variogram differs from one bandwidth to the next, but instead whether the fundamental *shapes* of the variograms differ. Generally, at Site 49 they did not.

A couple of additional technical points are important to the Temporal Variogram methodology. First, concentration outliers can skew the results of the Temporal Variogram as much as they can skew the Iterative Thinning routine (as explained in **Section 3.2.2**). Because of this possibility, Tukey's box plot rule (also described in **Section 3.2.2**) was run on the concentration data from each well, both on the raw and

logged scales of measurement. Again, as with Iterative Thinning, only data values that were tagged as outliers on *both* scales were excluded from the Temporal Variogram computations.

In addition, to avoid the problem of some wells having vastly different average concentration levels (and thus contributing vastly different squared-difference pair contributions to the Temporal Variogram), each well's data was temporarily re-scaled to have a maximum of one before doing the Temporal Variogram calculations and fitting. Thus, every well in the group was put more or less on an 'equal footing' in terms of its concentration range.

Another potential problem involved non-detects. Prior testing of the Temporal Variogram has shown that wells with too many non-detects exhibit too little temporal variation to be of help in estimating the Temporal Variogram. For this reason, all wells with less than a 30% detection rate are excluded from the variogram computations.

Finally, two different types of Temporal Variograms were computed on the Site 49 data: the *mean* variogram and the *median* variogram. In each case, the LWQR procedure looks at a neighborhood of half-squared-difference pairs surrounding a time lag point to be estimated. However, in the case of the mean variogram, the local regression estimate attempts to pinpoint the arithmetic average of the difference pairs, while in the case of the median variogram, a similar estimate is made on the *ranks* of the set of difference pairs rather than the pair values themselves. Comparisons of these variogram types showed that the mean variogram rarely offered interpretable results, mainly because it was too erratic, while the median variogram was typically more promising and well-behaved. Consequently, the Temporal Variograms of **Appendix 3-1** only include the median variogram results.

The ultimate goal when analyzing a Temporal Variogram is to identify an approximate *range* in its structure. That is, at what point (if any) does the variogram start to 'level out' and remain at roughly a constant level? Ideally, any variogram offers a measure of correlation between the measured data and either time or space. For cases of positive temporal or spatial correlation, such a linkage is evidenced on the variogram by small values for small lags (either *time* lags between sampling events for the Temporal Variogram or, more commonly, *distance* lags between well locations when constructing variograms for a geostatistical analysis) and larger values for large lags. Small values on a variogram are typically indicative of a high degree of correlation, while higher values represent a loss of correlation and greater statistical independence.

On many variograms, there is a point at which larger lags no longer lead to larger variogram values. It is at this point that the range is identified. The magnitude of the leveled-out portion of the variogram is known as its *sill*. Lags at least as large as the range — and thereby associated with the sill — are thought to represent sampling pairs having essentially no statistical correlation. Smaller lags on the other hand, having variogram values smaller than the sill, represent pairs which are correlated to some degree and therefore contain a certain level of statistical redundancy in the information they offer.

It is for this reason that GTS sets the optimal sampling interval for a group of wells as the *range* of the Temporal Variogram, if it can be identified. Sampling intervals smaller than the range are associated with somewhat correlated, and therefore redundant, sampling results. On the other hand, sampling intervals at least as large as the range tend to be uncorrelated, and therefore — from a statistical standpoint — optimal in the sense that consecutive samples collected at such lags will provide the shortest sampling interval at which the maximal statistical information per sample is achieved.

Bear in mind that while the Temporal Variogram is a useful tool, it is not without its caveats. Sometimes a range cannot be reliably identified, often because some of the wells in the group do not possess the same basic temporal correlation structure as other wells. In other cases, a range may be identified, yet the result is different from that estimated via Iterative Thinning. This can happen in part because the Temporal Variogram tries to optimize a group of locations *on average*, rather than individually. It can also occur if only a smaller number of wells have enough sampling data to be included in the Iterative Fitting analysis, yet are included in the Temporal Variogram computations.

### **Section 3.2.2. Iterative Thinning**

Iterative Thinning refers to the technique by which the well sampling frequencies at *individual* wells are optimized. Because each location is analyzed separately, it is quite possible to have a different recommended sampling interval for each well after applying the Iterative Thinning routine. Nevertheless, GTS looks at the optimized sampling intervals as a whole and adjusts the recommended common operational sampling frequency for either all the wells treated as a single group, or each subgroup of related wells, based on the median optimal sampling interval for that group or subgroup.

The Iterative Thinning process is based on a relatively simple idea: 1) take the existing, historical data for a given well location and constituent, 2) determine the current average sampling frequency and sampling interval, 3) fit a trend to these initial data along with statistical confidence bounds around this trend, 4) iteratively remove, at random, certain fractions of the original data, and 5) re-estimate the trend based on the reduced dataset to determine whether or not the trend still lies within the original confidence bounds. If too much of the new trend falls outside the confidence limits, stop removing data and compute a new, optimized sampling frequency and sampling interval based on the portion of data removed.

The original version of GTS fit trends during Iterative Thinning by way of Sen's slope statistic, a non-parametric estimate of the slope of a linear trend. Although useful, Sen's statistic is not highly informative for cases of more complicated, non-linear trends. Previously, this meant that the GTS analyst would have to 'screen out' those wells which did not exhibit roughly linear trends over time. Since then, GTS has been modified to estimate the initial trend via a statistical technique known as locally-weighted quadratic regression (LWQR; see Loader, 1999). This procedure is readily able to fit complex trends and confidence bounds around those trends. Moreover, the data requirements for using LWQR are quite similar to Sen's slope method, and the process can be automated to essentially the same degree.

To perform the Iterative Thinning, LWQR was used to construct an initial trend and 90% confidence bounds around this trend. Also, the baseline sampling frequency was computed over the entire record of sampling at the well, and the baseline sampling interval was estimated by averaging the set of intervals between consecutive samples. As will be noted below, greater emphasis was given to more recent sampling information when constructing these baselines, especially if any large gaps appeared within the sampling record. Still, it is quite possible that the baseline sampling interval for a given well may not directly correspond to the nominal operational sampling schedule currently being used. The Iterative Thinning routine is data driven, and includes as much useful trend information as is possible, even if contributed by, for instance, multiple contractors operating under different sampling schedules or goals.

Once the initial trend was fit, data points were removed at random in systematic increments of 5% at each level, up to a maximum of 95%. At each stage, the trend was re-estimated on the reduced dataset and then compared to the initial confidence bounds. Since data points were removed randomly, and it was therefore possible that only points from one portion of the existing sampling record might be removed, the same removal process was repeated 500 times at each removal level, each iteration with a new set of randomly chosen points. This step helped to ensure that the trend results were not artifacts of the removal process, but really reflected what kind of trend estimate was possible at each stage of removal.

Another advantage to using LWQR in this way is that it can readily account for seasonal fluctuations or seasonal trends. Because local regression is used to estimate non-linear trends in the original or baseline data at a given well, it does a good job of identifying seasonal patterns in the initial estimate. Then, since subsequent trends computed on the reduced data-sets are compared to the baseline estimate, if a dominant seasonal fluctuation cannot be identified in the reduced data, the iterative fitting procedure will register such a result as a loss of accuracy and perhaps conclude that too much data has been removed from that well.

Because 500 new trends were fit to the reduced data at each removal level, key statistical summaries were used to express the results. These include the median trend value (calculated at a series of dates throughout the sampling record), the lower quartile (i.e., 25<sup>th</sup> percentile) trend value, and the upper quartile (i.e., 75<sup>th</sup> percentile) trend value. The median trend summaries are plotted on the graphs in **Appendix 3-2** for two specific removal levels: the percentage at which too much data has been removed to adequately reconstruct the original trend, and the removal level just below this, which represents the optimal stopping point for the Iterative Thinning algorithm. Thus, for example, at well 49-5562(D) for DCA11, the initial trend is plotted in blue with 90% confidence bounds around this trend shaded in light blue, the median fit of the set of new trends when 35% of the data has been removed is plotted in red, and the median fit of the optimal stopping point of 30% removal is plotted in green. This same pattern and color scheme was used for all of the **Appendix 3-2** graphs.

The other summary plotted on each **Appendix 3-2** graph is the pair of upper and lower

quartile fits (identified by red dashed traces) on the reduced data when too much sampling information was removed. These statistics are quite important for a couple of reasons. First, the upper quartile represents the point which is exceeded by 25% of all the new trend values (and the same for the lower quartile on the low end of the concentration range). If this trace falls outside the original confidence bounds, it demonstrates that at least a quarter of the new trend values constructed from the reduced data were outside the initial confidence limits. This can happen even when the *median* trend fit doesn't look that bad, especially in the case where the new trend value is 'swinging wildly' from iteration to iteration above and below the initial fit, causing the median fit to fall somewhere near the original trend, but at the expense of substantial variability in the 500 trend fits at that removal level. Therefore it can be quite informative to compare the lower and upper quartile fit traces against the original confidence bounds. Sometimes there are key stretches of the data record where these fits lie outside the confidence band, indicating too much variability in the fitting process to allow for reliable trend reconstruction.

Second, the difference between the upper and lower quartile fits — also known as the *interquartile range* or IQR — was computed at each fitting point along the sampling record and averaged across the fitting points to form the *average* IQR. This statistic offers a numerical indication of the typical level of variation exhibited among the 500 trend fits computed at a given removal level. It is also plotted against removal level (i.e., fraction of data removed) for each well and parameter in the graphs of **Appendix 3-3**. There the average IQR typically increases as more of the data is removed, up until and often beyond the optimal stopping point.

Note however that the average IQR is not a fail-safe indicator. In some cases, this statistic begins to *drop* near to or beyond the optimal stopping point, rather than continuing to increase. The primary reason for such behavior is that when enough data is removed — and depending on the configuration of the original time series — the re-estimated trend can, instead of 'swinging' above and below the initial fit, merely stay either consistently above or below the original trend, leading to a lower than expected difference between the upper and lower quartile fits.

It is for this reason that the optimal stopping point was chosen not on the basis of the average IQR, but rather by determining what fraction of the new trend values fell outside the original 90% confidence band. For Site 49, a threshold of 25% was chosen, meaning that too much removal was judged to have occurred whenever at least 25% of the reduced-data trend values fell beyond the initial confidence bounds. While the choice of threshold is somewhat arbitrary, tests of the data at Site 49 and at other sites have shown that it gives generally good results. However, it may not be the *ideal* threshold for each and every time series. Remember, the overall goal in Iterative Thinning is to determine how much data can be removed (and thus how much the interval between sampling events can be lengthened) and still allow one to reconstruct the *major* features of the original trend. Some 'finer' features of the time series trend are undoubtedly lost when less data is collected, but often it is quite difficult to determine whether these features are 'real' or simply due to measurement and/or field variation in the data. It may also be the case that certain transient features are less important to the needs of the long-term

monitoring program and therefore do not need to be estimated as carefully.

To graphically illustrate at what point the ‘out-of-bounds’ fraction of new trend values exceeded the threshold of 25%, a graph of this measure plotted against removal level is provided for each well and COC in **Appendix 3-3**. Both this graph and the plot of the average IQR are denoted by red traces and set in the top panel of the page for each well. Also on these graphs is a vertical reference line indicating the optimal stopping point of data removal as determined by the Iterative Thinning routine. In the bottom panel are two graphs representing optimal sampling interval (in green) and optimal sampling frequency (in blue). These graphs were constructed by adjusting the baseline sampling interval and baseline frequency according to the amount of data ‘thinned’ at each removal level. Also included are two reference lines indicating the optimal stopping point and the optimal interval or sampling frequency associated with that stopping point. Hence, again referring to DCA11 at well 49-5562(D), the baseline sampling interval is just over 32 weeks between sampling events, while the optimal interval is found to be just greater than 38 weeks. Conversely, the baseline sampling frequency at this well is approximately 0.037 samples per week (approximately 1.9 samples per year), compared to a recommended optimal frequency of just over 0.026 samples per week (1.35 samples per year).

### Data Screening prior to LWQR

It is important to note certain steps that were necessary to apply the locally-weighted quadratic regression technique. While extremely flexible as a statistical tool, its flexibility comes with certain restrictions and assumptions. First, prior testing of the GTS algorithm has demonstrated that reliable fitting of an initial trend, and especially, confidence bounds around that trend, are almost impossible with less than 8 to 10 sample measurements (that is, data from distinct sampling events). Because of this, well locations with fewer sampling events at Site 49 were automatically screened out of the Iterative Thinning routine and do not appear in the graphs of **Appendices 3-2** and **3-3**.

Furthermore, large data gaps in the sampling record are also troublesome to the LWQR algorithm and tend to cause artifactual looking trends. For this reason, historical sampling data prior to a large gap were screened from that well’s time series before fitting. In this case, a large gap was defined as an outlier among the set of time-lags between consecutive sampling events using *Tukey’s box plot outlier rule*, where a sampling gap outlier is identified whenever the lag exceeds the upper ‘hinge’ of the box plot of time-lags. (The upper hinge is defined as the upper quartile plus 1.5 times the interquartile range [IQR] of the box plot.)

Another data feature that can significantly affect the trend estimate is the presence of concentration outliers. The modified GTS algorithm screens these values prior to fitting with LWQR by again using Tukey’s box plot rule, this time on the concentration values. To ensure that only very significant outliers are identified and removed, two passes of the box plot test are run, once on the raw data and once on the logged concentrations. Only samples that are identified as outliers on *both* scales are screened from the time series prior to fitting.

A final screening check is made for wells with no observable variation, typically in the

case where all the data for a time series are non-detects with a common reporting limit (RL). Although LWQR can estimate a (flat) trend to such data, it is impossible to construct a confidence band around the trend or to determine an optimal stopping point for data removal. These latter statistics require the measurements to exhibit some variation (the same is true of other trend estimation methods). Because of this, wells with no observable variation are screened from the Iterative Thinning routine. In addition, the data at some wells — after removing apparent concentration outliers and sampling events prior to large data gaps — only consist of a string of identically-valued non-detects. These wells are consequently also screened from Iterative Thinning.

After running these automated checks, the results are re-checked manually by the GTS analyst by examining a time series plot of each well with possible outliers, data gaps, and stretches of no variation identified. Occasionally, it is necessary to add or remove one or more outliers or data gaps, in order to improve the fitting process.

### Trend Fitting with LWQR

After screening the time series measurements for data gaps, concentration outliers, and observable variation, one final step was needed before constructing the initial trend estimates. That step was to choose a *bandwidth* for fitting. LWQR works by estimating the trend value at a given fitting point (i.e., a particular date within the range of dates between the start and end of the sampling record) using a weighted linear combination of the known sample values close to the fitting point. What must be selected by the analyst is how many neighboring sample measurements to use. In GTS this is done by selecting a *bandwidth parameter* that represents the fraction of known samples to be included in the neighborhood of any given fitting point. These bandwidths typically range from 40% to 80%, depending, among other things, on the number of points in the time series and its shape.

In order to automate the GTS routines as much as possible, especially when there are a large number of wells to analyze, every attempt is made to simplify the choice of bandwidth. In general, the higher the bandwidth, the greater the amount of ‘smoothing’ that will occur within the fitted trend. Too high a bandwidth and the trend may ‘miss’ important peaks and valleys in the time series. Too low a bandwidth and the trend may exhibit artifactual jumps and/or dips between known sample values. It can also occur that the fitted trend mostly ‘disregards’ the known data altogether, leading to highly inaccurate trend estimates.

To guard against these scenarios, it is important to run a ‘pre-flight’ check of the LWQR fits at several possible bandwidths prior to running the Iterative Thinning routine. This pre-fighting is done in two basic ways: 1) visually comparing the estimated fits obtained by systematically changing the bandwidth for each well, and 2) computing diagnostic checks of the *residuals* obtained when the trend is estimated at each known sample value and the known value is subtracted from this estimate. Again the goal is to automate this process as much as possible. However, some visual inspection of the pre-flight results at each well is still necessary.

As to the first pre-flight check, plots of the known sampling data can be overlaid with

LWQR trend estimates at several possible bandwidths. In this setting, one should look for a ‘visually pleasing’ fit, one that captures the major features of the overall trend, and especially to exclude fits that are clearly bad.

The second pre-flight check, that of residuals, includes the following calculations: Mallows’ CP statistic, correlation of the residuals with date of sampling, skewness of the residuals, and Filliben’s probability plot correlation coefficient. Each of these statistics is designed to provide a numerical indication of the goodness of the estimated trend relative to a given bandwidth. In GTS, these residual diagnostic measures are plotted simultaneously against bandwidth in order to search for the most appropriate fitting neighborhood. None of them, however, is fail-safe by themselves.

Mallows’ CP statistic is a scaled measure of the sum of squared residuals. Lower values of Mallows’ CP usually indicate a better fit. However, it is possible to have a very low Mallows’ CP and yet a visually unacceptable fit between known sample values. This occurs for instance when the estimated trend ‘goes right through’ each known sampling value, yet has improbable ‘squiggles’ or curves *between* sampling points. The correlation with sampling date is used to check whether the fit is worse over certain portions of the sampling record than others. Values close to zero are best. The skewness coefficient is used to check for ‘lopsidedness’ in the distribution of residuals. LWQR works best when the *residual* distribution is symmetric and normally distributed, so skewness values closer to zero are better. Along the same lines, Filliben’s correlation coefficient is a test of normality that can be used to check the shape of the residual distribution. Coefficient values closer to one are best.

As noted, none of the residual diagnostic measures are fool-proof by themselves. They can even give conflicting indications for the same time series in some situations. Nevertheless, examined together along with graphs of the possible fits by bandwidth, an acceptable initial trend estimate can almost always be found.

### Section 3.3. Trend Mapping

One of the natural by-products of constructing the initial trend fits at each well location during Iterative Fitting is the ability to create a *map* of the trend estimates for any specific time period. In order to construct the confidence band around the initial fit on the known sample data, LWQR creates an estimate not only of the trend value at each fitting point, but also the local *first derivative* or *slope*. These local slopes can then be averaged in an appropriate way to determine the general direction and magnitude of the trend for a given portion of the sampling record.

At Site 49, three different time windows were chosen for estimating average trend slopes: 1) the historical trend, based on all the available and usable data at a well location, 2) the recent trend, based on data collected since the start of 2000, and 3) the newest trend, based on the four latest sampling measurements. Each of these trends was also characterized as increasing (with an average slope  $> 0$ ) or decreasing/flat (with an average slope no greater than 0).

To actually estimate the typical slope, the *median* slope value is selected from the set of

fitting points falling within the specified time period. This is done to ensure that the dominant trend direction is identified. With non-linear trends, there can be short periods of very steep trends that do not represent the dominant direction of the trend over the time interval in question. The *mean* slope can be then skewed by a few very large local slope values, whereas the *median* slope tends to be resistant to this problem.

In addition, it is possible to compute a non-parametric confidence interval around the median slope, in order to characterize the *strength* of each trend. Using a 95% nominal target confidence level, each trend can then be characterized as either fairly ‘sure’ or ‘unsure,’ depending on whether the confidence interval around the slope contained the value zero.

Finally, all of this trend information can be mapped by well location. The maps presented in **Appendix 3-4** offer for each COC and designated time period a spatial representation of the types of trends at Site 49, along with an indication of their strength and relative magnitude. Specifically, increasing trends are listed in red and pink, with trends surely above 0 identified in red, and less sure increases in pink. Flat or decreasing trends are colored in blue and light blue, with surely decreasing trends in blue and less sure trends (including flat trends) in light blue.

Also on these maps is an indication of the *relative* magnitude of each trend. To do this, the actual slope estimates were divided into quintiles (each quintile representing 20% of the ranked slope estimates). Then, an increasing series of symbol sizes was assigned to the set of quintiles for plotting purposes. Consequently, the largest red symbols on the trend maps, for example, represent increases in the top 20% of magnitude, while the smallest red symbols designate increases in the lowest 20% of magnitude. The same patterns apply to the other trends. The largest blue symbols represent those trends that exhibited the largest decreases, while the smallest blue symbols represent the smallest downward trends. And so on.

It is important to note that the trend maps do not provide information specific to the optimal adjustment of sampling frequencies. Rather, the maps provide an overview of where at the site different kinds of trends are occurring and how probable it is that the trends represent something ‘real.’ They can also be used to potentially augment or confirm patterns of plume movement or change over time, and perhaps to help identify areas of the site where additional sampling might be helpful. Still, it must be remembered that the LWQR fits are only constructed at wells with at least 8 usable sampling events. At Site 49, since data was only available from 1997 onwards, this meant that most of the wells were screened from the Iterative Fitting component of GTS. Consequently, the trend maps are incomplete and somewhat sketchy.

### **Section 3.4. Temporal Optimization Results**

The temporal optimization results at Site 49 are contained in a series of graphs and tables. Overall, there is room to adjust and optimize sampling frequencies within the long-term monitoring (LTM) program. If thought feasible from an engineering and operational standpoint, at least a few of the monitoring wells could have their sampling frequencies reduced by at least 15-30% yet retain the most useful statistical information concerning

their long-term trends. However, too few of the wells retained presented enough data to make well-specific Iterative Thinning possible. More general conclusions about sampling frequency have to be derived from the Temporal Variogram results. These results indicate that it would also be possible to adjust the *common* sampling schedule for Site 49 as a whole. Temporal variograms generated by combining all the available sampling information suggest that the common sampling interval could be set to one sampling event every 8 to 9 quarters (or roughly once every 2 years) with little loss of statistical information.

### Section 3.4.1. Temporal Variograms

The Temporal Variograms for Site 49 are contained in the graphs of **Appendix 3-1**. There is one Temporal Variogram per COC. As can be seen from these graphs, especially for DCE12C, there appears to be a slight leveling off of the variogram at approximately a lag of 30 to 40 weeks. However, the ultimate sill does not occur until at least 90 to 100 weeks, and as late as 120 weeks for TCE. Consequently, there seems to be some statistical correlation, and therefore statistical redundancy, for pairs of samples collected within a two year span. Conversely, for all three COCs, no correlation is apparent between sample pairs collected more than 2 years apart. The recommended optimal sampling interval for Site 49 is then approximately one sampling event every 8 to 9 quarters. Results by COC are listed in **Table 3-3** below.

It should be noted that the recommendations on sampling frequency for Site 49 are strictly data driven. Other regulatory or engineering considerations may need to be accommodated in the assignment of final sampling schedules. Still, the sampling intervals listed below in **Table 3-3** offer a summary of the statistical information provided by the available data, and how that information can be used to adjust operations at the site.

**Table 3-3. Temporal Variogram Ranges and Recommended Sampling Interval**

Temporal Variogram Range			Optimal Sampling Interval
DCA11	DCE12C	TCE	
110 wks	90-100 wks	120 wks	8-9 qtrs

### Section 3.4.2. Iterative Thinning

Mention has already been made of the graphs in **Appendices 3-2** and **3-3**. These appendices provide the visual results of the Iterative Thinning process. As described above, **Appendix 3-2** includes a time series graph of each eligible well, overlaid with the initial trend fit, a confidence band around that trend, and selected results of the Iterative Thinning routine, including an indication of the optimal stopping point for data removal. These results are further detailed in the graphs of **Appendix 3-3**, where for each well and COC there are four plots: 1) the percentage of trend fits on the reduced data that fall outside the initial confidence band, plotted against the percent of data removed; 2) the average interquartile range (IQR) of the reduced-data trend fits, plotted against percent of data removed; 3) the optimal average sampling interval, plotted against percent of data removed; and 4) the optimal average sampling frequency, plotted against percent of data

removed.

Key numerical portions of this same information are summarized in **Table 3-4**. There for each well, the optimal and recommended sampling intervals and frequencies are summarized for the three COCs input into GTS. It will be noted that different stopping points sometimes occur for the same well depending on the COC utilized. Operationally, the minimum data removal percentage across the COCs could be chosen to select the optimal sampling interval and frequency, as shown in **Table 3-5**.

As is seen in this latter table, the suggested operational sampling interval for the wells that could be analyzed by Iterative Fitting is 2 to 3 quarters. This differs from the recommended sampling interval from the Temporal Variograms of approximately 2 years. The main reason for this difference is the small number of wells with sufficient data to perform the Iterative Fitting. Many more wells contributed sampling data to the Temporal Variograms, and therefore the results from the Temporal Variograms should be accorded more weight at Site 49.

**Table 3-4. Summary of Iterative Thinning Results, By COC and Well Location**

Notes: CUT = optimal data removal percentage; OUTPCT = fraction of estimated trend pts on reduced data falling outside baseline trend confidence bands; INTERVAL = optimal sampling interval (in weeks); FREQ = optimal sampling frequency per week; AVE-IQR = average interquartile range across 500 iterative LWQR fits on reduced dataset at specified removal level

WELL_ID	EASTING (ft)	NORTHING (ft)	COC	CUT	OUTPCT	INTERVAL (wks)	FREQ (#/wk)	AVE-IQR (ppb)
49-5562(D)	1212854	215270	DCA11	0.30	0.244	37.81	0.0262	0.299
49-5562(D)	1212854	215270	DCE12C	0.25	0.237	40.48	0.0249	0.297
49-5562(D)	1212854	215270	TCE	0.30	0.215	39.00	0.0258	0.407
49-5563(S)	1213011	215306	DCA11	0.10	0.203	33.41	0.0302	1.060
49-5563(S)	1213011	215306	DCE12C	0.20	0.207	37.30	0.0271	2.620
49-5563(S)	1213011	215306	TCE	0.15	0.245	34.81	0.0289	7.486
49-5564(D)	1212930	215180	DCA11	0.05	0.205	31.46	0.0321	1.594
49-5564(D)	1212930	215180	DCE12C	0.25	0.224	40.34	0.0250	0.280
49-5564(D)	1212930	215180	TCE	0.15	0.221	35.23	0.0286	1.852
49-5565(S)	1212924	215184	DCA11	0.10	0.202	33.67	0.0299	0.352
49-5565(S)	1212924	215184	DCE12C	0.10	0.240	33.23	0.0303	0.091
49-5565(S)	1212924	215184	TCE	0.20	0.201	37.45	0.0269	0.198
49-5566(S)	1212855	215266	DCA11	0.20	0.205	37.87	0.0266	0.189
49-5566(S)	1212855	215266	DCE12C	0.25	0.244	40.24	0.0252	0.267
49-5566(S)	1212855	215266	TCE	0.25	0.246	40.30	0.0253	0.266
49-5568(D)	1213344	215122	DCA11	0.10	0.211	29.93	0.0334	4.728
49-5568(D)	1213344	215122	DCE12C	0.10	0.224	29.62	0.0337	9.186
49-5568(D)	1213344	215122	TCE	0.05	0.169	28.55	0.0350	28.890
49-5573(D)	1213180	215177	DCA11	0.10	0.221	32.12	0.0314	7.129
49-5573(D)	1213180	215177	DCE12C	0.10	0.217	36.20	0.0283	6.754
49-5573(D)	1213180	215177	TCE	0.20	0.229	36.35	0.0277	112.000
49-5574(S)	1213181	215174	DCA11	0.15	0.194	34.24	0.0294	0.417
49-5574(S)	1213181	215174	DCE12C	0.15	0.220	34.55	0.0294	0.447
49-5574(S)	1213181	215174	TCE	0.15	0.193	34.44	0.0294	9.864
49-5577(D)	1212915	215277	DCA11	0.20	0.197	32.79	0.0305	0.150
49-5577(D)	1212915	215277	DCE12C	0.40	0.228	48.61	0.0208	1.198
49-5577(D)	1212915	215277	TCE	0.20	0.244	33.02	0.0301	46.750
49-5578(S)	1212919	215278	DCA11	0.35	0.246	44.44	0.0225	2.941
49-5578(S)	1212919	215278	DCE12C	0.55	0.248	65.97	0.0154	1.931
49-5578(S)	1212919	215278	TCE	0.05	0.176	30.78	0.0329	0.447
49-6515(S)	1212858	215262	DCA11	0.15	0.186	34.14	0.0295	0.159
49-6515(S)	1212858	215262	DCE12C	0.15	0.205	34.46	0.0293	0.161
49-6515(S)	1212858	215262	TCE	0.20	0.248	36.63	0.0276	0.206
49-6516(S)	1213093	215386	DCA11	0.20	0.230	36.66	0.0276	0.222
49-6516(S)	1213093	215386	DCE12C	0.05	0.148	30.77	0.0329	0.043
49-6516(S)	1213093	215386	TCE	0.20	0.226	36.91	0.0275	0.224
49-MW01	1213408	215440	DCA11	0.30	0.229	40.49	0.0248	0.488
49-MW01	1213408	215440	DCE12C	0.30	0.247	40.88	0.0246	0.523
49-MW01	1213408	215440	TCE	0.45	0.233	52.24	0.0193	1.381

**Table 3-5. Optimal Sampling Intervals and Frequencies Measured Across All COCs**

**Notes:** N-COCs = Number of COCs with Results; REMOVAL = Minimum fraction of data removed  
 INTERVAL = Minimum Optimal Sampling Interval (in weeks); FREQ = Maximum Optimal  
 Sampling Frequency (samples/week); PROPOSED = closest operational sampling interval (in quarters) to  
 the minimum optimal sampling interval (e.g., 3Q = 3 quarters)

WELL_ID	EASTING (ft)	NORTHING (ft)	N-COCs	REMOVAL	INTERVAL (wks)	FREQ (#/wk)	PROPOSED
49-5562(D)	1212854	215270	3	0.25	37.81	0.0262	3Q
49-5563(S)	1213011	215306	3	0.10	33.41	0.0302	3Q
49-5564(D)	1212930	215180	3	0.05	31.46	0.0321	2Q
49-5565(S)	1212924	215184	3	0.10	33.23	0.0303	3Q
49-5566(S)	1212855	215266	3	0.20	37.87	0.0266	3Q
49-5568(D)	1213344	215122	3	0.05	28.55	0.0350	2Q
49-5573(D)	1213180	215177	3	0.10	32.12	0.0314	2Q
49-5574(S)	1213181	215174	3	0.15	34.24	0.0294	3Q
49-5577(D)	1212915	215277	3	0.20	32.79	0.0305	3Q
49-5578(S)	1212919	215278	3	0.05	30.78	0.0329	2Q
49-6515(S)	1212858	215262	3	0.15	34.14	0.0295	3Q
49-6516(S)	1213093	215386	3	0.05	30.77	0.0329	2Q
49-MW01	1213408	215440	3	0.30	40.49	0.0248	3Q

### Section 3.4.3. Trend Maps

The trend maps themselves have been described above (a graph for each COC and each time period is contained in **Appendix 3-4**). One thing immediately apparent is that relatively few wells were actually mapped. Like the Iterative Fitting results, most of the wells at Site 49 had insufficient data to allow the estimation of reliable trends.

Consequently, the trend maps are rather sketchy and may not offer an accurate picture of trends at the site.

Concerning the wells that are mapped, very few show definite trends in either direction. Most of the estimated trends are fairly uncertain, as denoted by the light pink and light blue shading. This is true for the historical trends, as well as more recent ones. Overall, all three COCs exhibit many more decreasing trends instead of increasing ones. This is consistent with the observation that the original plume appears to be dissipating over time or perhaps moving beyond the range of the Site 49 well locations.

In any event, numerical information about the estimated trend magnitudes — including confidence bounds around each trend — by well and COC is listed in **Table 3-6**.



**Table 3-6. Estimated Trend Magnitudes and Confidence Intervals by COC and Well Location**

Notes: Historical = all data; Latest = last 4 sampling events  
 CONF-LEV = Achieved confidence level of non-parametric confidence interval around median slope  
 TREND = estimated magnitude of median slope (ppb/week);  
 LOWER-LIMIT = lower 95% confidence bound on trend magnitude (ppb/week)  
 UPPER-LIMIT = upper 95% confidence bound on trend magnitude (ppb/week)

WELLID	EASTING	NORTHING	COC	TYPE	CONF-LEV	TREND	LOWER-LIMIT	UPPER-LIMIT
49-5562(D)	1212854	215270	DCA11	Historical	0.962	-0.0013	-0.0034	0.0003
49-5562(D)	1212854	215270	DCA11	Post-1999	0.983	-0.0050	-0.0072	-0.0011
49-5562(D)	1212854	215270	DCA11	Latest	0.979	-0.0060	-0.0193	0.0001
49-5562(D)	1212854	215270	DCE12C	Historical	0.953	-0.0007	-0.0026	0.0008
49-5562(D)	1212854	215270	DCE12C	Post-1999	0.959	-0.0011	-0.0051	0.0011
49-5562(D)	1212854	215270	DCE12C	Latest	0.961	-0.0002	-0.0031	0.0024
49-5562(D)	1212854	215270	TCE	Historical	0.962	0.0000	-0.0025	0.0002
49-5562(D)	1212854	215270	TCE	Post-1999	0.983	0.0000	-0.0140	0.0009
49-5562(D)	1212854	215270	TCE	Latest	0.979	0.0003	0.0000	0.0023
49-5563(S)	1213011	215306	DCA11	Historical	0.953	-0.1352	-0.2967	-0.0338
49-5563(S)	1213011	215306	DCA11	Post-1999	0.959	-0.0323	-0.1285	0.0104
49-5563(S)	1213011	215306	DCA11	Latest	0.961	0.0104	-0.0309	0.0645
49-5563(S)	1213011	215306	DCE12C	Historical	0.953	-0.0750	-0.1776	-0.0279
49-5563(S)	1213011	215306	DCE12C	Post-1999	0.959	-0.0340	-0.0750	0.0351
49-5563(S)	1213011	215306	DCE12C	Latest	0.961	0.0351	-0.0279	0.1337
49-5563(S)	1213011	215306	TCE	Historical	0.953	-0.1758	-0.5867	-0.0397
49-5563(S)	1213011	215306	TCE	Post-1999	0.959	-0.0360	-0.1445	0.0553
49-5563(S)	1213011	215306	TCE	Latest	0.961	0.0553	-0.0324	0.1346
49-5564(D)	1212930	215180	DCA11	Historical	0.953	-0.1437	-0.1765	-0.0960
49-5564(D)	1212930	215180	DCA11	Post-1999	0.959	-0.0942	-0.1437	-0.0474
49-5564(D)	1212930	215180	DCA11	Latest	0.961	-0.1437	-0.2199	-0.0732
49-5564(D)	1212930	215180	DCE12C	Historical	0.953	-0.0015	-0.0030	0.0000
49-5564(D)	1212930	215180	DCE12C	Post-1999	0.959	-0.0028	-0.0072	-0.0001
49-5564(D)	1212930	215180	DCE12C	Latest	0.961	-0.0024	-0.0072	0.0000
49-5564(D)	1212930	215180	TCE	Historical	0.953	0.0137	0.0041	0.0414
49-5564(D)	1212930	215180	TCE	Post-1999	0.959	0.0595	0.0223	0.0824
49-5564(D)	1212930	215180	TCE	Latest	0.961	-0.0130	-0.0764	0.0776
49-5565(S)	1212924	215184	DCA11	Historical	0.953	-0.0070	-0.0186	-0.0007
49-5565(S)	1212924	215184	DCA11	Post-1999	0.959	-0.0041	-0.0191	0.0001
49-5565(S)	1212924	215184	DCA11	Latest	0.961	-0.0007	-0.0070	0.0047
49-5565(S)	1212924	215184	DCE12C	Historical	0.953	-0.0006	-0.0010	0.0011
49-5565(S)	1212924	215184	DCE12C	Post-1999	0.959	-0.0010	-0.0035	0.0001
49-5565(S)	1212924	215184	DCE12C	Latest	0.961	-0.0035	-0.0101	0.0022
49-5565(S)	1212924	215184	TCE	Historical	0.953	-0.0006	-0.0021	0.0007

WELLID	EASTING	NORTHING	COC	TYPE	CONF-LEV	TREND	LOWER-LIMIT	UPPER-LIMIT
49-5565(S)	1212924	215184	TCE	Post-1999	0.959	-0.0012	-0.0028	0.0010
49-5565(S)	1212924	215184	TCE	Latest	0.961	-0.0002	-0.0028	0.0025
49-5566(S)	1212855	215266	DCA11	Historical	0.953	-0.0007	-0.0021	0.0008
49-5566(S)	1212855	215266	DCA11	Post-1999	0.959	-0.0011	-0.0029	0.0010
49-5566(S)	1212855	215266	DCA11	Latest	0.961	-0.0002	-0.0027	0.0024
49-5566(S)	1212855	215266	DCE12C	Historical	0.953	-0.0007	-0.0021	0.0008
49-5566(S)	1212855	215266	DCE12C	Post-1999	0.959	-0.0011	-0.0029	0.0010
49-5566(S)	1212855	215266	DCE12C	Latest	0.961	-0.0002	-0.0027	0.0024
49-5566(S)	1212855	215266	TCE	Historical	0.953	-0.0007	-0.0021	0.0008
49-5566(S)	1212855	215266	TCE	Post-1999	0.959	-0.0011	-0.0029	0.0010
49-5566(S)	1212855	215266	TCE	Latest	0.961	-0.0002	-0.0027	0.0024
49-5568(D)	1213344	215122	DCA11	Historical	0.962	-0.0015	-0.0118	0.0457
49-5568(D)	1213344	215122	DCA11	Post-1999	0.983	-0.0383	-0.0775	-0.0013
49-5568(D)	1213344	215122	DCA11	Latest	0.979	-0.0012	-0.0972	0.1555
49-5568(D)	1213344	215122	DCE12C	Historical	0.962	0.0340	-0.0844	0.1489
49-5568(D)	1213344	215122	DCE12C	Post-1999	0.983	-0.2368	-0.5944	-0.0012
49-5568(D)	1213344	215122	DCE12C	Latest	0.979	-0.1147	-0.8066	0.0677
49-5568(D)	1213344	215122	TCE	Historical	0.962	-0.1436	-0.2263	0.0091
49-5568(D)	1213344	215122	TCE	Post-1999	0.983	-0.2269	-0.3072	-0.0706
49-5568(D)	1213344	215122	TCE	Latest	0.979	-0.0537	-0.3072	0.0459
49-5573(D)	1213180	215177	DCA11	Historical	0.953	-0.4729	-0.5998	-0.3860
49-5573(D)	1213180	215177	DCA11	Post-1999	0.959	-0.3802	-0.4645	-0.2890
49-5573(D)	1213180	215177	DCA11	Latest	0.961	-0.2956	-0.6418	-0.1915
49-5573(D)	1213180	215177	DCE12C	Historical	0.965	-0.1391	-0.2482	-0.0079
49-5573(D)	1213180	215177	DCE12C	Post-1999	0.969	-0.1620	-0.8716	0.0630
49-5573(D)	1213180	215177	DCE12C	Latest	0.992	-0.0638	-1.1946	0.0630
49-5573(D)	1213180	215177	TCE	Historical	0.953	-2.9872	-4.5367	-1.7470
49-5573(D)	1213180	215177	TCE	Post-1999	0.959	-1.2983	-1.9107	-0.0904
49-5573(D)	1213180	215177	TCE	Latest	0.961	-1.7470	-2.4055	-0.8444
49-5574(S)	1213181	215174	DCA11	Historical	0.953	-0.0114	-0.0211	-0.0024
49-5574(S)	1213181	215174	DCA11	Post-1999	0.959	-0.0168	-0.0211	-0.0044
49-5574(S)	1213181	215174	DCA11	Latest	0.961	-0.0044	-0.0155	0.0012
49-5574(S)	1213181	215174	DCE12C	Historical	0.953	0.0089	-0.0016	0.0136
49-5574(S)	1213181	215174	DCE12C	Post-1999	0.959	0.0097	-0.0030	0.0136
49-5574(S)	1213181	215174	DCE12C	Latest	0.961	0.0011	-0.0281	0.0192
49-5574(S)	1213181	215174	TCE	Historical	0.953	-0.1251	-0.2020	0.0224
49-5574(S)	1213181	215174	TCE	Post-1999	0.959	-0.0463	-0.1553	0.0407
49-5574(S)	1213181	215174	TCE	Latest	0.961	-0.0774	-0.2954	0.0224
49-5577(D)	1212915	215277	DCA11	Historical	0.962	-0.0075	-0.0117	-0.0051
49-5577(D)	1212915	215277	DCA11	Post-1999	0.965	-0.0044	-0.0064	-0.0025
49-5577(D)	1212915	215277	DCA11	Latest	0.979	-0.0015	-0.0043	0.0011
49-5577(D)	1212915	215277	DCE12C	Historical	0.953	-0.0079	-0.0107	-0.0062
49-5577(D)	1212915	215277	DCE12C	Post-1999	0.959	-0.0054	-0.0173	0.0048
49-5577(D)	1212915	215277	DCE12C	Latest	0.961	0.0086	-0.0009	0.0232

WELLID	EASTING	NORTHING	COC	TYPE	CONF-LEV	TREND	LOWER-LIMIT	UPPER-LIMIT
49-5577(D)	1212915	215277	TCE	Historical	0.962	-0.0391	-0.4091	0.1263
49-5577(D)	1212915	215277	TCE	Post-1999	0.965	-0.0292	-0.2290	0.2170
49-5577(D)	1212915	215277	TCE	Latest	0.979	0.3060	-0.2290	0.5535
49-5578(S)	1212919	215278	DCA11	Historical	0.953	-0.0123	-0.0230	0.0145
49-5578(S)	1212919	215278	DCA11	Post-1999	0.959	-0.0127	-0.0442	0.0176
49-5578(S)	1212919	215278	DCA11	Latest	0.961	-0.0229	-0.0628	0.0166
49-5578(S)	1212919	215278	DCE12C	Historical	0.953	0.0067	-0.0098	0.0164
49-5578(S)	1212919	215278	DCE12C	Post-1999	0.959	-0.0212	-0.0340	0.0031
49-5578(S)	1212919	215278	DCE12C	Latest	0.961	-0.0340	-0.0612	0.0204
49-5578(S)	1212919	215278	TCE	Historical	0.953	-0.0009	-0.0085	0.0048
49-5578(S)	1212919	215278	TCE	Post-1999	0.959	-0.0052	-0.0133	0.0089
49-5578(S)	1212919	215278	TCE	Latest	0.961	-0.0133	-0.0577	0.0128
49-6515(S)	1212858	215262	DCA11	Historical	0.953	-0.0009	-0.0020	0.0007
49-6515(S)	1212858	215262	DCA11	Post-1999	0.959	-0.0014	-0.0029	0.0007
49-6515(S)	1212858	215262	DCA11	Latest	0.961	-0.0003	-0.0023	0.0024
49-6515(S)	1212858	215262	DCE12C	Historical	0.953	-0.0009	-0.0020	0.0007
49-6515(S)	1212858	215262	DCE12C	Post-1999	0.959	-0.0014	-0.0029	0.0007
49-6515(S)	1212858	215262	DCE12C	Latest	0.961	-0.0003	-0.0023	0.0024
49-6515(S)	1212858	215262	TCE	Historical	0.953	-0.0009	-0.0020	0.0007
49-6515(S)	1212858	215262	TCE	Post-1999	0.959	-0.0014	-0.0029	0.0007
49-6515(S)	1212858	215262	TCE	Latest	0.961	-0.0003	-0.0023	0.0024
49-6516(S)	1213093	215386	DCA11	Historical	0.953	-0.0010	-0.0020	0.0006
49-6516(S)	1213093	215386	DCA11	Post-1999	0.959	-0.0012	-0.0024	0.0007
49-6516(S)	1213093	215386	DCA11	Latest	0.961	-0.0003	-0.0024	0.0024
49-6516(S)	1213093	215386	DCE12C	Historical	0.953	-0.0005	-0.0019	0.0014
49-6516(S)	1213093	215386	DCE12C	Post-1999	0.959	-0.0016	-0.0037	0.0029
49-6516(S)	1213093	215386	DCE12C	Latest	0.961	0.0037	-0.0026	0.0060
49-6516(S)	1213093	215386	TCE	Historical	0.953	-0.0010	-0.0020	0.0006
49-6516(S)	1213093	215386	TCE	Post-1999	0.959	-0.0012	-0.0024	0.0007
49-6516(S)	1213093	215386	TCE	Latest	0.961	-0.0003	-0.0024	0.0024
49-MW01	1213408	215440	DCA11	Historical	0.953	-0.0013	-0.0025	-0.0003
49-MW01	1213408	215440	DCA11	Post-1999	0.959	-0.0021	-0.0030	-0.0006
49-MW01	1213408	215440	DCA11	Latest	0.961	-0.0011	-0.0023	0.0001
49-MW01	1213408	215440	DCE12C	Historical	0.953	-0.0052	-0.0109	-0.0012
49-MW01	1213408	215440	DCE12C	Post-1999	0.959	-0.0104	-0.0203	-0.0013
49-MW01	1213408	215440	DCE12C	Latest	0.961	-0.0065	-0.0180	0.0030
49-MW01	1213408	215440	TCE	Historical	0.953	-0.0059	-0.0126	-0.0034
49-MW01	1213408	215440	TCE	Post-1999	0.959	-0.0050	-0.0101	-0.0026
49-MW01	1213408	215440	TCE	Latest	0.961	-0.0126	-0.0184	-0.0013

## Section 4. Spatial Optimization

This section summarizes the spatial statistical analyses conducted at Site 49 on long-term groundwater monitoring (LTM) data using the spatial component of the GTS algorithm. The main goal of this portion of the study was to determine whether there are statistical redundancies within the spatial network of well locations being monitored at Site 49, and to make recommendations as to which current wells might be “pulled out” of the network, or at least sampled very infrequently. The purpose in doing so is to optimize the LTM program by determining whether there are resources being poured into sampling and analysis that might be pared without sacrificing critical information.

A secondary goal of the spatial analysis is to determine whether there are specific areas at Site 49 where the siting of additional wells would provide important, unknown information about contaminant extent. By “eliminating” redundant wells from “over-sampled” areas and then potentially adding wells to other areas of “undercoverage,” the spatial network can be optimized in the sense that monitoring wells are effectively placed to capture key information about the contaminant plume(s).

This section includes descriptions of 1) what data preparations were made for input to the GTS spatial algorithm; 2) the GTS spatial algorithm itself, including changes made to the algorithm since the last published version (Cameron and Hunter, 2002); and 3) results of the Site 49 spatial analysis.

### Section 4.1. Data Preparation

As discussed in **Section 3.1**, data queries were made for all chemical analytical data collected from wells Site 49. Exploratory statistical analyses were then performed to pare the initial list of possible constituents to 2 to 3 candidate constituents of concern (COC). As mentioned previously, including a large number of COCs significantly increases the amount of work required to run the GTS algorithm without typically improving the results. So the goal was to include only those parameters in the optimization routine that offer *the most statistical information* concerning temporal and spatial redundancy. The best such parameters typically exhibit larger detection rates and more widespread spatial occurrence.

Overall, the most promising candidates at Site 49 were TCE (the single best candidate and the main source contaminant of the known plume), DCA11, and DCE12C. These three were chosen for the optimization analysis. Other COCs had much lower detection rates and/or poorer spatial distributions.

Unlike the temporal analysis, where sampling data at a given well and date but collected over multiple depths were averaged so as to ensure that there was only one value per sampling event per well, the spatial analysis was designed to be three-dimensional in nature. What that meant was that every sample measurement was assigned not only an easting and northing, but also a depth and elevation value. Only data that could be placed within three-dimensional space could be utilized in the analysis. Data points missing any of these components were excluded.

Because a small number of existing well locations were either missing the depth or surface elevation component, attempts were made to “fill in” missing information where possible. After obtaining the most up-to-date information from Montgomery Watson, only 12 of 92 locations were still missing necessary depth information. All of these wells were associated with historical sampling events, but were not currently being sampled at the site. Of the more recent data, a total of 67 wells had sampling information and were used as a baseline for the spatial analysis.

The other major step in the data preparation was to divide the available data for each COC into two separate “time slices.” The first time slice consisted of all measurements procured during 2001. The second covered all measurements sampled from 2002. No measurements were available in the database from the year 2000. Data prior to this were not used in the spatial analysis in part to ensure that the most current well network was optimized, especially as the list of wells being monitored changed substantially between 1997 through 1999 and the period from 2001 to 2002. It was also apparent that the magnitude of the plume of contamination had dropped substantially between these two periods.

The reason for analyzing separate time slices was three-fold: 1) because the character and extent of contamination is likely to change over time, yet maps of a site represent only “snapshots,” it is important to analyze data from a limited time frame in order to create reasonably accurate maps; 2) unless sampling events are highly regimented and all wells are sampled at the same time and during the same sampling event, it may be impossible to include a full representation of the spatial well network if only a specific sampling event is analyzed, as opposed to a “slice” of time that includes a limited range of events; 3) to help ensure that well locations are optimized over the life of the LTM program and not simply for a given sampling event, wells are only identified as potentially redundant if they exhibit redundancy across time slices (note, however, that newer wells might not have any data for earlier time slices; such wells would exhibit redundancy only in more recent time slices).

In practical terms at Site 49, with 3 COCs and two time slices per COC, six distinct data sets were analyzed under the spatial optimization algorithm. This allowed for a six-fold comparison of redundancy in identifying wells that were either “essential” or potentially “redundant” in their statistical information. On a final note, as in the temporal analysis, non-detects were handled by converting them to half the listed reporting limit (RL).

## **Section 4.2. Methodology**

The heart of the spatial optimization analysis in GTS consists of the following basic steps: 1) estimation of a declustered, univariate cumulative distribution of concentration values for each COC; 2) determination of an appropriate spatial bandwidth; 3) creation of a base map using locally-weighted quadratic regression and all existing site data; 4) calculation of a global regression weight at each well; and 5) iterative elimination of wells with the lowest global regression weights and re-estimation of the site map based on the reduced data set. Each of these steps is explained below.

### Section 4.2.1. Declustered CDF

The first task of the spatial analysis was to determine an appropriate univariate distribution of concentration values for each COC. At many contaminated sites, the measurement data may range over several orders of magnitude. As importantly, there is a complex, three-dimensional spatial distribution associated with these values, dependent both on the nature of the subsurface and the intensity and location of the contaminant plume(s). High concentrations tend to cluster together, although not uniformly and not necessarily in a predictable fashion. Because of this reality, most standard geospatial techniques, including typical forms of kriging, can suffer in their ability to produce reasonable site maps. Univariate and parametric forms of kriging, in particular, such as ordinary or lognormal kriging, often have great difficulty accurately reproducing the highs and lows of widely spread concentration ranges. Except that is, at known data locations, where kriging “honors” the data by exactly reproducing it.

A better strategy is to use a non-parametric form of spatial analysis, such as probability kriging or perhaps even quantile kriging. Probability kriging transforms the original concentration data into a series of indicator variables and another variable representing the uniform scores of the original data. Each indicator is a binary 0-1 variable associated with a particular reference concentration level. All samples with values no greater than the reference level are converted to ones and all values larger than the reference level are converted to zeros. The basic idea is to convert each data value into known probabilities: if the reference level is, for example, 10 ppb, an indicator value of one means it is certain that the data point in question does not exceed 10 ppb (the probability of not exceeding the reference level being equal to one), while an indicator value of zero means that the actual concentration is certainly greater than 10 ppb (the probability of not exceeding the reference being zero).

Typically in probability kriging a series of increasing reference levels is used to define key portions of the actual concentration range (e.g., 5 ppb, 100 ppb, 1,000 ppb, 5,000 ppb, 10,000 ppb). Indicator variables are defined for each reference level and kriging is performed on each indicator. The ultimate goal at each unknown map location is to form a weighted combination of the known 0's and 1's to estimate a probability that the unknown location does not exceed the reference level. Then, by having such probabilities in hand for the entire series of indicators, a reasonable estimate can be made of the actual concentration at the unknown location (more on that below).

To improve these estimates, probability kriging employs an extra variable computed as the *uniform scores* of the original concentration distribution. This transformation simply orders the data and converts each value to its rank divided by the data set sample size, thus giving a transformed value between 0 and 1. Higher values thus have uniform scores closer to 1 while low values have uniform scores closer to 0.

The same strategy is used in quantile kriging. While no indicator variables are formed as in probability kriging, kriging is performed on the uniform scores directly instead of the actual concentrations, leading to kriged estimates between 0 and 1. These estimates can then be thought of as percentiles, since they represent a probability of not exceeding a certain concentration level. The concentration level itself is known as the *quantile*

associated with the particular percentile, hence the name quantile kriging. So for example, if the kriged estimate were 0.7, the estimated value at that location would represent the 70<sup>th</sup> percentile of the possible distribution of concentration measurements.

To actually re-transform these percentile estimates back to the original concentration scale, some form of the cumulative distribution of concentration measurements must be used. Unfortunately, because sampling in contaminated areas is often done to “chase the plume,” clusters of high values are often over-represented in the raw, univariate concentration distribution, biasing the results. A better solution is to make use of the *declustered cumulative distribution* or declustered CDF for short. The declustered CDF adjusts the raw distribution for spatial clustering and generally offers a more accurate estimate of the true concentration distribution.

While a variety of techniques exist to form the declustered CDF, the one utilized in GTS is based on a method for finding declustering weights (Bourgault, 1999). In this method, simple quantile kriging is performed on the set of known measurements, not to estimate *unknown* locations, but rather to *cross-validate* the *known* ones. This is done by temporarily removing a known value from the data set and then calculating a kriged estimate at that spot using the remaining data (otherwise known as “leave-one-out” cross-validation or jackknifing). As it turns out, the local kriging variance associated with each data location being cross-validated can be considered a *declustering weight*: higher variances represent locations with minimal spatial clustering while lower variances represent locations with significant clustering. By then weighting the original concentrations according to these declustering weights, the declustered CDF is formed as the resulting weighted univariate distribution.

To perform the actual cross-validation and simple quantile kriging, two preparation steps had to be accomplished. One was to convert the original data into uniform scores. The other was to develop a three-dimensional model of spatial covariance for the uniform scores. This was accomplished by analyzing omnidirectional variograms of the uniform scores for each of the three COCs and fitting appropriate spatial correlation models to these plots. Parameters for each model are provided in **Table 4-1** below.

**Table 4-1. Parameters of Final Spatial Correlation Models**

COC	Nugget	Spherical Component		Exponential Component		Gaussian Component	
		Sill	Range	Sill	Range	Sill	Range
DCA11	0.74	0.30	180	—	—	—	—
DCE12C	0.69	0.36	170	—	—	—	—
TCE	0.625	0.36	120	0.05	500	—	—

The result of this step was a declustered univariate CDF for each COC. Note that this cumulative distribution of concentration values was designed to represent the range of concentrations that could be observed at Site 49. As such, the declustered CDF includes data from the entire time period under consideration, from 1997 until the present.

Furthermore, as will be explained below, the declustered CDF was ultimately used to derive concentration estimates of each COC along a grid of unknown locations encompassing what will be termed the *optimization box*.

#### **Section 4.2.2. Spatial Bandwidth and Search Radius**

An important step to building an estimated site map is to choose a *spatial bandwidth*. The fitting procedure used in the current version of GTS, namely *locally-weighted quadratic regression* (LWQR), works by estimating the surface value at a given unknown grid location using a weighted linear combination of the known sample values close to the grid point. The analyst must select, however, how many neighboring sample measurements to use. In GTS this is done by selecting a *bandwidth parameter* that represents the fraction of known samples to be included in the neighborhood of any given grid point. For a one-dimensional time series, these bandwidths typically range from 40% to 80%. With volumetric or three-dimensional data, roughly equivalent bandwidths (in terms of data density included in the neighborhood per unit of volume) are on the order of 10% to 40%.

In general, the higher the bandwidth, the greater the amount of ‘smoothing’ that will occur over the estimated surface. Too high a bandwidth and the surface trend may ‘miss’ important peaks and valleys. Too low a bandwidth and the surface trend may exhibit artifactual jumps and/or dips between known sample values.

To guard against these scenarios, it is important to run a ‘pre-flight’ check of the LWQR fits at several possible bandwidths prior to constructing a base map of the site. This pre-flighting is done by computing diagnostic checks of the *residuals* obtained when the surface trend is estimated at each known sample location and the known value is subtracted from this estimate.

Using GTS, several tests of the surface residuals are made, including the following calculations: Mallow’s CP statistic, correlation of the residuals with the estimated surface trend, average bias of the residuals, and Filliben’s probability plot correlation coefficient. Each of these statistics is designed to provide a numerical indication of the goodness of the estimated trend relative to a given bandwidth. In GTS, these residual diagnostic measures are plotted simultaneously against bandwidth in order to search for the most appropriate fitting neighborhood. The residuals are also plotted in space to look for obvious anomalies or areas of substantial lack of fit.

Mallow’s CP statistic is a scaled measure of the sum of squared residuals. Lower values of Mallow’s CP usually indicate a better fit. The correlation with the estimated surface trend is used to check whether the fit is worse over certain ranges of the variable being estimated than others. Values close to zero are best. Values close to zero are also good when examining the average bias, which simply measures the average difference between the estimated surface value and the known measurement. Filliben’s correlation coefficient is a test of normality that can be used to check the shape and symmetry of the residual distribution. LWQR works best when the *residual* distribution is symmetric and normally distributed. Coefficient values closer to one are best.

Taken together, it is usually possible to find an acceptable bandwidth with which to construct the surface maps. At Site 49, a value of 20% was deemed a reasonably good choice for TCE and DCE12C. That simply means that the nearest one-fifth of the data measurements were used to help estimate the unknown grid point, regardless of their distance from that location. For DCA11, a bandwidth of 15% was used.

### **Section 4.2.3. Creating Base Maps with LWQR**

Once a bandwidth is chosen, the next task is to create a three-dimensional base map for each COC and time slice. The base map under GTS serves as the primary means by which degrees of spatial redundancy are assessed. Not only is a baseline established as each COC is mapped across the site area, but measures of local and global variance are also computed. At each further iteration of the GTS algorithm, new maps created from reductions in the original data set are compared to the base map to determine how much plume information has been lost and at what price in increased map uncertainty. For this reason, it is important to try and build as accurate a base map as possible.

The previously published version of GTS employed a fairly simple strategy for creating base maps (and subsequent maps). In order to 1) avoid data complexity, 2) handle large fractions of non-detect values, and to 3) aid in the fitting of spatial covariance models, all measurements were converted to a single indicator variable (i.e., zeros and ones), where the reference concentration level was taken as either the detection/reporting limit or a regulatory limit (such as an MCL). Base maps constructed from these indicators were not re-converted to concentrations, but rather represented maps of the probability that the true concentration was below the reference level. As such, these maps did not provide detailed information about plume intensity, but still were useful for assessing spatial redundancy. However, a significant amount of statistical information concerning the spatial distribution of contaminants was not utilized.

In the current version of GTS, the attempt is made to map the plume or contaminant distribution more completely. This is done by converting the sample concentrations into a series of 10 indicator variables, with each reference concentration representing a key quantile of the original, univariate declustered CDF, as shown in **Table 4-2** below. The goal here is not to choose specific regulatory limits as reference values, but rather levels that adequately ‘divide’ or ‘span’ the univariate distribution of COC concentrations, paying particular attention to the often highly skewed upper end of these distributions.

It should also be noted that at the lower end of the concentration range, the reference percentiles are not always equally distributed. At many sites, including Site 49, there is often a significant fraction of non-detects at a common reporting limit. This can lead to large jumps in the declustered CDF.

**Table 4-2. Reference Concentrations and Corresponding Percentiles of Declustered CDF for Each COC**

Indicator Variable	DCA11		DCE12C		TCE	
	Reference Conc (ppb)	Percentile	Reference Conc (ppb)	Percentile	Reference Conc (ppb)	Percentile
I-1	0.25	0.130	0.25	0.122	0.5	0.416
I-2	0.5	0.442	0.5	0.442	1	0.530
I-3	1	0.592	1	0.562	5	0.632
I-4	3.5	0.695	3.5	0.652	10	0.712
I-5	10	0.795	10	0.776	30	0.799
I-6	20	0.863	20	0.848	80	0.855
I-7	40	0.926	45	0.900	120	0.901
I-8	60	0.951	70	0.948	240	0.951
I-9	90	0.978	90	0.978	700	0.974
I-10	150	0.992	200	0.993	2000	0.990

Another facet of the previous version of GTS was that all analyses were conducted in two-dimensional (2D) space. Depth information was simply ignored or collapsed so that all well locations were treated as if they resided in a 2D plane. Furthermore, the technique used to estimate the base map (and all subsequent maps) was ordinary indicator kriging. Kriging takes a neighborhood of known values around an unknown grid point and solves a set of simultaneous linear equations to find the “best” estimate for that grid point. The known locations are “honored” in the sense that a kriged estimate at a known location returns the original data value. In this way, kriging can be thought of as a kind of *spatial interpolator*, where grid points between known locations are interpolated based on the known values.

A key aspect of the kriging method is that it fundamentally depends on having a spatial covariance model that adequately describes the strength of the spatial correlation between adjacent sample points. Much effort in fact can be devoted to analyzing the empirical spatial correlation measure (typically called the variogram or semi-variogram) and then developing an appropriate mathematical model of the spatial covariance.

In order to streamline this process, a different technique has been incorporated into the GTS algorithm: *locally-weighted quadratic regression* (LWQR). Like kriging, LWQR takes a neighborhood of sample values located near an unknown grid point and solves a system of linear equations to determine the optimal estimate. Like kriging, LWQR is a kind of linear estimator. Both techniques assign numerical weights to the sample values in the neighborhood and form the new estimate as a weighted average of the sample values. However, there are also a number of differences.

For one, kriging requires that all the sample data have distinct locations in space. Otherwise the kriging algorithm does not return a solution. In practice, if some locations have multiple measurements during a given time slice (say from distinct sampling

events), these values must first be averaged or pre-processed in such a way that only a single value is used for kriging. Some information about the individual measurements and data variability is necessarily lost in this step. LWQR has no similar requirement. So multiple values at a given well or given sampling location are OK.

Second, kriging, as mentioned above, is a spatial interpolator which honors the known data values. LWQR is instead a *smoother*. Applied to spatial fields, LWQR attempts to find the best overall surface to *fit* the available sample points, but it does not require that any individual data value be honored. The best analogy is standard linear regression. When a best-fitting line is estimated for a time series or an XY-scatterplot, the line may or may not exactly pass through any given individual value. Nevertheless, the line is chosen to minimize the sum of squared deviations from it and to fit the overall trend. In a similar way, the standard version of LWQR is designed to determine the best-fitting quadratic surface through the sample points, but will not *necessarily* pass through any one of them exactly.

In practical terms, LWQR attempts to fit the best overall surface to the sample data while implicitly assuming that the measured samples may not precisely fit the surface trend either due to error or some other source of variation. Standard forms of kriging basically assume that all sample data are known exactly. Of course, there is no guarantee that some measurements might not include elements of laboratory or sampling error. Variation is also introduced by the fact that the groundwater quality and/or plume intensity may change slightly from one sampling event to the next.

A third difference is that LWQR does not require prior development of a spatial covariance model. With LWQR, a locally-quadratic surface is fit to each grid point. Spatial correlation is incorporated in this method not through an explicit prior correlation model, but rather through the apparent *curvature* in the sample points themselves. The quadratic surface is fit to this curvature, the degree of curvature potentially changing with each grid point. In this way, spatial clustering *is* accommodated by the LWQR technique.

#### **Section 4.2.4. Constructing the Base Map**

To actually build the base maps at Site 49, a volume surrounding the site was constructed and a rectangular grid imposed on this volume. This volume is termed the *optimization box* in GTS. Often the optimization box will not precisely coincide with the site boundaries, or may not include some peripheral wells, but the aim is to have the box match the site boundaries fairly closely. Peripheral wells are included in the neighborhoods of sample points associated with some of the nearby grid locations. In this way, those wells do get included in the optimization analysis.

The specific coordinate ranges of the optimization box for Site 49 are listed in **Table 4-3** below. Note that due to the surface topography, it may occur that nodes on the upper layer of the grid are sometimes higher than ground level. Fortunately at Site 49, the surface gradients are quite mild, so that the optimization grid nodes almost always corresponded to real subsurface locations.

**Table 4-3. Boundaries of Optimization Box**

Direction	Minimum	Maximum	Step Size
Easting	1,212,850 ft	1,213,850 ft	40 ft
Northing	215,000 ft	215,450 ft	30 ft
Elevation	0 ft	60 ft	10 ft

At each grid node, an LWQR estimate was made using each of the ten indicator variables in turn. At each indicator level, the zeros and ones corresponding to the sample data were employed to compute an estimate of the probability that the reference concentration level had not been exceeded. Repeating this process for each indicator then gave a series of ten probability values at each grid node, representing updated information helping to “bracket” the best estimate of the concentration at that node. As an example of this process, consider the following hypothetical results for TCE at node 10 as shown in **Table 4-4**:

**Table 4-4. Hypothetical LWQR Results for TCE**

COC	Indicator Variable	Reference Level (ppb)	LWQR Result
TCE	I-1	0.5	0.10
TCE	I-2	1	0.20
TCE	I-3	5	0.25
TCE	I-4	10	0.28
TCE	I-5	30	0.36
TCE	I-6	80	0.45
TCE	I-7	120	0.78
TCE	I-8	240	0.95
TCE	I-9	700	0.99
TCE	I-10	2000	0.99

Based on the LWQR results, there would be only a 10% probability that the true concentration fell below 0.5 ppb, a 20% chance that the true concentration was below 1 ppb, a 25% chance that the true value was below 5 ppb, a 28% chance that the true value was below 10 ppb, a 36% chance that the true value was below 30 ppb, a 45% chance that the true value was below 80 ppb, a 78% chance that the value was below 120 ppb, a 95% chance that the true value was below 240 ppb, and a 99% probability that the value was below 700 ppb or greater. The most likely range would therefore be between 80 ppb and 120 ppb.

To actually determine a concentration estimate for this hypothetical grid node, the approach taken in GTS is to update the univariate declustered CDF using the LWQR results for the series of indicators. This leads to what is known as the *conditional* cumulative distribution function or CCDF. The basic idea is to *condition* or *adjust* the overall univariate distribution of measured values using the updated information provided by the LWQR indicator results. So, for instance, in the hypothetical example above, the declustered CDF for TCE indicates that 90.1% of all the available TCE measurements at

Site 49 were no greater than 160 ppb (see previous table). At the hypothetical grid node being estimated, however, the probability that the true value does not exceed 160 ppb is only 78%. Therefore, the overall univariate CDF must be updated so that values less than 160 ppb only occur 78% of the time *at this grid node*. In this manner, an updated CCDF can be calculated independently for each grid node and estimates of the (locally-varying) true mean concentration made across the site using the formula:

$$\hat{v} = \sum_i v_i (CCDF(v_i) - CCDF(v_{i-1}))$$

where  $v_i$  indexes the observed concentration values from the declustered, univariate CDF, and  $CCDF(v_i)$  represents the updated or conditional CDF probability associated with  $v_i$ .

### Section 4.2.5. Global Regression Weights

In addition to the base map built from the LWQR estimates, another key output is the computation of global regression weights. The vector of global regression weights associates each known well location with a numerical index representing that well's overall relative contribution to the base map. Positive global regression weights represent wells that are more influential in the base map estimation; negative or zero weights represent wells which play a smaller, more redundant statistical role in the creation of the map. Thus, the global regression weights serve to identify degrees of spatial redundancy among the set of existing well locations.

The global regression weights are calculated by accumulating in an appropriate way a series of intermediate vectors known as the *local* regression weights. These intermediate weights are a by-product formed when computing the estimated probability of non-exceedance for each indicator variable at a given grid node: the LWQR results are manipulated to compute what is known as the *local weight diagram*. The weight diagram is a vector of numerical weights, one per sample measurement in the search neighborhood, such that the probability of non-exceedance for a specific indicator level is proportional to a weighted average of the product of the sample indicator values and the weight diagram. Thus the weight diagram represents the set of local regression weights that gets applied to the observed indicator data to produce the LWQR estimate.

There are two important things to note about the local weight diagram. First, each grid node involves a different set of neighborhood samples, but across the site as a whole, any given sample value is likely to be used in the neighborhood of a number of distinct grid nodes. Thus, the search neighborhoods tend to overlap as one "moves about" the grid. Second, the local weights in LWQR, while they sum to one, are not necessarily positive.

With these items in mind, how are the global regression weights then computed from the local weights? First, the local weight vectors are augmented to give *zero* weight to any sample location located outside the search neighborhood for that grid node. This numerically represents the fact that samples outside the neighborhood have no influence (positive or negative) on the LWQR result for the node being estimated. Second, the augmented local weight vectors are averaged across all the grid nodes *by* sample location. This means that given a known sample location at well X, the local weights associated with that location (one per grid node, with some possibly equaling zero) are summed and

then divided by the total number of nodes. Finally the averaged weights are adjusted for wells with multiple sampling depths. Here the weights are summed across depths for each well. Weights at wells with only a single sampling depth remain unchanged.

After all these steps are completed, *there is exactly one weight per well location*, and it is this numerical vector that is deemed the set of global regression weights. The term global is used because the final weights are built by averaging the local influence on the base map of each sample across the grid, and hence, across the site as a whole. With this vector in hand, the wells are then ranked according to their statistical influence on the base map. Wells with higher global regression weights are deemed more essential to the map estimate, while those with lower weights are deemed least essential and thus potentially redundant.

### Section 4.2.6. Local and Global Variance Measures

In addition to forming the basis for the global regression weights, the local regression weights are also useful for estimating relative local and global variance measures. These measures provide a way to assess the relative degree of statistical uncertainty associated with a given map estimate. First, a local uncertainty measure is computed at each grid node using the local weight diagram and the following formula:

$$locvar(w_k) = \sum_i |lx^i(w_k)|^2$$

where  $w_k$  denotes the  $k$ th grid node,  $i$  indexes the sample values in the search neighborhood around the  $k$ th node, and  $lx$  represents the local regression weight vector.

Because a different relative local variance is computed at each grid node, the set of local variances can be mapped, much like the base map of concentration estimates. One can also determine from such a variance map whether there are certain areas of the site where the local variance is particularly high, representing places of greater statistical uncertainty connected with the mapped concentration estimate.

With the local variances in hand, GTS also computes a global variance measure for the site as a whole. To do this, the local variances are simply summed across the set of grid nodes, using the following formula:

$$gvar = \sum_k locvar(w_k)$$

where, as before,  $w_k$  denotes the  $k$ th grid node and the summation is taken over the entire grid.

The reason why the global variance is valuable is that it provides a single numerical summary of the total relative statistical uncertainty associated with a given configuration of well locations. In other words, the global variance from the base map — utilizing all the original well locations — can be compared against the global variance computed from estimating the same map on a reduced or different set of well locations. Increases in global uncertainty then represent configurations that are less statistically reliable.

### Section 4.2.7. Iterative Elimination of Wells

Given that the global regression weights provide a *relative* but not an *absolute* measure of spatial redundancy, it is important to use other measures to test how many wells are actually redundant and what degree of redundancy should be tolerated. The global regression weights therefore provide a *strategy* for identifying potentially redundant wells. However, the acid test is to see how accurately maps can be estimated when these possibly redundant wells are temporarily removed from the data set.

To accomplish this goal in a systematic fashion, GTS uses the following procedure. First, the remaining wells are sorted by global regression weight. Second, the subset with the lowest five to ten percent of global regression weight scores are flagged and removed from the data. Then LWQR is used on the reduced data set to re-estimate the site map. Comparing this re-estimated map to the original base map, three basic statistical quantities are measured: 1) change in global regression variance; 2) changes in local node-specific variances, including tracking of the percentage of nodes with local variances greater than a pre-defined threshold; and 3) changes in the mapped concentration estimates.

The same process is repeated several times by removing five to ten percent of the lowest ranked well locations (that is, ranked by global regression weight) at each incremental iteration. In this fashion, a small number of wells is temporarily eliminated at each step, until the map estimates show obvious deterioration and the variance measures show substantial change.

The final step in the spatial analysis is to review the results of the iterative well location removal algorithm and to decide at what point the re-estimated maps have deteriorated beyond a reasonable level. Such a decision is necessarily somewhat subjective. However, it is often helpful to examine the rate of deterioration in the maps and the rate of change in the global and local variance measures as a function of the percentage of well locations that has been removed.

Once a “stopping point” has been decided, only wells deemed potentially redundant at the *previous* removal step are ultimately tagged as redundant for that COC and time slice. Then the lists of redundant wells are compared across the COCs and time slices in order to determine that subset of locations which is consistently redundant. These wells then make up the final redundancy list for the site.

One final thing to note is that the global regression weights are recomputed at each stage of removal and therefore are not “fixed” measures of redundancy. Wells with higher global weights at one stage, and thus considered important enough to “keep in the mix” of essential wells, might have low global weights at a subsequent stage. Because of this, rankings based on the global regression weights are only meaningful relative to the particular removal stage at which they are computed.

### Section 4.3. Spatial Optimization Results

The spatial optimization results are contained in a series of graphs and tables. Overall, the spatial analysis of the two time slices (2001 and 2002) and the three COCs at Site 49

revealed varying levels of spatial redundancy. For TCE, a ‘safe’ level of redundancy appeared to be about 25% of the total well network for the first time slice and approximately 35-40% for the second. For DCA11, this safe level dropped to only about 20% of the wells. DCE12C fell in-between the other two at 20-30%. Because of the importance of TCE as the main source contaminant and as the COC with the greatest spatial spread and intensity, the overall recommendation from the GTS analysis identifies 35-40% of the well network locations as redundant.

When matching lists of redundant wells across the COCs that were analyzed, only 7 wells among the baseline of 67 were commonly listed, amounting to 10 percent of the total baseline well set. However, when using the most recent data (that is, sampling events from 2002), 24 wells might be considered redundant or 36% of the baseline LTM network.

Potentially, *from strictly a statistical point of view*, all of these redundant wells ought to be eliminated from the Site 49 LTM network. However, other considerations must be factored in before making any such decisions. The spatial analysis here only considers statistical contributions of each well to concentration maps of the site. It does not consider other purposes for these wells. Some of them may be essential for other engineering or site characterization reasons. Each potentially redundant well should be reviewed by site geologists and hydrologists to determine if such overriding factors exist.

#### **Section 4.3.1. Global Measures of Redundancy**

To help assess redundancy at a global level, the graphs in **Appendix 4-1** were prepared. These graphs plot selected summary statistics from the spatial mapping exercise against the percentage of wells that was removed from the data for each COC. Examination of these graphs can provide one indication of when ‘too much’ data has been removed (that is, when a reasonable level of statistical redundancy has been exceeded), especially if the trend is flat or very gentle at first (say for lower fractions of data removal), but then begins to trend more sharply at some increased level of data removal.

The first measure of global redundancy is given in the first figure for each COC in **Appendix 4-1**. These graphs plot the trend in global variance for each COC and each time slice. In general, the global variance might be expected to increase as more data is removed and the maps are re-estimated. In other words, less data equals less certainty and higher variance. However, this pattern does not always occur. At some grid nodes, the estimated variance tends to ‘blow up,’ leading to a much higher global variance value even at low removal levels. This artifact makes the global variance measures harder to interpret. In other cases, say for DCA11, the global variance is rather high on the base map, but then drops with increasing removal level. On occasion, this can occur if pairs of closely spaced wells report very different concentration levels for a given time period, leading to high uncertainty in the local estimates near these wells. If one of the pair is removed on a subsequent iteration, the local variance (and hence the global variance also) will tend to drop from what it was on the base map.

Overall, the global variance patterns, while not ideal, show a substantial jump for DCA11 after a 20% removal in both time slices. For DCE12C, a jump also occurs after 20%

removal for 2001, but does not occur until approximately a 40-45% removal for sample data from 2002. A similar pattern is evident for TCE: for 2001, the largest jump in global variance occurs after 25% removal; for 2002, the jump occurs after 40% removal.

Additional measures of global redundancy are shown the second two figures for each COC in **Appendix 4-1**. The first of these documents the change in two measures: the percentage of voxels (i.e., three-dimensional pixels) with very high grid-node-specific local variances (denoted REDUCED-VARPCT on the plots) and the average level of difference between the estimated indicator values from the reduced data set and those of the base map (denoted AVE-IDIFF). The first of these (i.e., REDUCED-VARPCT) simply counts across the site grid the percentage of estimated nodes where the local variance value was determined to be in the extreme upper tail of the distribution of local variances. As the fraction of data removal increases, the percentage of extreme local variances would also be expected to increase.

The second measure (i.e., AVE-IDIFF) was computed by taking the difference at each of the five indicator levels between the reduced data set indicator estimate and the corresponding base map indicator estimate. These indicator differences were then averaged across the five indicator levels and finally averaged again across all the nodes on the site grid. The interpretation of the average indicator difference is as follows: each indicator variable corresponds to a particular concentration level from the overall declustered CDF (for instance, the first indicator for TCE corresponds to a concentration value of 0.5 ppb). The indicator estimate after mapping the site with LWQR is the probability of not exceeding this reference concentration value. To the extent that the indicator estimates at a particular grid node for both the base map and the reduced-data map are the same, both maps then provide the same statistical information about the expected concentration level at that node. On the other hand, if the indicator estimates differ, the estimated concentration values will also differ, leading the reduced-data map to differ in pattern and magnitude from the base map. Averaged across all the nodes on the site grid, the average indicator difference then provides a summary measure of how much change is to be expected between the base and reduced-data maps.

For DCA11 and DCE12C, there is no particular pattern to the REDUCED-VARPCT measure. In fact it is generally flat to declining in overall trend as more data is removed. The reason for this appears to be connected with how the LWQR method estimates variance. Because the estimated variability depends fundamentally on the observed concentration values, if enough of the pre-existing variation has been removed at a given step (by not including wells with more variable sampling data), the local variances may begin to drop, leading sometimes to a lower overall global variance, and a smaller percentage of grid nodes with very high local variance values. This pattern can be seen for instance in some of the graphs in **Appendix 4-3**. The only case for which the REDUCED-VARPCT measure makes a significant jump is for TCE during 2002. This jump occurs after approximately a 40% removal.

The average indicator difference measure (AVE-IDIFF) traces a more complicated, but also more informative, pattern. *Negative* values of this measure signify an overall *over-*estimation of the site grid on the reduced-data set compared to the base map. *Positive*

values signify an overall *under*-estimation. For all three COCs, low levels of data removal correspond to values of AVE-IDIFF that are slightly negative. This suggests that the reduced-data maps tend to somewhat over-estimate the base maps even if a small number of wells has been removed.

For DCA11, the only significant change in AVE-IDIFF occurs for the first time slice after about 30% removal. For DCE12C, AVE-IDIFF tends to drop after about 20-25% removal for 2001, and after about 40-45% removal for 2002. For TCE, the pattern in AVE-IDIFF is somewhat murky for 2001, but rapidly increases above zero during 2002 after a 40% removal.

The final set of global redundancy measures are denoted by MEAN-MISCLASS, TRIM-MISCLASS, and PCT-IDIFF. MEAN-MISCLASS refers to the percentage of voxels or nodes that were classified one way relative to a regulatory limit or other pre-specified concentration level on the base map but are classified the *opposite* way on the reduced-data map. For example, using the MCL of 5 ppb for TCE, approximately 17% of all the estimated grid nodes were *misclassified* when 5% of the wells were removed in time slice one. That percentage rises to about 33% by the time 25% of the wells have been removed. TRIM-MISCLASS is a measure closely related to MEAN-MISCLASS, except that instead of classifying voxels on the basis of the estimated mean concentration, the classification is done using the estimated *trimmed mean*, cutting off 10% of the lower and upper tails of the updated, conditional CDF. For the most part, MEAN-MISCLASS and TRIM-MISCLASS tend to give similar results at Site 49.

For all the COCs, while the percentage of such misclassifications increases as expected with increased data removal, the trends generally provide no obvious way to measure a specific degree of acceptable redundancy. Instead of flat or nearly flat trend followed at greater levels of removal by a sharp increase, the majority of the increase often occurs right away at the lowest removal levels. The only possible exception to this at Site 49 is for DCA11, where there appears to be a small jump in misclassifications after a removal of 30% during 2001.

PCT-IDIFF is an additional measure of how much the reduced-data map indicator estimates differ from the base map indicator estimates. It counts the percentage of nodes at which at least one reduced-data indicator differs from the corresponding base map indicator by at least 0.5 (remember that all the indicator estimates are between 0 and 1; a difference of at least 0.5 is thus a large change in the estimated probability of non-exceedance for the associated reference concentration level). Unfortunately, while PCT-IDIFF again trends upward with increased data removal for all three COCs and both time slices, there is little evidence of any ‘flat’ portions of the trends upon which to judge degrees of redundancy.

### **Section 4.3.2. Local Indications of Redundancy**

While global measures of redundancy can be useful, they do not provide the full story. Global misclassification rates for example do not indicate *where* the misclassification is occurring or to what degree. Only actual maps of the site can provide this type of information. To this end, two sets of maps are provided for each COC and time slice. The

first documents, at each level of data removal, the differences in the local indicator values between the base map and each reduced-data map (see **Appendix 4-2**) Local areas of overestimation (corresponding to *negative* indicator differences) are shaded in orange and red. Local areas of underestimation (corresponding to *positive* indicator differences) are shaded in blue. By comparing these maps relative to the increase in the amount of data removed, one can assess at what point too many local areas of over- and under-estimation ‘pop-up.’

The second set of maps (see **Appendix 4-3**) details in a similar way what changes occur in the local variance with increasing data removal. Are there particular areas of the site at which the local uncertainty is unacceptably high? Do the areas with high local variance change as more data is removed? Do new areas emerge? All these questions can be assessed by viewing the maps in **Appendix 4-3**.

In general, the maps in **Appendices 4-2** support the conclusion that too much local information is lost from the base map when the data removal fraction rises above approximately 20% for all three COCs during 2001. For the second time slice, the results are more varied, but suggest a ‘safe’ level of redundancy of perhaps 20-25% for DCA11 and DCE12C, and perhaps 40% for TCE.

The maps in **Appendix 4-3** are more problematic. The overriding pattern exhibited by the local variance maps is an increase in areas of both very high variability and, simultaneously, areas of very low variability. As noted in **Section 4.3.1**, this is probably due to the fact that when a larger percentage of the wells have been removed, there are large swatches of the site where the nearest sample measurements are fairly uniform in concentration level, leading to a low variability estimate. At other locations, there is less data available to use in the estimates (or perhaps the remaining data do not vary in a continuous manner) and so the variation is quite high. In any event, the local variance maps, with a couple exceptions, do not provide much help at Site 49 in assessing degrees of redundancy. The exceptions are for DCE12C in the first time slice, where a number of local variance ‘hotspots’ appear at the 25% removal stage, and for TCE in the second time slice, where local variance ‘hotspots’ are not widespread until approximately 45-50% removal.

One important thing to note about the maps in **Appendices 4-2** and **4-3** is that they are presented as two-dimensional “plan-view” contour surfaces. The actual map estimates at Site 49 were three-dimensional, as noted earlier. However, it is difficult to adequately visualize three-dimensional data within a static report. To solve this difficulty, all the indicator difference and local variance maps were first *averaged over depth* in order to provide two-dimensional projections of the three-dimensional surface estimates. Some information is of course lost when such averaging is done. Nevertheless, the results can be presented and visualized much more easily.

### **Section 4.3.3. Base Map Accuracy**

In **Appendix 4-4**, there is a base map of the estimated concentrations for each COC, overlaid with a scatter plot of the actual data locations used in the analysis. Both the base map and the scatter plot of actual data are colored by contour level. One can see from this

representation that most of the observed data levels correspond reasonably well with the surrounding nearby base map estimates. There are, however, a few exceptions.

A couple of major reasons account for areas where there appears to be poor base map accuracy. First, the two-dimensional base map representation is again averaged over depth, but is in reality three-dimensional. Often the plume areas lie below the ground surface, but appear to be at ground level on the 2D surface map. Although unavoidable, this averaging process affects to some degree how well the observed data appear to “match” the estimated contours on the base map. Along the same lines, many more individual samples were used in the base map construction than show up on the base maps in **Appendix 4-4**. Deeper sample values are sometimes ‘hidden’ by shallower, but nearby, locations due to the scaling and size of the maps.

Second, locally-weighted quadratic regression is, as was noted earlier, a smoothing technique rather than a spatial interpolator. Because of this, the estimated surface may not precisely equal the value of any given observed data point. This will especially be true in those cases where one nearby sample is quite high while its neighbor is quite low. At Site 49, there is one noticeable area to the northwest of the primary source area where little sample information is available. In this case, LWQR graduates the estimated plume from the high values near the source down to the much lower values farther to the northwest.

Ultimately, having an accurate base map is an important key to a successful spatial optimization analysis using GTS. As noted, all assessments of redundancy flow from a comparison between the base map and subsequent maps constructed from reduced-data sets. Although it is likely that the GTS algorithm is ‘robust’ to some base map inaccuracy, it is certainly the case that spatial redundancy cannot be judged fairly unless the base map matches the actual data to a reasonable degree.

The base maps generated using LWQR may or may not adequately coincide with similar hand-drawn maps created by project geologists. The estimated base maps from the spatial analysis are strictly data driven and do not account for special features of the terrain or hydrogeology.

## **Section 5. Recommendations for Pease AFB, Site 49**

### **Section 5.1 Recommendations Regarding Sampling Frequency**

It has already been noted in **Section 3** from the temporal analysis that the operational sampling frequency at Site 49 ought to be reduced from annually to once every 2 years. This recommendation is based on the Temporal Variograms discussed in **Section 3.2**. What was not discussed is how this sampling schedule can be translated into a site-specific sampling plan. The recommended sampling strategy is discussed in more detail below.

With regard to sampling frequency, construction of the Temporal Variograms requires pairs of measurements from any given well with a variety of inter-event time intervals. If the wells are sampled at regular intervals (e.g., every seven quarters) after

implementation, then the range of between-sample intervals would not have the required variety of inter-event time intervals, and consequently it would be much harder to construct a future Temporal Variogram to test the original recommendation. Therefore, a key goal of the sampling strategy is to ensure that each well is sampled at irregular intervals over time. This involves ‘mixing up’ or randomizing the distribution of inter-event sampling intervals to facilitate a similar follow-up analysis after 3 to 5 years to assess whether or not the initial recommendations would still hold.

***Full implementation of the sampling strategy may not, however, be practical for certain wells that need to be sampled together or in a particular sequence. To make the sampling procedure as operationally efficient as possible, but without sacrificing the goal of at least partially ‘mixing up’ or randomizing the distribution of inter-event sampling intervals, one could also group the wells into clusters that would be sampled simultaneously.*** This might be needed, for instance, if ‘cleaner’ wells needed to be sampled prior to ‘dirtier’ wells, or perhaps for other logistical reasons. In this case, each cluster would be treated as a single well in the randomization scheme discussed below. Care should be taken, however, to ensure that individual clusters are not so large as to make the final sampling groups highly unbalanced.

It is recommended that a sampling plan be developed using the following three-step process to ensure sufficient variety of inter-event sampling intervals:

**Step 1** – Randomly divide the group of essential monitoring wells into four approximately equal-size groups (e.g., Group 1, Group 2, Group 3, and Group 4). This process would be akin to representing each well as a ball, and then randomly dropping each ball into one of four different urns, until all the balls are used up. In practical terms, the easiest way to achieve such random assignment — and to ensure that each group is of roughly equal size — is to list the wells in any order (say on a spreadsheet), draw a random number between 0 and 1 for each well from either a computer, calculator, or random number table, list the random numbers beside each well, sort the list in order of the random values, then assign the wells at the top of the sorted list comprising the first one-fourth of the total to the first urn (Group 1), the second listed chunk of one-fourth to the second urn (Group 2), and so on.

**Step 2** - Randomly assign Group 1 wells to one of the eight quarters that comprise the first two-year interval of the new sampling program. Next, randomly assign Group 2 to one of the eight quarters that comprise the first two years of the new sampling program. Repeat this process until all four well groups have been assigned to one of the eight quarters.

**Step 3** – At the start of each successive eight-quarter (two-year) interval, repeat steps 1 and 2. This step ensures that no single well will be sampled at precisely the same time during each sampling round.

**Example Sampling Schedule for Wells Listed in Table 5-2 (60 wells):**

**Step 1-** Divide the set of wells (60 wells) into four equal groups. To do this, assign a random number between 0 and 1 to each well, sort the list of wells in order by the random numbers, place the first 15 of the sorted wells in Group 1, the next 15 in Group 2, etc.), as shown in the example below. *Note that this table is for illustrative purposes, and site managers should construct their own well grouping to address any site-specific operational considerations (such as the need to sample certain wells together or in a particular sequence).*

<b>Example of Random Grouping of Wells Listed in Table 5-2</b>			
<b>Group 1</b>	<b>Group 2</b>	<b>Group 3</b>	<b>Group 4</b>
49-MW04	49-PZ001(SBR)	49-MW008(SBR)	49-PZ004(SBR)
49-MW006(SOB)	49-5564(D)	49-6663(S)	49-PZ002(SBR)
49-5567(D)	49-MW013(SBR)	49-MW014(SBR)	49-6517(S)
49-PZ002(DOB)	49-6701	49-PZ005(SBR)	49-6516(S)
49-5578(S)	49-MW006(DOB)	49-PZ004(SOB)	49-5970(D)
49-MW009(SBR)	49-5969(S)	49-5971(D)	49-5566(S)
49-MW009(DOB)	49-6700	49-6515(S)	49-MW02
49-MW014(DOB)	49-MW03	49-5973(D)	49-MW006(SBR)
49-6665(S)	49-MW013(DOB)	49-MW012(SBR)	49-6670(DBR)
49-PZ004(DOB)	49-5967(D)	49-5562(D)	49-5577(D)
49-MW011(SBR)	49-5980(D)	49-MW010(SBR)	49-MW010(DOB)
49-6667(S)	49-PZ003(SOB)	49-MW011(DOB)	49-5982(D)
49-PZ003(SBR)	49-6669(S)	49-MW01	49-MW002(SBR)
49-6666(DBR)	49-PZ002(SOB)	49-PZ003(DOB)	49-6668(S)
49-W013A(SBR)	49-5981(D)	49-5565(S)	49-5563(S)

**Step 2** – Randomly assign each group to one of eight quarters to develop the two-year sampling schedule. See **Table 5-1**. To create the sampling schedule table, pick a random sampling quarter – e.g., using a handheld calculator – between one and eight, and assign the Group 1 wells to that quarter. Repeat this process for each of the remaining Groups. Note that during some quarters, no sampling will be conducted.

**Table 5-1. Example Sampling Plan for the First Two-Year Sampling Interval of the Optimized LTM Sampling Program**

<b>Year</b>	<b>First Quarter</b>	<b>Second Quarter</b>	<b>Third Quarter</b>	<b>Fourth Quarter</b>
<b>1</b>	Group 1 Group 4	Group 3	No sampling	No sampling
<b>2</b>	No sampling	Group 2	No sampling	No sampling

Thus, all wells will be sampled once over the two-year period. Per **Step 3**, the process is repeated to develop a new sampling schedule for Years 3 and 4, again for Years 5 and 6, and so on.

## Section 5.2 Recommendations Regarding Spatial Redundancy

The ultimate decision about when ‘too much’ data has been removed is somewhat subjective. But, based on the GTS spatial analysis, and considering both the global measures of redundancy and the maps of local indicator differences, at least 7 wells and perhaps as many as 24, could be considered as redundant to the Site 49 LTM program. This leaves 43 to 60 wells from the baseline list as ones that should remain in the monitoring program. Specific lists of wells essential to the LTM program are provided in **Tables 5-2** and **5-4**. **Table 5-2** is a list of essential wells based on using all three COCs from the spatial analysis. **Table 5-4** is a similar, but slightly smaller, list based on the results of most recent TCE data. Given the importance of TCE as a ‘plume driver’ at Site 49, this analysis recommends that the second of these monitoring networks be implemented.

Note that in each of these tables, the last column assigns a relative ranking of the statistical importance of each well, classified as HIGH, MED(IUM), or LOW. These rankings (at least for **Table 5-2**) reflect whether or not the well was consistently deemed essential in each time slice for at least one COC and had a positive average global regression weight (HIGH), was consistently deemed essential but had a non-positive average global regression weight (MED), or was deemed essential only in certain time slices (LOW).

Complementing these tables are lists of statistically redundant wells culled from each thread of the analysis. **Table 5-3** lists the redundant wells derived from an analysis using all three COCs, while **Table 5-5** is a longer list of redundant wells derived from the results of the TCE analysis.

It should be noted that for the purposes of long-term follow-up analysis, if redundant wells are removed from regular long-term monitoring, they should ideally not be decommissioned. Rather, prior to a multi-year follow-up review, the same wells ought to be sampled again to determine whether or not the original recommendations are still valid. Thus, these wells would still be sampled very infrequently, say once every 3 to 5 years.

Lastly, it is important to reiterate that the recommendations concerning redundant wells are highly data-driven. Groundwater wells can serve multiple purposes and may be important for reasons other than long-term monitoring. Because of this, all of the potentially redundant wells should be evaluated by site geologists and regulators to ensure that other goals of the Site 49 LTM program are not compromised.

**Table 5-2. Essential Monitoring Network Based on Analysis of All COCs (All measurements in feet)**

Note: RANKING refers to relative statistical importance; HIGH = wells deemed essential in both time slices and having positive average global regression weights at optimal removal stage; MED = wells deemed essential in both time slices but having non-positive average global regression weights; LOW = wells deemed essential in only one of two time slices

WELL_ID	EASTING	NORTHING	DEPTH	SCREEN ELEVATION	RANKING
49-5565(S)	1212924	215184	10	63.74	HIGH
49-5566(S)	1212855	215266	8	67.2	HIGH
49-5967(D)	1213634.39	215132.89	25.5	44.34	HIGH
49-5969(S)	1213634.39	215132.58	8.05	58.505	HIGH
49-5973(D)	1213015	215231.3	12.8	59.065	HIGH
49-5981(D)	1212903.02	215321.5	19.5	55.5955	HIGH
49-6515(S)	1212858	215262	39.3	35.7	HIGH
49-6516(S)	1213093	215386	21.6	50	HIGH
49-6663(S)	1213456.96	215130.93	31.5	38.55	HIGH
49-6665(S)	1213183.89	215178.03	18.3	52.425	HIGH
49-6666(DBR)	1213017	215220.6	78	-6.41	HIGH
49-6667(S)	1213015	215226.2	18	53.71	HIGH
49-6670(DBR)	1213640	215134.9	70	-3.425	HIGH
49-MW008(SBR)	1213210	215002	30	43.425	HIGH
49-MW009(SBR)	1213510	215017	22.5	47.015	HIGH
49-MW01	1213408	215440	12	56.62	HIGH
49-MW013(SBR)	1213860	215081	19	47.78	HIGH
49-MW014(SBR)	1213526	215666	32	34.185	HIGH
49-MW02	1212932	215409	11.5	64.61	HIGH
49-PZ001(SBR)	1213007	215303	17.2	55.945	HIGH
49-PZ002(SBR)	1213030	215225	19	53.205	HIGH
49-PZ005(SBR)	1213052	215130	21.7	49.495	HIGH
49-5982(D)	1213283.75	215067.61	16.5	53.135	MED
49-6668(S)	1213408	215433.3	35.8	32.7	MED
49-6669(S)	1212908	215266.5	28	47.515	MED
49-6700	1213536.408	215817.0246	20.5	46.27	MED
49-6701	1214189.944	215982.6607	14.5	48.64	MED
49-MW006(SOB)	1212996	215237	6.5	65.4	MED
49-MW011(SBR)	1213590	215433	20.5	46.16	MED
49-W013A(SBR)	1213804	215076	14.5	50.385	MED
49-MW014(DOB)	1213530	215668	22.5	42.815	MED
49-MW03	1213431	215248	12	57.1	MED
49-PZ003(DOB)	1213045	215173	12.7	59.75	MED
49-PZ004(SBR)	1213024	215182	22	49.835	MED
49-PZ004(SOB)	1213022	215183	7.5	64.275	MED
49-5562(D)	1212854	215270	21.5	55.28	LOW
49-5563(S)	1213011	215306	9.5	64.625	LOW
49-5564(D)	1212930	215180	20.5	53.11	LOW
49-5567(D)	1213430	215244	19	49.6	LOW
49-5577(D)	1212915	215277	19.5	56.51	LOW
49-5578(S)	1212919	215278	11.5	64.33	LOW
49-5970(D)	1213403.93	215426.31	29.5	39.515	LOW
49-5971(D)	1213003.18	215303.58	9.7	63.525	LOW
49-5980(D)	1213087.06	215385.48	11.5	59.715	LOW
49-6517(S)	1213338	215120	23	45.67	LOW
49-MW002(SBR)	1213145.92	215153	34.5	34.94	LOW
49-MW006(DOB)	1212997.33	215233	17	54.63	LOW
49-MW006(SBR)	1212999.33	215230.7	29.5	42.265	LOW
49-MW009(DOB)	1213509	215013	15	54.71	LOW
49-MW010(DOB)	1213103	215352	7.5	63.26	LOW
49-MW010(SBR)	1213107	215353	15.5	55.21	LOW
49-MW011(DOB)	1213592	215429	12.5	54.075	LOW
49-MW012(SBR)	1213464	215197	28	41.2	LOW
49-MW013(DOB)	1213865	215081	14.5	51.285	LOW
49-MW04	1213047	215134	10.5	60.63	LOW

WELL_ID	EASTING	NORTHING	DEPTH	SCREEN ELEVATION	RANKING
49-PZ002(DOB)	1213031	215223	12	60.15	LOW
49-PZ002(SOB)	1213029	215228	6.5	65.585	LOW
49-PZ003(SBR)	1213044	215176	21.5	50.935	LOW
49-PZ003(SOB)	1213044	215178	6.5	65.84	LOW
49-PZ004(DOB)	1213023	215184	14	57.92	LOW

**Table 5-3. Redundant Monitoring Wells Based on Analysis of All COCs (All measurements in ft)**

WELL_ID	EASTING	NORTHING	DEPTH	SCREEN ELEVATION
49-5568(D)	1213344	215122	13	55.455
49-5573(D)	1213180	215177	15.5	53.65
49-5574(S)	1213181	215174	8.5	60.665
49-6664(S)	1213628.7	215131.26	17	49.52
49-MW003(SBR)	1213141.15	215116.65	29.5	40.58
49-MW008(DOB)	1213211	214999	22.5	51.055
49-PZ005(DOB)	1213051	215133	14	57.17

**Table 5-4. Essential Monitoring Network Based on Analysis of TCE in 2002 (All measurements in feet)**

Note: RANKING refers to relative statistical importance; HIGH = wells with highest (positive) global regression weights; MED = wells with mid-range, non-negative global regression weights; LOW = wells with negative global regression weights

WELL_ID	EASTING	NORTHING	DEPTH	SCREEN ELEVATION	RANKING
49-5565(S)	1212924	215184	10	63.74	HIGH
49-5567(D)	1213430	215244	19	49.6	HIGH
49-5967(D)	1213634.39	215132.89	25.5	44.34	HIGH
49-5969(S)	1213634.39	215132.58	8.05	58.505	HIGH
49-5970(D)	1213403.93	215426.31	29.5	39.515	HIGH
49-5982(D)	1213283.75	215067.61	16.5	53.135	HIGH
49-6516(S)	1213093	215386	21.6	50	HIGH
49-6663(S)	1213456.96	215130.93	31.5	38.55	HIGH
49-6665(S)	1213183.89	215178.03	18.3	52.425	HIGH
49-MW006(DOB)	1212997.33	215233	17	54.63	HIGH
49-MW010(SBR)	1213107	215353	15.5	55.21	HIGH
49-MW011(SBR)	1213590	215433	20.5	46.16	HIGH
49-MW012(SBR)	1213464	215197	28	41.2	HIGH
49-MW013(SBR)	1213860	215081	19	47.78	HIGH
49-PZ001(SBR)	1213007	215303	17.2	55.945	HIGH
49-PZ002(SBR)	1213030	215225	19	53.205	HIGH
49-PZ005(SBR)	1213052	215130	21.7	49.495	HIGH
49-5566(S)	1212855	215266	8	67.2	MED
49-5973(D)	1213015	215231.3	12.8	59.065	MED
49-5981(D)	1212903.02	215321.5	19.5	55.5955	MED
49-6666(DBR)	1213017	215220.6	78	-6.41	MED
49-6669(S)	1212908	215266.5	28	47.515	MED
49-6670(DBR)	1213640	215134.9	70	-3.425	MED
49-6700	1213536.408	215817.0246	20.5	46.27	MED
49-6701	1214189.944	215982.6607	14.5	48.64	MED
49-MW008(SBR)	1213210	215002	30	43.425	MED
49-MW009(SBR)	1213510	215017	22.5	47.015	MED
49-MW01	1213408	215440	12	56.62	MED
49-MW013A(SBR)	1213804	215076	14.5	50.385	MED

WELL_ID	EASTING	NORTHING	DEPTH	SCREEN ELEVATION	RANKING
49-MW014 (SBR)	1213526	215666	32	34.185	MED
49-MW02	1212932	215409	11.5	64.61	MED
49-PZ003 (DOB)	1213045	215173	12.7	59.75	MED
49-PZ004 (SBR)	1213024	215182	22	49.835	MED
49-6515 (S)	1212858	215262	39.3	35.7	LOW
49-6517 (S)	1213338	215120	23	45.67	LOW
49-6667 (S)	1213015	215226.2	18	53.71	LOW
49-6668 (S)	1213408	215433.3	35.8	32.7	LOW
49-MW006 (SOB)	1212996	215237	6.5	65.4	LOW
49-MW013 (DOB)	1213865	215081	14.5	51.285	LOW
49-MW014 (DOB)	1213530	215668	22.5	42.815	LOW
49-MW03	1213431	215248	12	57.1	LOW
49-PZ002 (DOB)	1213031	215223	12	60.15	LOW
49-PZ004 (SOB)	1213022	215183	7.5	64.275	LOW

**Table 5-5. Redundant Monitoring Wells Based on Analysis of TCE in 2002 (All measurements in ft)**

WELL_ID	EASTING	NORTHING	DEPTH	FINAL ELEV
49-5562 (D)	1212854	215270	21.5	55.28
49-5563 (S)	1213011	215306	9.5	64.625
49-5564 (D)	1212930	215180	20.5	53.11
49-5568 (D)	1213344	215122	13	55.455
49-5573 (D)	1213180	215177	15.5	53.65
49-5574 (S)	1213181	215174	8.5	60.665
49-5577 (D)	1212915	215277	19.5	56.51
49-5578 (S)	1212919	215278	11.5	64.33
49-5971 (D)	1213003.18	215303.58	9.7	63.525
49-5980 (D)	1213087.06	215385.48	11.5	59.715
49-6664 (S)	1213628.7	215131.26	17	49.52
49-MW002 (SBR)	1213145.92	215153	34.5	34.94
49-MW003 (SBR)	1213141.15	215116.65	29.5	40.58
49-MW006 (SBR)	1212999.33	215230.7	29.5	42.265
49-MW008 (DOB)	1213211	214999	22.5	51.055
49-MW009 (DOB)	1213509	215013	15	54.71
49-MW010 (DOB)	1213103	215352	7.5	63.26
49-MW011 (DOB)	1213592	215429	12.5	54.075
49-MW04	1213047	215134	10.5	60.63
49-PZ002 (SOB)	1213029	215228	6.5	65.585
49-PZ003 (SBR)	1213044	215176	21.5	50.935
49-PZ003 (SOB)	1213044	215178	6.5	65.84
49-PZ004 (DOB)	1213023	215184	14	57.92
49-PZ005 (DOB)	1213051	215133	14	57.17

### Section 5.3 Recommendations Regarding Siting of New Wells

While the primary motivation for the spatial analysis at Site 49 was to identify potentially redundant wells, a secondary goal was to locate areas of the site where additional wells might provide significant improvements in accuracy of the estimated site maps and thus improved information on the nature and extent of the groundwater plume(s). In GTS, the most straightforward way to do this is to examine the local variance *base maps* for each time slice and COC. There the local variances offer an indication of the relative *local uncertainty* associated with the mapped grid estimates. The higher the local uncertainty at a particular spot, the greater the benefit to siting a new well in that location.

It should be noted that high local uncertainty arises from two basic sources using the LWQR estimation technique. First, there may be areas of data sparsity, such as the

locations northeast of the contaminant source area. Estimates in these spots tend to be uncertain because few wells are sited there. Secondly, there may be areas of data inconsistency, where nearby wells exhibit strongly different concentration levels. This second phenomenon occurs wells with very low concentrations are located near wells with much higher measurements. High local uncertainty at grid nodes in these areas is then a result of the inconsistency of the known data located within the search neighborhood. In such cases, it may not be advantageous to site a new well nearby to several existing well locations, especially since the inconsistency might be due to the complex pattern of groundwater flow through the subsurface.

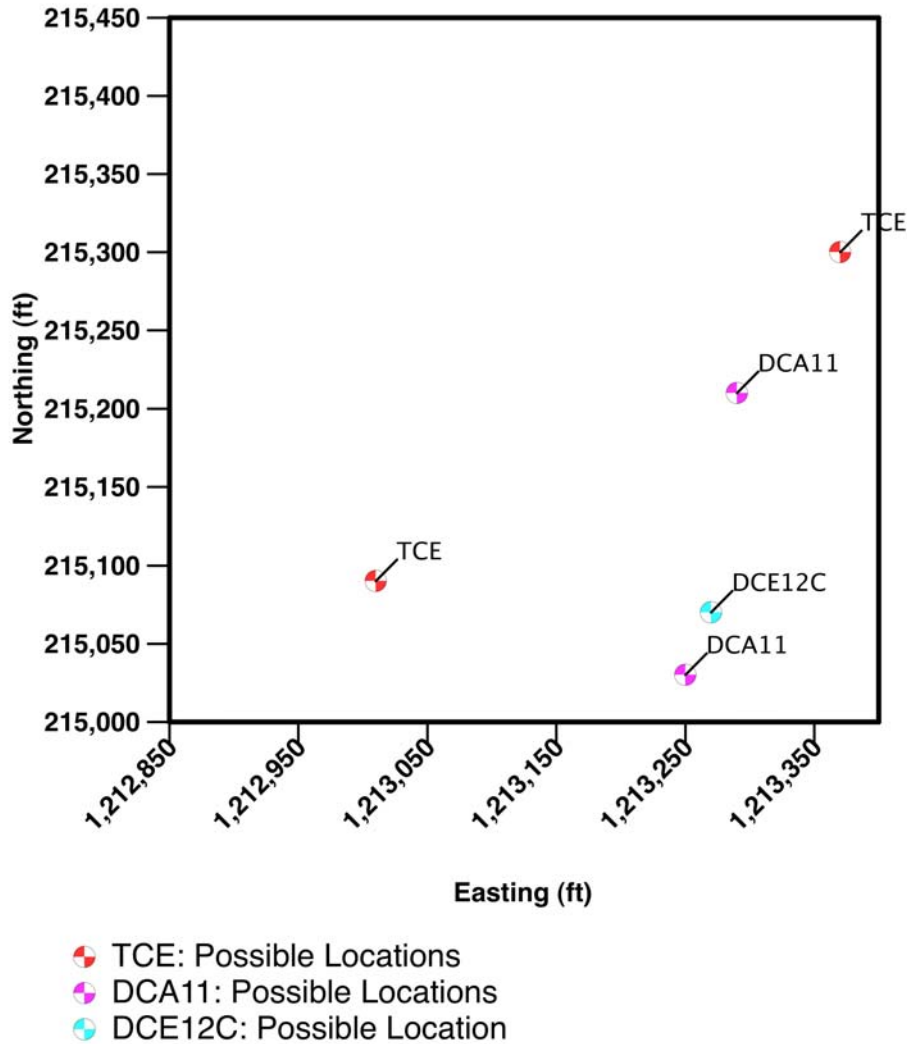
The approximate locations exhibiting the greatest local uncertainty are listed below in **Table 5-6** and graphed in **Figure 5-1**. Any of these spots might serve as locations for the siting of additional wells, but particularly those locations where nearby wells are sparse. Please note, however, that since the determination of local variance depends *both* upon the spatial configuration of the well network *and* the actual concentration values at those locations, it cannot be determined *a priori* exactly which additional sites would provide the greatest informational benefit, nor to what degree the accuracy would be improved. In addition, **Table 5-6** and **Figure 5-1** take no account of physical obstacles at the site (e.g., buildings) that might preclude siting of wells in the listed locations.

It should also be noted that the locations in **Table 5-6** are not ranked in any particular order. Operationally, more weight could be given to those two locations found to exhibit high local uncertainty when using the more recent data of time slice two (2002). At this point, though, there is no reliable way within the GTS algorithm to reliably rank or distinguish between locations of uncertainty found from the TCE analysis versus the DCA11 analysis or the DCE12C analysis. Furthermore, high local uncertainty, for instance in TCE, does not mean there is high local uncertainty for other COCs not included in the optimization at those locations. However, given the fact that COCs are chosen for optimization in part because they exhibit more frequent and widespread spatial occurrence than other available chemical parameters, it is not unreasonable to assume that these same locations would be good candidates for sampling of other pertinent COCs.

**Table 5-6. Approximate Locations of Greatest Local Relative Uncertainty**

COC	Time Slice	Easting (ft)	Northing (ft)
DCA11	2001	1,213,290	215,210
		1,213,250	215,030
	2002	1,213,410	215,030
DCE12C	2002	1,213,270	215,070
TCE	2001	1,213,010	215,090
		1,213,370	215,300

**Figure 5-1. Approximate Locations of Greatest Local Uncertainty**



## Section 5.4. Cost Analysis and Summary

This section describes the methodology for developing credible estimates of annualized cost savings that might result from the implementation of a GTS-optimized monitoring program. The approach is based on a simple cost model. To calculate a cost savings, two cost estimates are required for comparison. The first is the baseline (current) costs, including fixed and variable costs; the second is the projected cost under the optimized program. Cost savings are estimated based on the difference between baseline monitoring costs and projected costs under the optimized program, expressed in terms of current dollars and percent reduction from baseline.

### Section 5.4.1. Initial Monitoring and Cost Information

Monitoring data from 2001 and 2002 shows that 67 wells are currently being monitored at Site 49 and these 67 wells were the subject of the optimization study. The current monitoring cost for the 67 wells serve as the baseline by which to measure cost savings.

Current annual costs for the groundwater monitoring programs at Pease AFB were obtained from MWH Americas, Incorporated, an Air Force O&M contractor. The cost data that were provided, however, only accounted for monitoring of 65 of the 67 wells. These cost data showed that there were 11 COCs currently being monitored at the site. 65 wells were monitored for Volatile Organic Compounds (VOCs), while only 17 of the wells were monitored for the other listed COCs. Therefore, it was assumed that the two additional wells included in the optimization study, but not included in the MWH Americas cost data, were also monitored for VOCs only.

The costs data provided by MWH Americas formed the baseline monitoring costs by which optimization costs could be compared to determine potential costs savings. The cost data provide sample analysis costs on a per-sample basis. These cost estimates are provided in **Table 5-7.A1** in **Appendix 5-1**. The cost data include estimates for sample management and labor costs, sample cooler shipping charges, as well as the costs for rental and purchase of material and equipment. These costs were provided on an annual basis rather than per COC sampled basis. The cost data also include estimates of costs for activities that support the sampling and analysis, such as: providing chemistry data management; preparing monitoring reports and attending meetings; updating and revising documents; and overall project management and administration. All baseline costs, including a summary of sample analysis costs can be found in **Tables 5-7.B1a** and **5-7.B1b** in **Appendix 5-1**.

#### **Section 5.4.2. Scenario Cost Estimates**

The optimization study results produced two lists of essential wells. The first list, which takes into account all monitoring and all COCs since 2001, shows the elimination of seven redundant wells. However, the TCE plume at Site 49 is actively lessening and changing over time. Therefore, when only TCE data from 2002 were considered, the optimization results showed that 24 wells could be retired from the monitoring program.

The information sent by MWH Americas did not list which COCs are monitored at each well. Therefore, assumptions had to be made as to how much of a reduction in sampling would occur as a result of eliminating wells from the site based on the two optimization scenarios. As mentioned, it is assumed that all wells are monitored for VOCs. Therefore, any reduction in the number of wells monitored would result in a corresponding reduction in VOC sampling and analysis. To be conservative, the 17 wells sampled for pollutants other than VOCs were assumed to not be included in the set of wells eliminated under each optimization scenario.

Coincident with the available sampling data, the current monitoring program at Site 49 is conducted on a semiannual basis, with each well being sampled in the Spring and Fall. The temporal optimization study indicates that sampling could be reduced at Site 49 to once every 100 to 120 weeks, or once every eight to nine quarters. For the cost analysis, it was assumed then that under each optimized scenario the monitoring frequency would be reduced to once every eight quarters, or two years.

In **Appendix 5-1**, **Table 5-7.BA2** shows the reduction in annual samples taken and the resulting sampling cost estimates for the optimization based on all the COCs. Similarly,

**Table 5-7.A3** shows annual samples taken and sampling cost estimates for the optimization based on 2002 TCE data only. These two tables also show reductions in labor, equipment, and shipping costs. Since these initial baseline cost estimates were not expressed in terms of samples taken or wells monitored, assumptions had to be made regarding how much these costs would change under each optimization scenario. It was assumed that the amount of labor required was directly associated with the number of samples taken. So these costs were reduced proportionally to the total reduction in the number of samples taken annually.

Rental and purchase costs were considered less sensitive to the number of samples taken. The cost of sample vials will vary proportionately to samples taken, but the rental cost for a purge pump will not. Therefore, the initial baseline equipment and materials cost of \$4,600 was divided into a fixed and a variable cost. One half (\$2,300) is considered a fixed cost that does not vary. The other half of the baseline cost was divided by the total number of baseline samples to derive a per sample cost (\$4.14). The per-sample cost is then multiplied by the total samples under each scenario, to derive the variable portion of the equipment and materials cost.

Sample cooler shipping charges vary directly with the number of wells monitored rather than with the number of samples taken. The reason is that shipping is typically done at the end of each day after all wells have been sampled for that day. The number of samples in each shipment will vary depending on the wells sampled, but each day's shipping costs will be relatively the same.

**Tables 5-7.B2b** and **5-7.B3b** in **Appendix 5-1** show the monitoring project costs not directly related to sampling analysis. Most of these costs are assumed to be less sensitive to the number of samples taken. Chemistry data management cost is the one exception, as it is assumed to vary proportionally to the number of samples taken annually. Monitoring reports and meetings are considered to have both fixed and variable components. So it was assumed that 70% of the initial baseline costs for reports and meetings was fixed, while the other 30% varied directly with the total number of samples taken. The updating and revision of documents was assumed to be a fixed cost regardless of changes to the number of annual samples. Finally, overall project management and administration costs were assumed to be half fixed and half variable, like the equipment and materials costs.

### **Section 5.4.3 Resulting Cost Savings**

Although the measurement data at Site 49 are somewhat challenging, the temporal and spatial analyses demonstrate that the GTS optimization algorithm can offer potentially significant cost savings over the existing LTM program. Decent estimates of plume magnitude and extent can be made using fewer wells than the current network and sampling at a lower frequency than presently in place. Estimates of specific potential cost savings of course depend on how many wells are actually deemed redundant after further review by project managers and regulators, and to what extent sampling frequencies can be reduced to levels recommended in the temporal analysis.

Nevertheless, **Table 5-6** below outlines the two estimates of the savings that might be achieved, based on costs of the current network, and also assuming that one of the two

reduced monitoring networks is implemented at Site 49.

The baseline for Site 49 estimates that 556 samples will be taken from 67 wells annually at a total cost of approximately \$172,000. Under the first optimization scenario, 155 samples would be taken from 30 wells annually for a total cost of approximately \$86,000 (an annual cost savings of 49.7 percent). Under the second optimization scenario, an estimated 144 samples would be taken from 22 wells annually for a total cost of approximately \$82,000 (an annual cost savings of 52.2 percent).

**Table 5-7. Estimate of Cost Savings**

<b>Pease - Site 49</b>			
	Baseline	Optimization 1 (All COCs)	Optimization 2 (2002 TCE)
<b>Samples Collected Annually</b>	<b>556</b>	<b>155</b>	<b>144</b>
<b>Annual Costs</b>			
Analytical Cost for Annual Sampling	\$38,456	\$10,394	\$8,807
Sampling and Analysis Labor Costs	\$27,298	\$7,610	\$7,045
Sample Shipping Costs	\$3,450	\$3,555	\$2,548
Materials and Equipment Costs	\$4,600	\$2,941	\$2,894
<b>Subtotal Sampling and Analysis Costs</b>	<b>\$73,804</b>	<b>\$24,500</b>	<b>\$21,293</b>
Chemistry Data Management	\$19,720	\$5,497	\$5,090
Reports and Meetings	\$42,500	\$33,304	\$33,041
Update & Revise Documents	\$600	\$600	\$600
Professional Site Visits & QA/QC Audits	\$5,000	\$3,197	\$3,145
Project Management and Administration	\$30,125	\$19,262	\$18,950
<b>Total Annual Project Cost</b>	<b>\$171,749</b>	<b>\$86,360</b>	<b>\$82,119</b>
<b>Potential Cost Savings</b>		<b>\$85,389</b>	<b>\$89,630</b>
<b>Percent Reduction in Annual Monitoring Costs</b>		<b>49.72%</b>	<b>52.19%</b>

## Section 6. References

Bourgault, G. (1997) Spatial declustering weights. *Mathematical Geology*, 29:277-290.

Cameron, K. & Hunter, P. (2002) Using spatial models and kriging techniques to optimize long-term groundwater monitoring networks: a case study. *Environmetrics*, 13:629-656.

Loader, C. (1999) *Local Regression and Likelihood*. New York: Springer-Verlag.

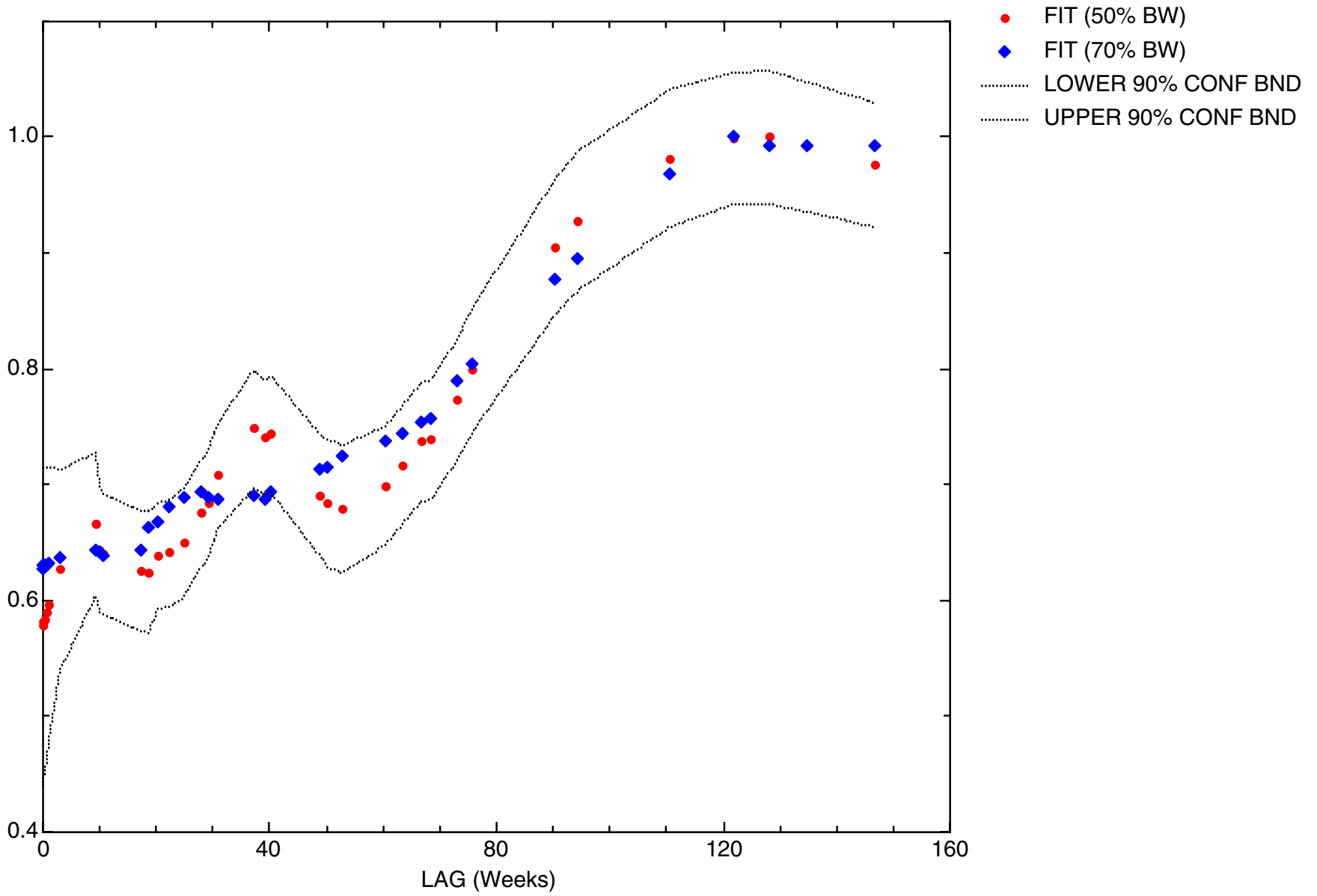
United States Air Force Base Conversion Agency (AFBCA) (1999). First Five-Year Review Report: Pease Air Force Base.

([www.epa.gov/region01/superfund/sites/pease/35074sect3-5.pdf](http://www.epa.gov/region01/superfund/sites/pease/35074sect3-5.pdf))

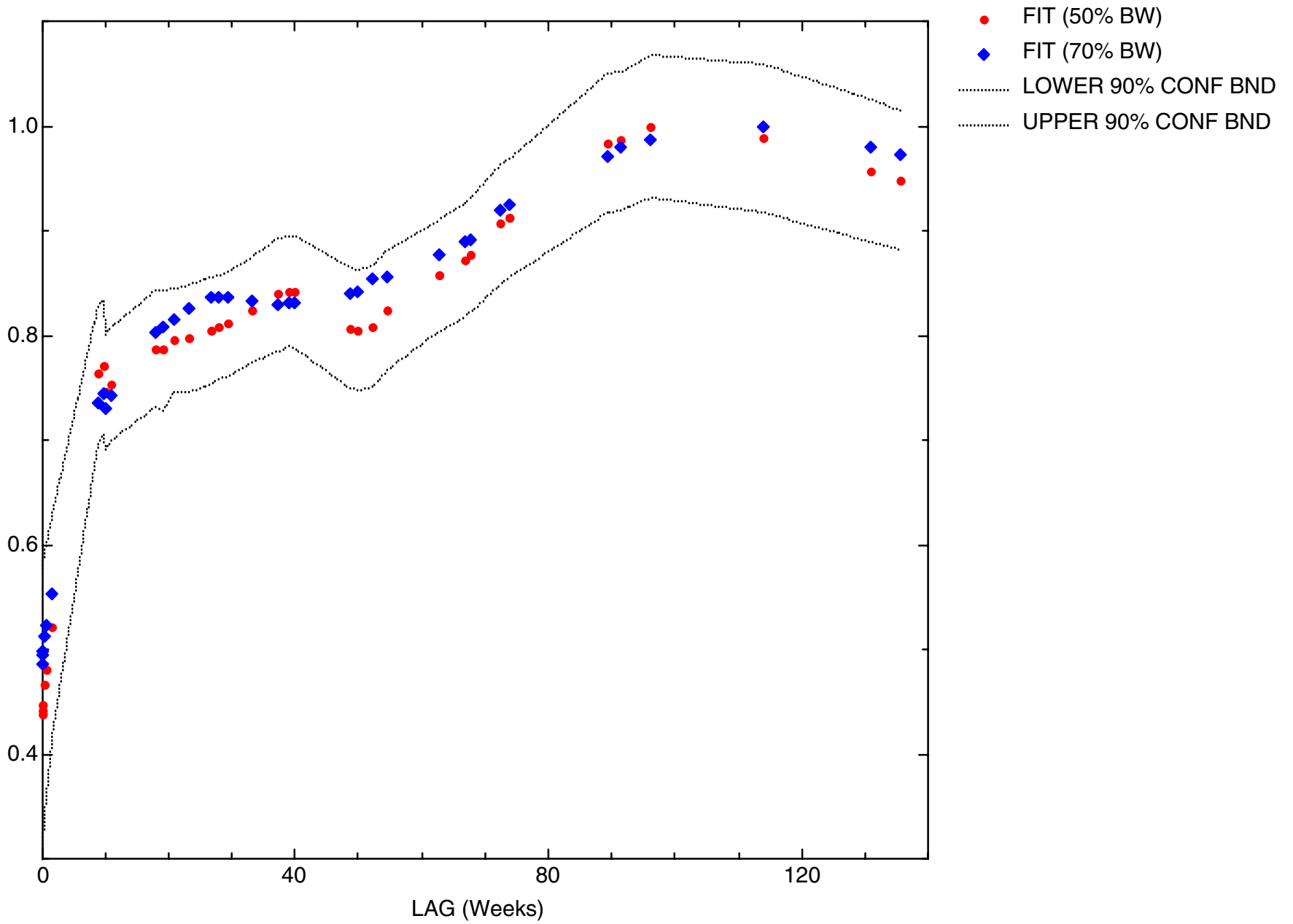
# Appendix 3.1

## Temporal Variograms

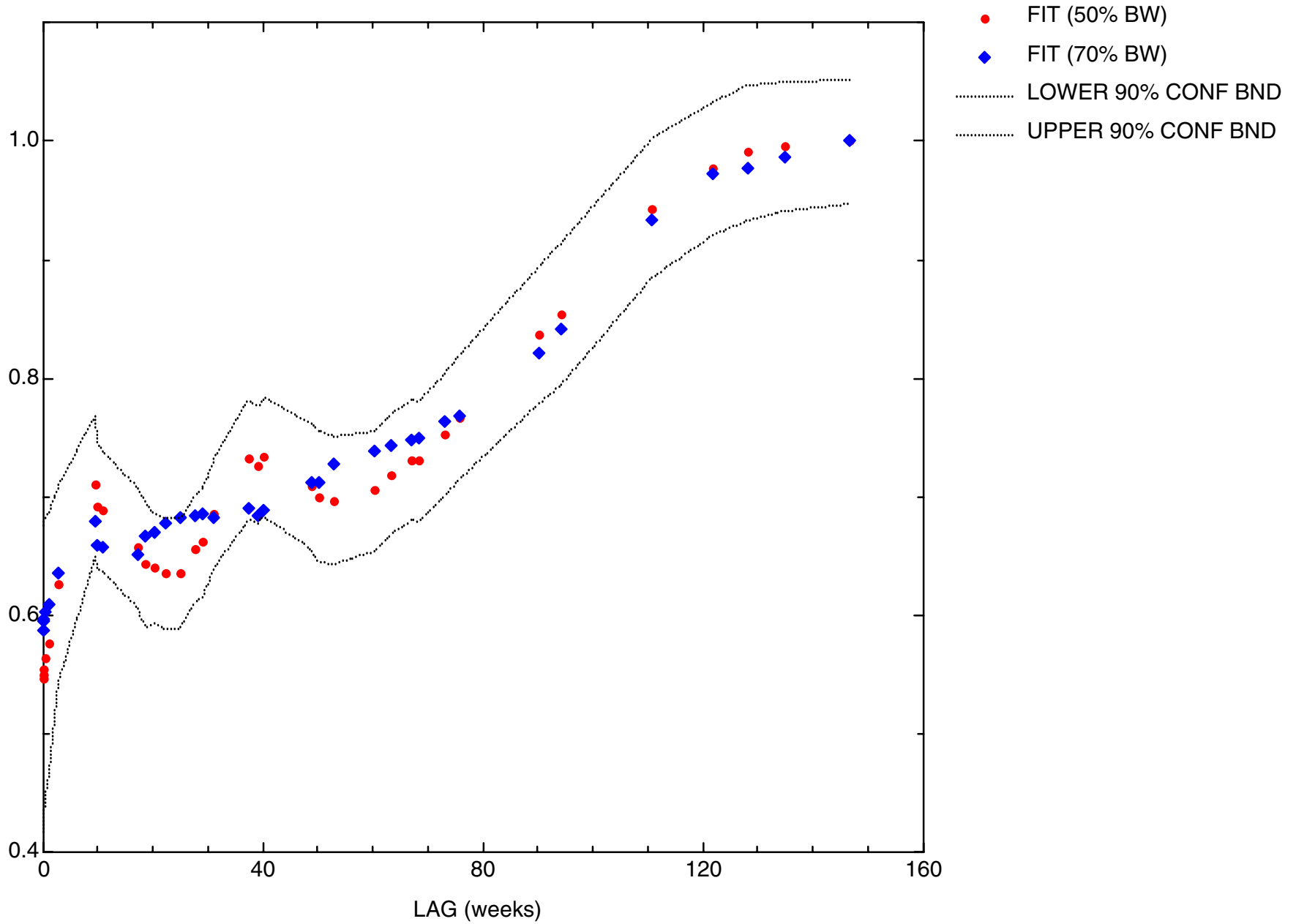
PEASE AFB, SITE 49: DCA11 TEMPORAL VARIOGRAM



PEASE AFB, SITE 49: DCE12C TEMPORAL VARIOGRAM



PEASE AFB, SITE 49: TCE TEMPORAL VARIOGRAM

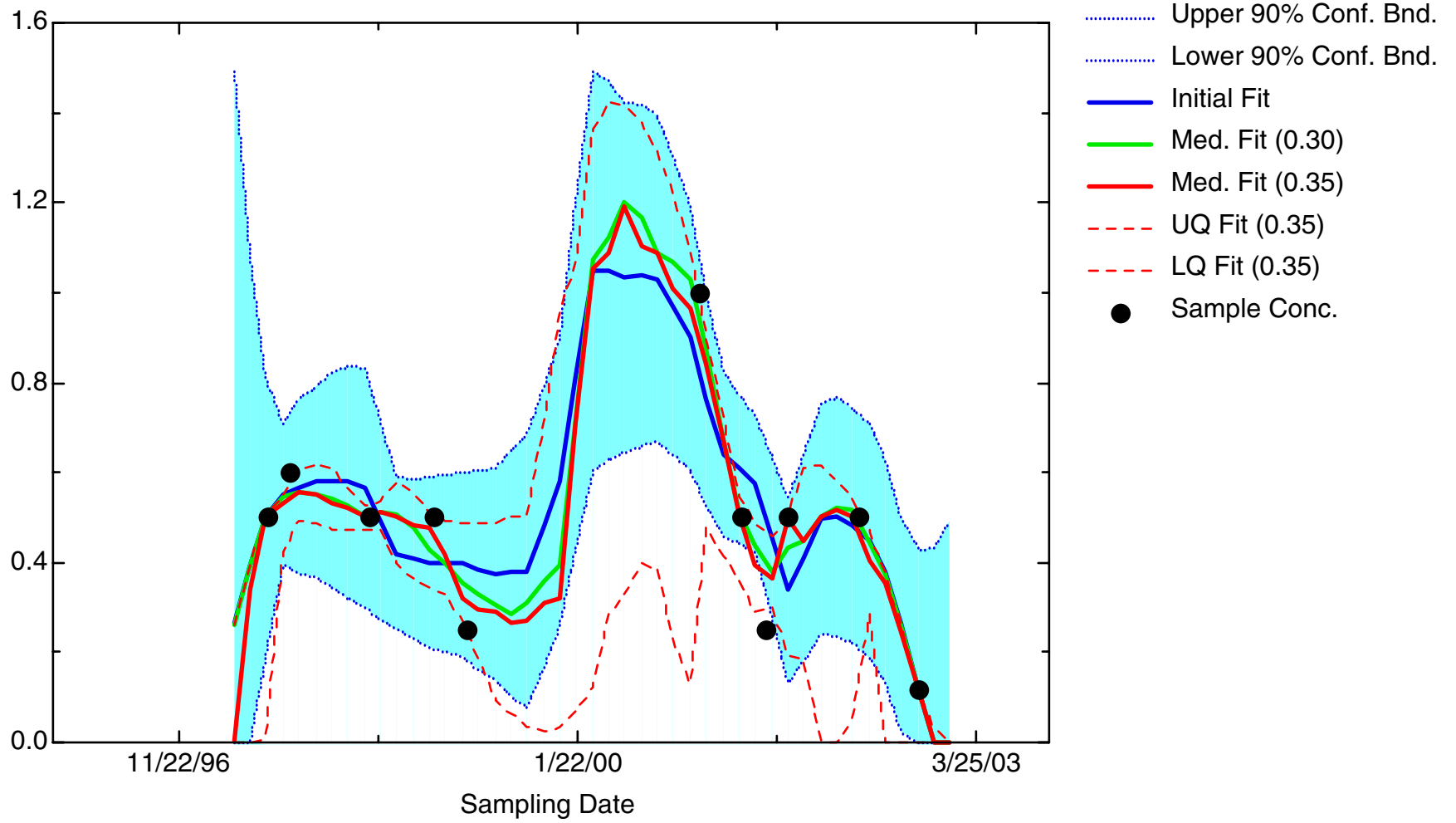


# Appendix 3.2

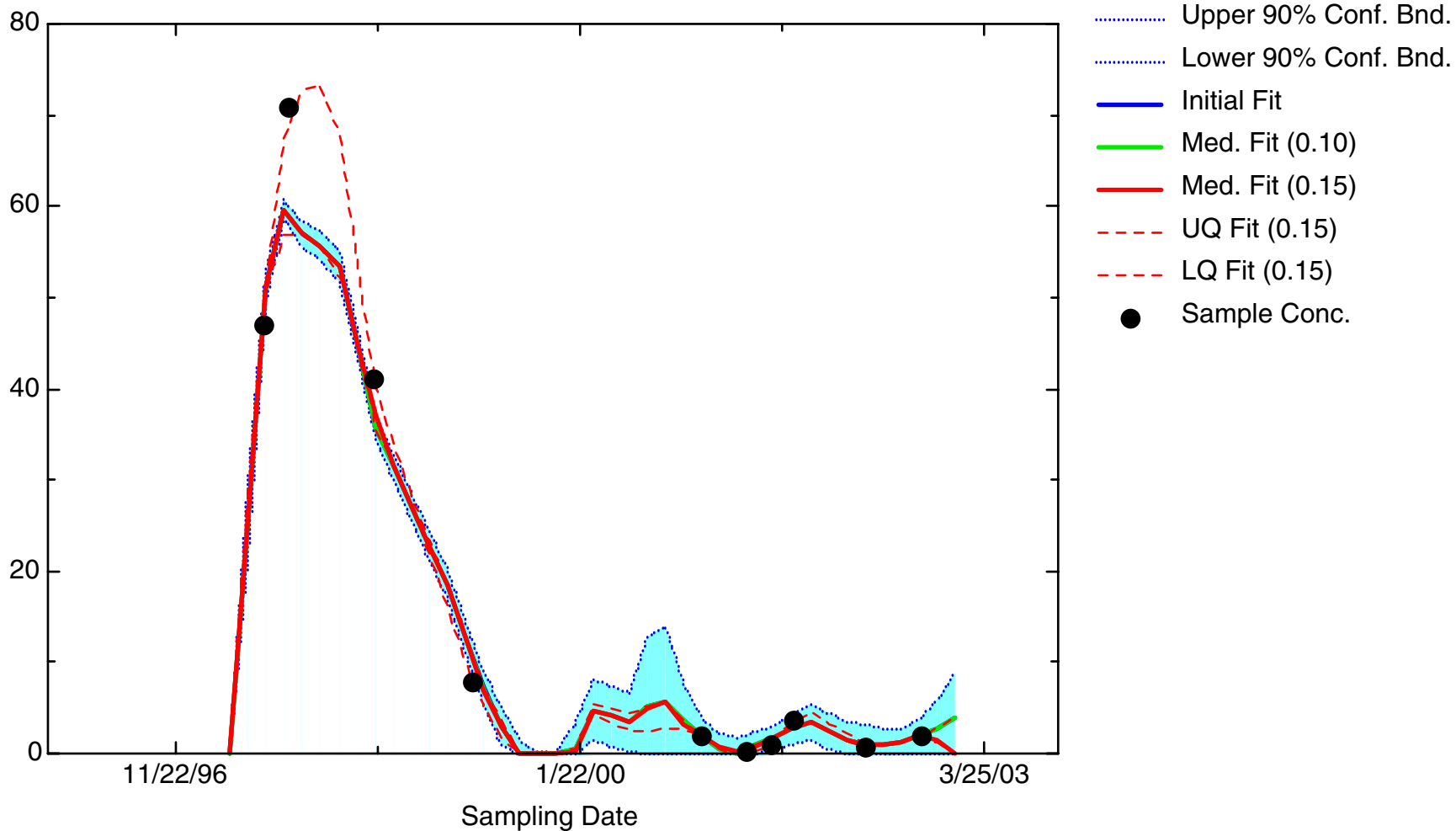
## Iterative Fitting Trend Overlays

DCA11

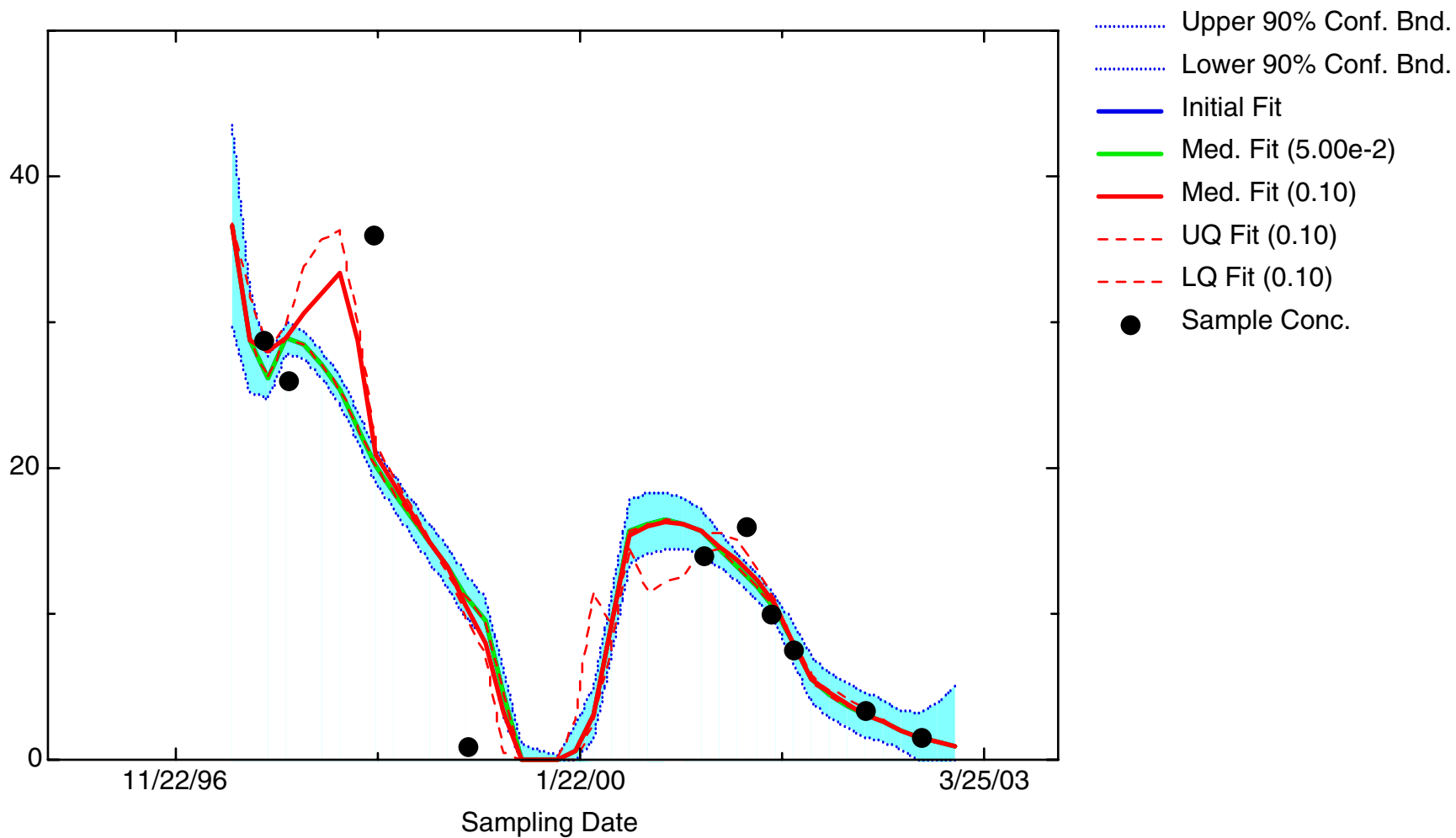
DCA11: Well 49-5562(D)



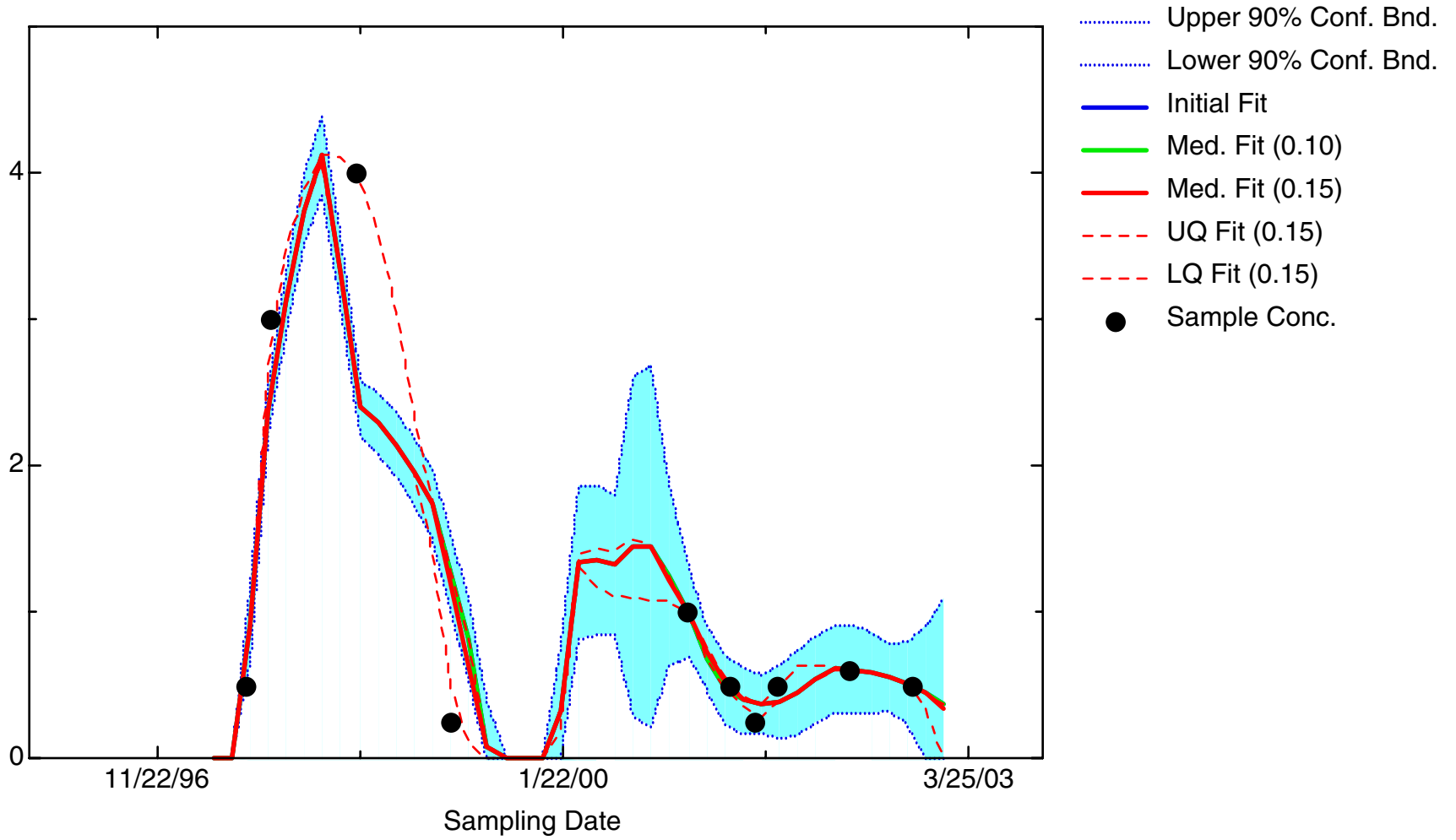
DCA11: Well 49-5563(S)



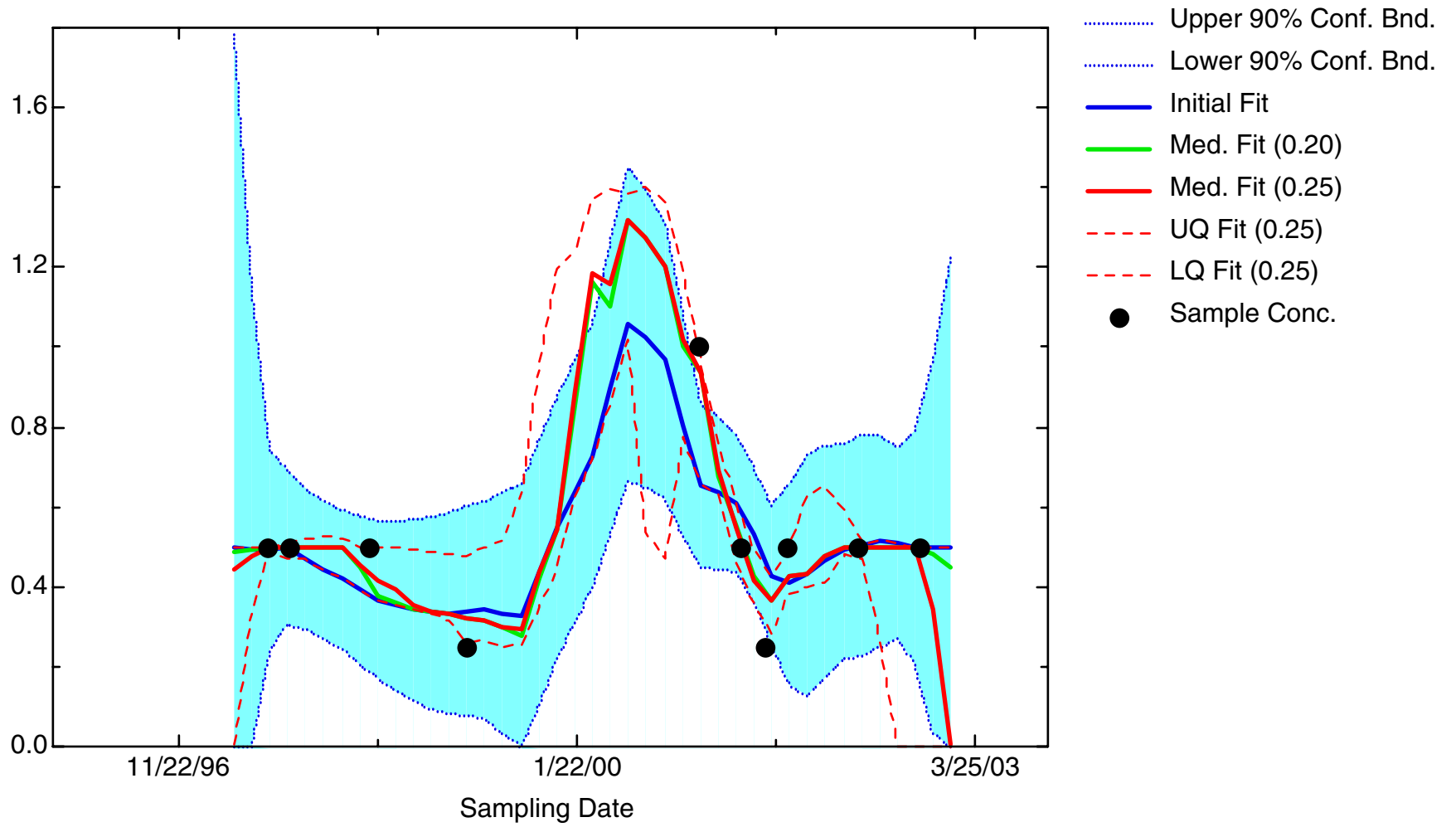
DCA11: Well 49-5564(D)



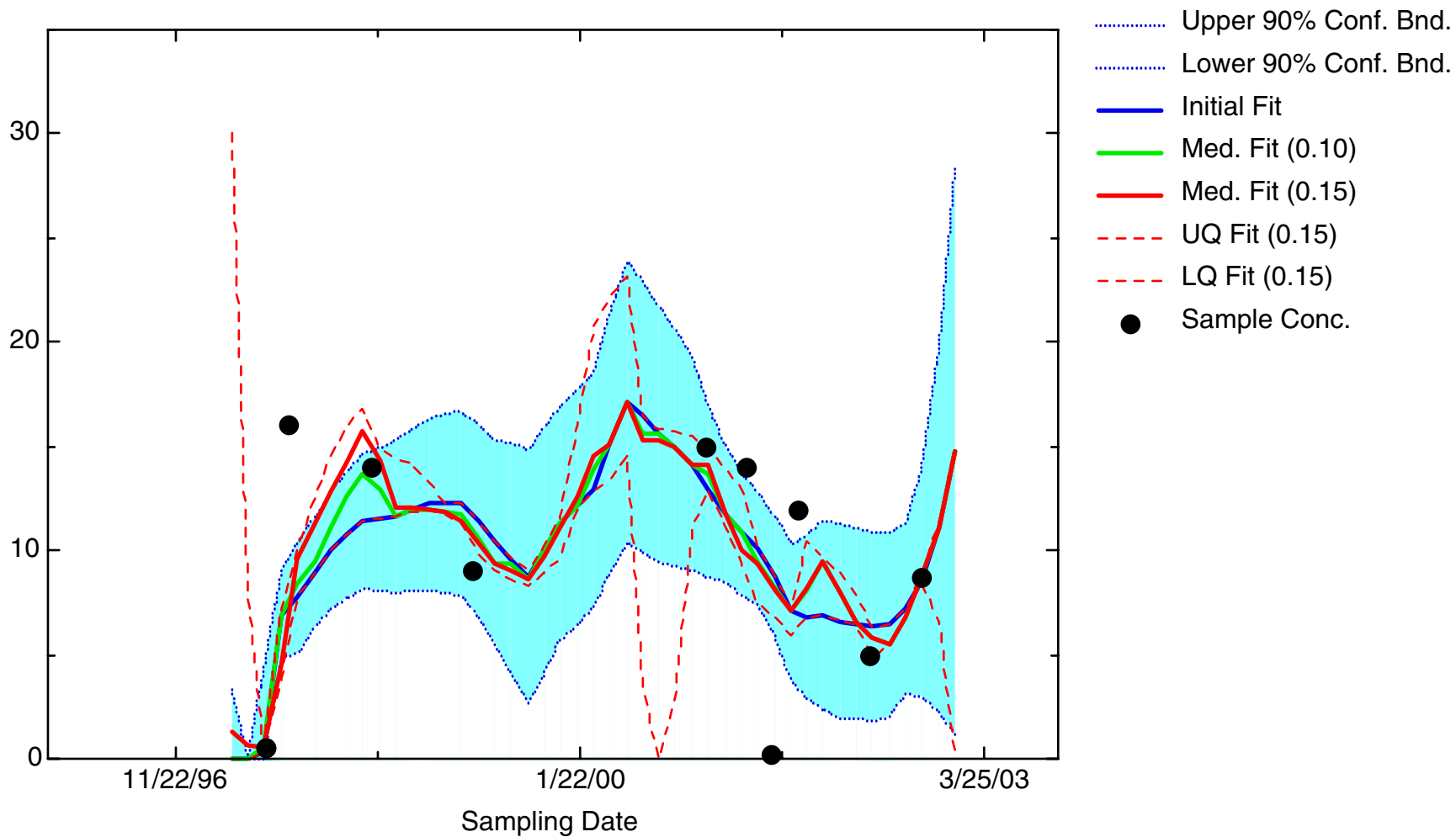
DCA11: Well 49-5565(S)



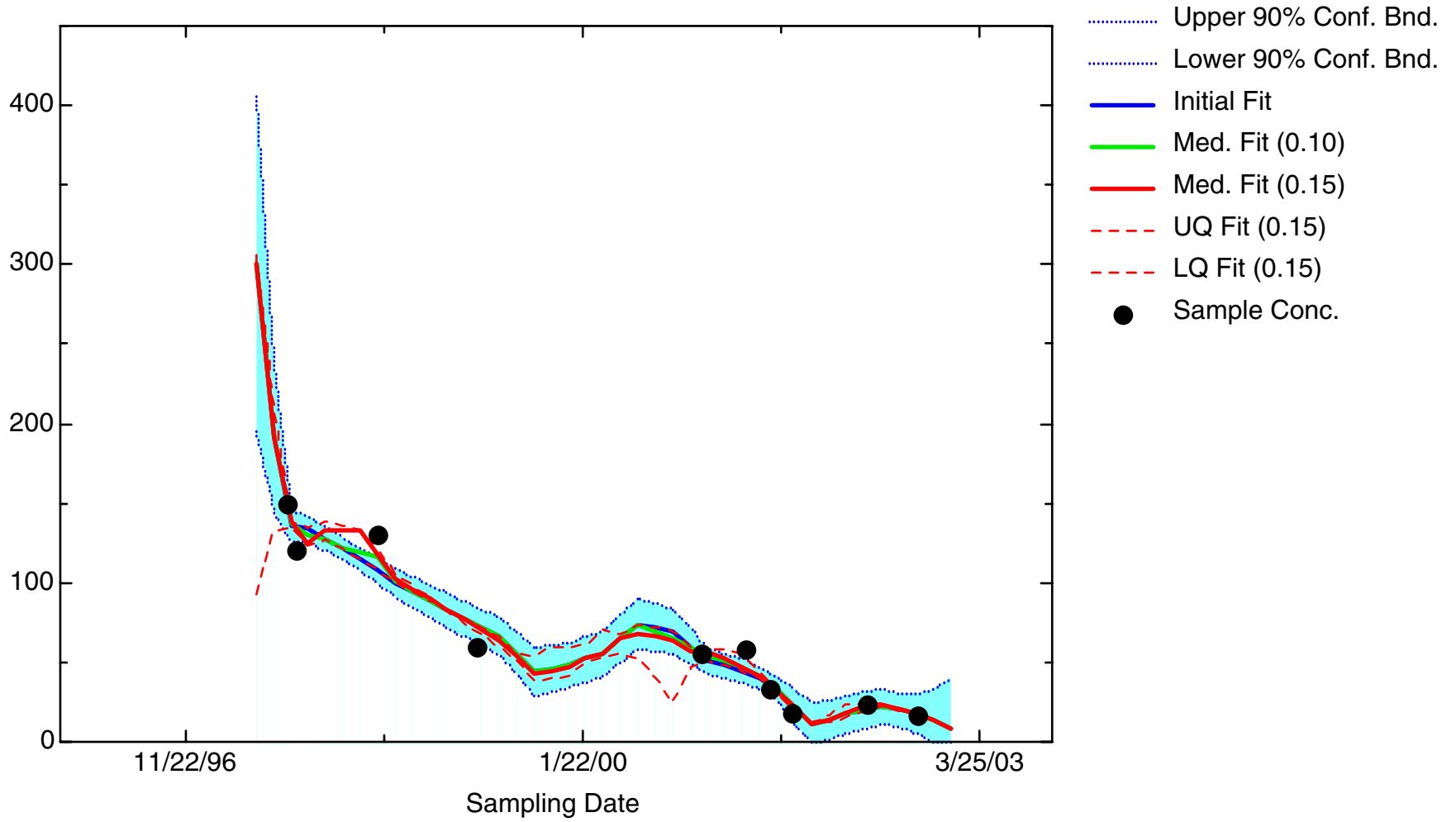
DCA11: Well 49-5566(S)



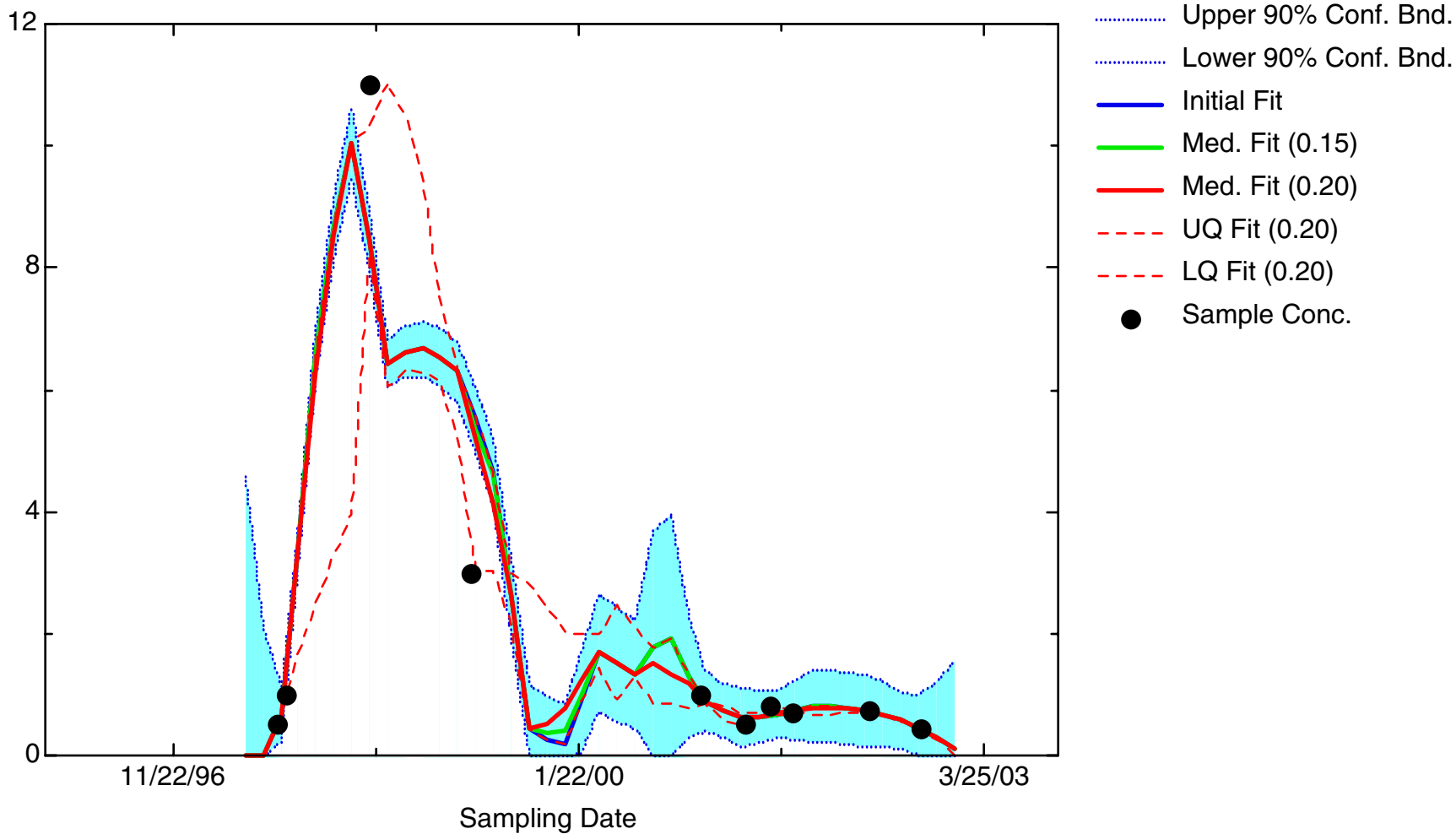
DCA11: Well 49-5568(D)



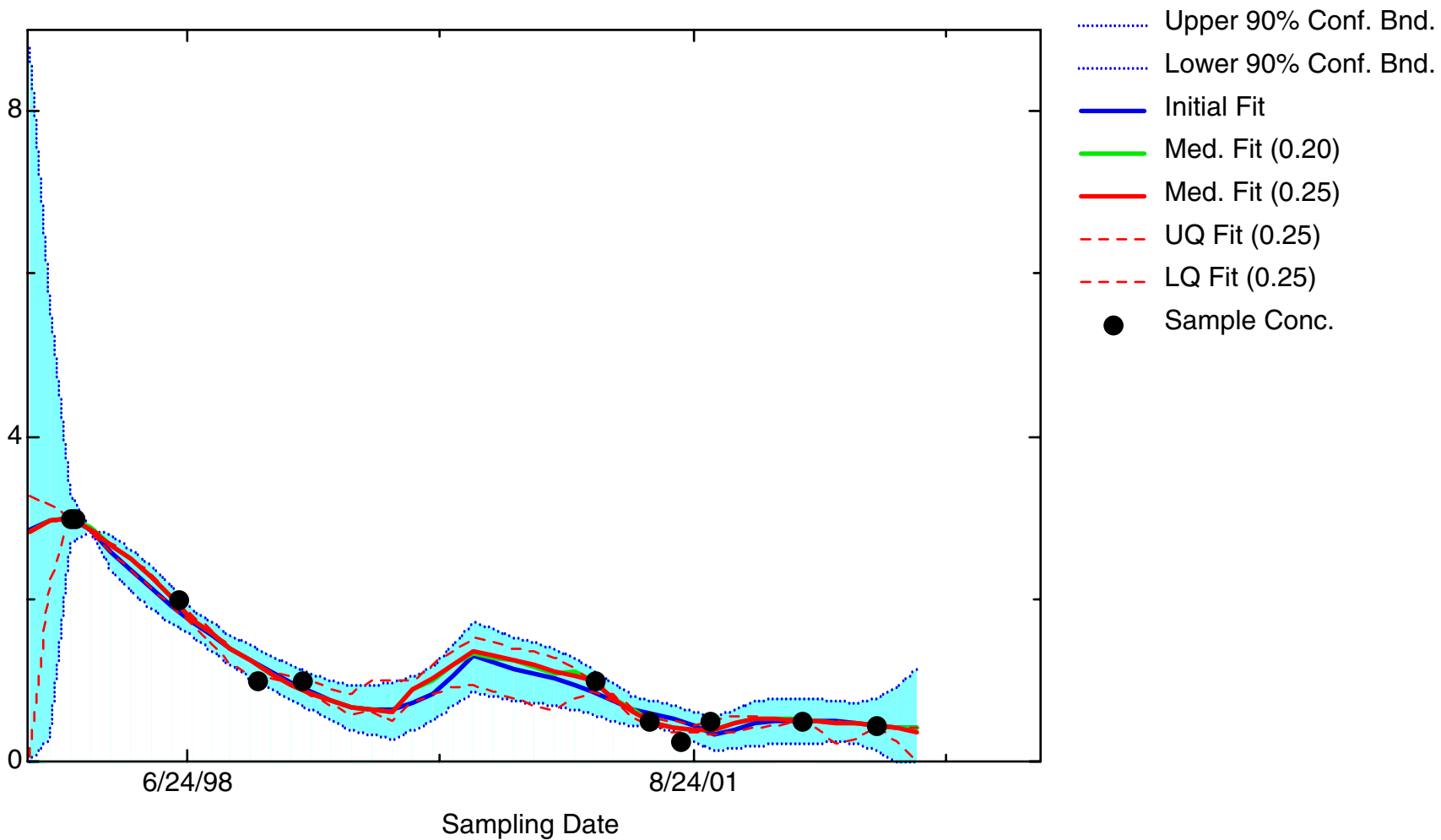
DCA11: Well 49-5573(D)



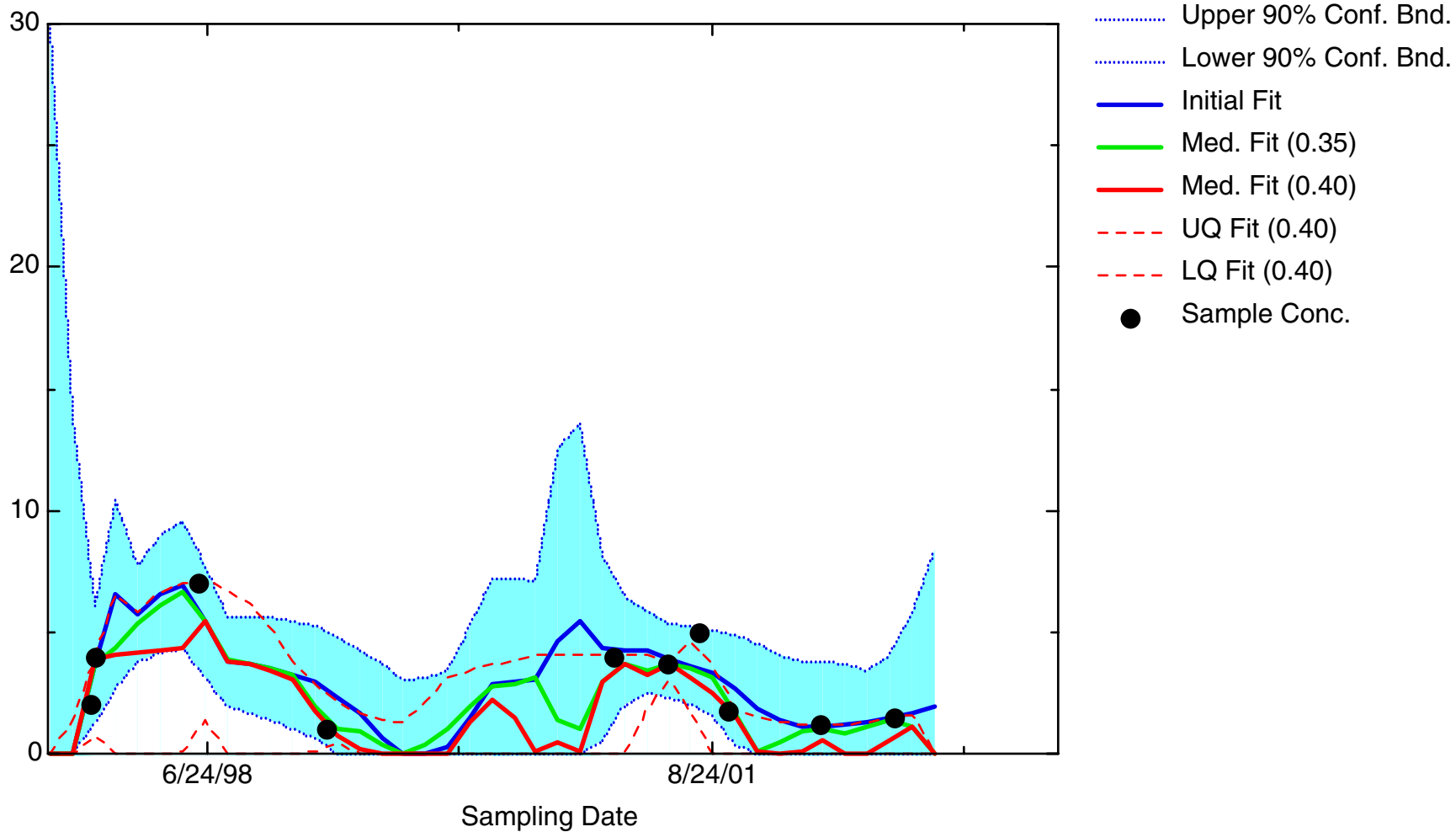
DCA11: Well 49-5574(S)



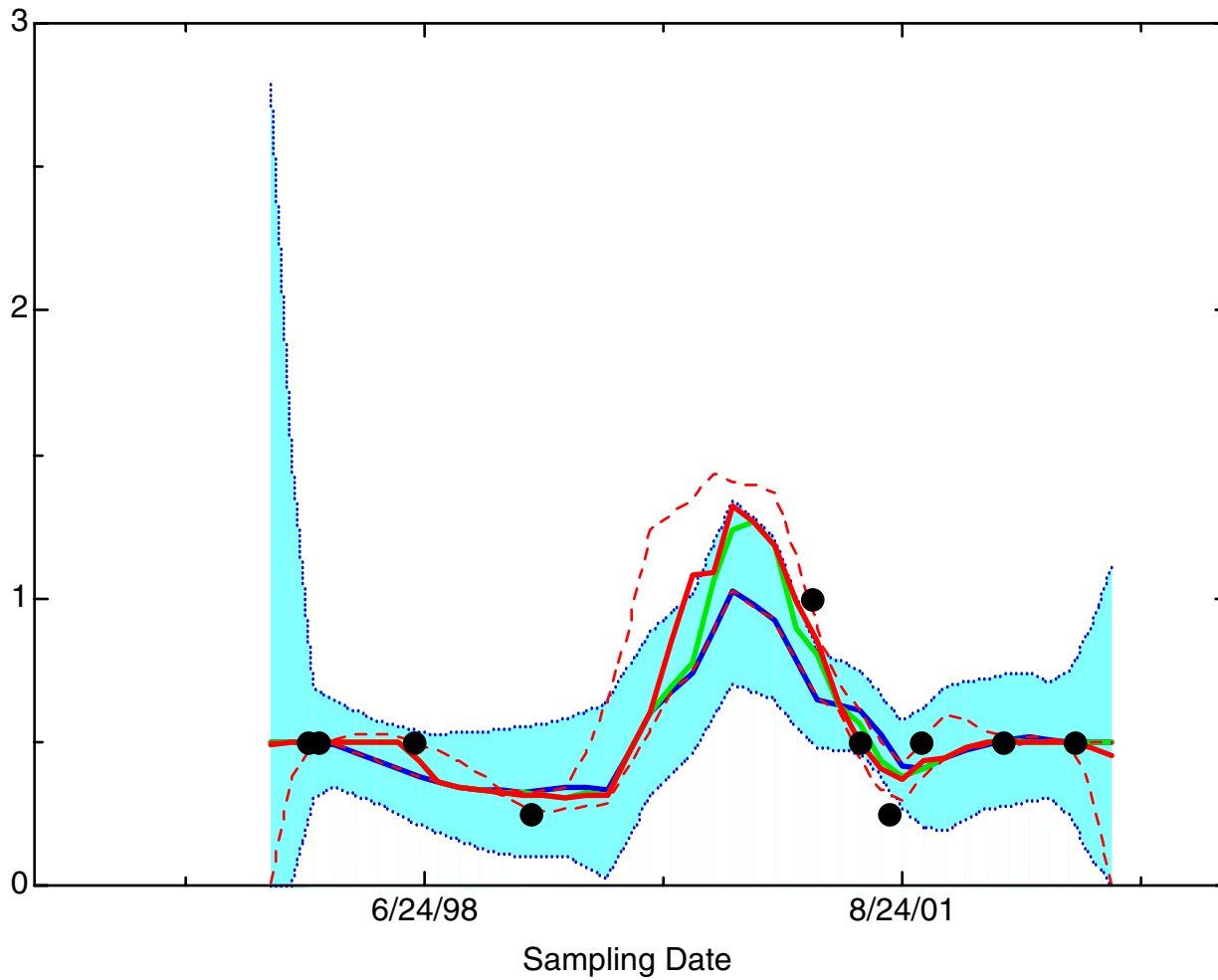
DCA11: Well 49-5577(D)



DCA11: Well 49-5578(S)

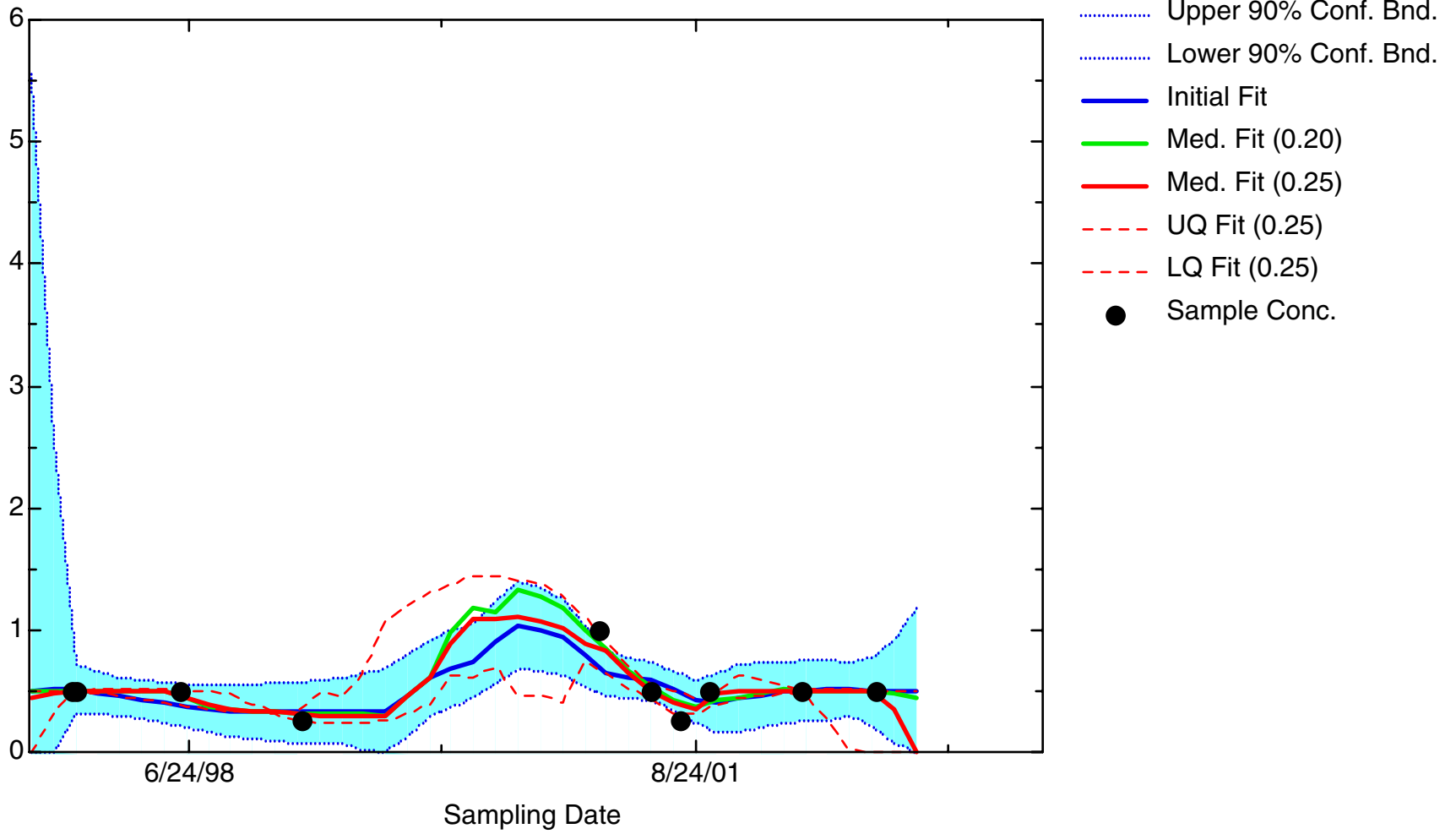


DCA11: Well 49-6515(S)

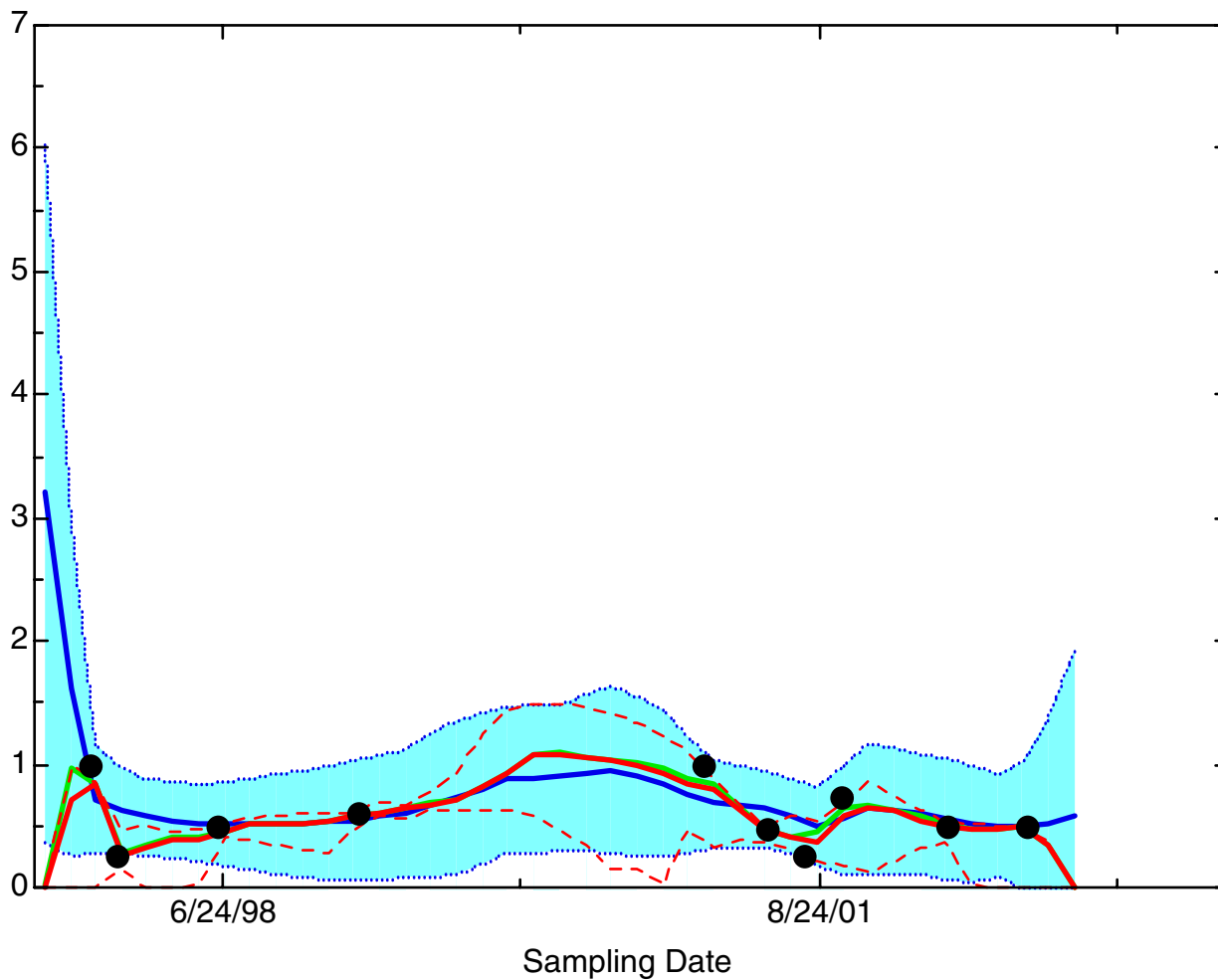


- ..... Upper 90% Conf. Bnd.
- ..... Lower 90% Conf. Bnd.
- Initial Fit
- Med. Fit (0.15)
- Med. Fit (0.20)
- - - UQ Fit (0.20)
- . - LQ Fit (0.20)
- Sample Conc.

DCA11: Well 49-6516(S)



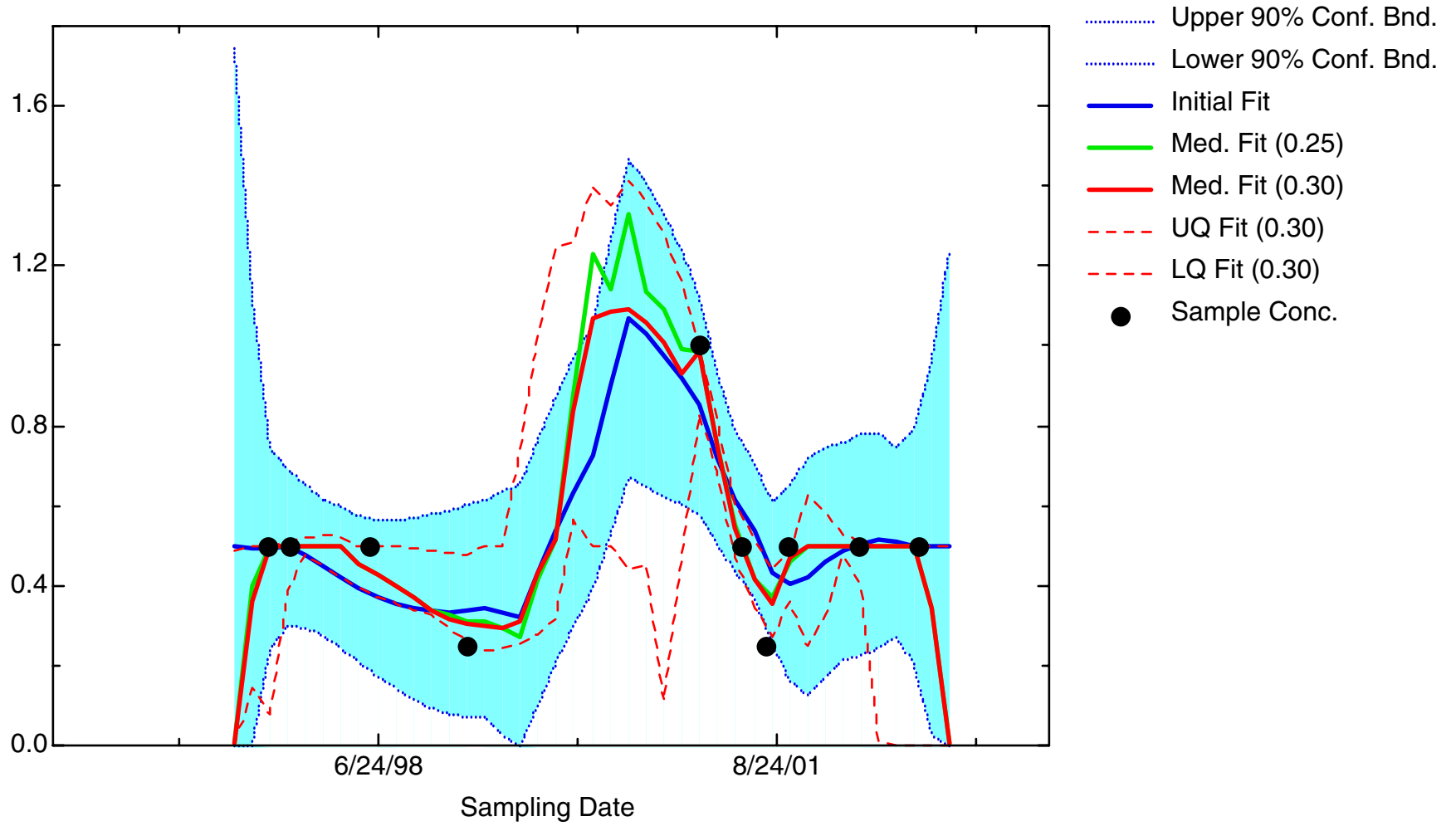
DCA11: Well 49-MW01



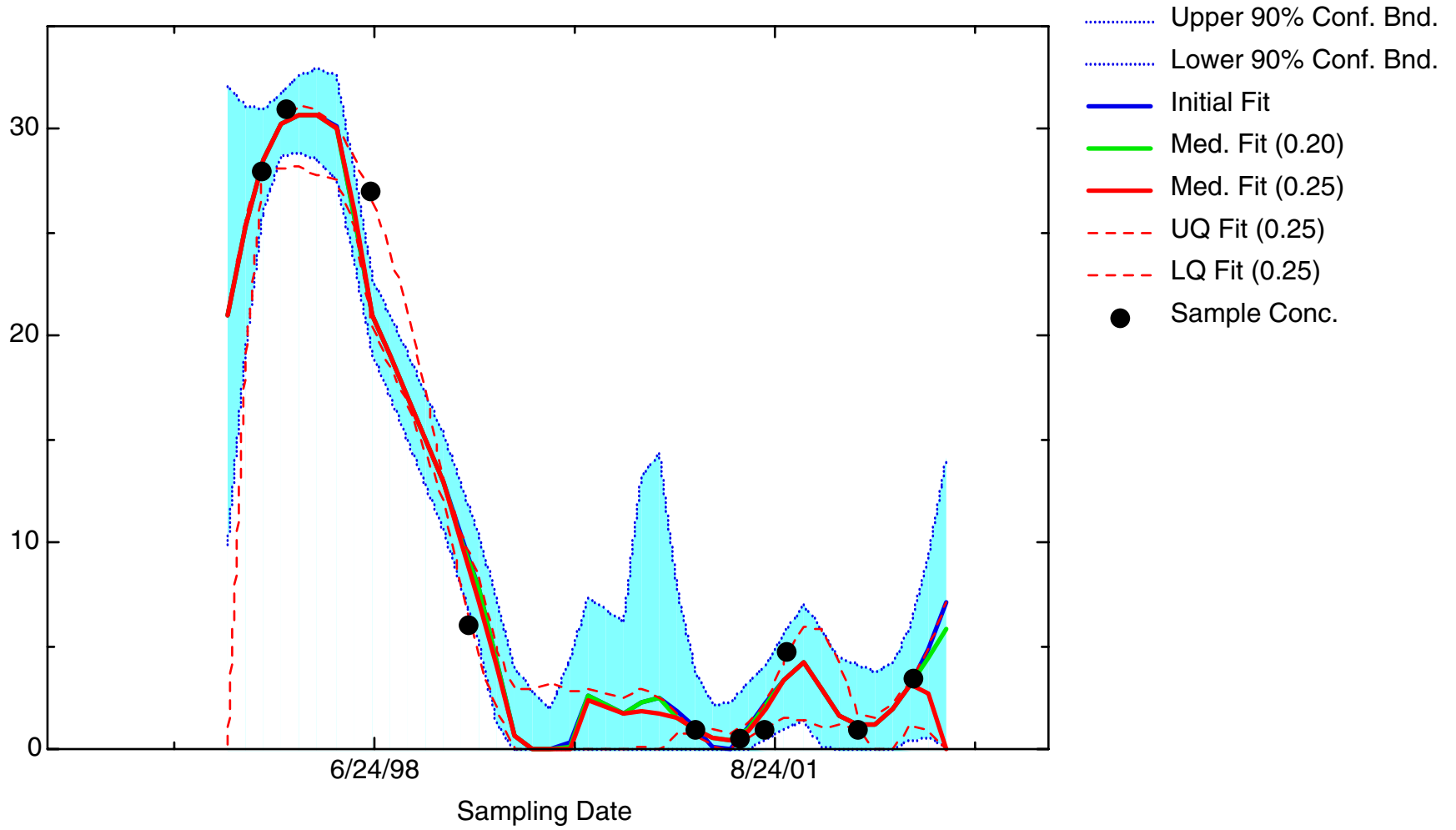
- ..... Upper 90% Conf. Bnd.
- ..... Lower 90% Conf. Bnd.
- Initial Fit
- Med. Fit (0.30)
- Med. Fit (0.35)
- - - UQ Fit (0.35)
- - - LQ Fit (0.35)
- Sample Conc.

DCE12C

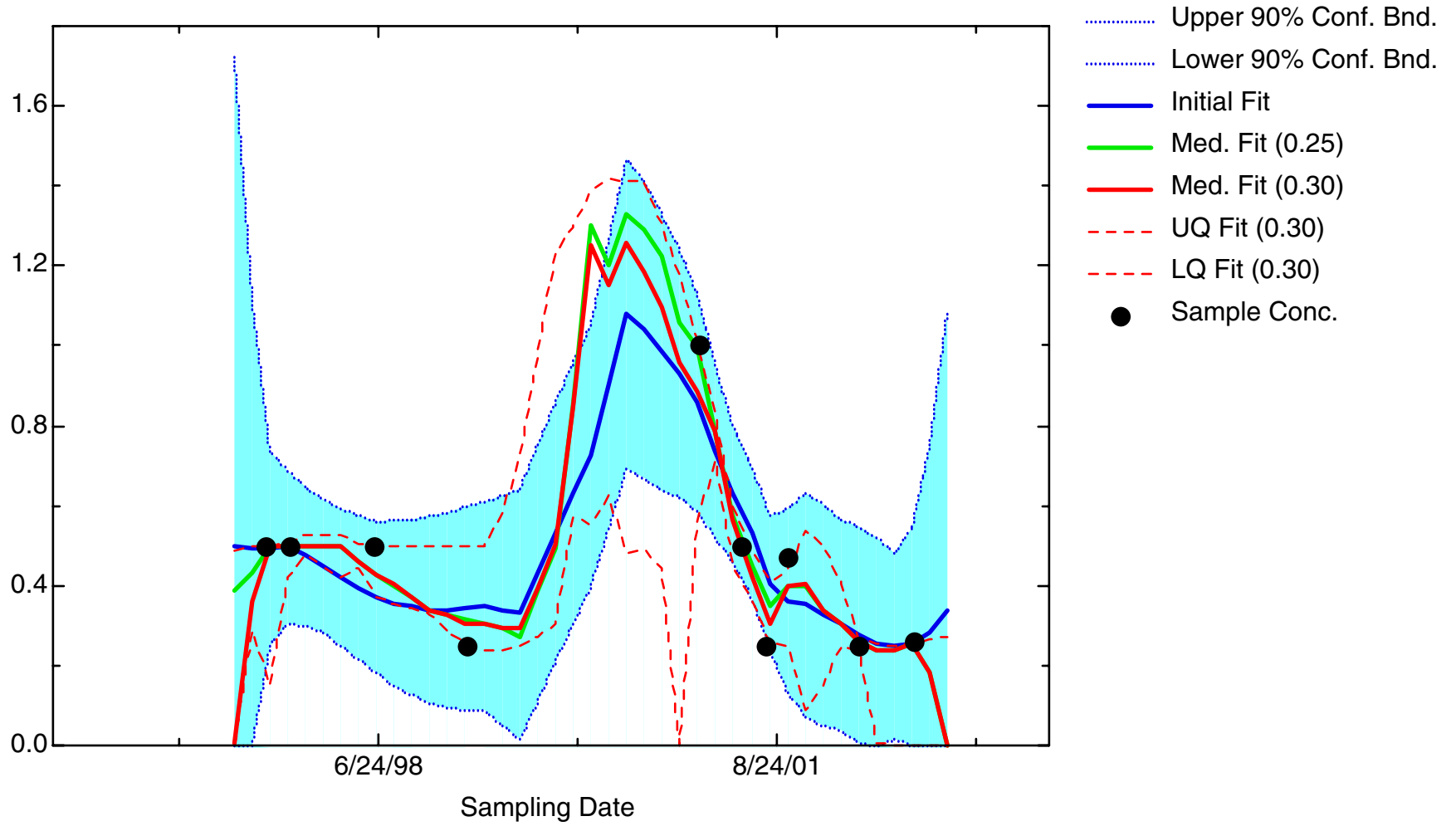
DCE12C: Well 49-5562(D)



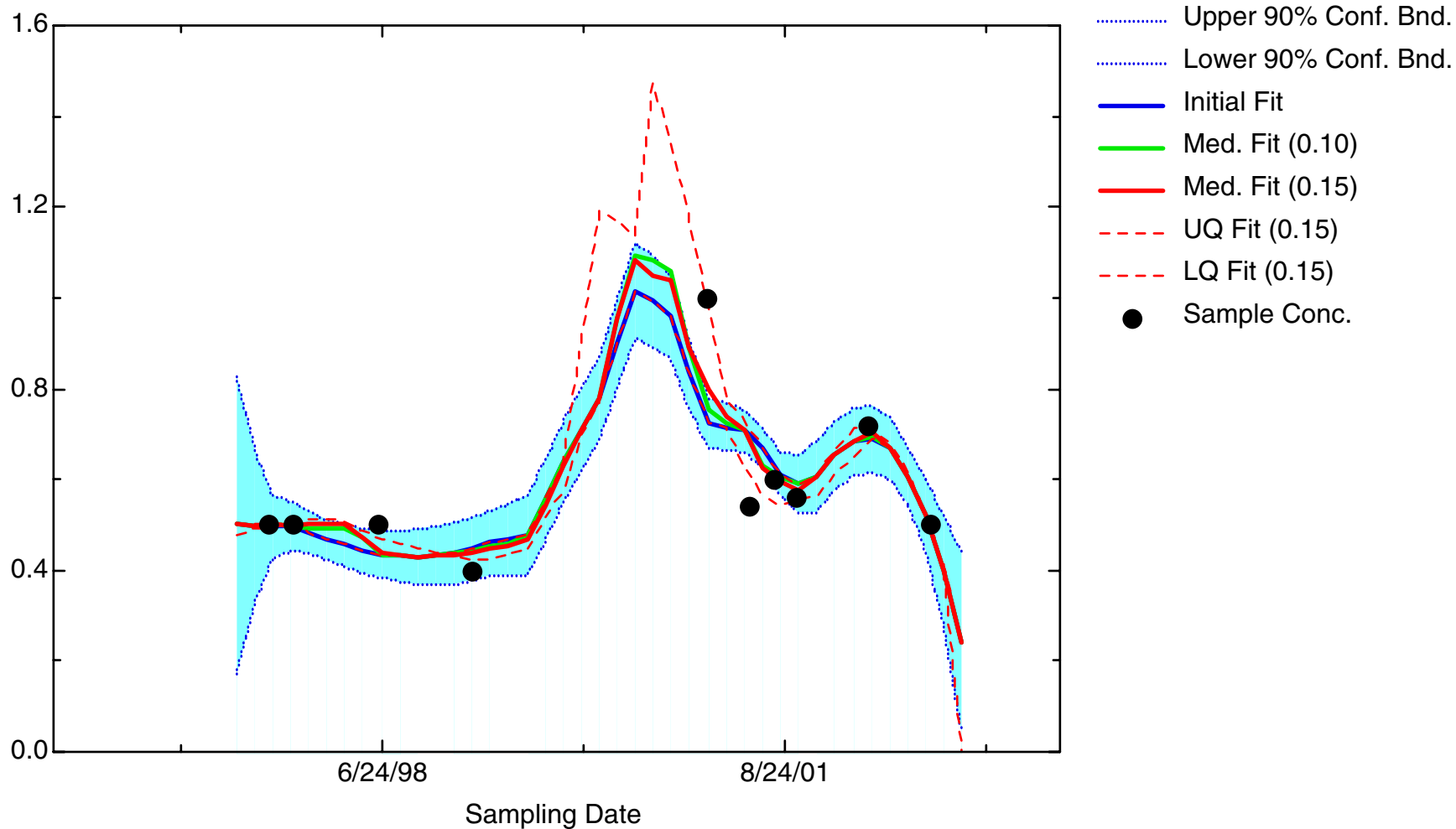
DCE12C: Well 49-5563(S)



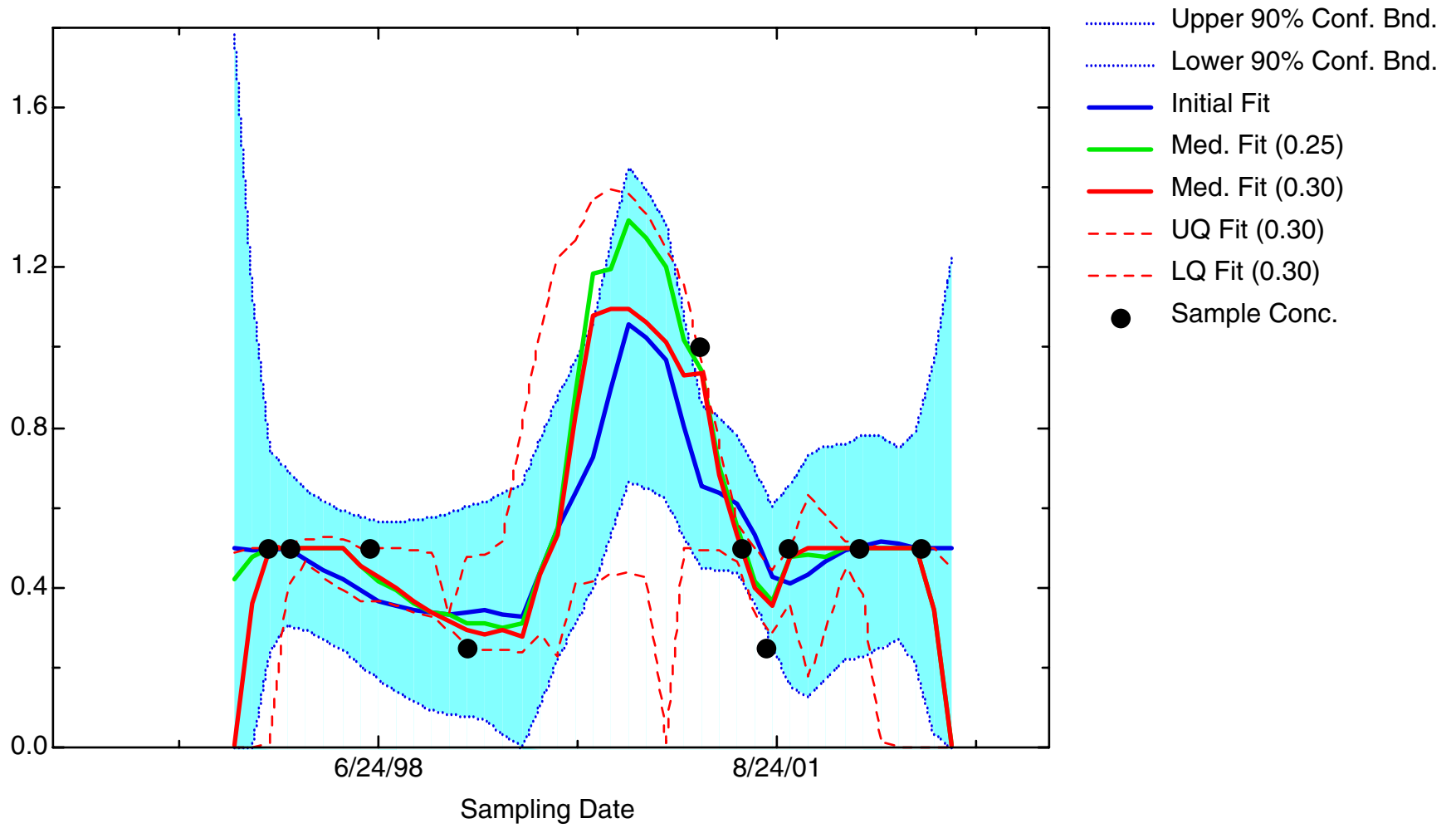
DCE12C: Well 49-5564(D)



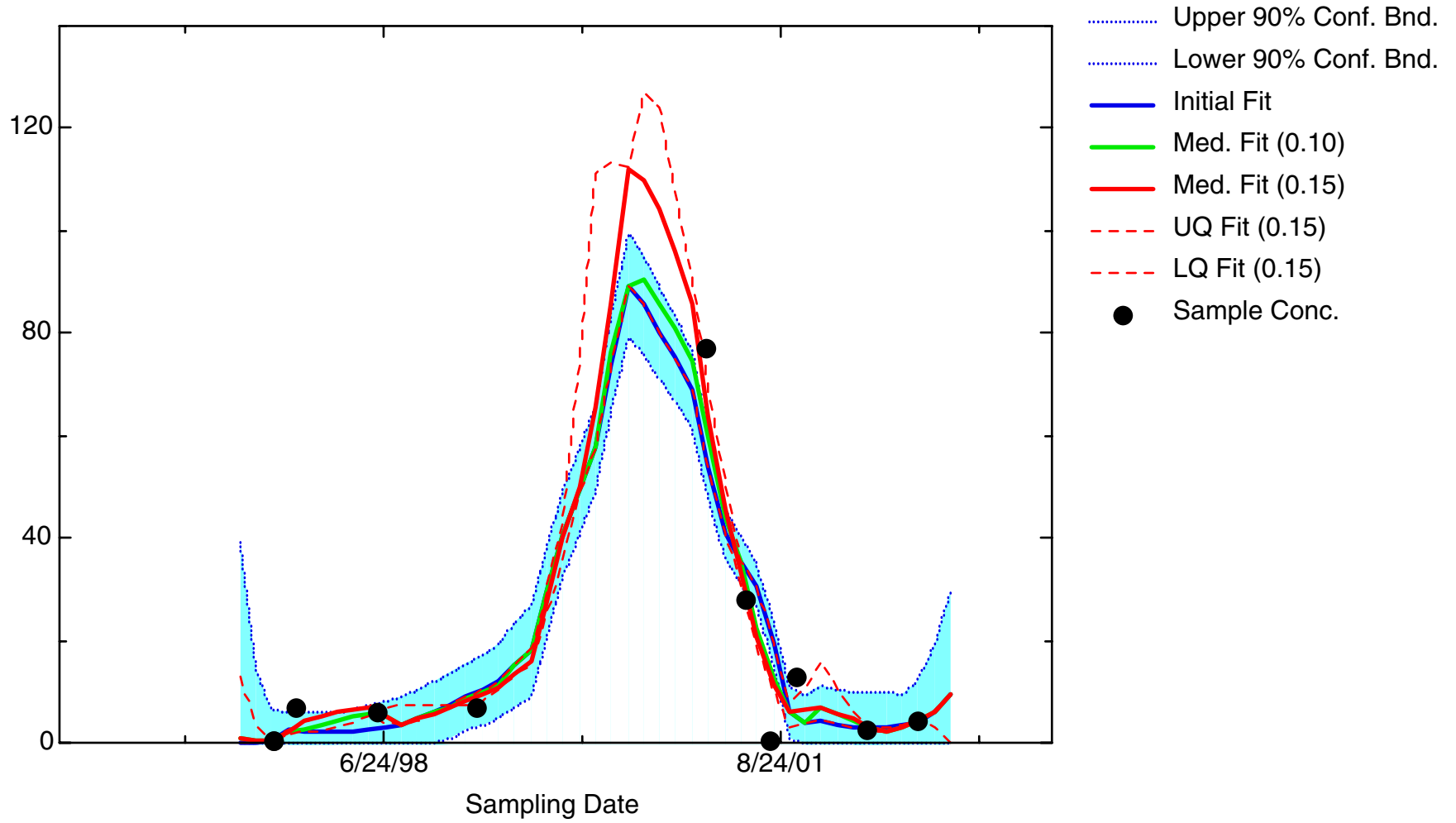
DCE12C: Well 49-5565(S)



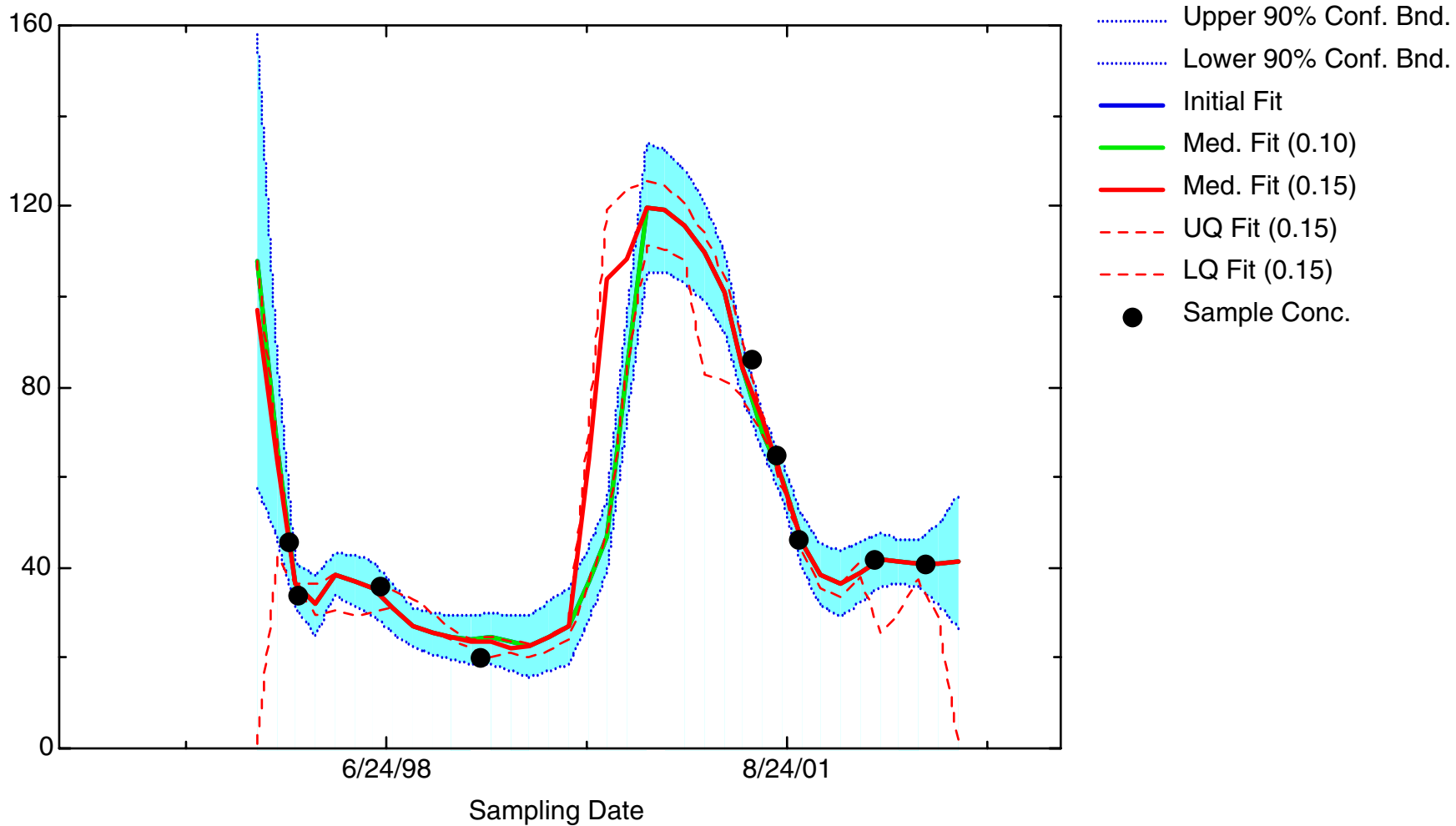
DCE12C: Well 49-5566(S)



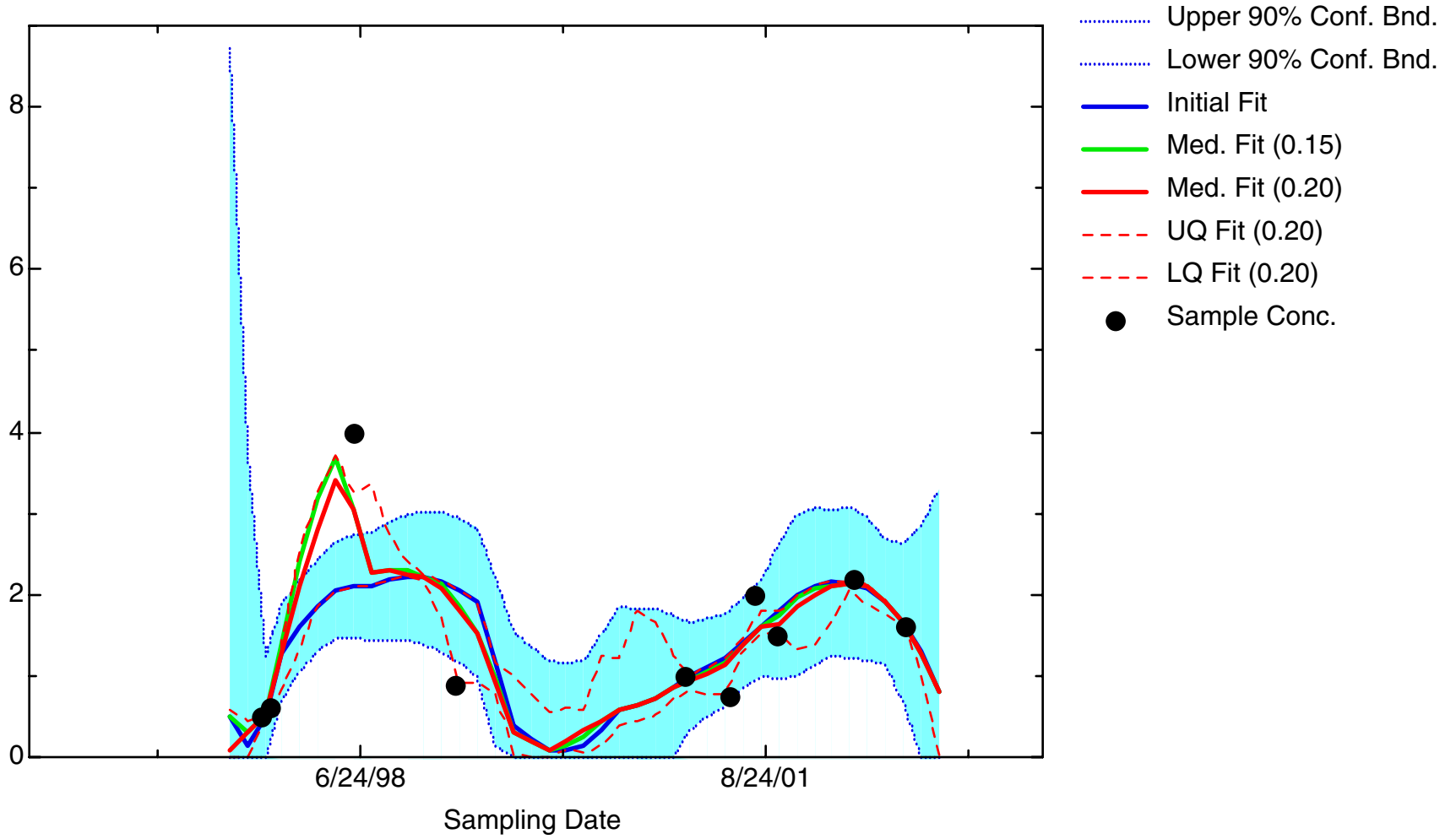
DCE12C: Well 49-5568(D)



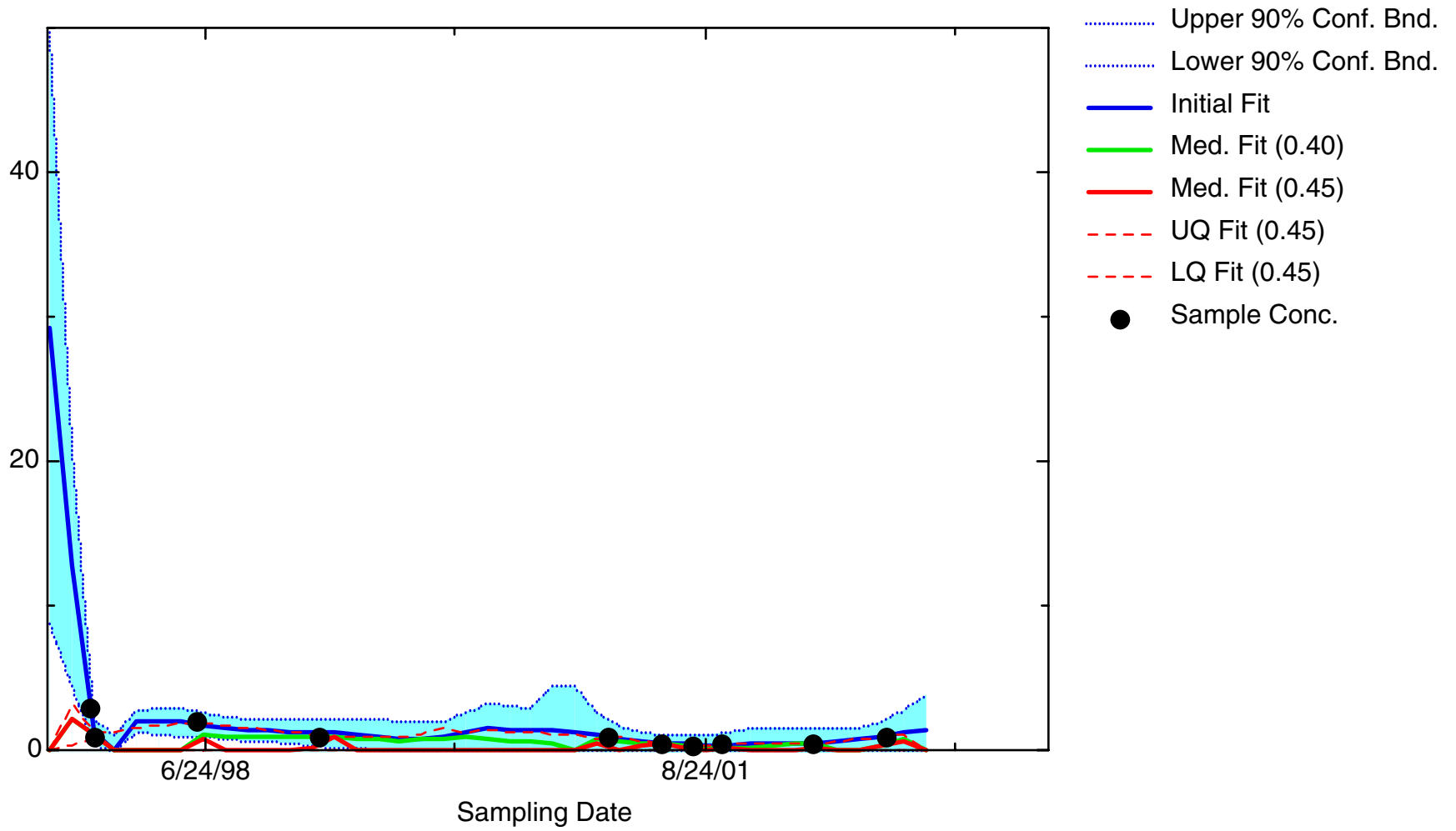
DCE12C: Well 49-5573(D)



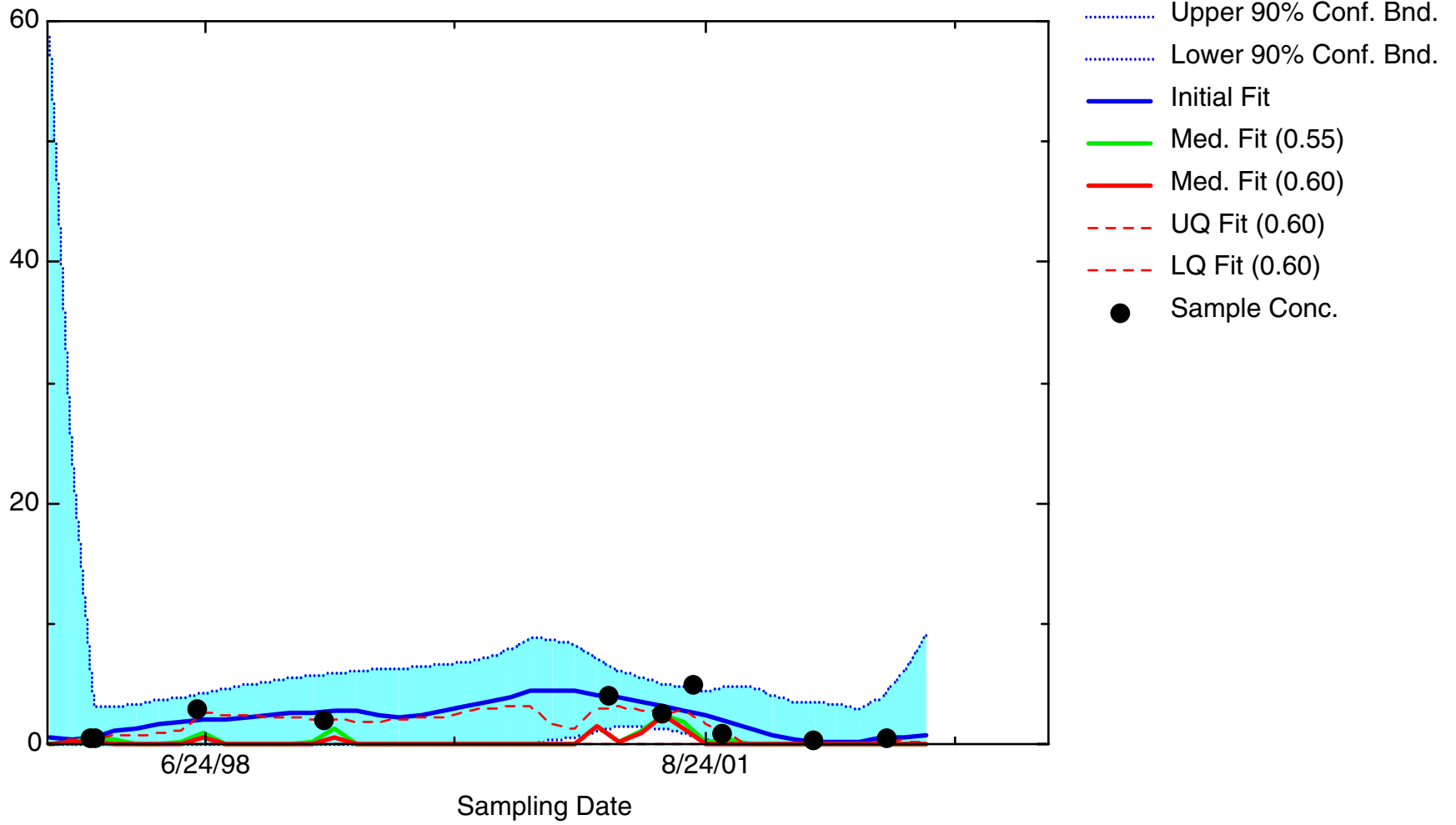
DCE12C: Well 49-5574(S)



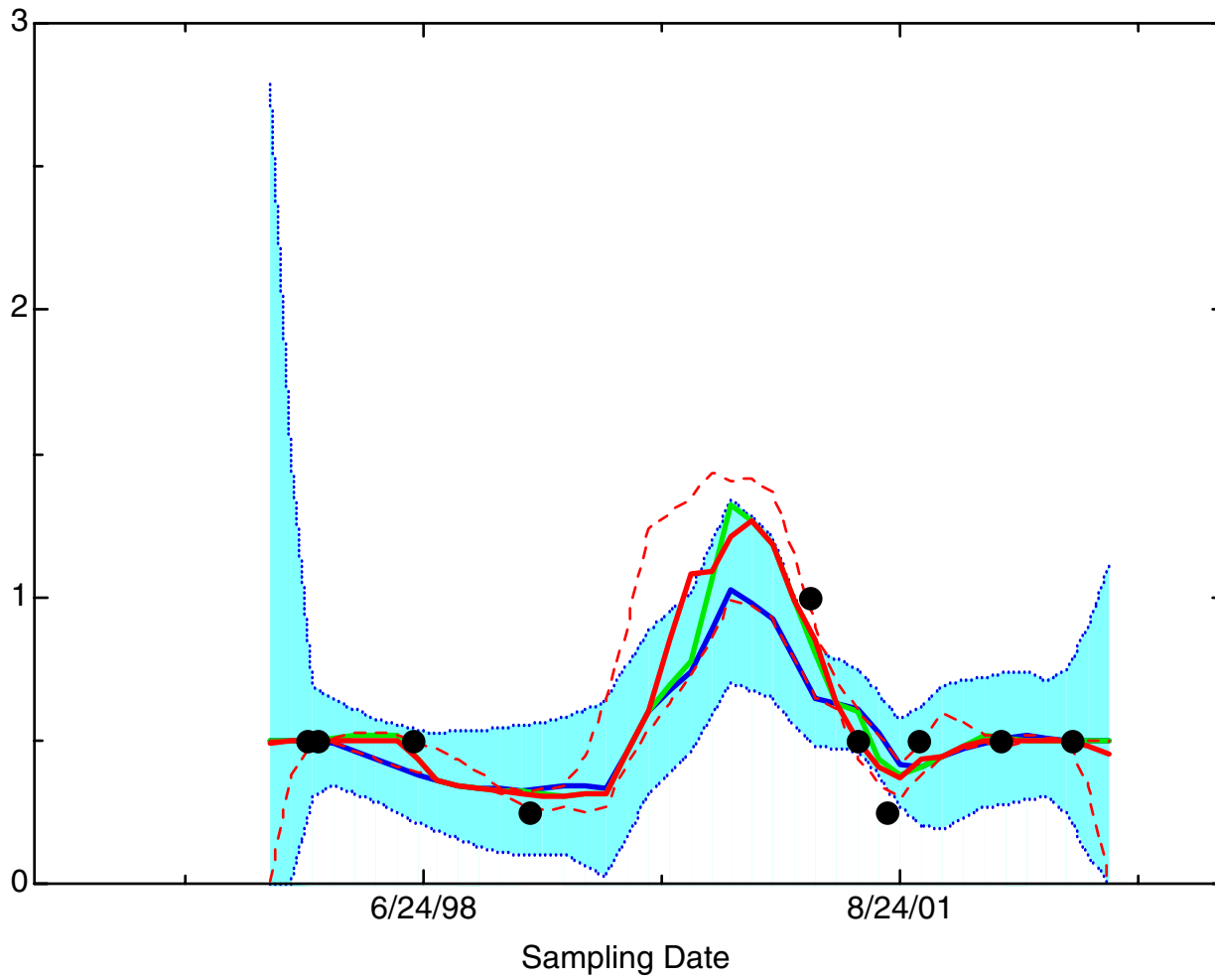
DCE12C: Well 49-5577(D)



DCE12C: Well 49-5578(S)

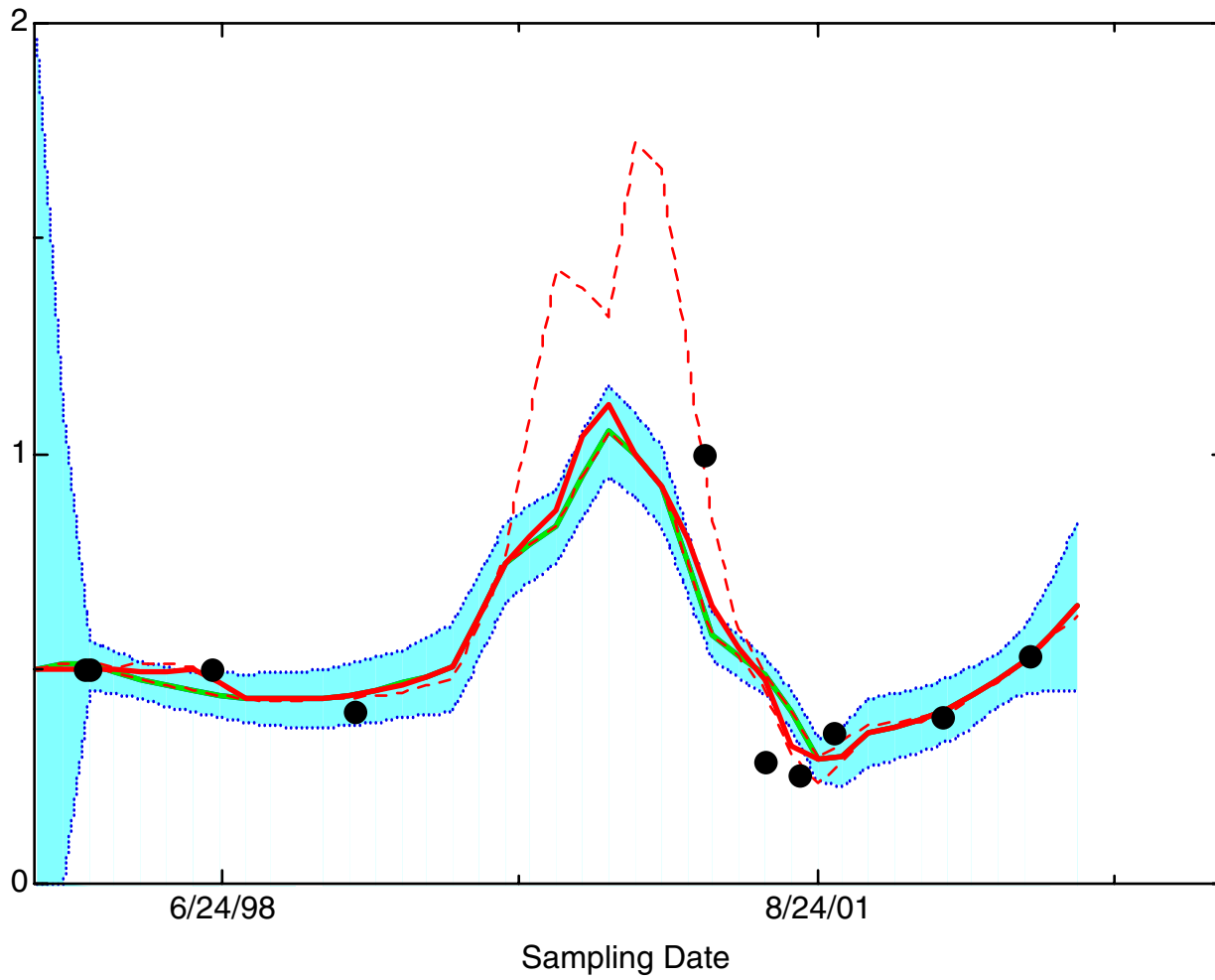


DCE12C: Well 49-6515(S)



- ..... Upper 90% Conf. Bnd.
- ..... Lower 90% Conf. Bnd.
- Initial Fit
- Med. Fit (0.15)
- Med. Fit (0.20)
- - - UQ Fit (0.20)
- . - LQ Fit (0.20)
- Sample Conc.

DCE12C: Well 49-6516(S)

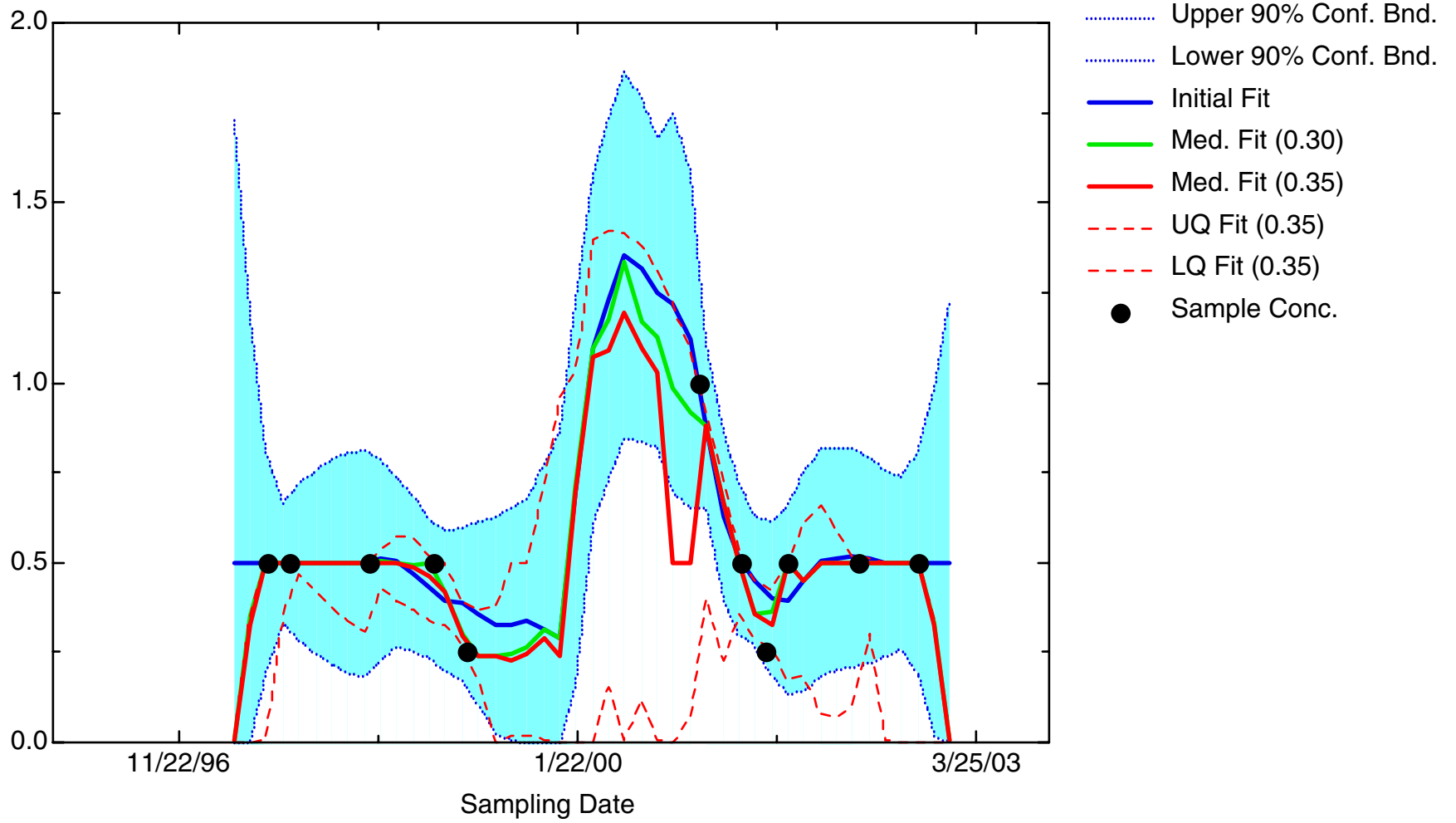


- ..... Upper 90% Conf. Bnd.
- ..... Lower 90% Conf. Bnd.
- Initial Fit
- Med. Fit (5.00e-2)
- Med. Fit (0.10)
- - - UQ Fit (0.10)
- - - LQ Fit (0.10)
- Sample Conc.

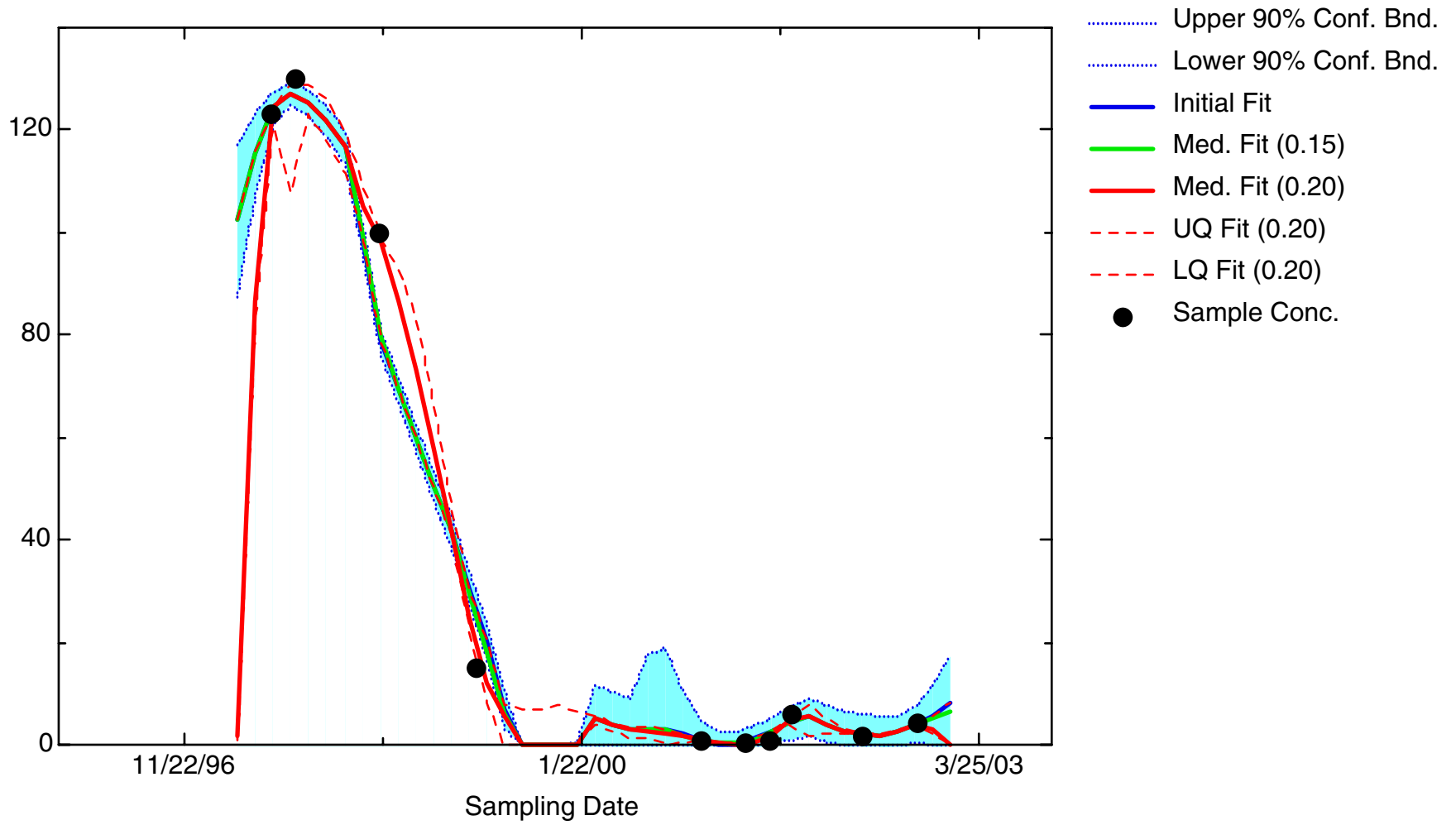


TCE

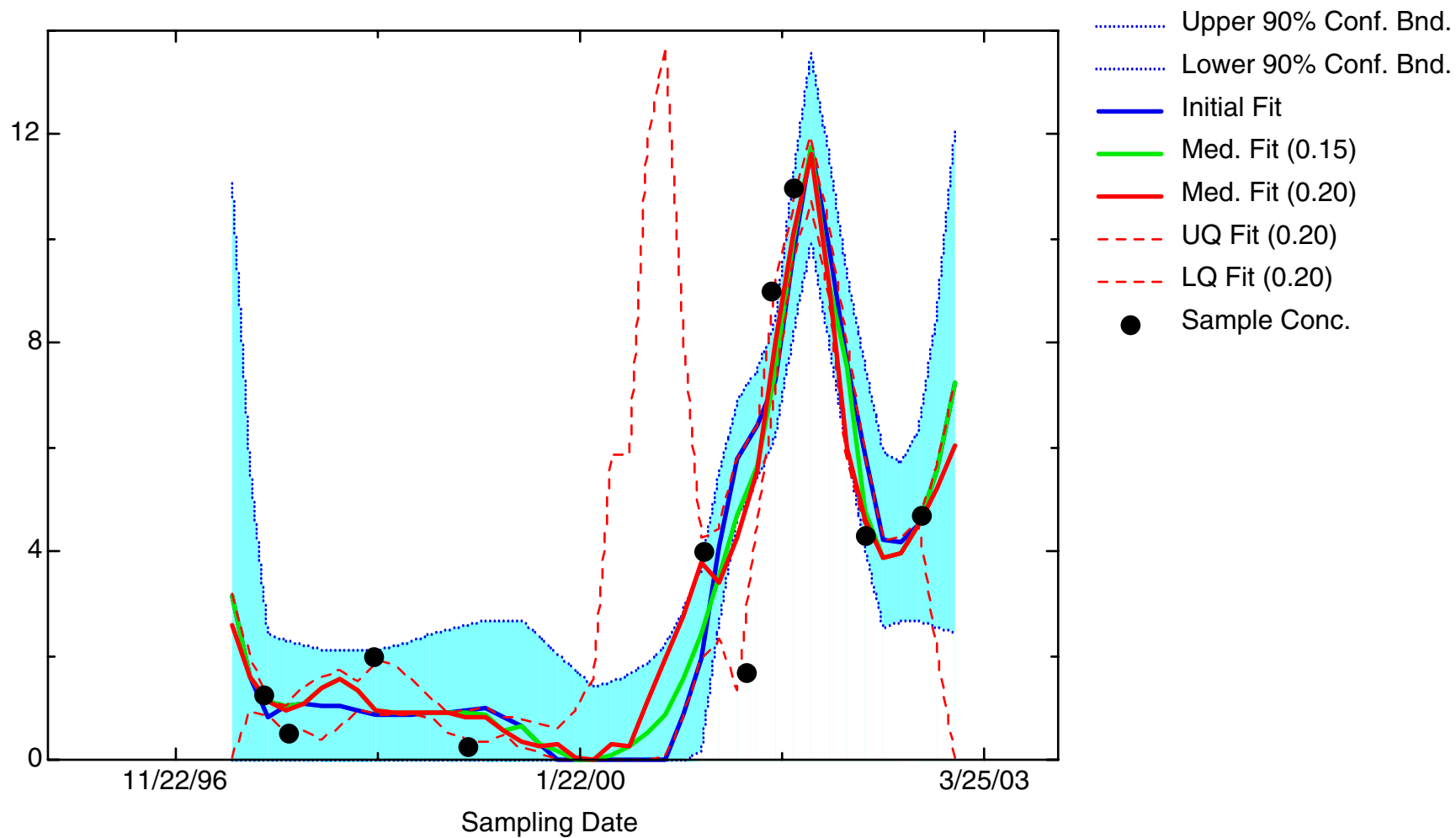
TCE: Well 49-5562(D)



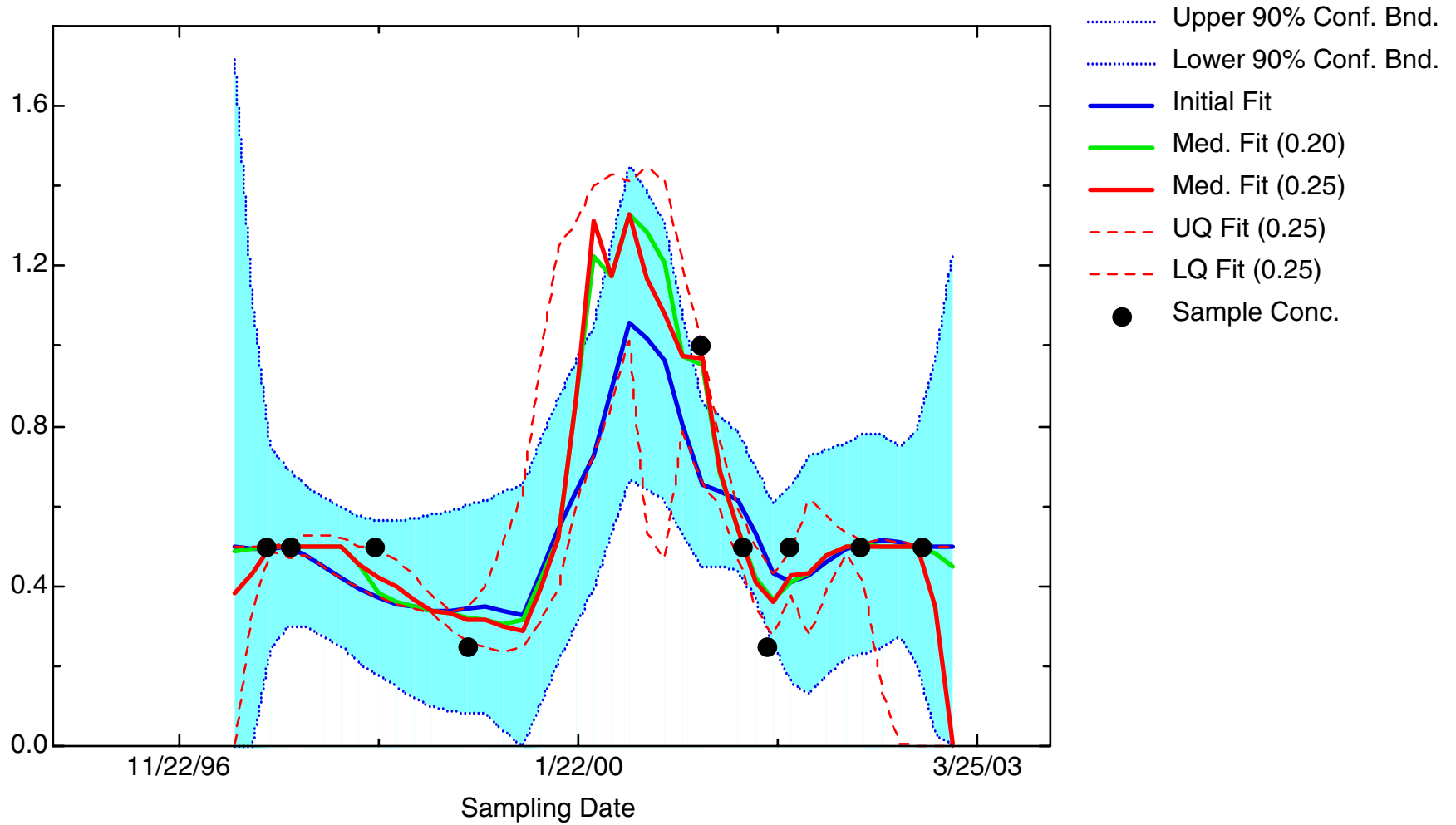
TCE: Well 49-5563(S)



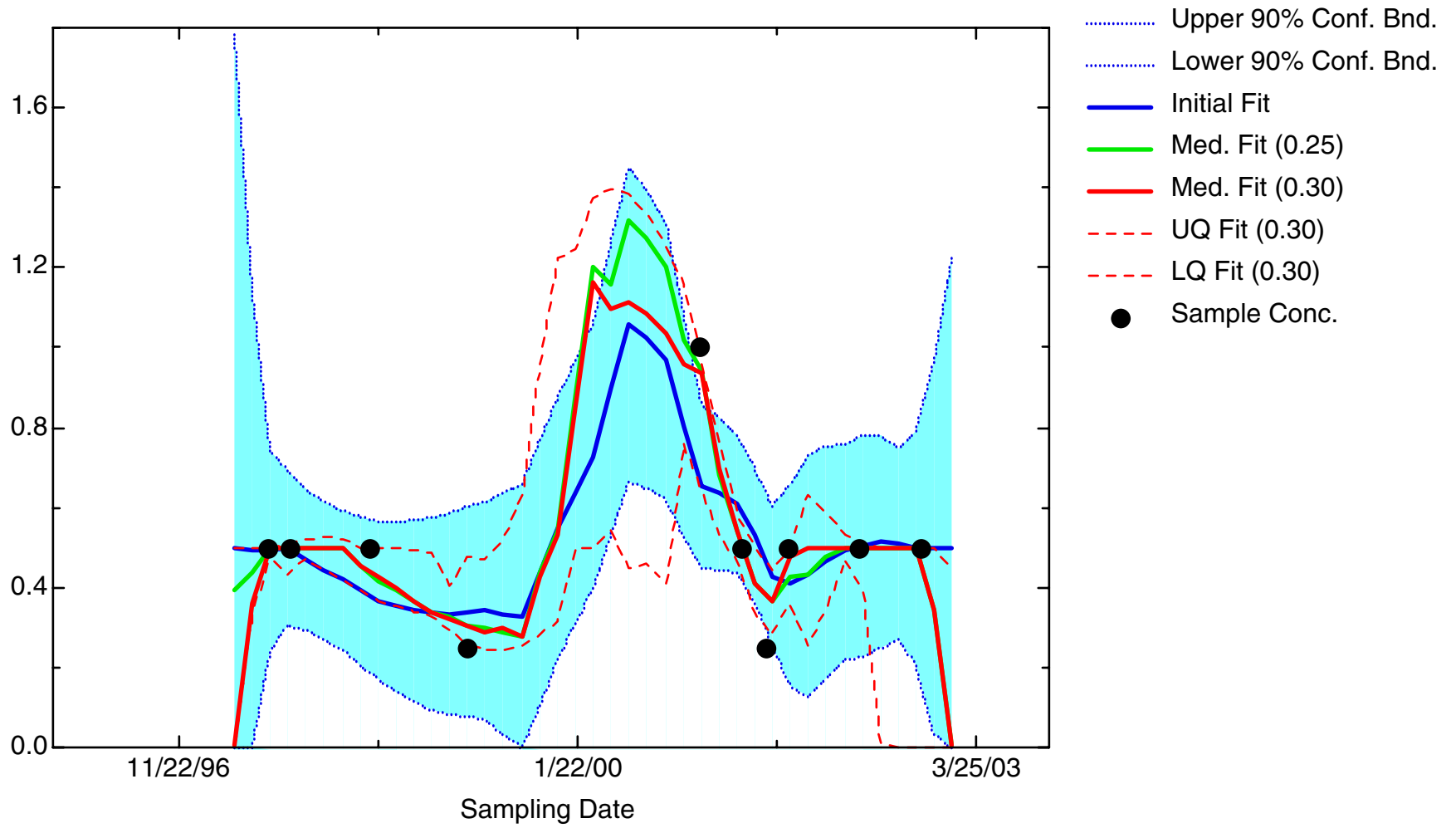
TCE: Well 49-5564(D)



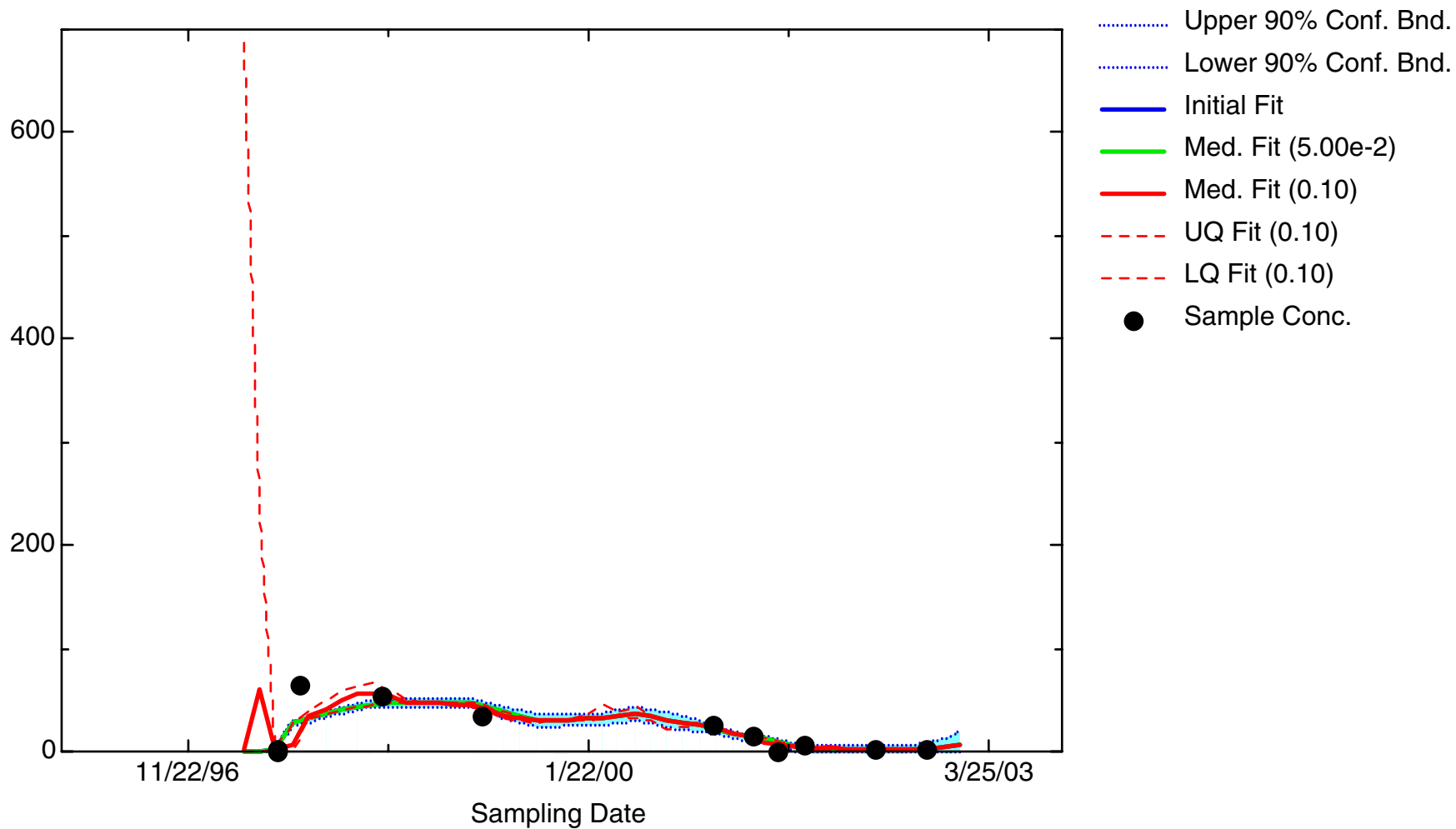
TCE: Well 49-5565(S)



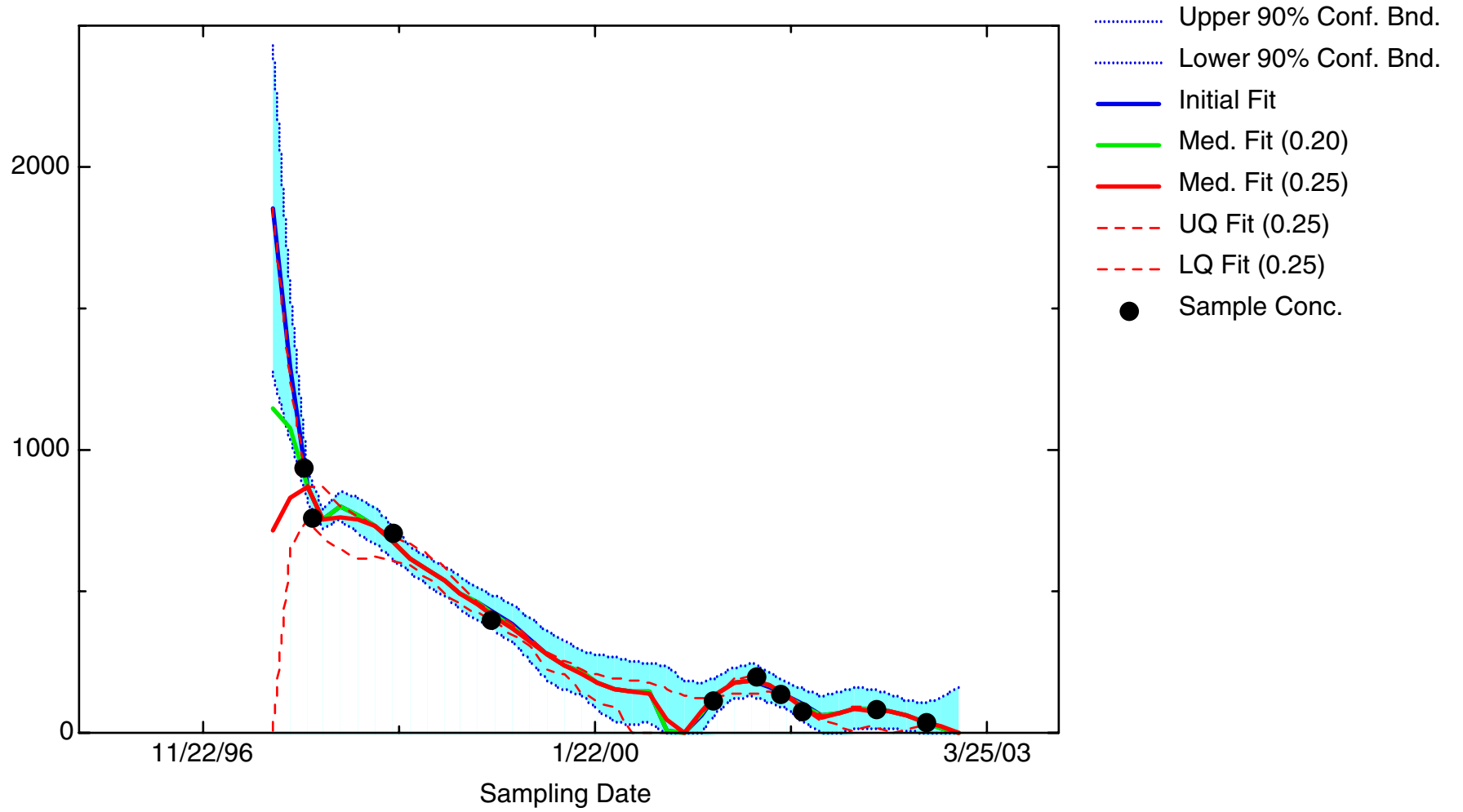
TCE: Well 49-5566(S)



TCE: Well 49-5568(D)

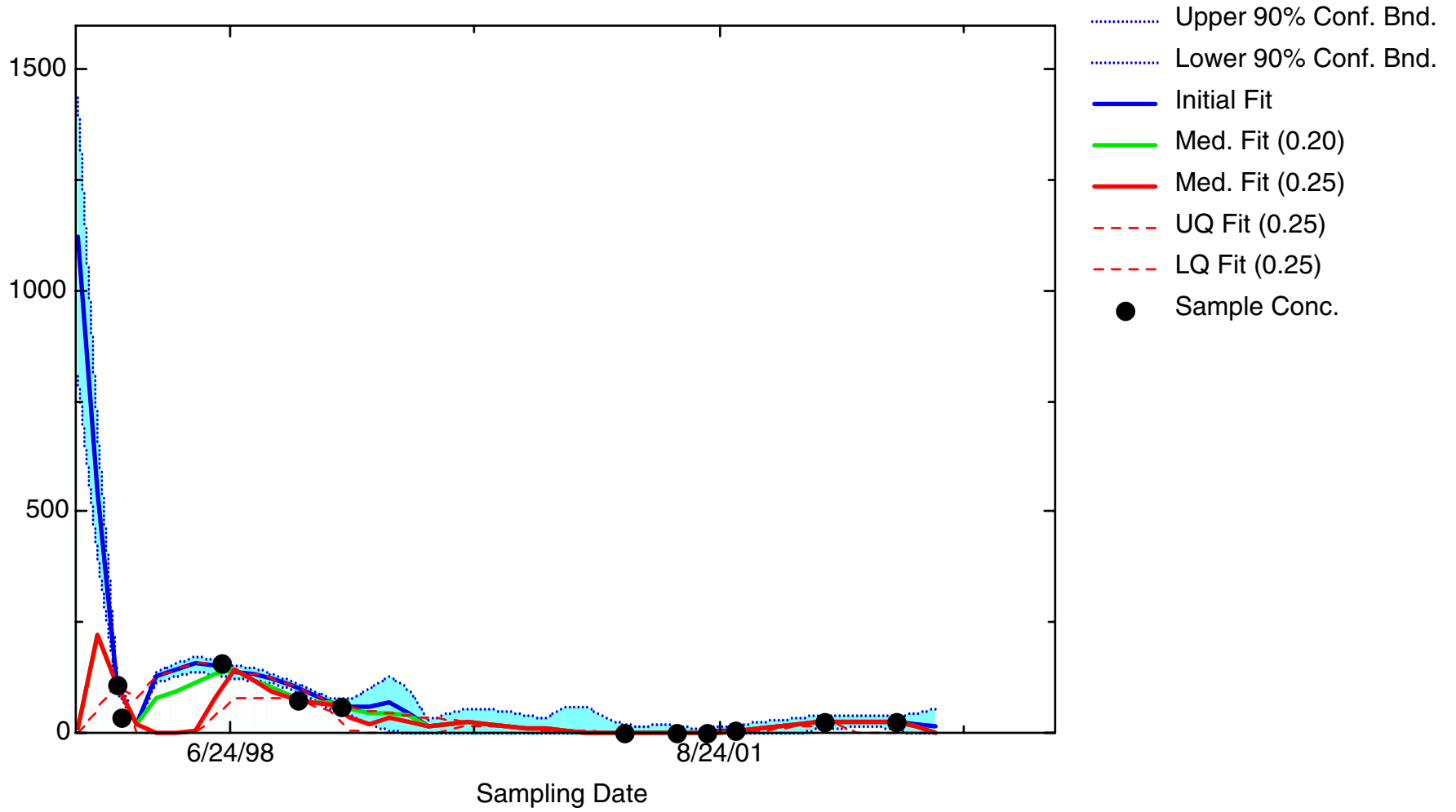


TCE: Well 49-5573(D)

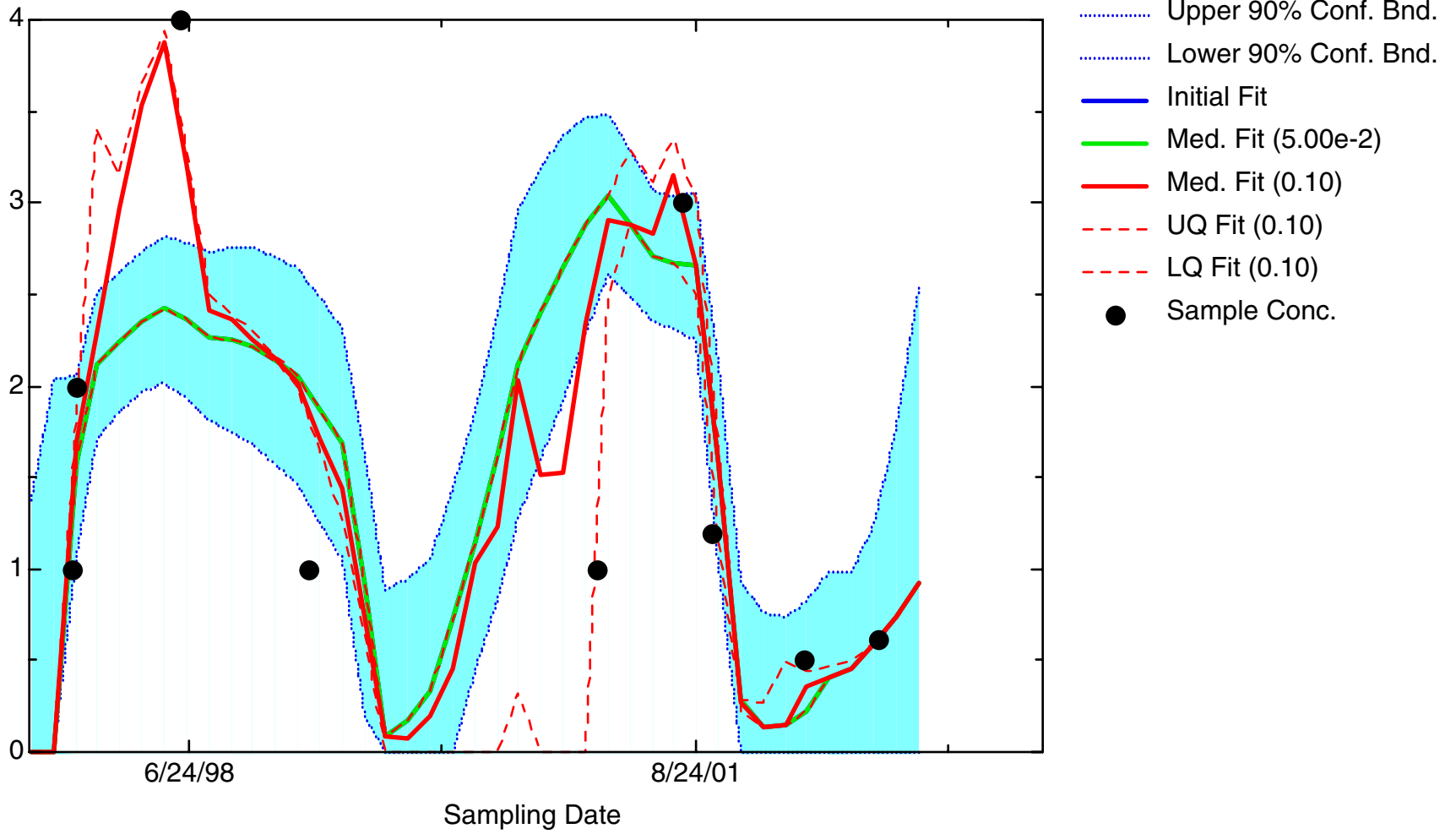




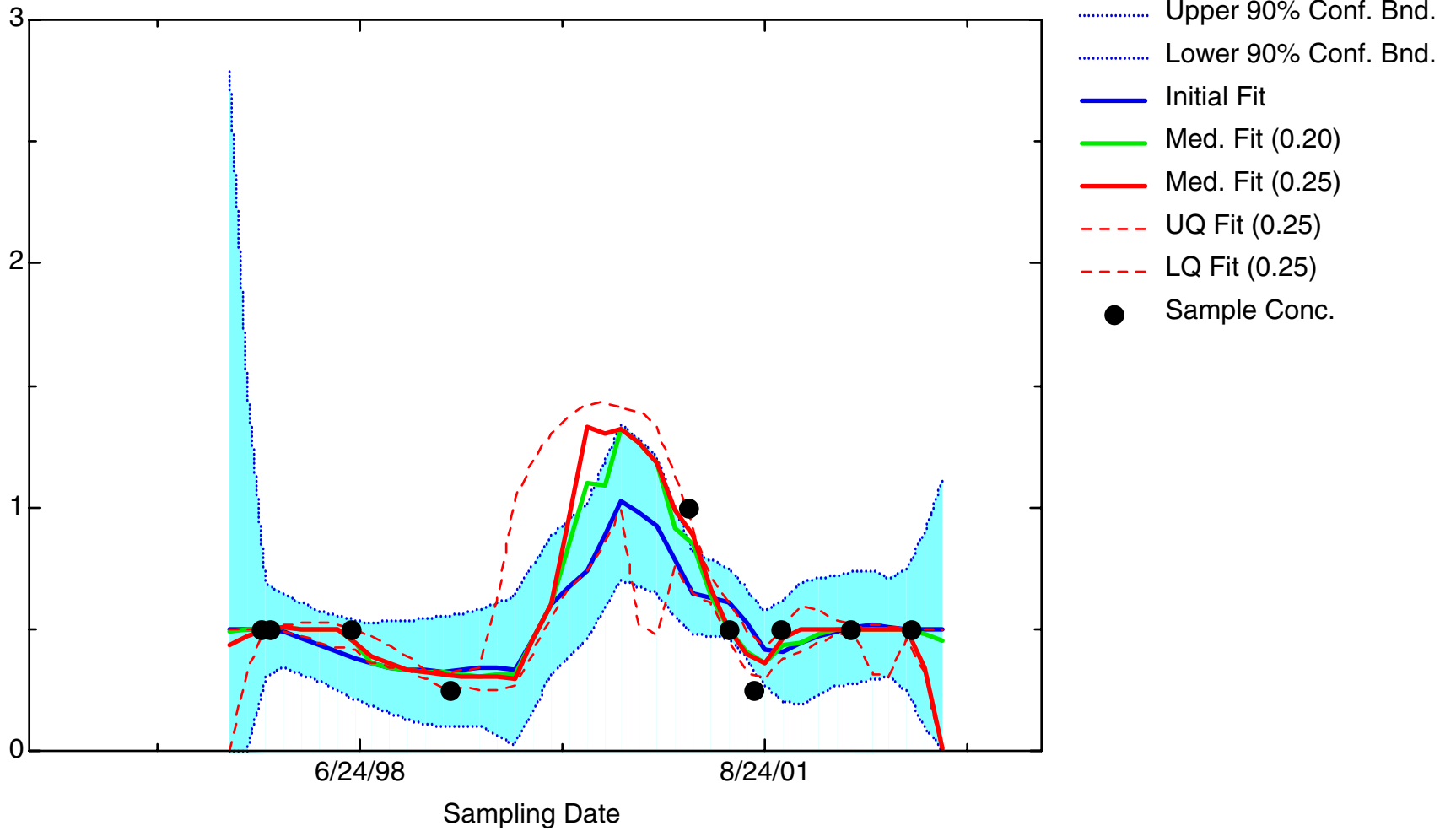
TCE: Well 49-5577(D)



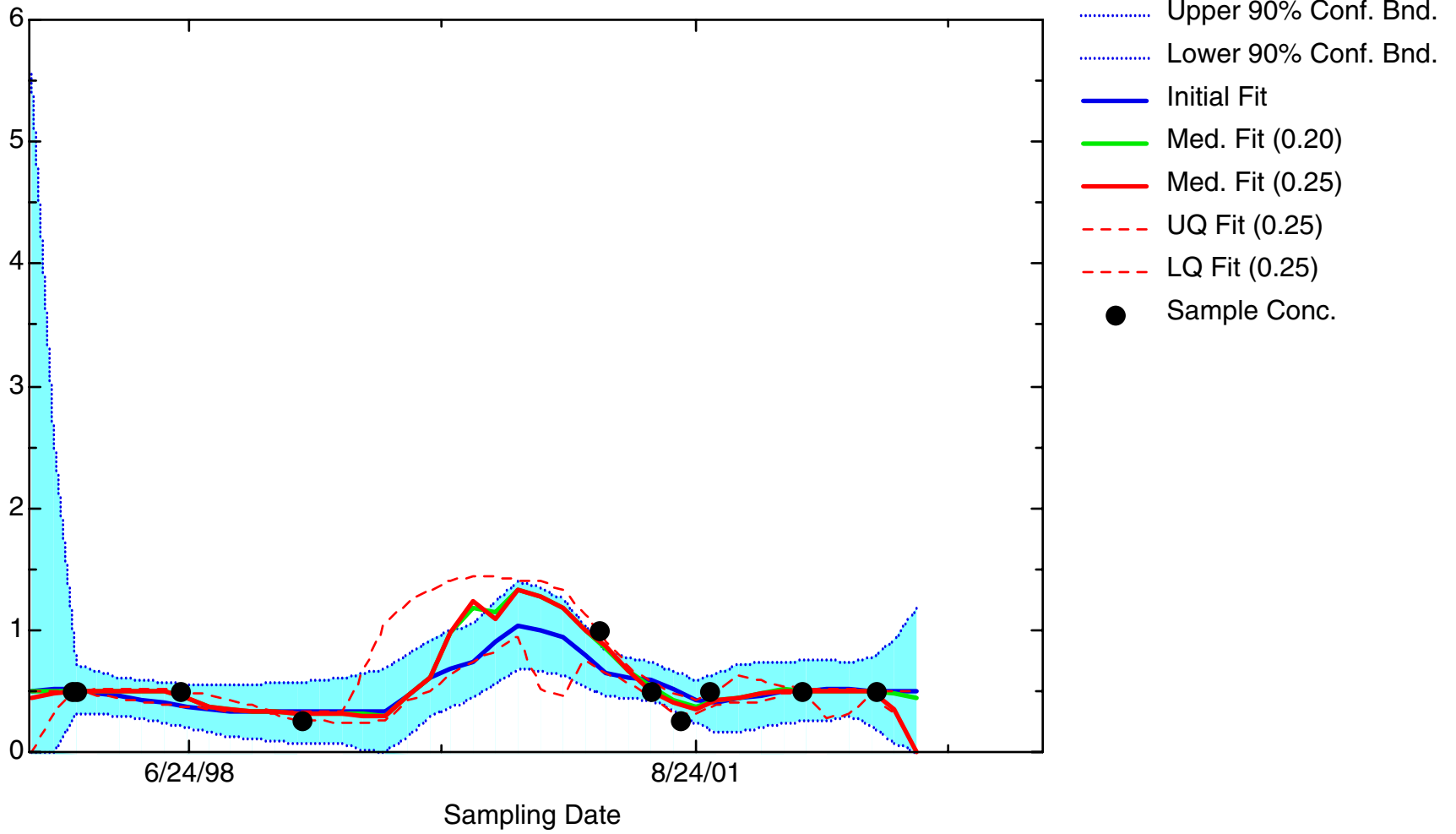
TCE: Well 49-5578(S)



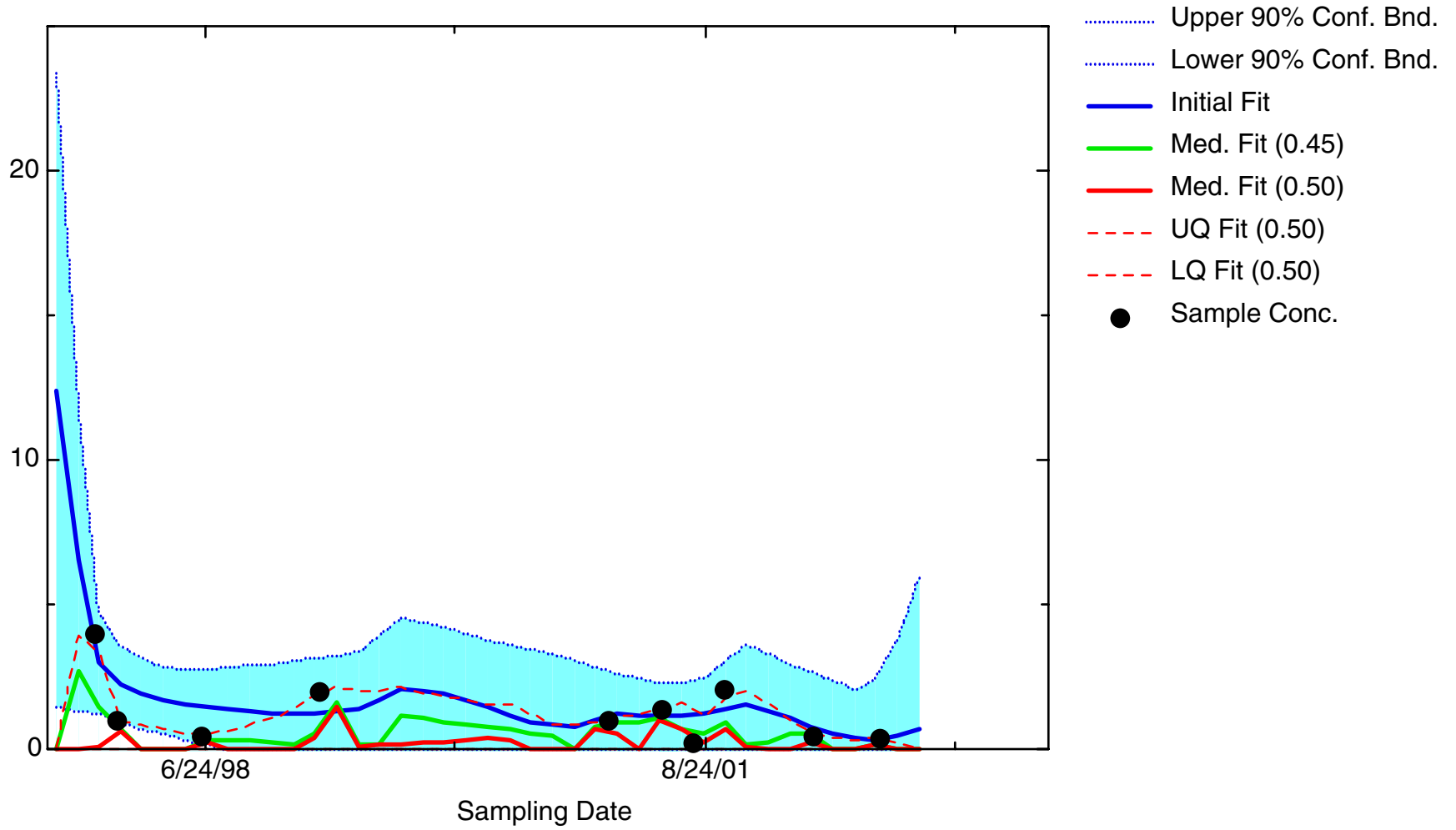
TCE: Well 49-6515(S)



TCE: Well 49-6516(S)



TCE: Well 49-MW01

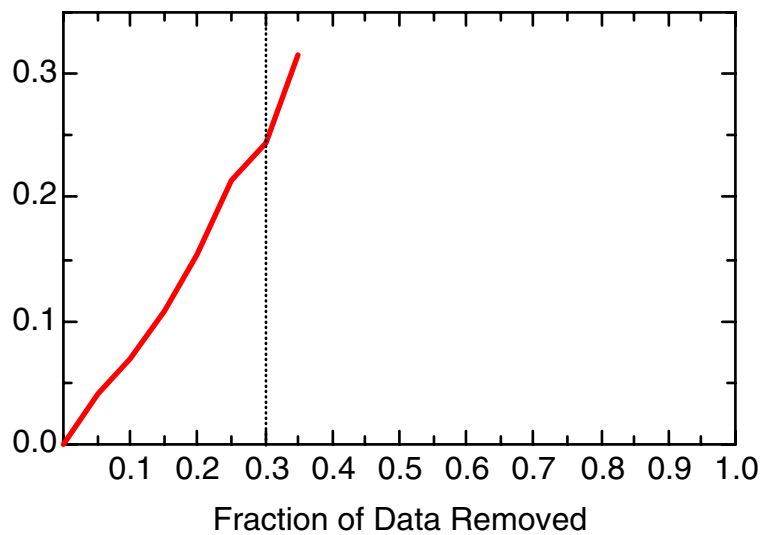


# Appendix 3.3

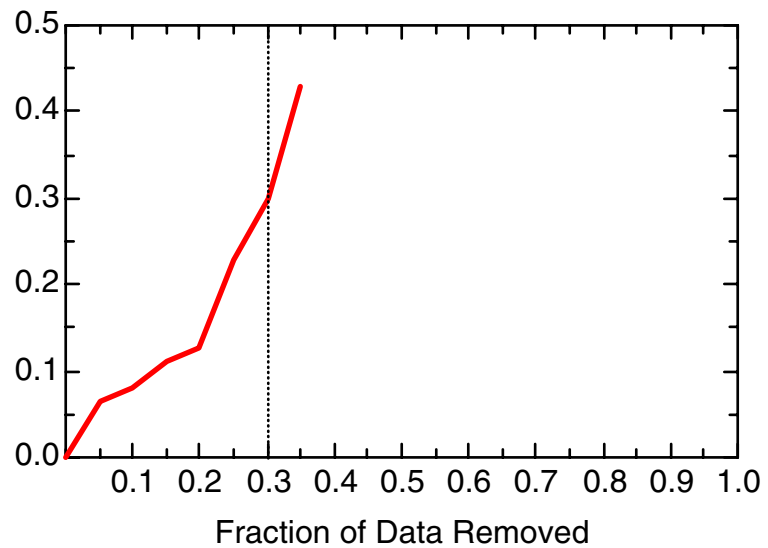
## Iterative Fitting Result Graphs

DCA11

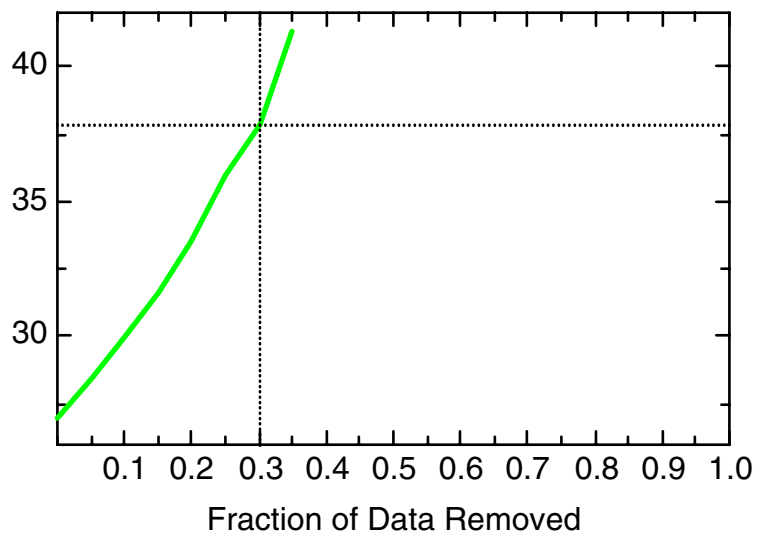
DCA11: Well 49-5562(D)



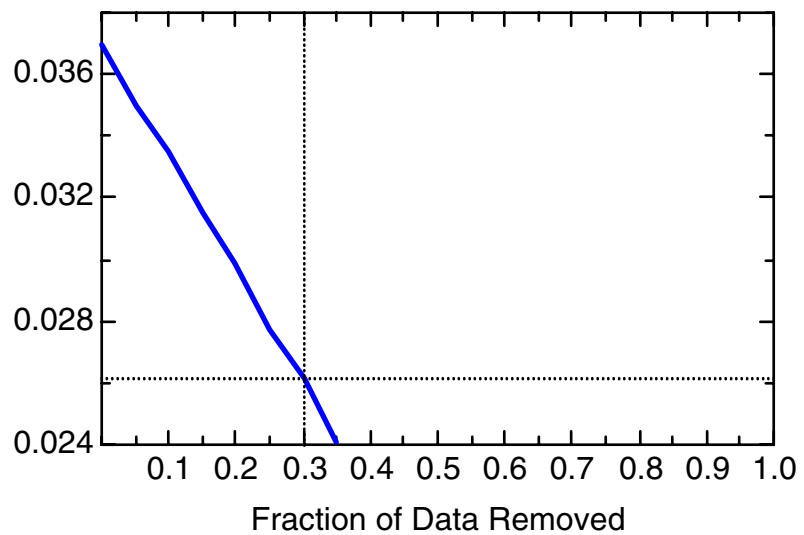
DCA11: Well 49-5562(D)



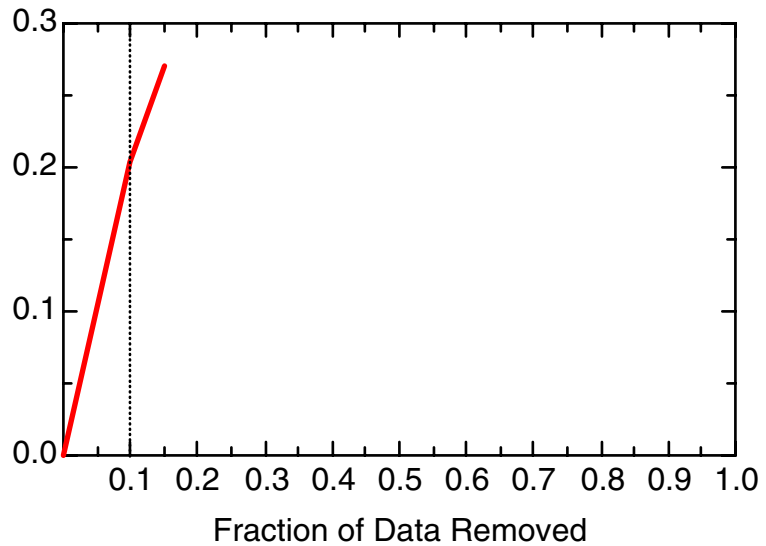
DCA11: Well 49-5562(D)



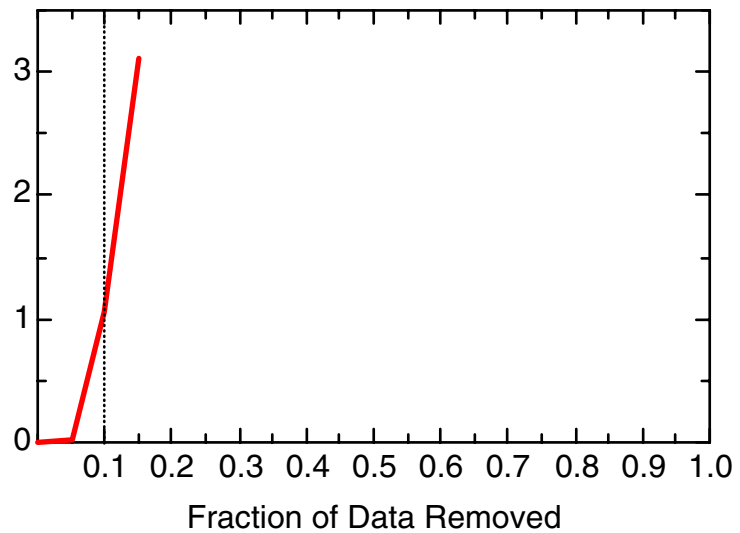
DCA11: Well 49-5562(D)



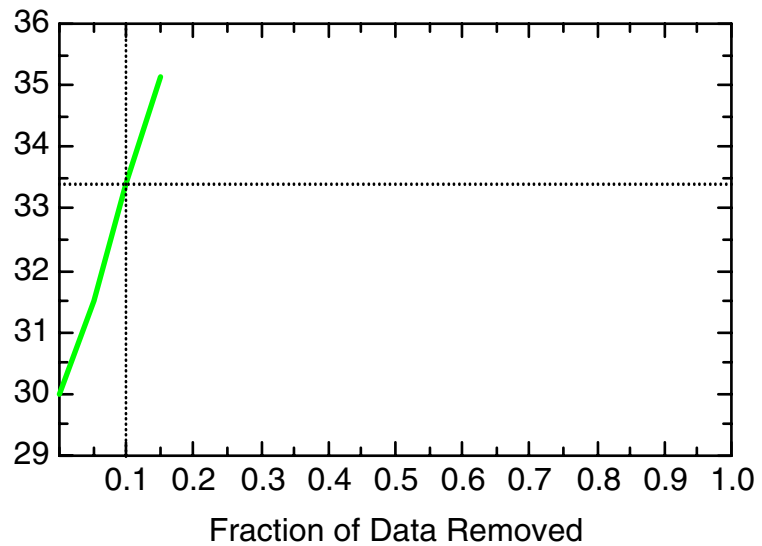
DCA11: Well 49-5563(S)



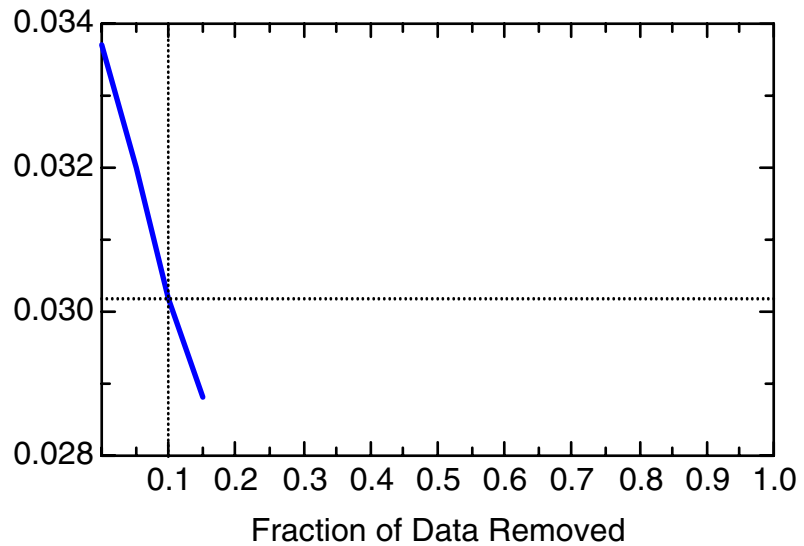
DCA11: Well 49-5563(S)



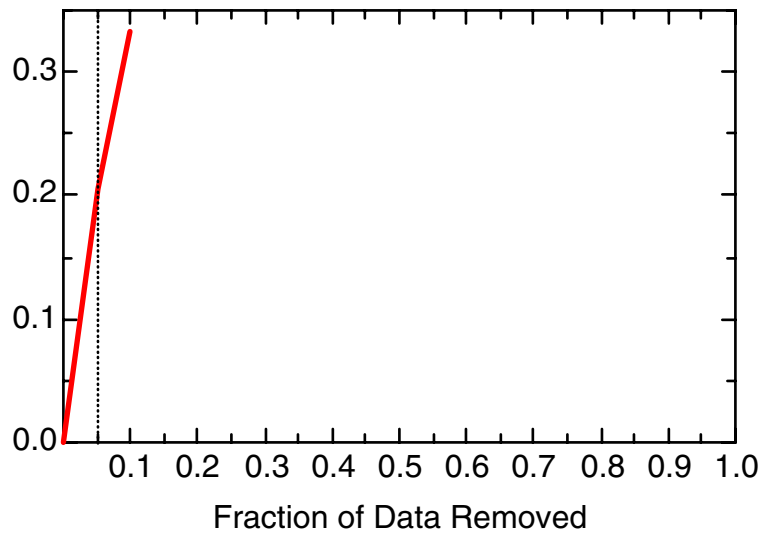
DCA11: Well 49-5563(S)



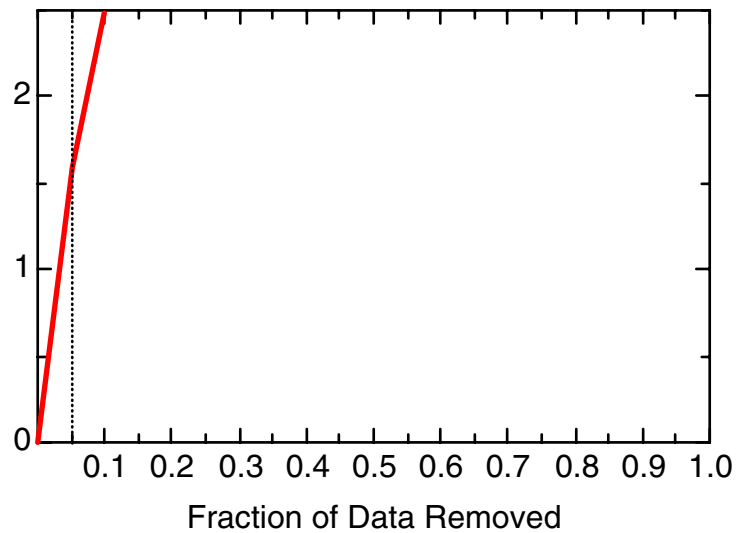
DCA11: Well 49-5563(S)



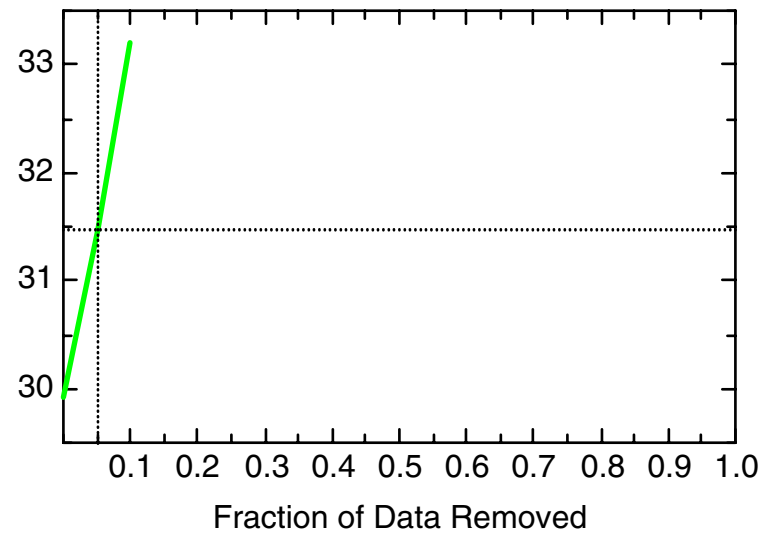
DCA11: Well 49-5564(D)



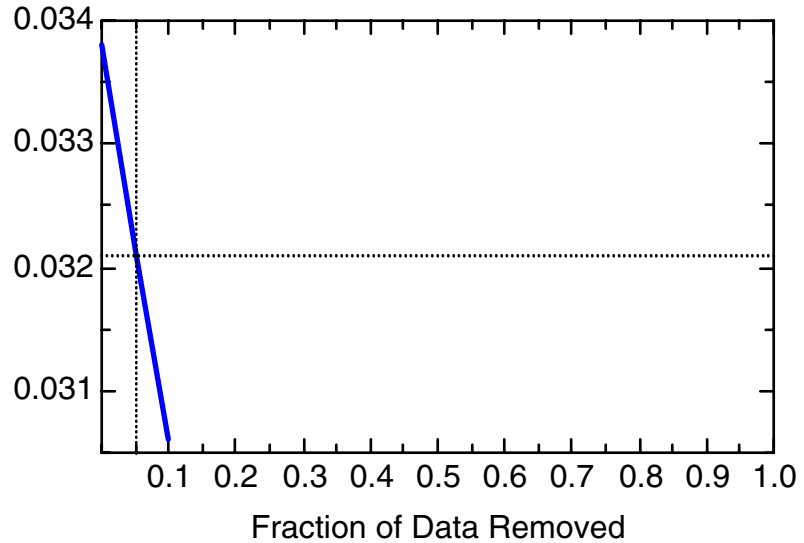
DCA11: Well 49-5564(D)



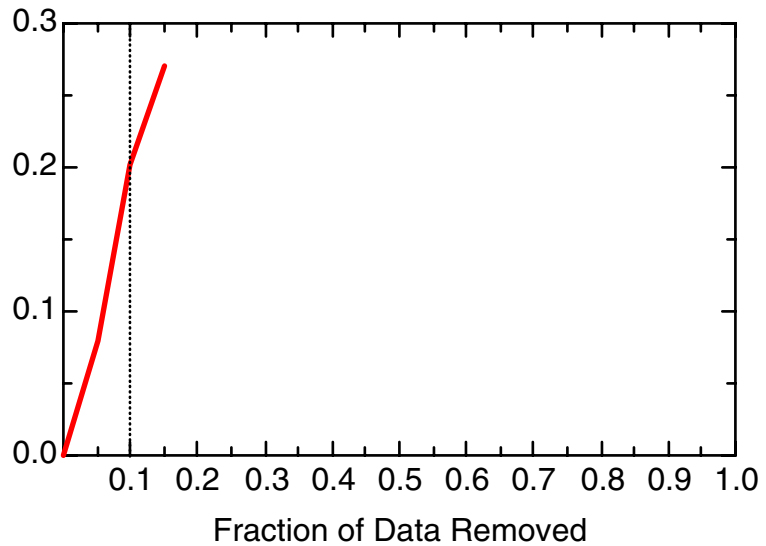
DCA11: Well 49-5564(D)



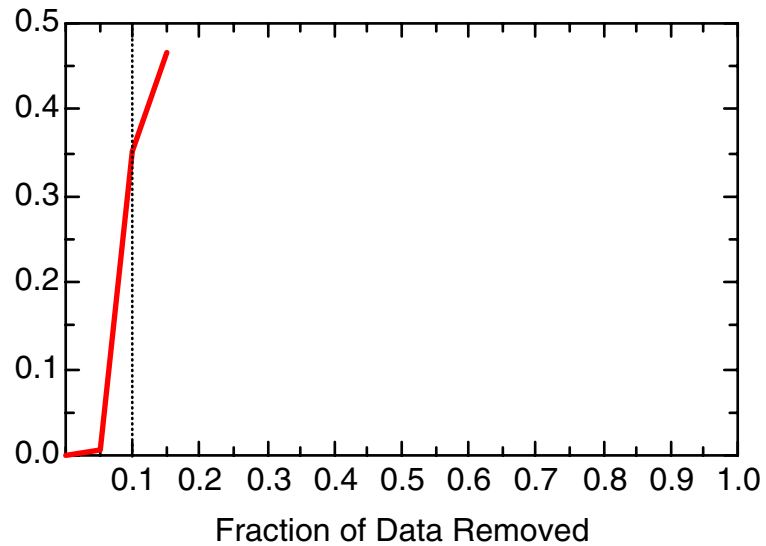
DCA11: Well 49-5564(D)



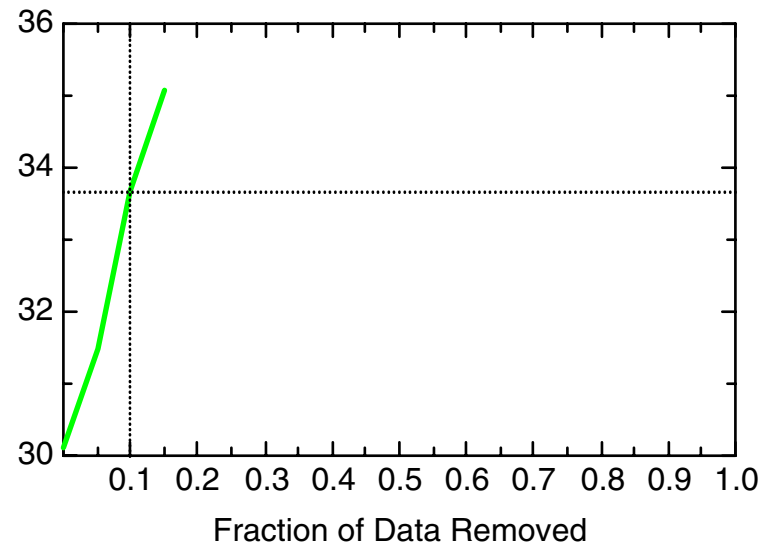
DCA11: Well 49-5565(S)



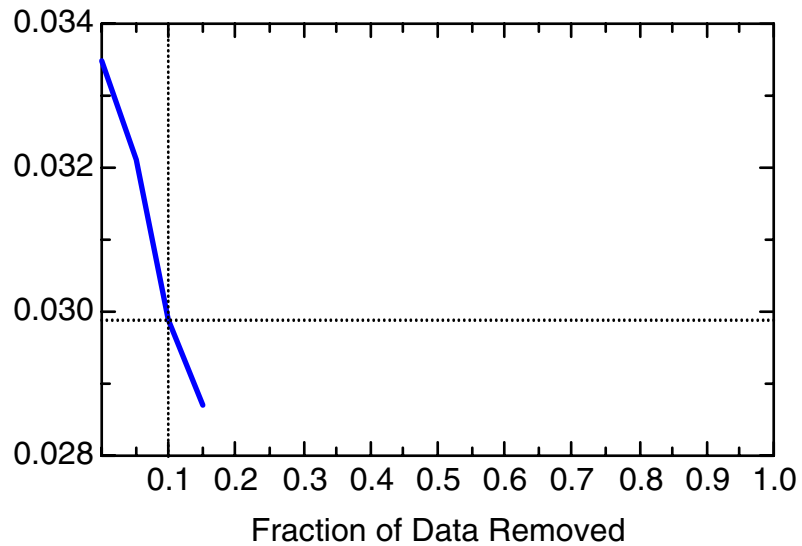
DCA11: Well 49-5565(S)



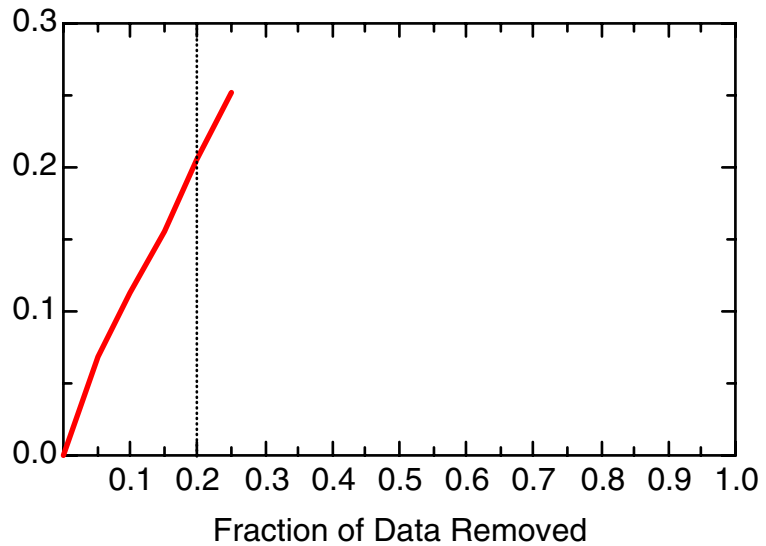
DCA11: Well 49-5565(S)



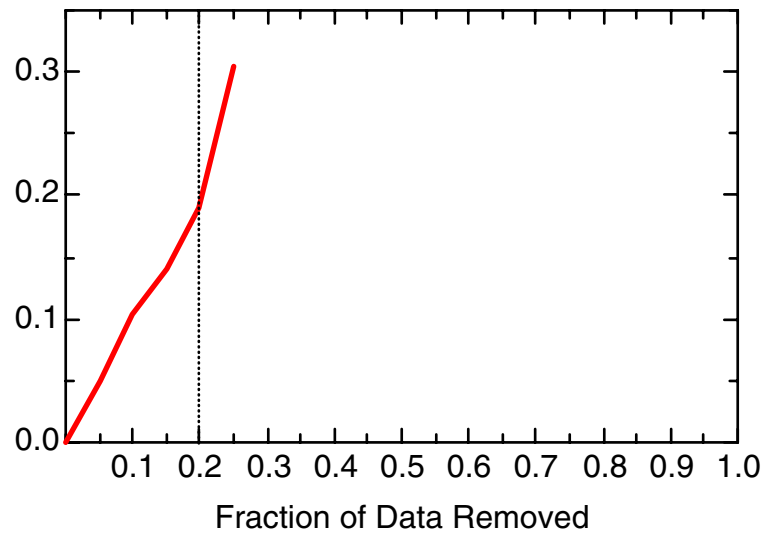
DCA11: Well 49-5565(S)



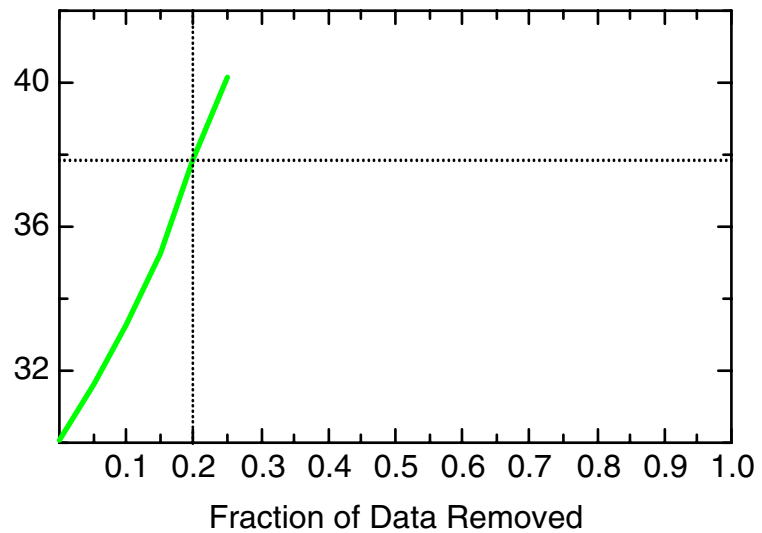
DCA11: Well 49-5566(S)



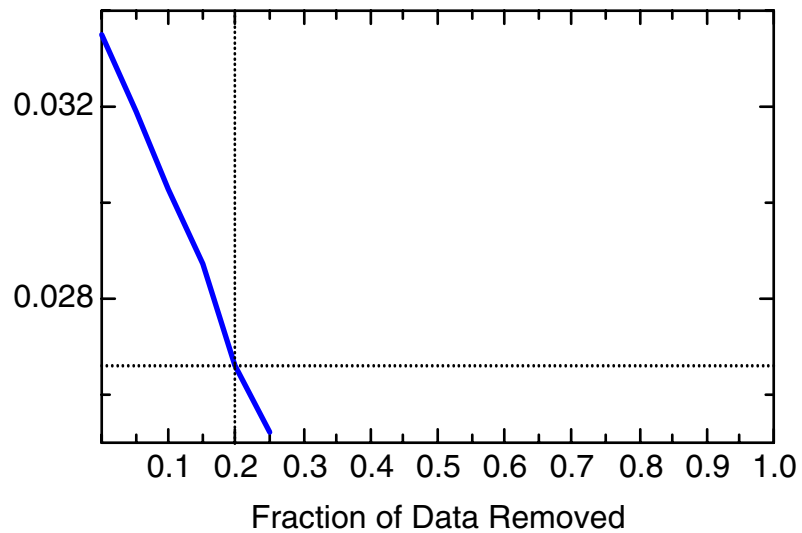
DCA11: Well 49-5566(S)



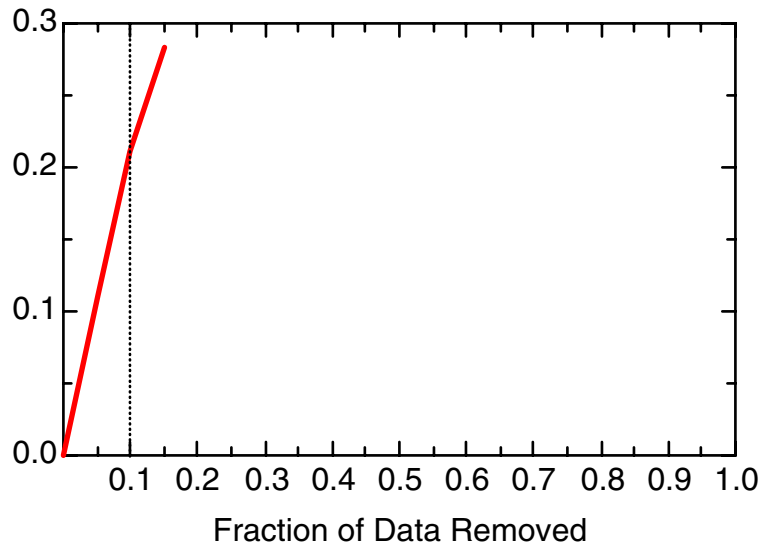
DCA11: Well 49-5566(S)



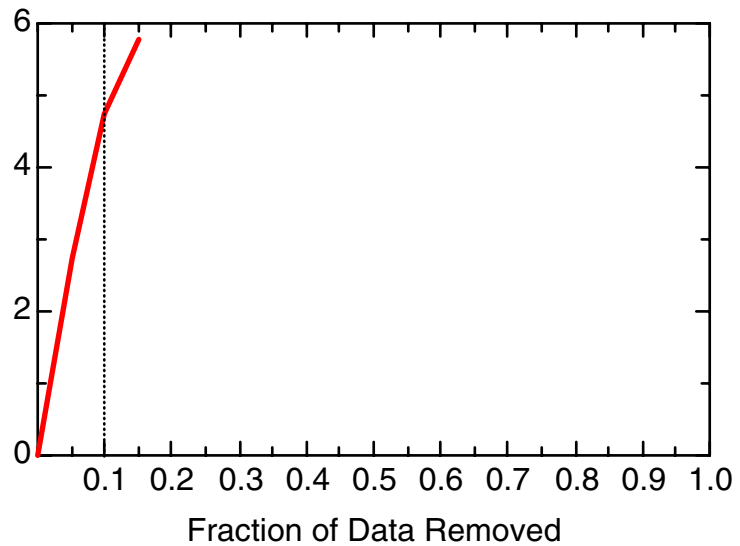
DCA11: Well 49-5566(S)



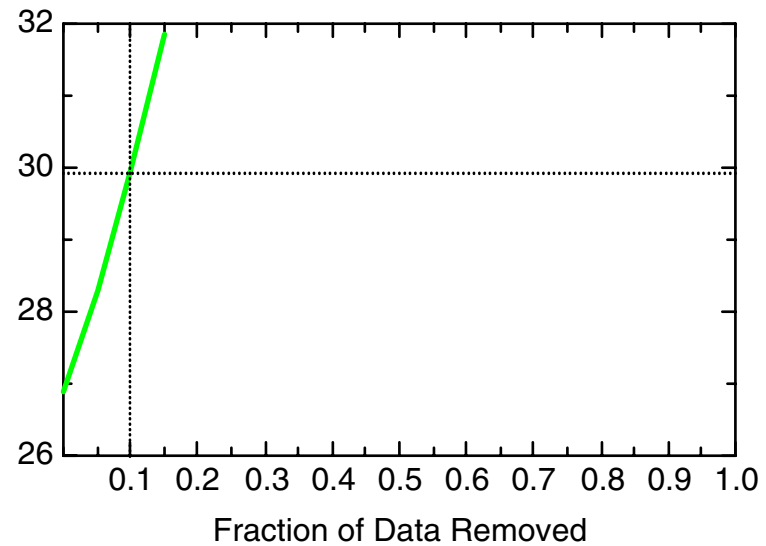
DCA11: Well 49-5568(D)



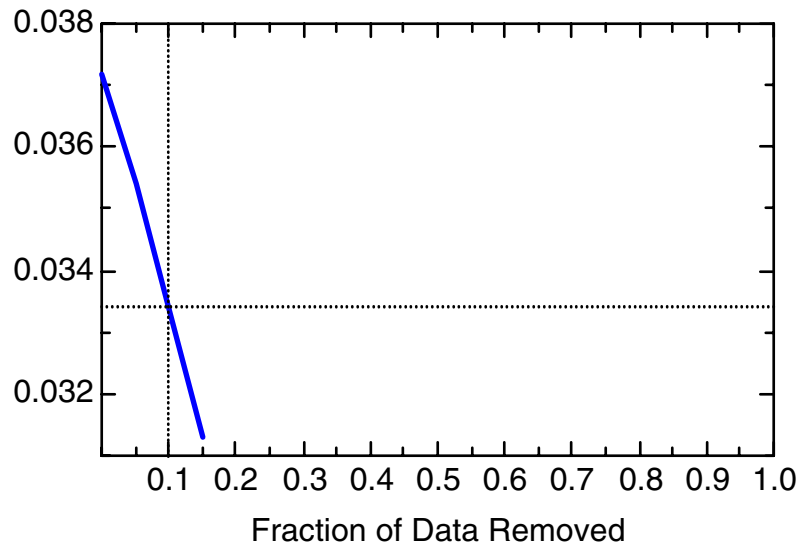
DCA11: Well 49-5568(D)



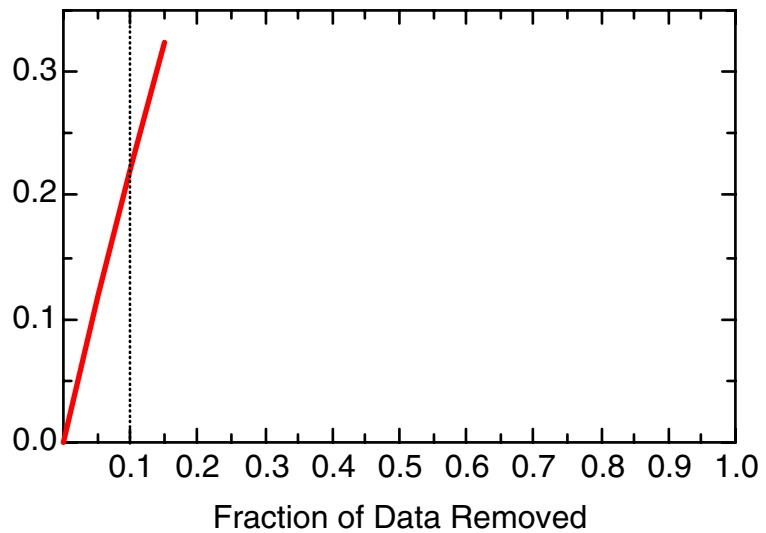
DCA11: Well 49-5568(D)



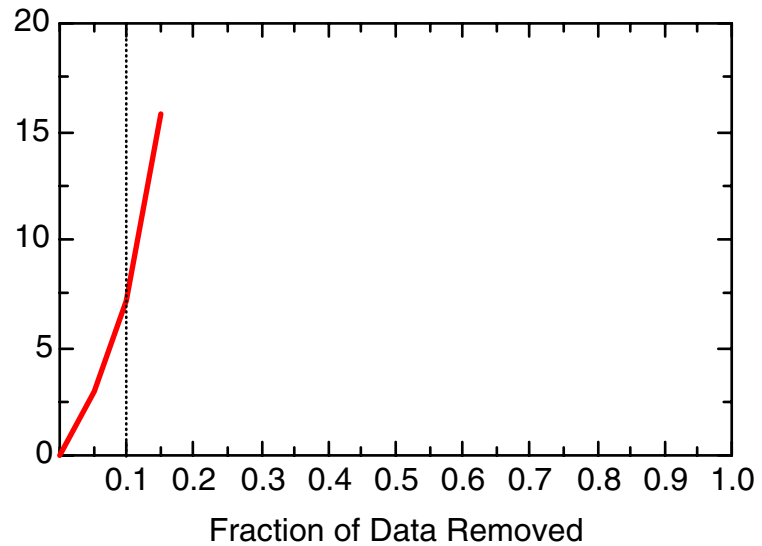
DCA11: Well 49-5568(D)



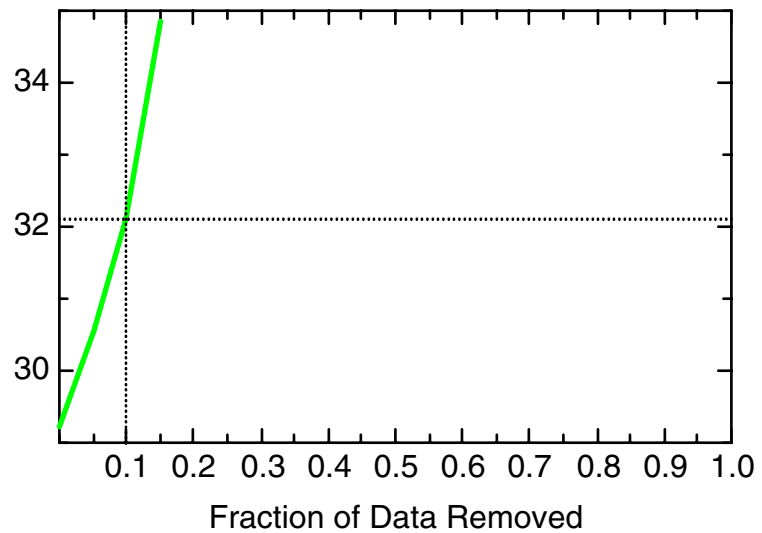
DCA11: Well 49-5573(D)



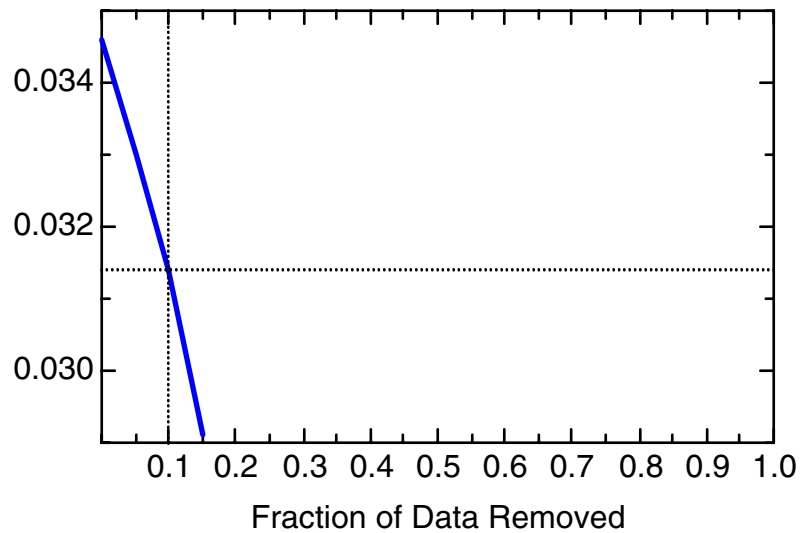
DCA11: Well 49-5573(D)



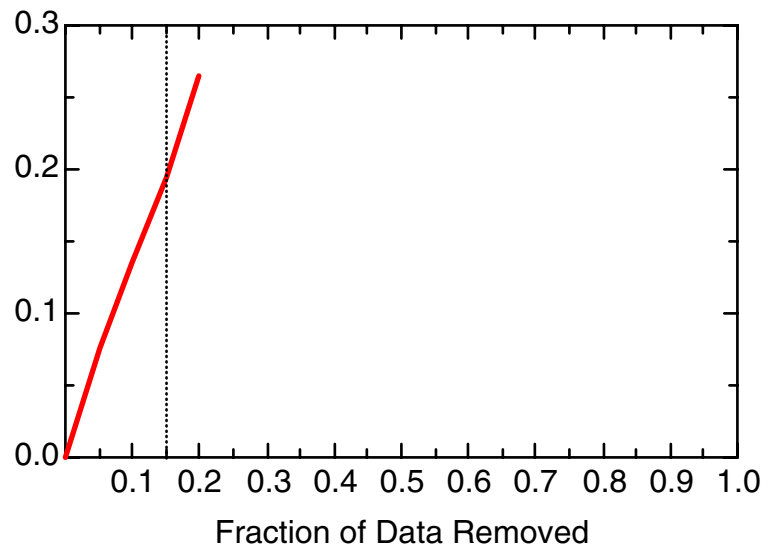
DCA11: Well 49-5573(D)



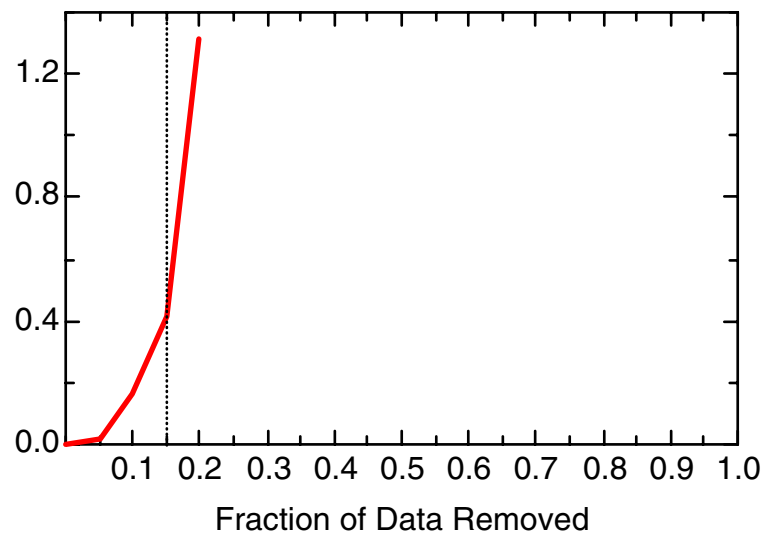
DCA11: Well 49-5573(D)



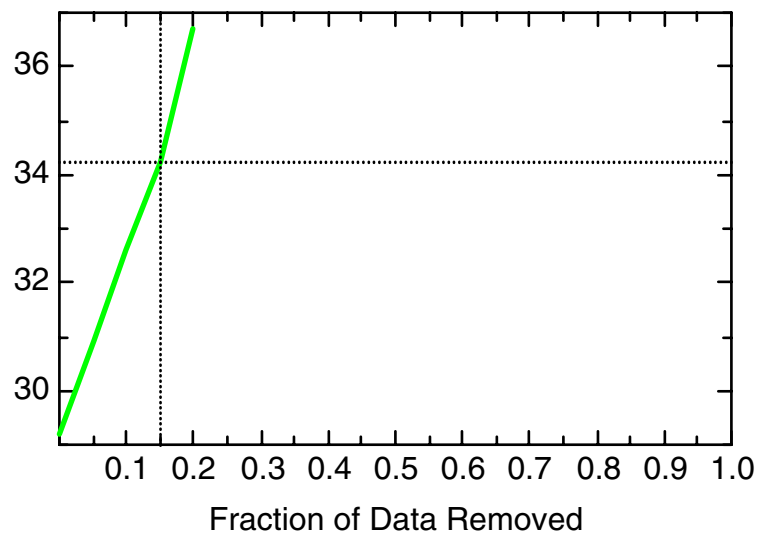
DCA11: Well 49-5574(S)



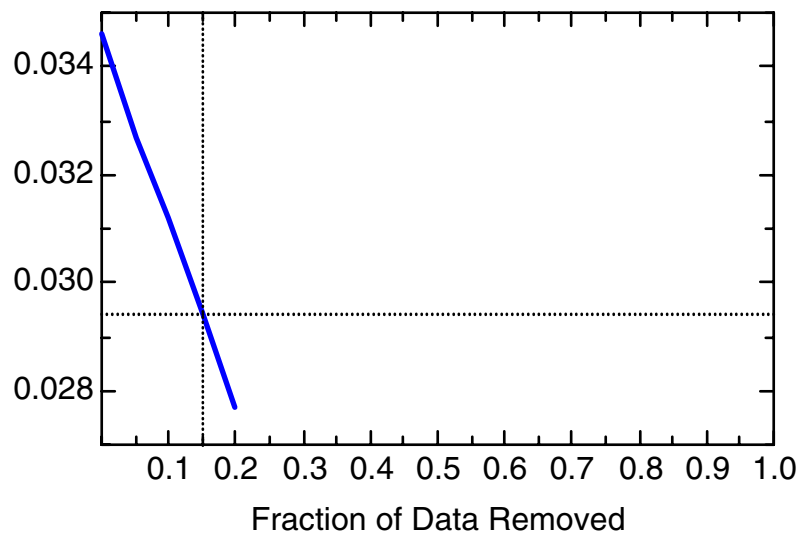
DCA11: Well 49-5574(S)



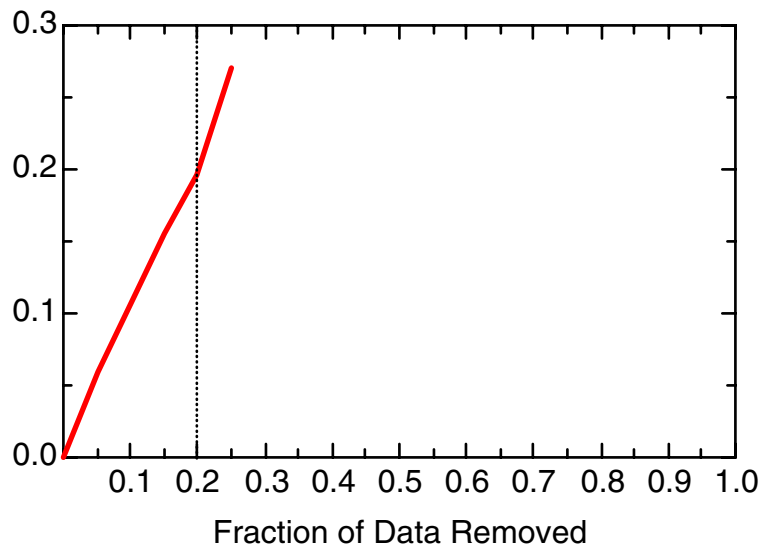
DCA11: Well 49-5574(S)



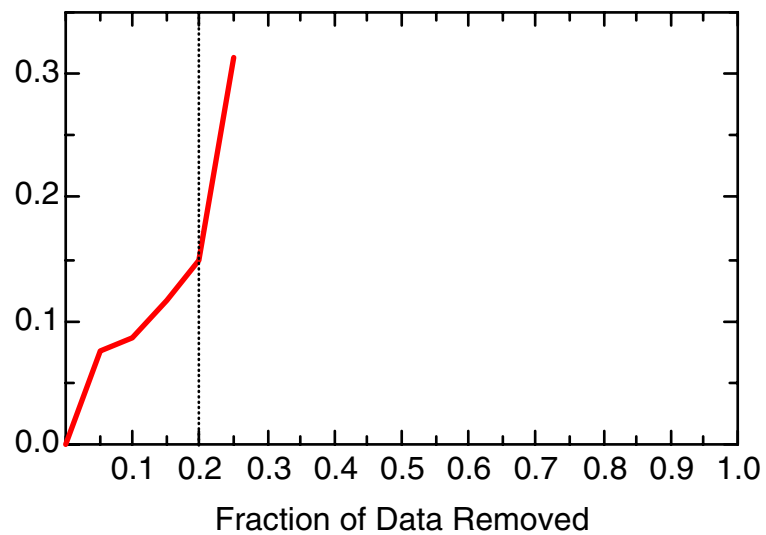
DCA11: Well 49-5574(S)



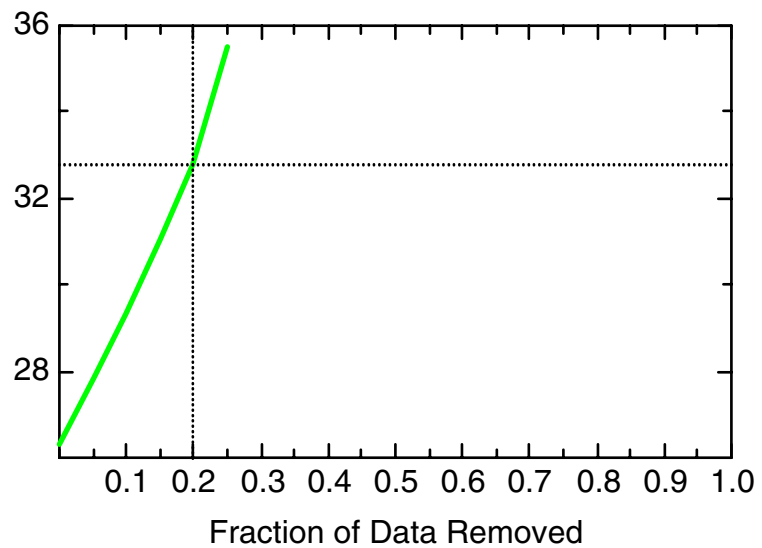
DCA11: Well 49-5577(D)



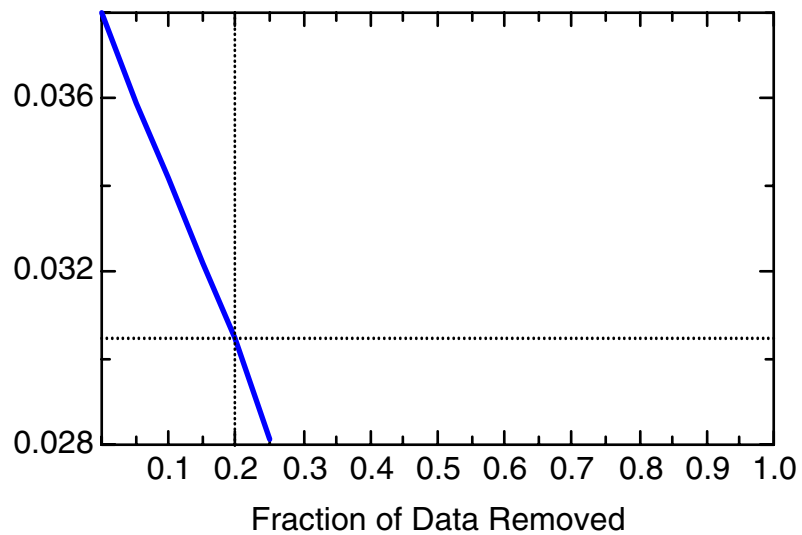
DCA11: Well 49-5577(D)



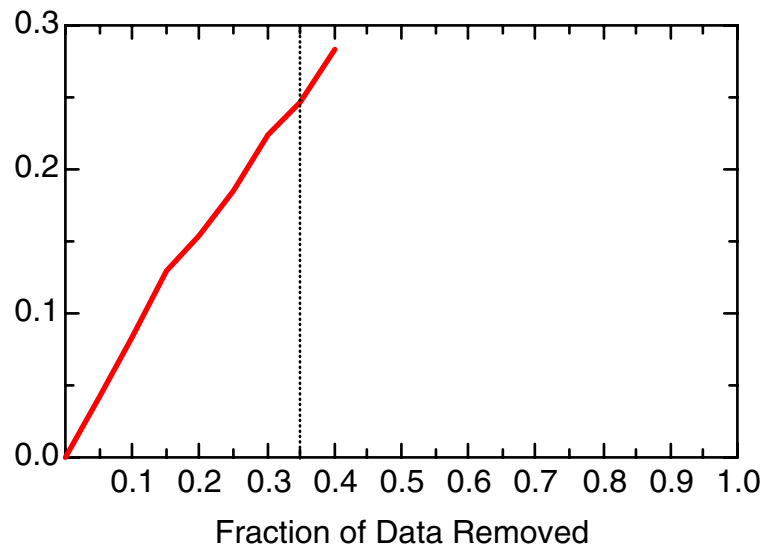
DCA11: Well 49-5577(D)



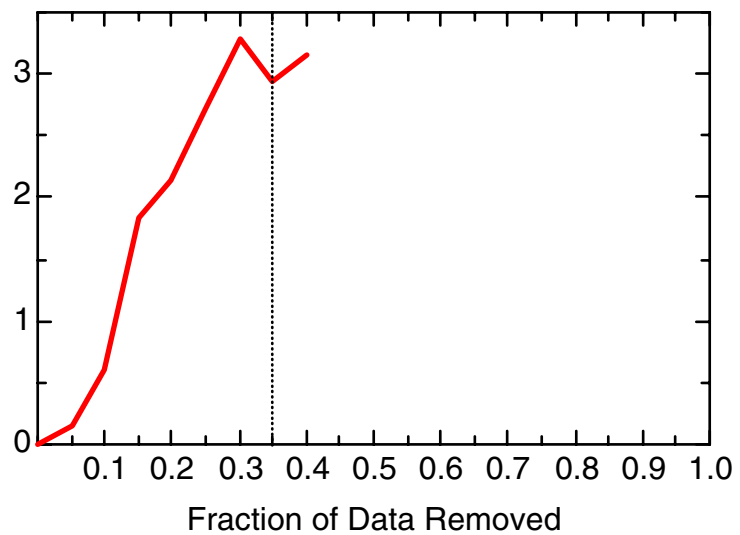
DCA11: Well 49-5577(D)



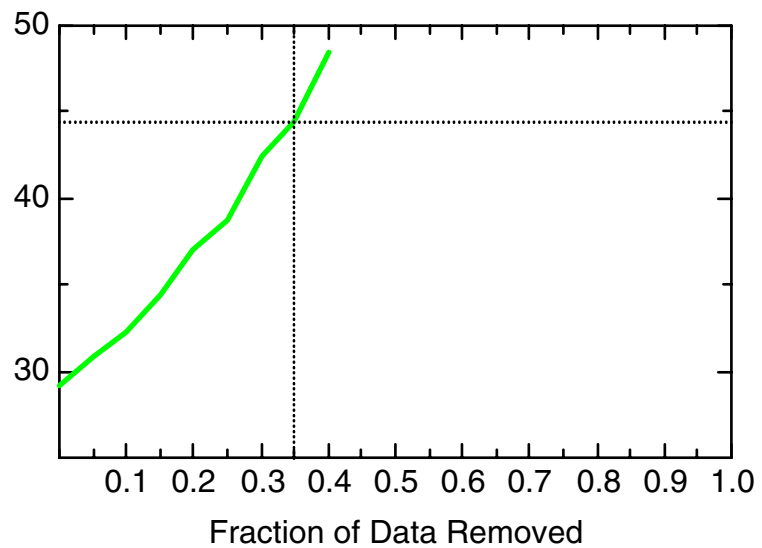
DCA11: Well 49-5578(S)



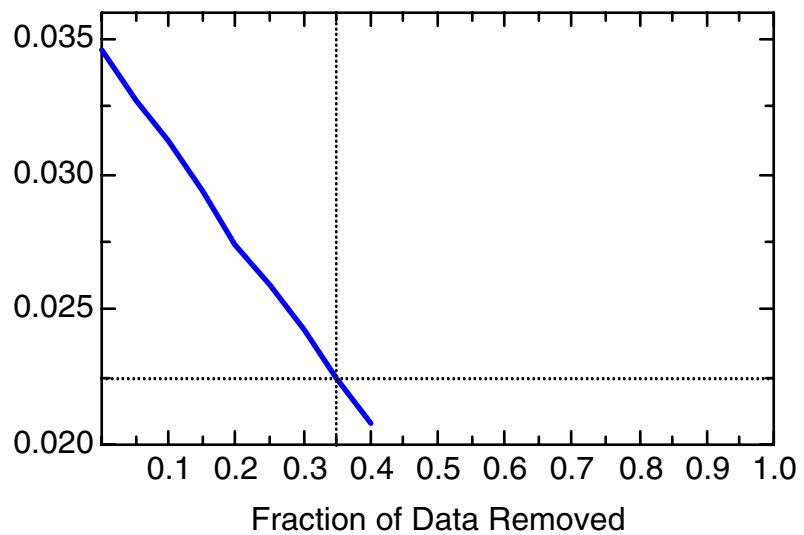
DCA11: Well 49-5578(S)



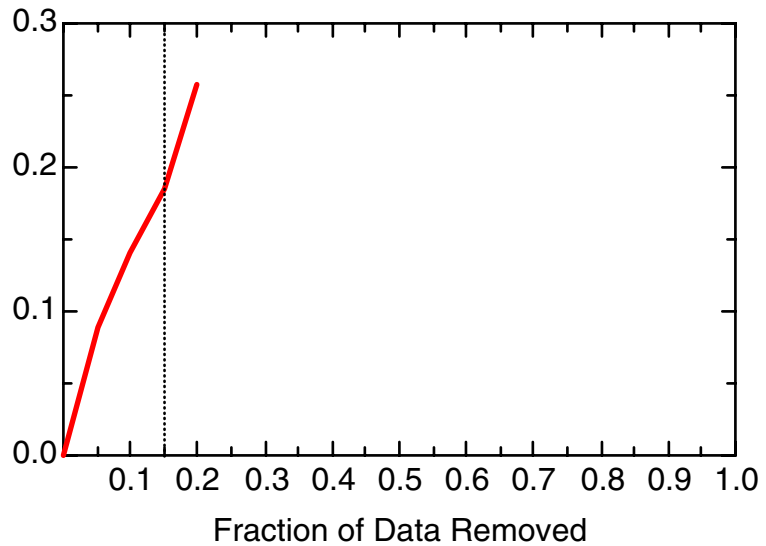
DCA11: Well 49-5578(S)



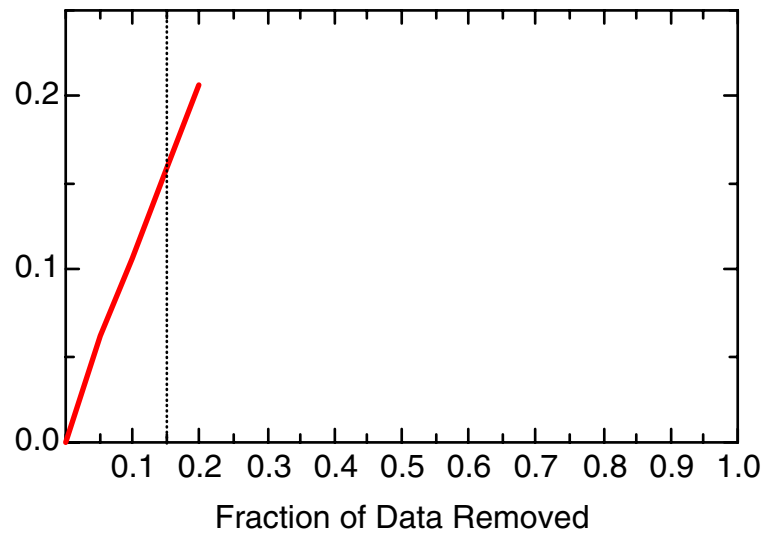
DCA11: Well 49-5578(S)



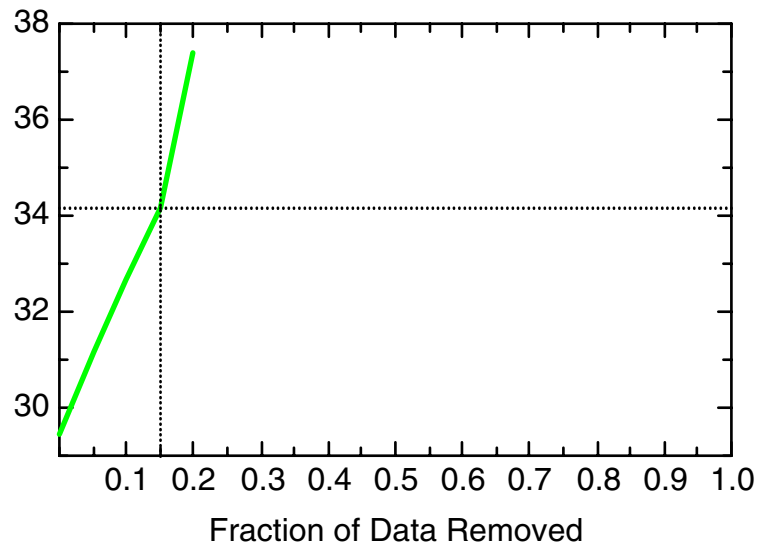
DCA11: Well 49-6515(S)



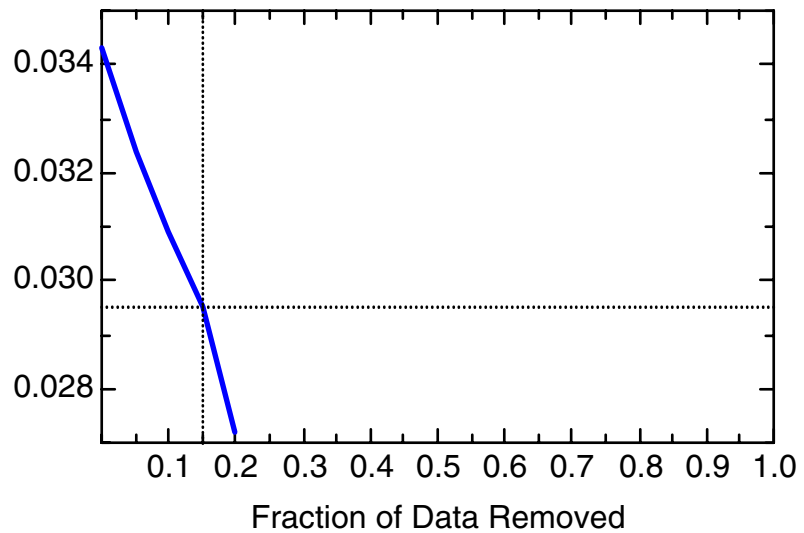
DCA11: Well 49-6515(S)



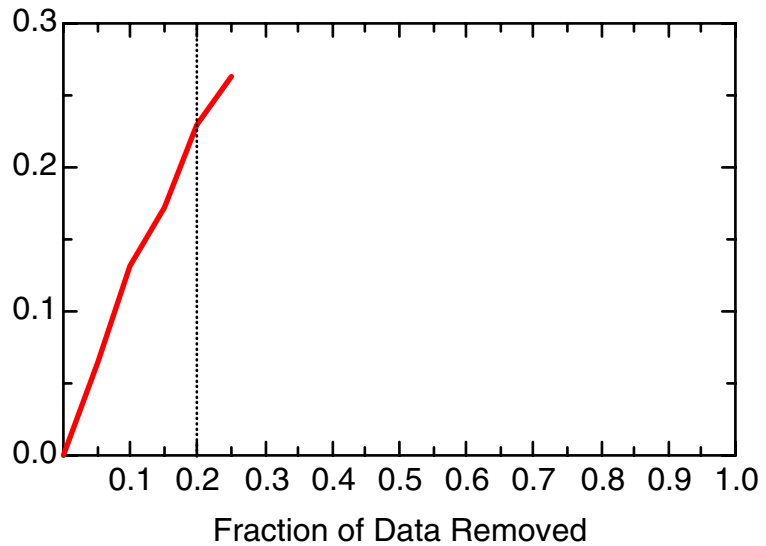
DCA11: Well 49-6515(S)



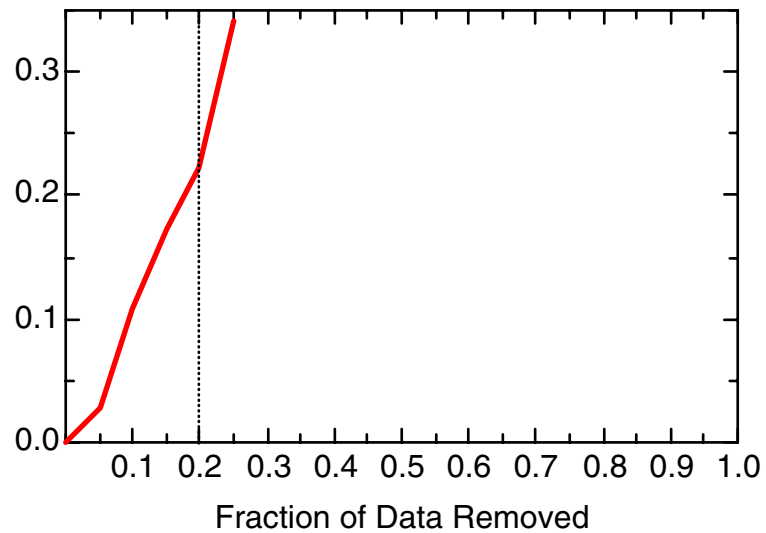
DCA11: Well 49-6515(S)



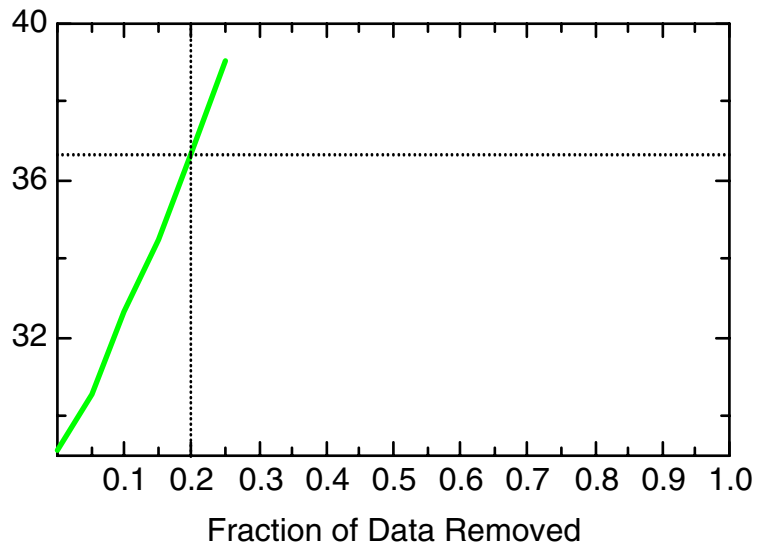
DCA11: Well 49-6516(S)



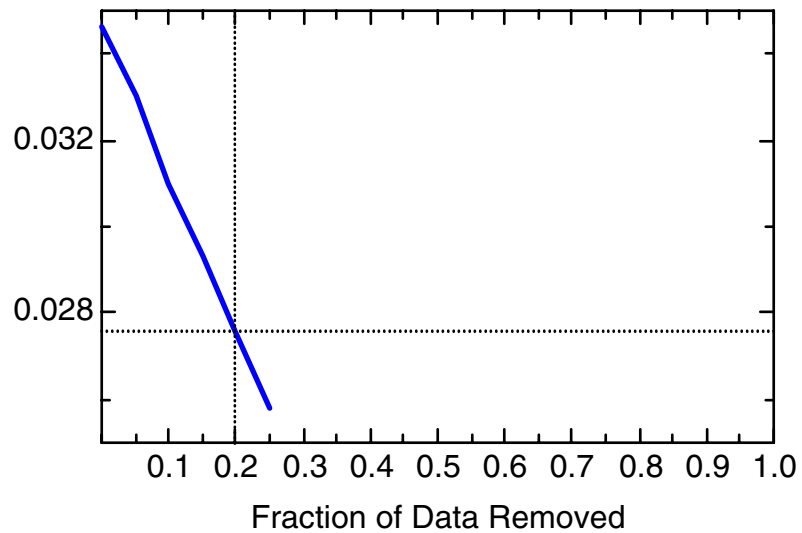
DCA11: Well 49-6516(S)



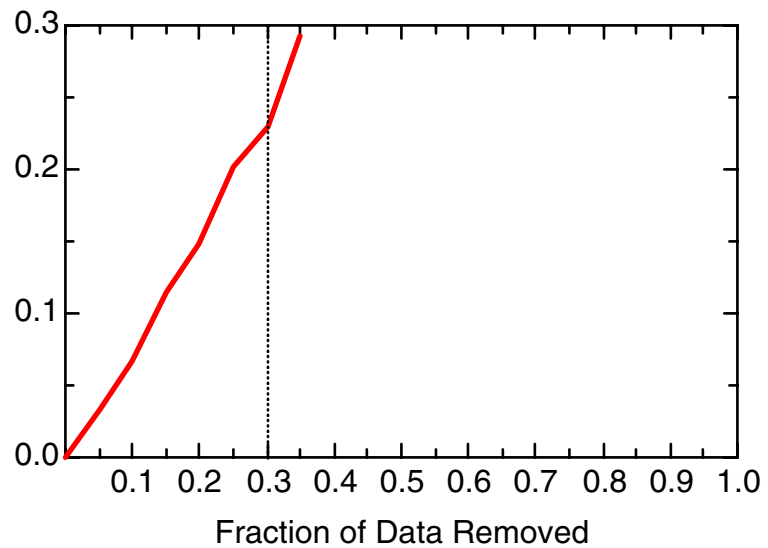
DCA11: Well 49-6516(S)



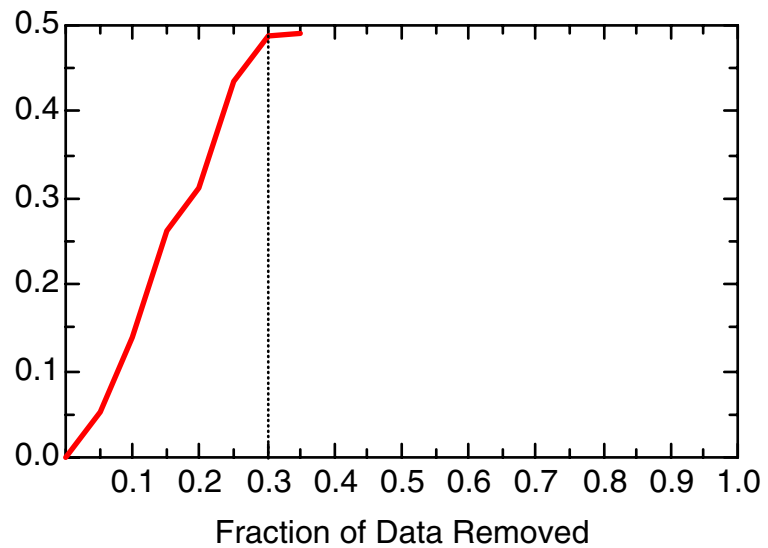
DCA11: Well 49-6516(S)



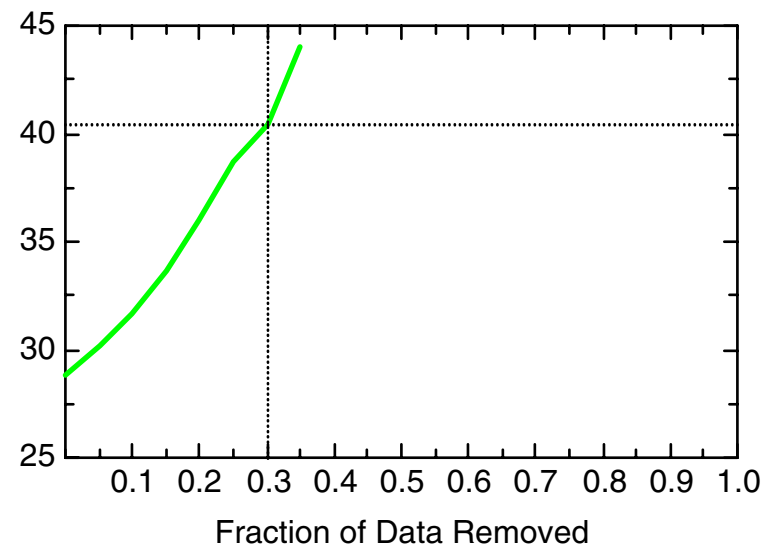
DCA11: Well 49-MW01



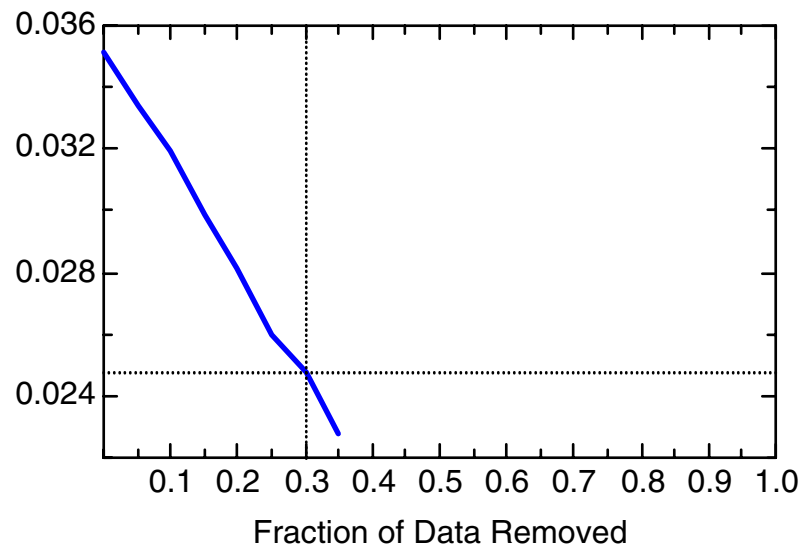
DCA11: Well 49-MW01



DCA11: Well 49-MW01

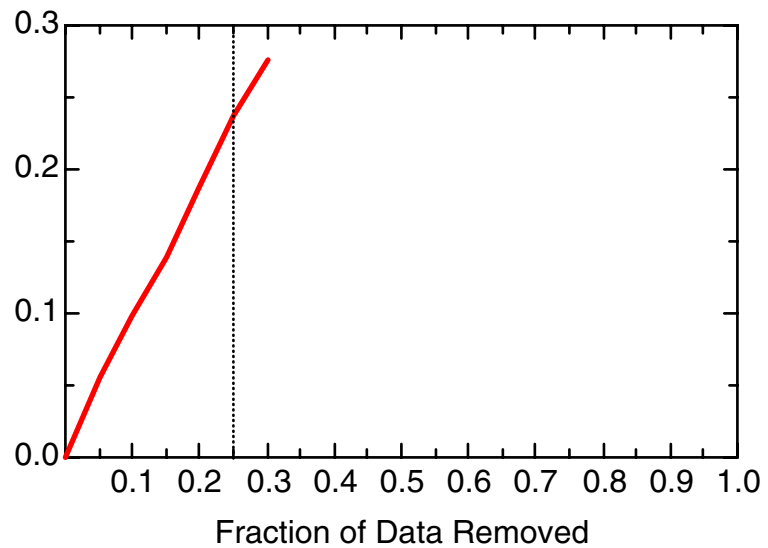


DCA11: Well 49-MW01

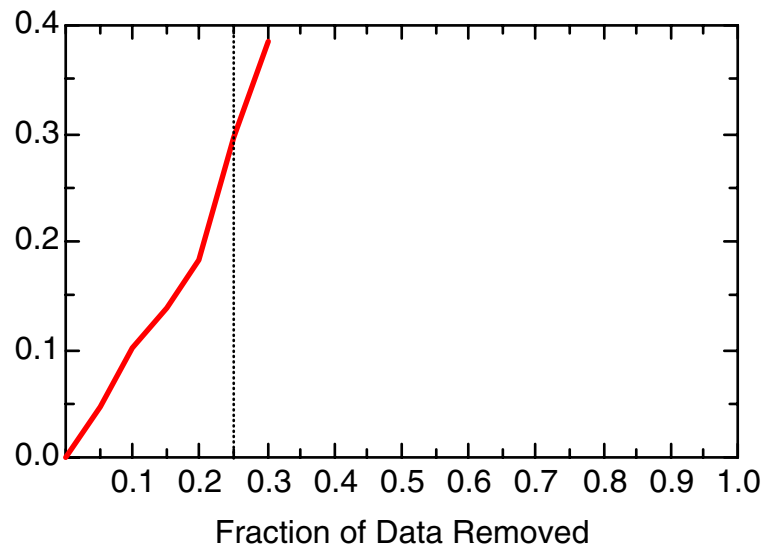


DCE12C

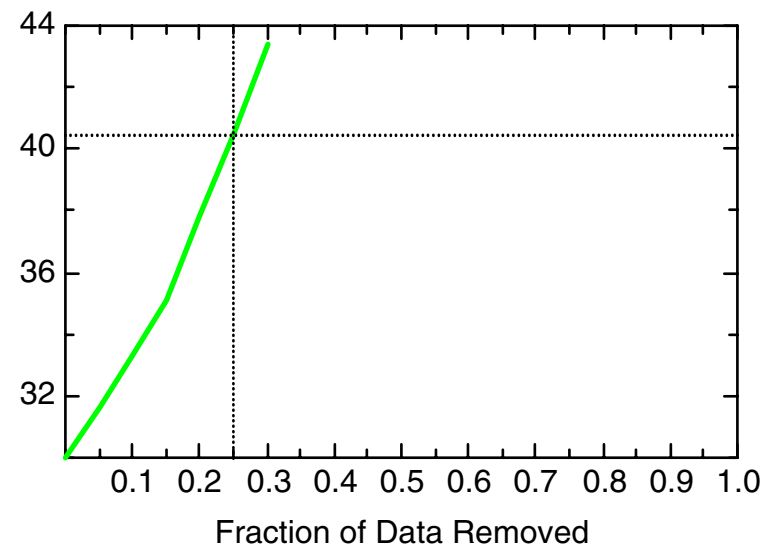
DCE12C: Well 49-5562(D)



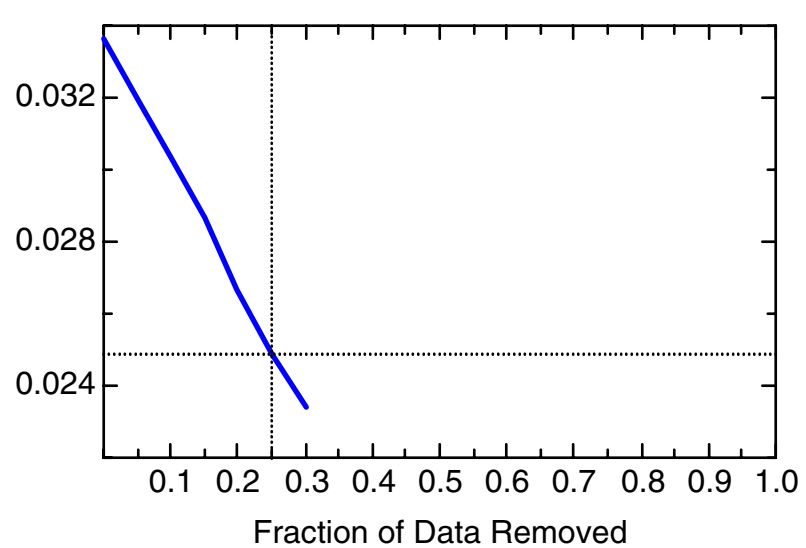
DCE12C: Well 49-5562(D)



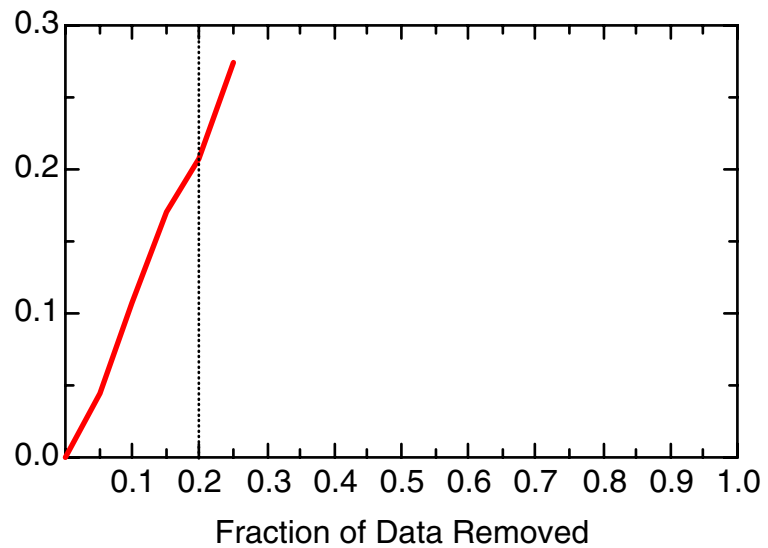
DCE12C: Well 49-5562(D)



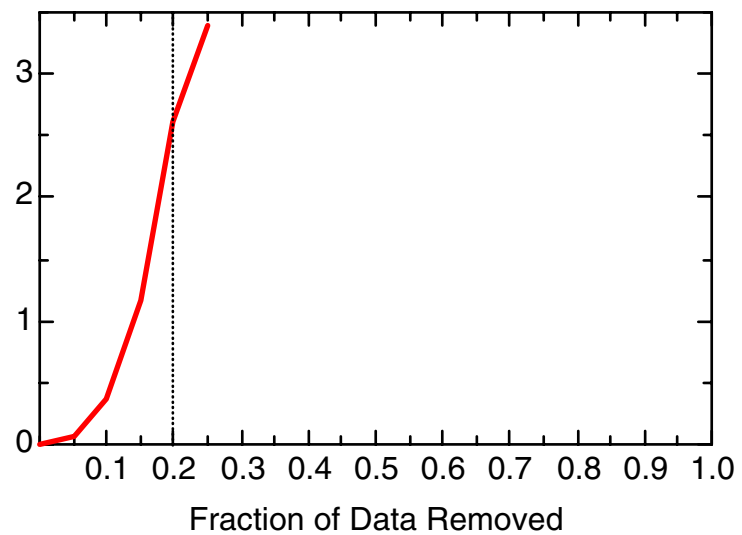
DCE12C: Well 49-5562(D)



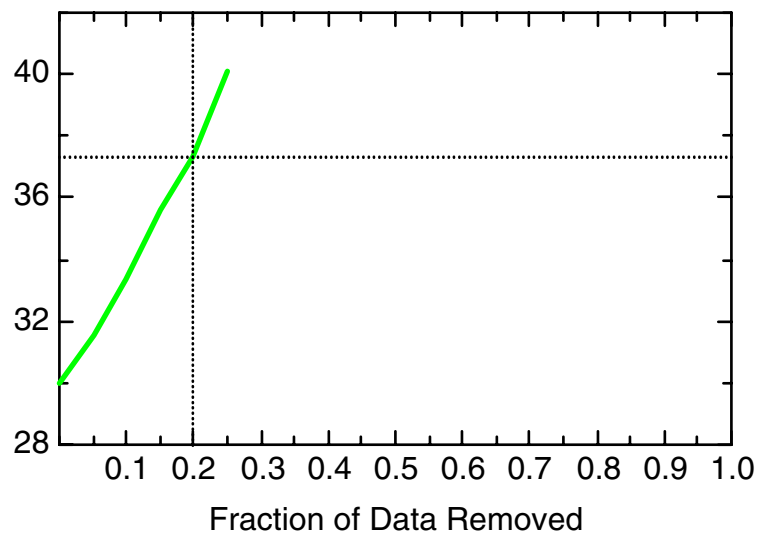
DCE12C: Well 49-5563(S)



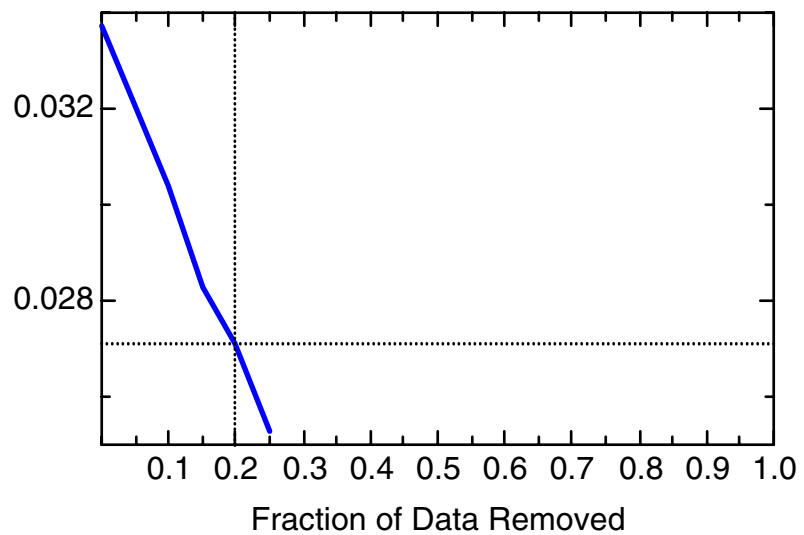
DCE12C: Well 49-5563(S)



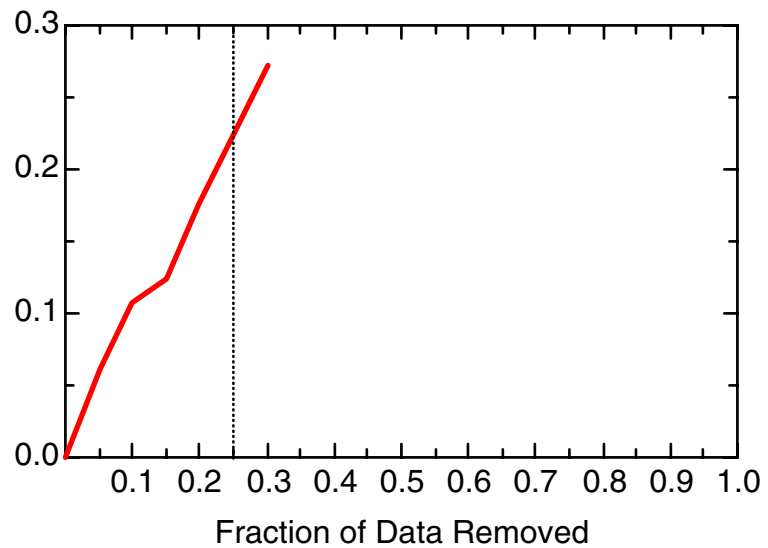
DCE12C: Well 49-5563(S)



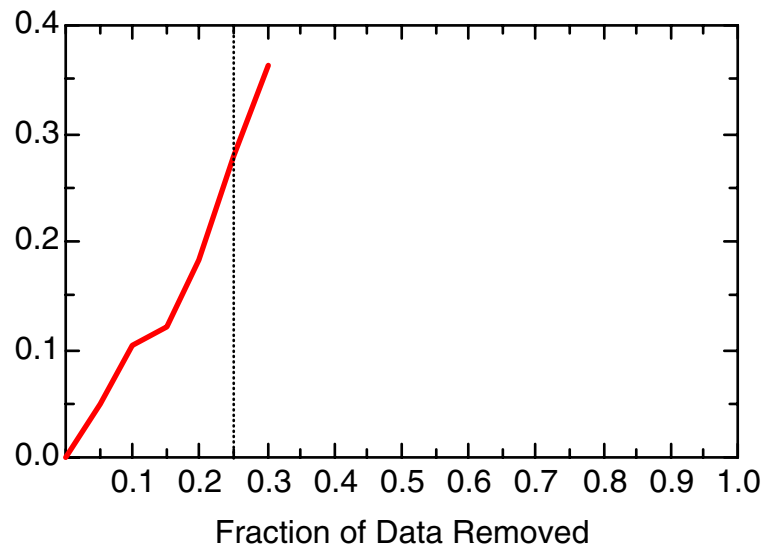
DCE12C: Well 49-5563(S)



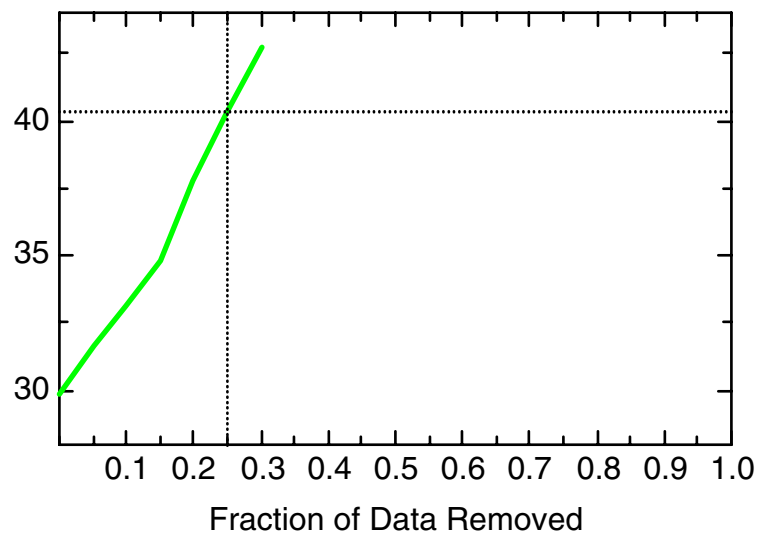
DCE12C: Well 49-5564(D)



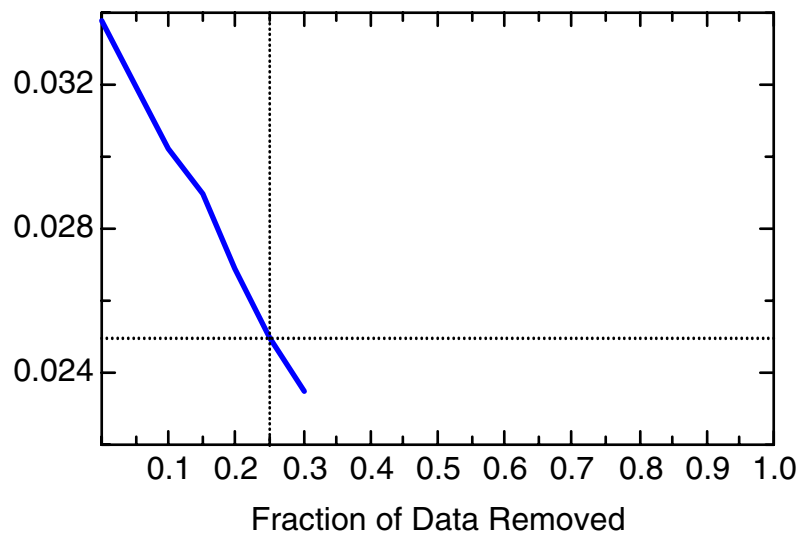
DCE12C: Well 49-5564(D)



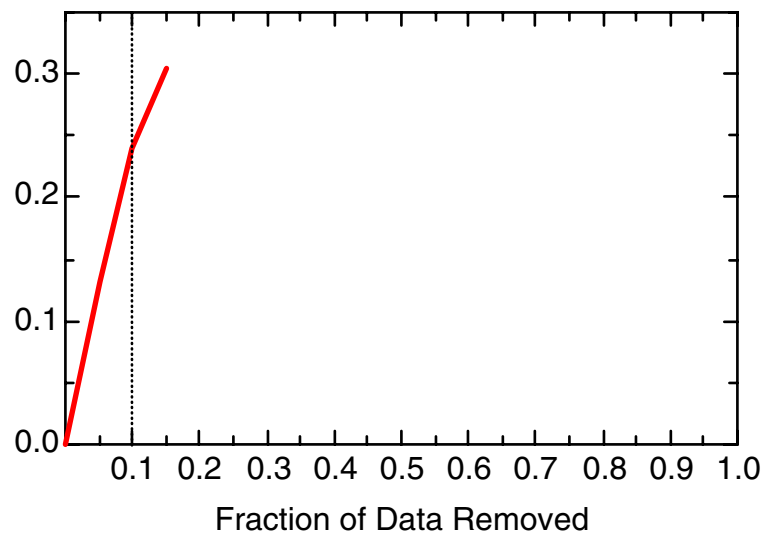
DCE12C: Well 49-5564(D)



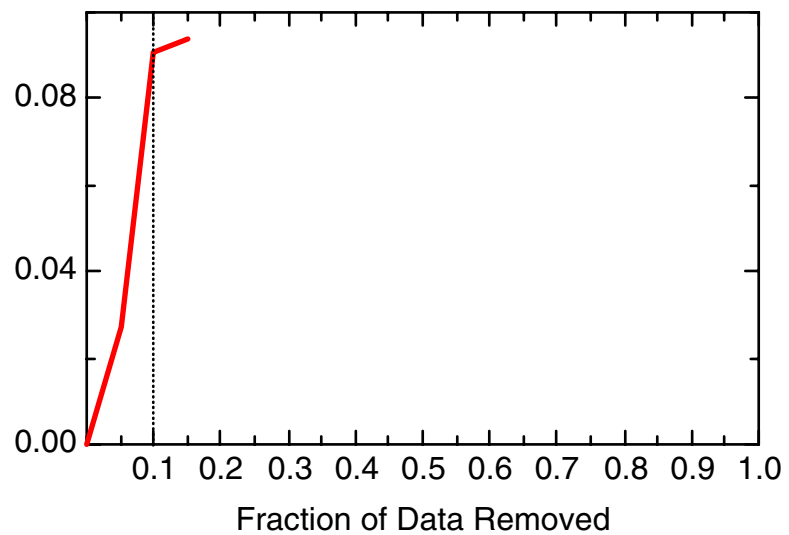
DCE12C: Well 49-5564(D)



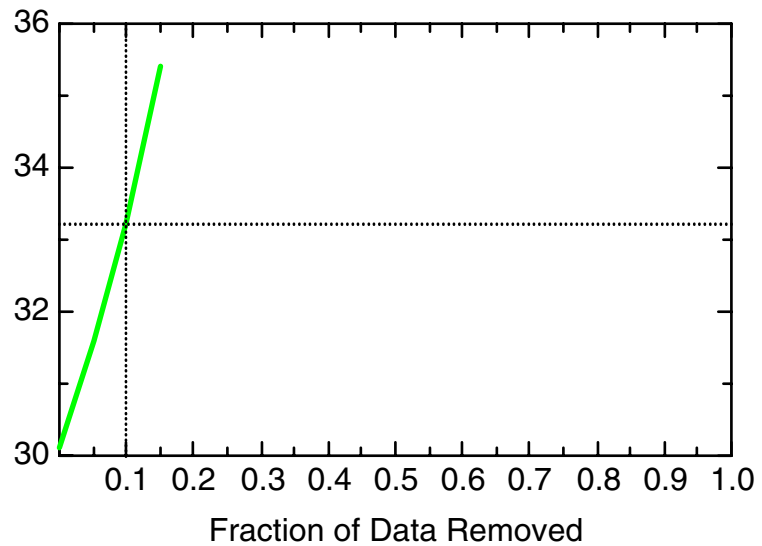
DCE12C: Well 49-5565(S)



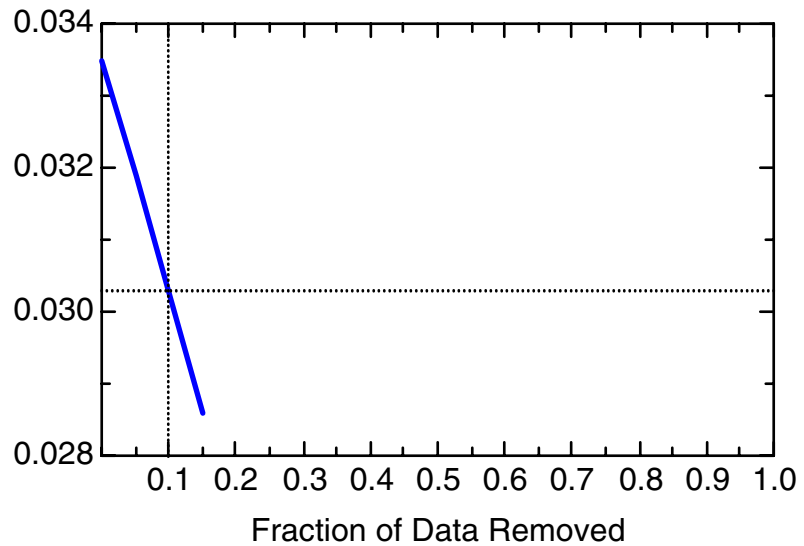
DCE12C: Well 49-5565(S)



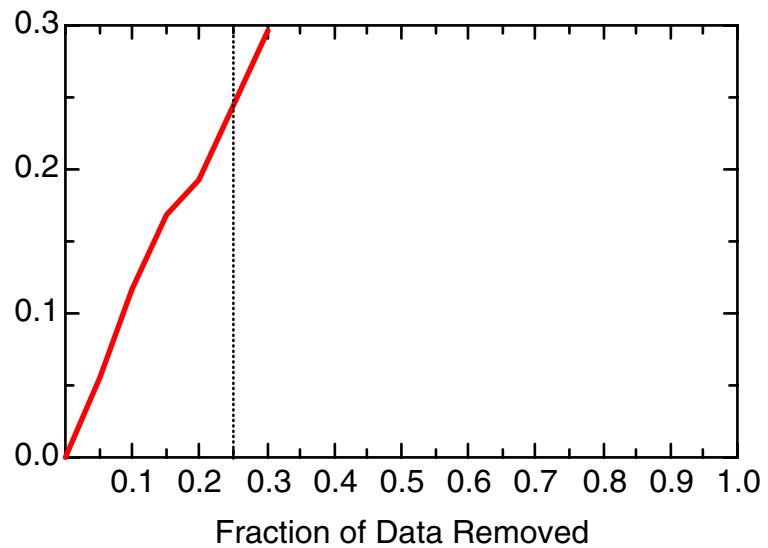
DCE12C: Well 49-5565(S)



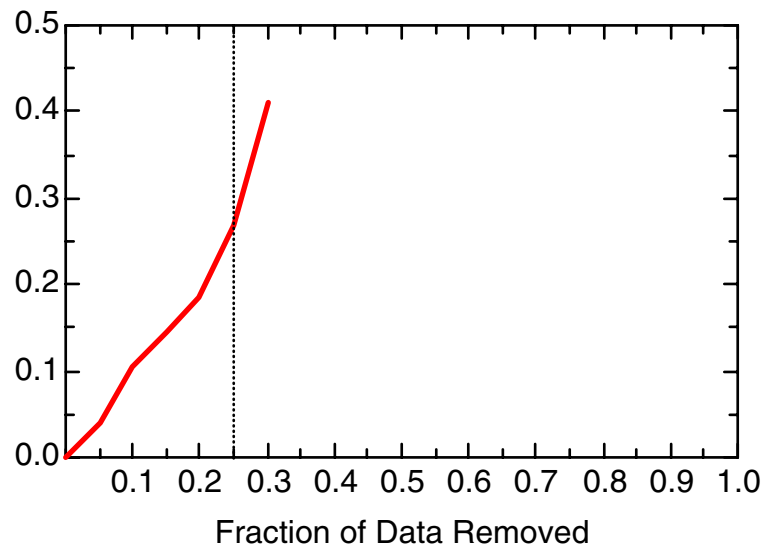
DCE12C: Well 49-5565(S)



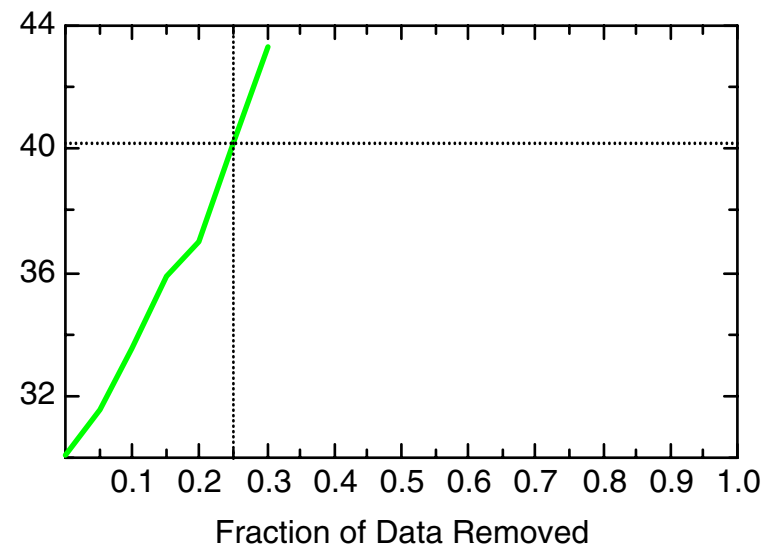
DCE12C: Well 49-5566(S)



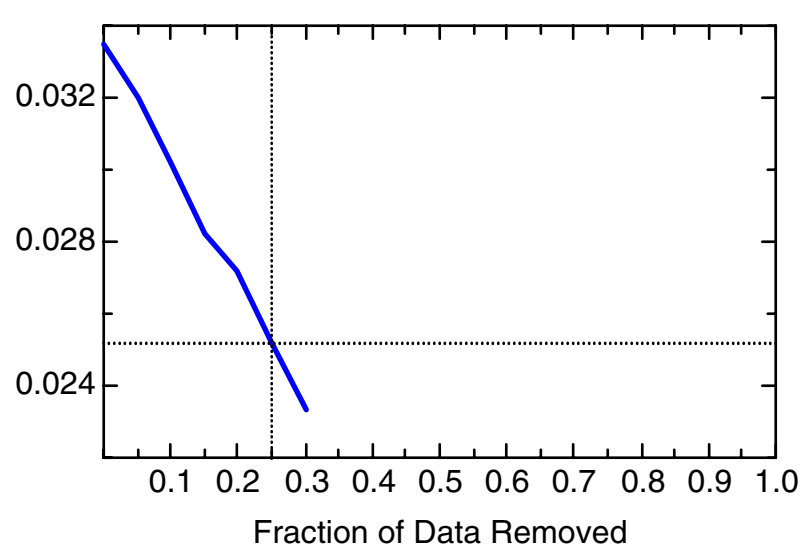
DCE12C: Well 49-5566(S)



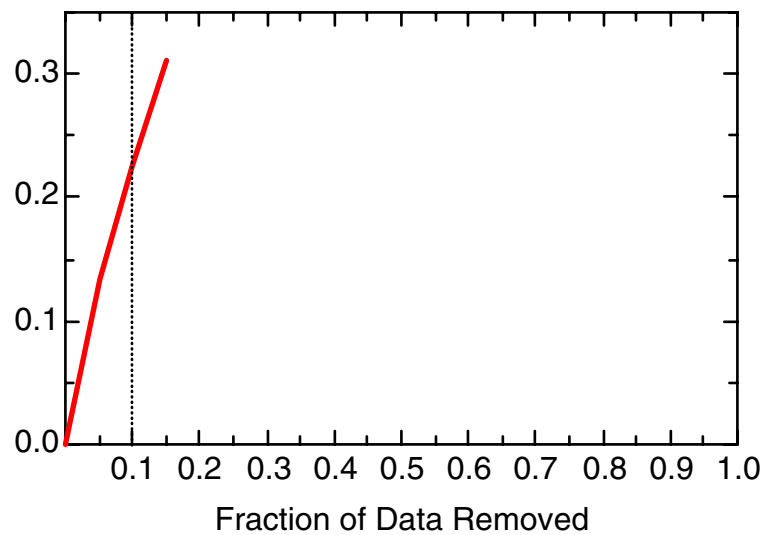
DCE12C: Well 49-5566(S)



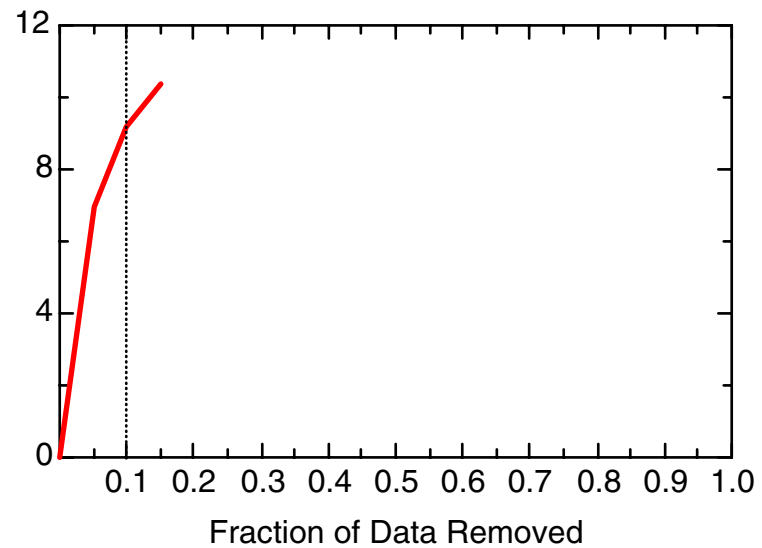
DCE12C: Well 49-5566(S)



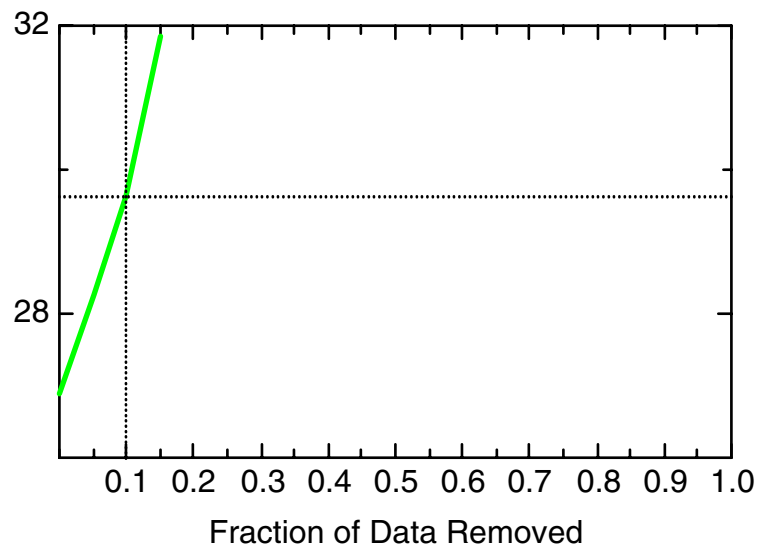
DCE12C: Well 49-5568(D)



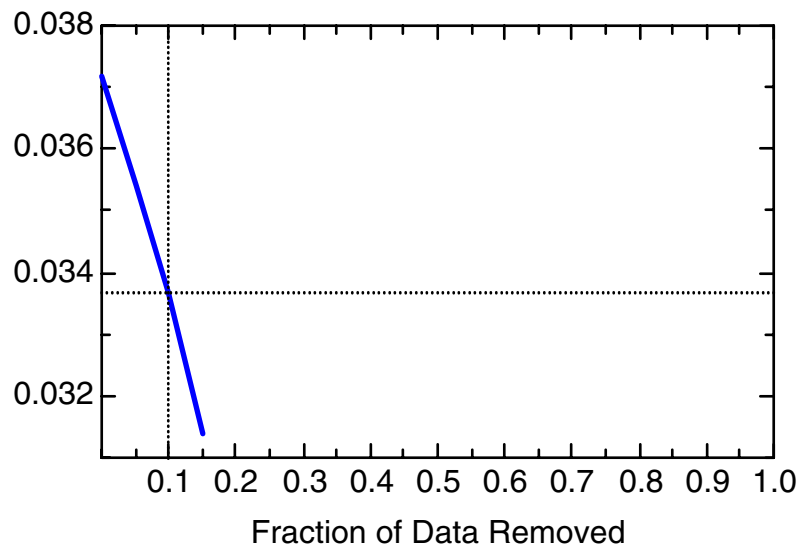
DCE12C: Well 49-5568(D)



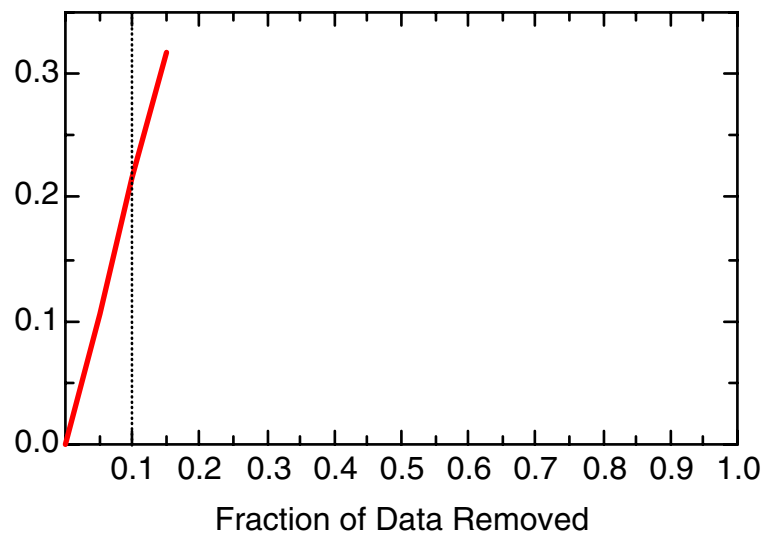
DCE12C: Well 49-5568(D)



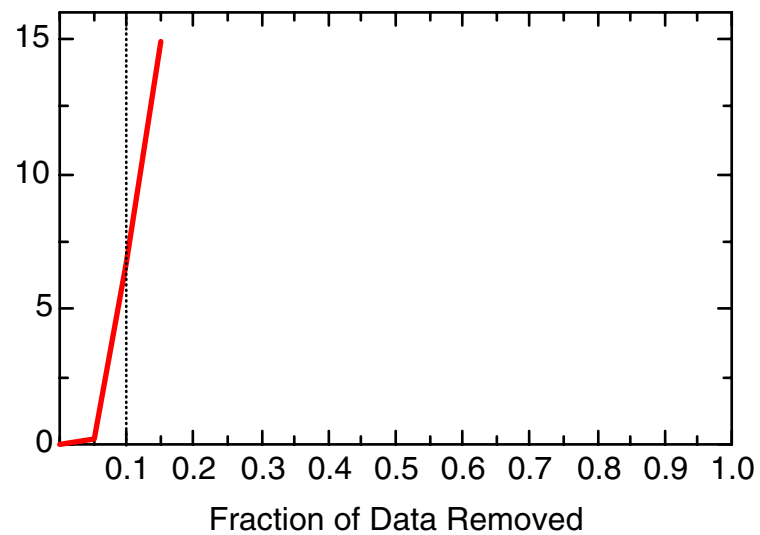
DCE12C: Well 49-5568(D)



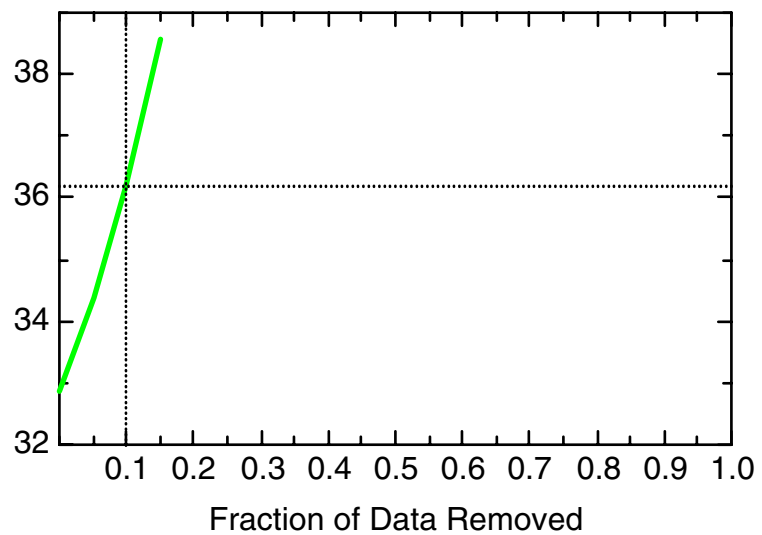
DCE12C: Well 49-5573(D)



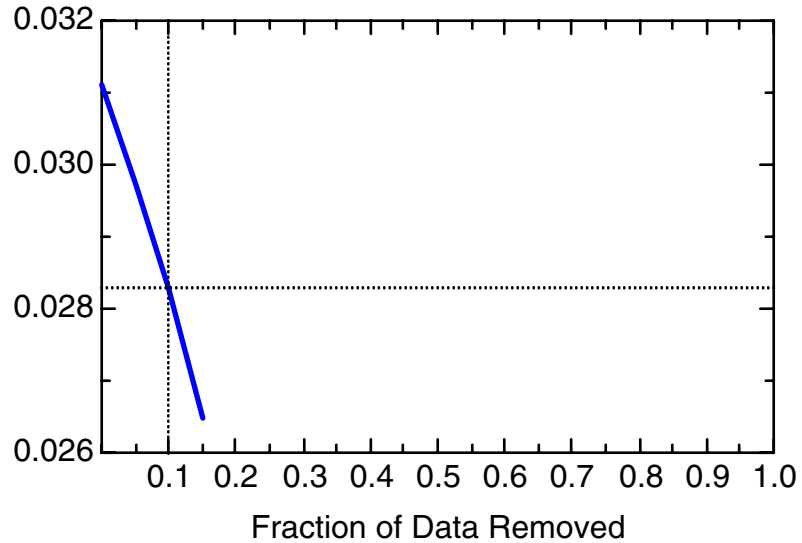
DCE12C: Well 49-5573(D)



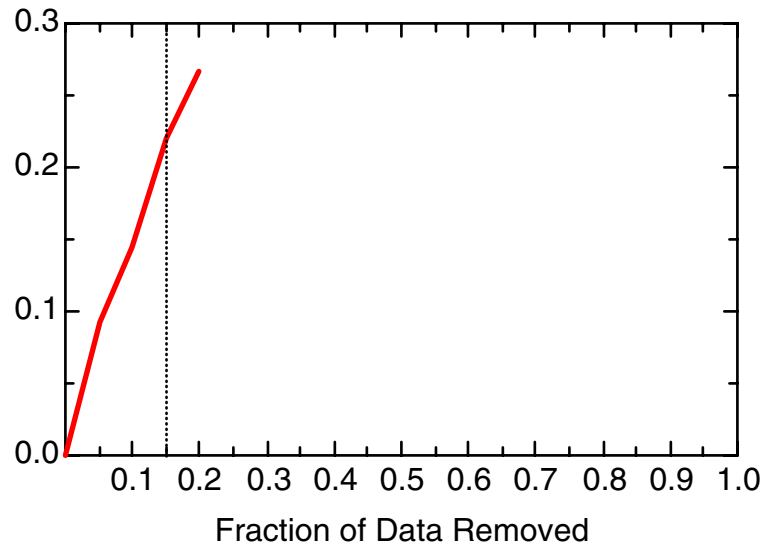
DCE12C: Well 49-5573(D)



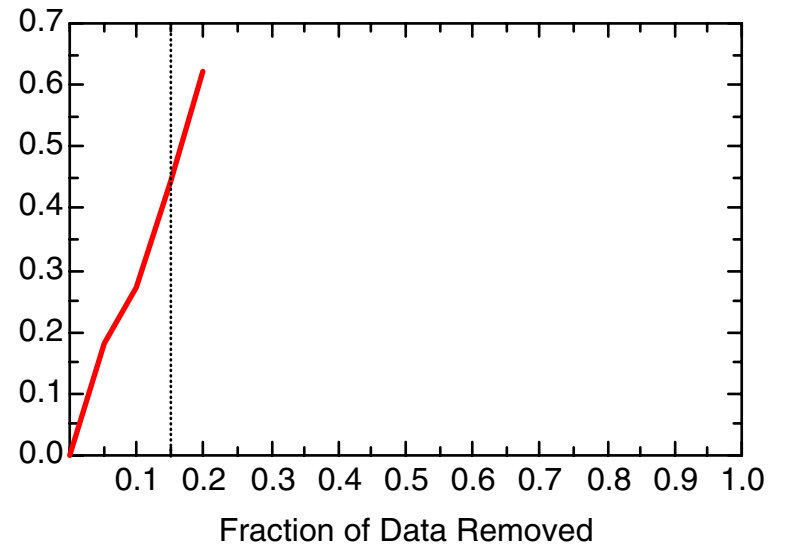
DCE12C: Well 49-5573(D)



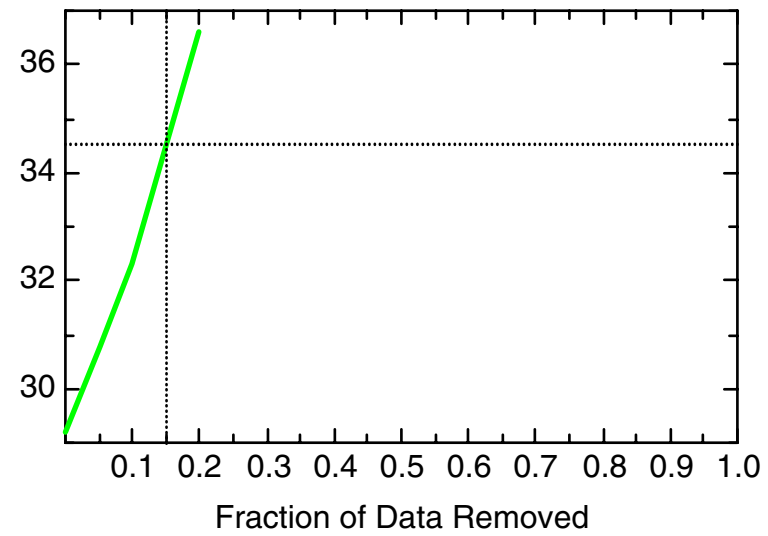
DCE12C: Well 49-5574(S)



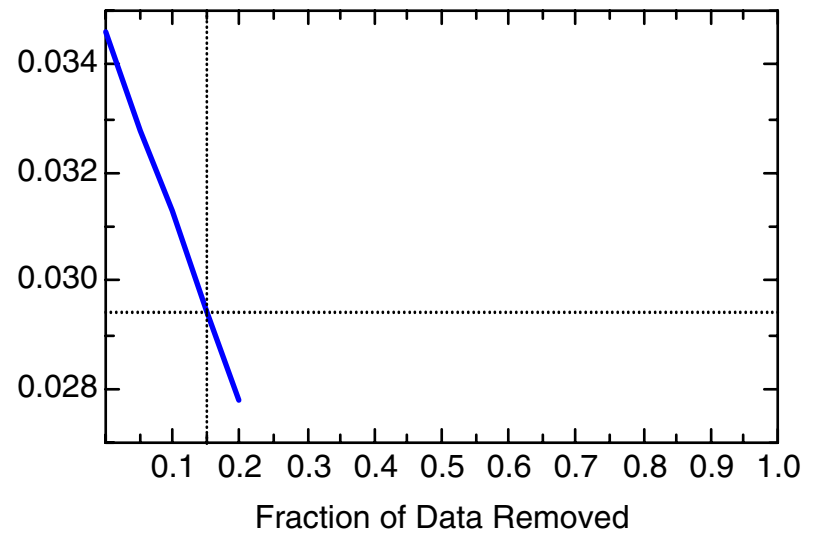
DCE12C: Well 49-5574(S)



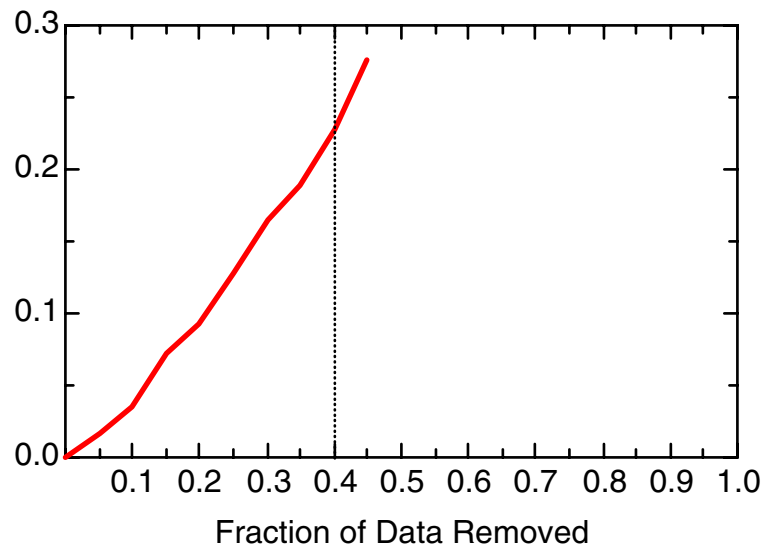
DCE12C: Well 49-5574(S)



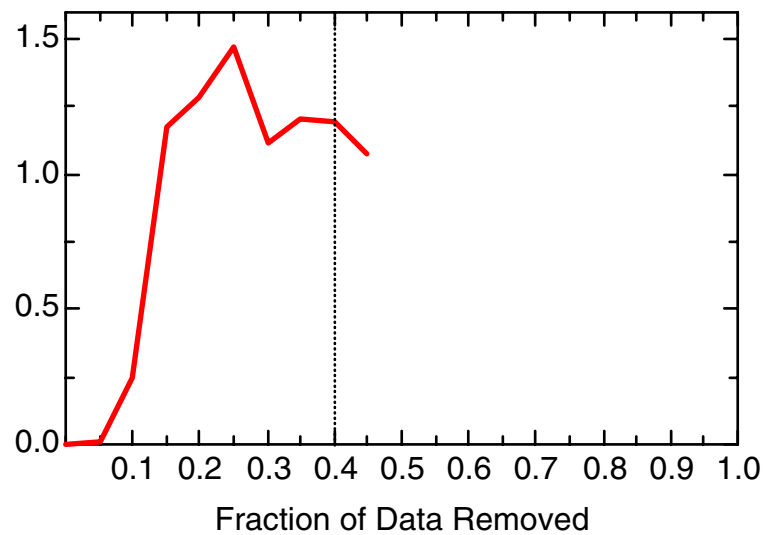
DCE12C: Well 49-5574(S)



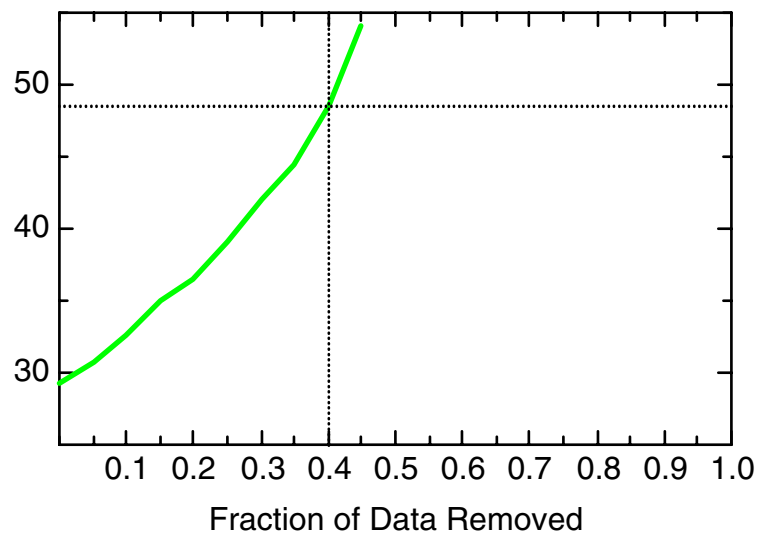
DCE12C: Well 49-5577(D)



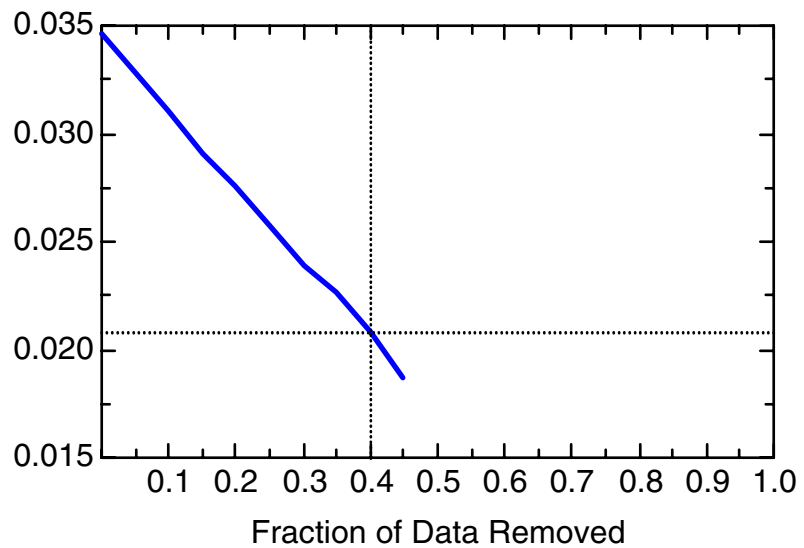
DCE12C: Well 49-5577(D)



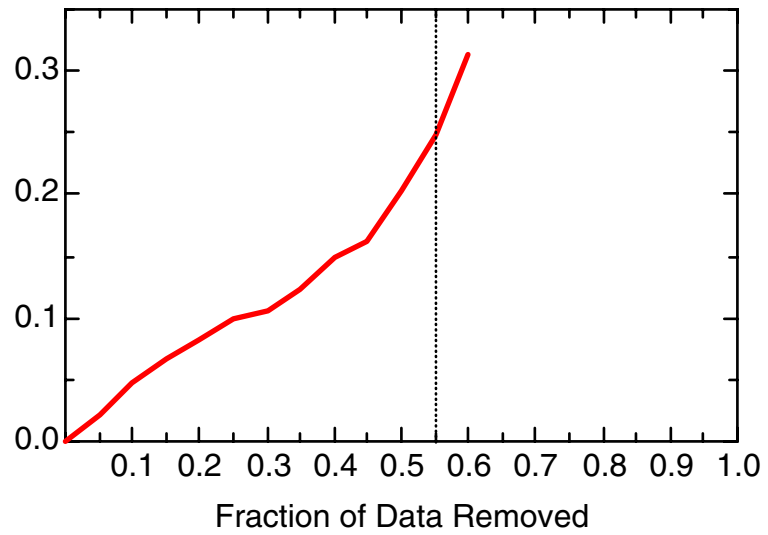
DCE12C: Well 49-5577(D)



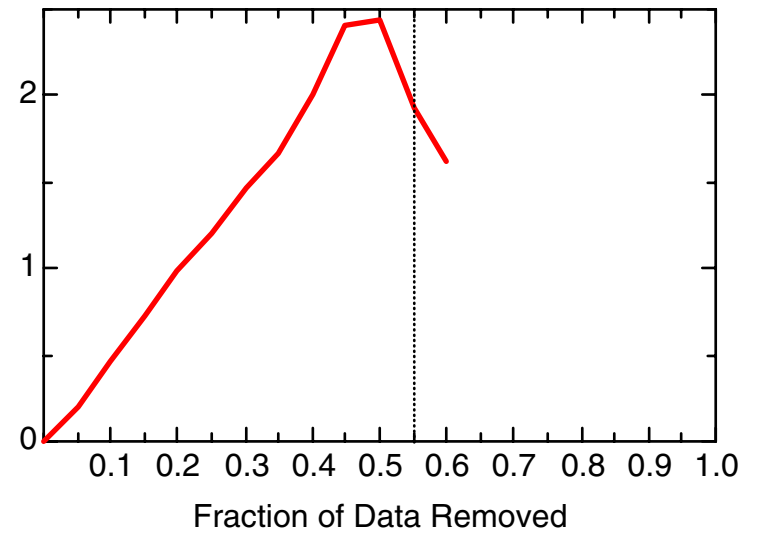
DCE12C: Well 49-5577(D)



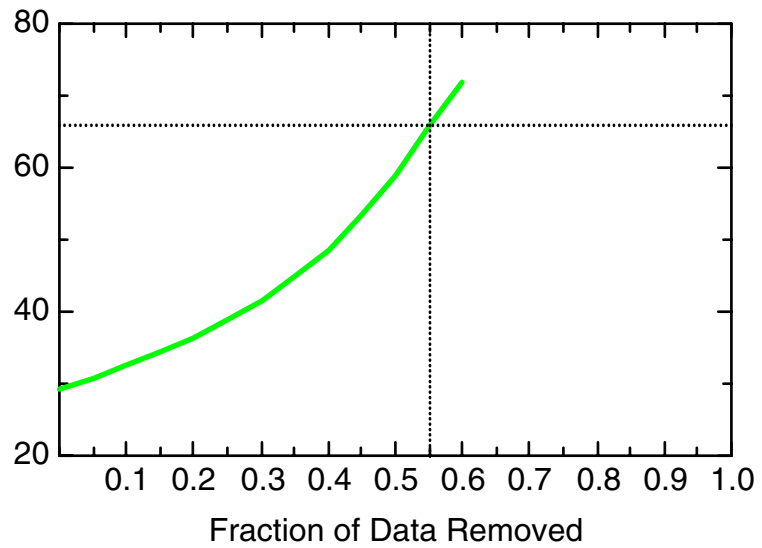
DCE12C: Well 49-5578(S)



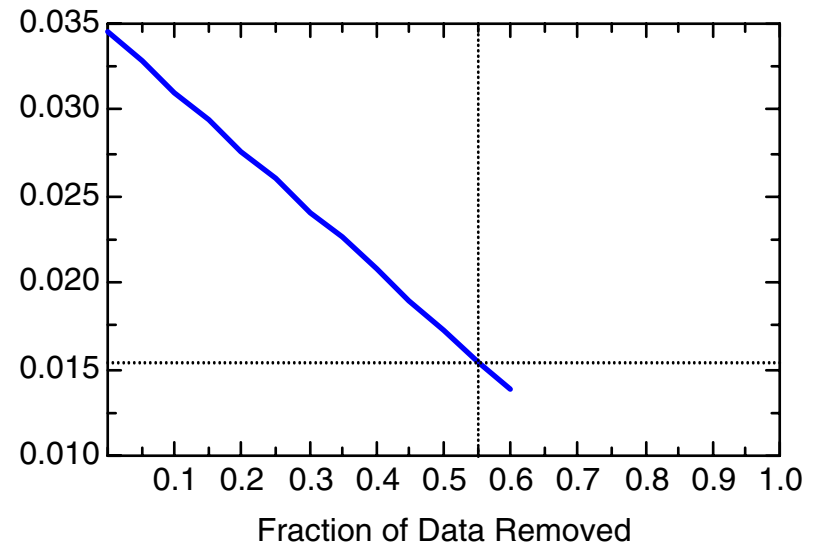
DCE12C: Well 49-5578(S)



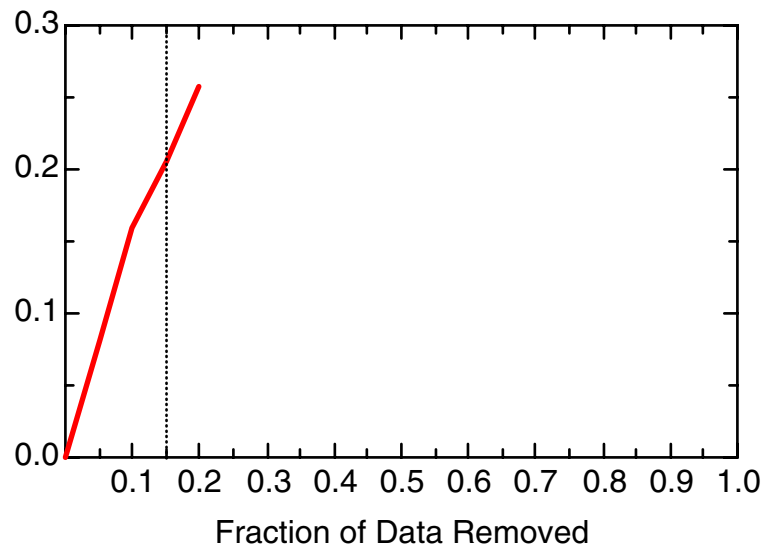
DCE12C: Well 49-5578(S)



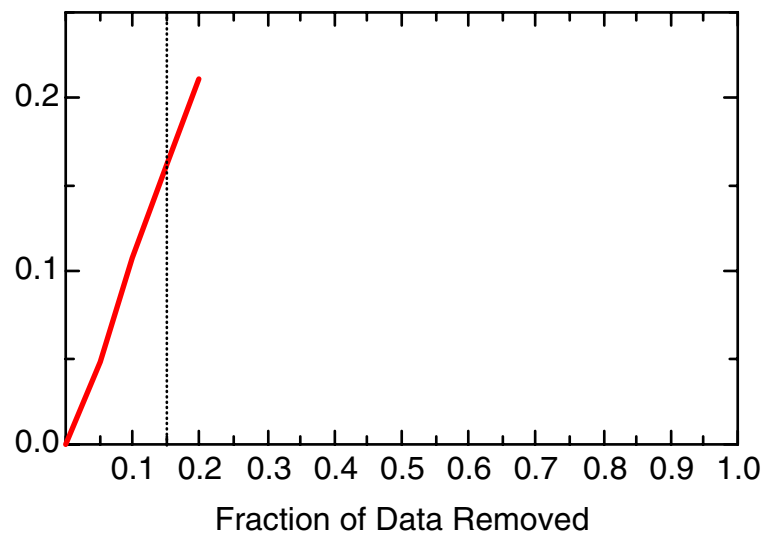
DCE12C: Well 49-5578(S)



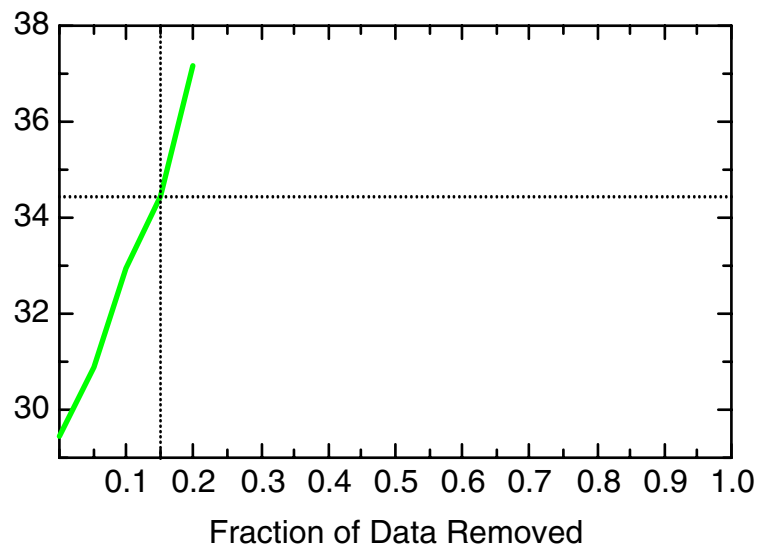
DCE12C: Well 49-6515(S)



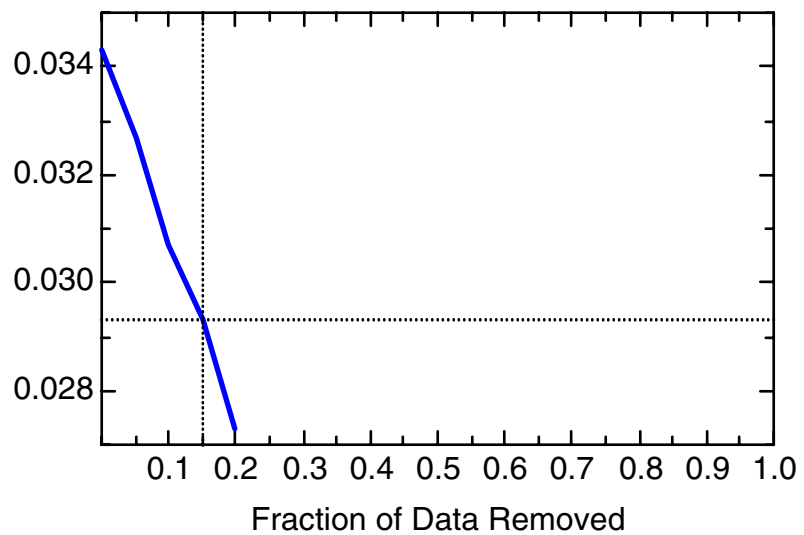
DCE12C: Well 49-6515(S)



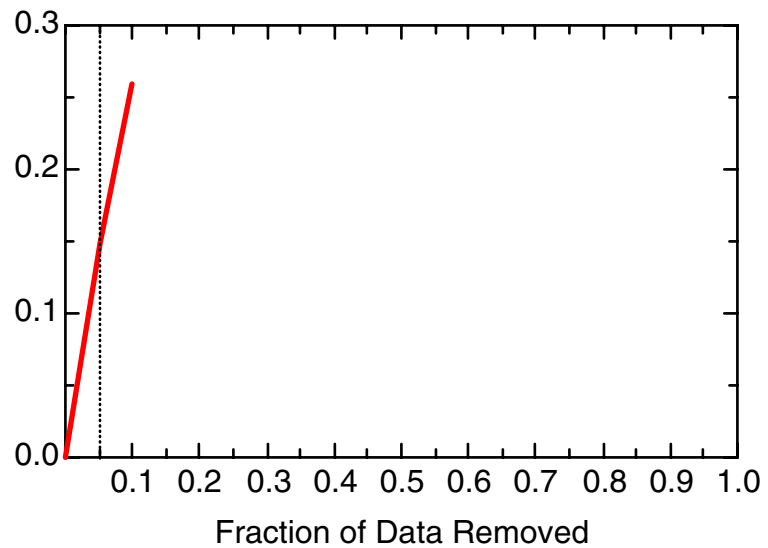
DCE12C: Well 49-6515(S)



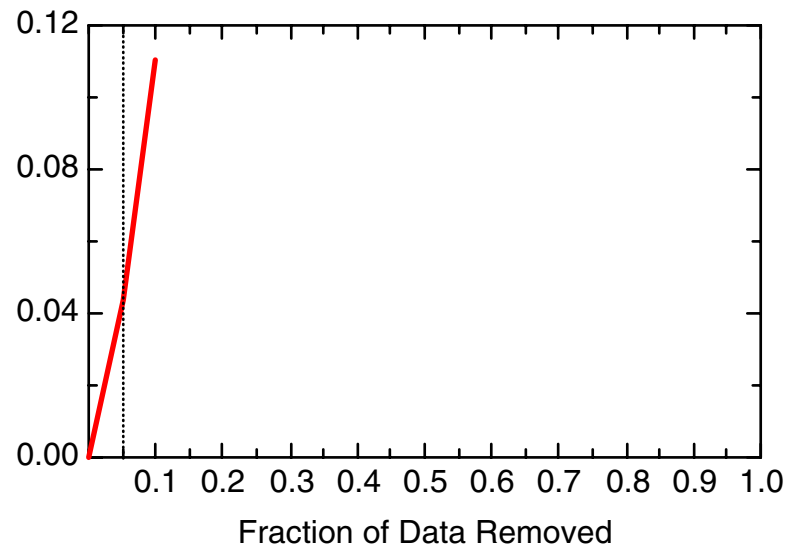
DCE12C: Well 49-6515(S)



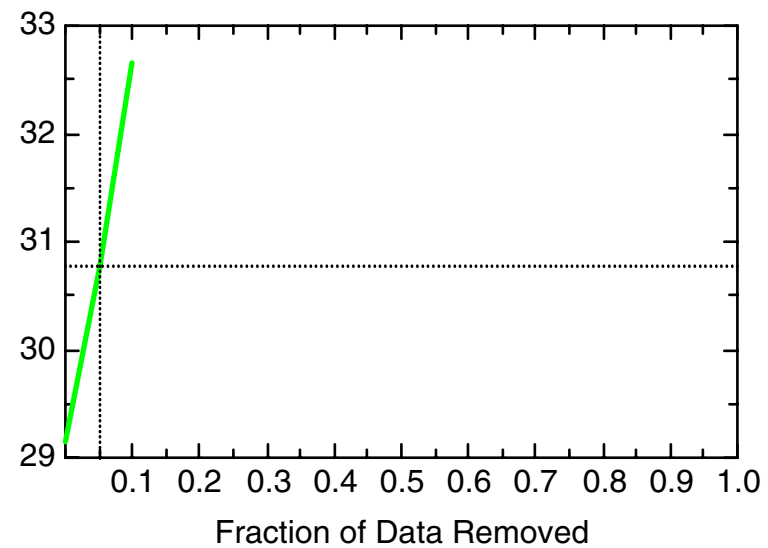
DCE12C: Well 49-6516(S)



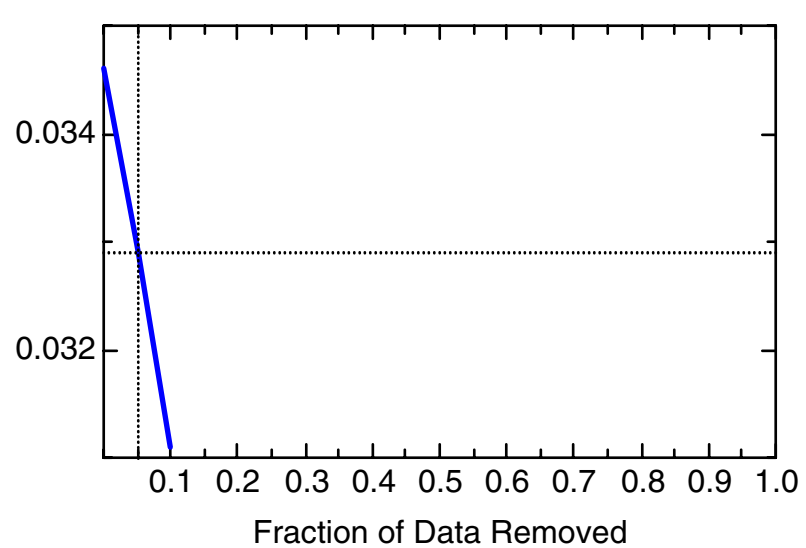
DCE12C: Well 49-6516(S)



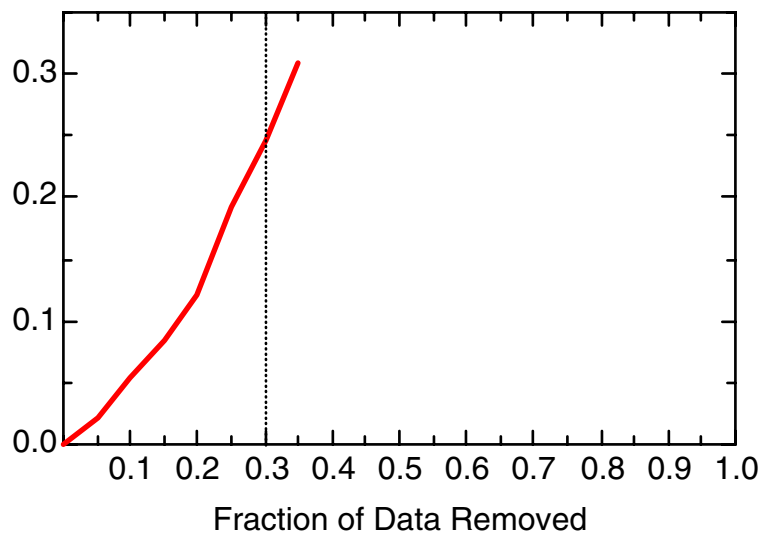
DCE12C: Well 49-6516(S)



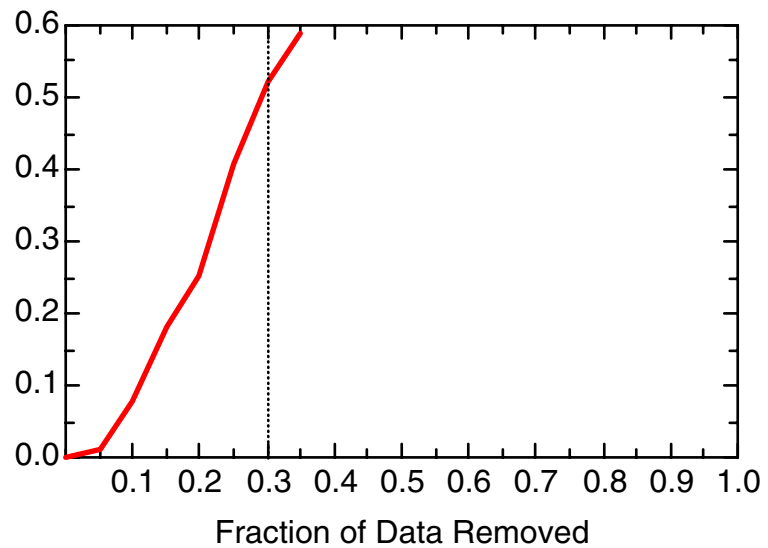
DCE12C: Well 49-6516(S)



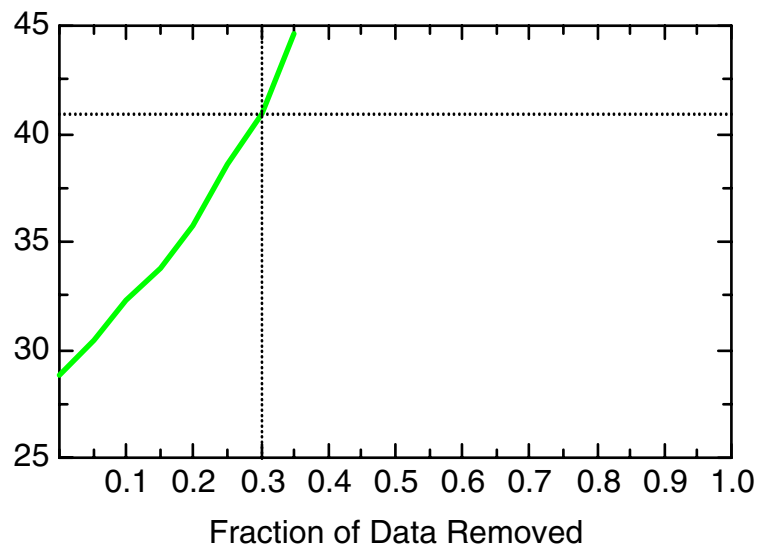
DCE12C: Well 49-MW01



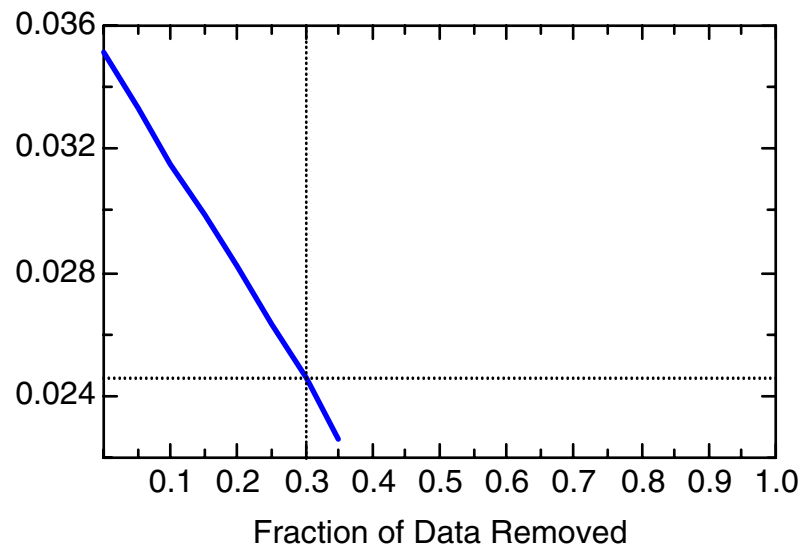
DCE12C: Well 49-MW01



DCE12C: Well 49-MW01

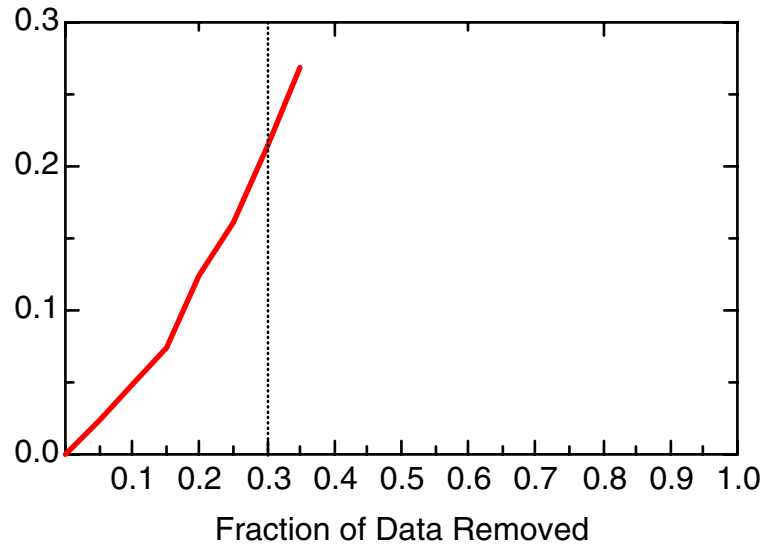


DCE12C: Well 49-MW01

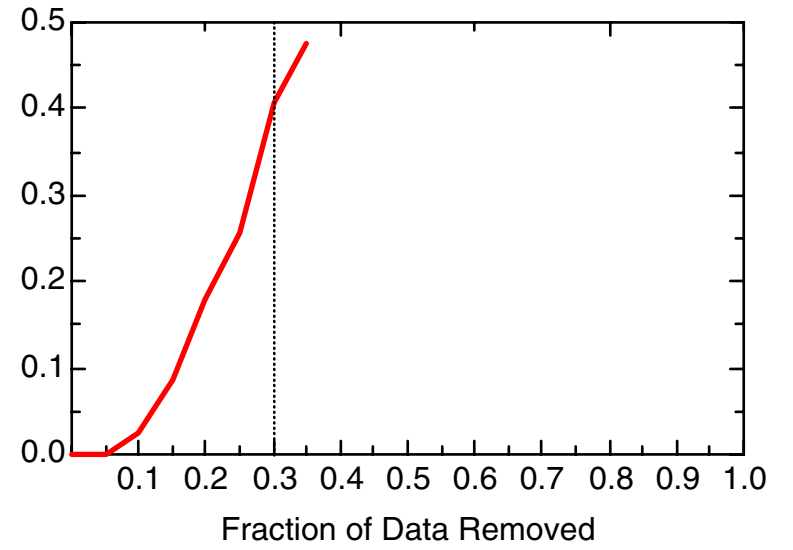


TCE

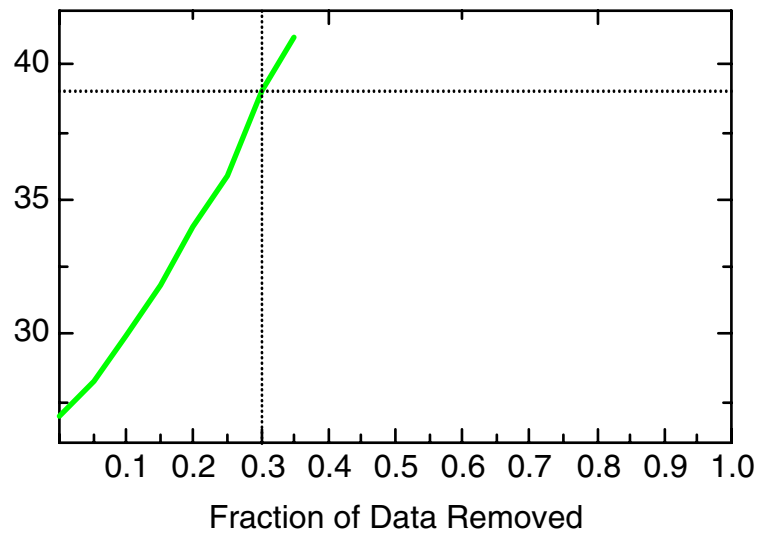
TCE: Well 49-5562(D)



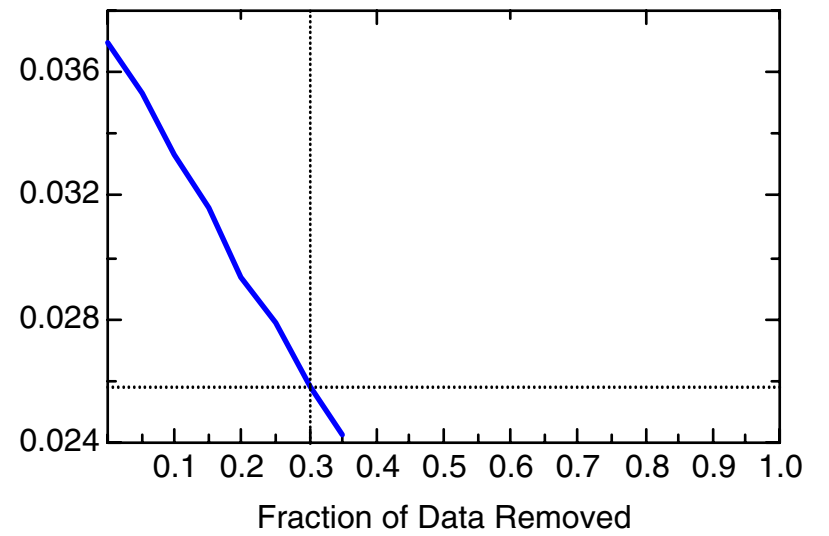
TCE: Well 49-5562(D)



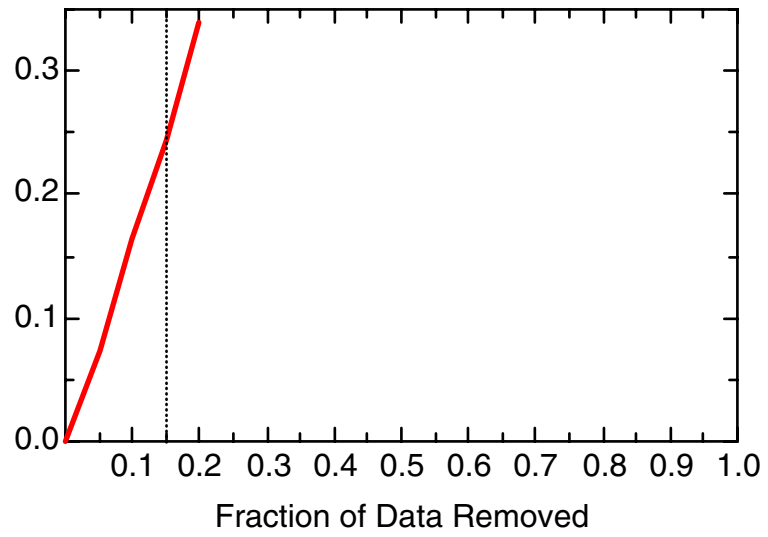
TCE: Well 49-5562(D)



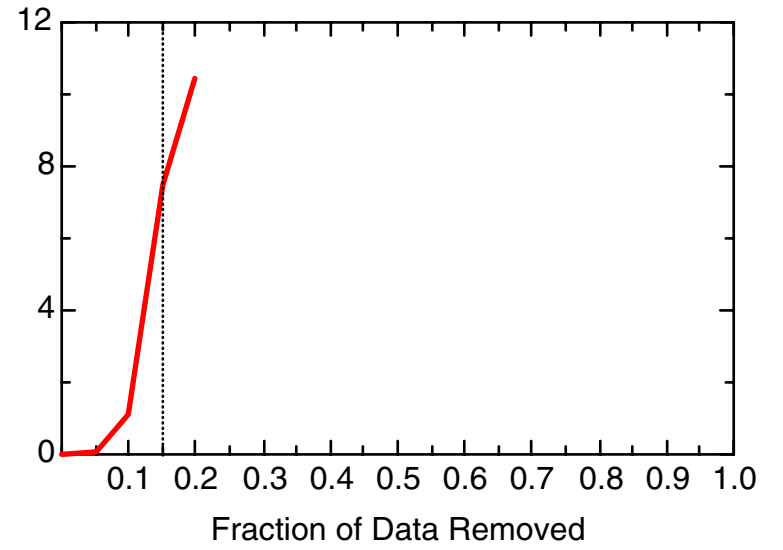
TCE: Well 49-5562(D)



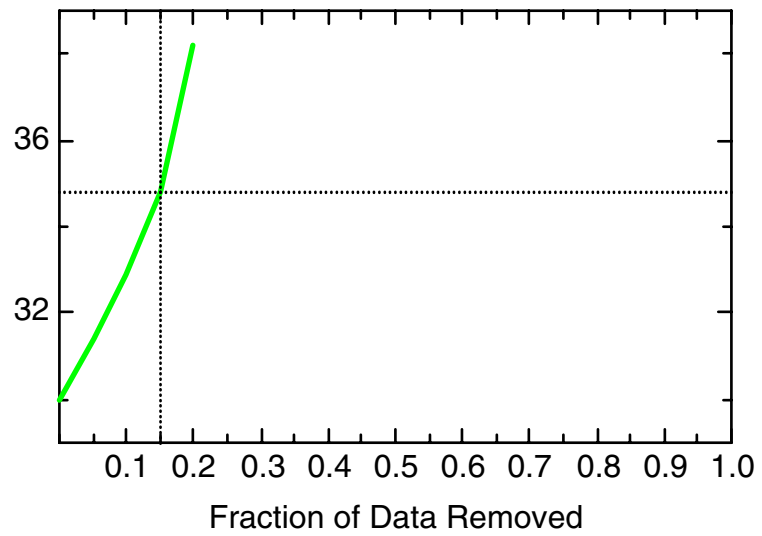
TCE: Well 49-5563(S)



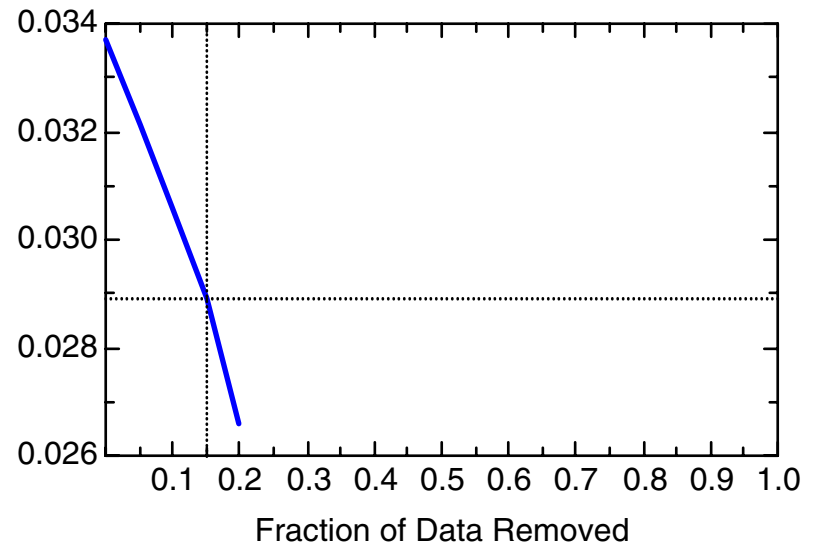
TCE: Well 49-5563(S)



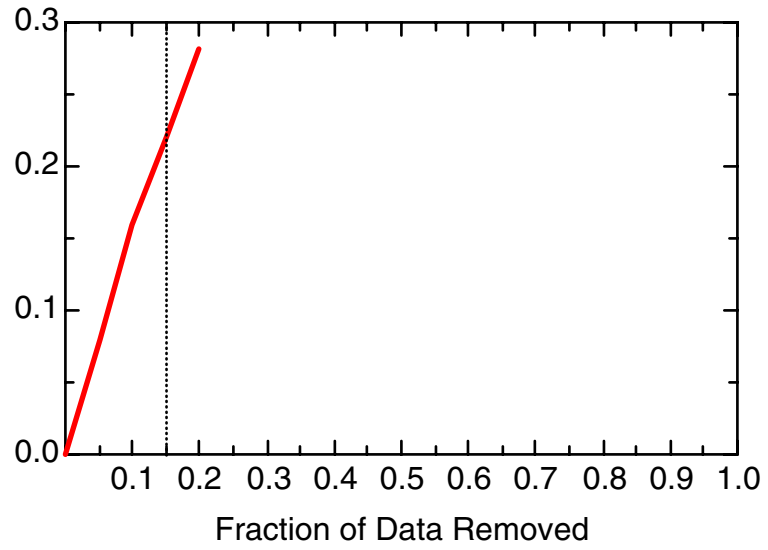
TCE: Well 49-5563(S)



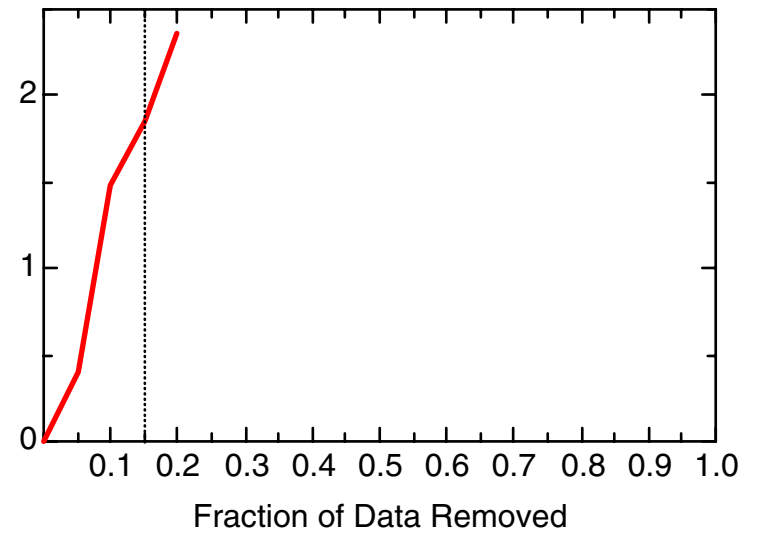
TCE: Well 49-5563(S)



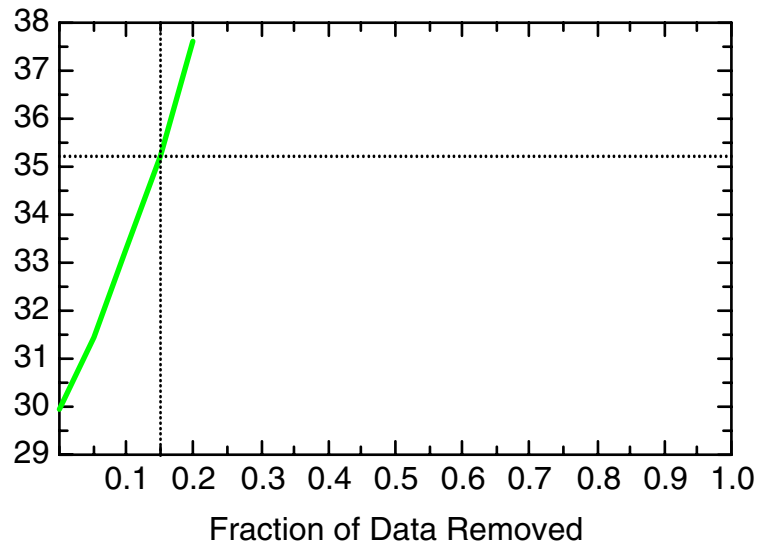
TCE: Well 49-5564(D)



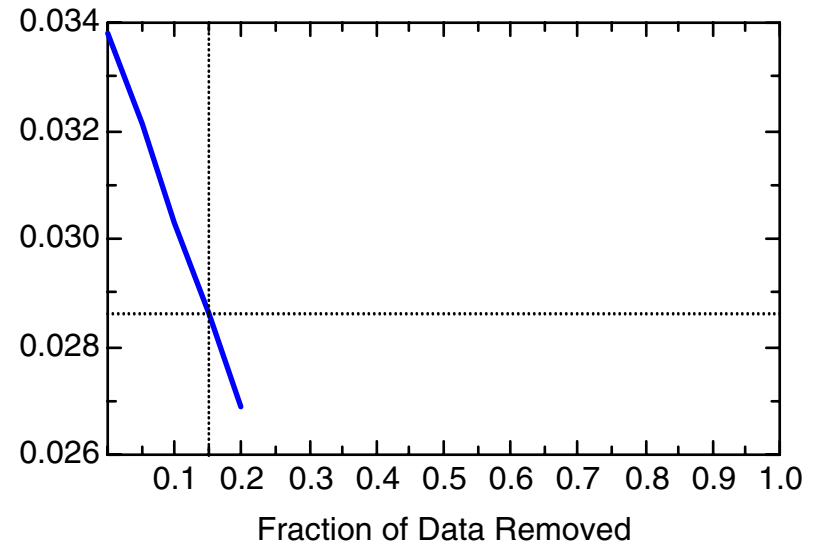
TCE: Well 49-5564(D)



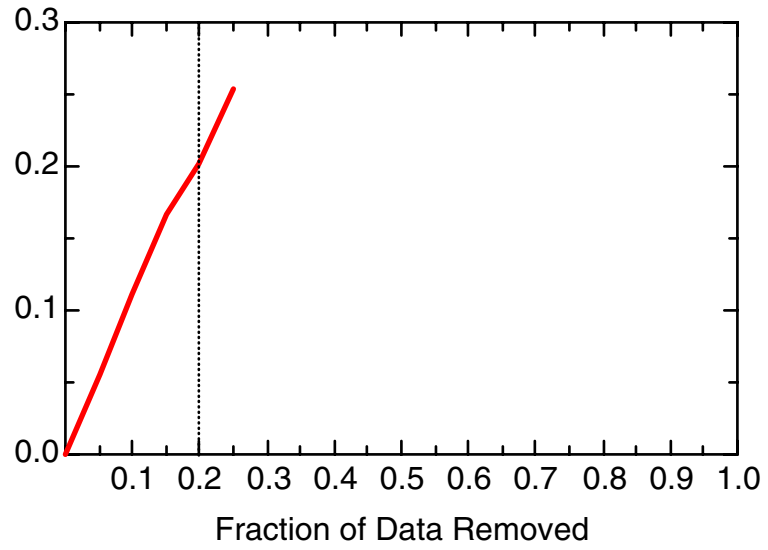
TCE: Well 49-5564(D)



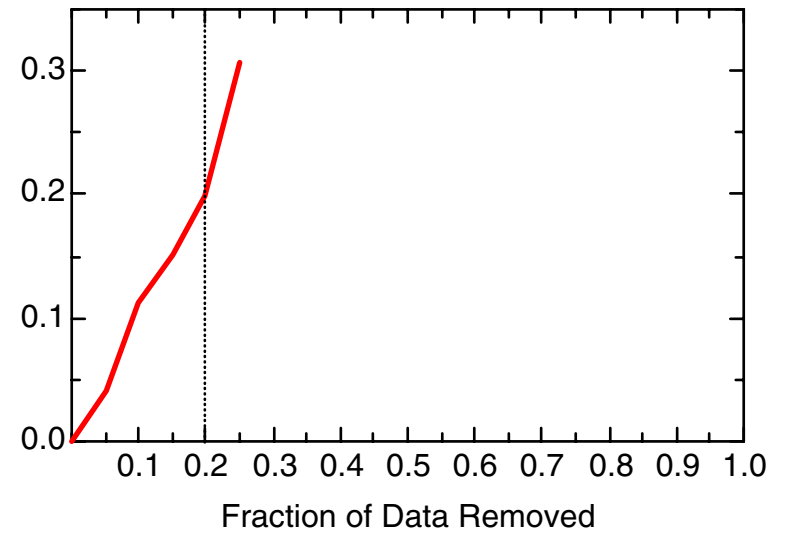
TCE: Well 49-5564(D)



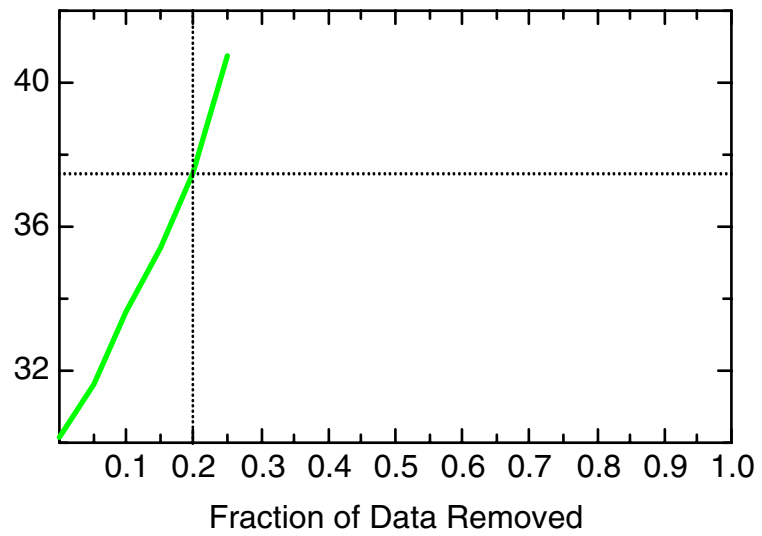
TCE: Well 49-5565(S)



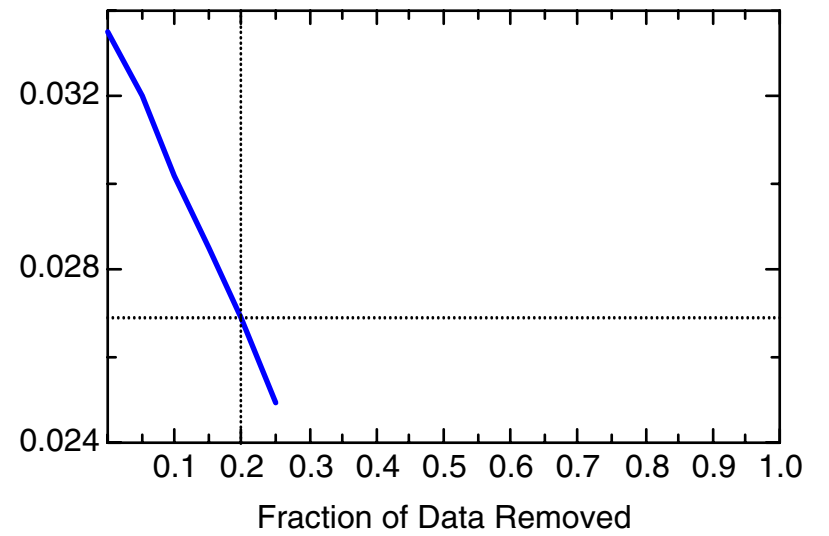
TCE: Well 49-5565(S)



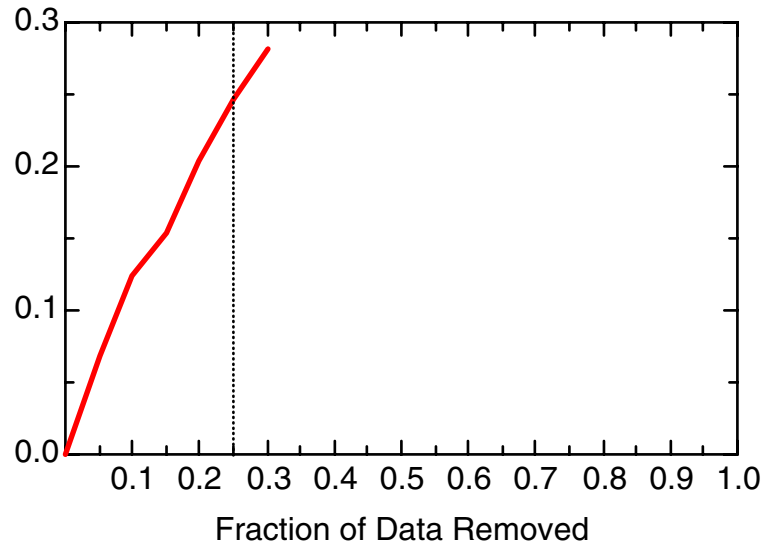
TCE: Well 49-5565(S)



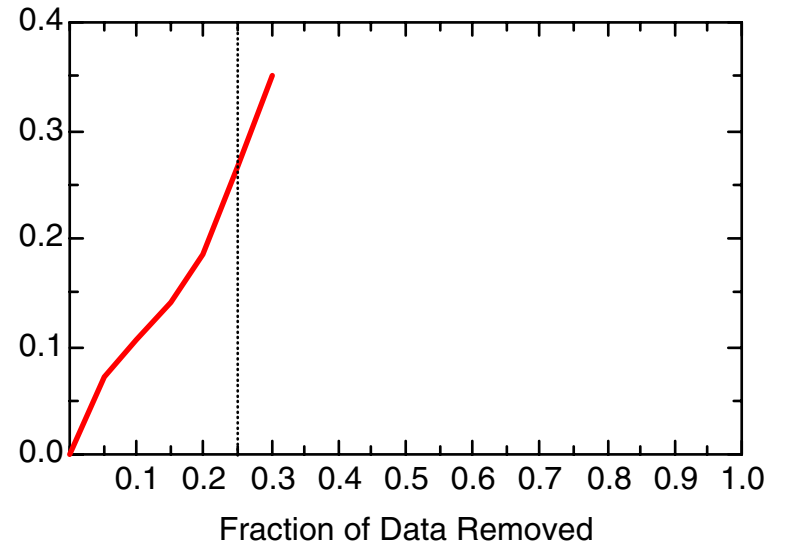
TCE: Well 49-5565(S)



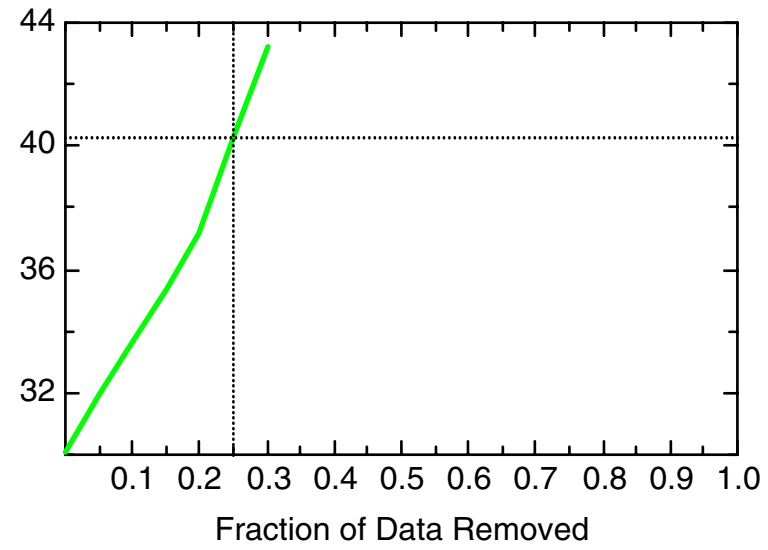
TCE: Well 49-5566(S)



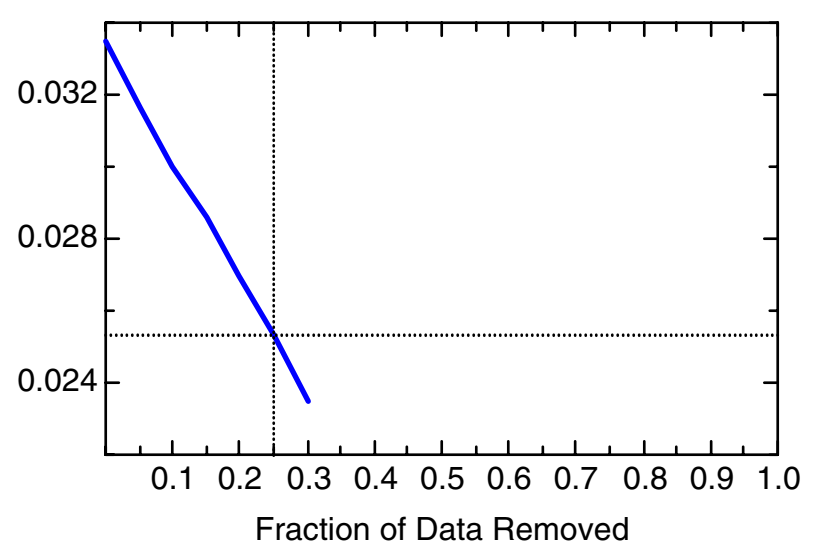
TCE: Well 49-5566(S)



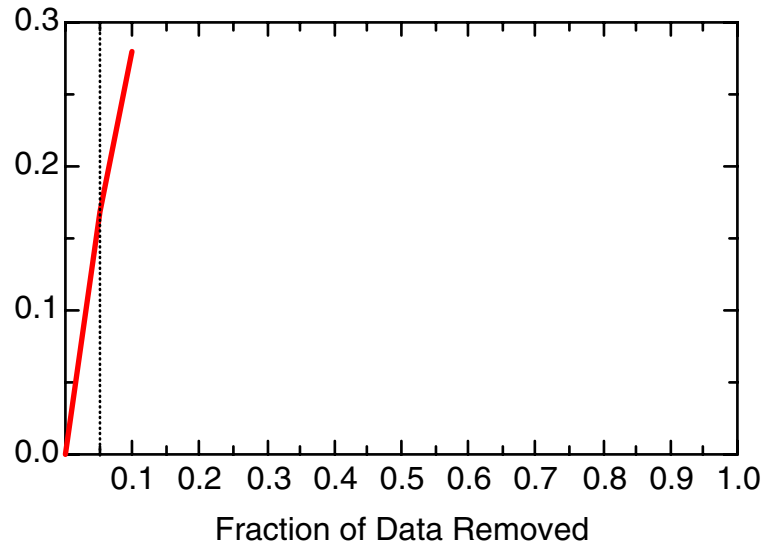
TCE: Well 49-5566(S)



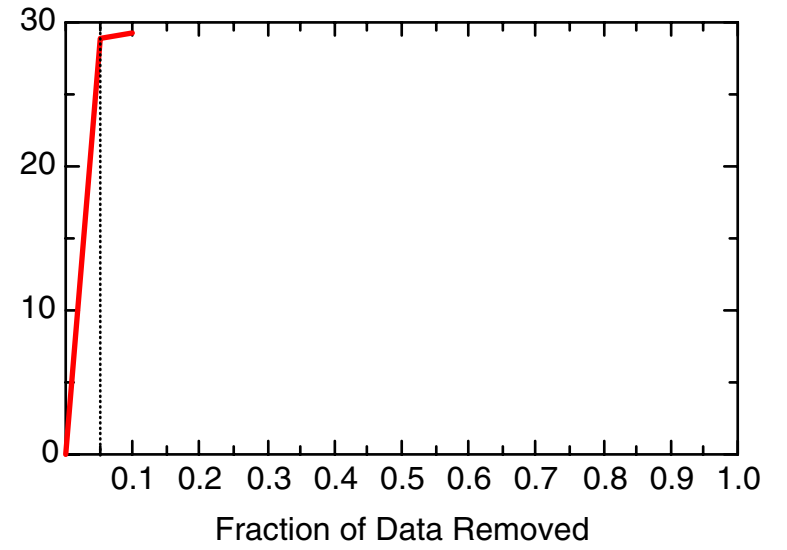
TCE: Well 49-5566(S)



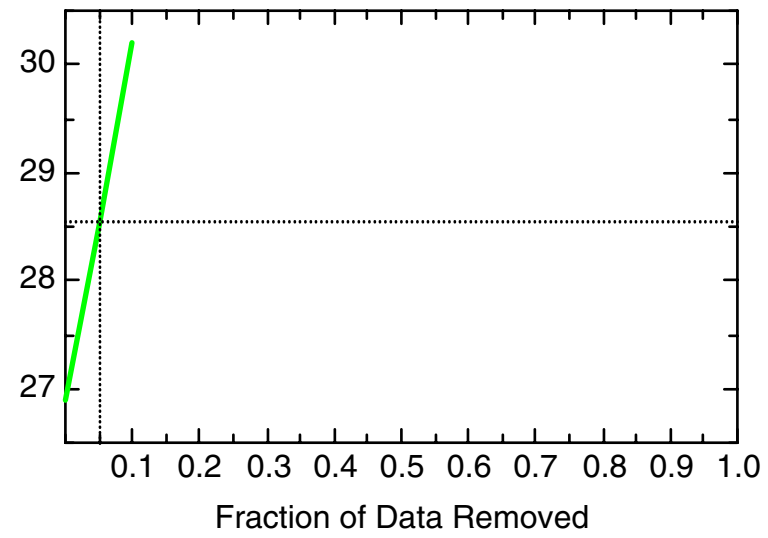
TCE: Well 49-5568(D)



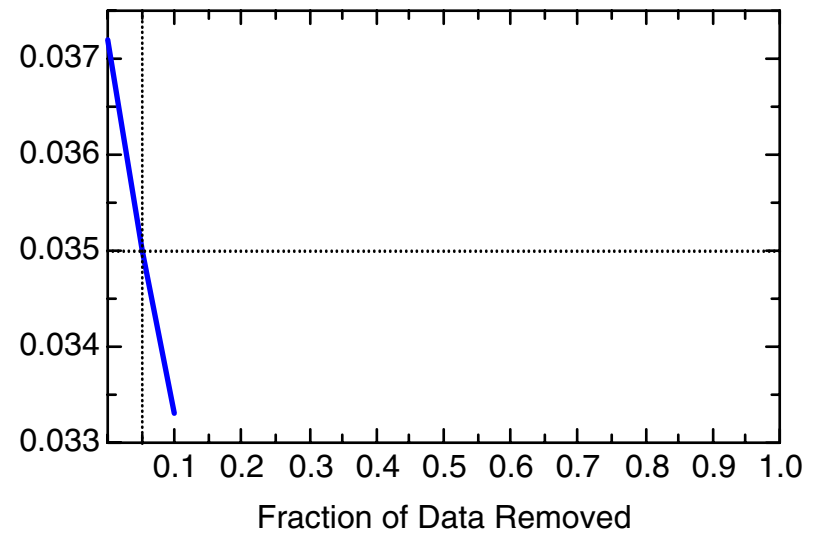
TCE: Well 49-5568(D)



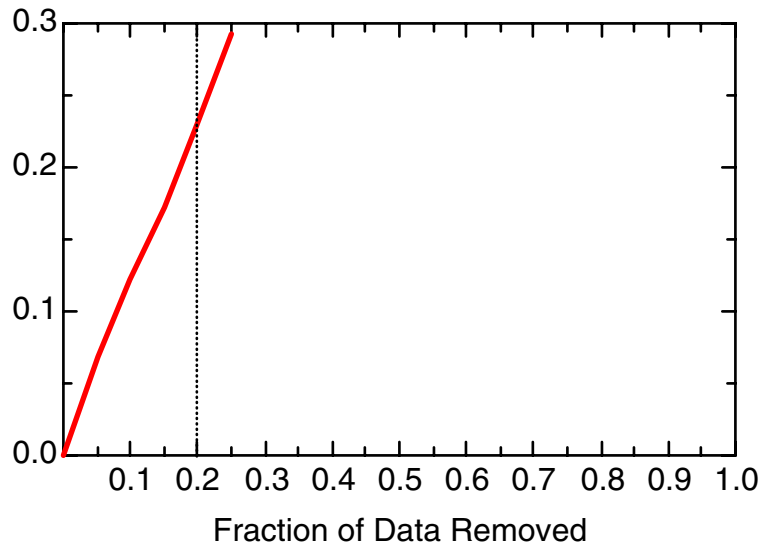
TCE: Well 49-5568(D)



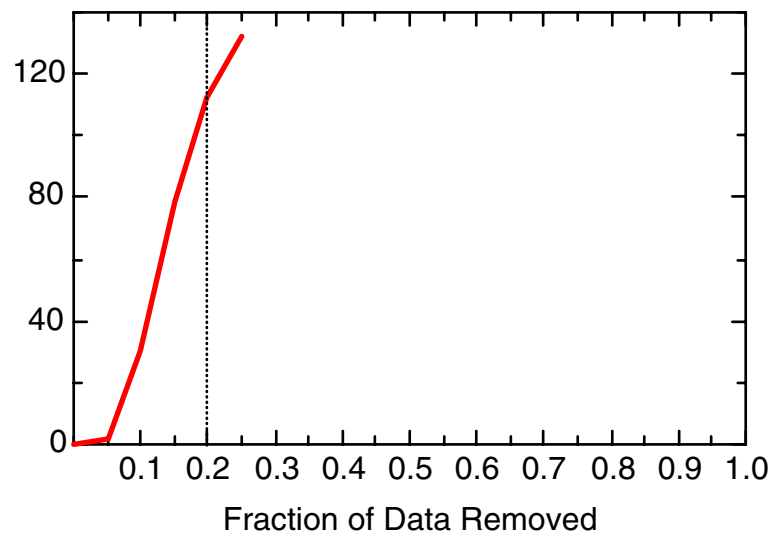
TCE: Well 49-5568(D)



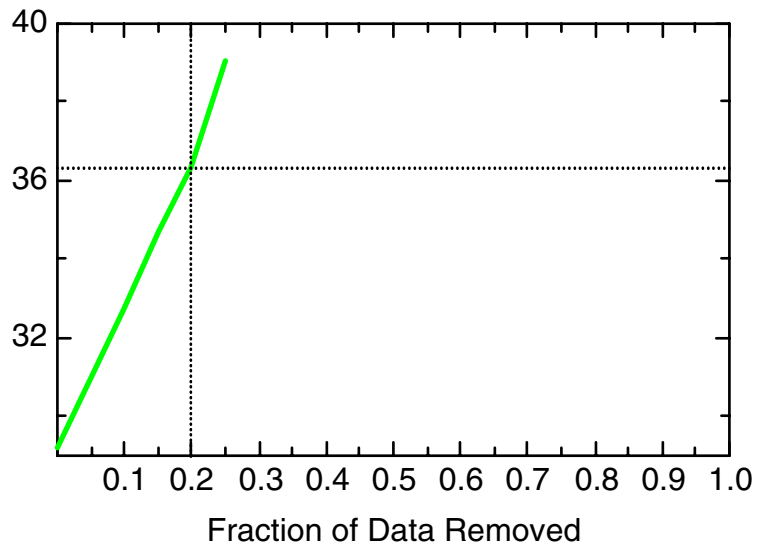
TCE: Well 49-5573(D)



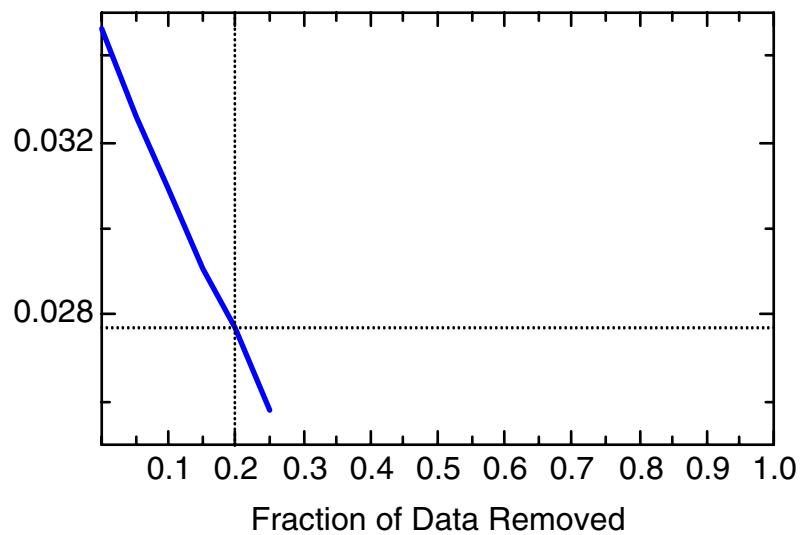
TCE: Well 49-5573(D)



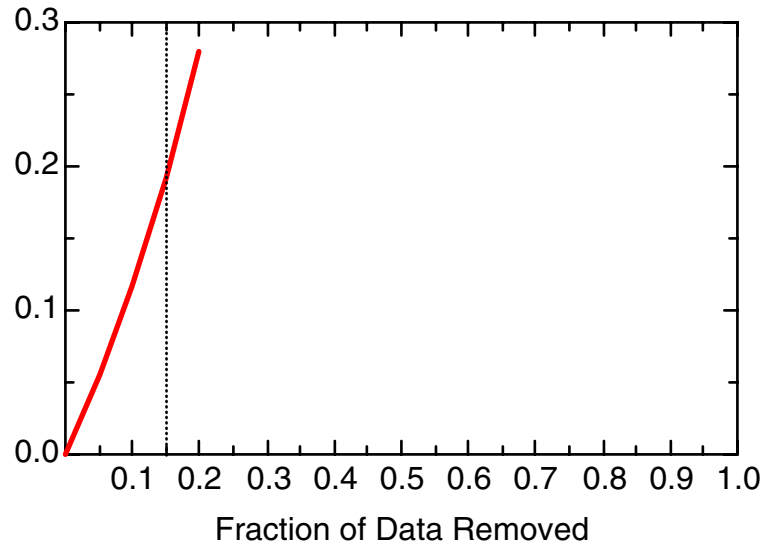
TCE: Well 49-5573(D)



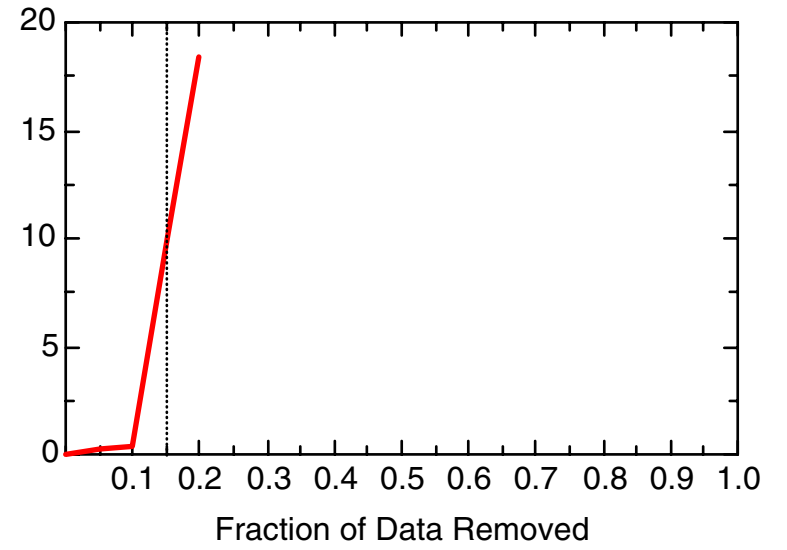
TCE: Well 49-5573(D)



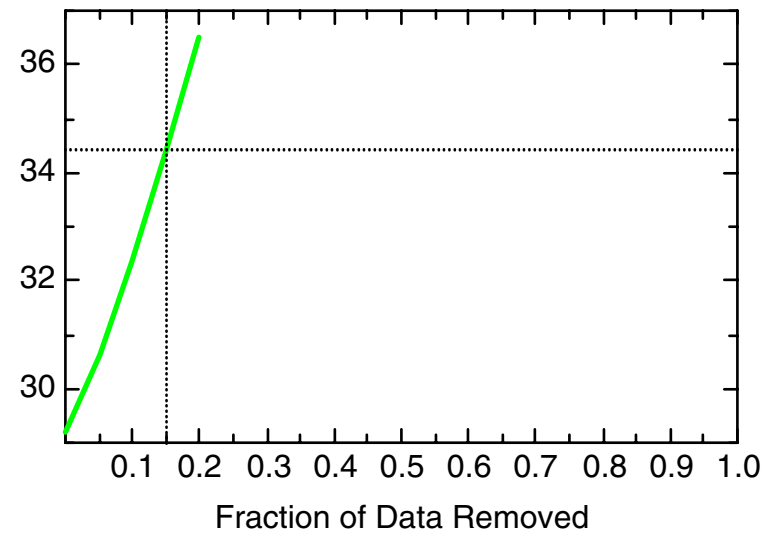
TCE: Well 49-5574(S)



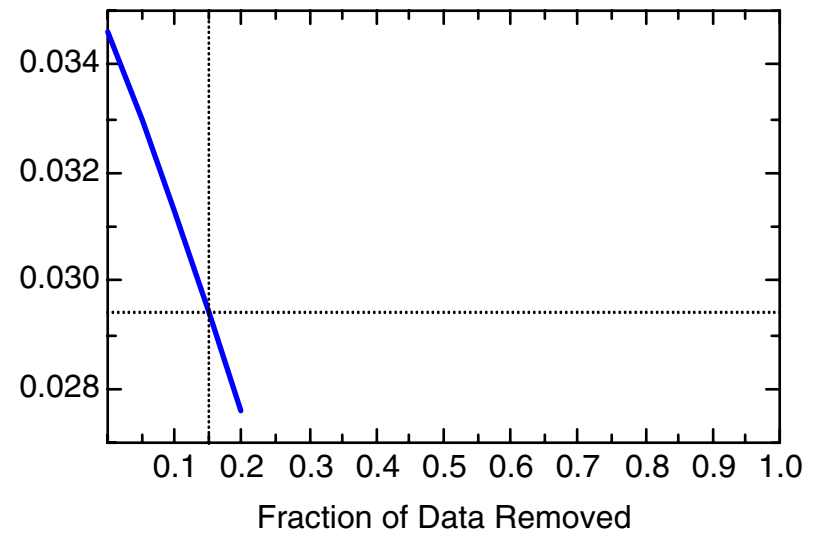
TCE: Well 49-5574(S)



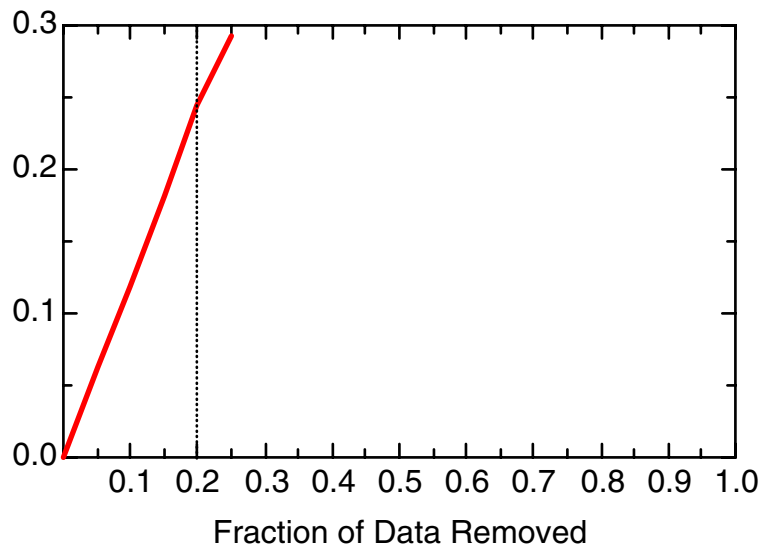
TCE: Well 49-5574(S)



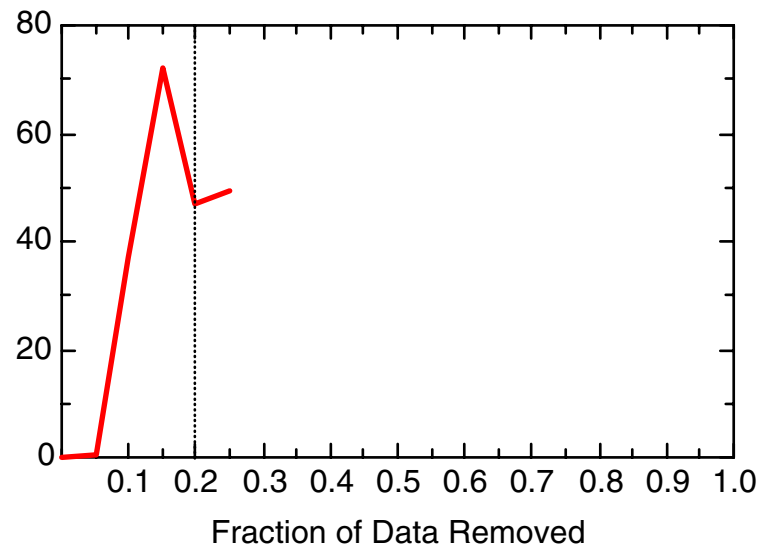
TCE: Well 49-5574(S)



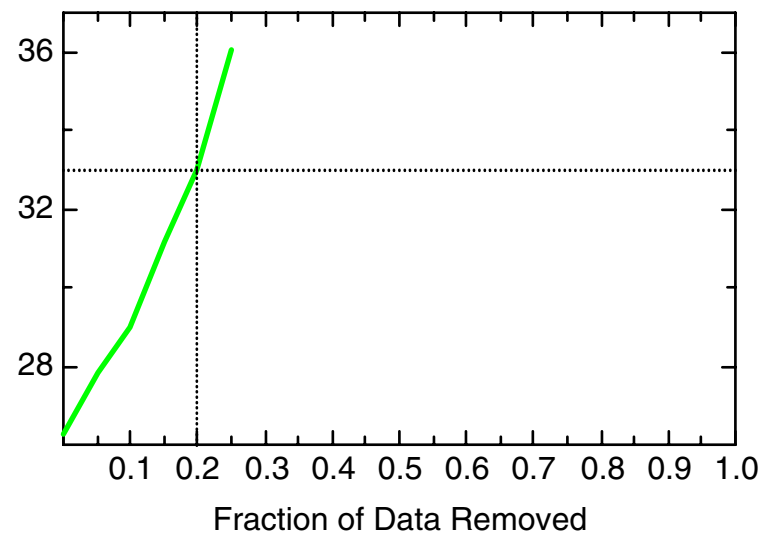
TCE: Well 49-5577(D)



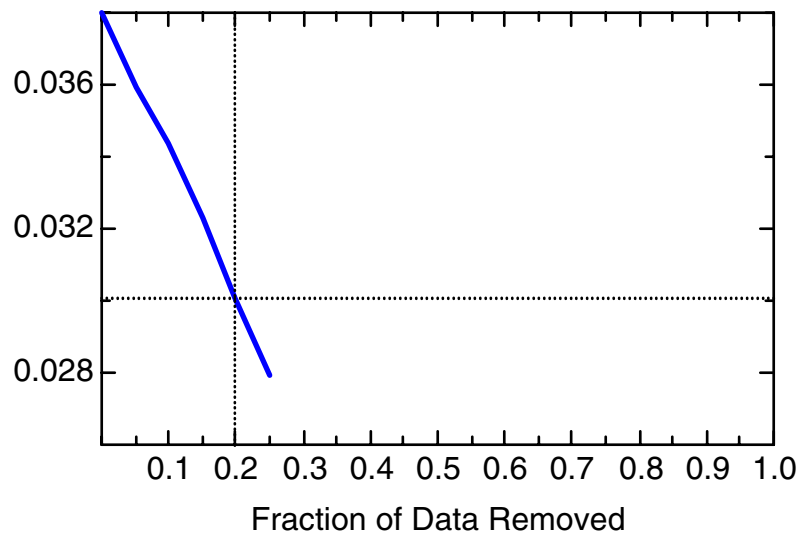
TCE: Well 49-5577(D)



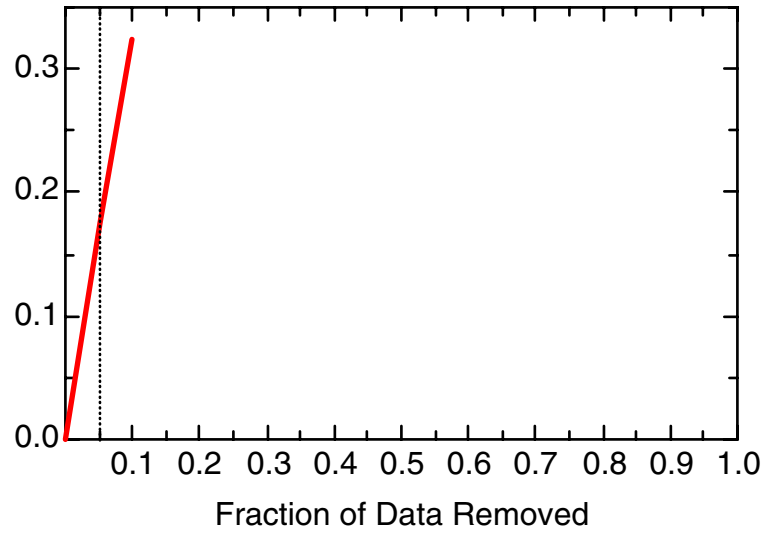
TCE: Well 49-5577(D)



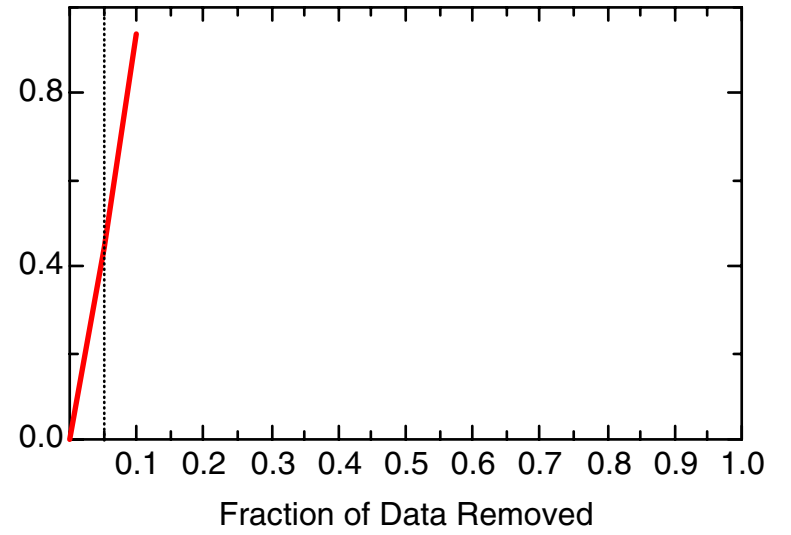
TCE: Well 49-5577(D)



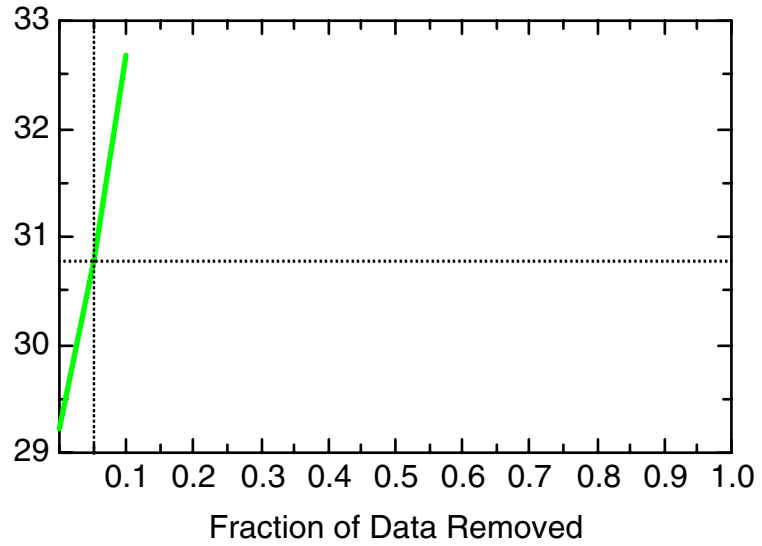
TCE: Well 49-5578(S)



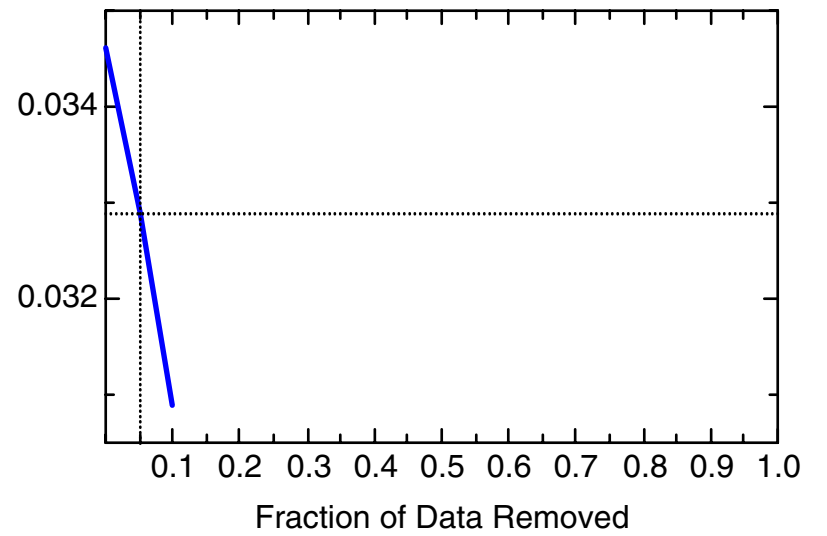
TCE: Well 49-5578(S)



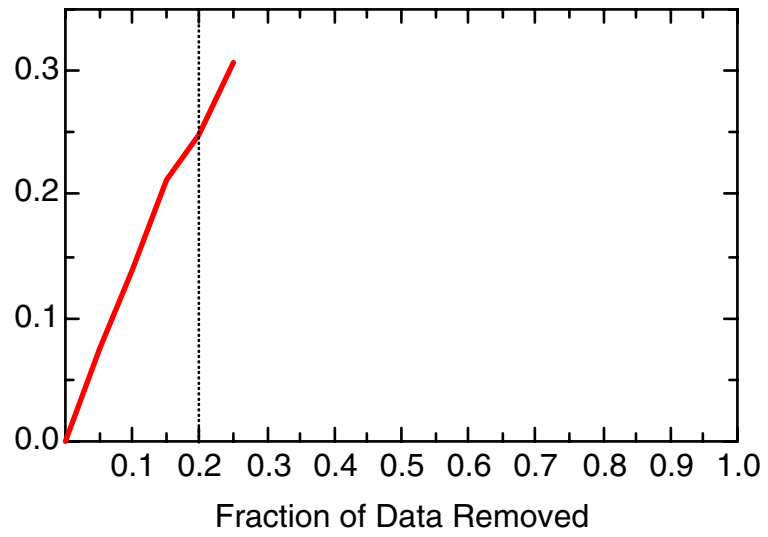
TCE: Well 49-5578(S)



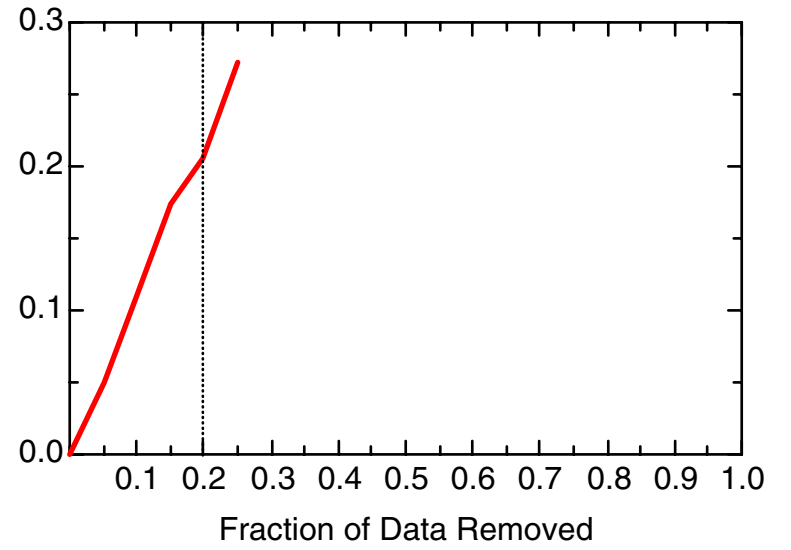
TCE: Well 49-5578(S)



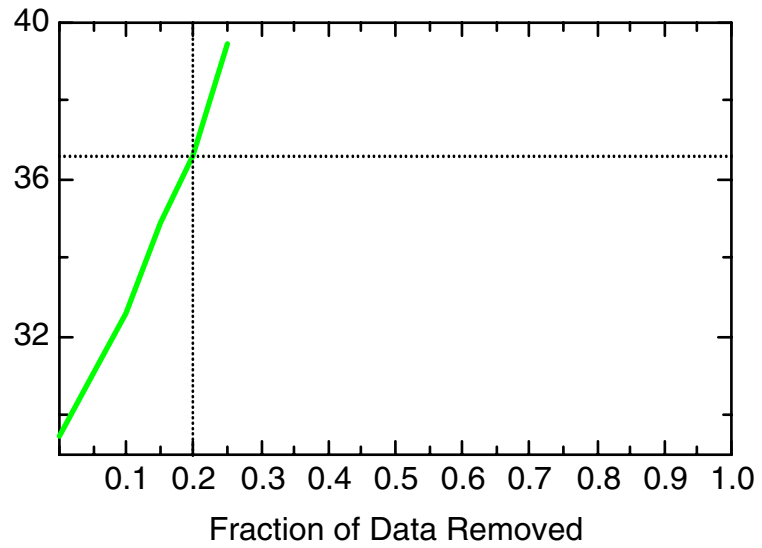
TCE: Well 49-6515(S)



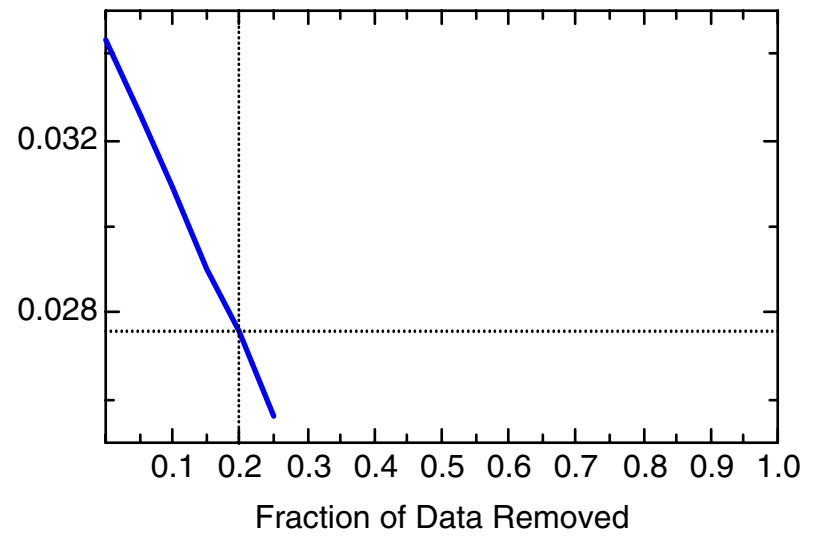
TCE: Well 49-6515(S)



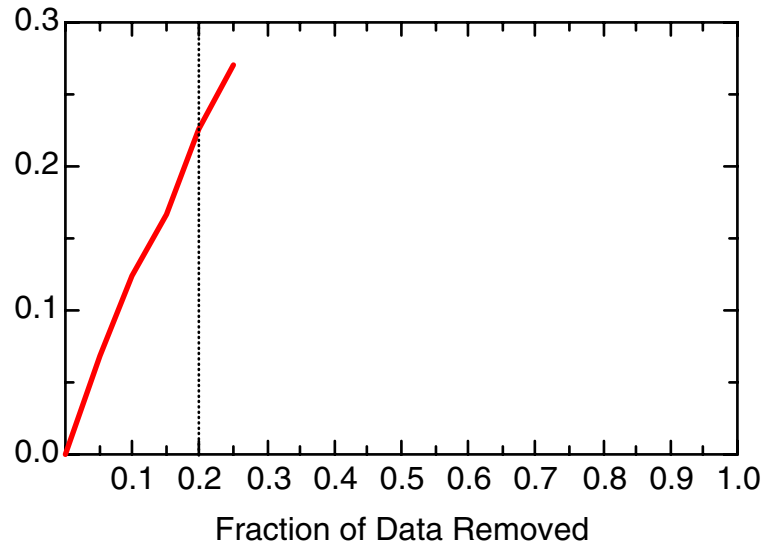
TCE: Well 49-6515(S)



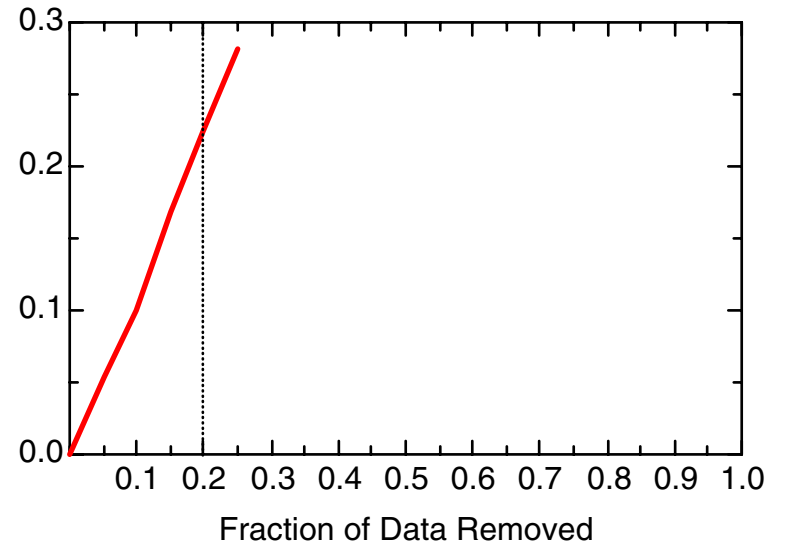
TCE: Well 49-6515(S)



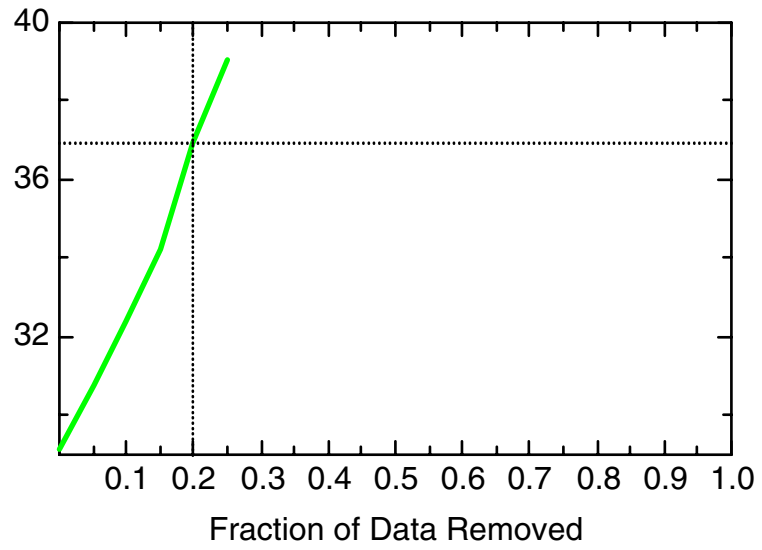
TCE: Well 49-6516(S)



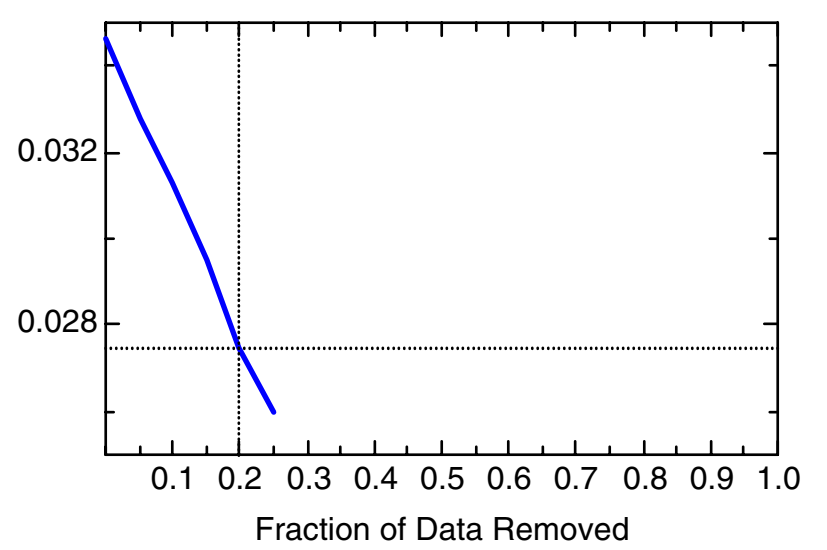
TCE: Well 49-6516(S)



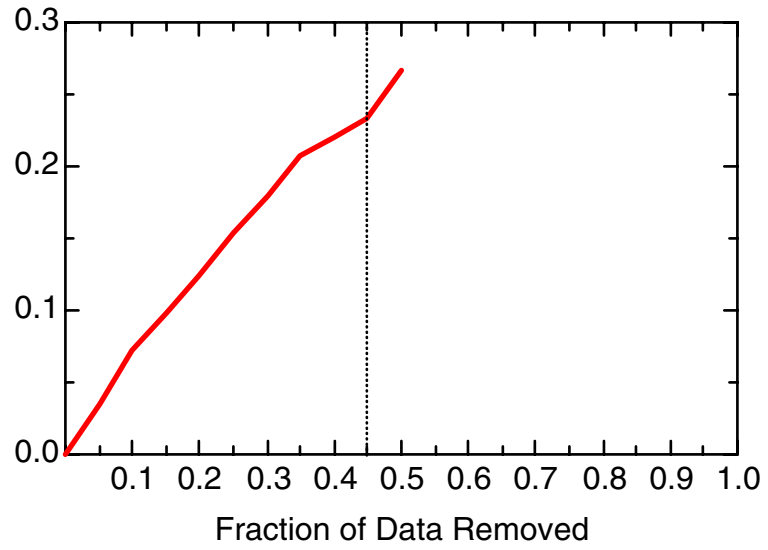
TCE: Well 49-6516(S)



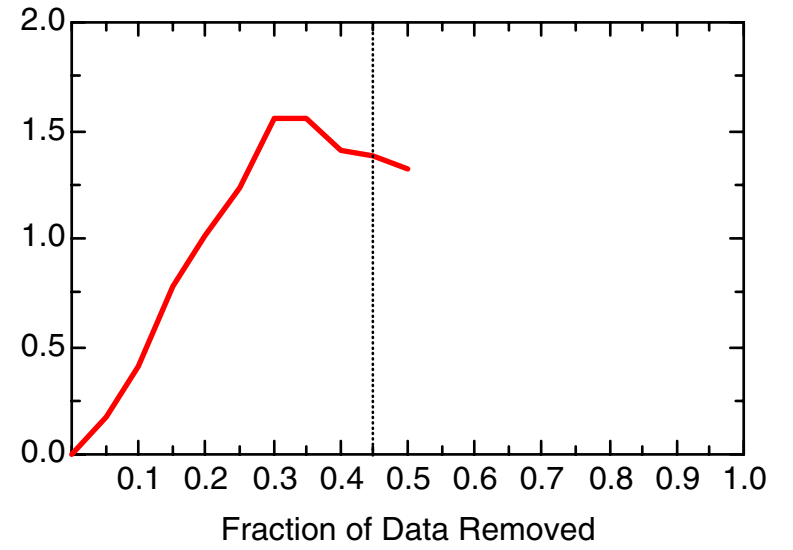
TCE: Well 49-6516(S)



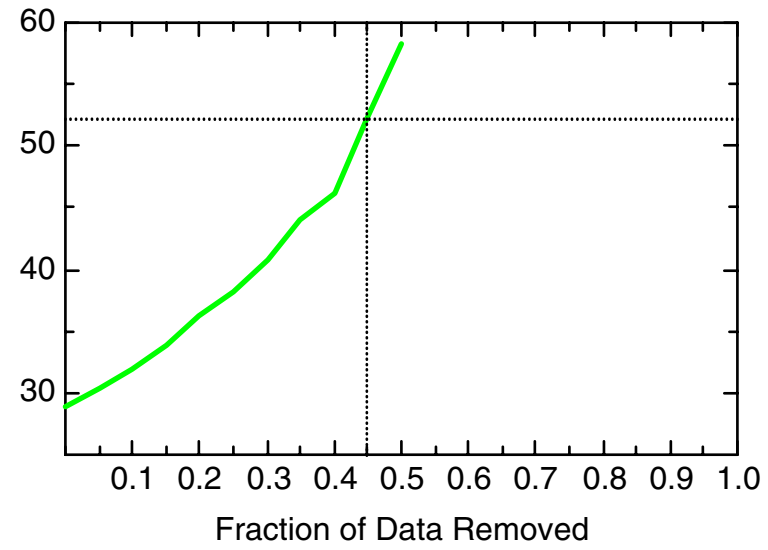
TCE: Well 49-MW01



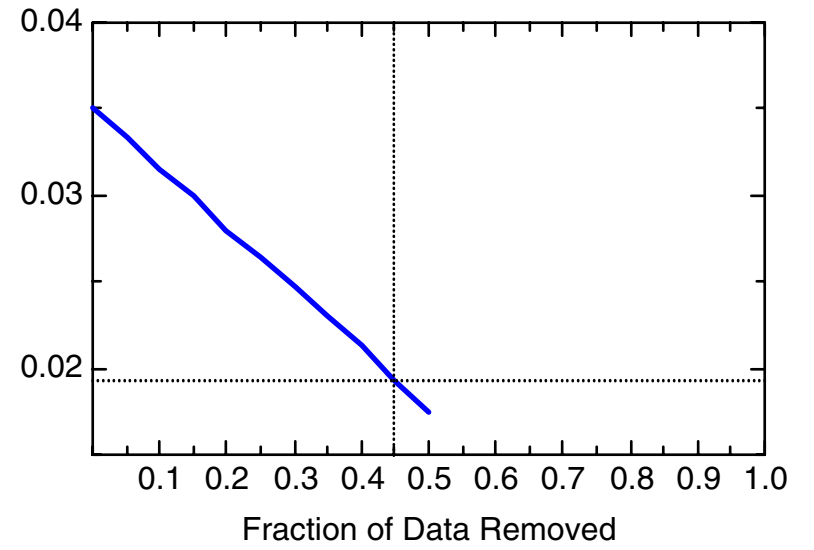
TCE: Well 49-MW01



TCE: Well 49-MW01



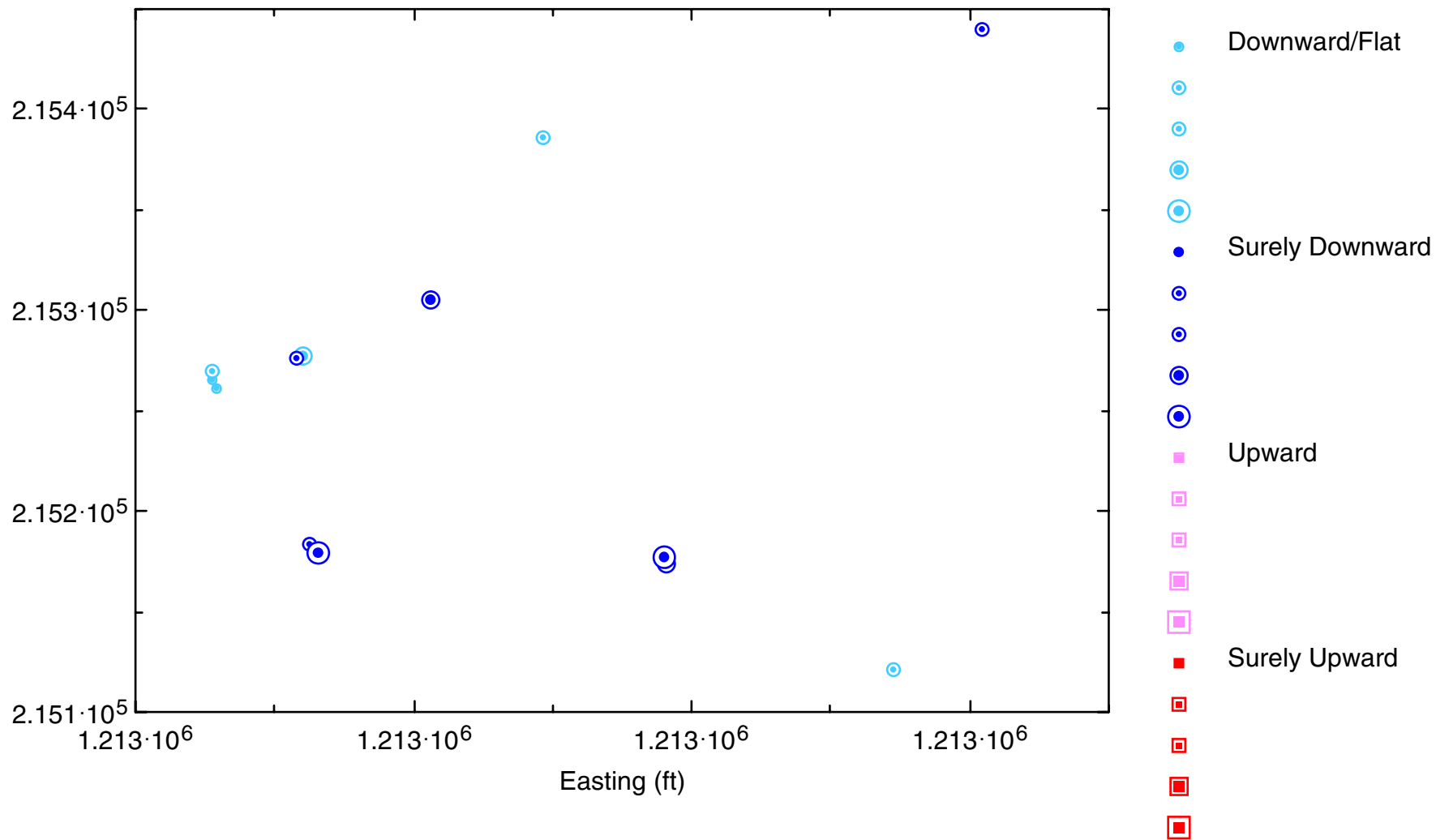
TCE: Well 49-MW01



# Appendix 3.4

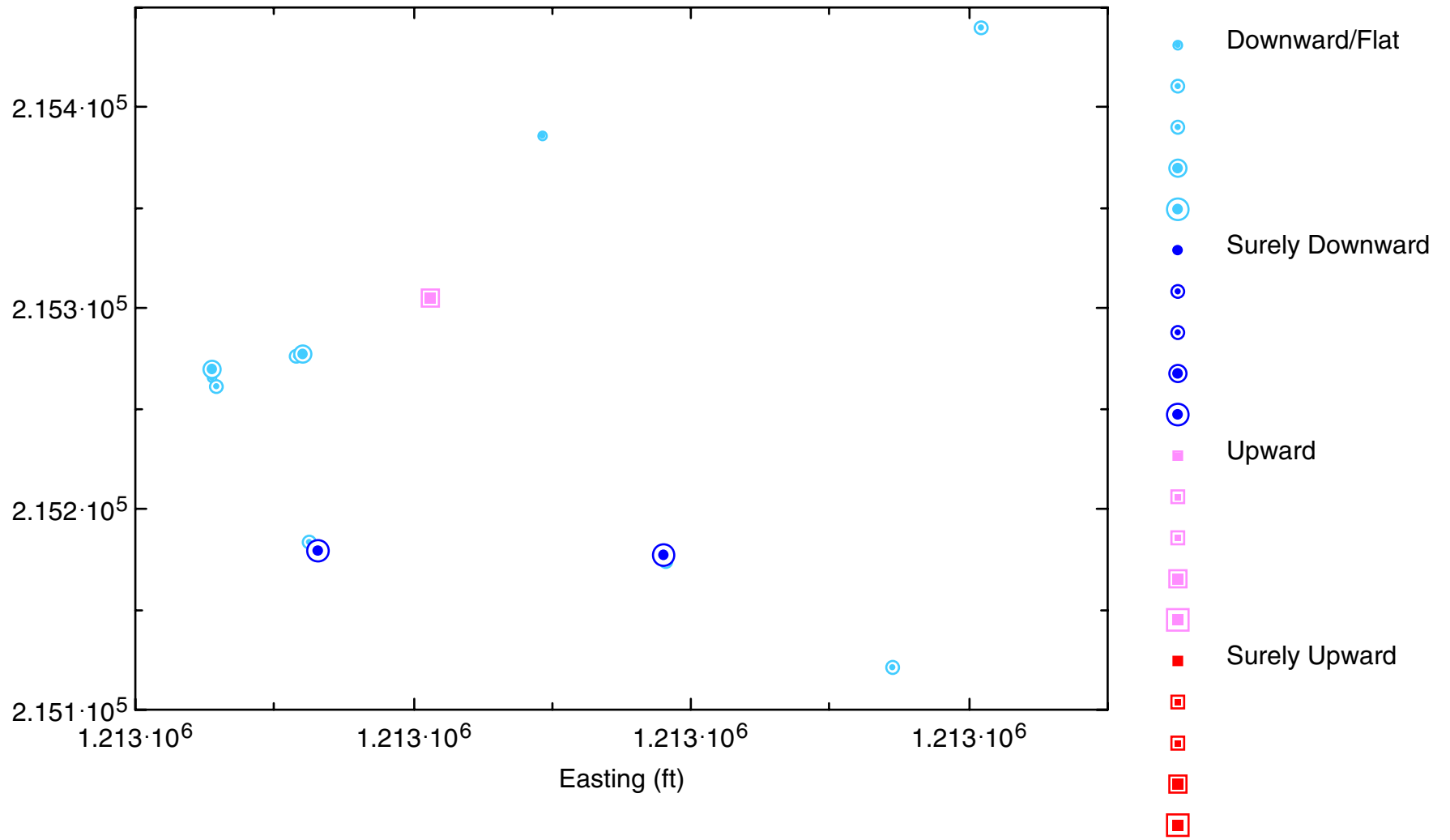
## Trend Maps

Post-Plot of Historical Median Trends for DCA11

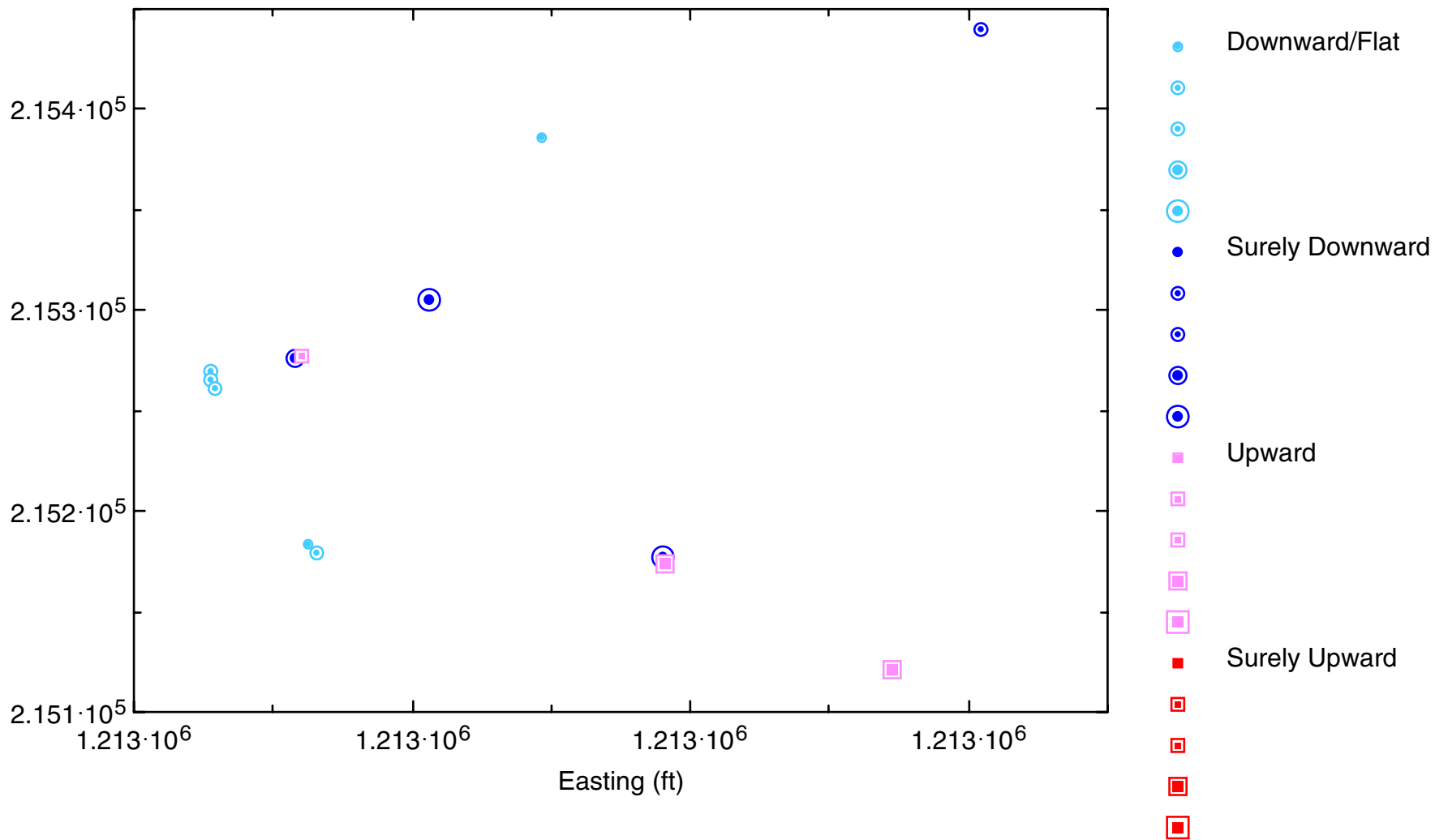




Post-Plot of New (Last 4 Sampling Events) Median Trends for DCA11

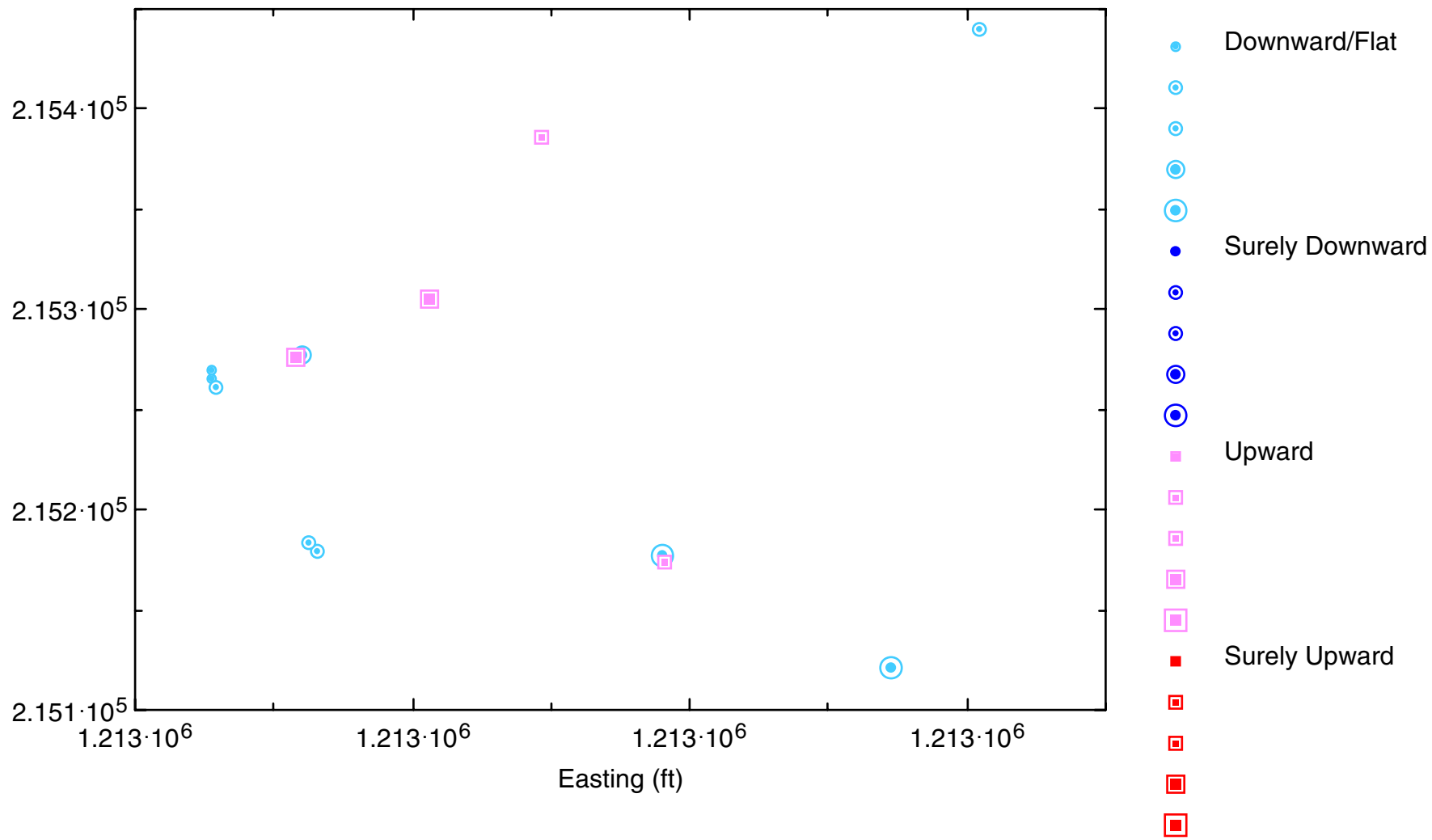


Post-Plot of Historical Median Trends for DCE12C

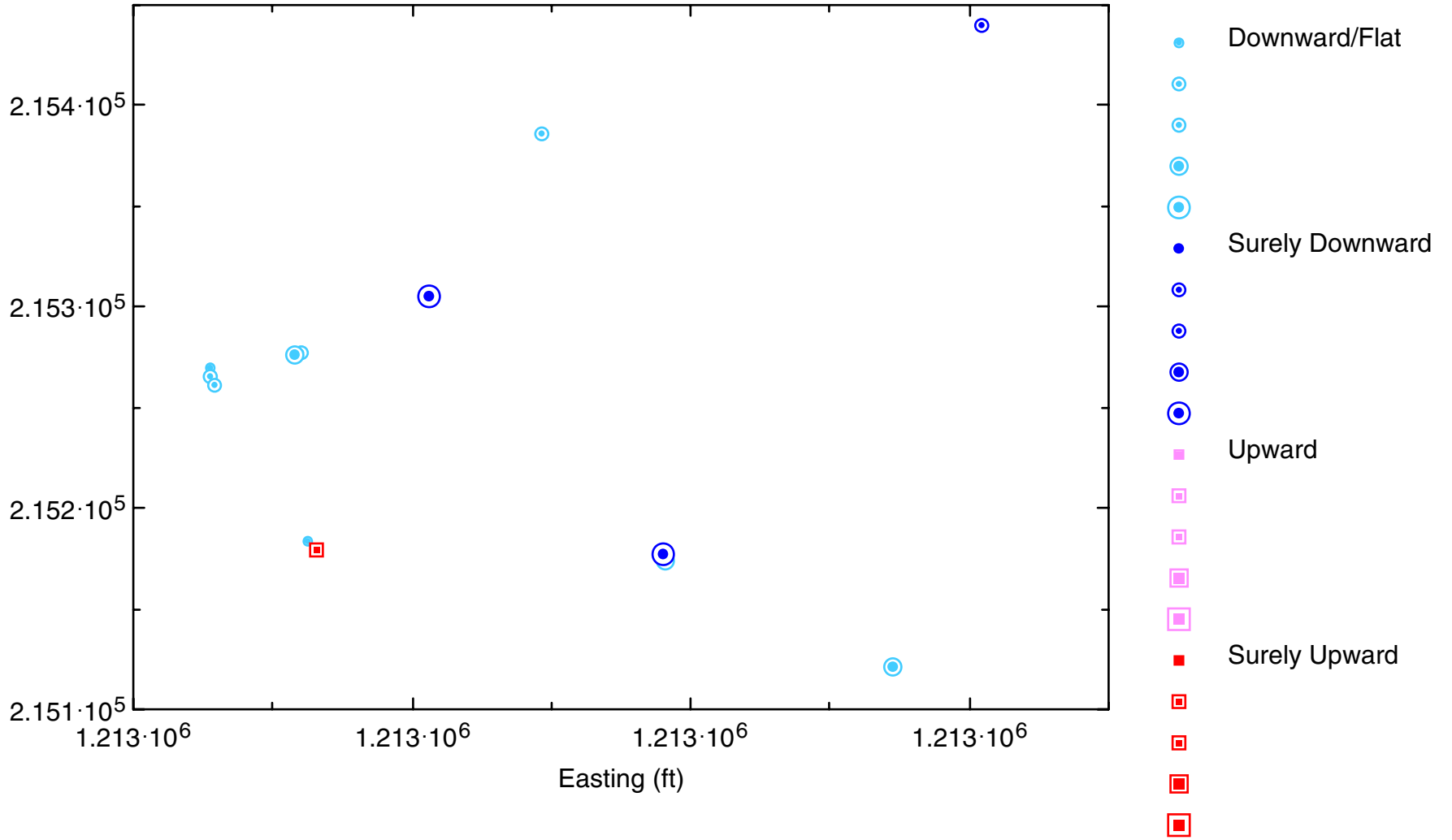




Post-Plot of New (Last 4 Sampling Events) Median Trends for DCE12C



Post-Plot of Historical Median Trends for TCI





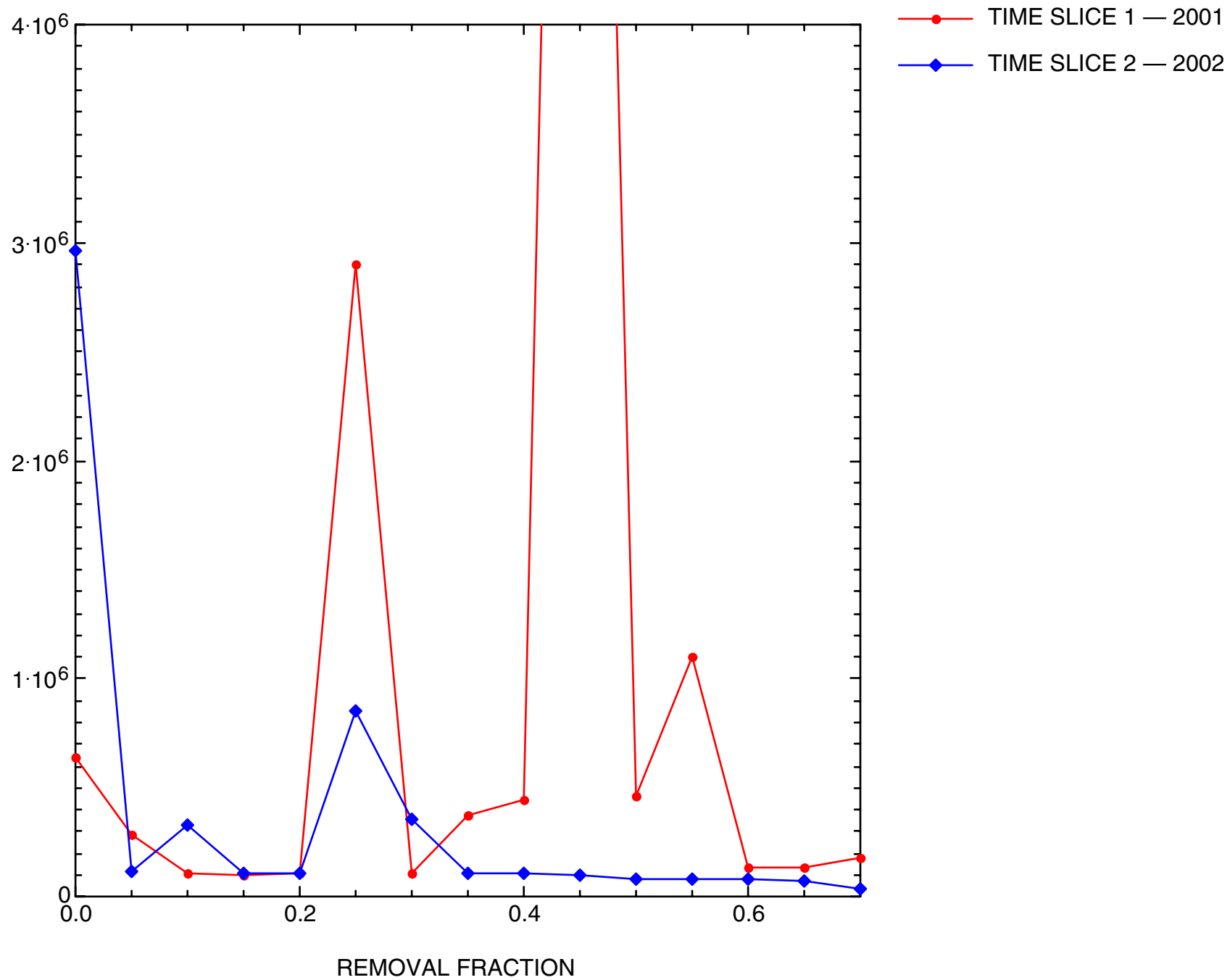


# Appendix 4.1

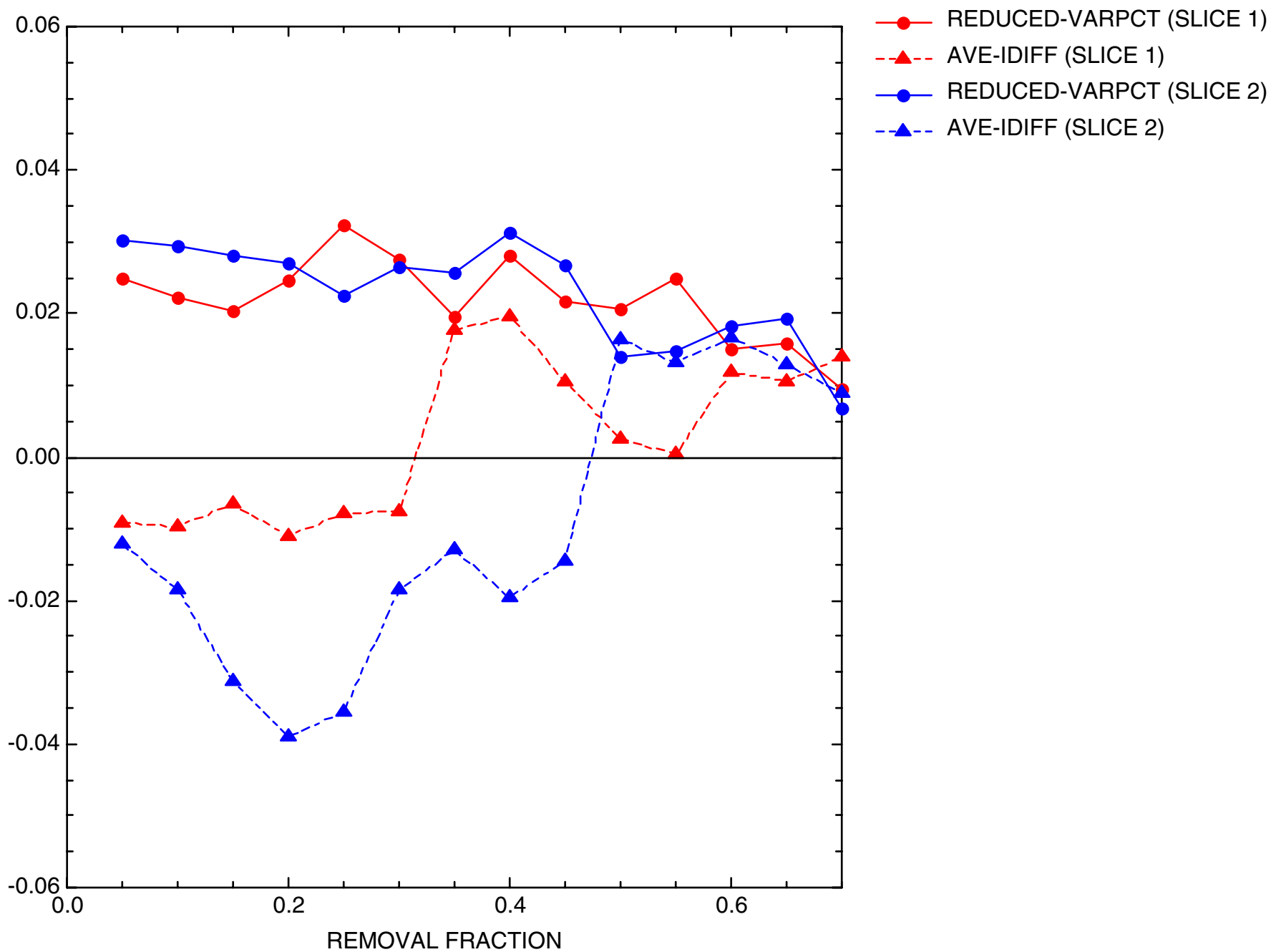
## Global Redundancy Measures

DCA11

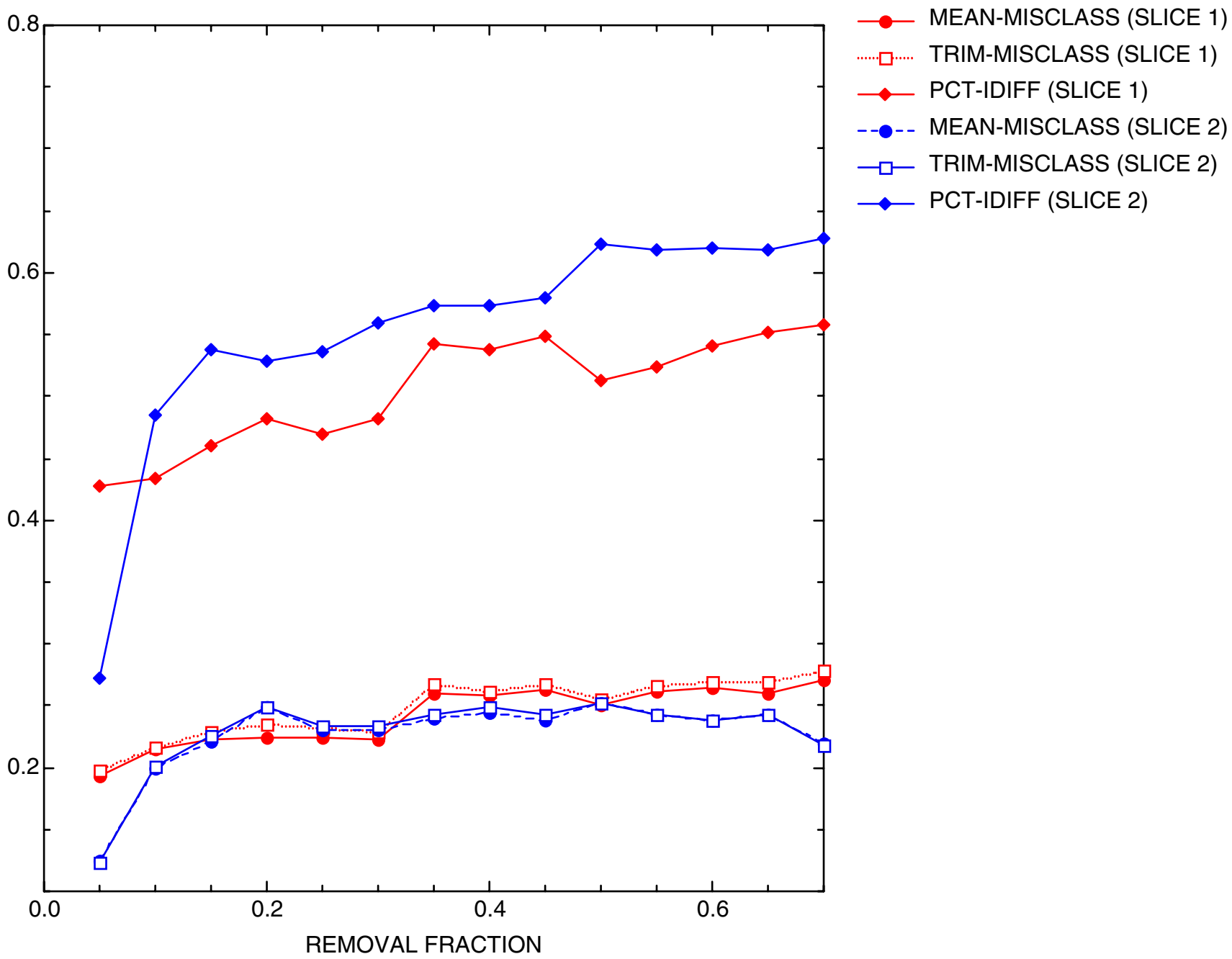
PEASE AFB, SITE 49: DCA11 TRENDS IN GLOBAL VARIANCE



PEASE AFB, SITE 49: DCA11 GLOBAL REDUNDANCY MEASURES, PART 1

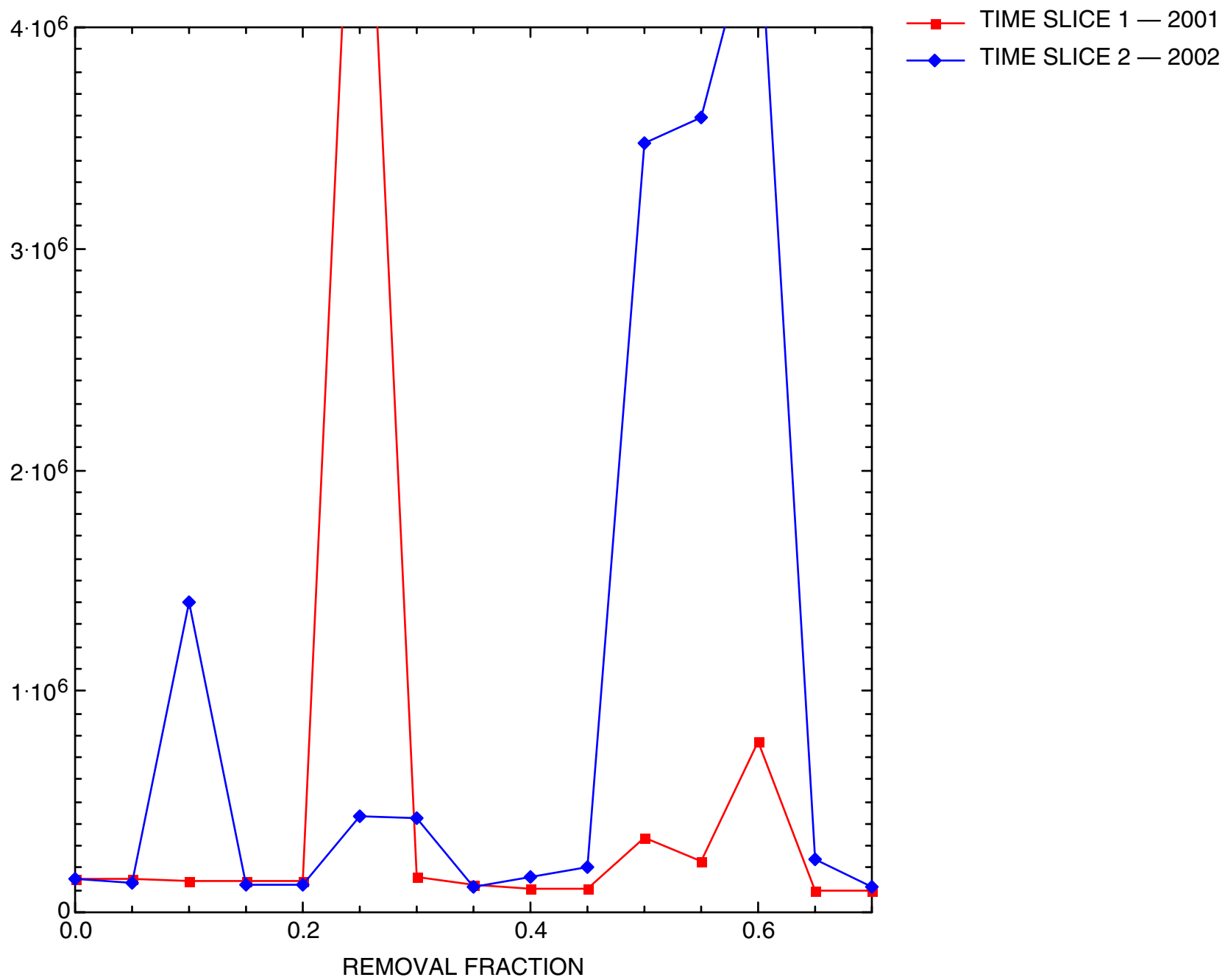


PEASE AFB, SITE 49: DCA11 GLOBAL REDUNDANCY MEASURES, PART 2

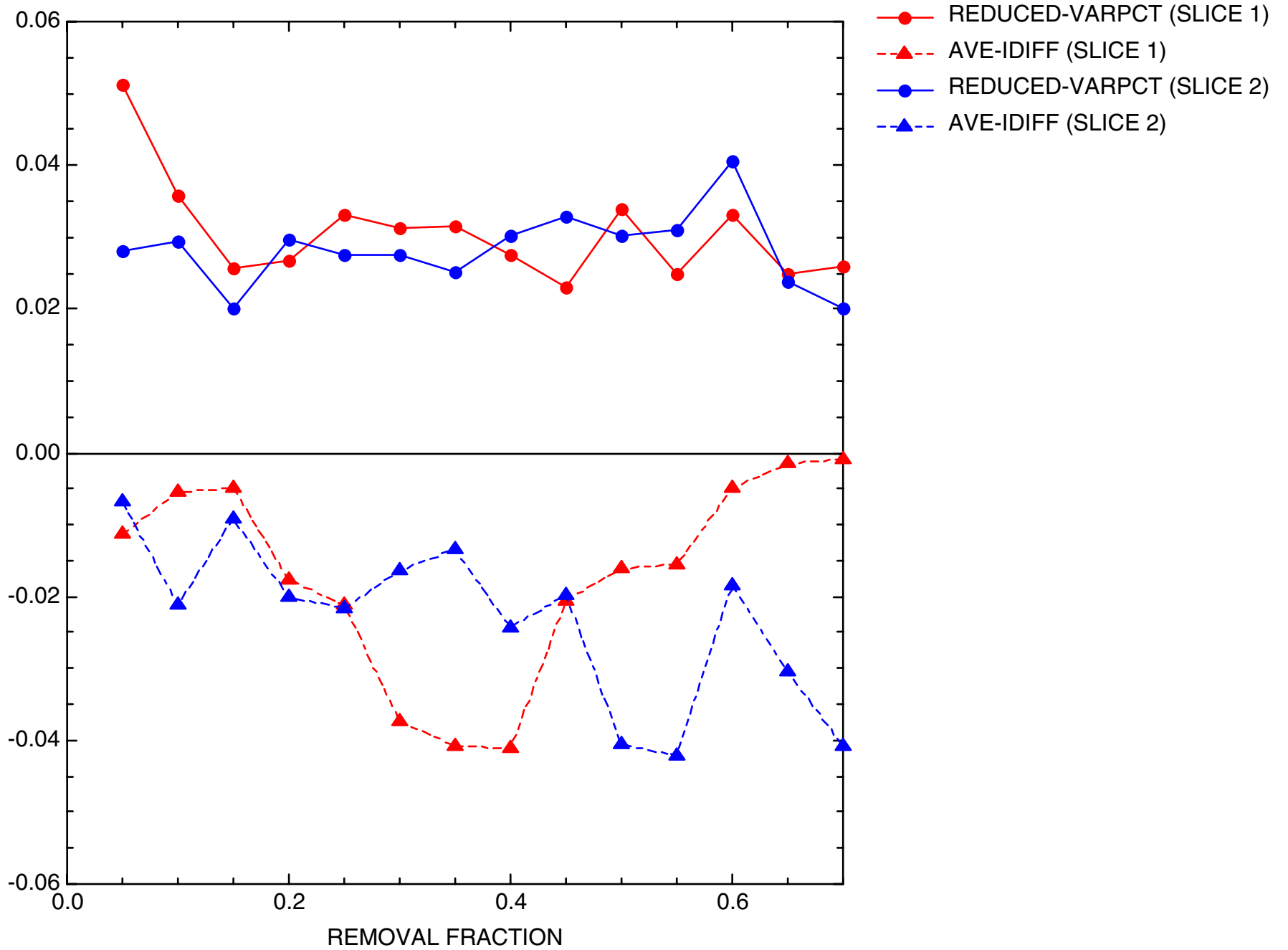


DCE12C

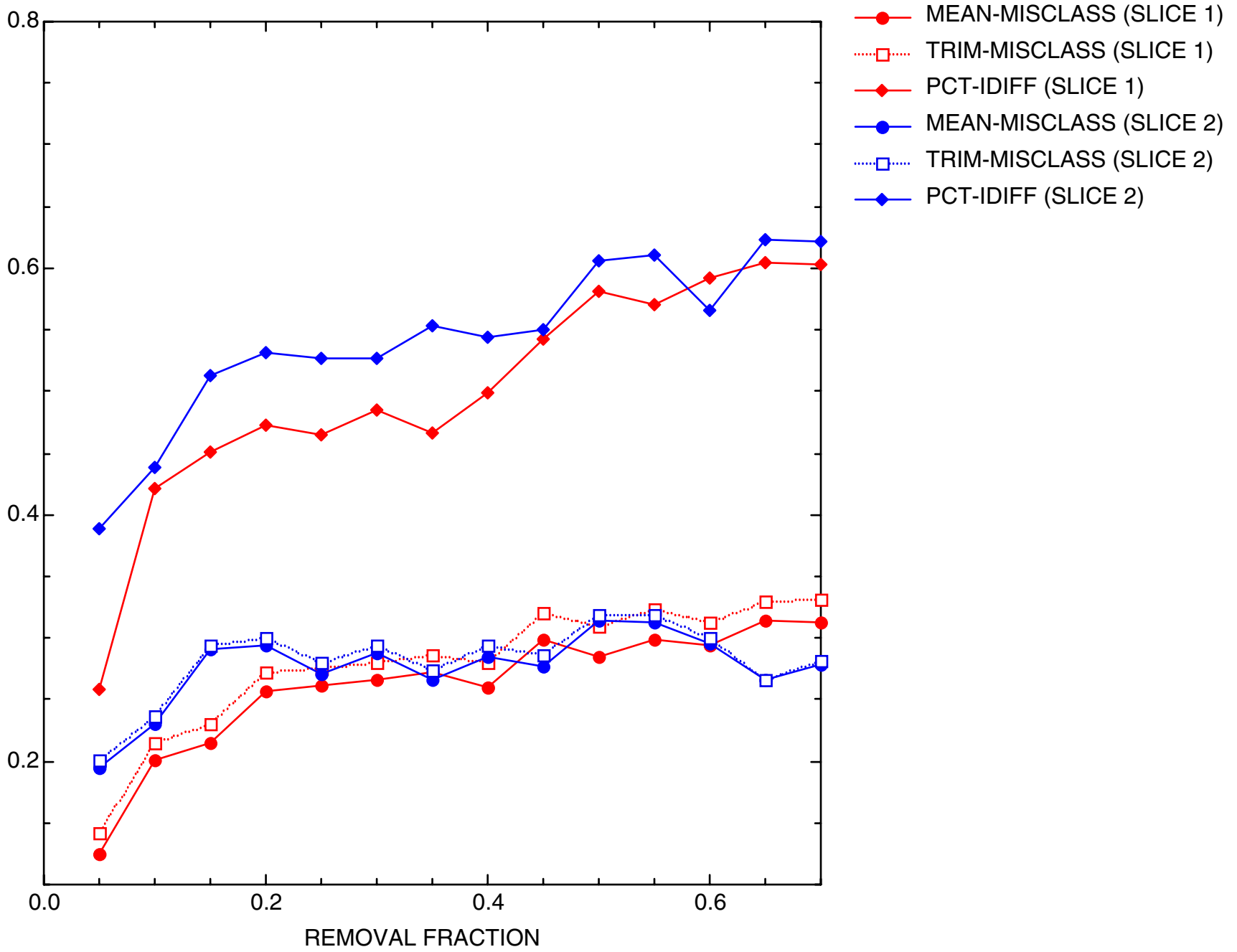
PEASE AFB, SITE 49: DCE12C TRENDS IN GLOBAL VARIANCE



PEASE AFB, SITE 49: DCE12C GLOBAL REDUNDANCY MEASURES, PART 1

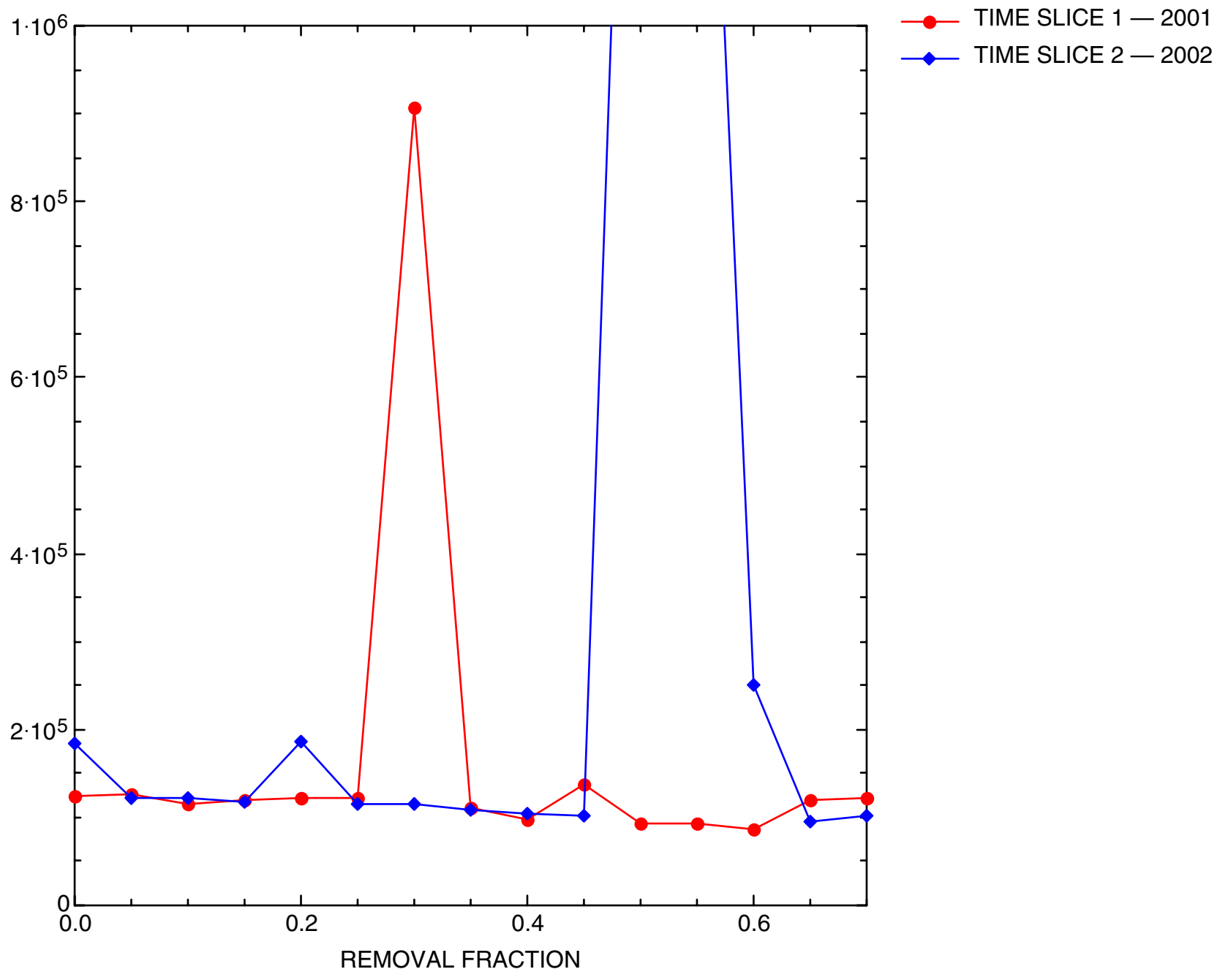


PEASE AFB, SITE 49: DCE12C GLOBAL REDUNDANCY MEASURES, PART 2

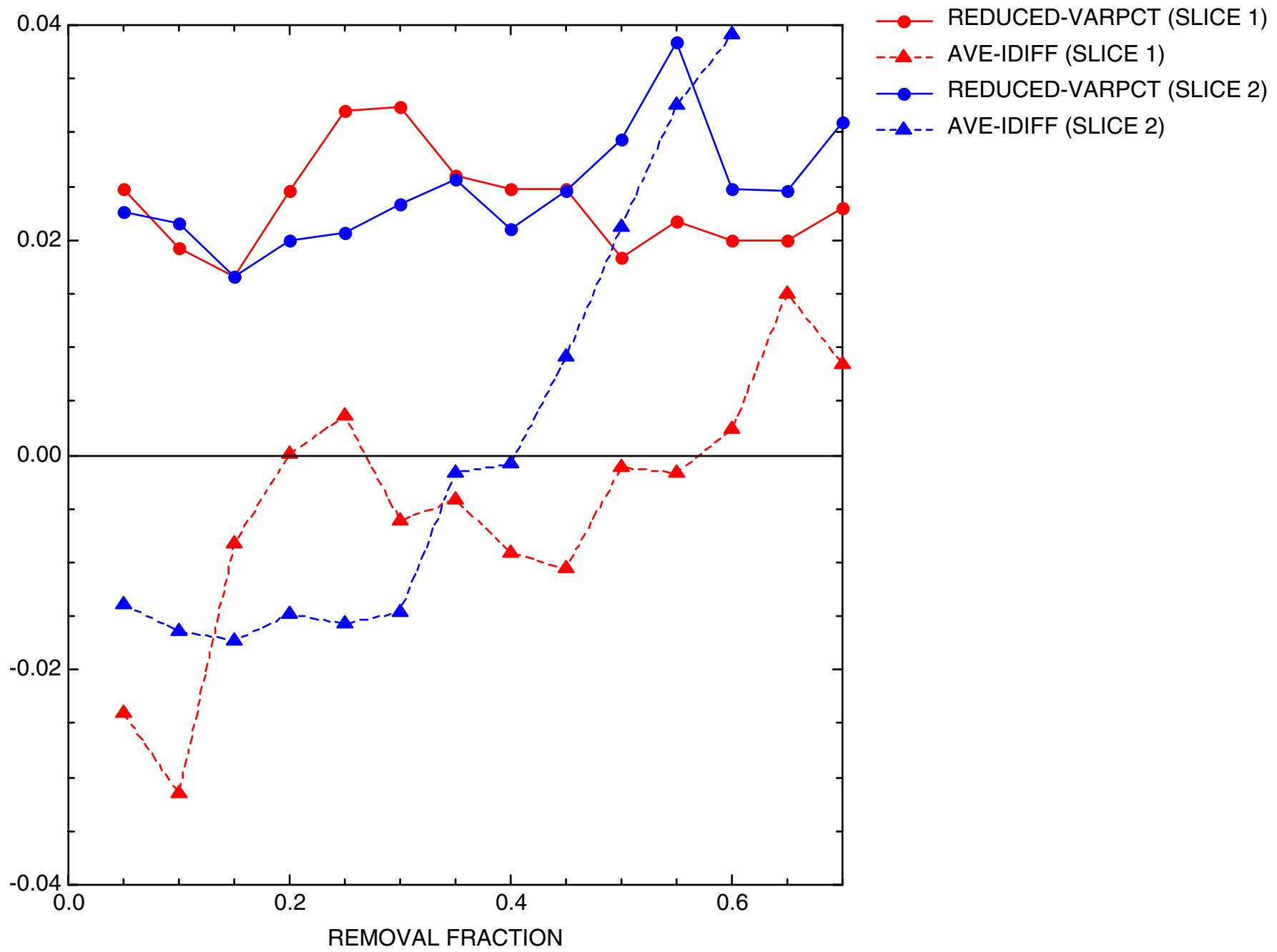


TCE

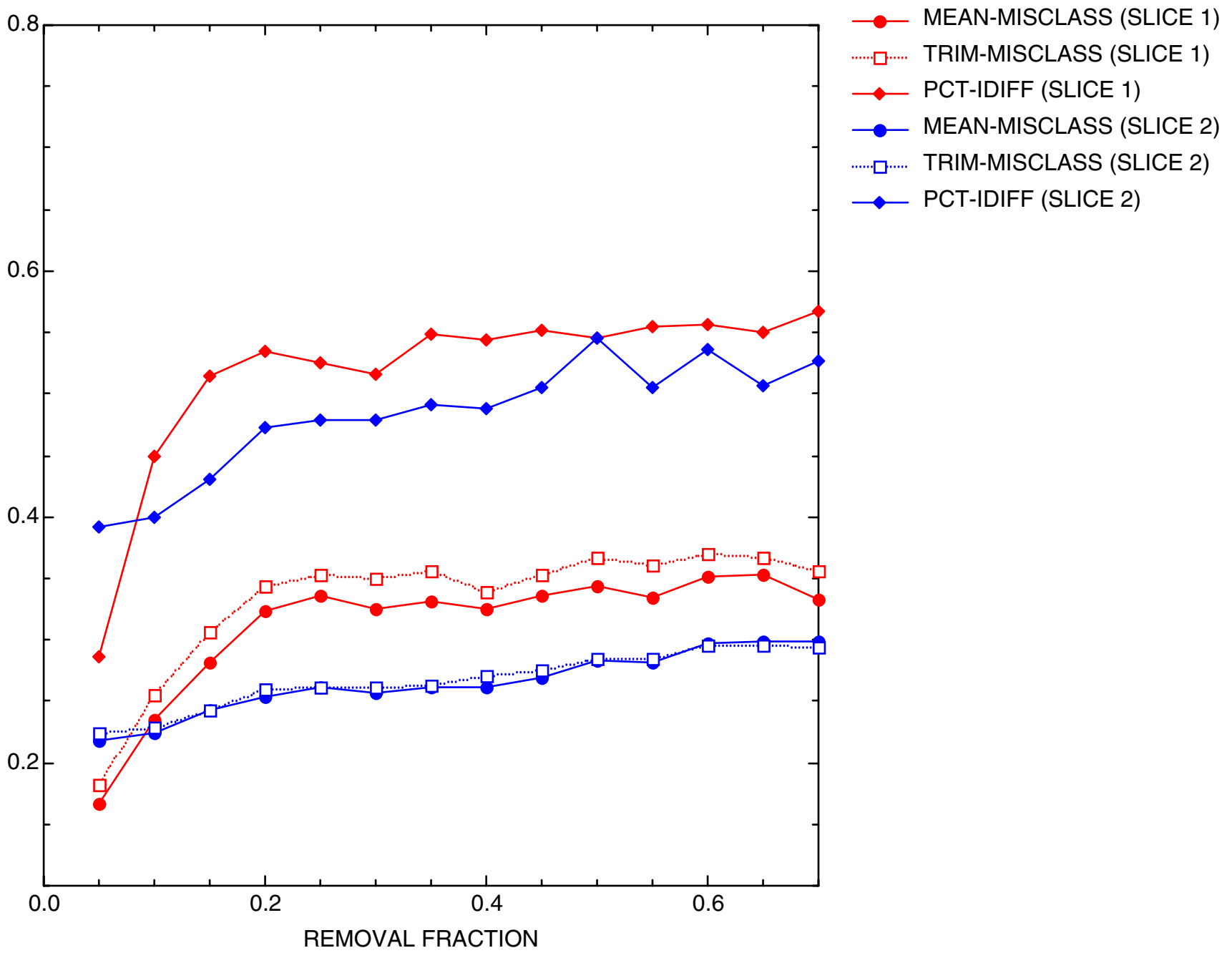
PEASE AFB, SITE 49: TCE TRENDS IN GLOBAL VARIANCE



PEASE AFB, SITE 49: TCE GLOBAL REDUNDANCY MEASURES, PART 1

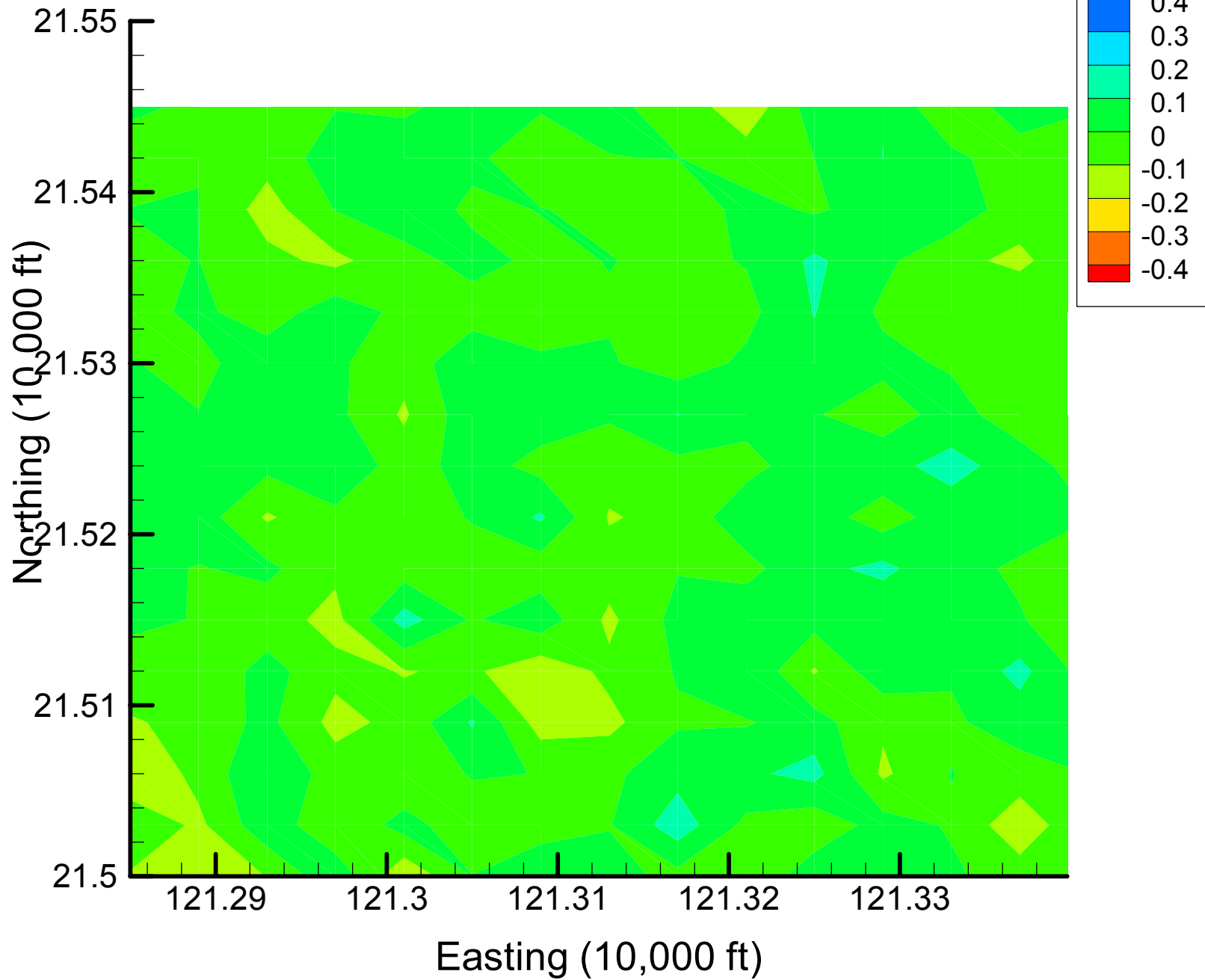


PEASE AFB, SITE 49: TCE GLOBAL REDUNDANCY MEASURES, PART 2

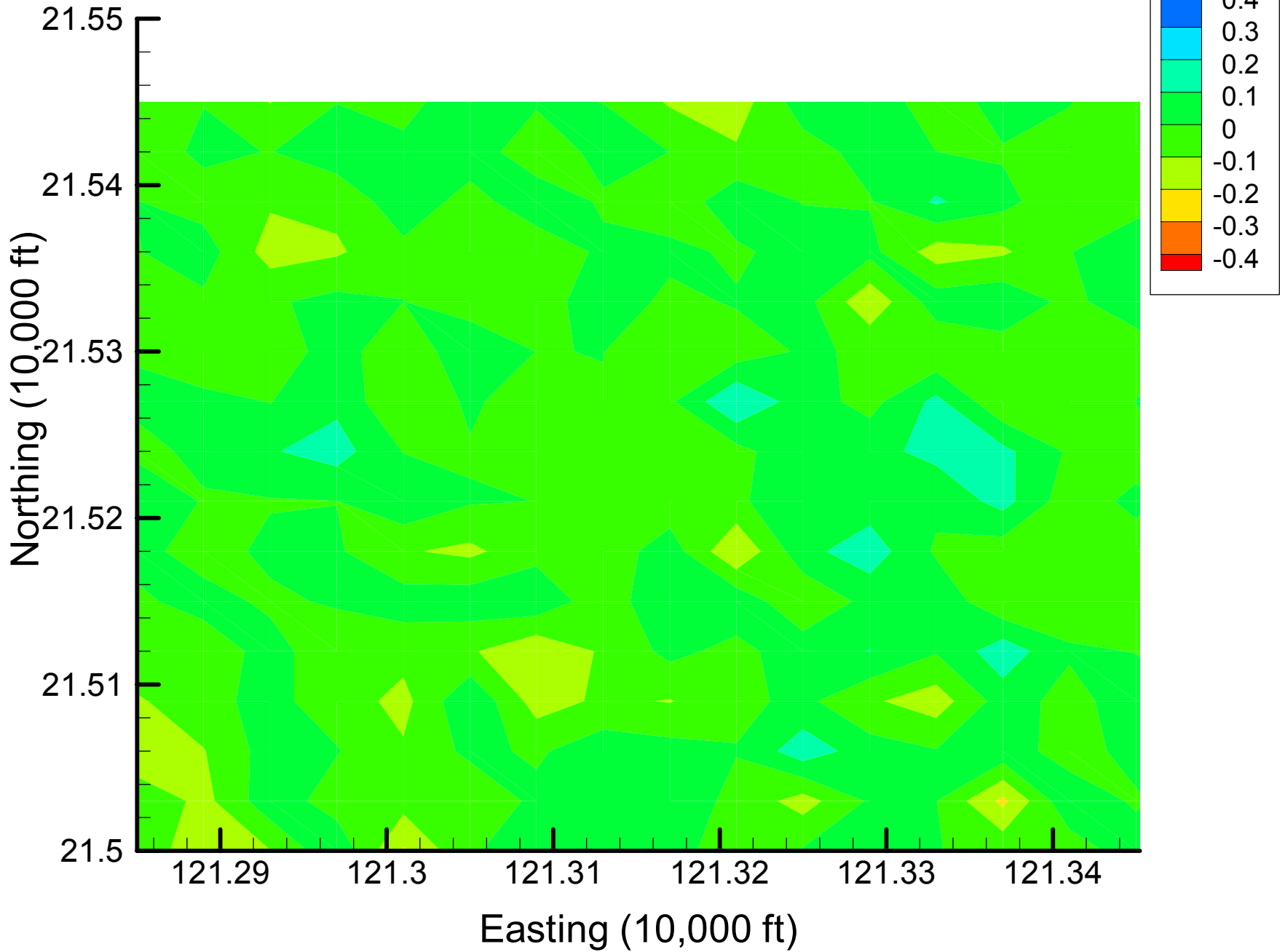


Appendix 4.2  
DCA11 Indicator Difference  
Maps  
Time Slice 1 — 2001

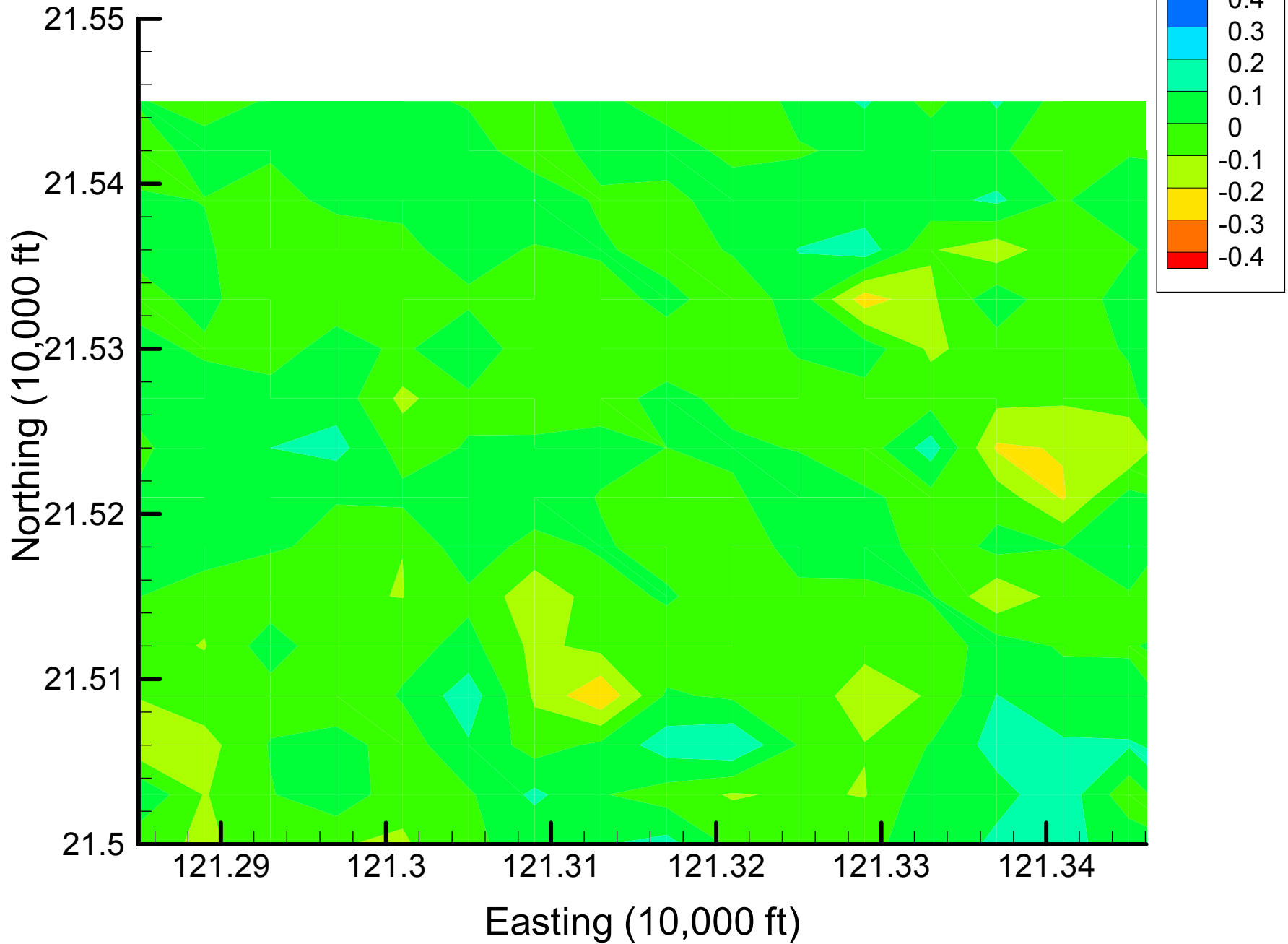
Site 49: DCA11 Indicator Differences, 2001, 5% Removal



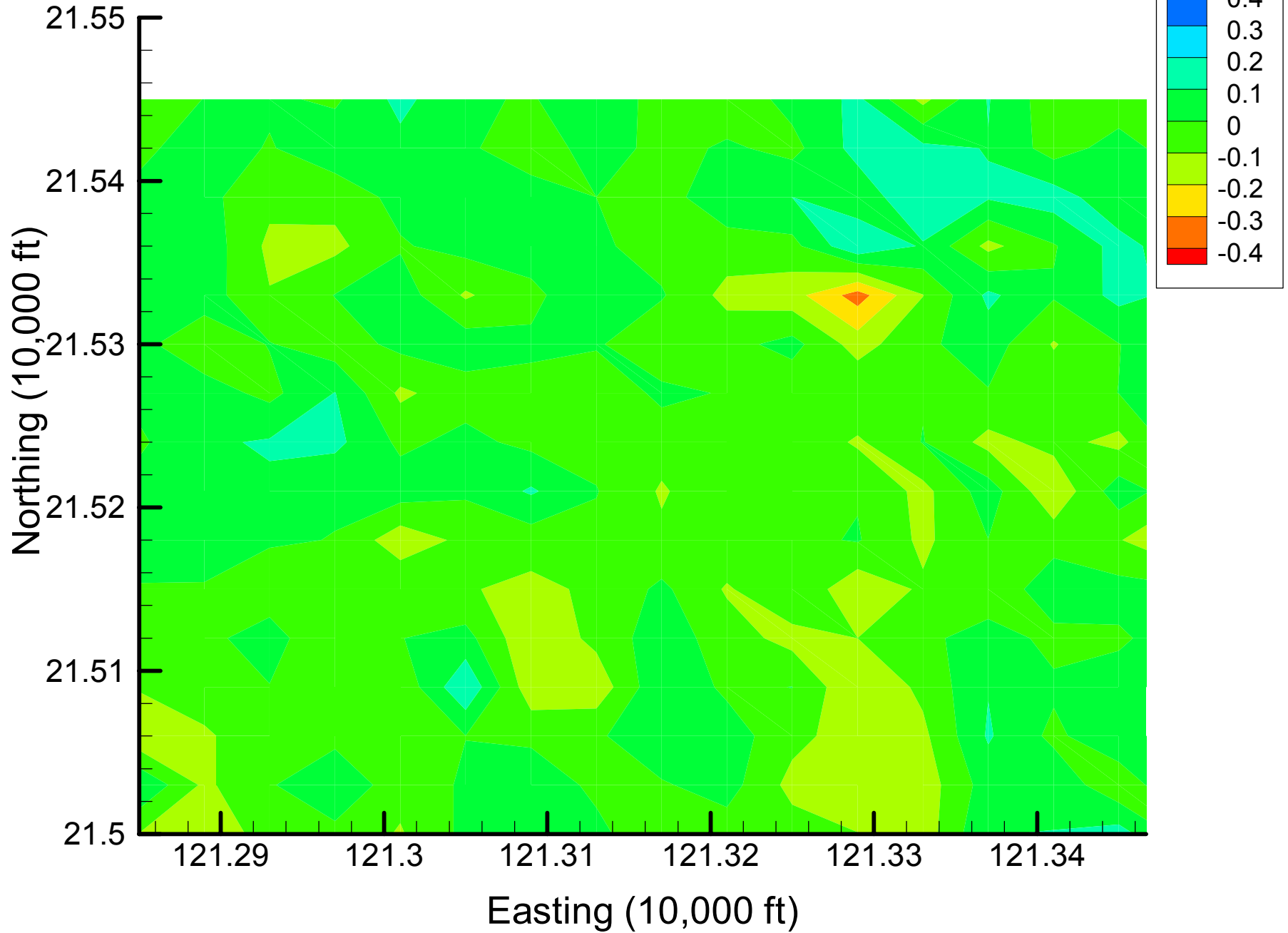
Site 49: DCA11 Indicator Differences, 2001, 10% Removal



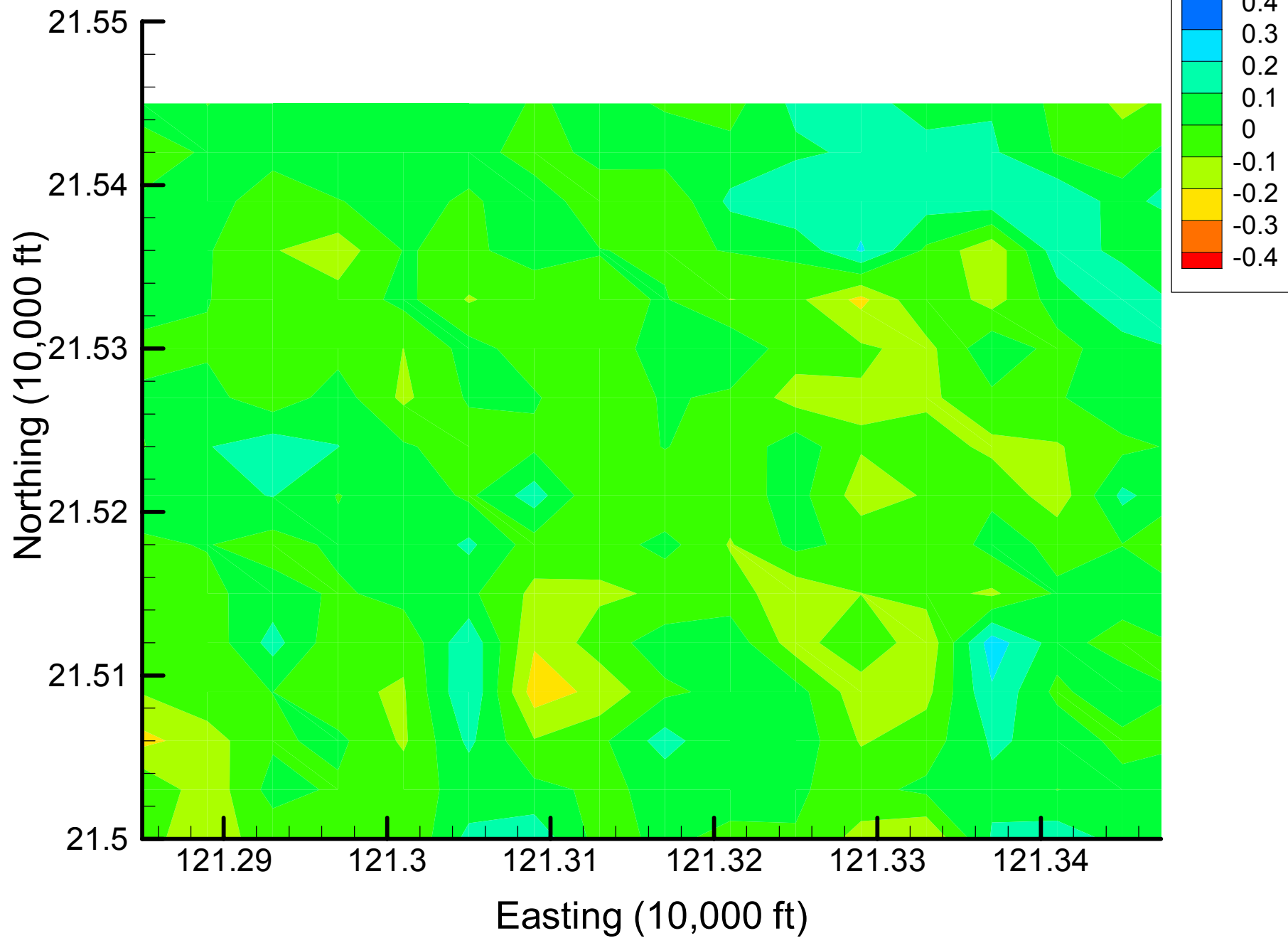
Site 49: DCA11 Indicator Differences, 2001, 15% Removal



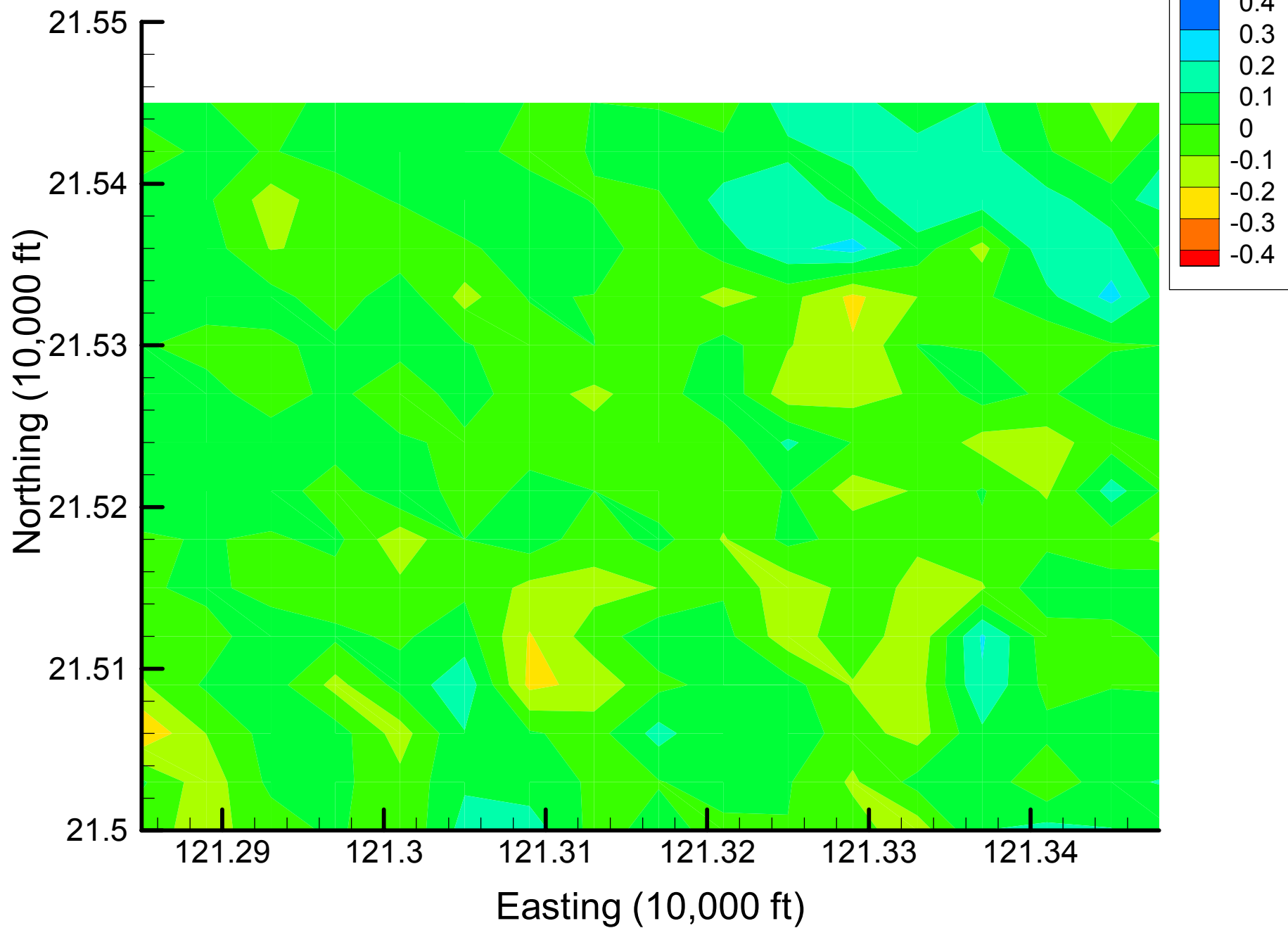
Site 49: DCA11 Indicator Differences, 2001, 20% Removal



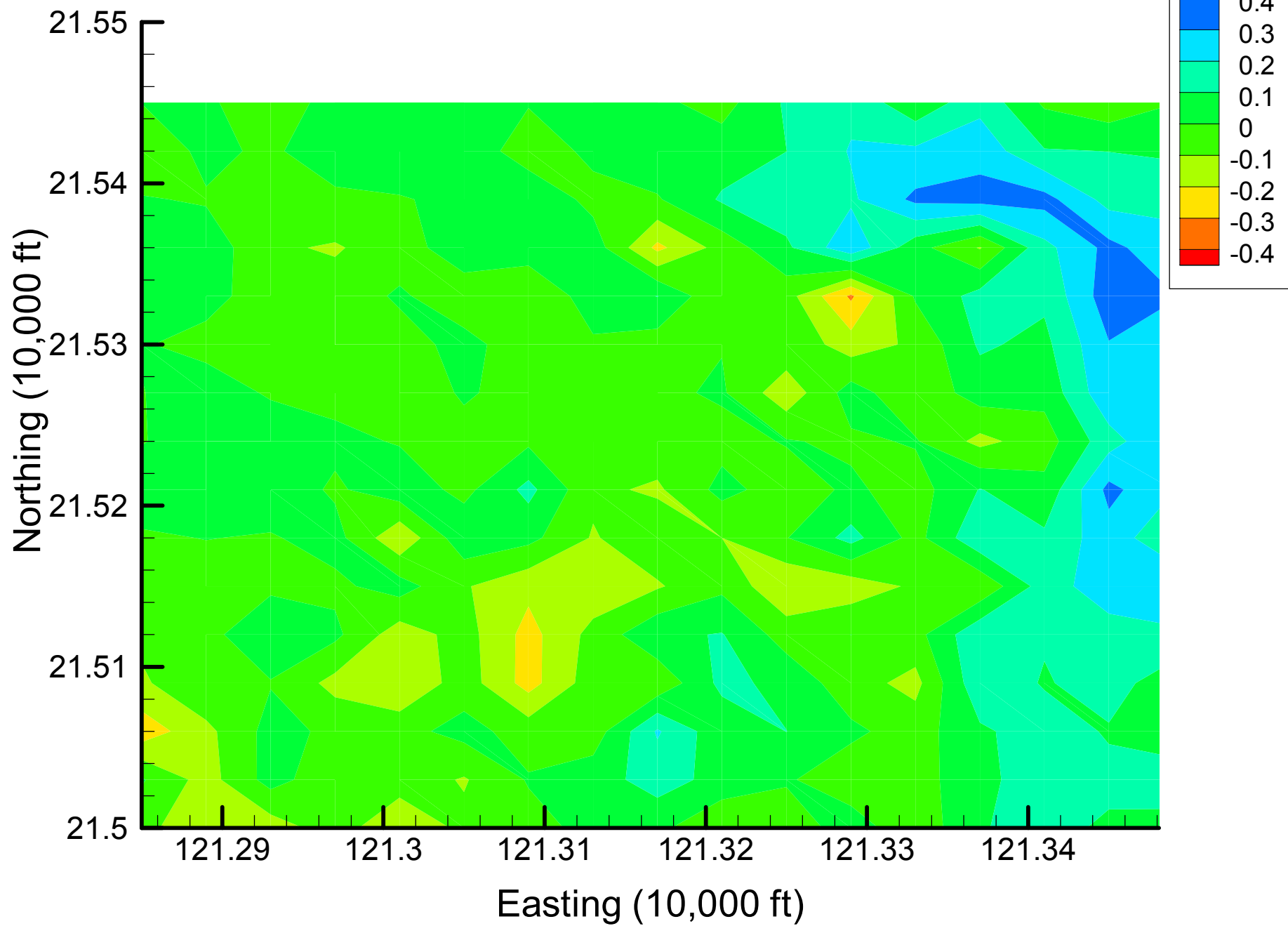
Site 49: DCA11 Indicator Differences, 2001, 25% Removal



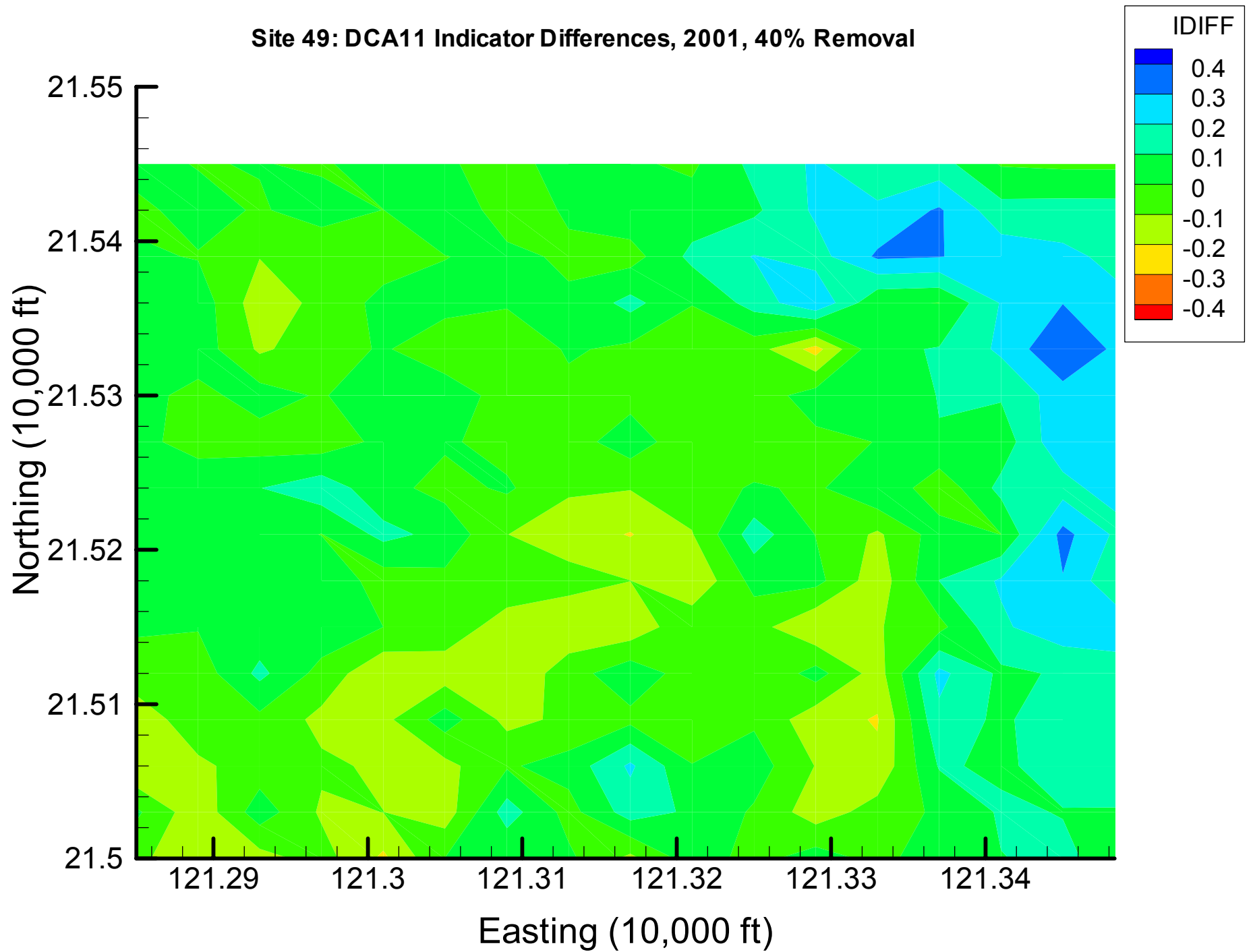
Site 49: DCA11 Indicator Differences, 2001, 30% Removal



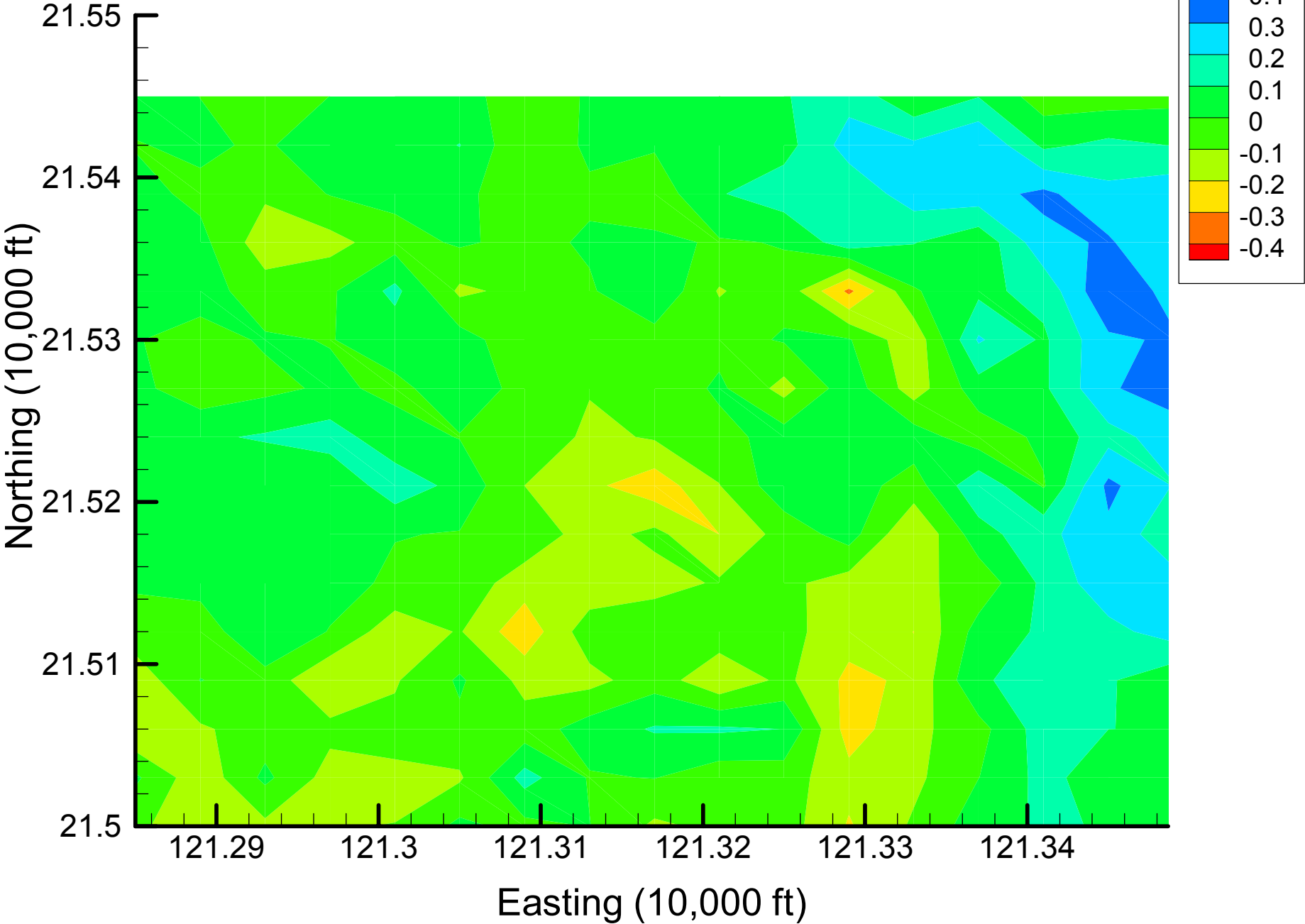
Site 49: DCA11 Indicator Differences, 2001, 35% Removal



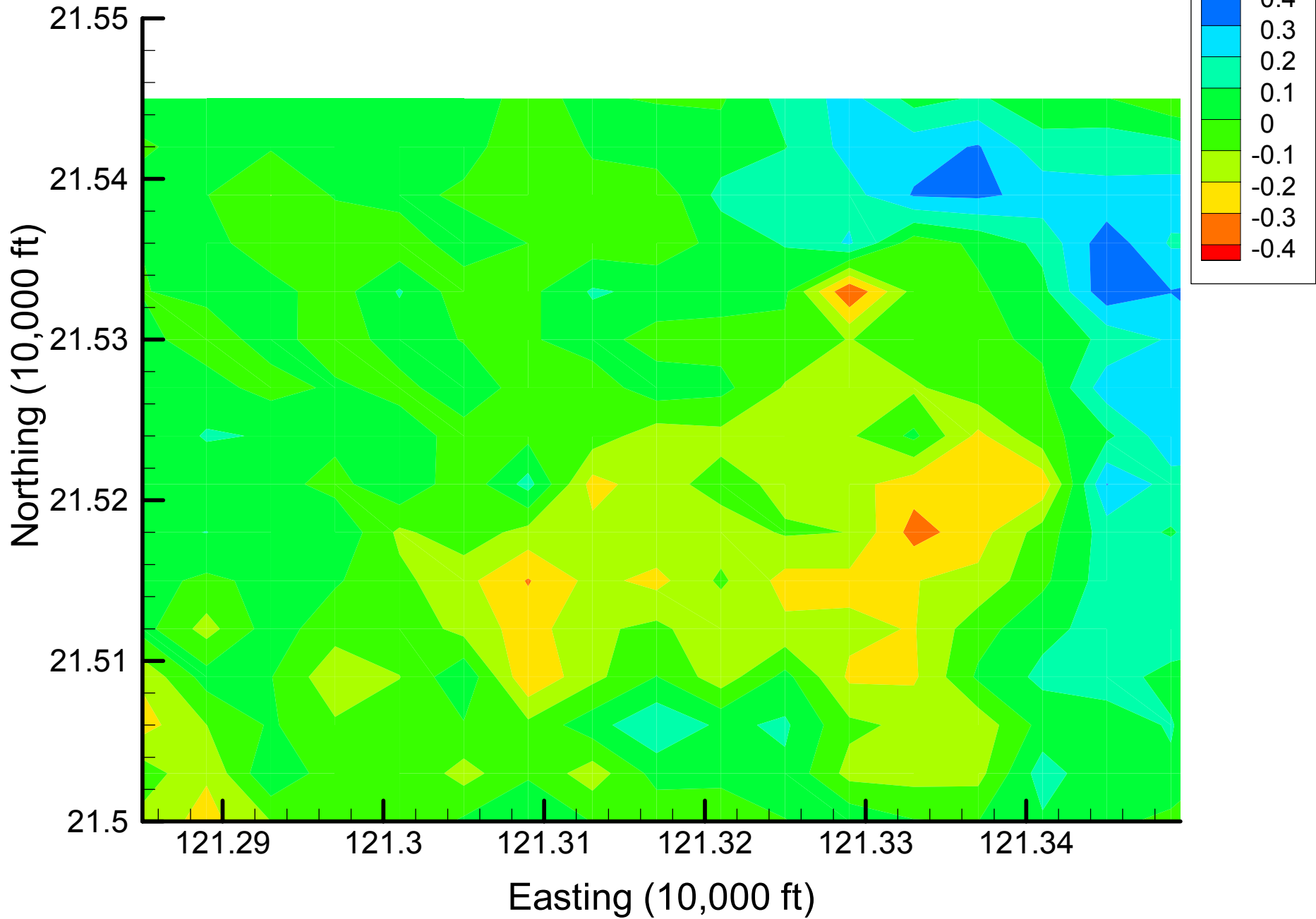
Site 49: DCA11 Indicator Differences, 2001, 40% Removal



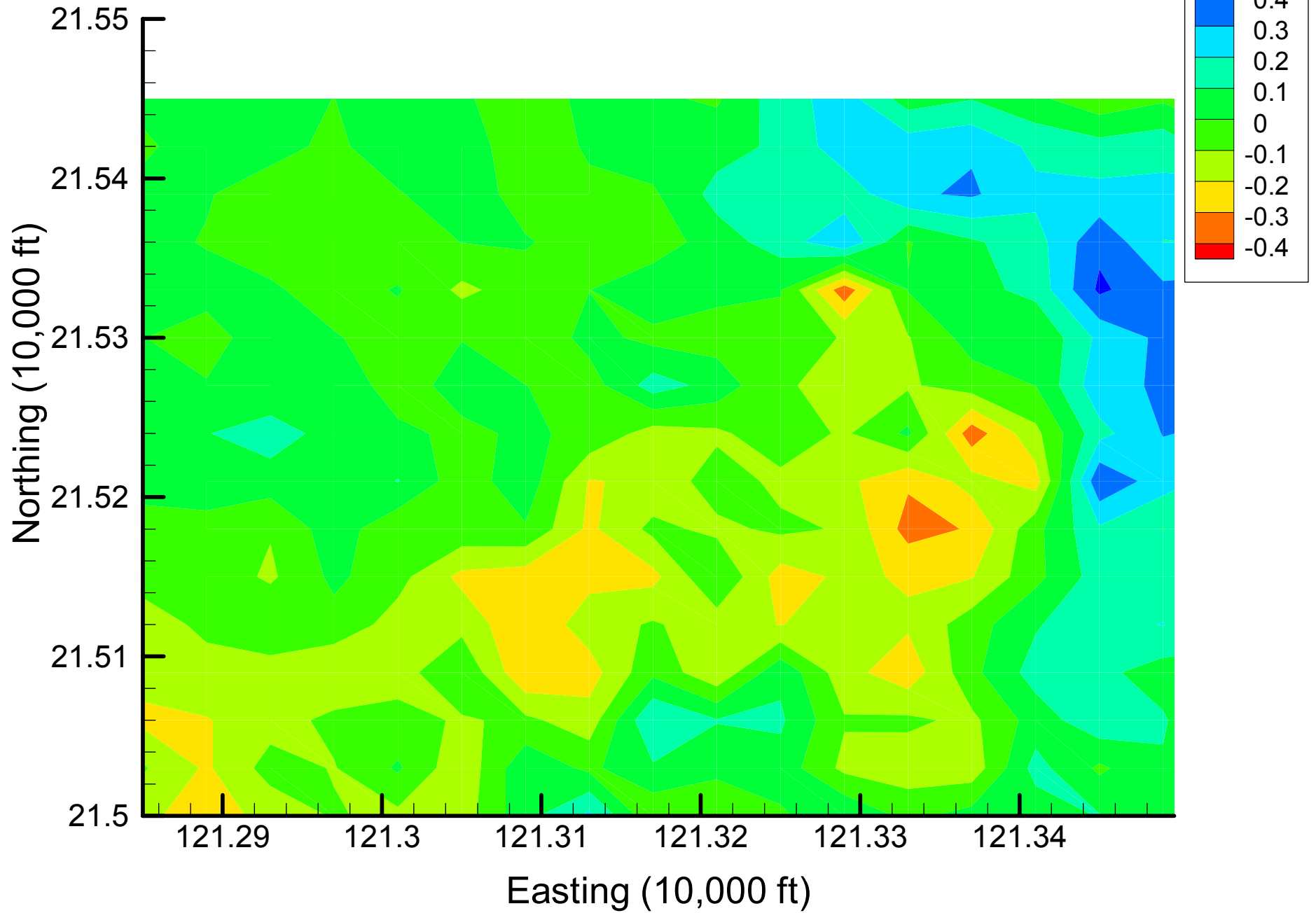
Site 49: DCA11 Indicator Differences, 2001, 45% Removal



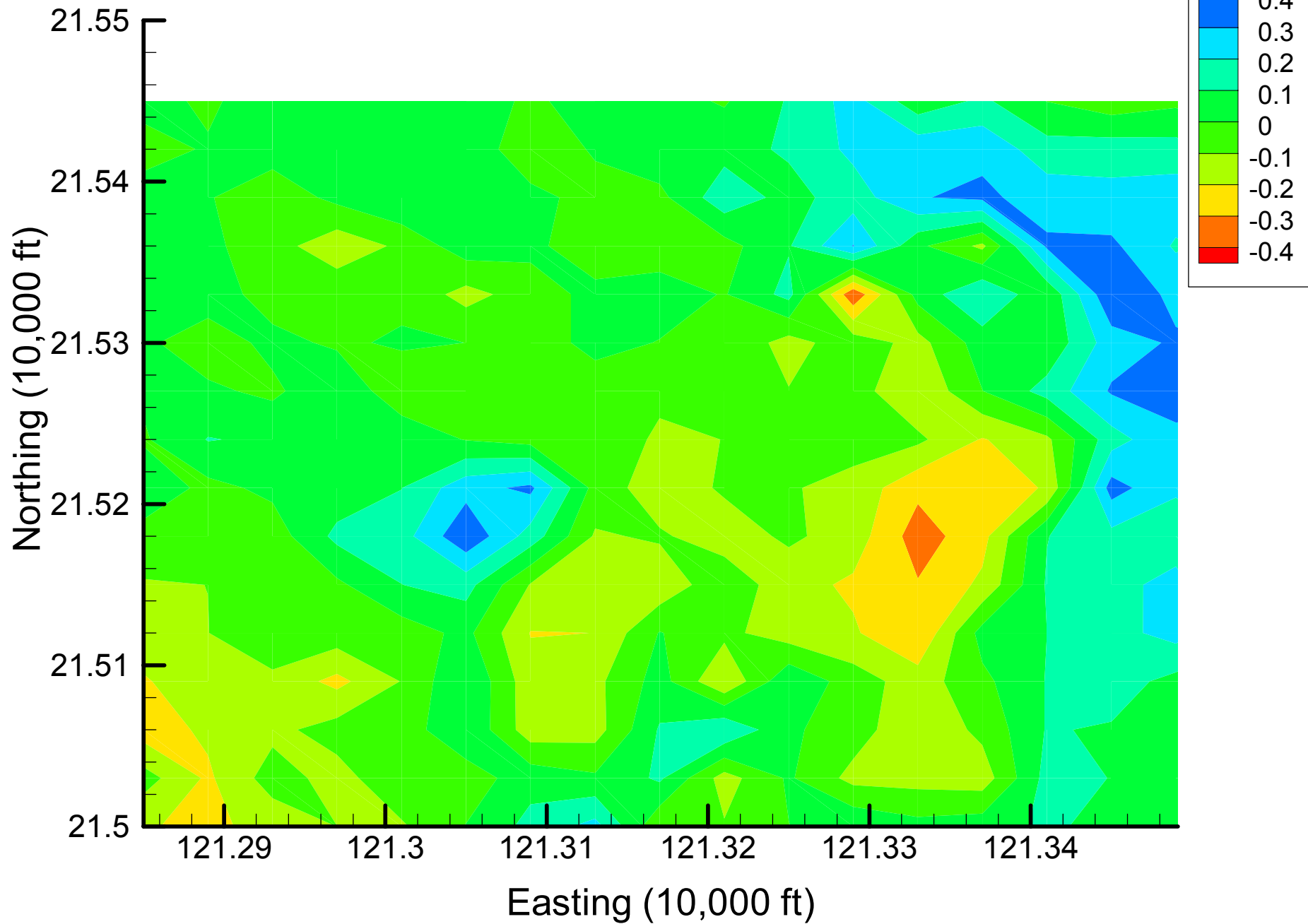
Site 49: DCA11 Indicator Differences, 2001, 50% Removal



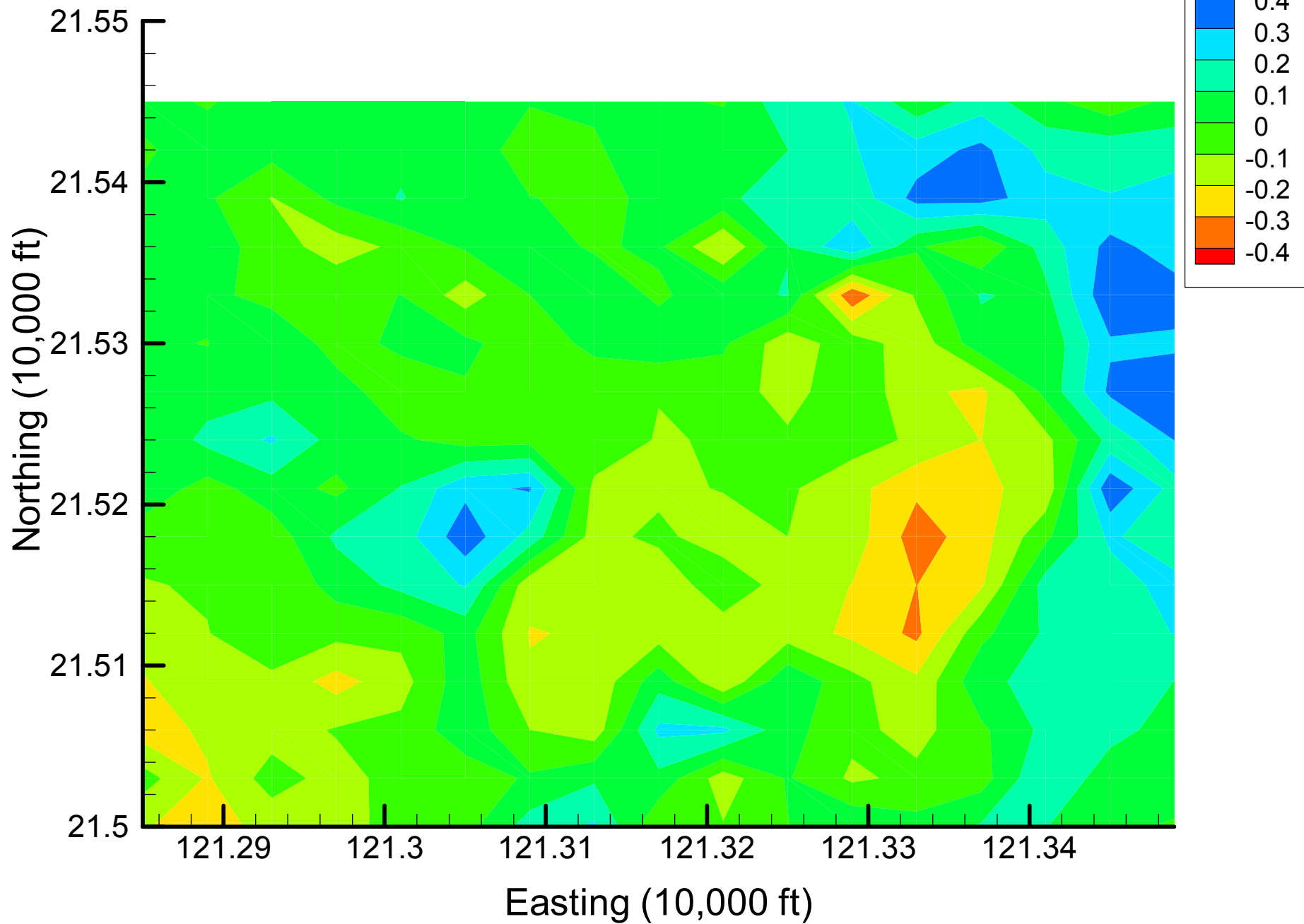
Site 49: DCA11 Indicator Differences, 2001, 55% Removal



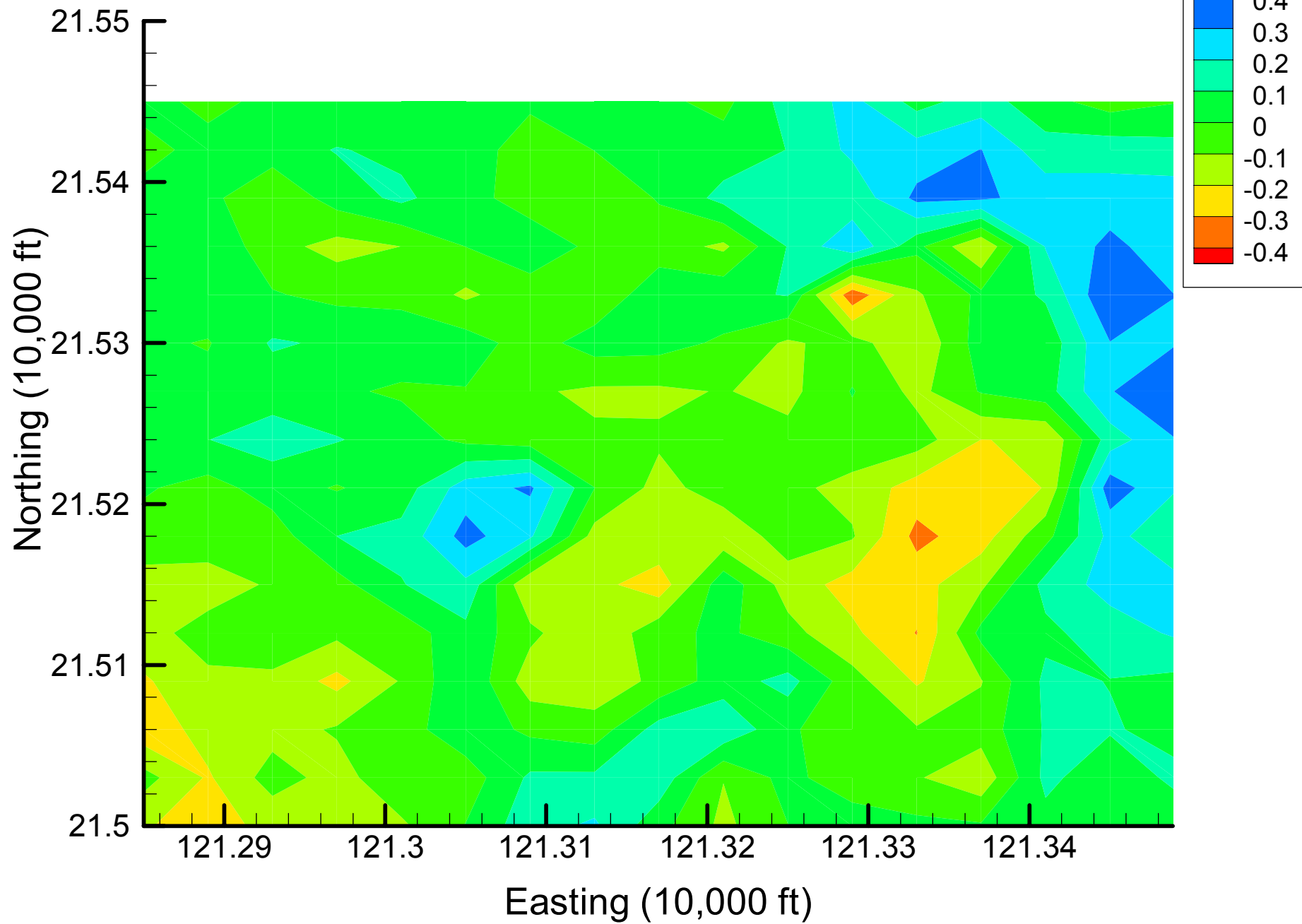
Site 49: DCA11 Indicator Differences, 2001, 60% Removal



Site 49: DCA11 Indicator Differences, 2001, 65% Removal



Site 49: DCA11 Indicator Differences, 2001, 70% Removal

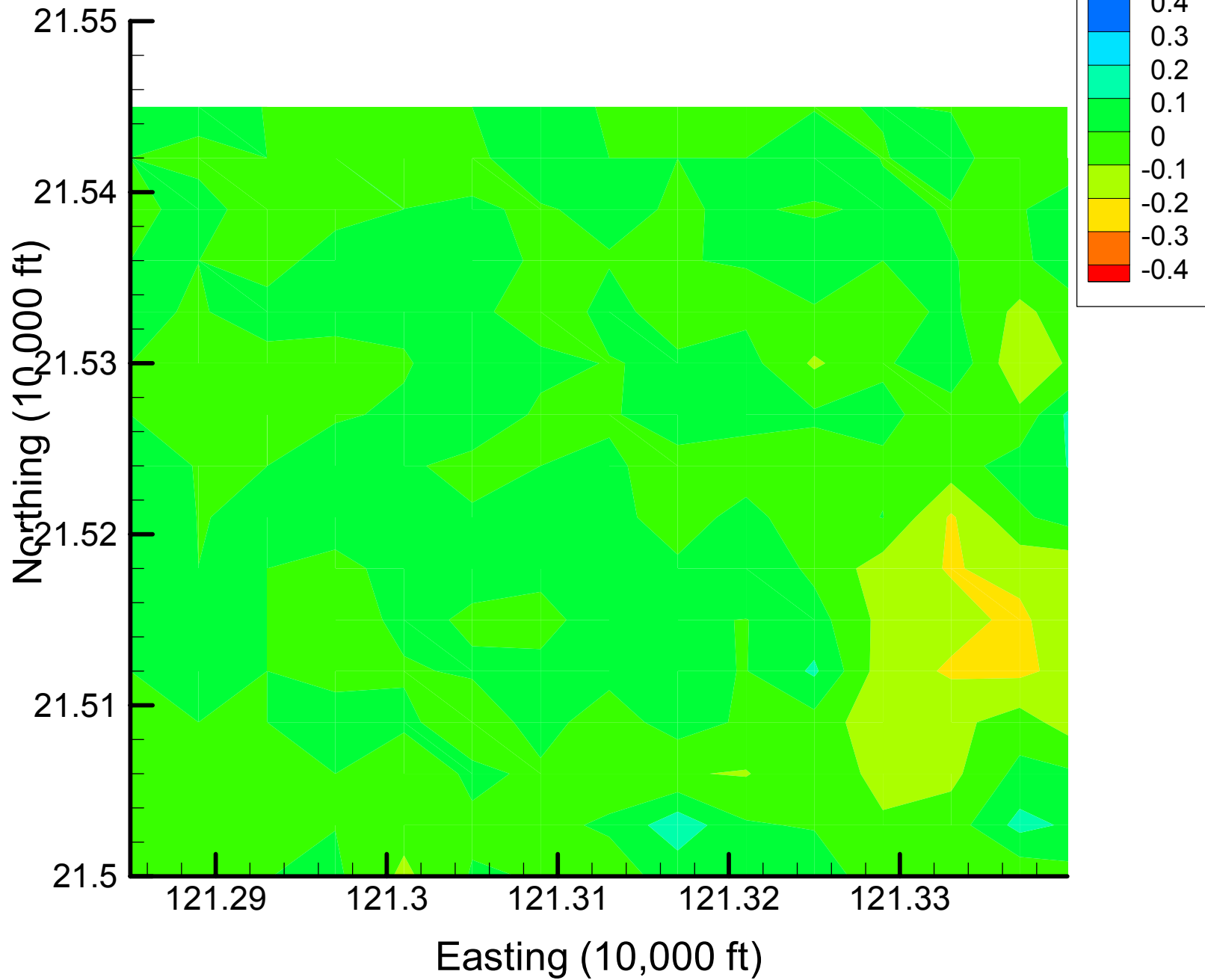


## Appendix 4.2

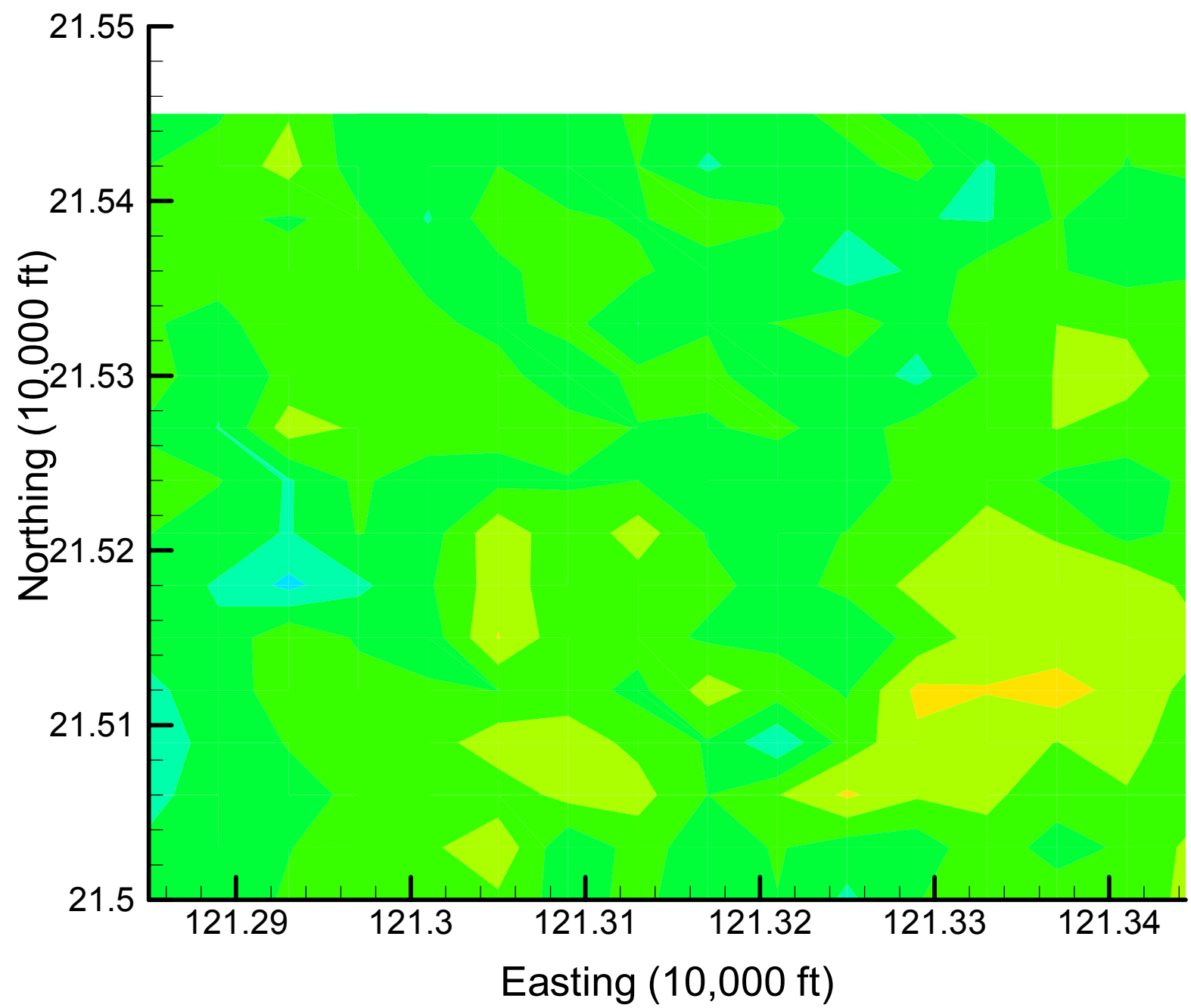
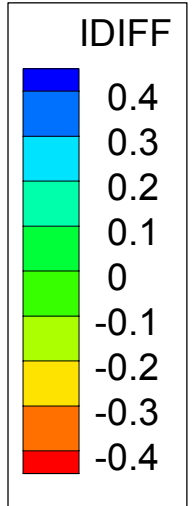
# DCA11 Indicator Difference Maps

Time Slice 2 — 2002

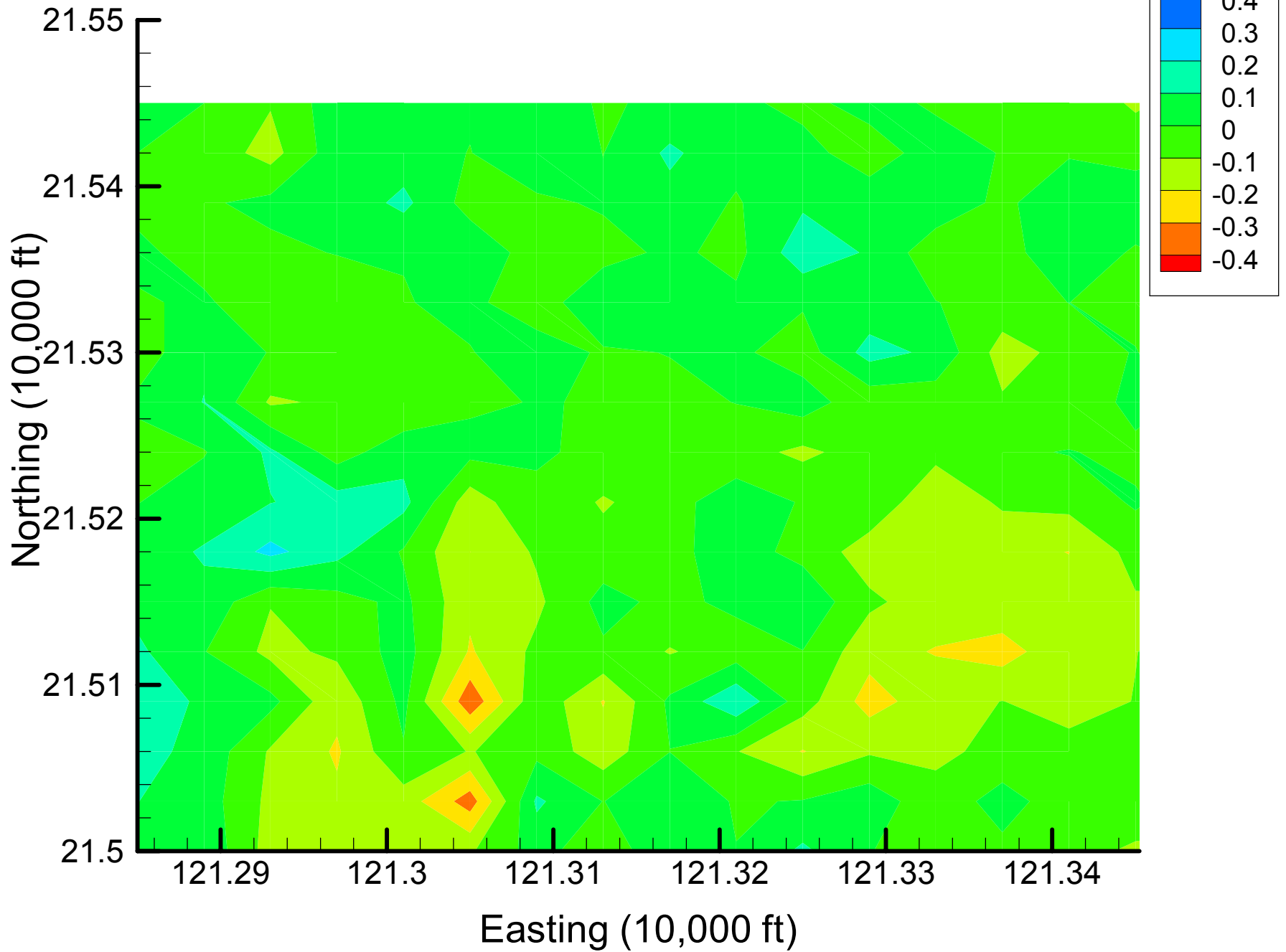
Site 49: DCA11 Indicator Differences, 2002, 5% Removal



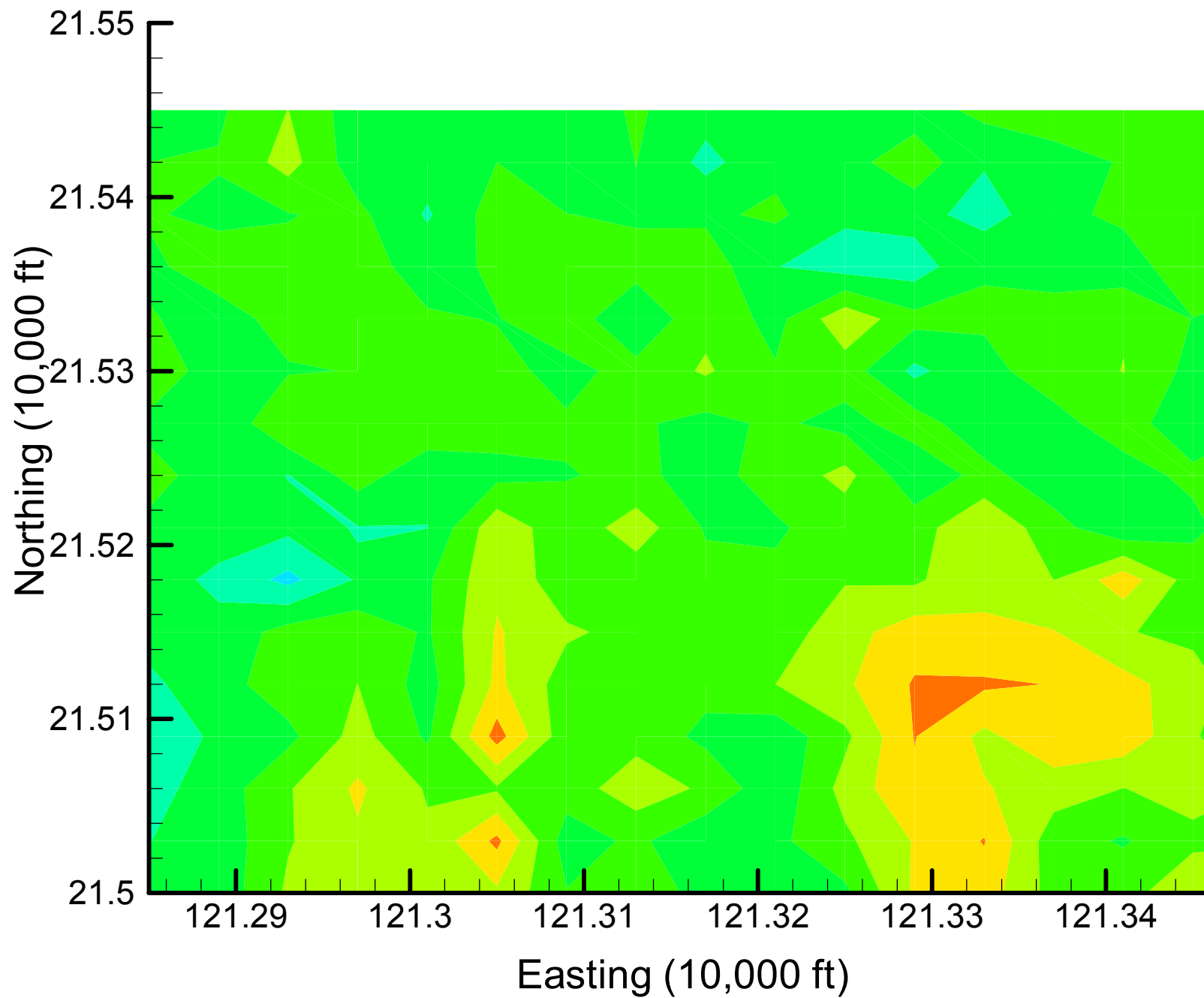
Site 49: DCA11 Indicator Differences, 2002, 10% Removal



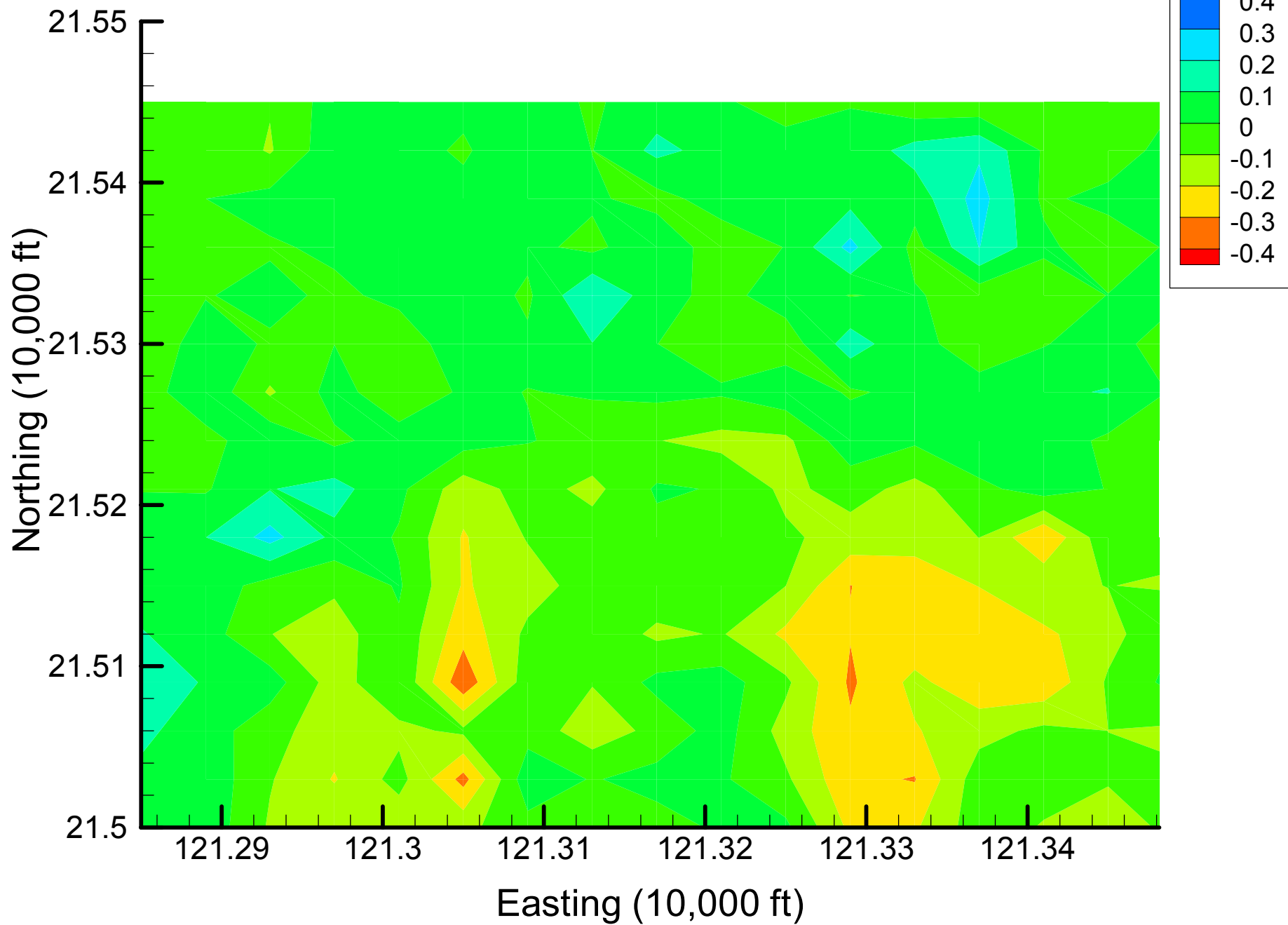
Site 49: DCA11 Indicator Differences, 2002, 15% Removal



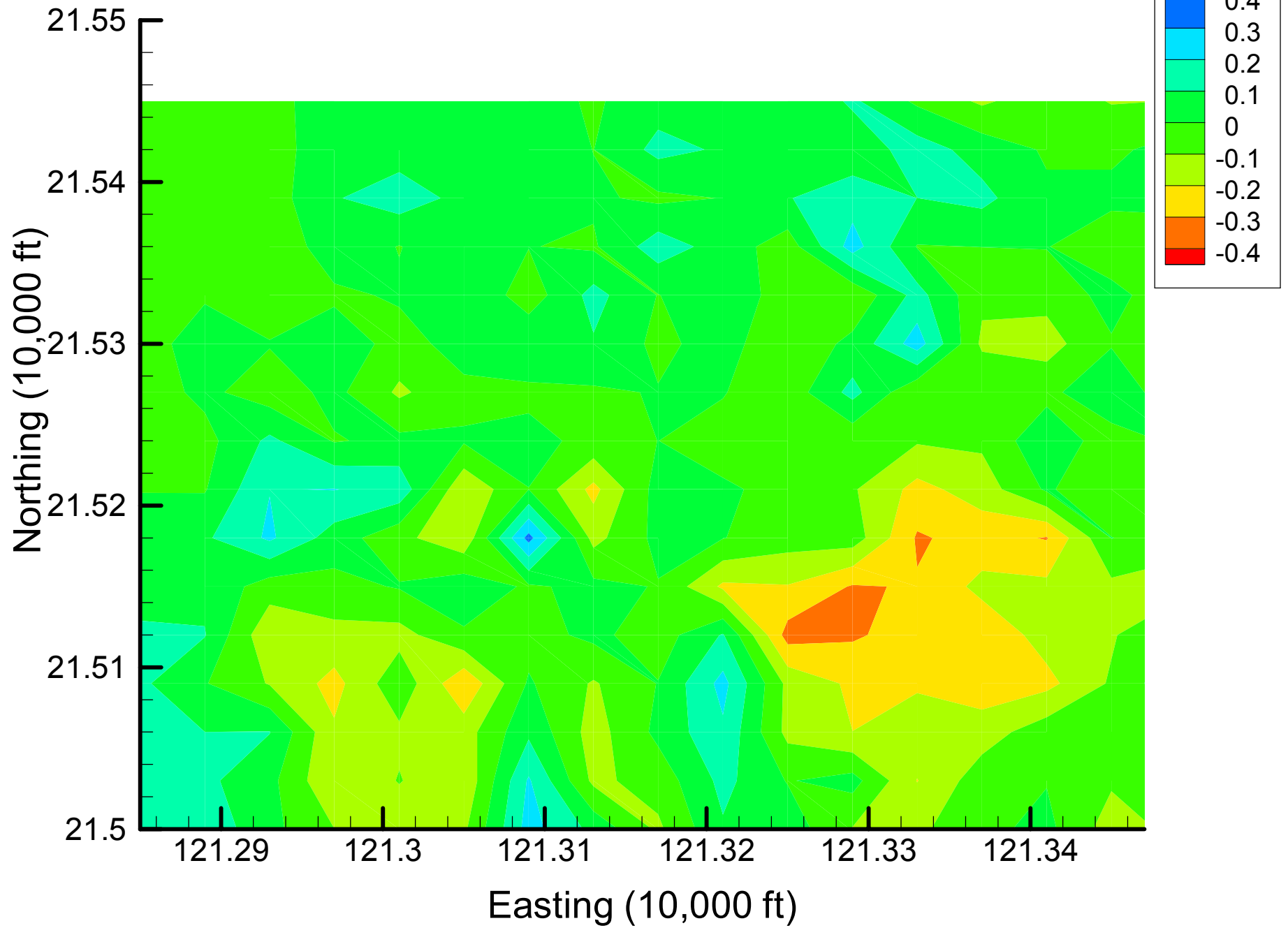
Site 49: DCA11 Indicator Differences, 2002, 20% Removal



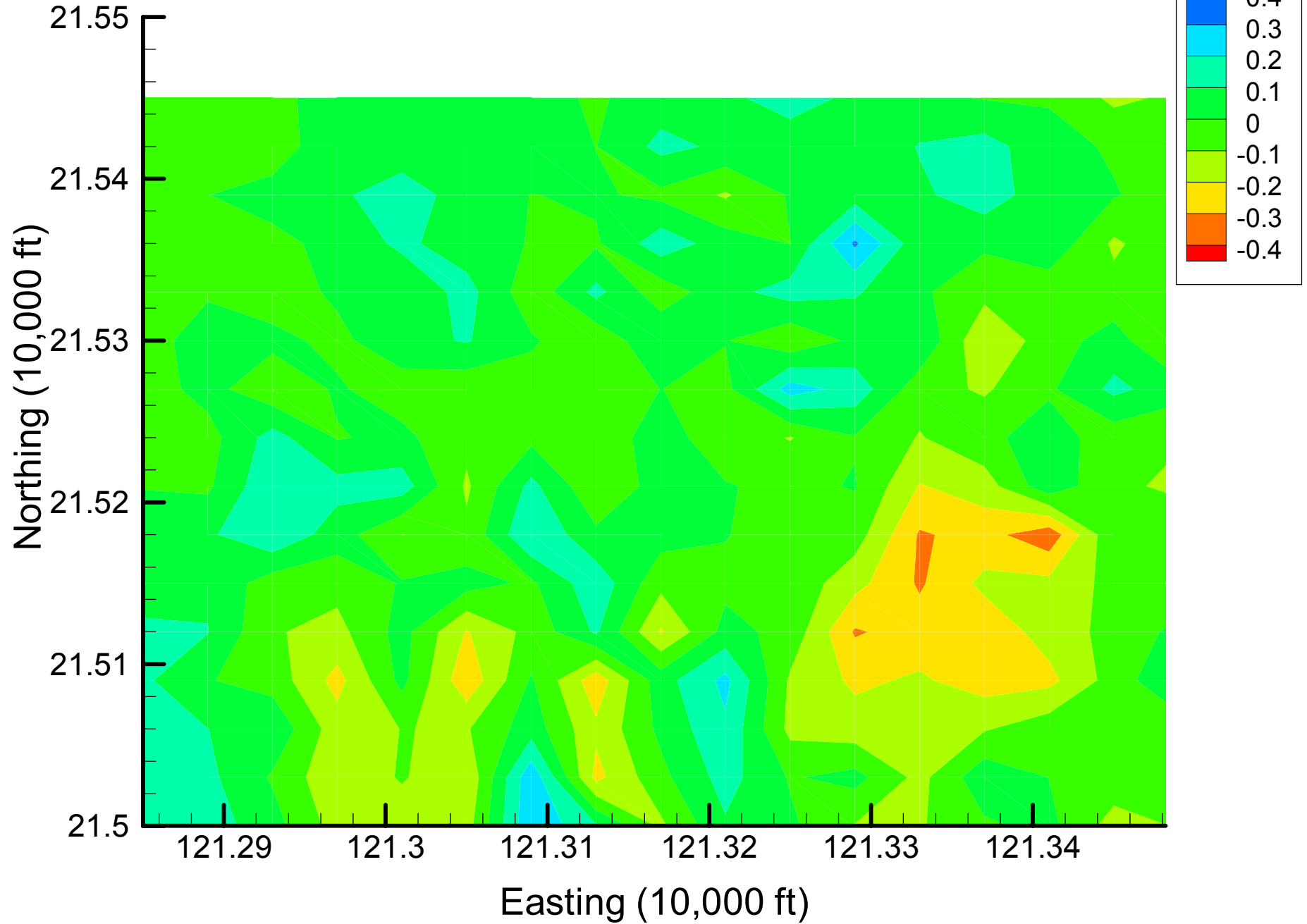
Site 49: DCA11 Indicator Differences, 2002, 25% Removal



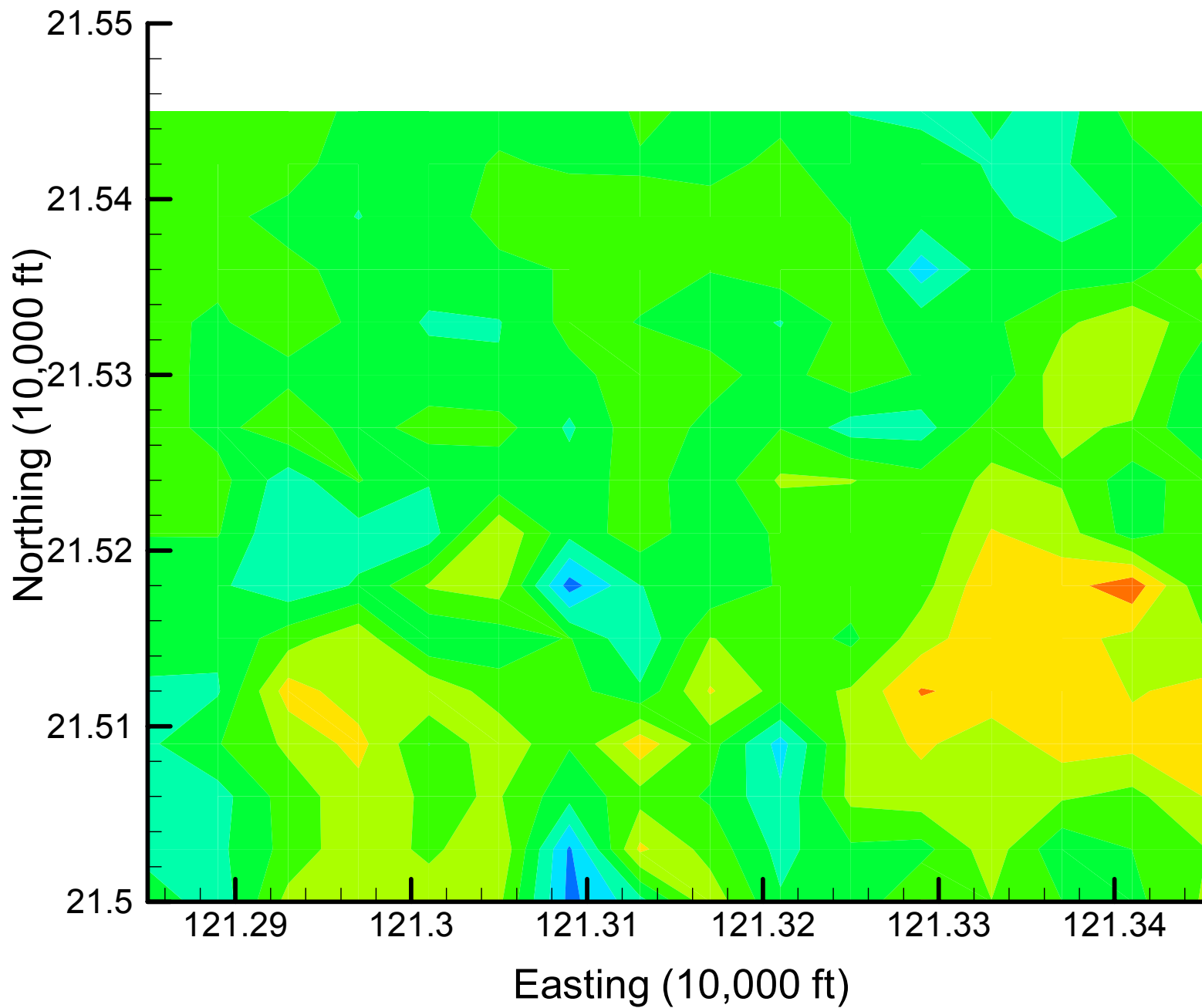
Site 49: DCA11 Indicator Differences, 2002, 30% Removal



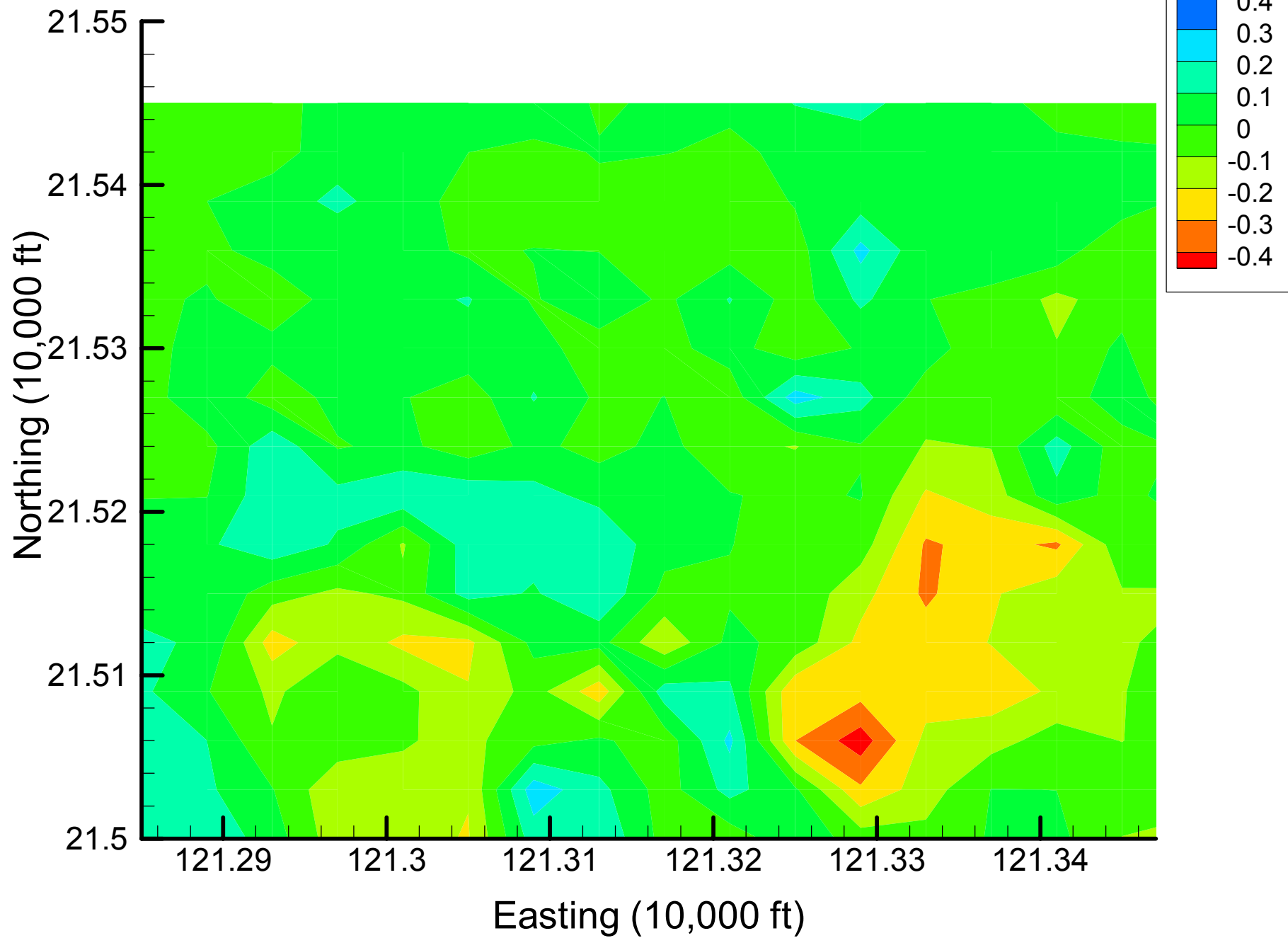
Site 49: DCA11 Indicator Differences, 2002, 35% Removal



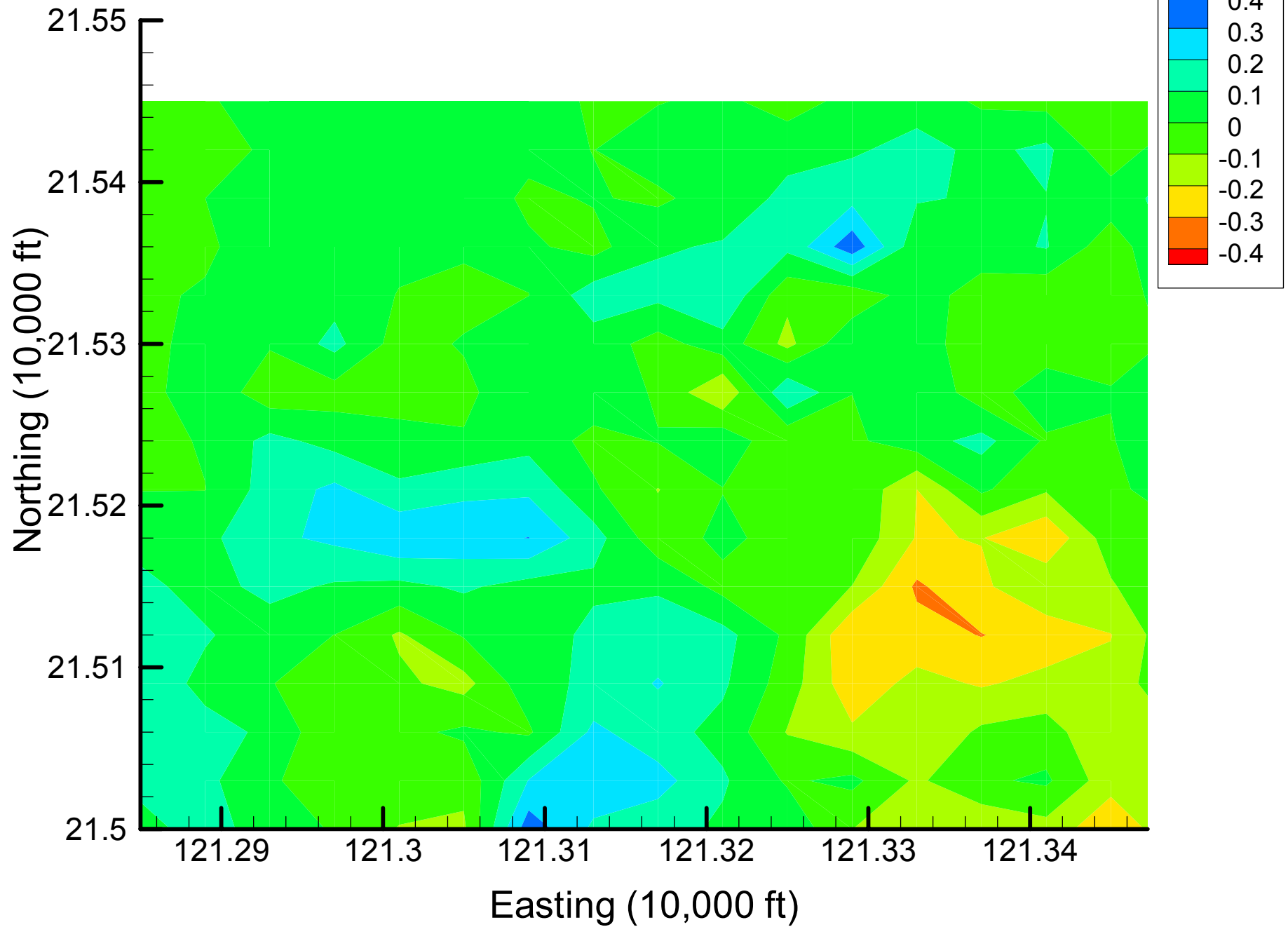
Site 49: DCA11 Indicator Differences, 2002, 40% Removal



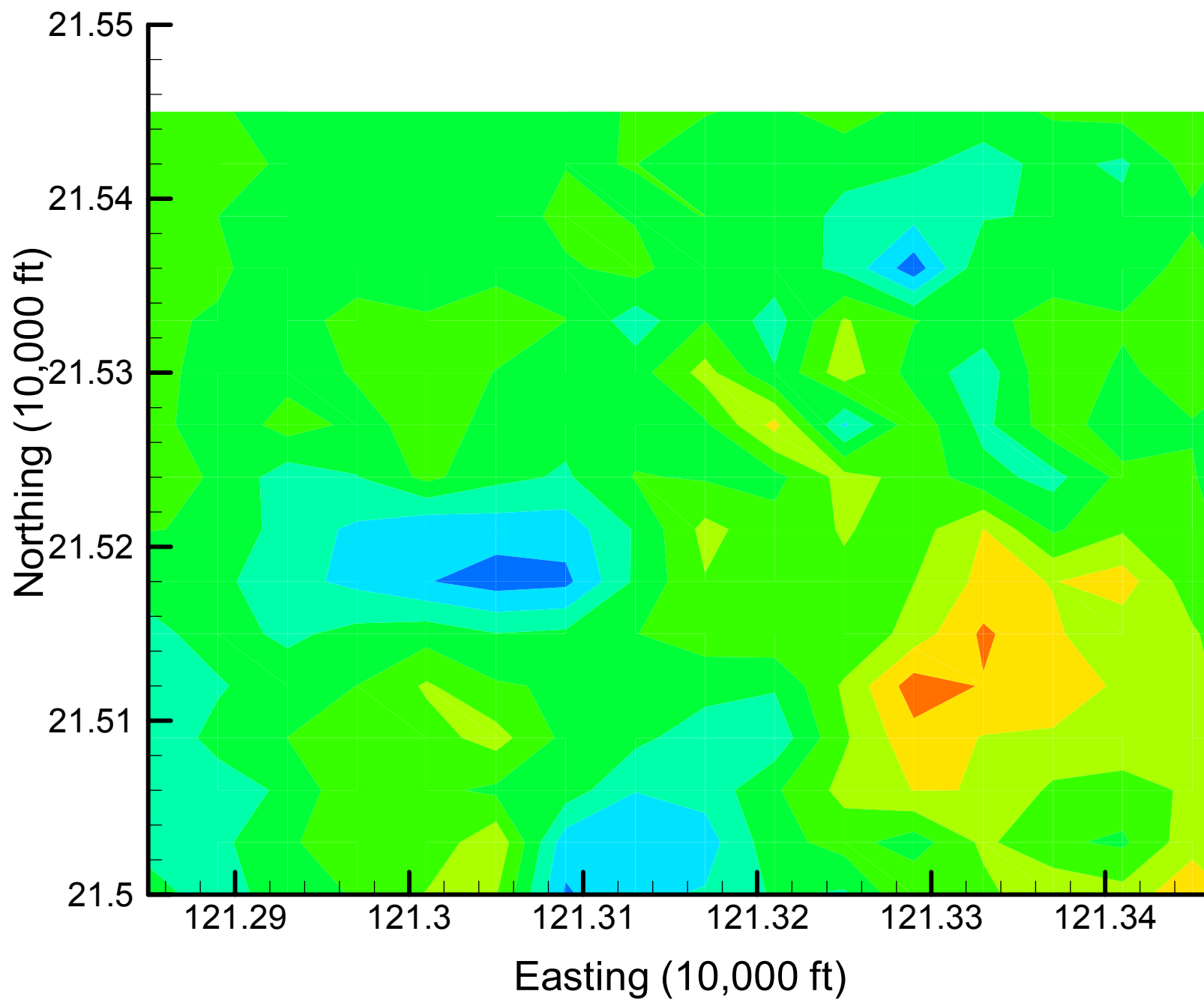
Site 49: DCA11 Indicator Differences, 2002, 45% Removal



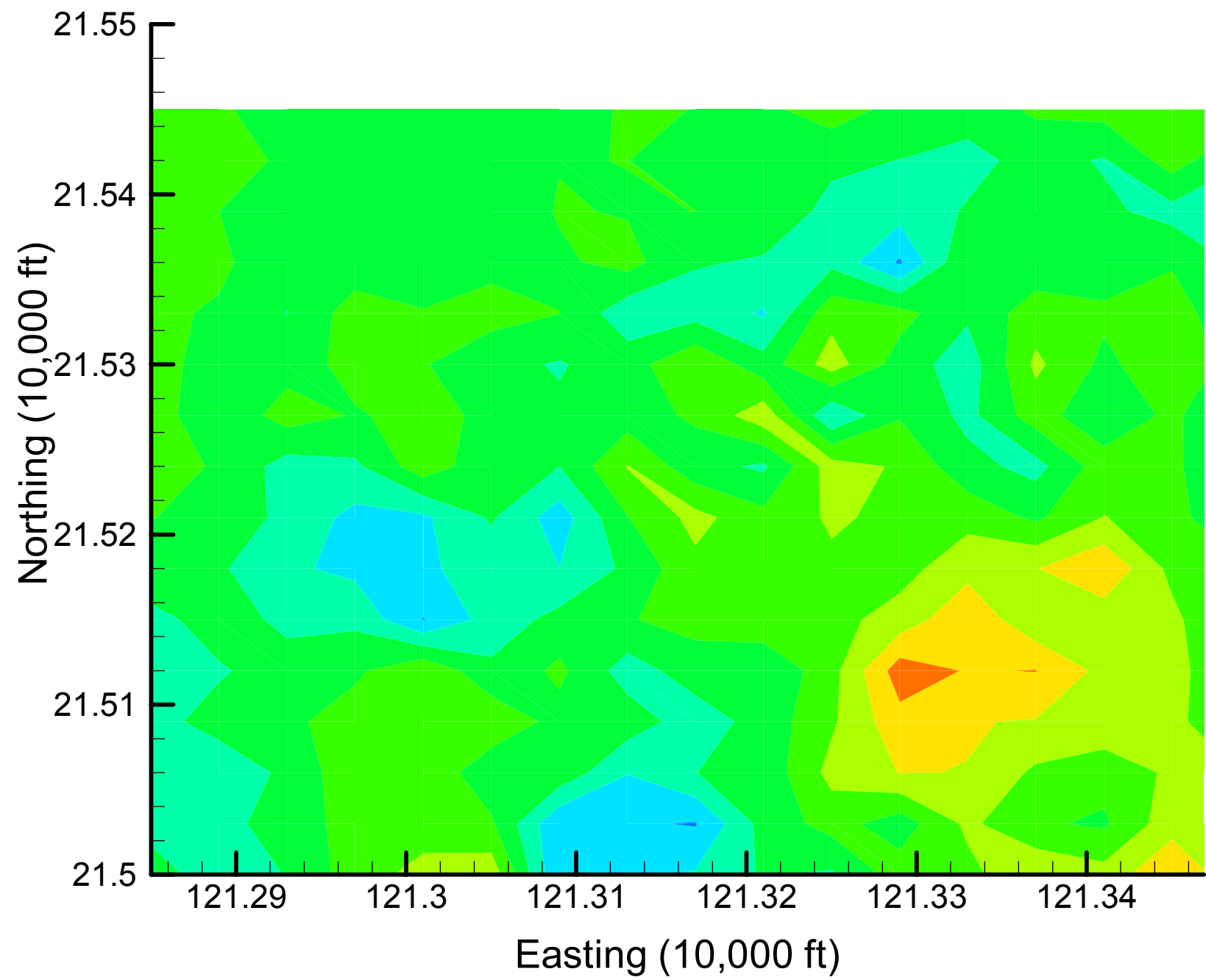
Site 49: DCA11 Indicator Differences, 2002, 50% Removal



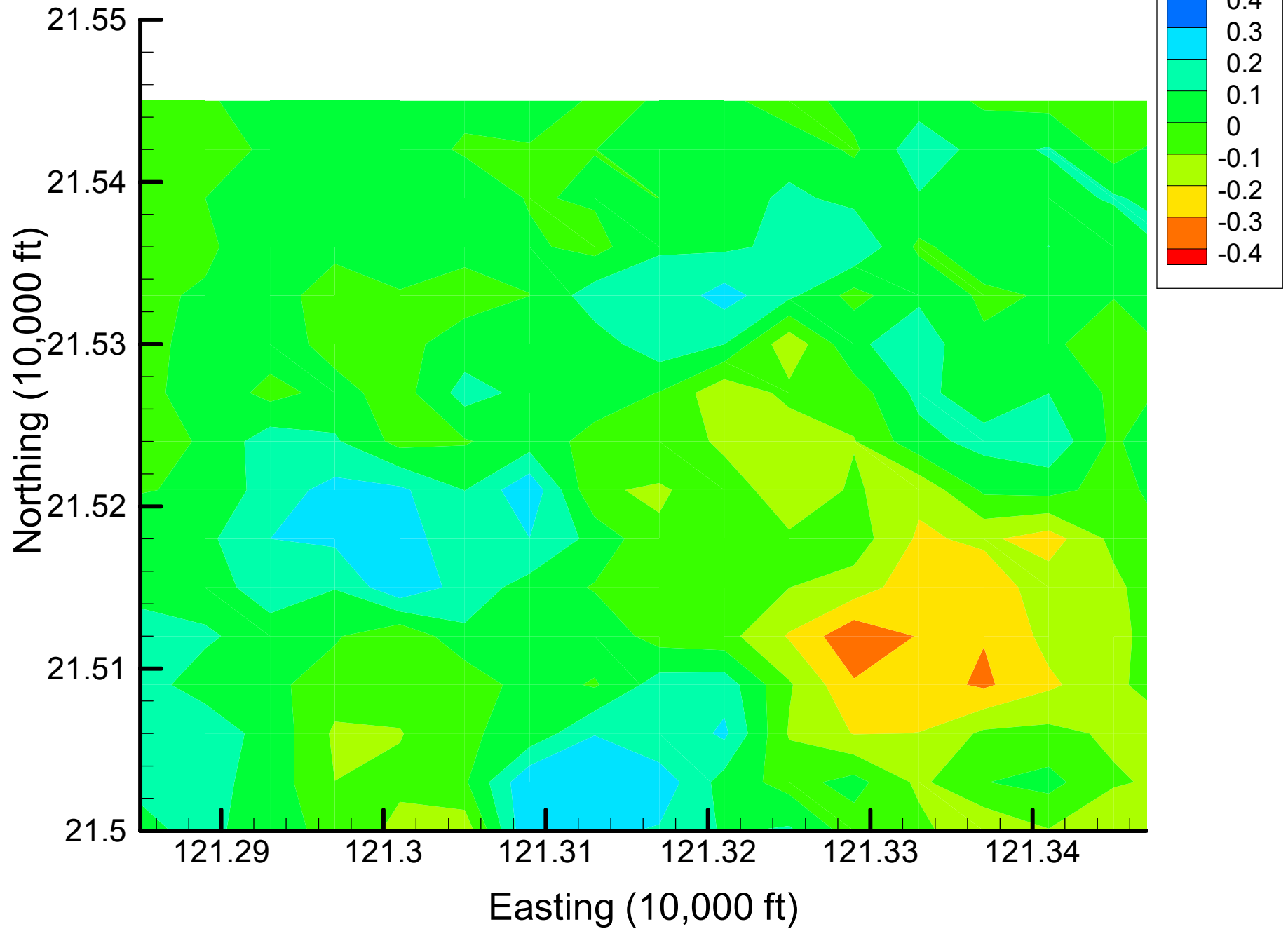
Site 49: DCA11 Indicator Differences, 2002, 55% Removal



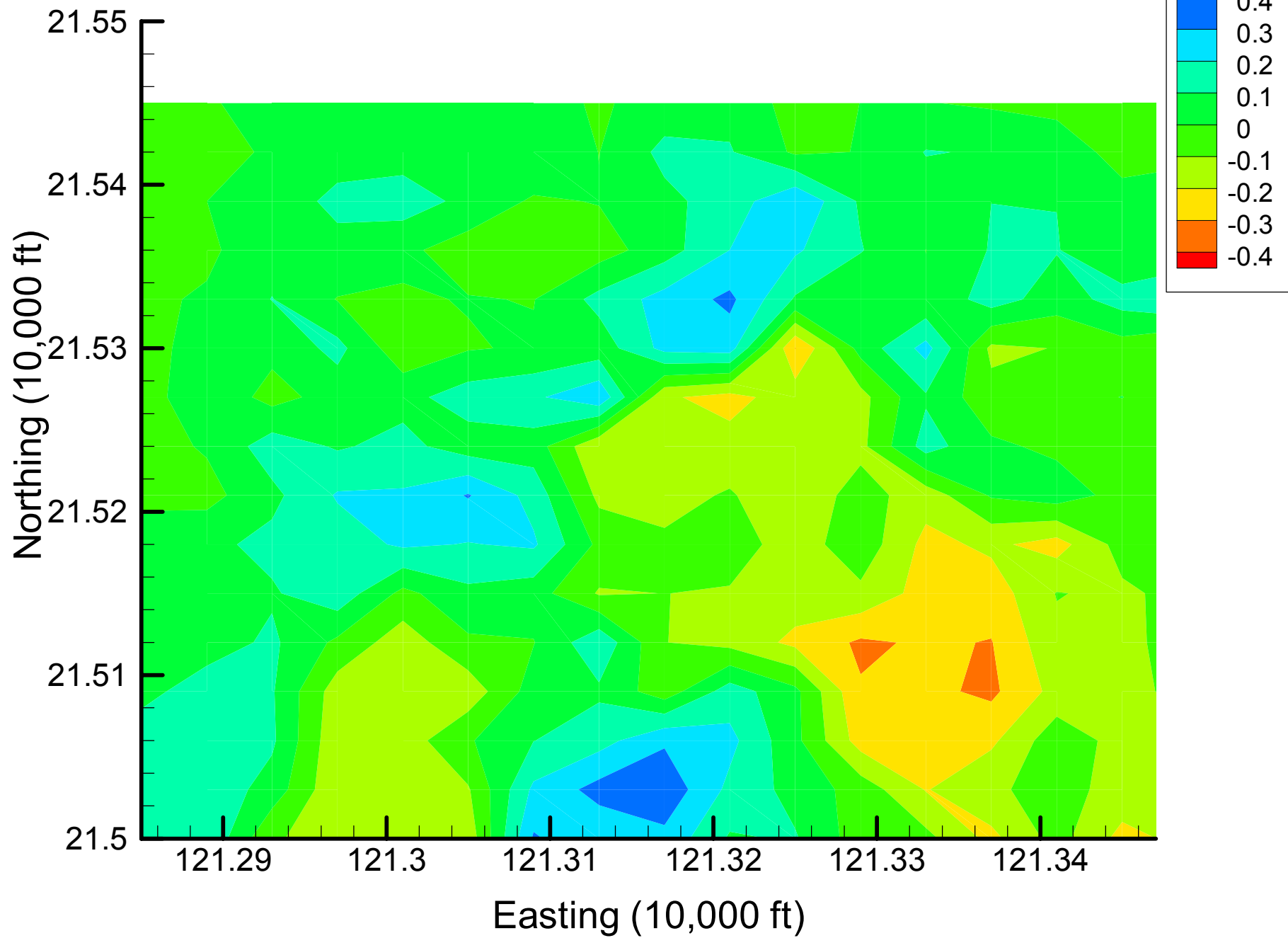
Site 49: DCA11 Indicator Differences, 2002, 60% Removal



Site 49: DCA11 Indicator Differences, 2002, 65% Removal



Site 49: DCA11 Indicator Differences, 2002, 70% Removal

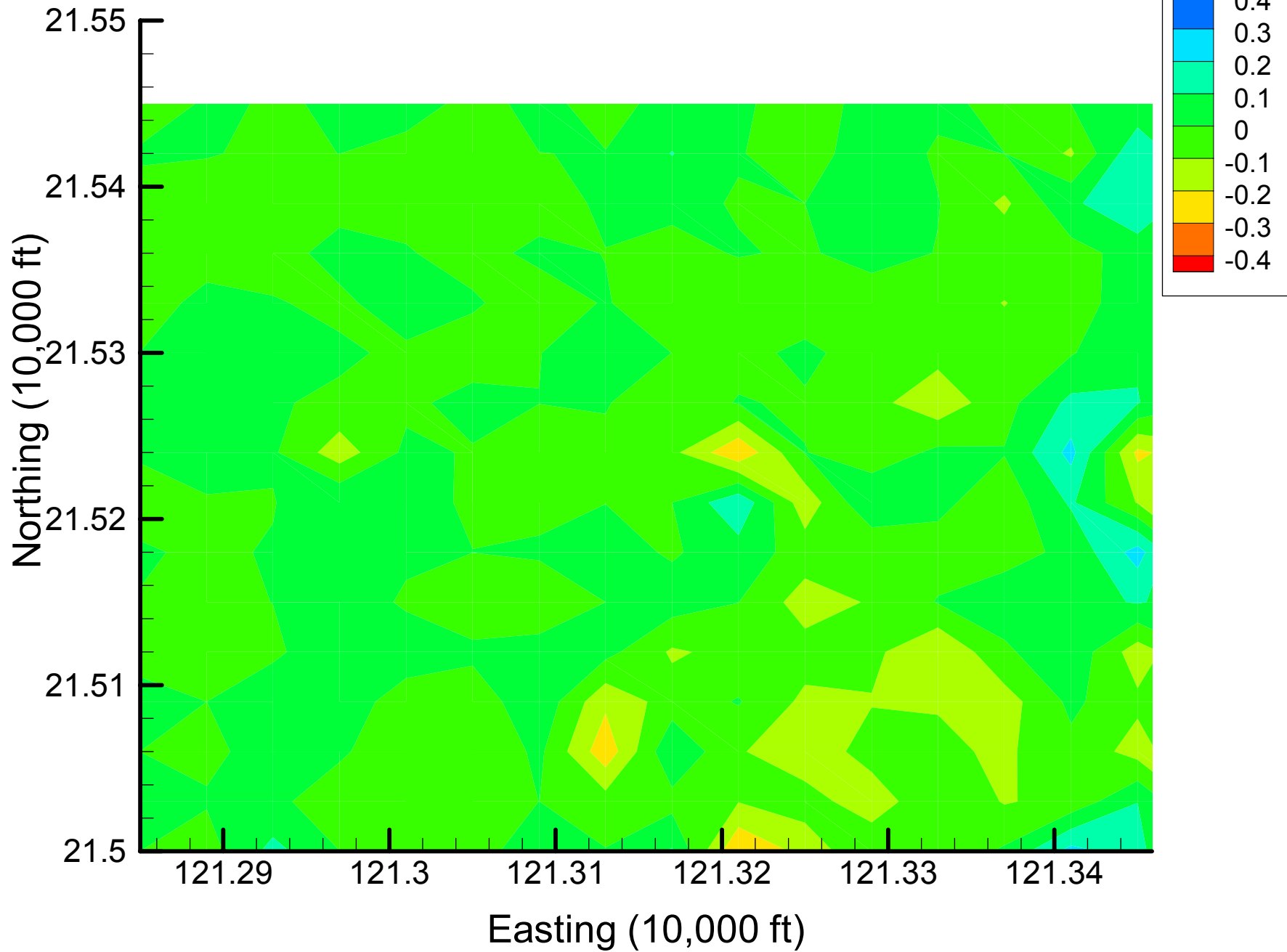


# Appendix 4.2

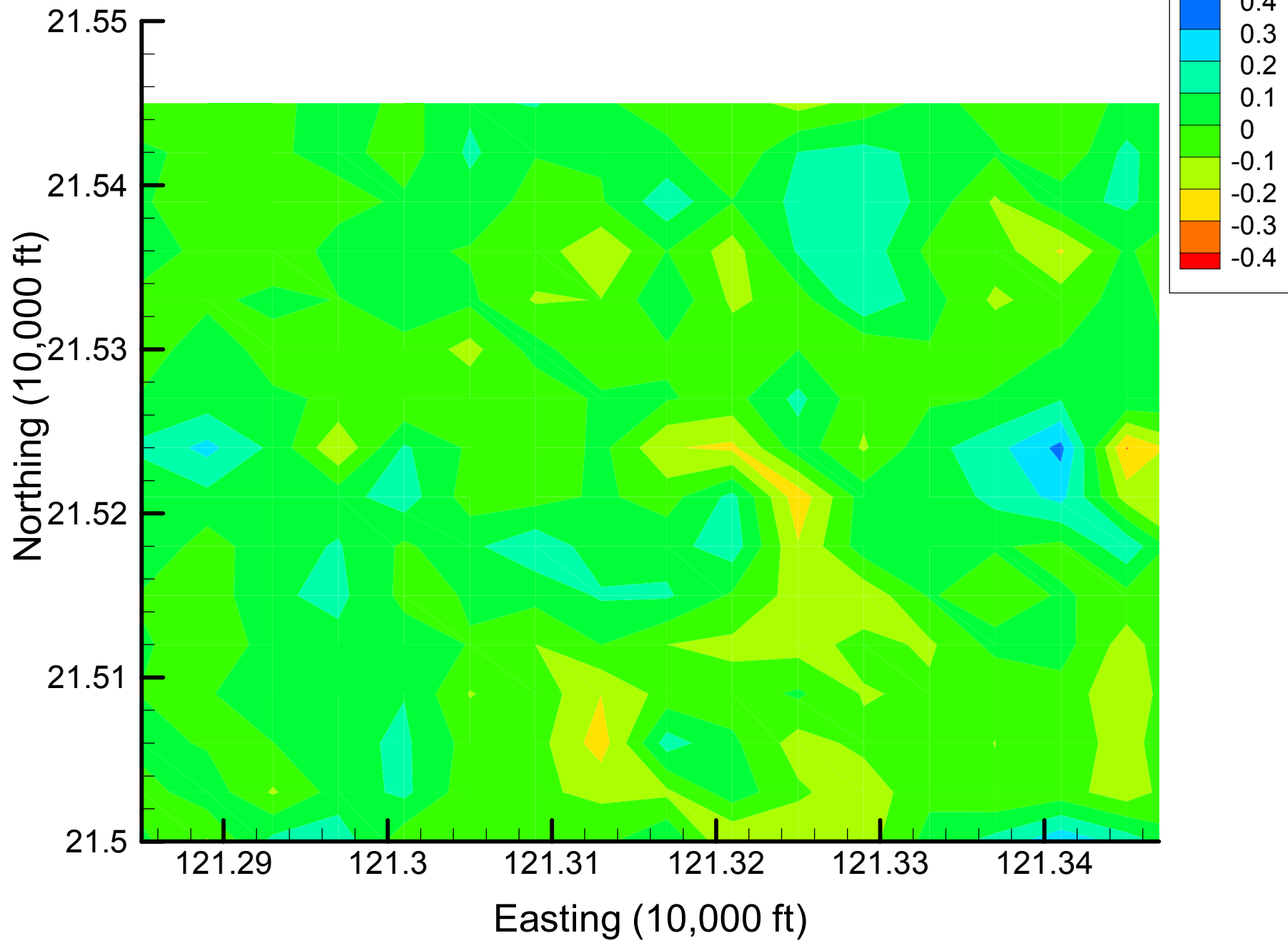
## DCE12C Indicator Difference Maps

Time Slice 1 — 2001

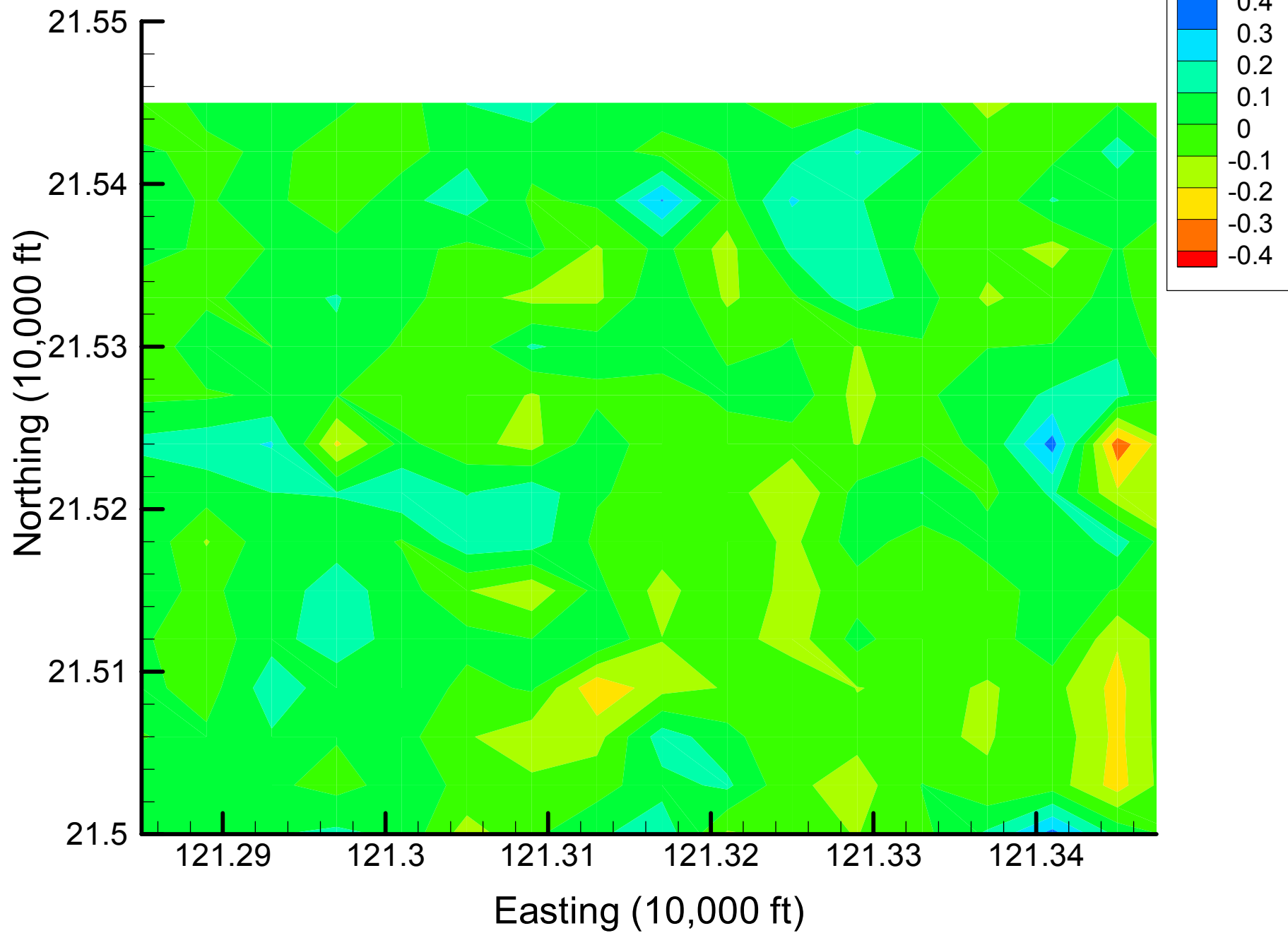
Site 49: DCE12C Indicator Differences, 2001, 5% Removal



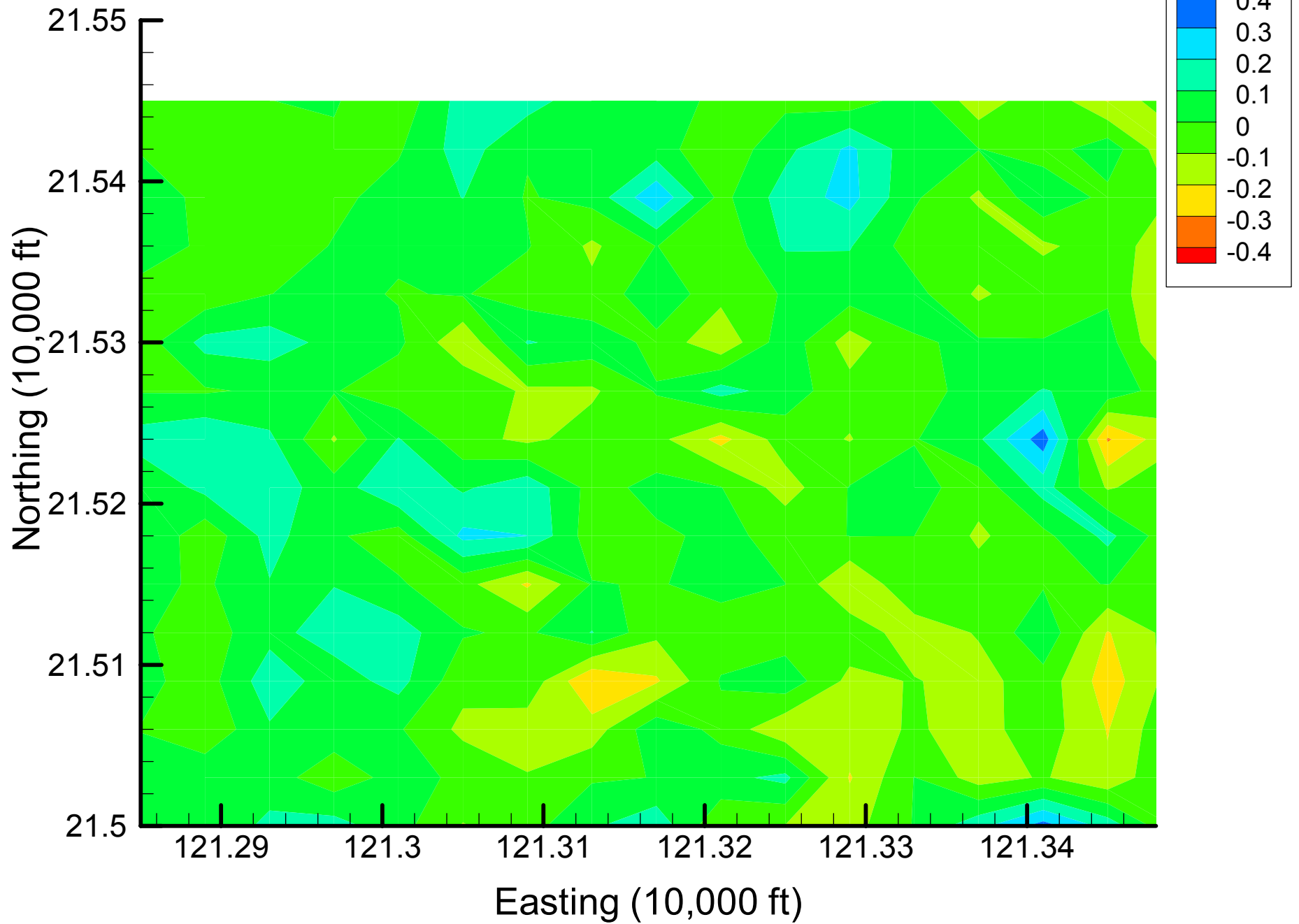
Site 49: DCE12C Indicator Differences, 2001, 10% Removal



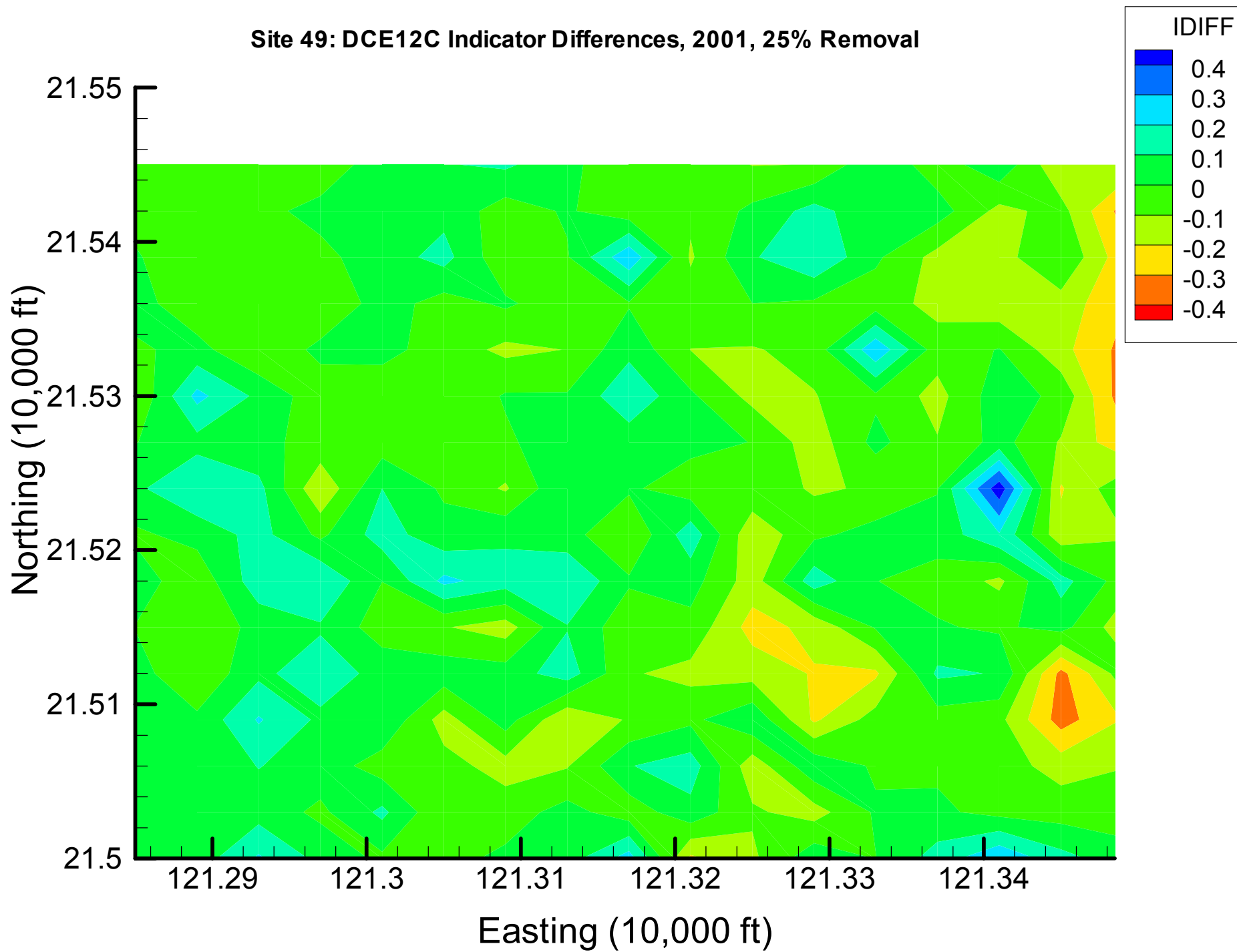
Site 49: DCE12C Indicator Differences, 2001, 15% Removal



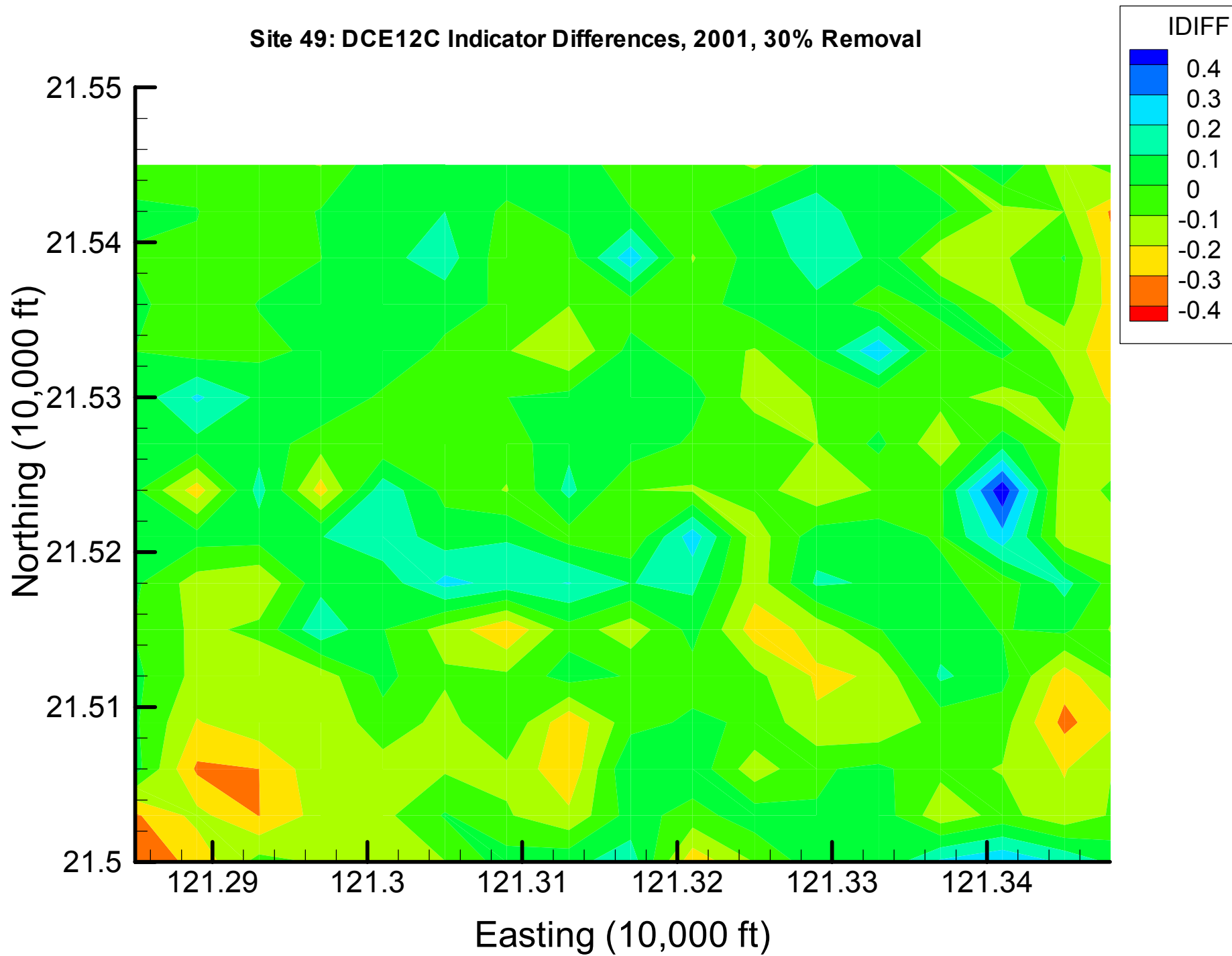
Site 49: DCE12C Indicator Differences, 2001, 20% Removal



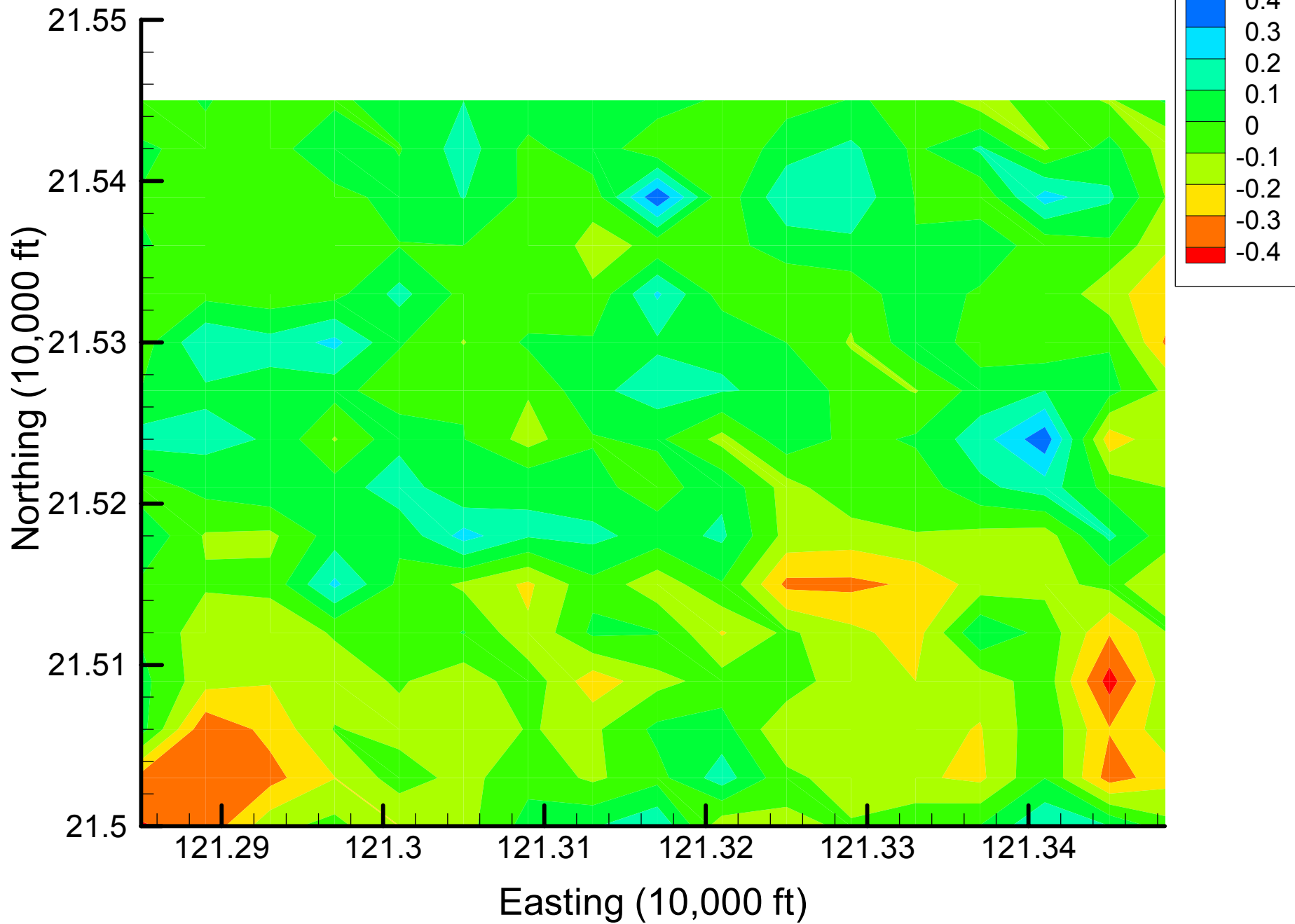
Site 49: DCE12C Indicator Differences, 2001, 25% Removal



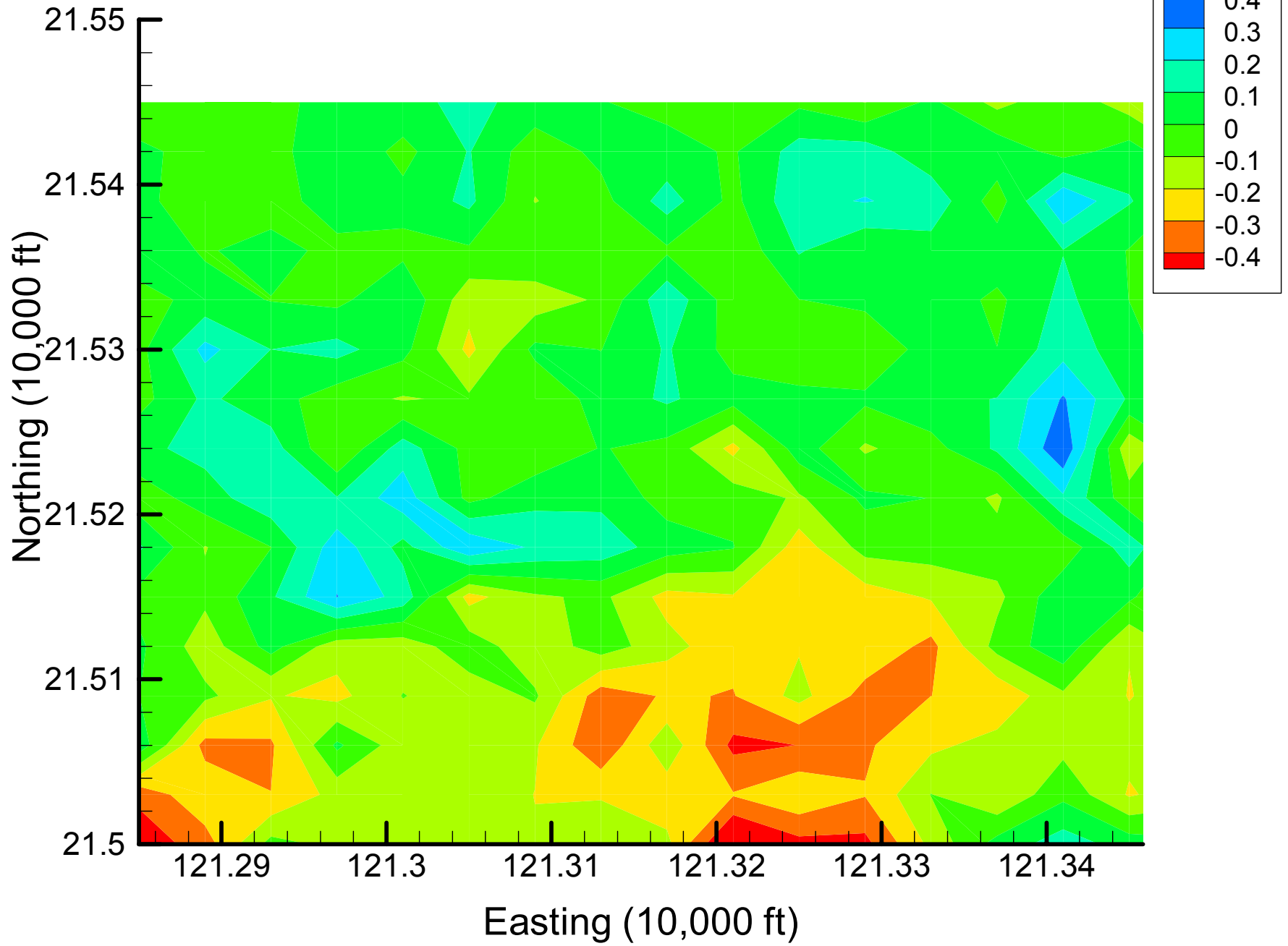
Site 49: DCE12C Indicator Differences, 2001, 30% Removal



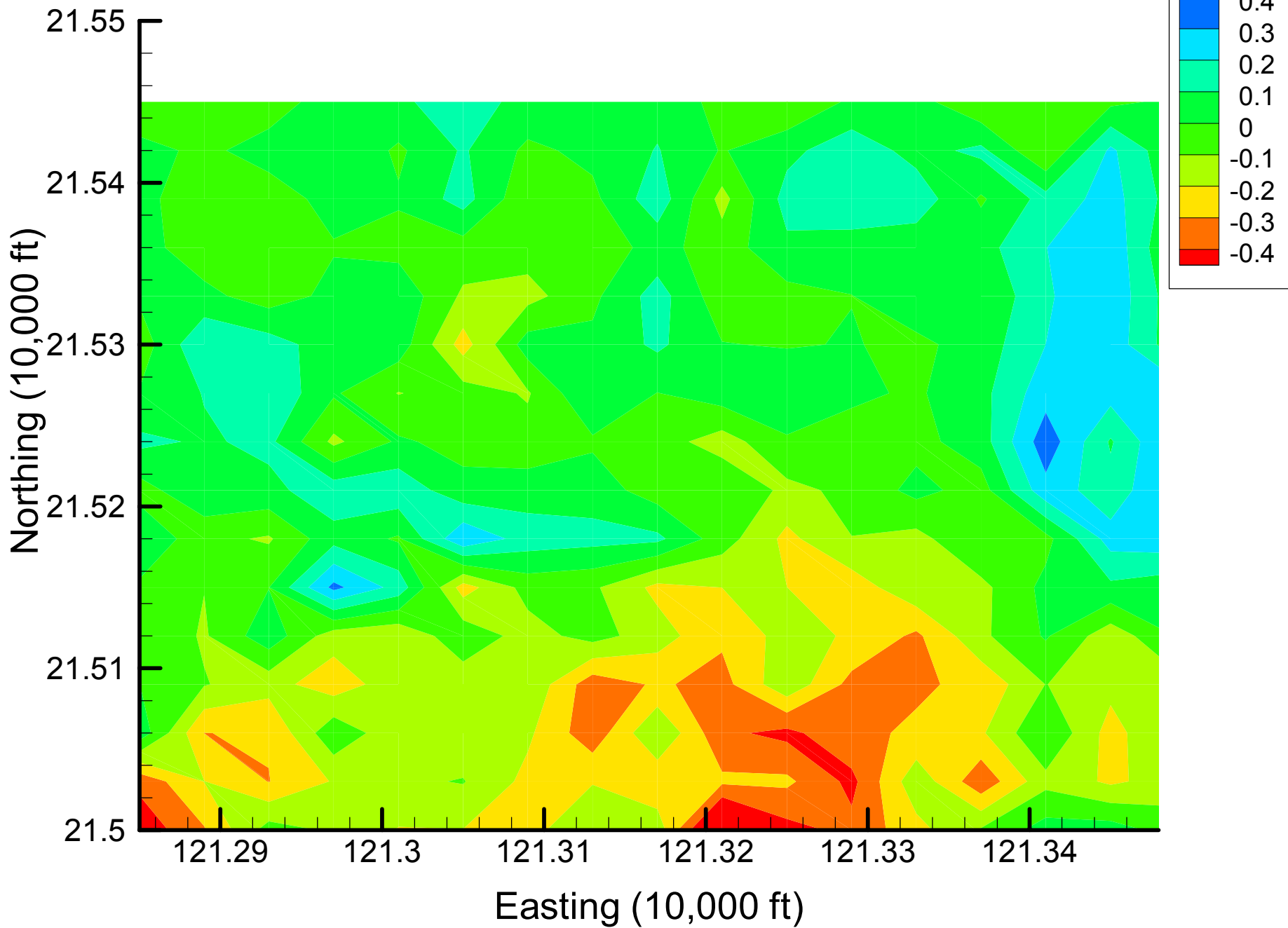
Site 49: DCE12C Indicator Differences, 2001, 35% Removal



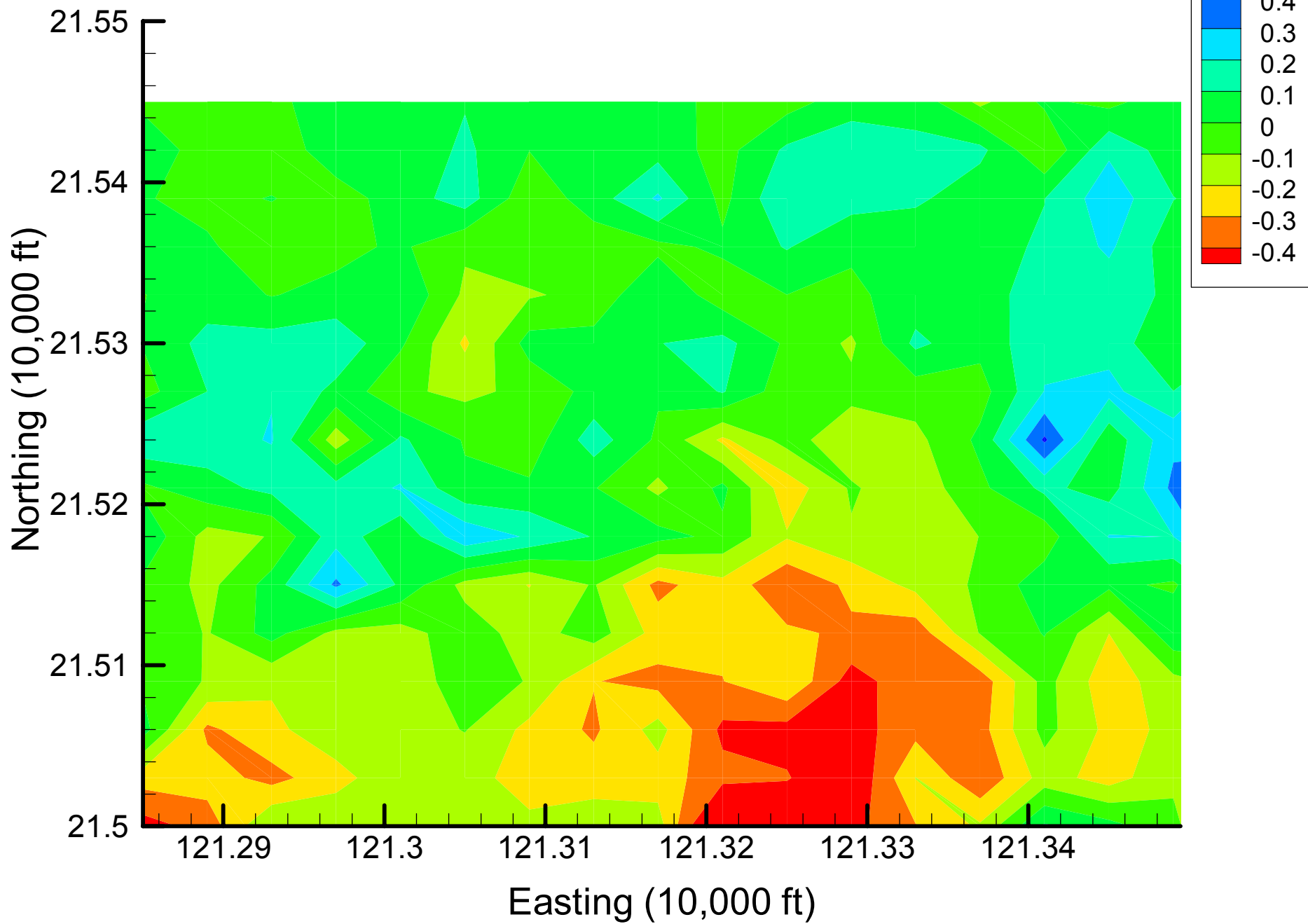
Site 49: DCE12C Indicator Differences, 2001, 40% Removal



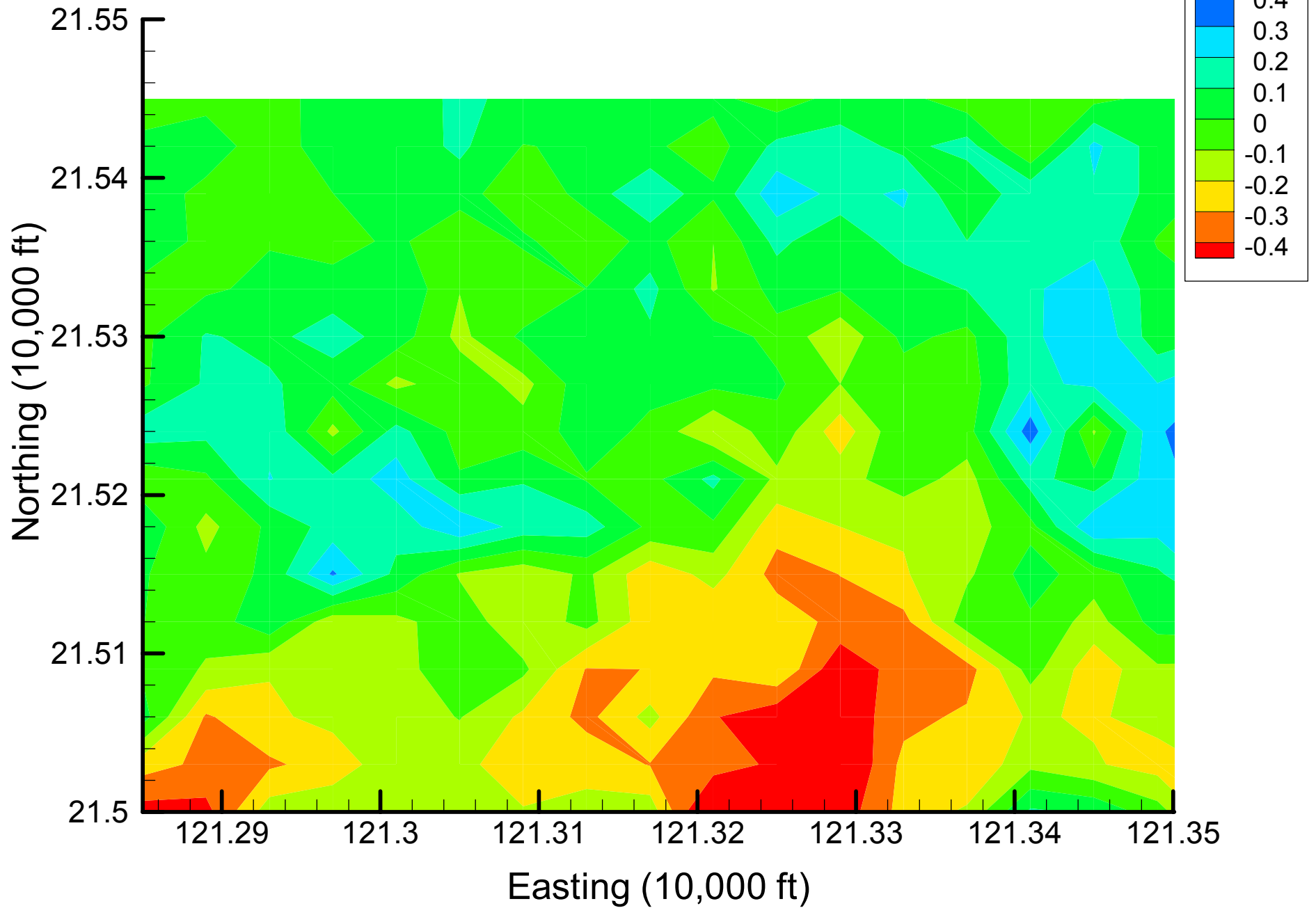
Site 49: DCE12C Indicator Differences, 2001, 45% Removal



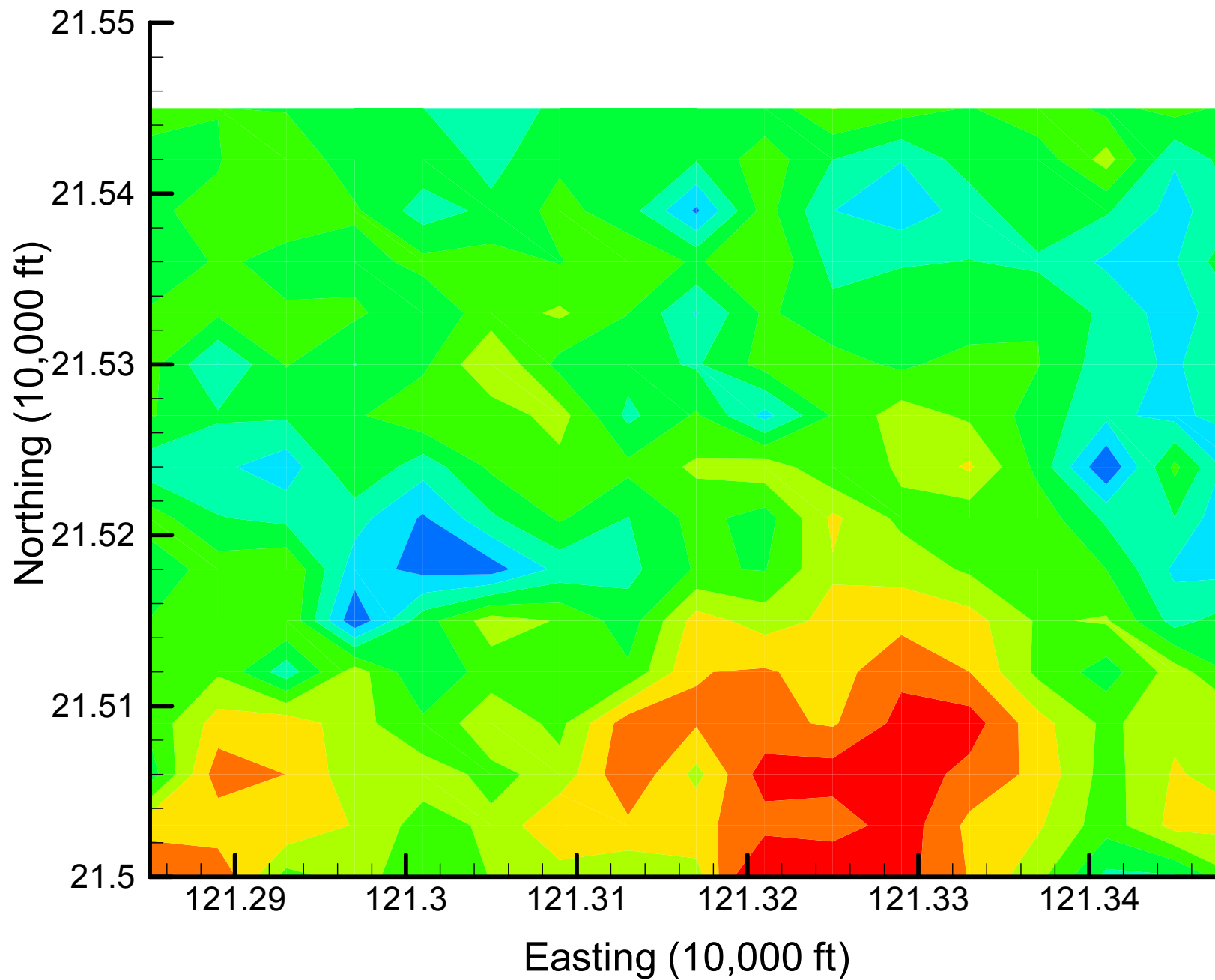
Site 49: DCE12C Indicator Differences, 2001, 50% Removal



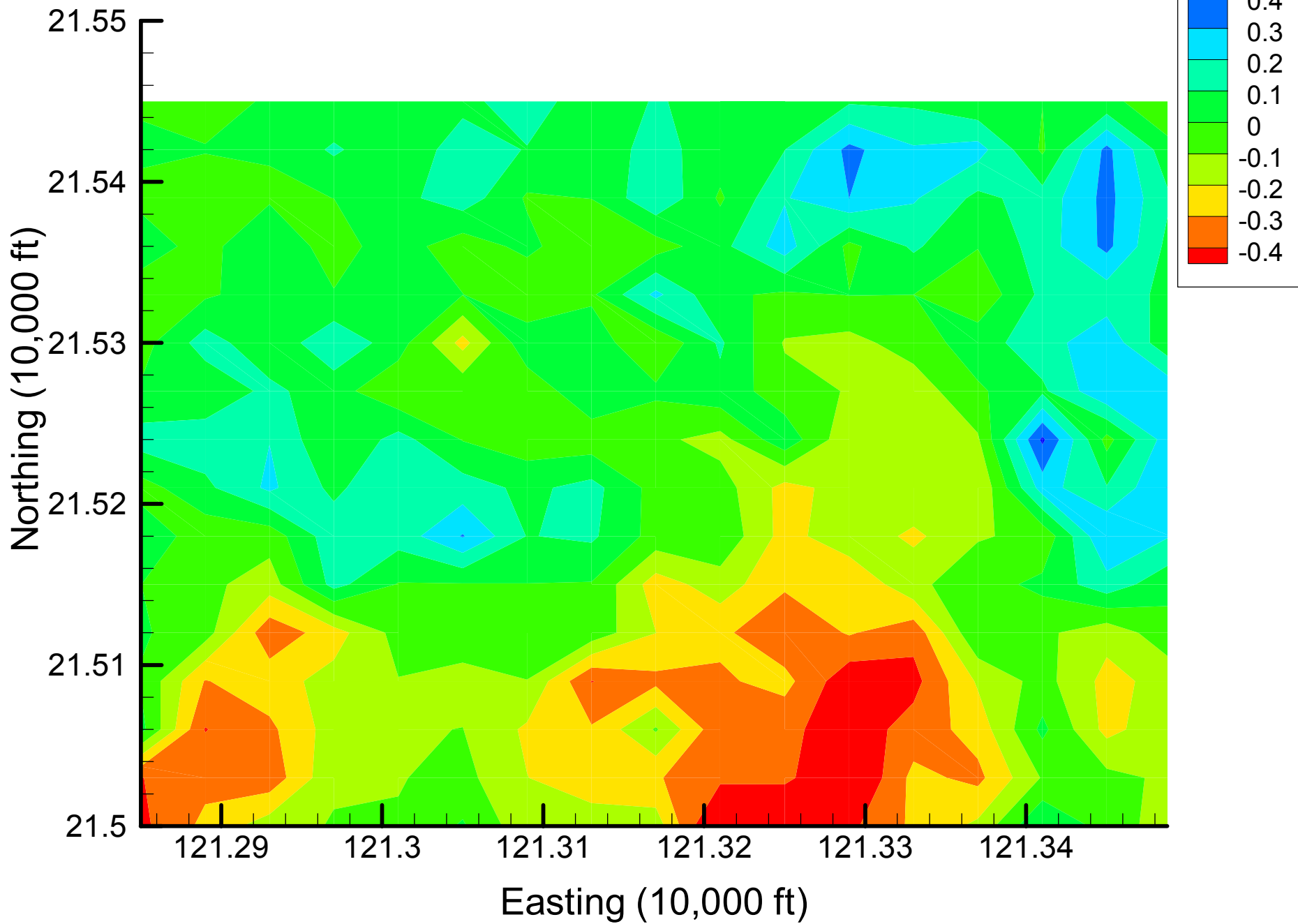
Site 49: DCE12C Indicator Differences, 2001, 55% Removal



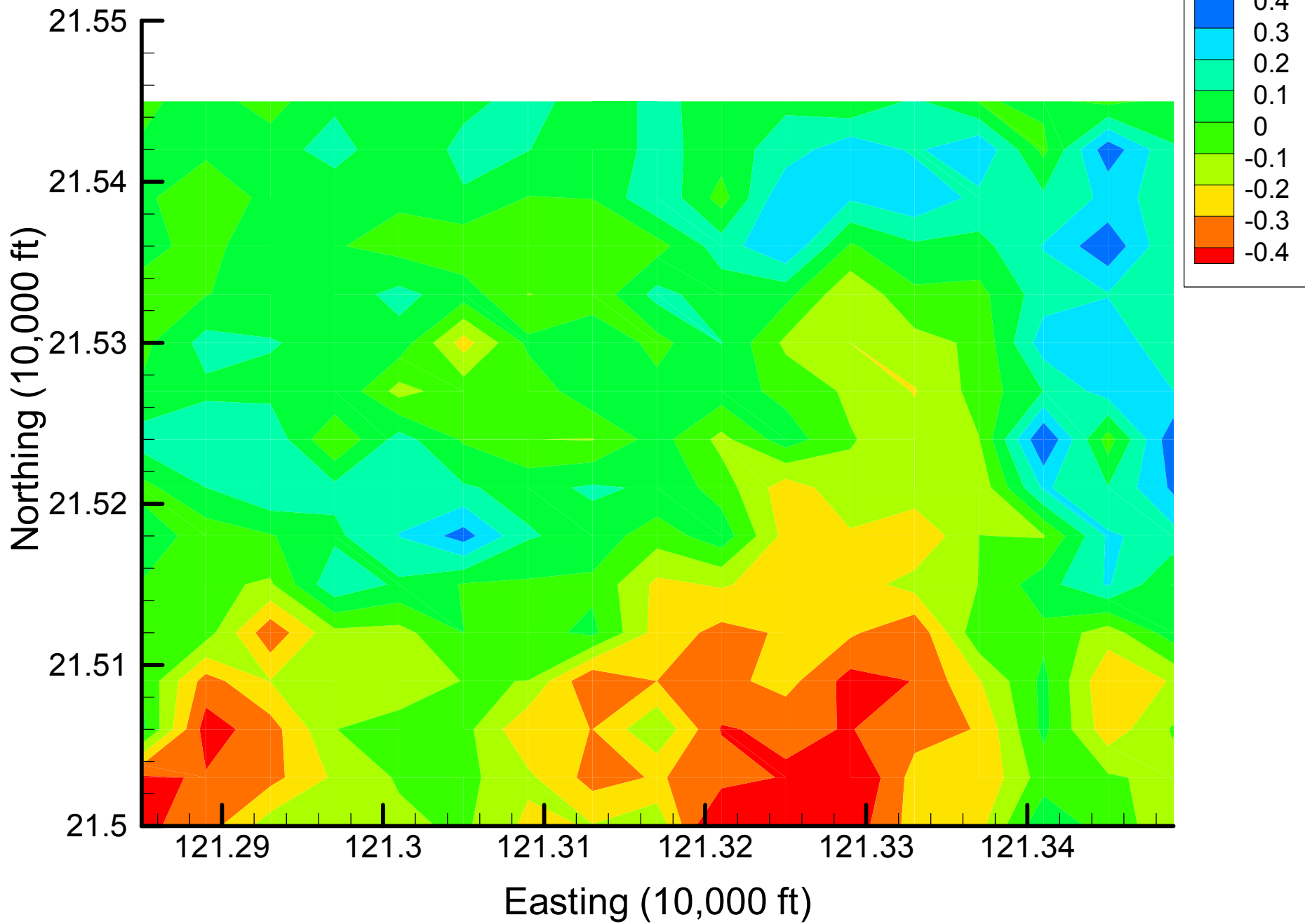
Site 49: DCE12C Indicator Differences, 2001, 60% Removal



Site 49: DCE12C Indicator Differences, 2001, 65% Removal



Site 49: DCE12C Indicator Differences, 2001, 70% Removal

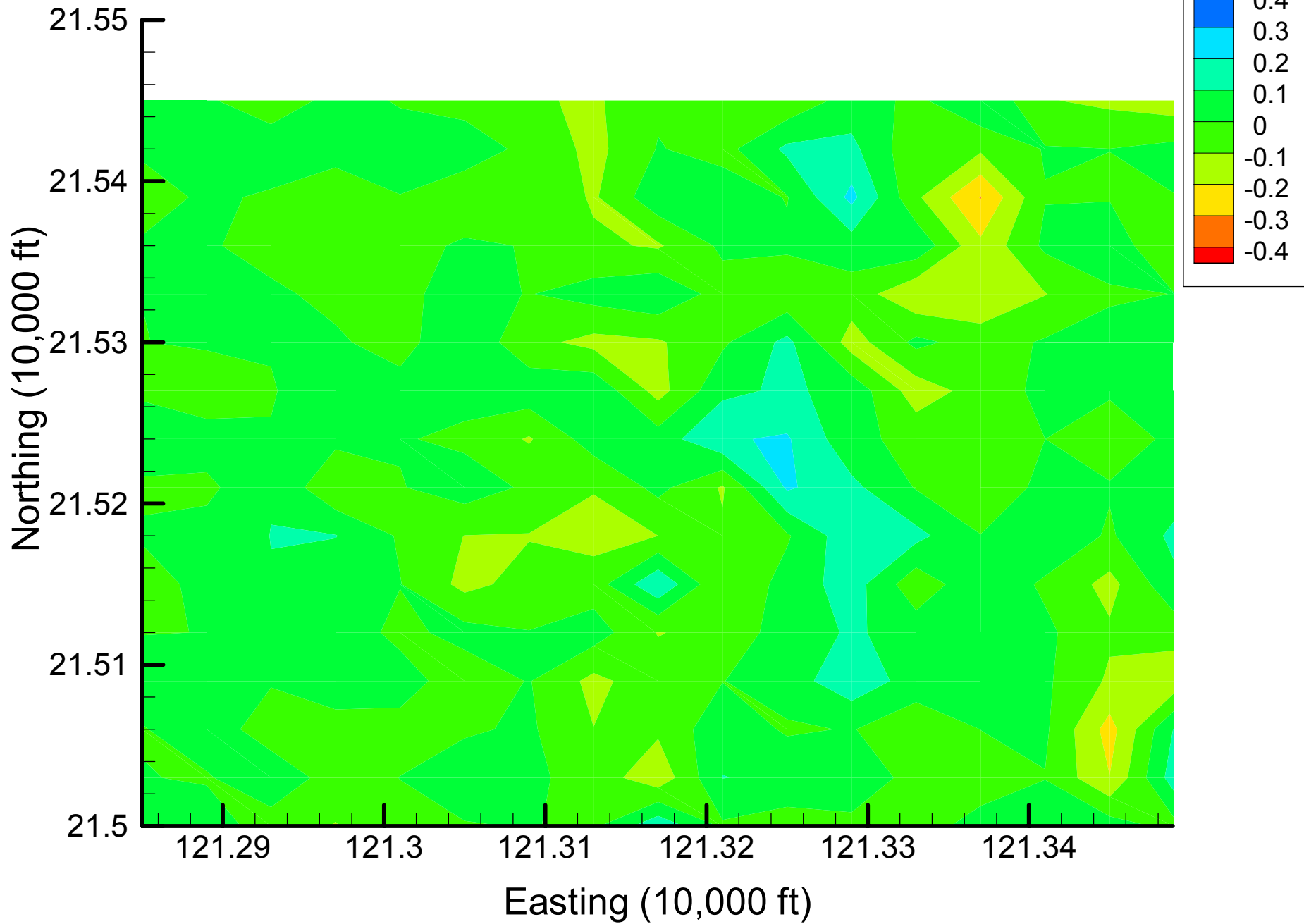


## Appendix 4.2

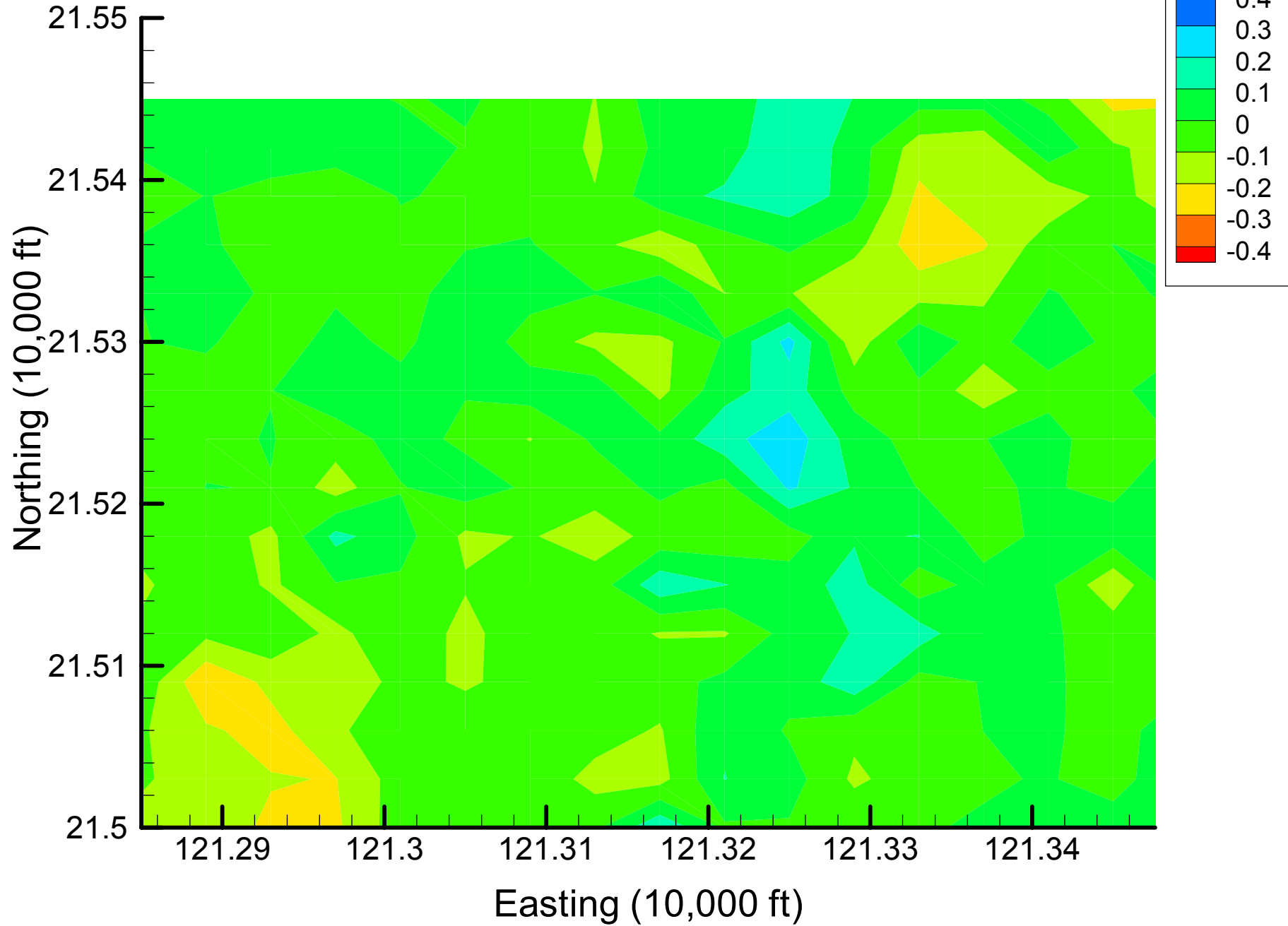
# DCE12C Indicator Difference Maps

Time Slice 2 — 2002

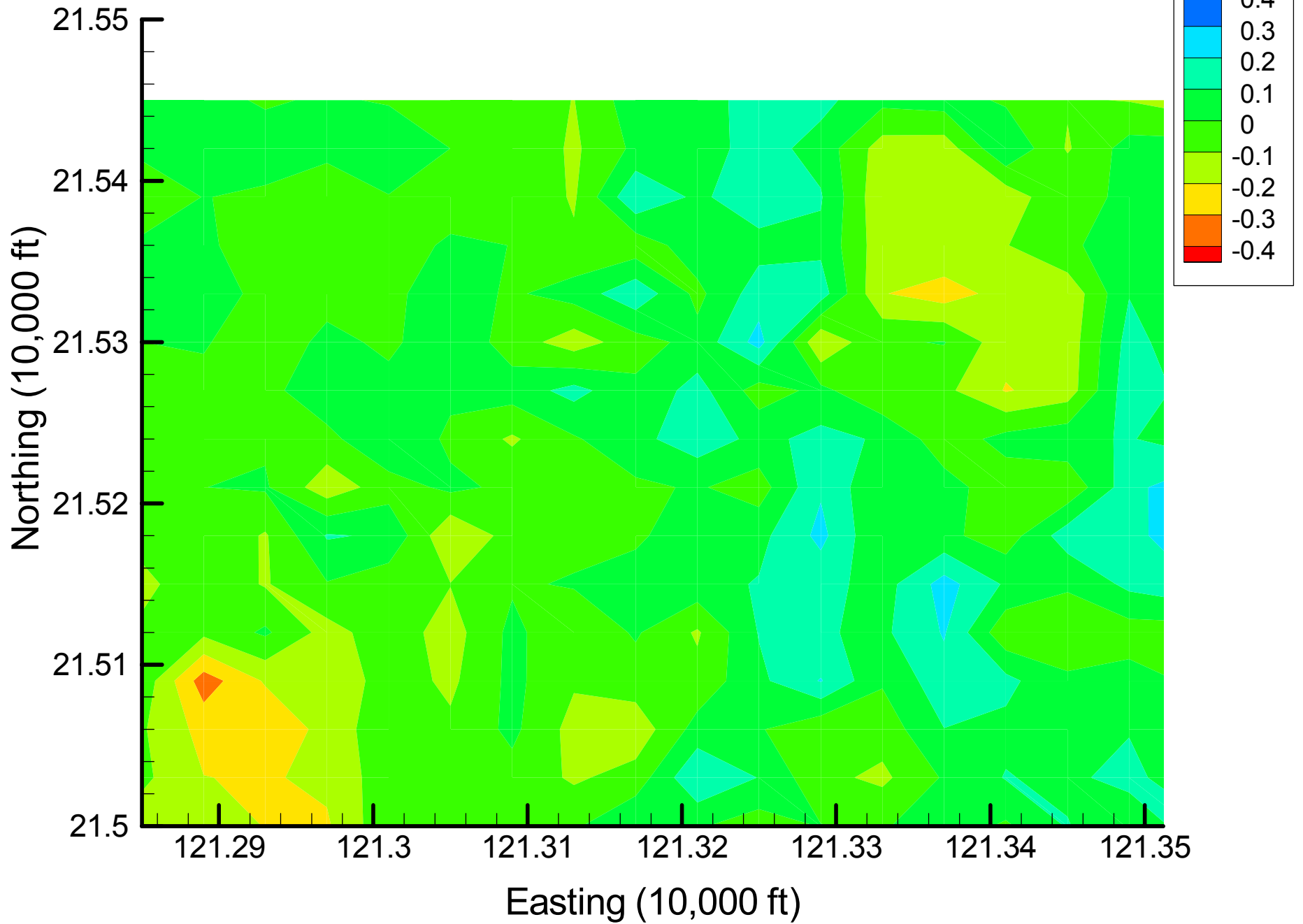
Site 49: DCE12C Indicator Differences, 2002, 5% Removal



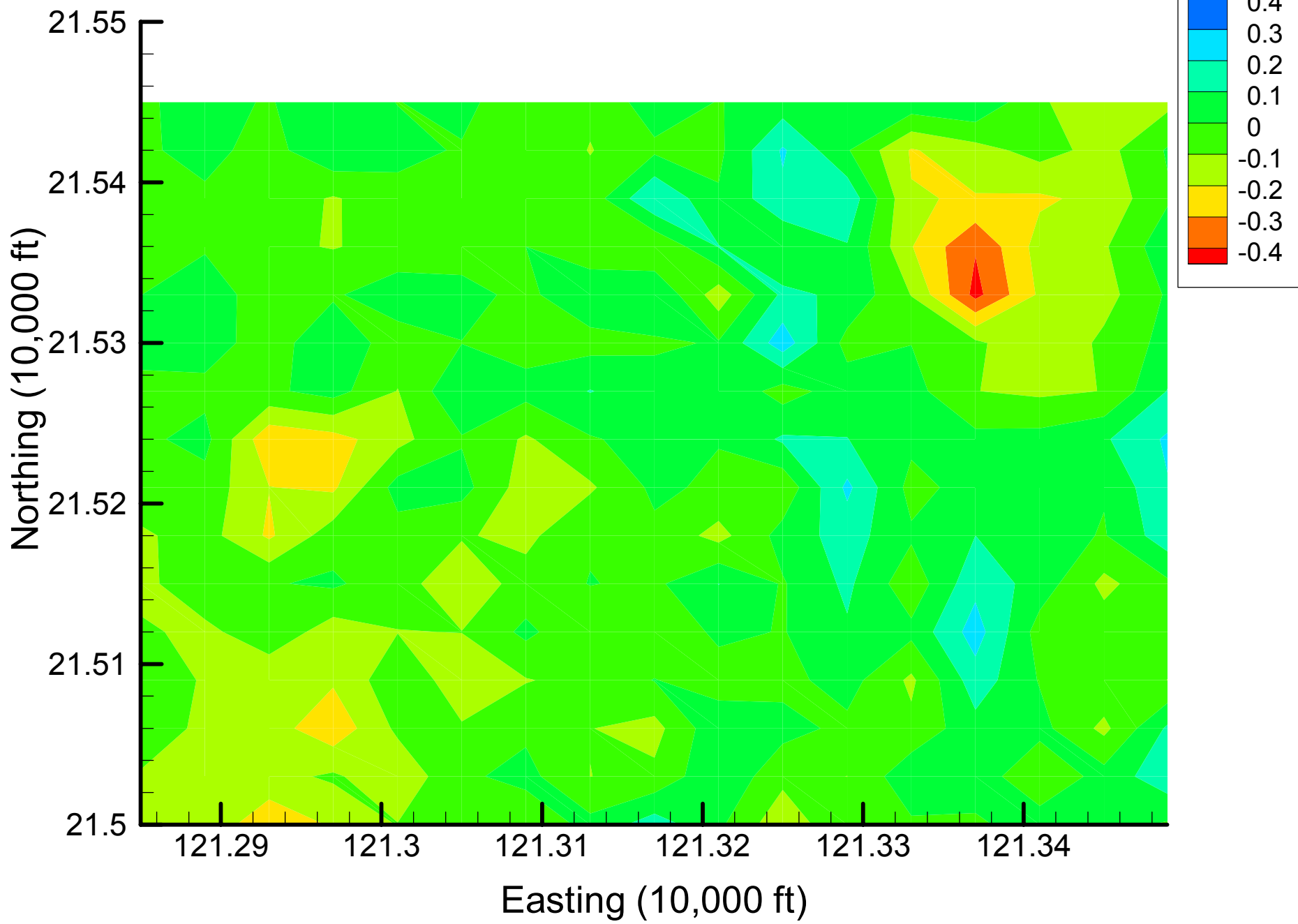
Site 49: DCA11 Indicator Differences, 2002, 10% Removal



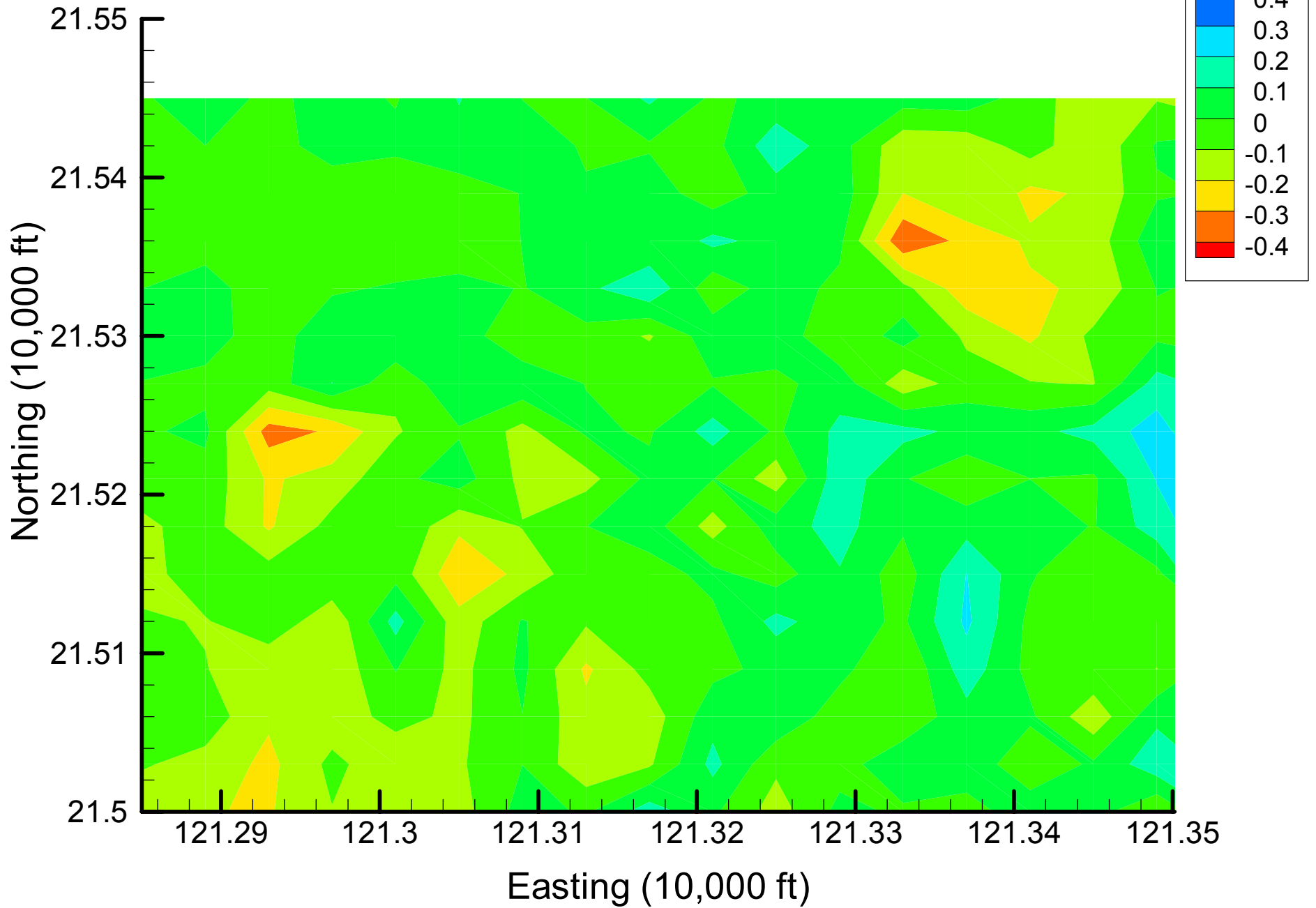
Site 49: DCE12C Indicator Differences, 2002, 15% Removal



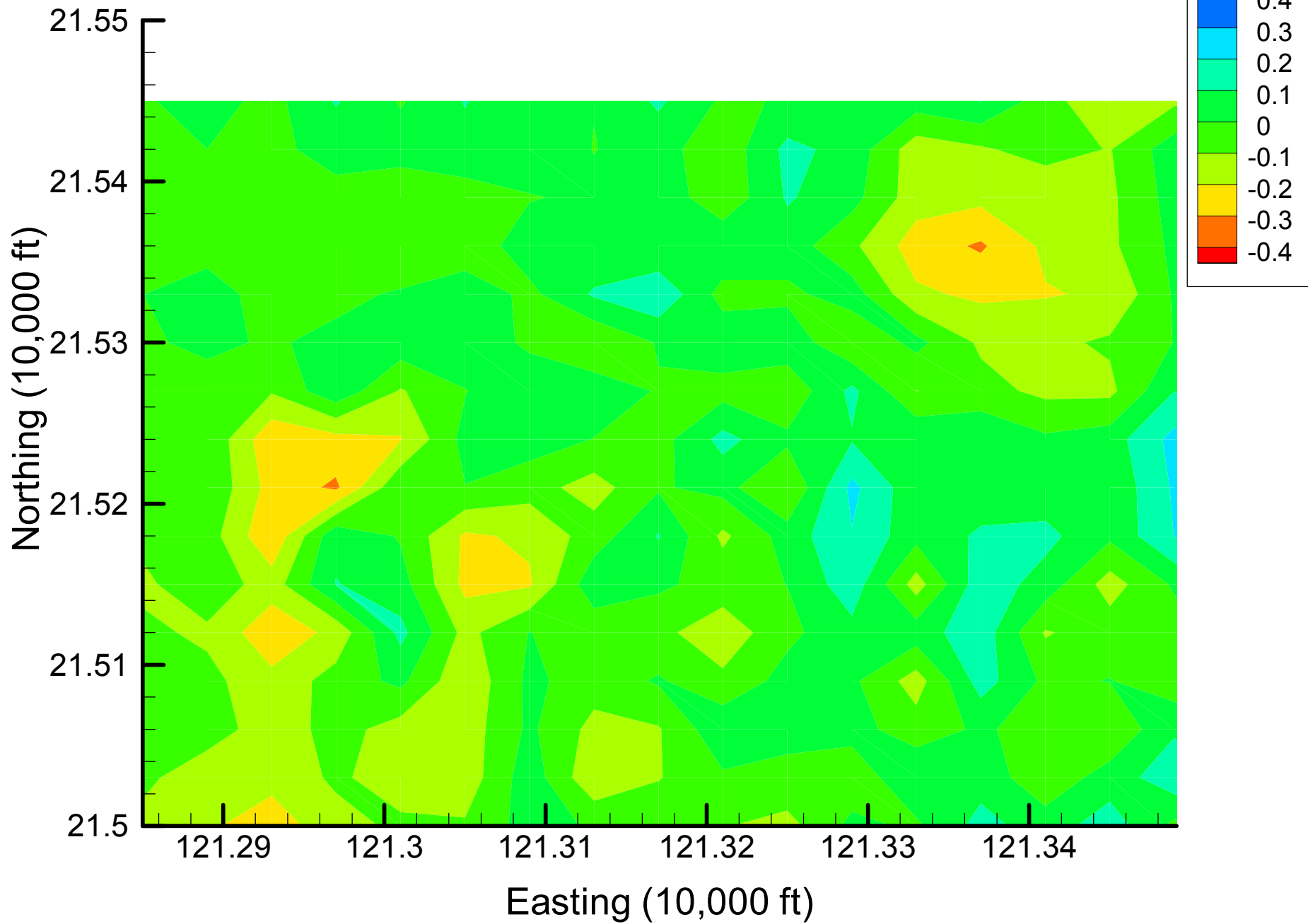
Site 49: DCA11 Indicator Differences, 2002, 20% Removal



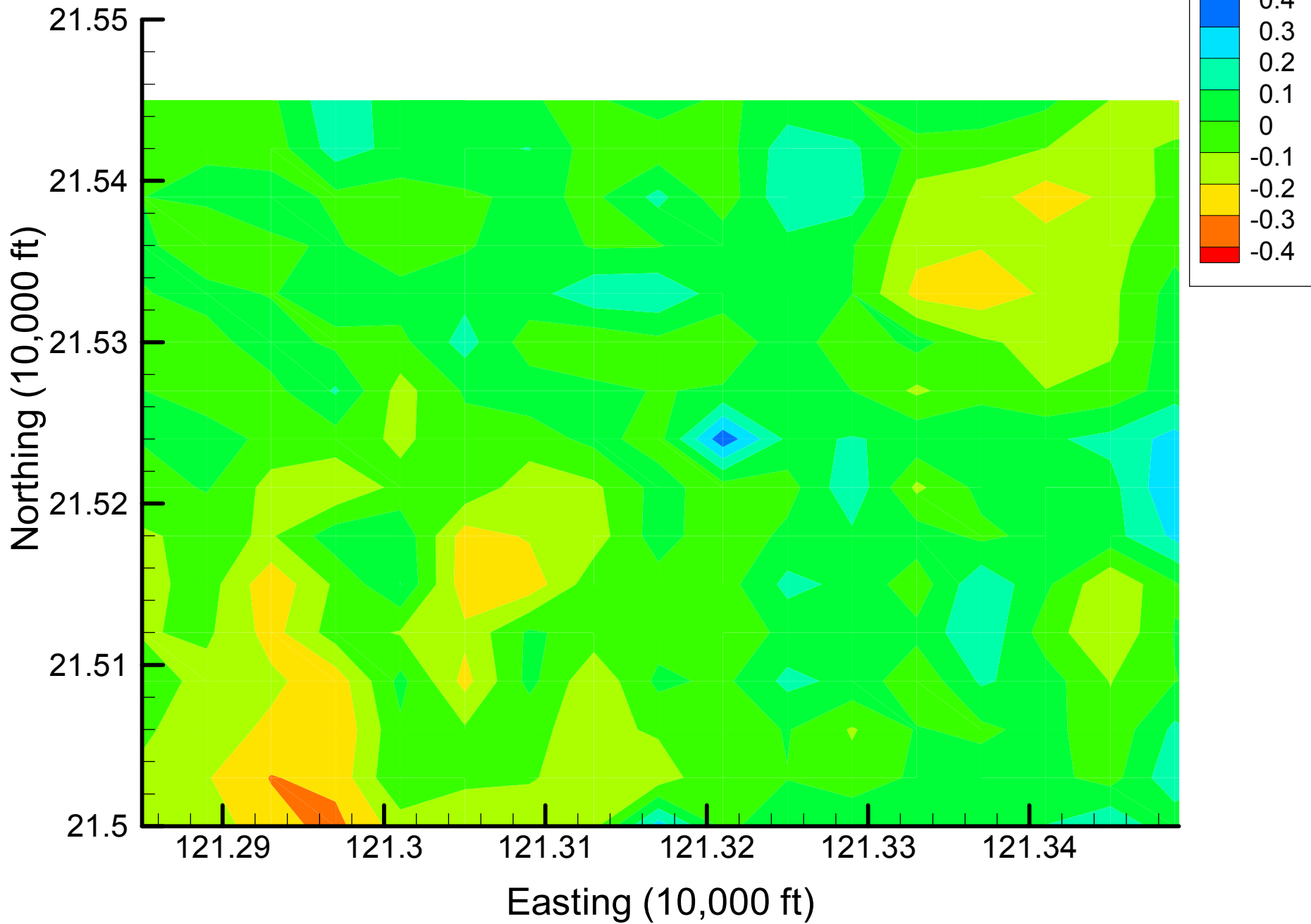
Site 49: DCE12C Indicator Differences, 2002, 25% Removal



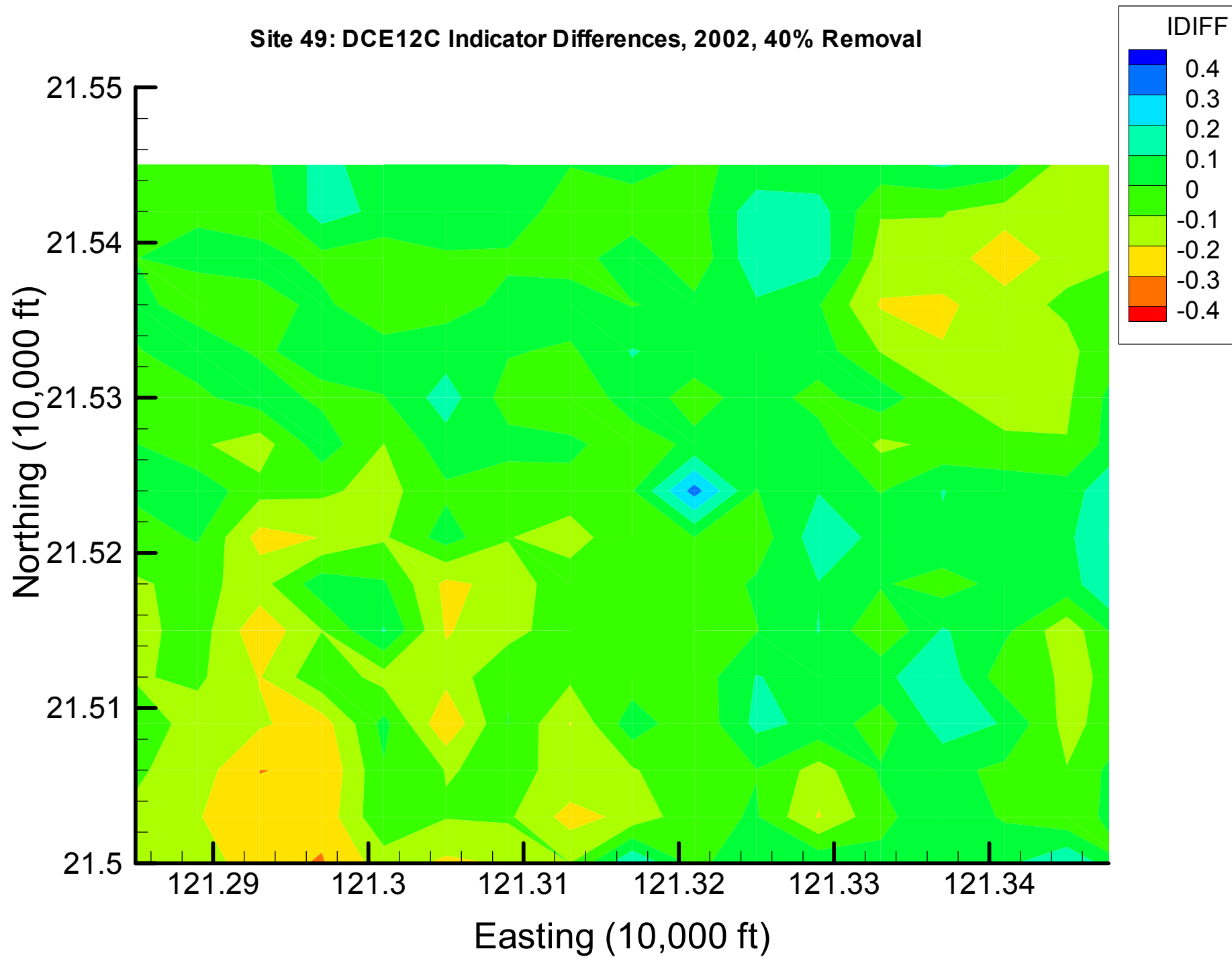
Site 49: DCE12C Indicator Differences, 2002, 30% Removal



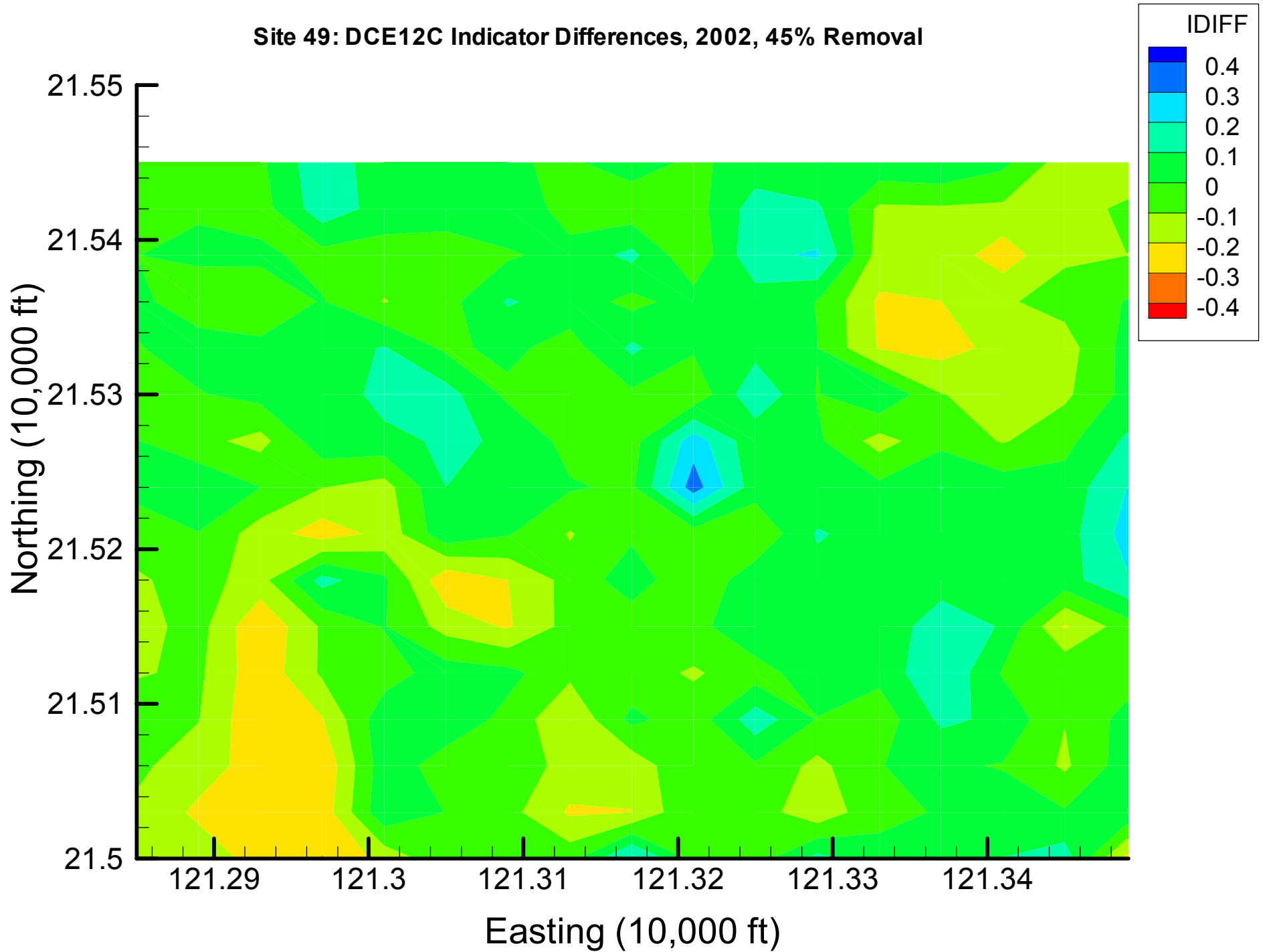
Site 49: DCE12C Indicator Differences, 2002, 35% Removal



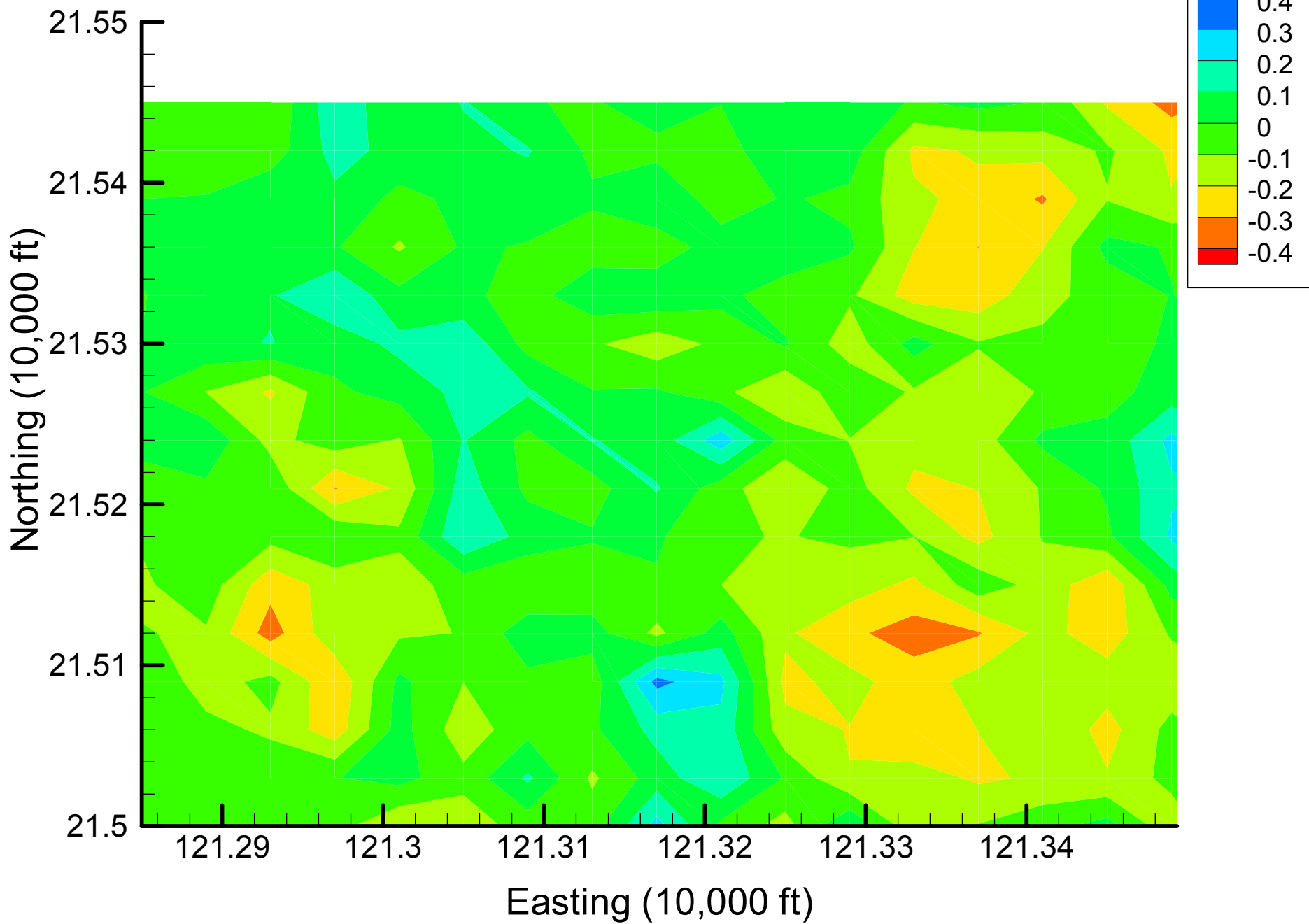
Site 49: DCE12C Indicator Differences, 2002, 40% Removal



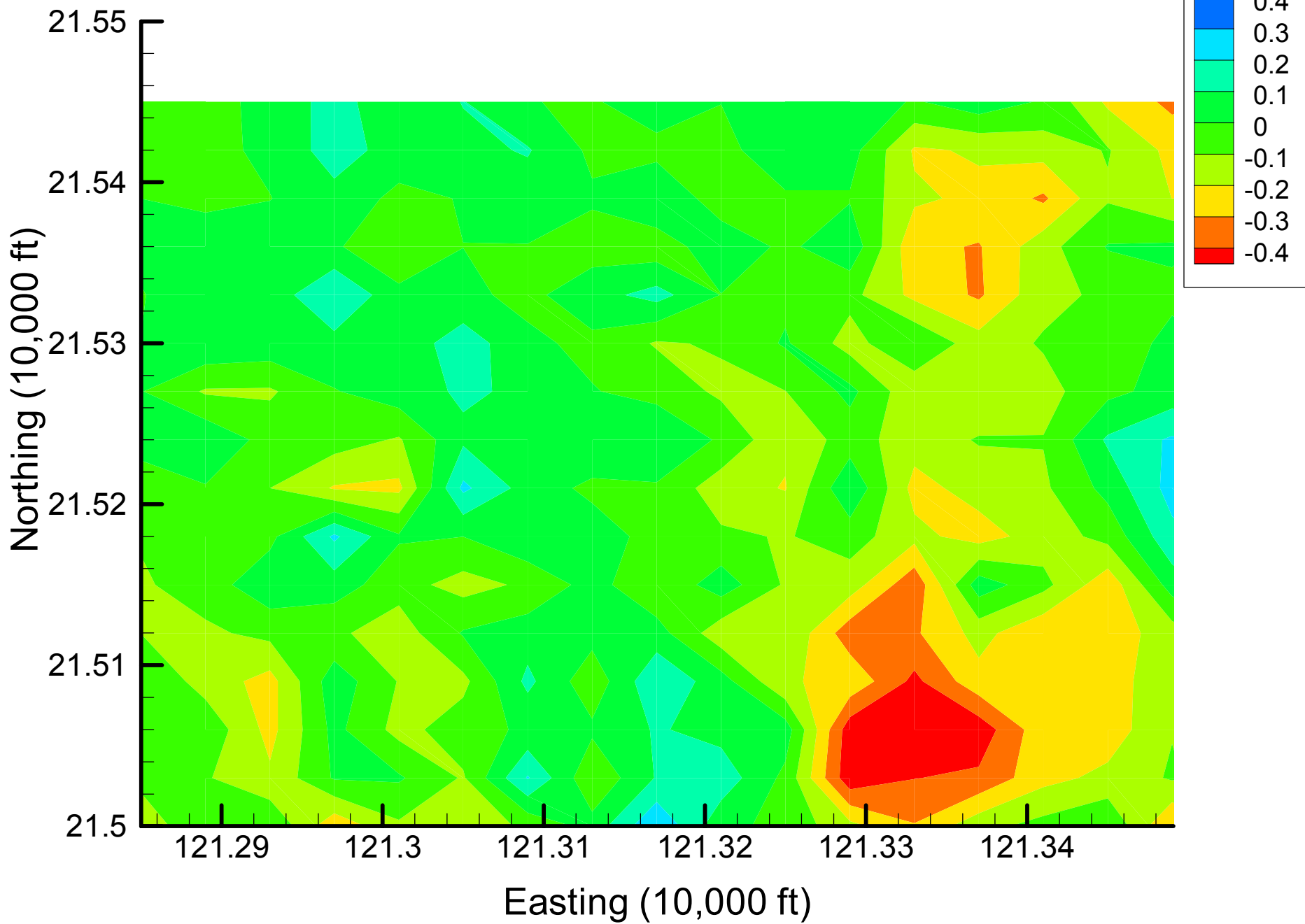
Site 49: DCE12C Indicator Differences, 2002, 45% Removal



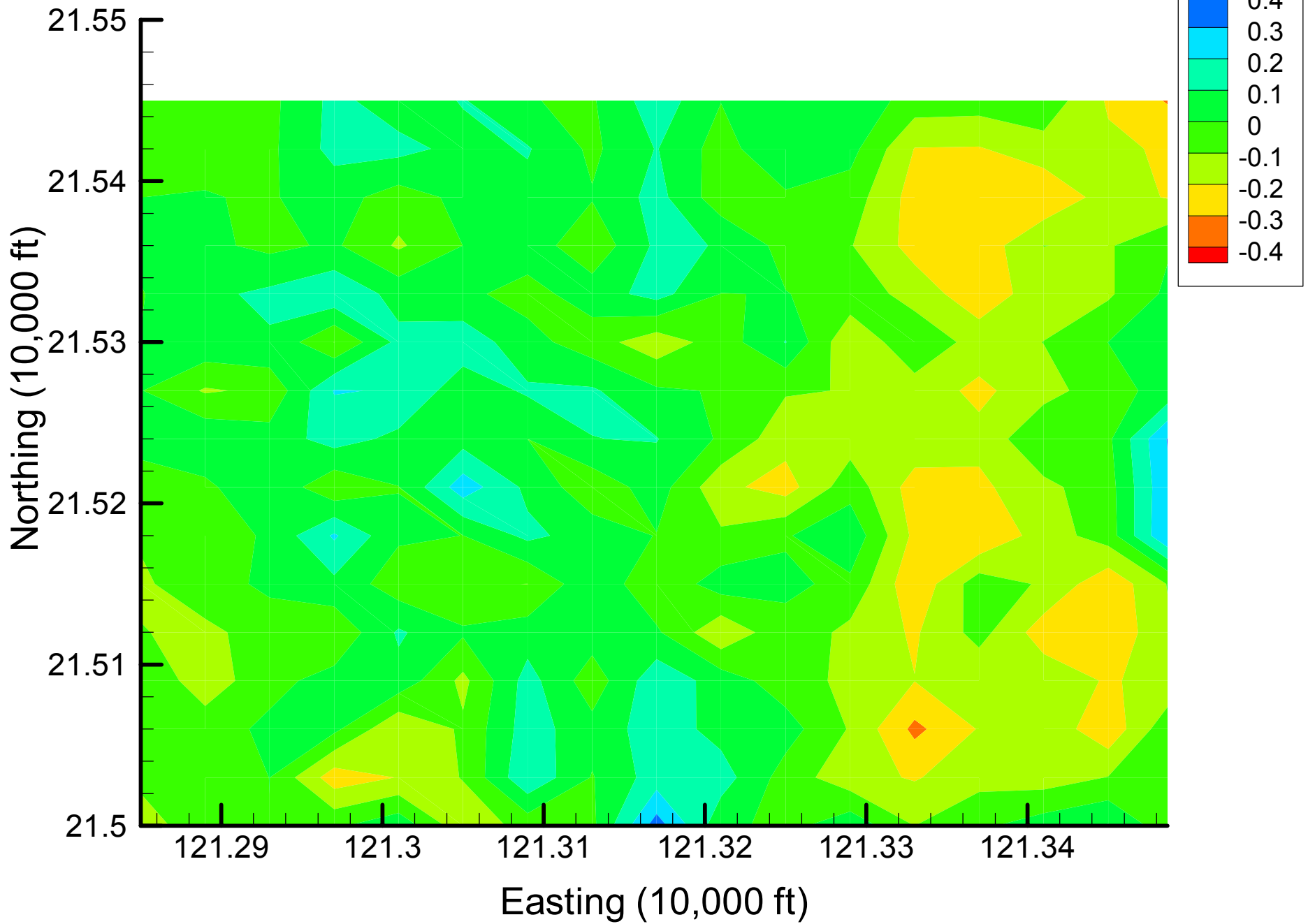
Site 49: DCE12C Indicator Differences, 2002, 50% Removal



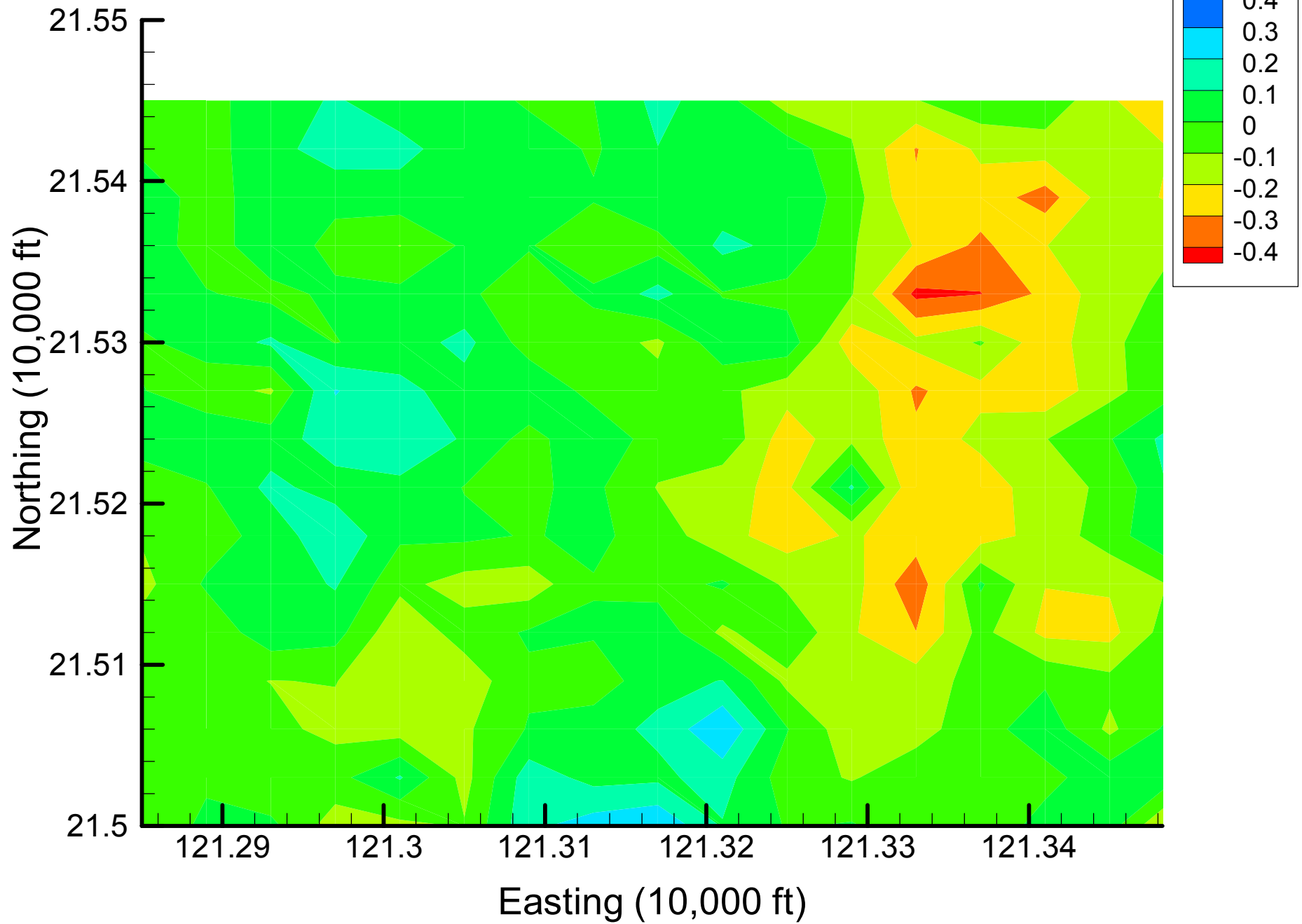
Site 49: DCE12C Indicator Differences, 2002, 55% Removal



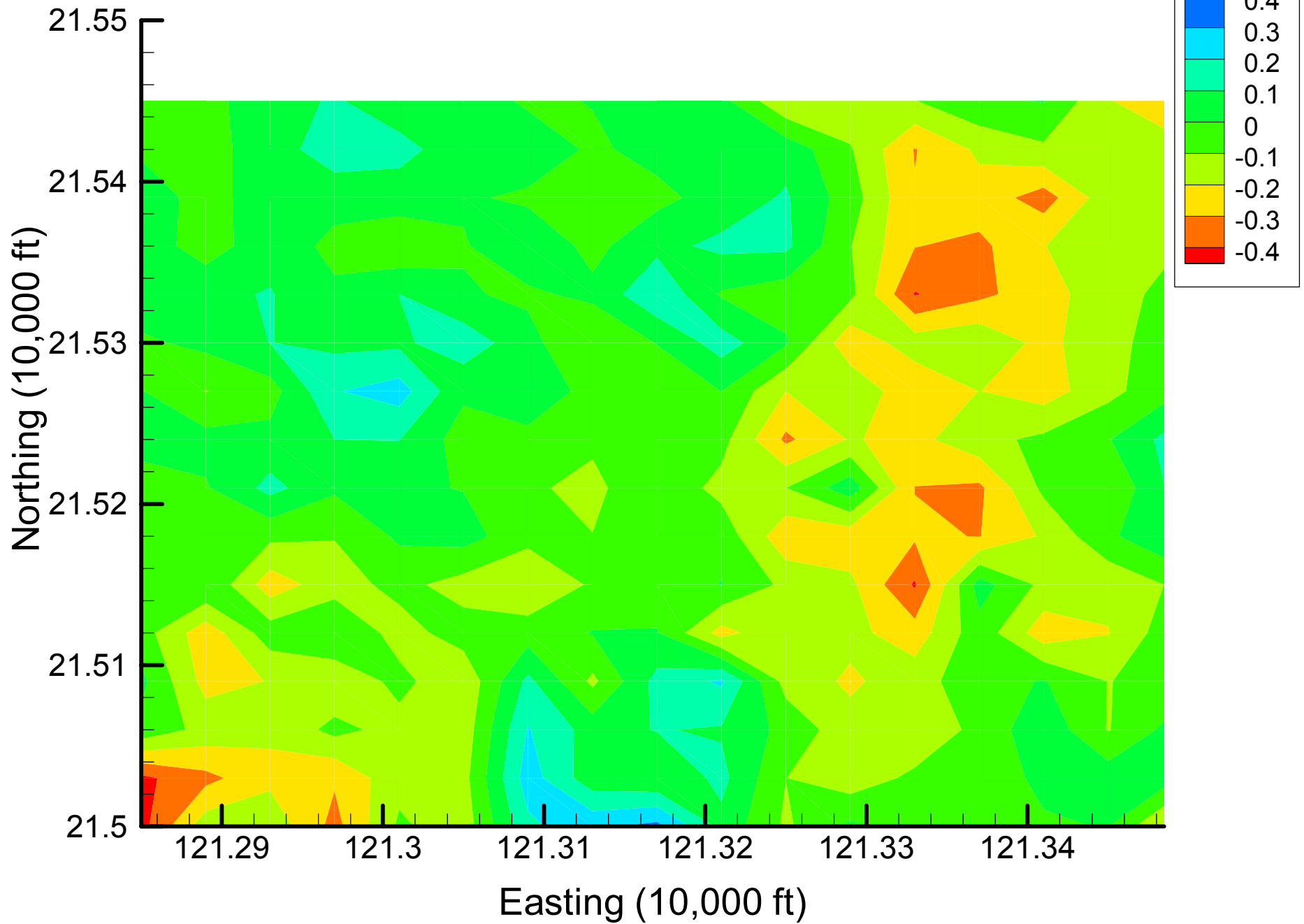
Site 49: DCE12C Indicator Differences, 2002, 60% Removal



Site 49: DCE12C Indicator Differences, 2002, 65% Removal

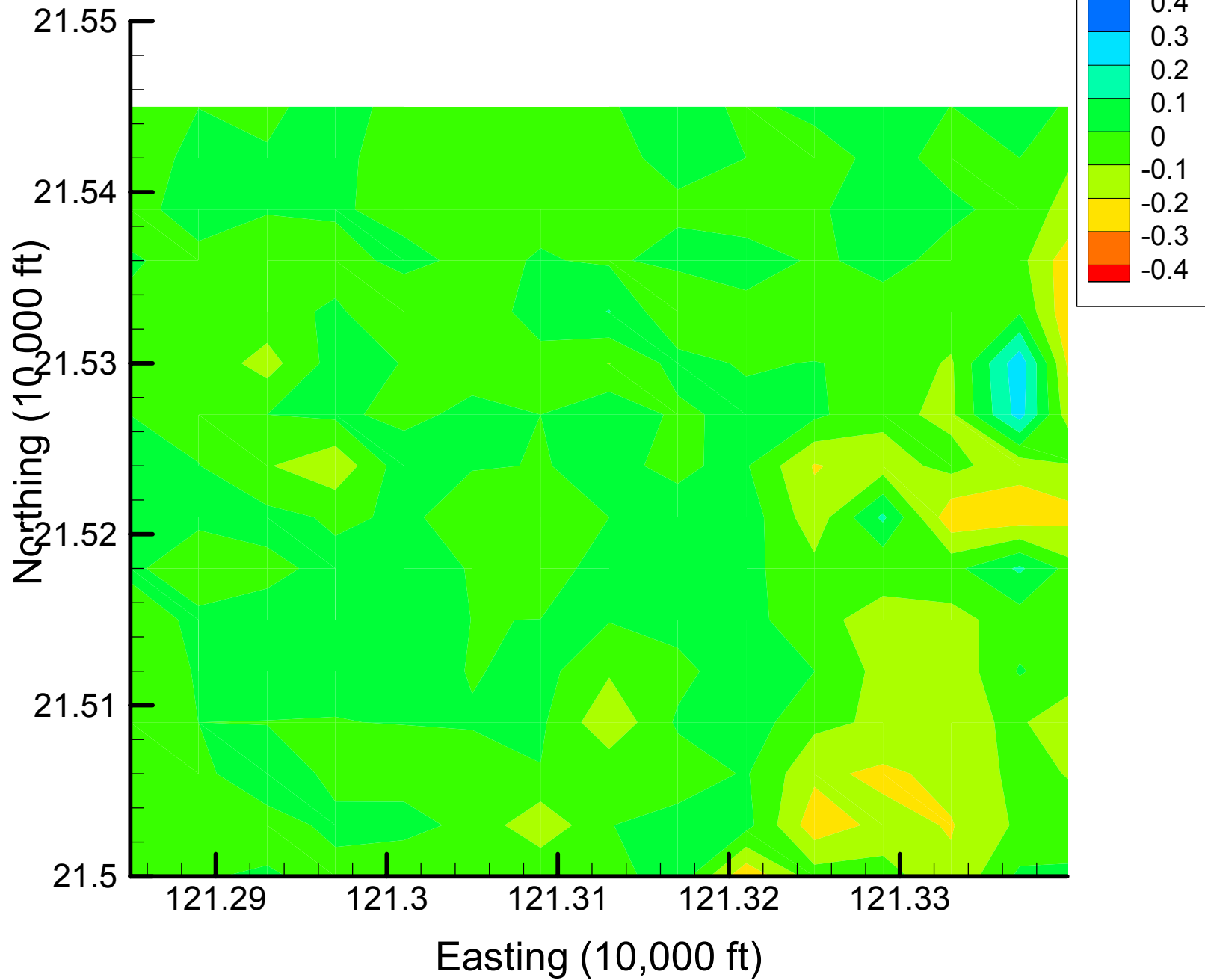


Site 49: DCE12C Indicator Differences, 2002, 70% Removal

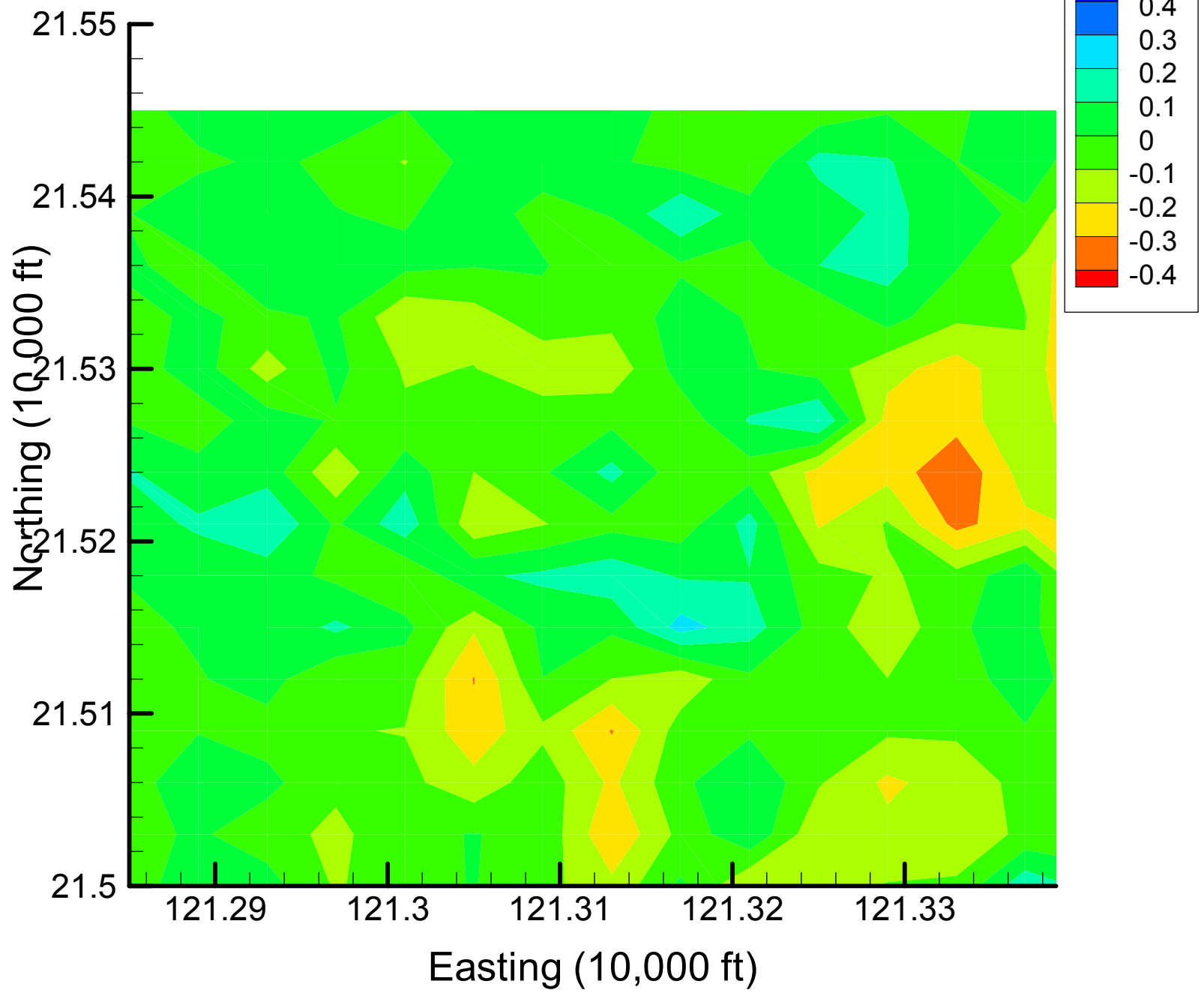


Appendix 4.2  
TCE Indicator Difference Maps  
Time Slice 1 — 2001

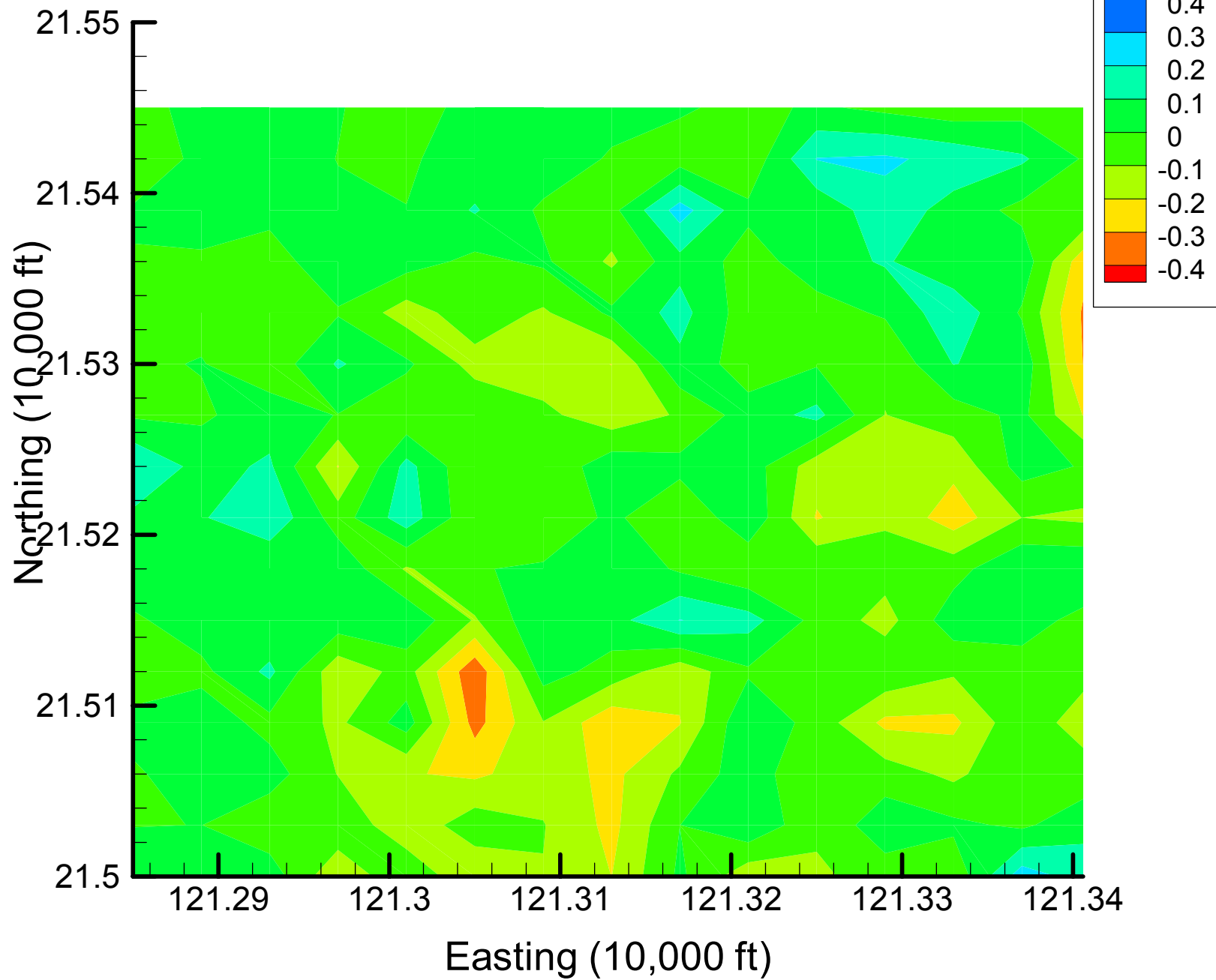
Site 49: TCE Indicator Differences, 2001, 5% Removal



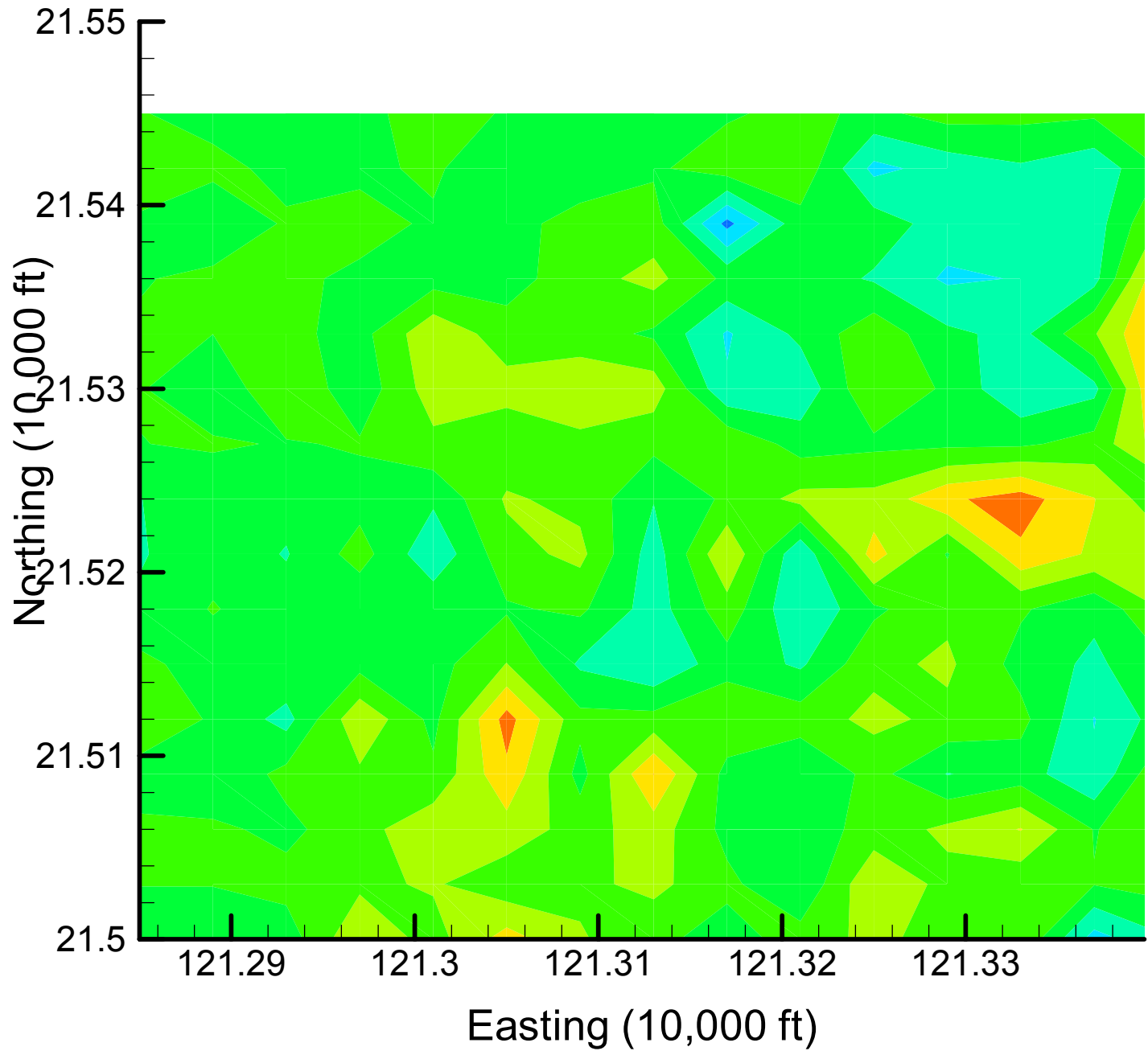
Site 49: TCE Indicator Differences, 2001, 10% Removal



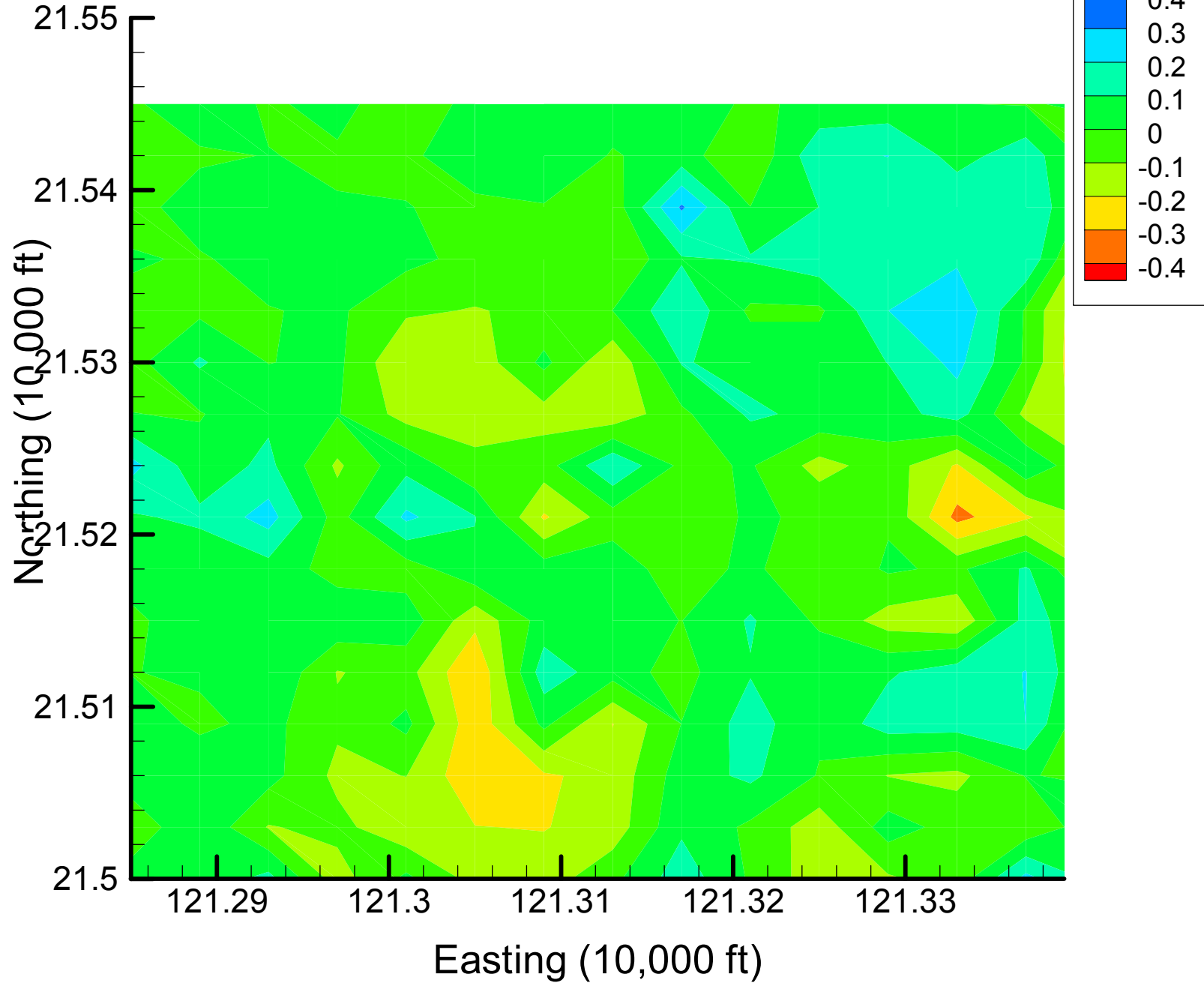
### Site 49: TCE Indicator Differences, 2001, 15% Removal



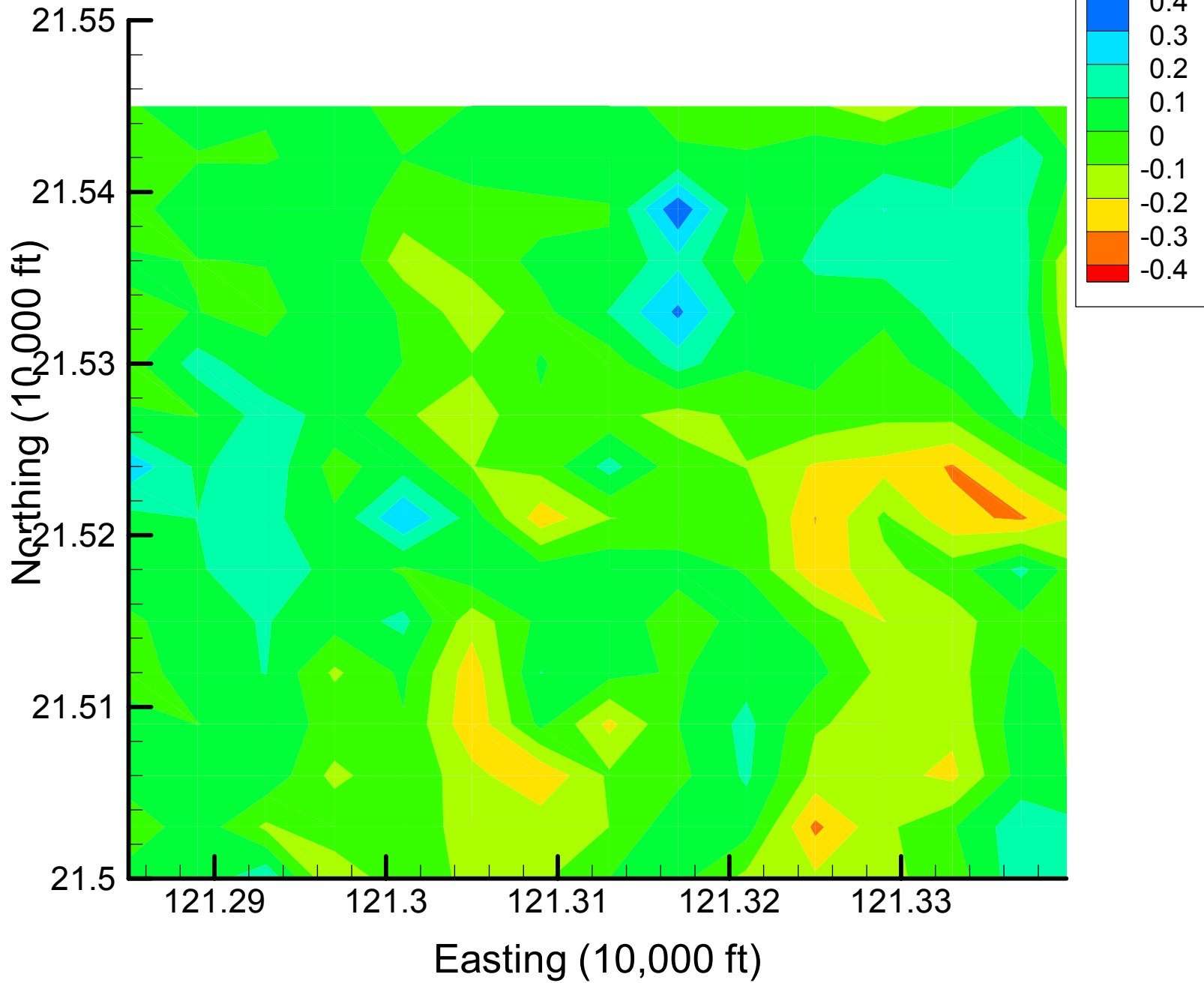
Site 49: TCE Indicator Differences, 2001, 20% Removal



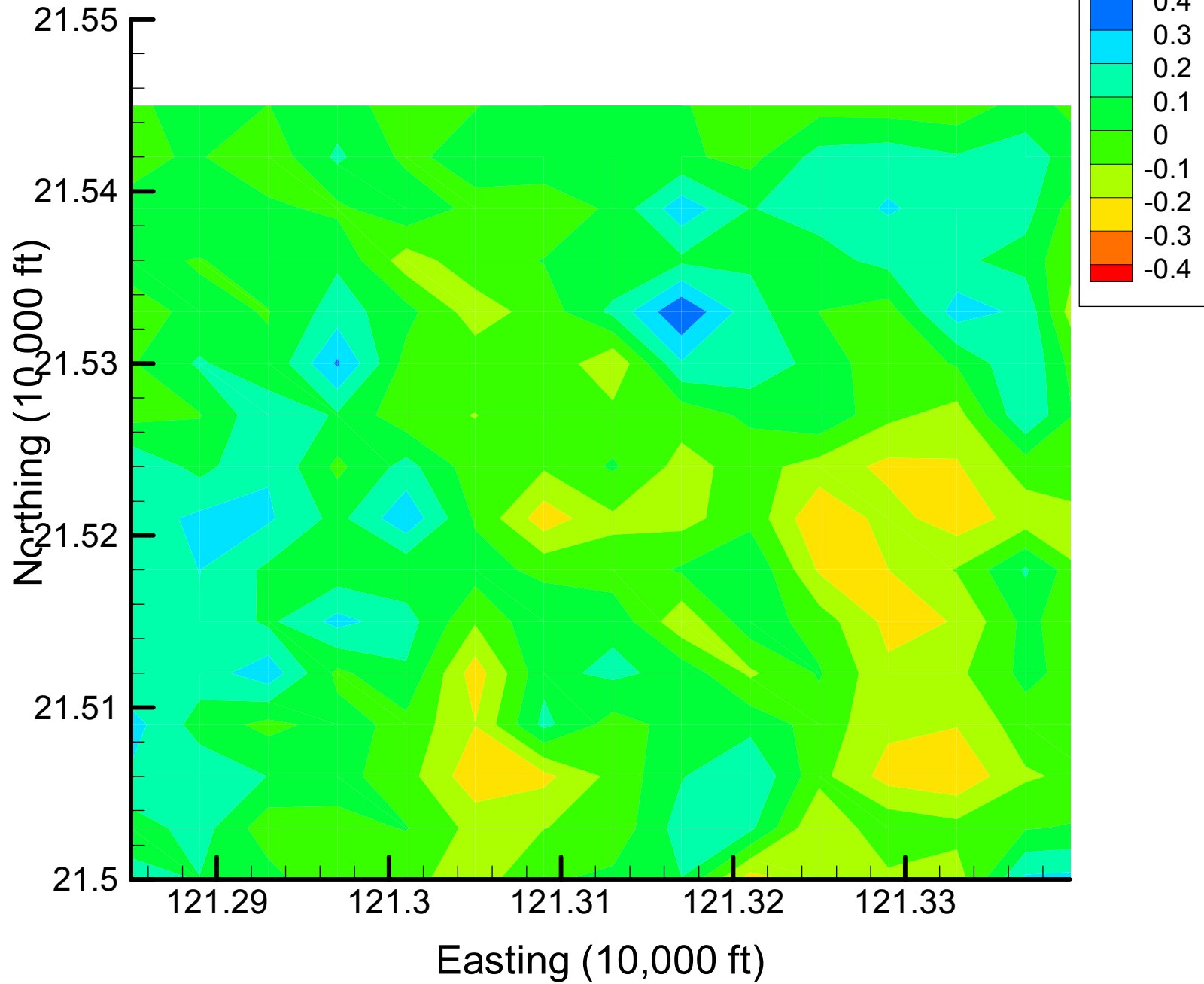
Site 49: TCE Indicator Differences, 2001, 25% Removal



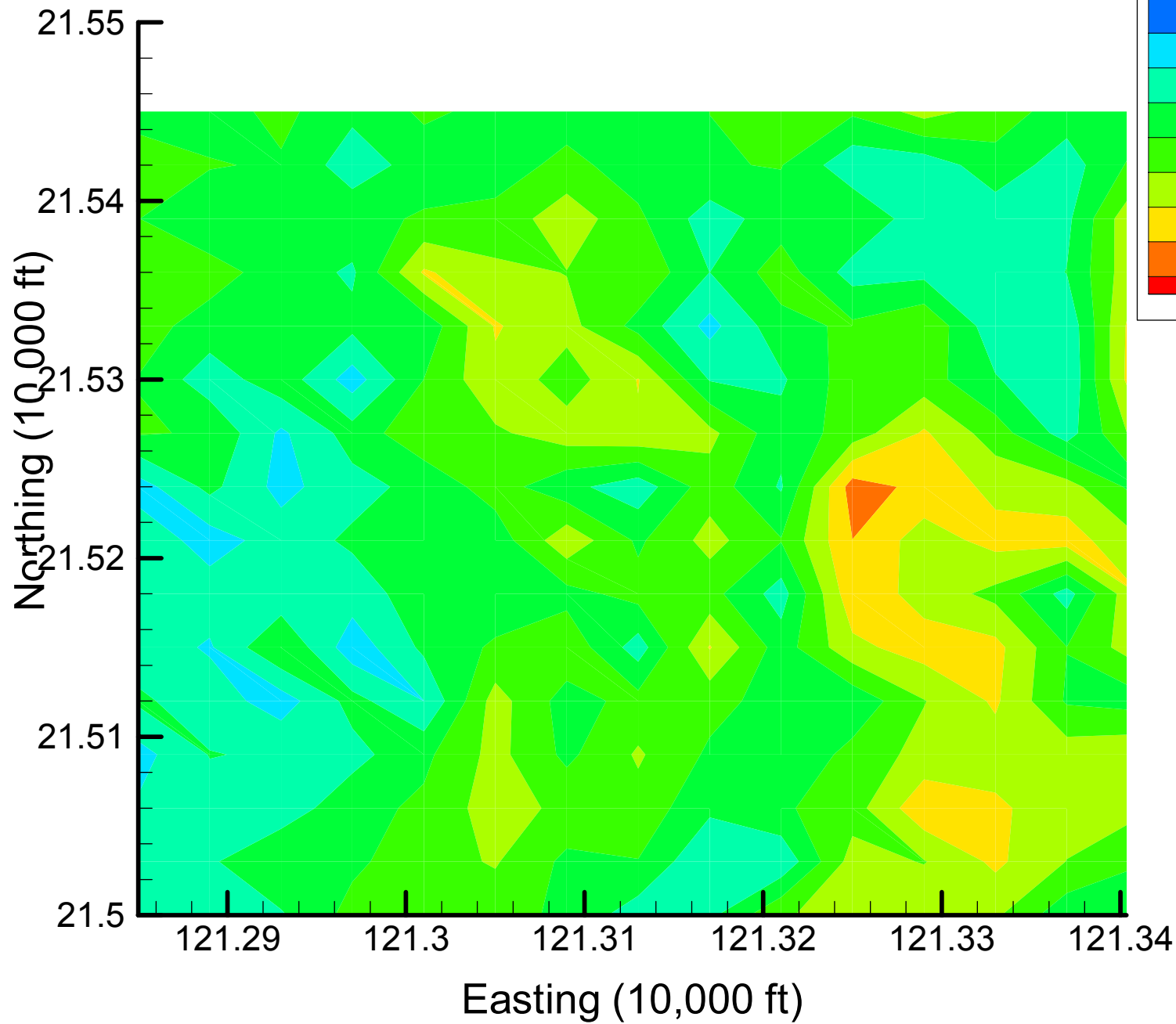
Site 49: TCE Indicator Differences, 2001, 30% Removal



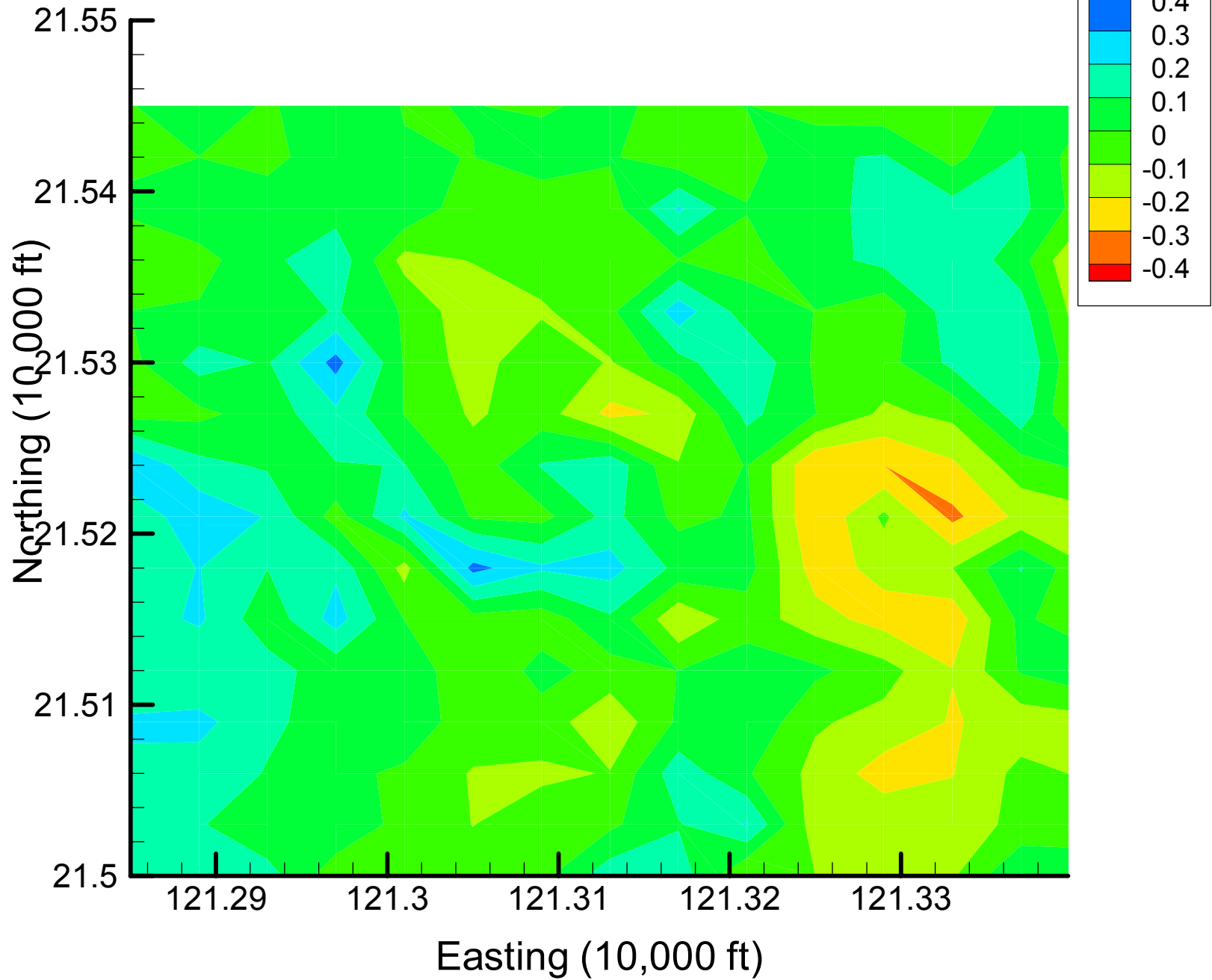
Site 49: TCE Indicator Differences, 2001, 35% Removal



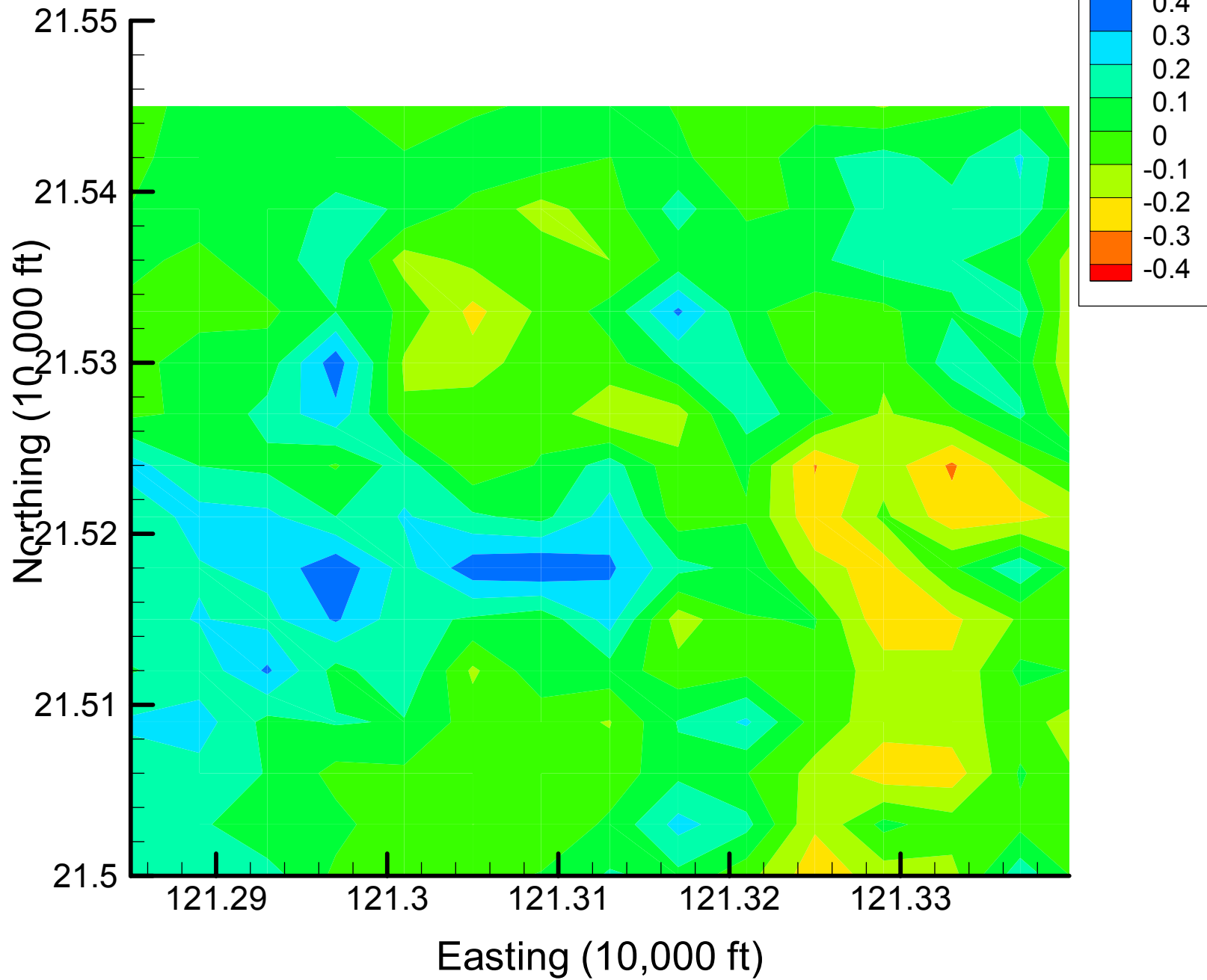
Site 49: TCE Indicator Differences, 2001, 40% Removal



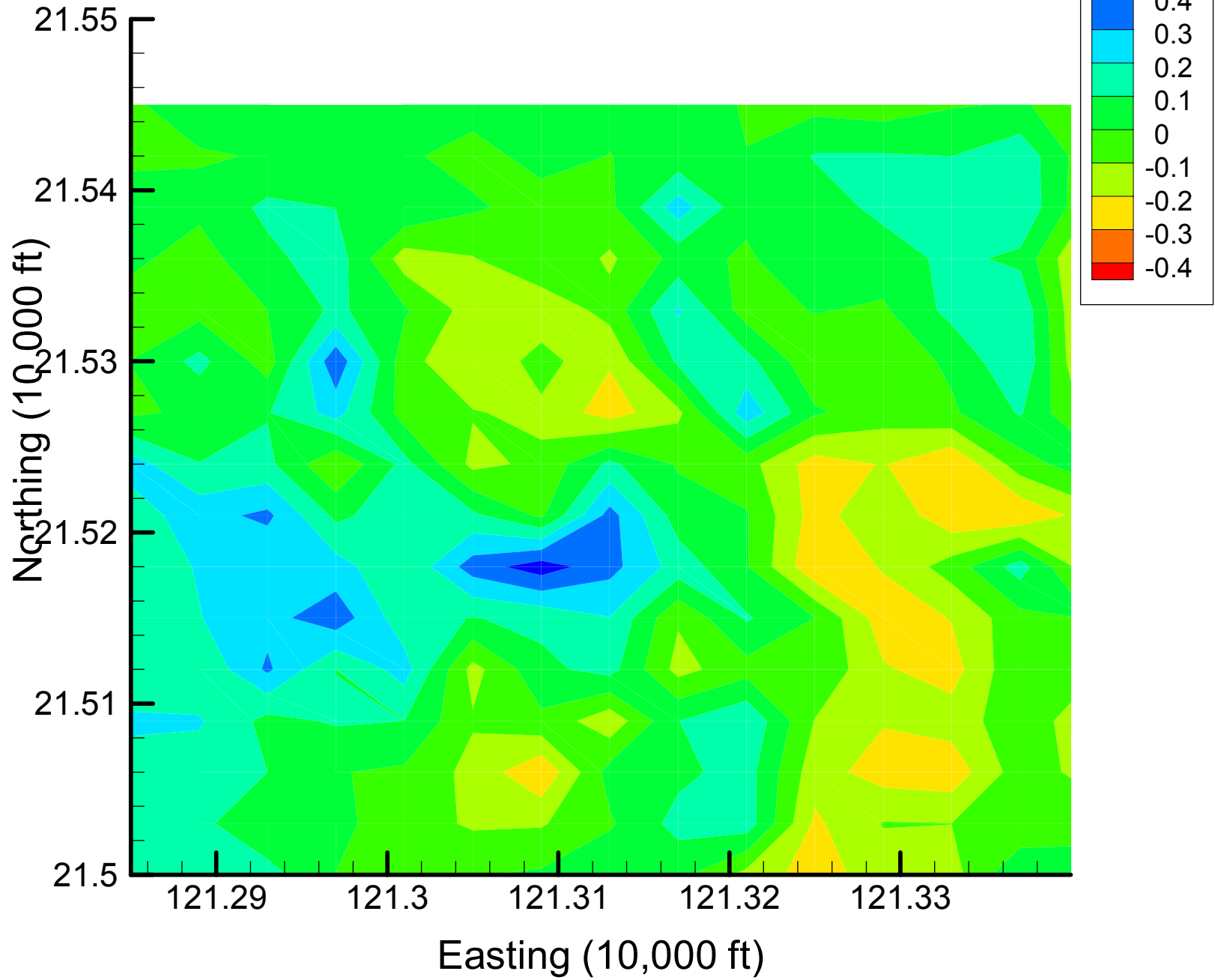
Site 49: TCE Indicator Differences, 2001, 45% Removal



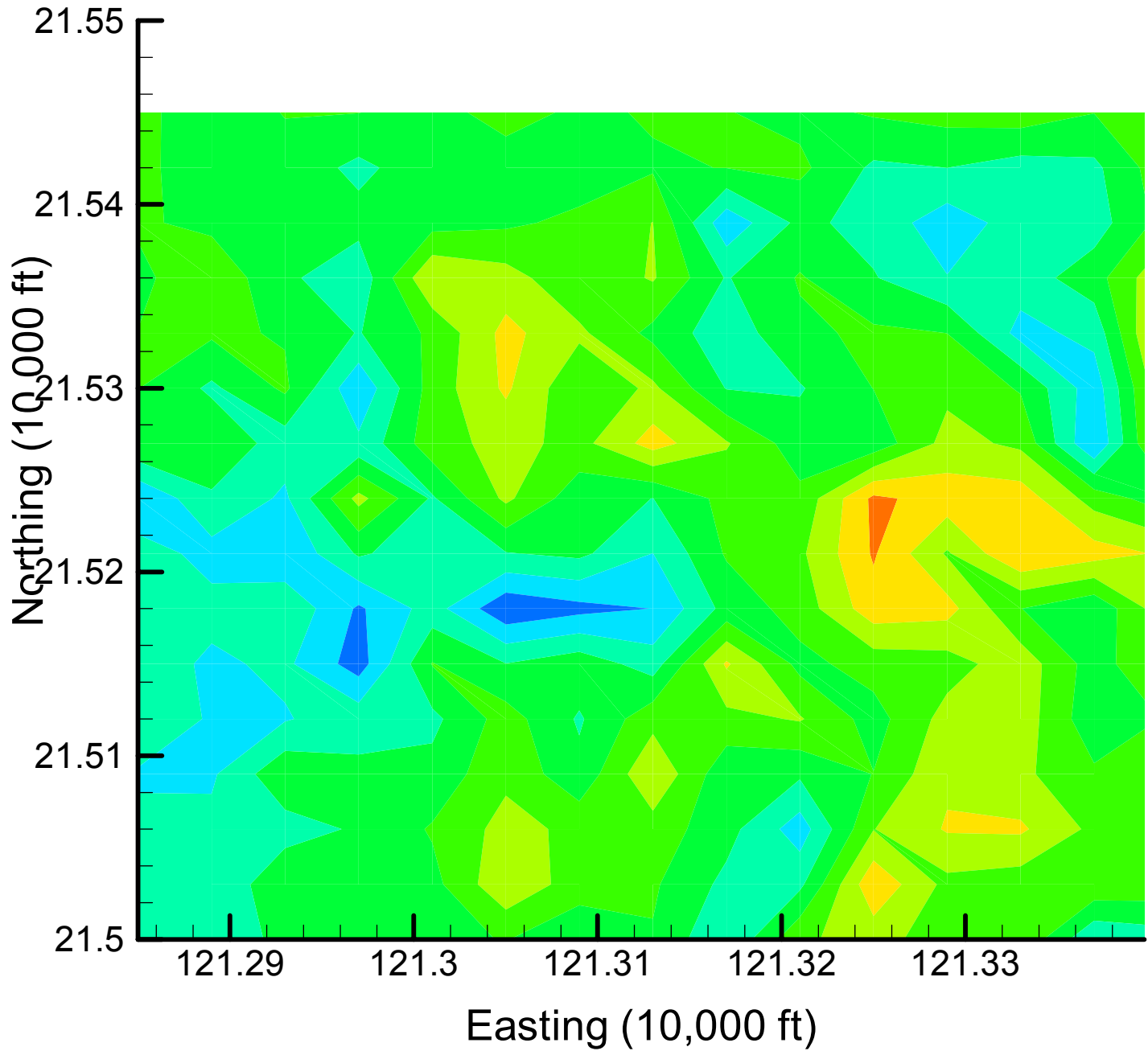
Site 49: TCE Indicator Differences, 2001, 50% Removal



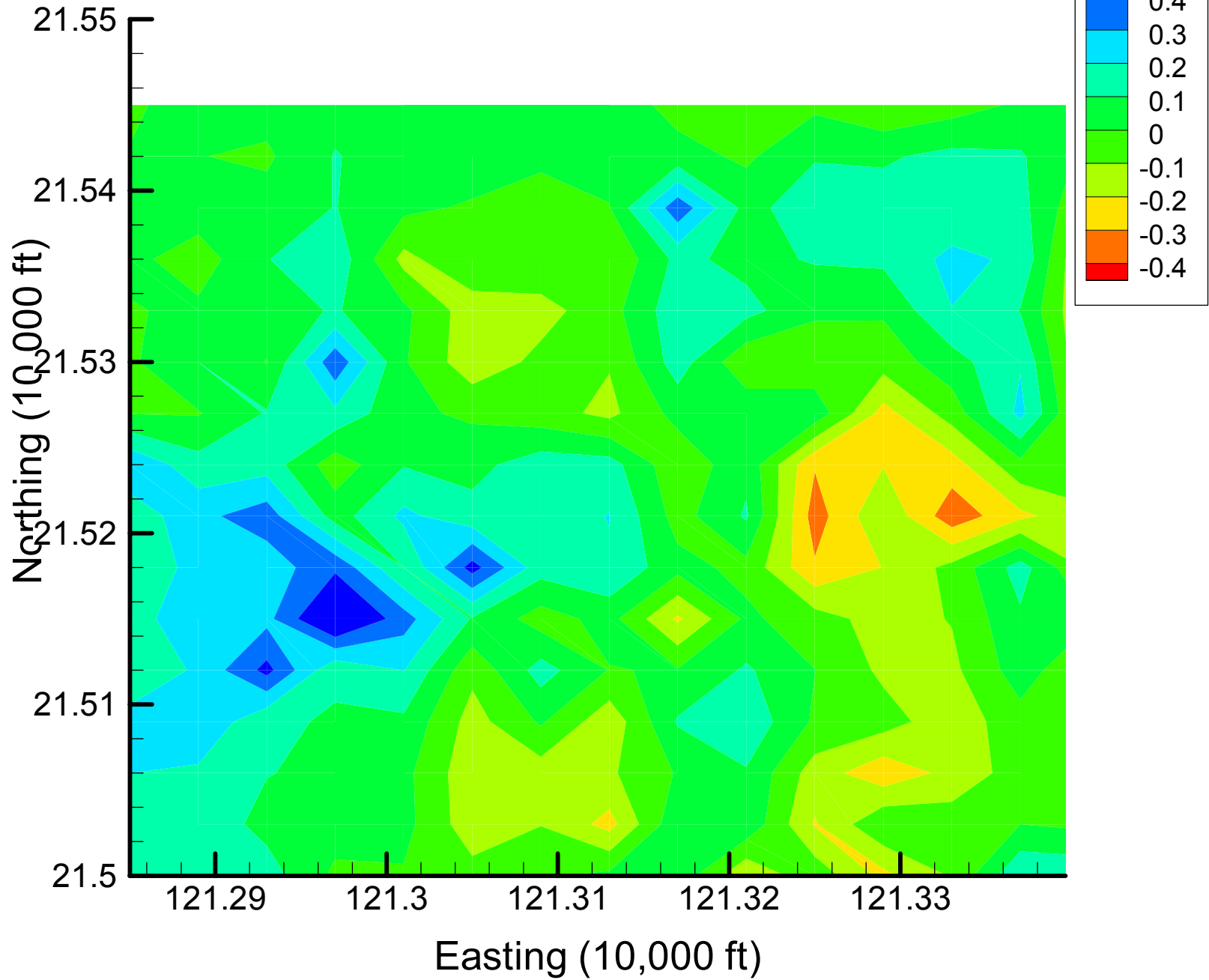
Site 49: TCE Indicator Differences, 2001, 55% Removal



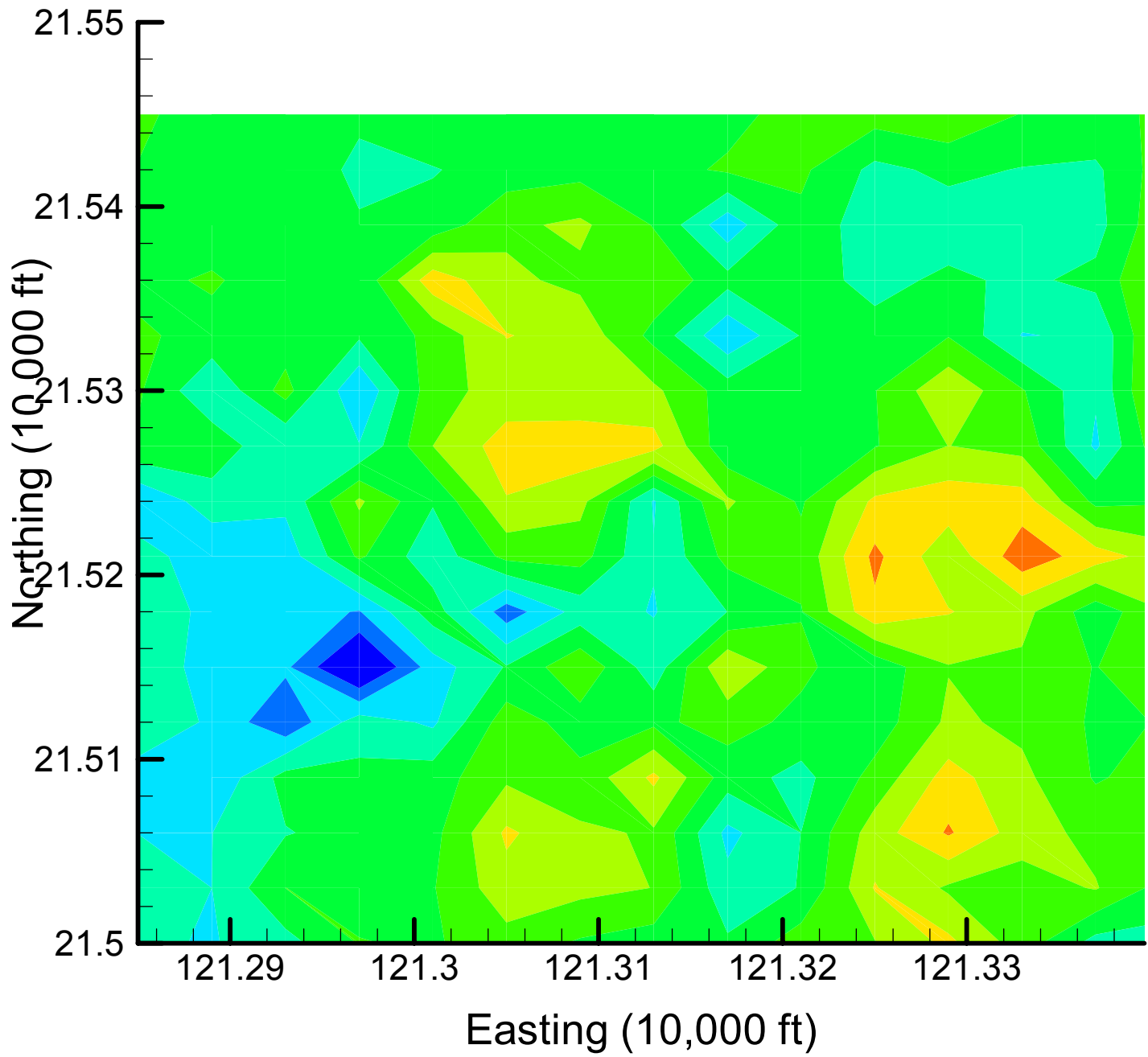
Site 49: TCE Indicator Differences, 2001, 60% Removal



Site 49: TCE Indicator Differences, 2001, 65% Removal

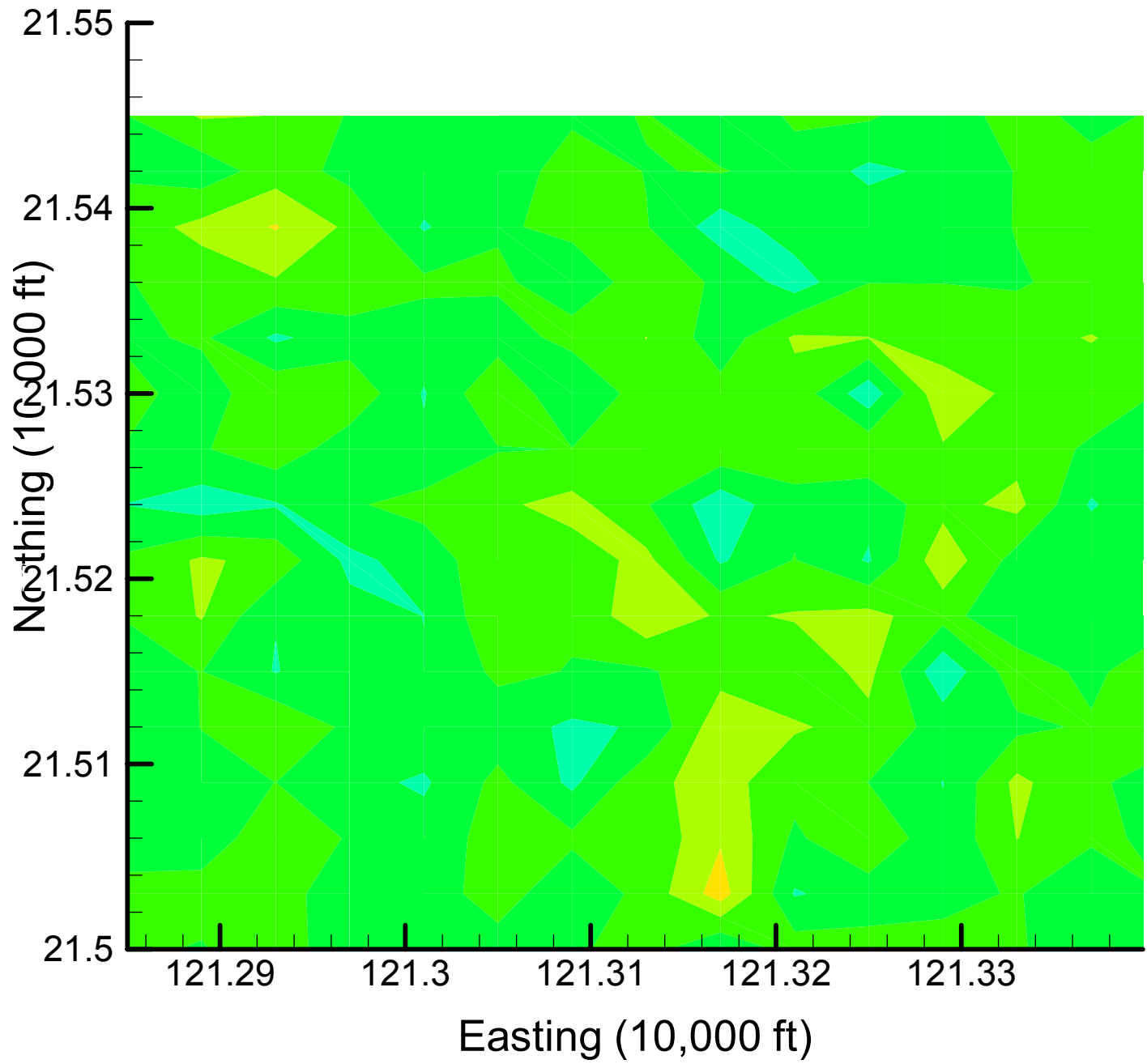


Site 49: TCE Indicator Differences, 2001, 70% Removal

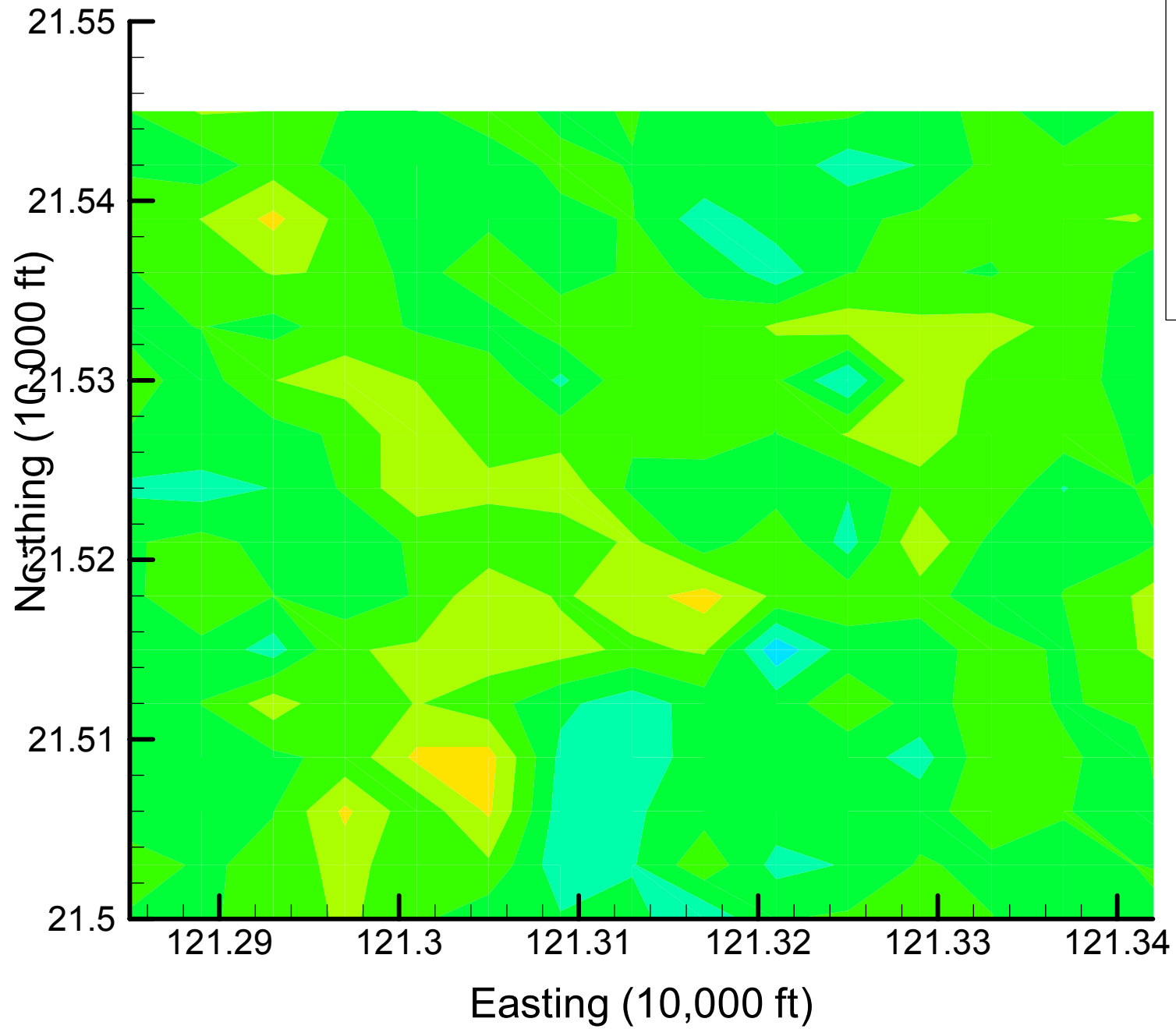


Appendix 4.2  
TCE Indicator Difference Maps  
Time Slice 2 — 2002

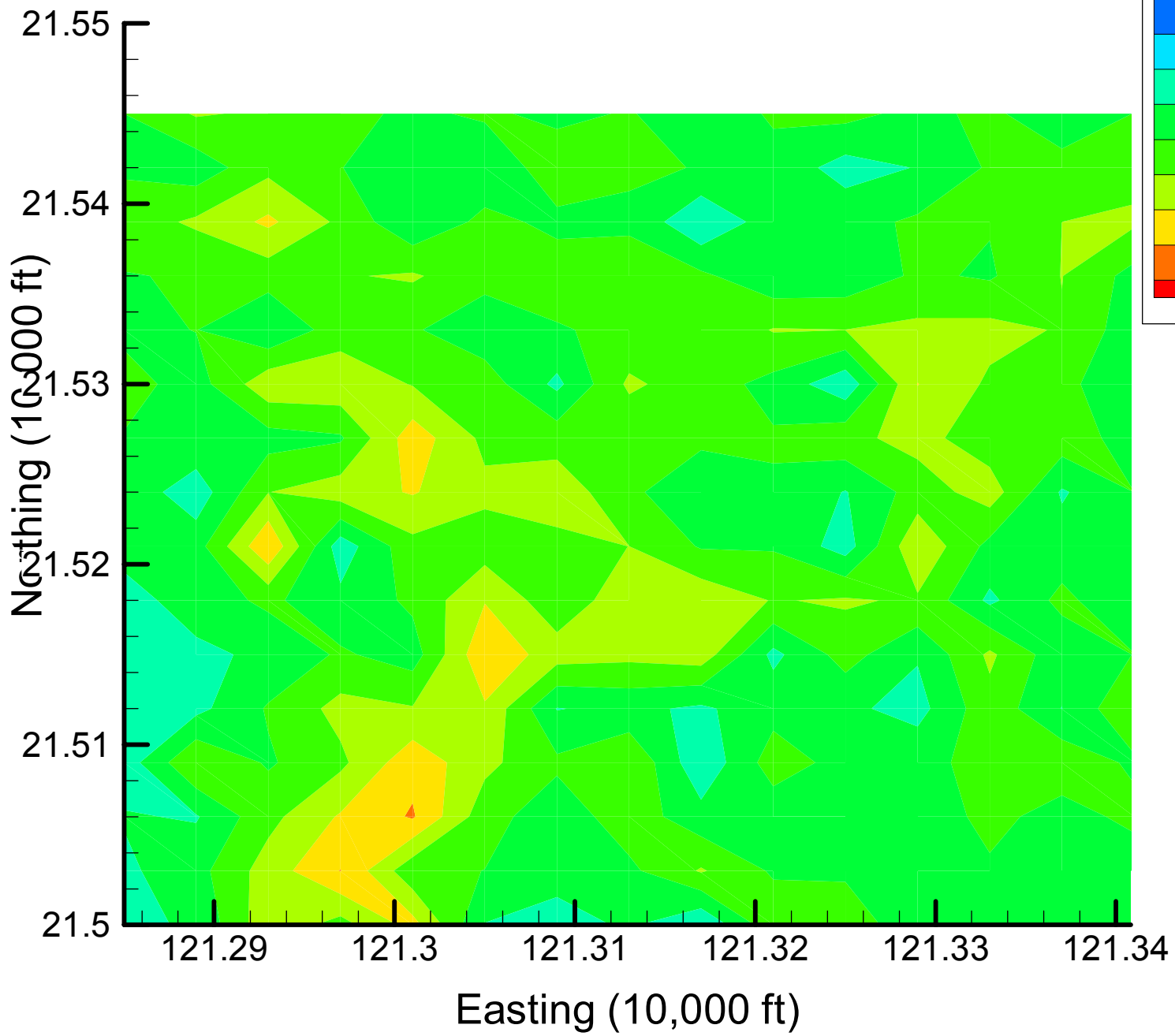
Site 49: TCE Indicator Differences, 2002, 5% Removal



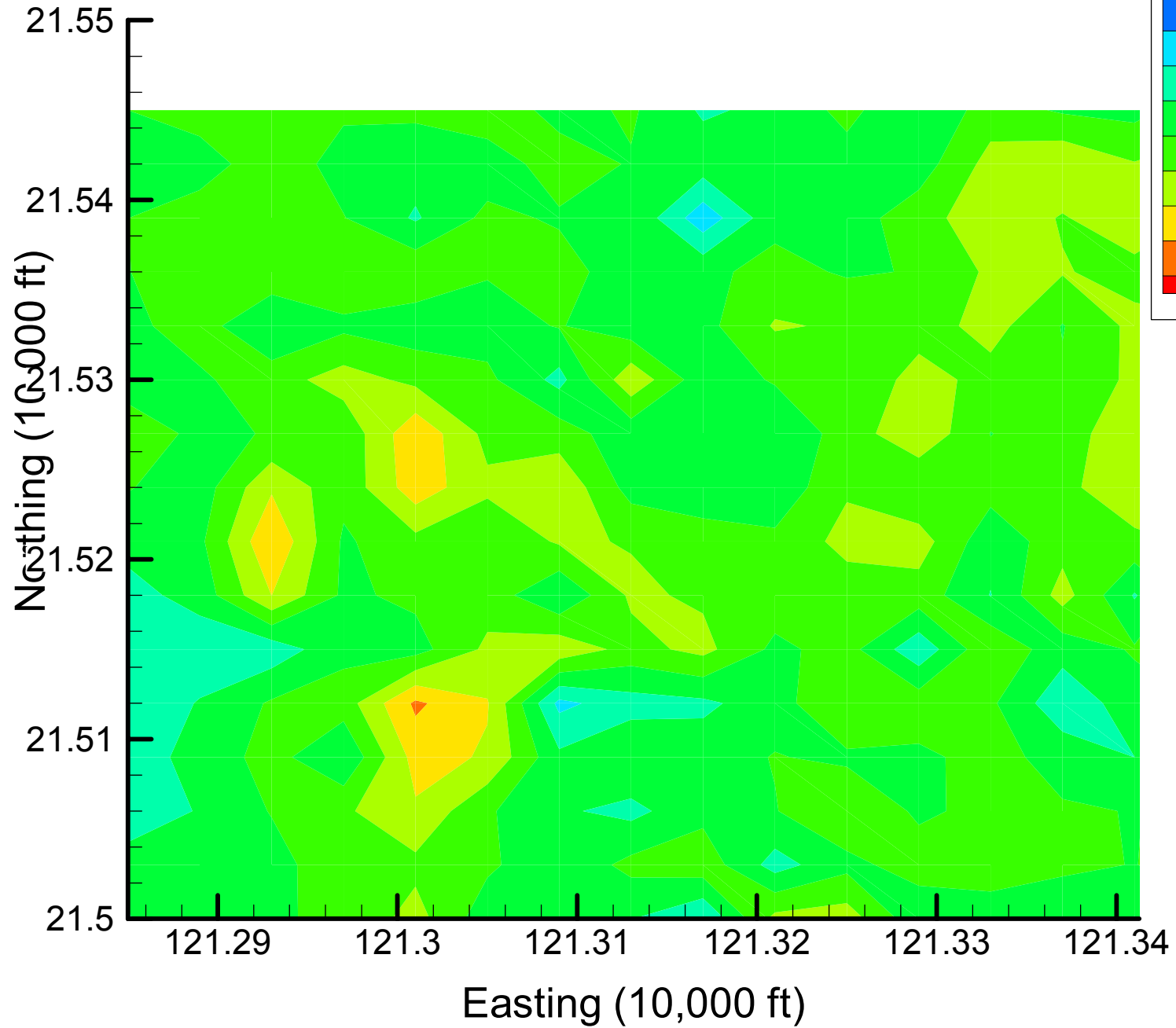
Site 49: TCE Indicator Differences, 2002, 10% Removal



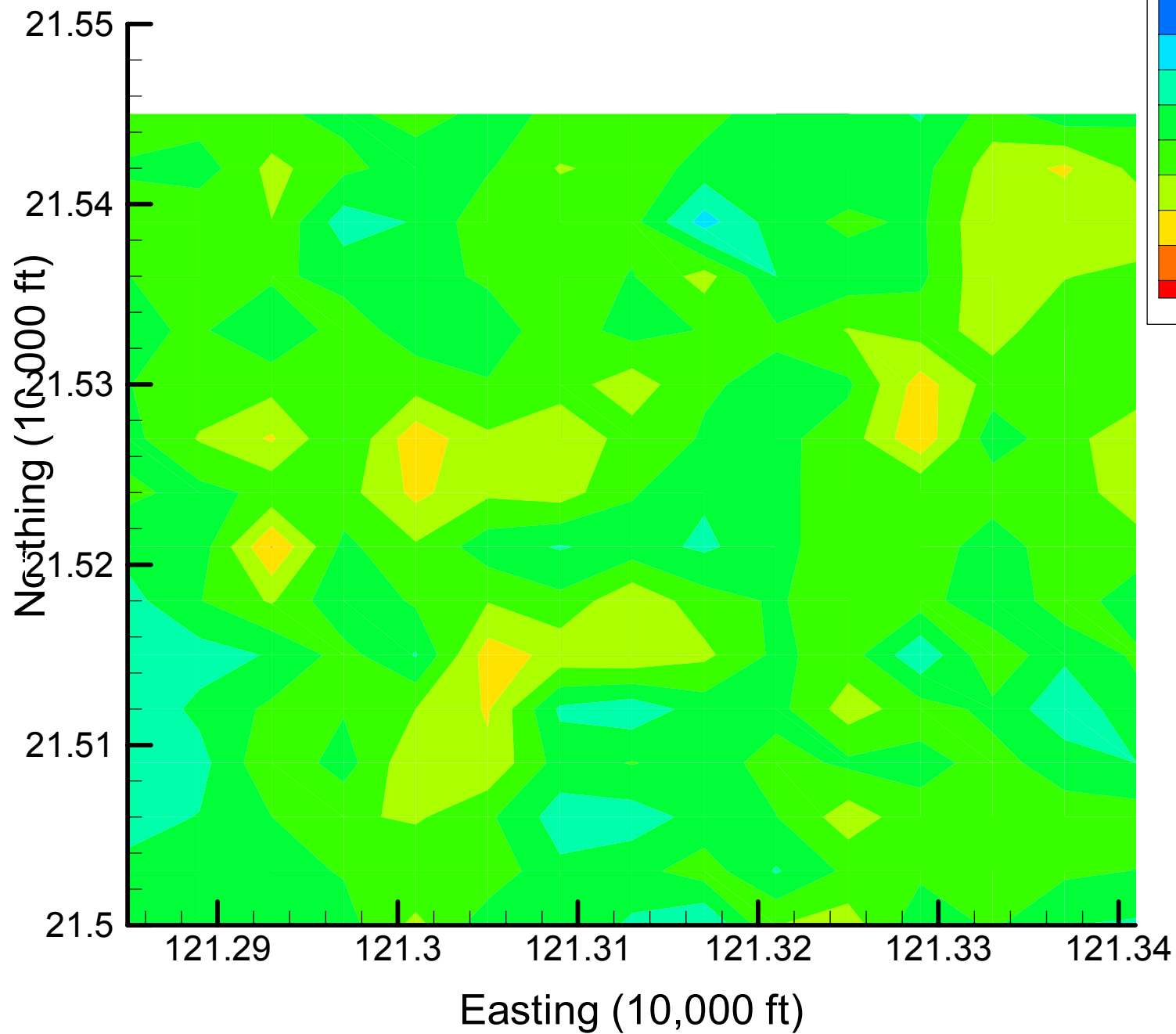
Site 49: TCE Indicator Differences, 2002, 15% Removal



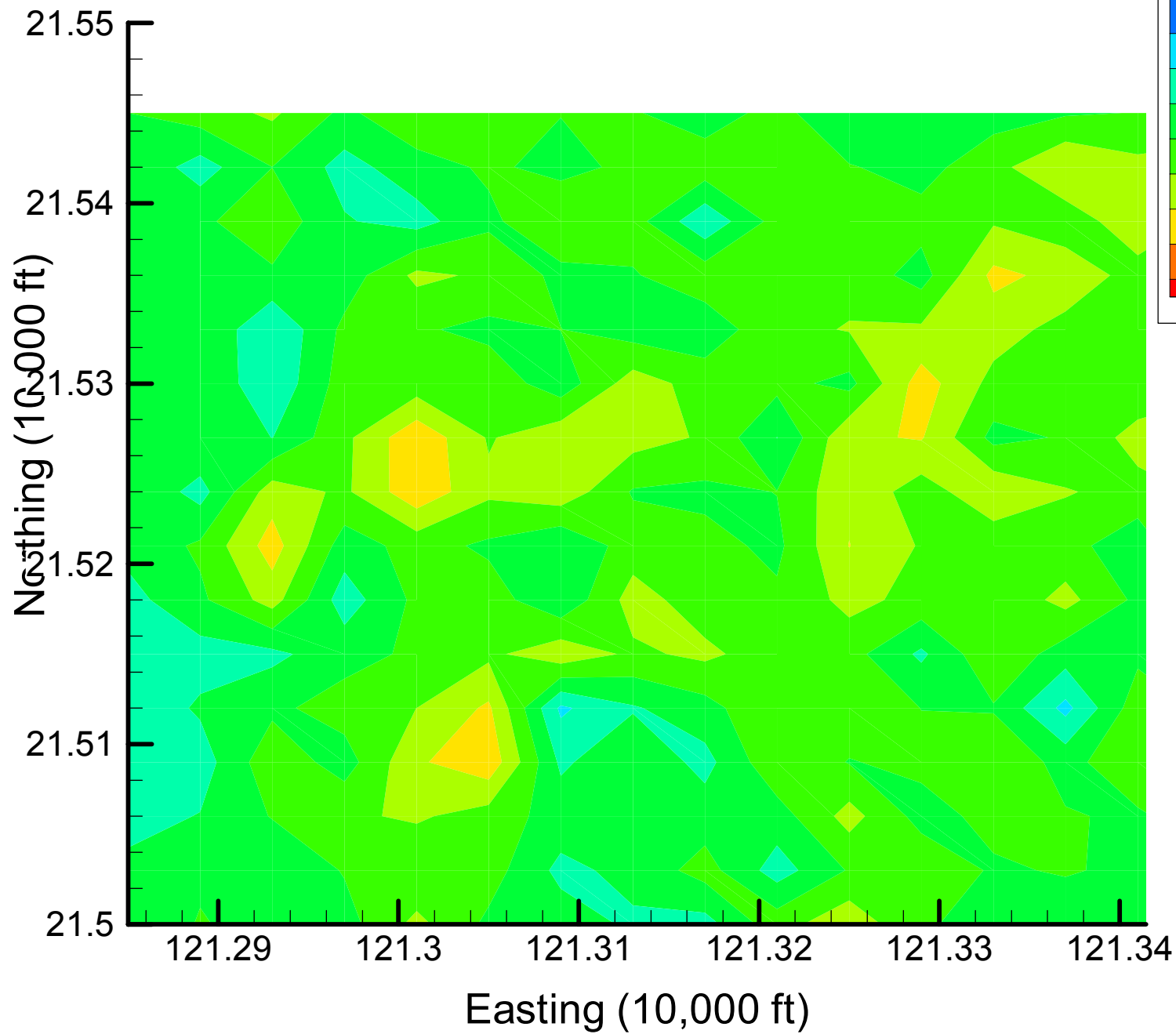
Site 49: TCE Indicator Differences, 2002, 20% Removal



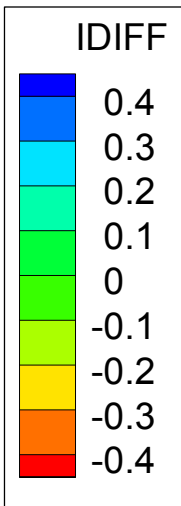
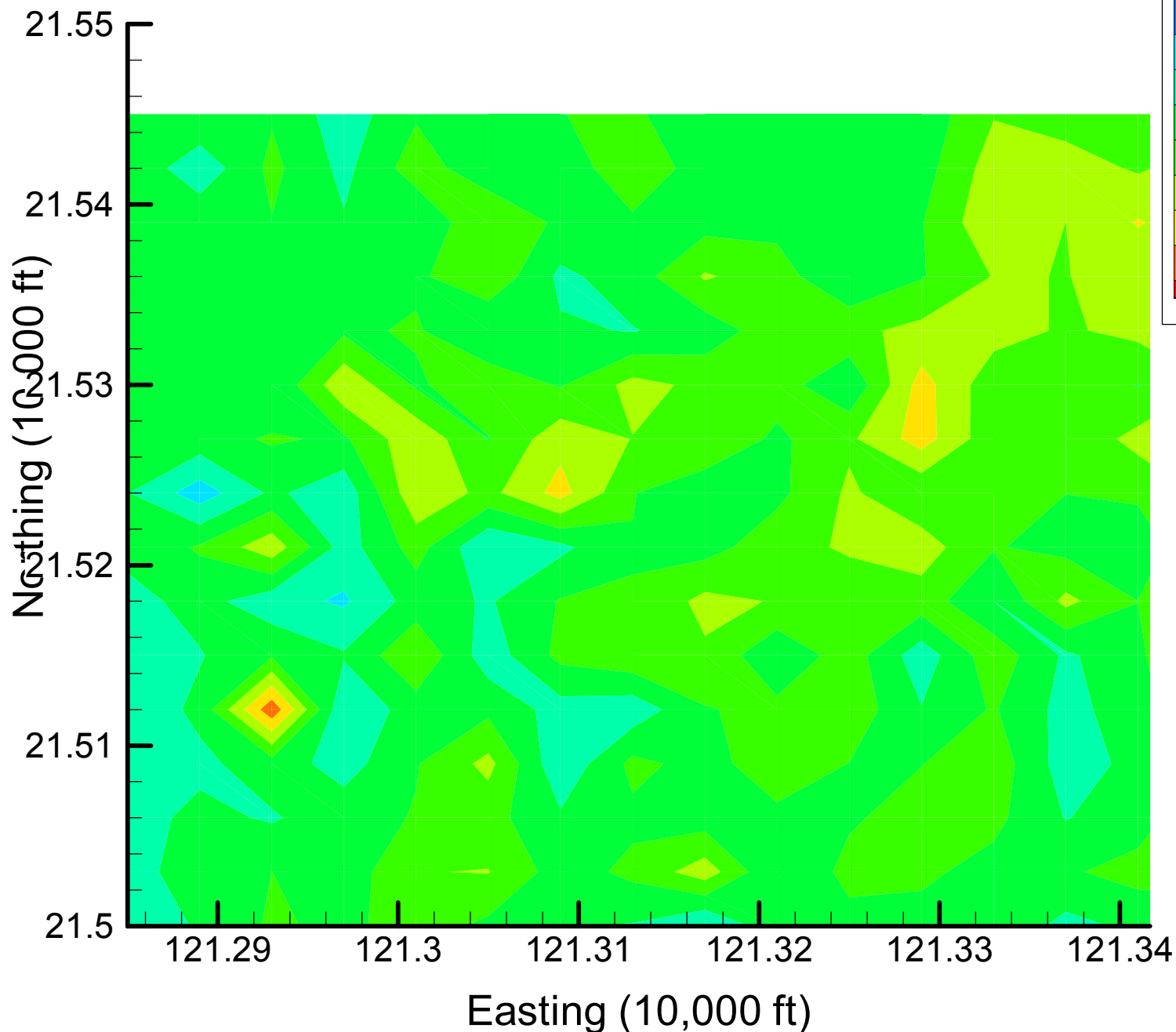
Site 49: TCE Indicator Differences, 2002, 25% Removal



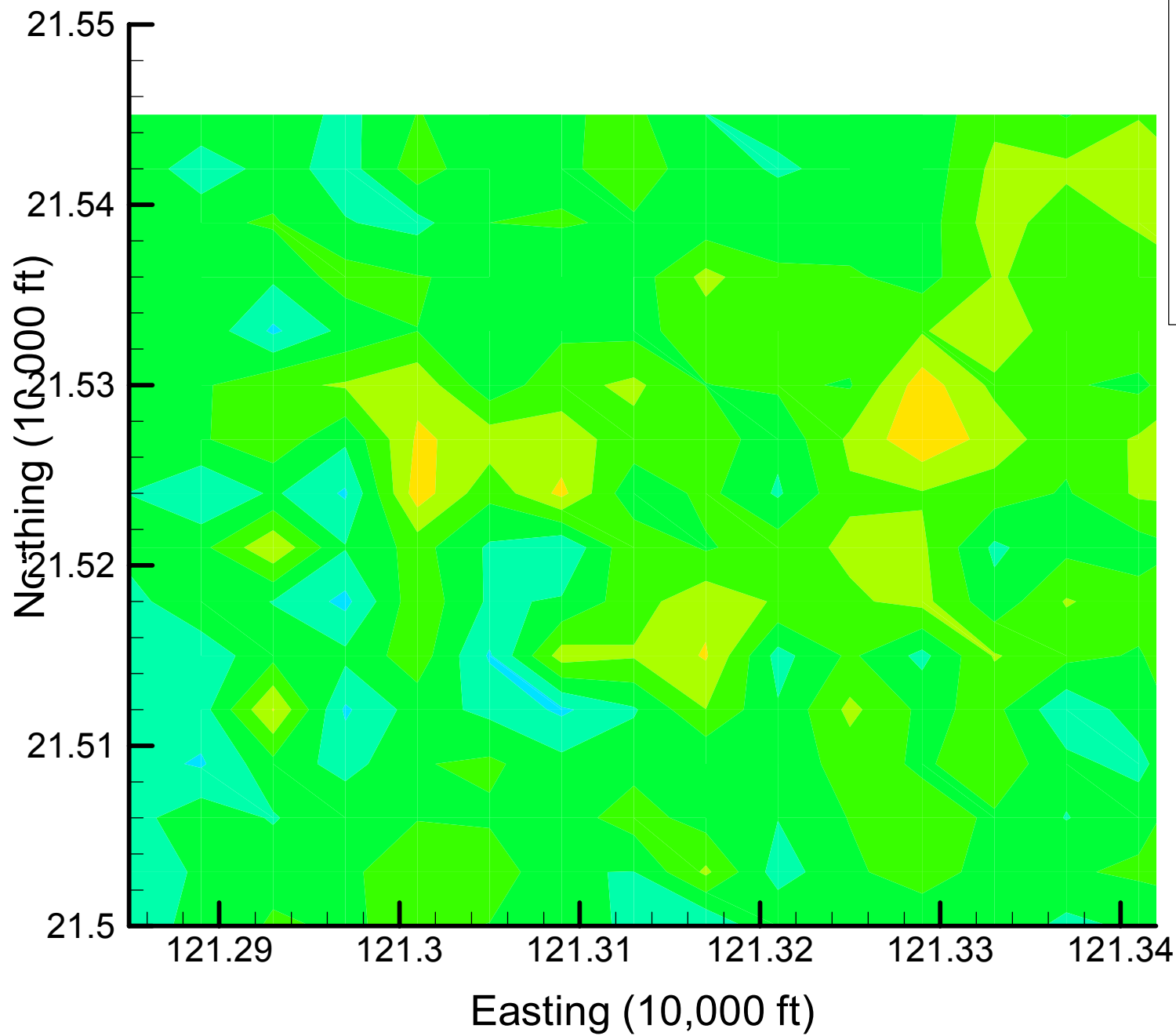
Site 49: TCE Indicator Differences, 2002, 30% Removal



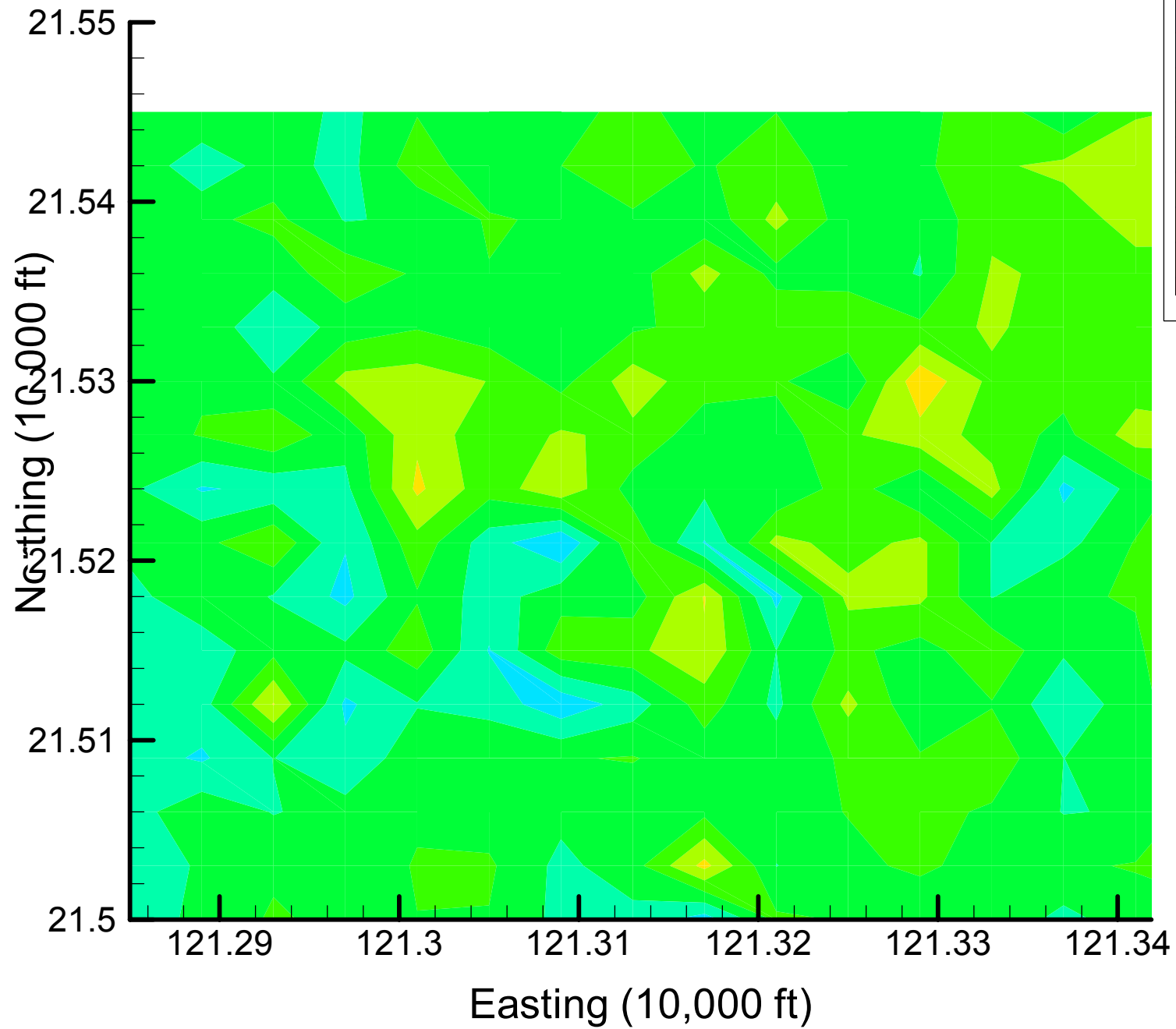
Site 49: TCE Indicator Differences, 2002, 35% Removal



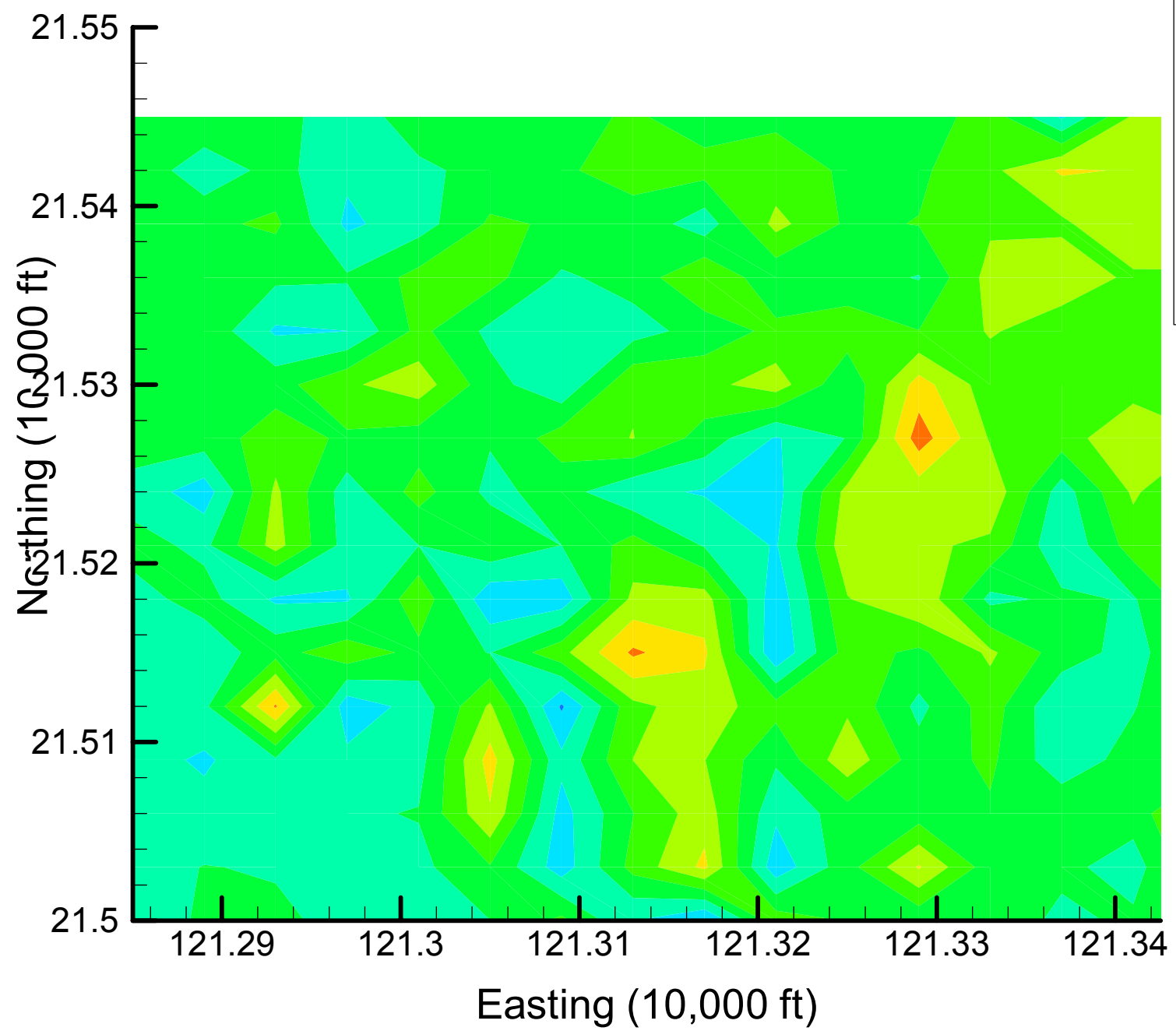
Site 49: TCE Indicator Differences, 2002, 40% Removal



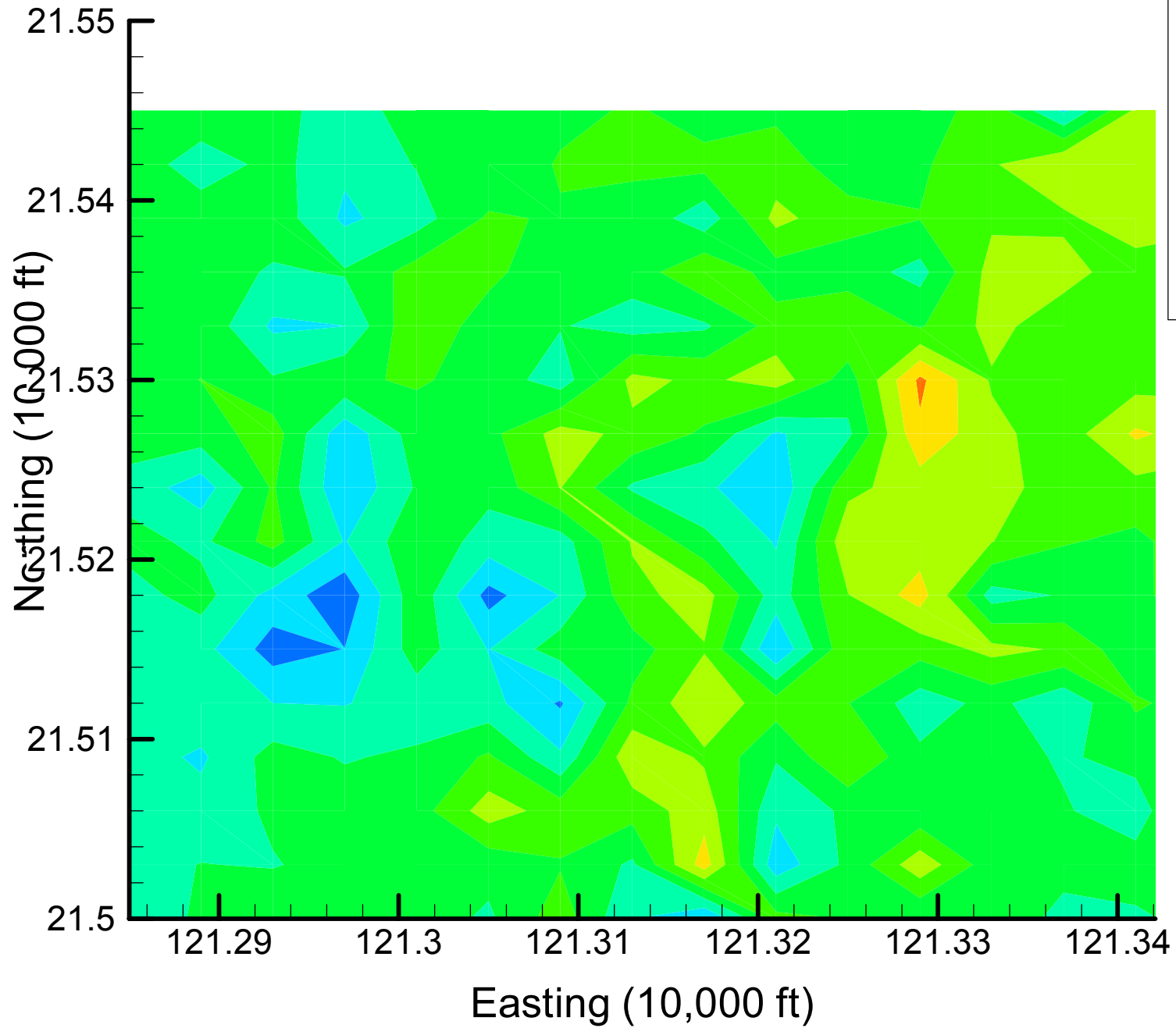
Site 49: TCE Indicator Differences, 2002, 45% Removal



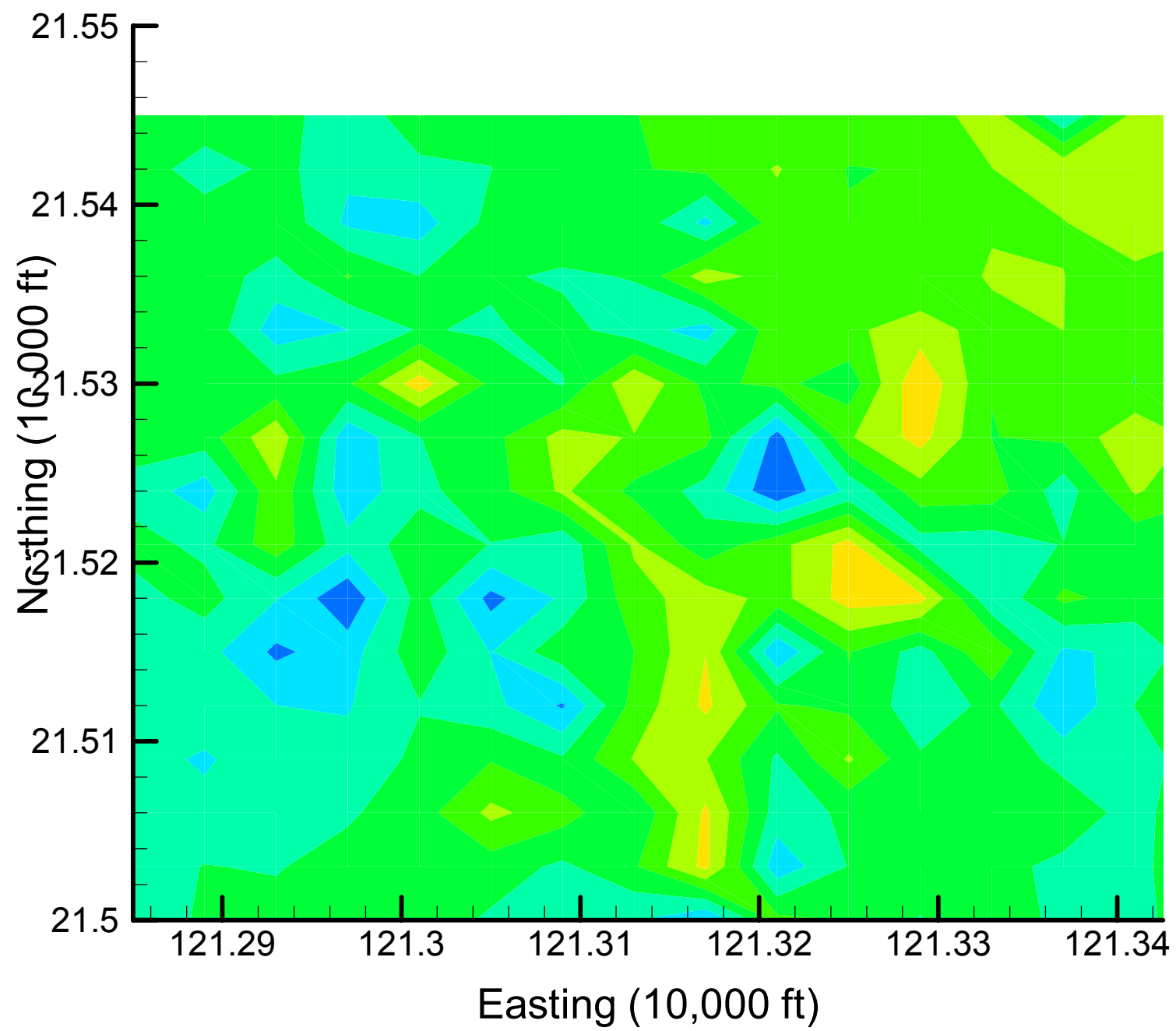
Site 49: TCE Indicator Differences, 2002, 50% Removal



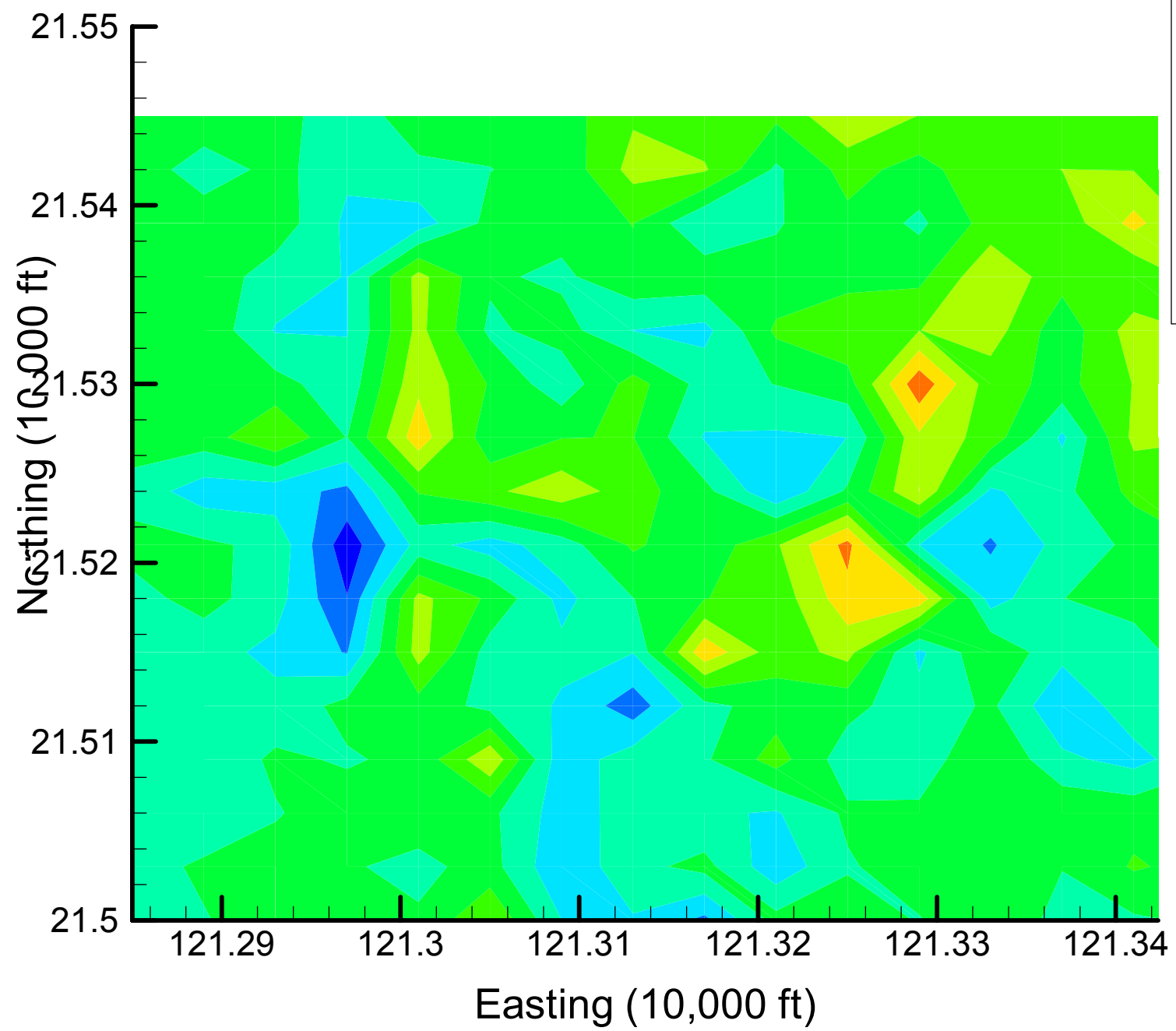
Site 49: TCE Indicator Differences, 2002, 55% Removal



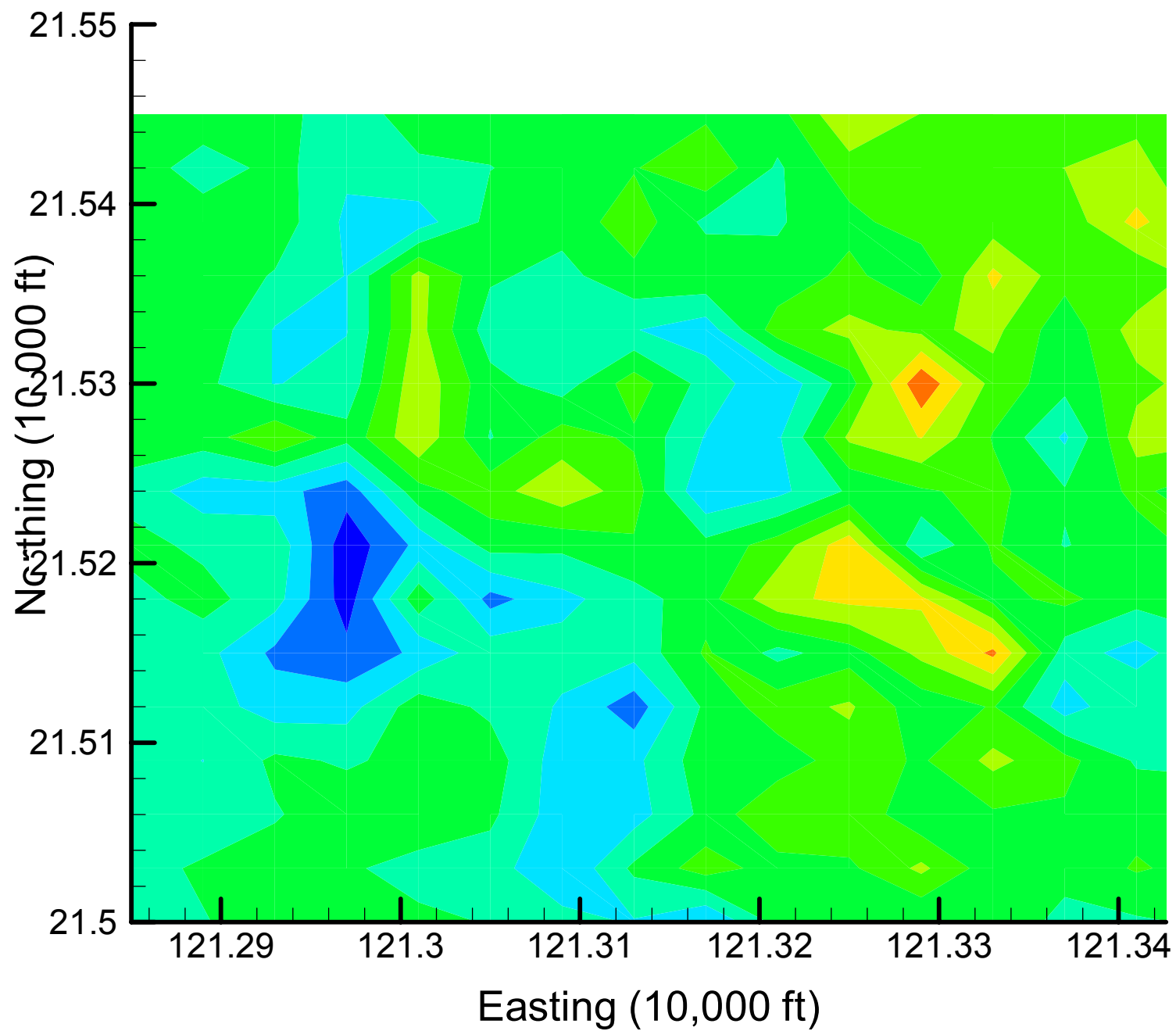
Site 49: TCE Indicator Differences, 2002, 60% Removal



Site 49: TCE Indicator Differences, 2002, 65% Removal

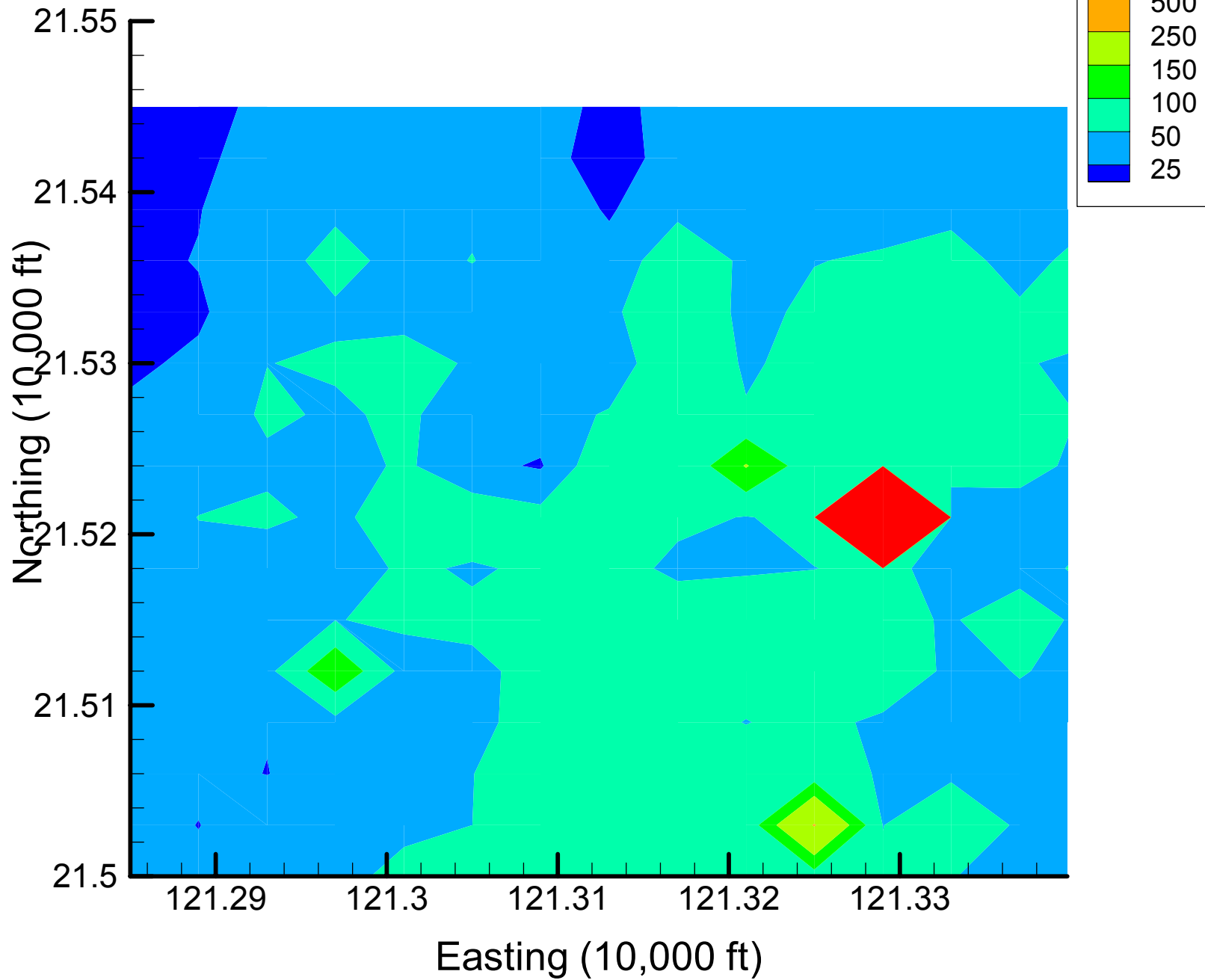


Site 49: TCE Indicator Differences, 2002, 70% Removal

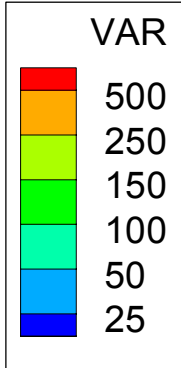
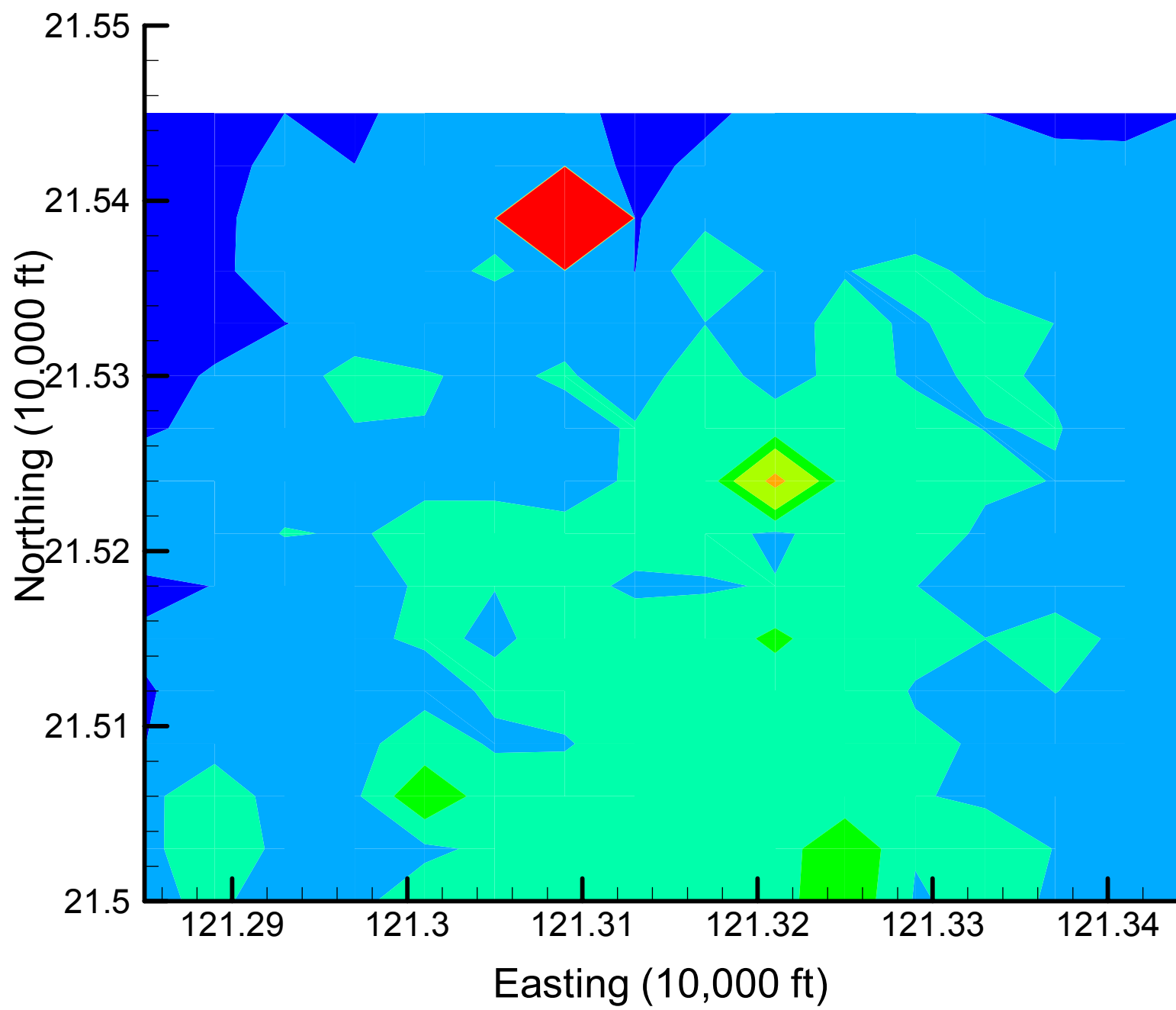


Appendix 4.3  
DCA11 Local Variance Maps  
Time Slice 1 — 2001

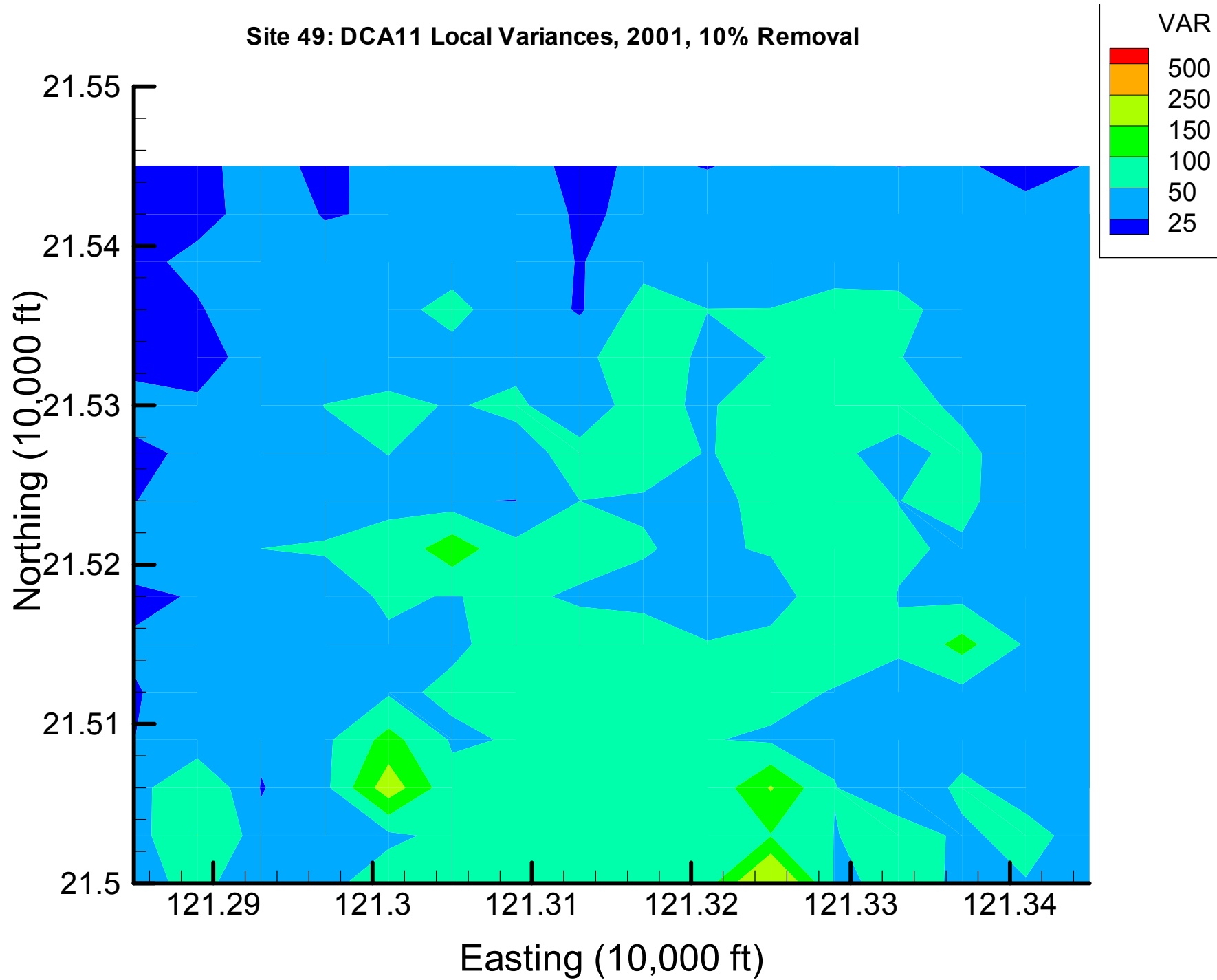
Site 49: DCA11 Local Variances, 2001, Base Map



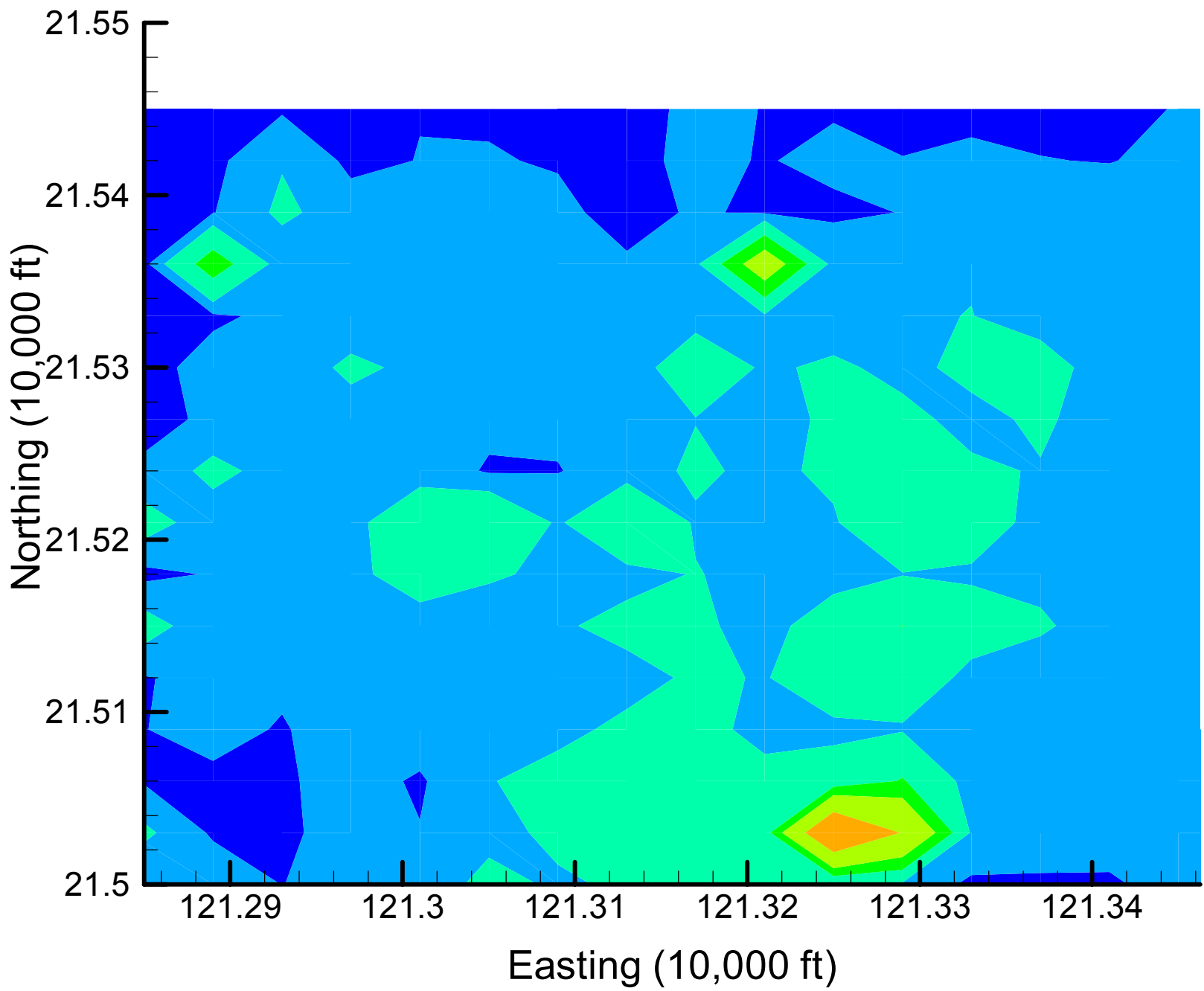
Site 49: DCA11 Local Variances, 2001, 5% Removal



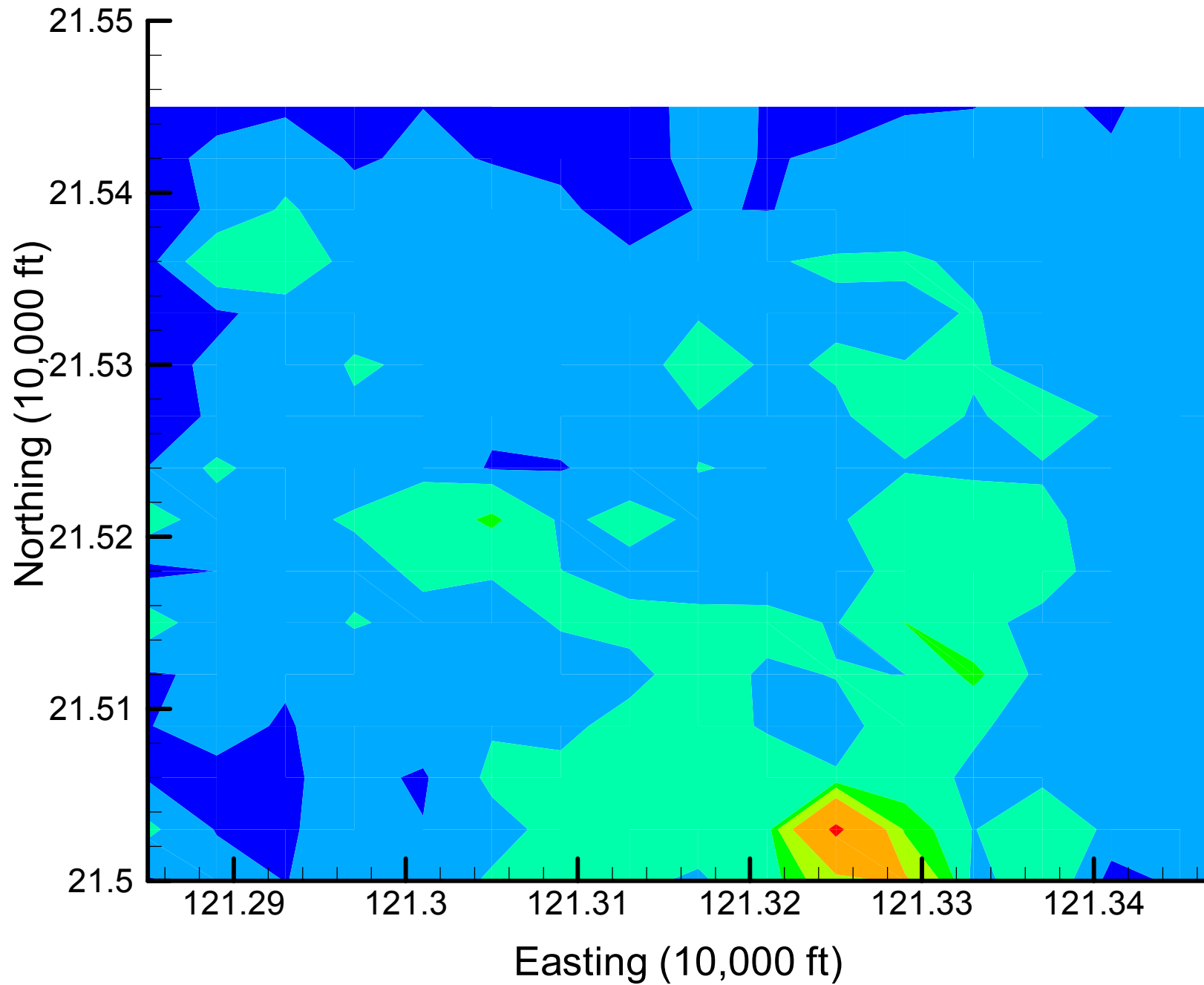
Site 49: DCA11 Local Variances, 2001, 10% Removal



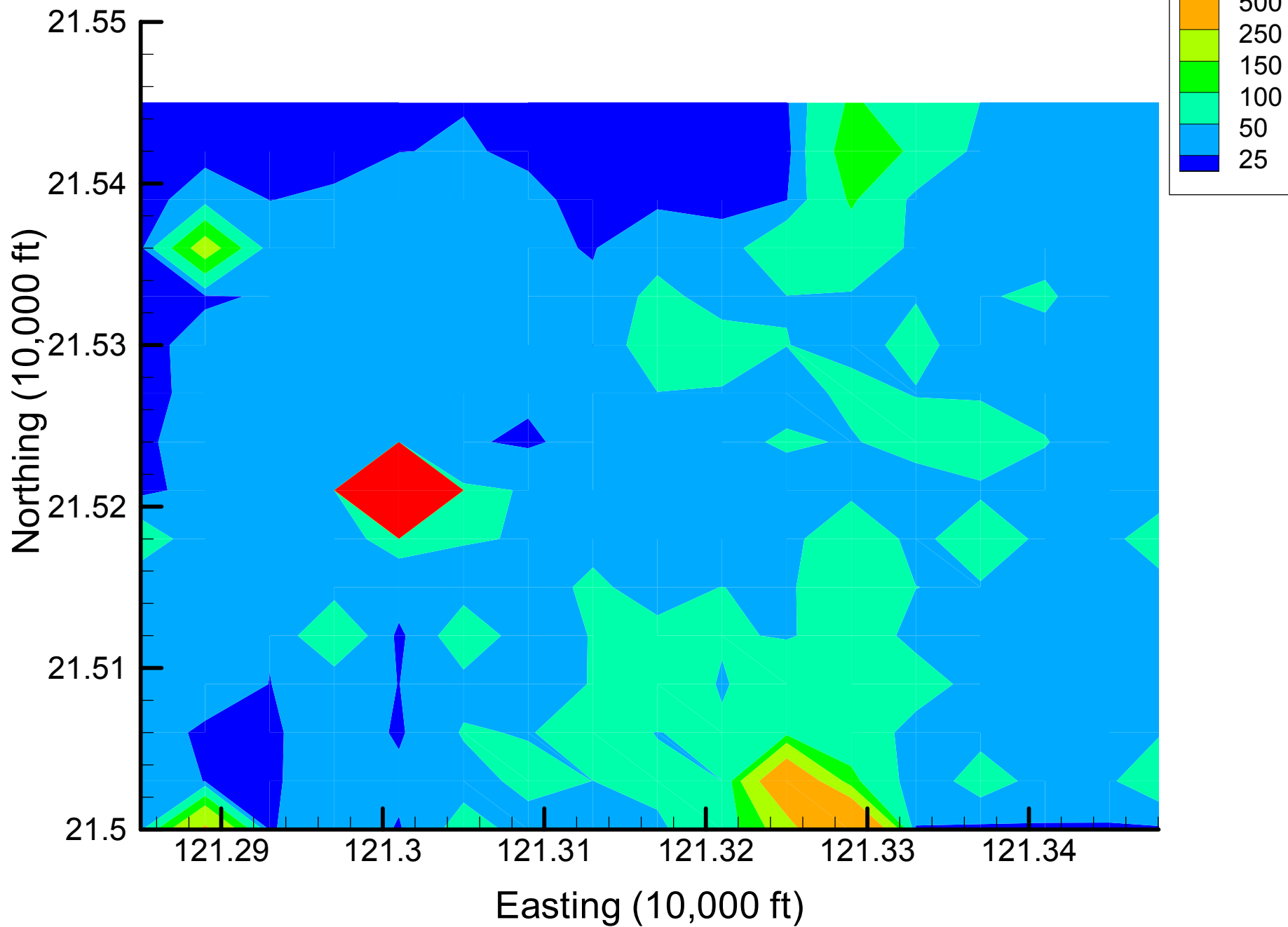
Site 49: DCA11 Local Variances, 2001, 15% Removal



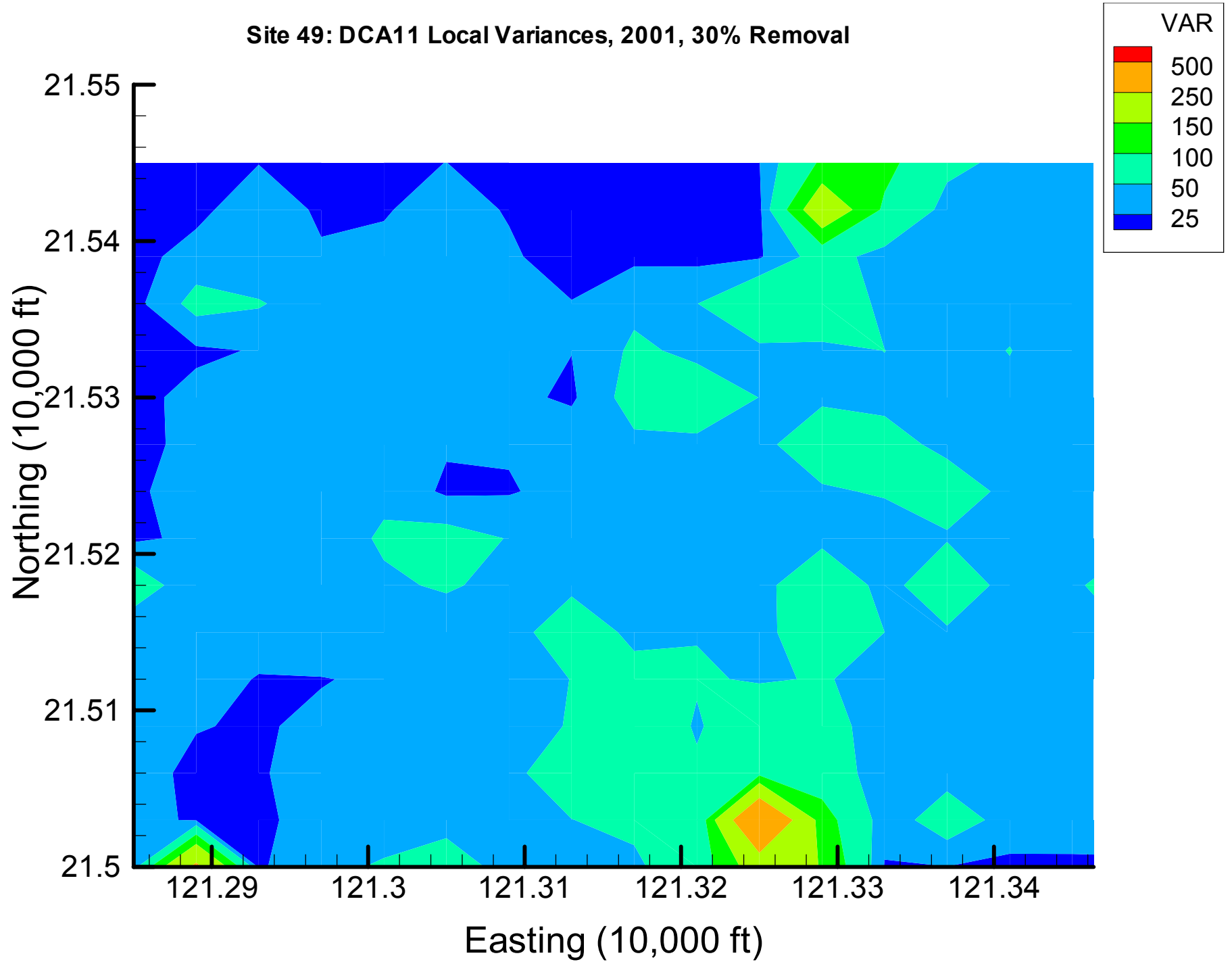
Site 49: DCA11 Local Variances, 2001, 20% Removal



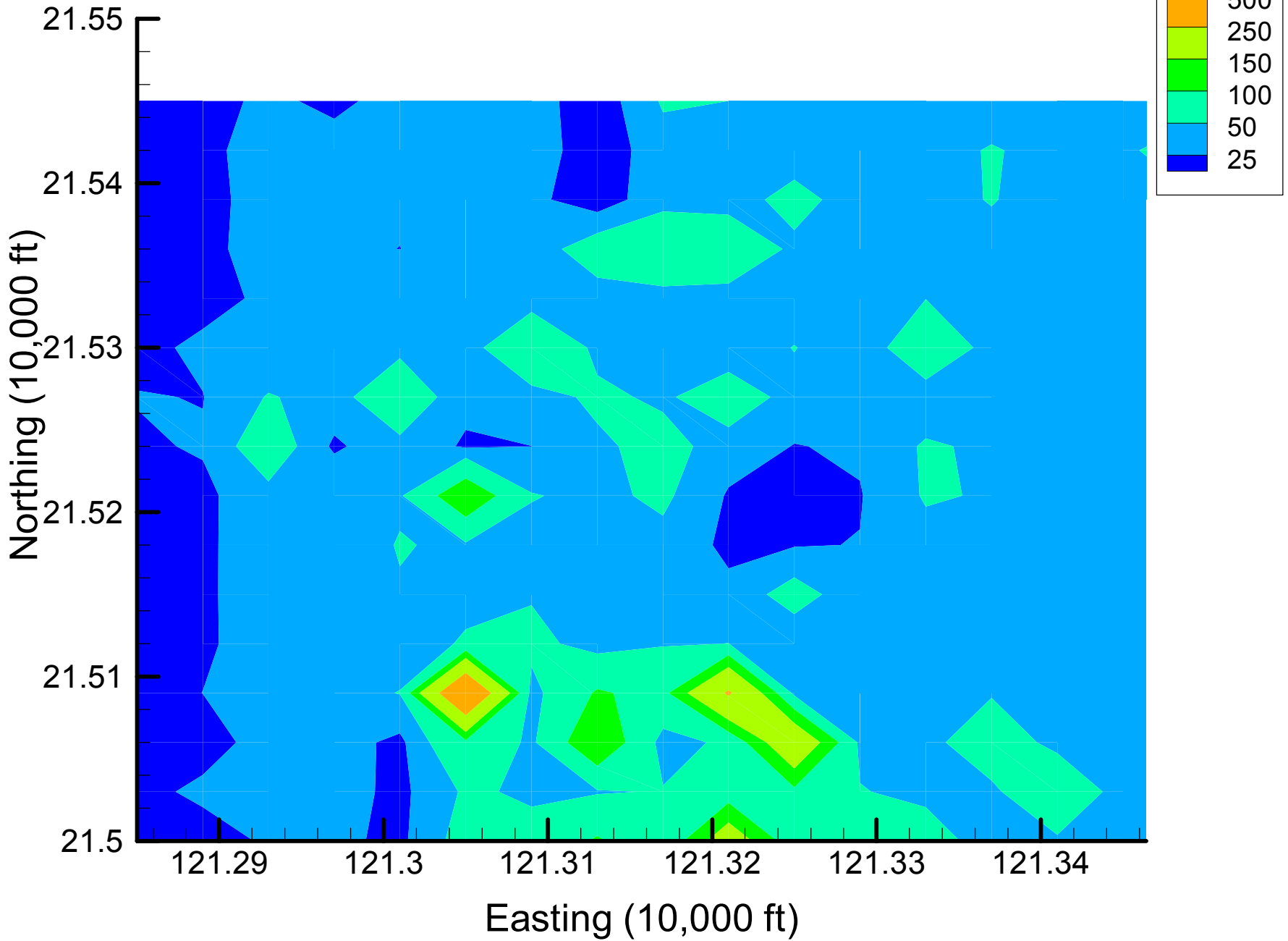
Site 49: DCA11 Local Variances, 2001, 25% Removal



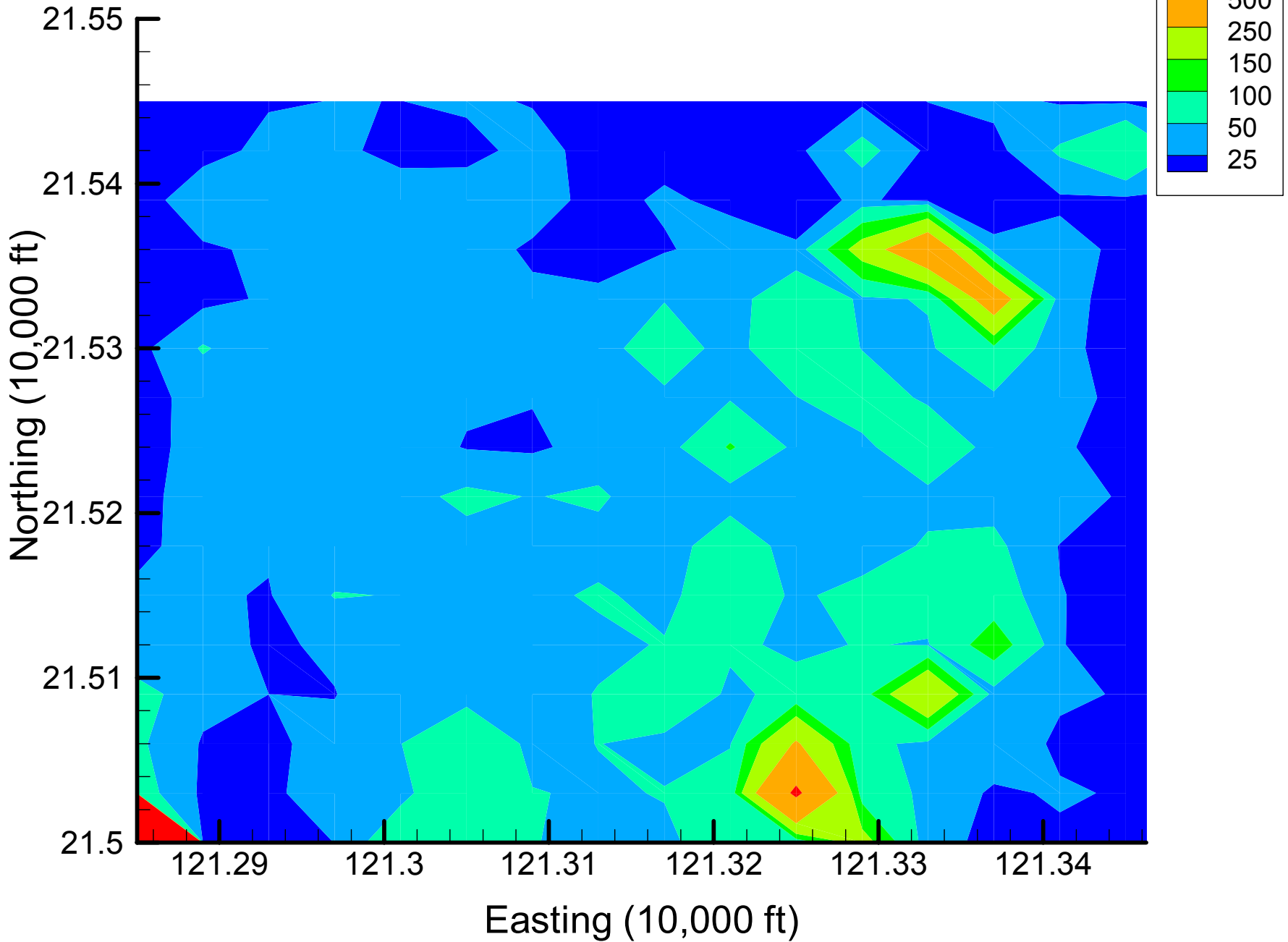
Site 49: DCA11 Local Variances, 2001, 30% Removal



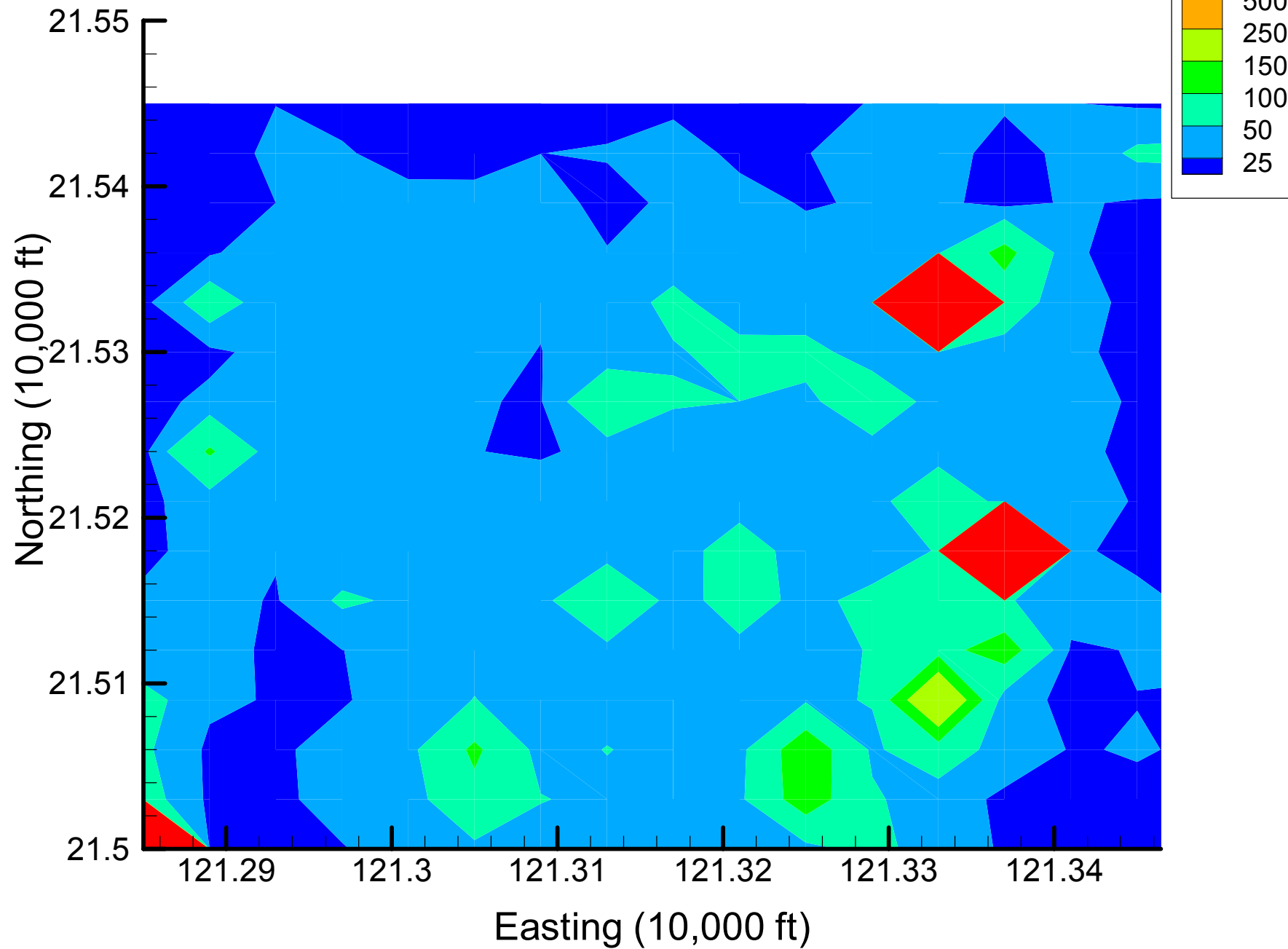
Site 49: DCA11 Local Variances, 2001, 35% Removal



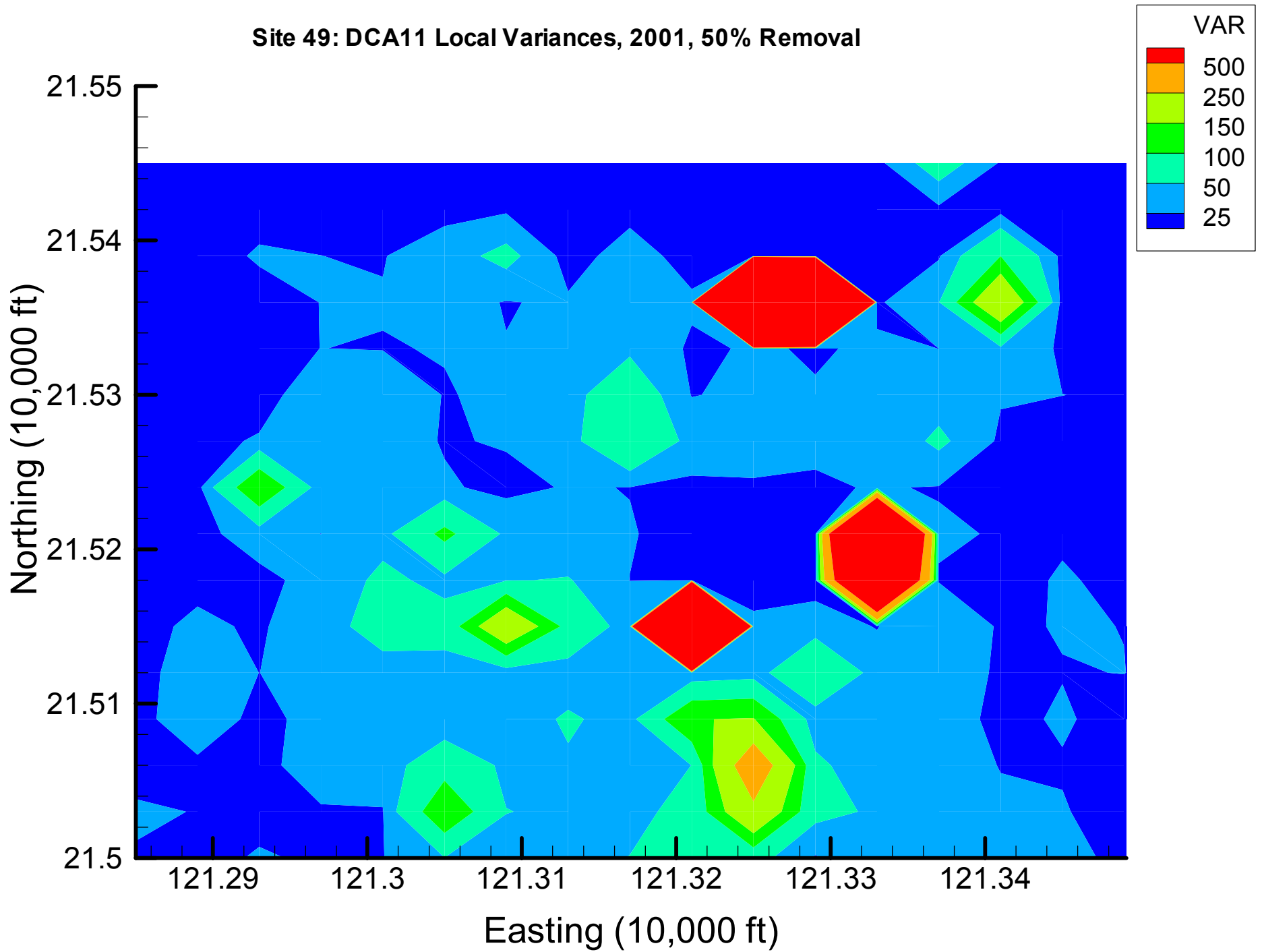
Site 49: DCA11 Local Variances, 2001, 40% Removal



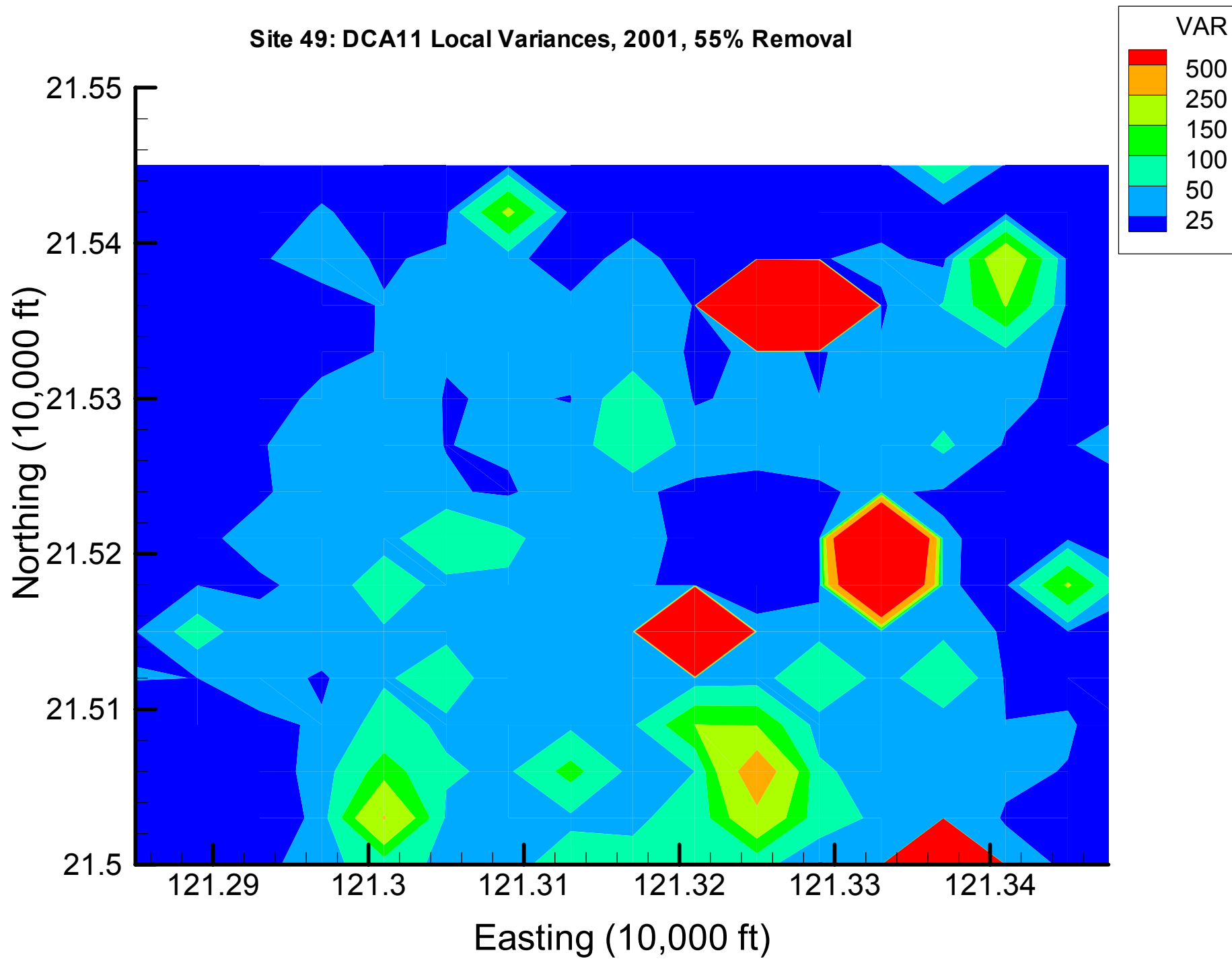
Site 49: DCA11 Local Variances, 2001, 45% Removal



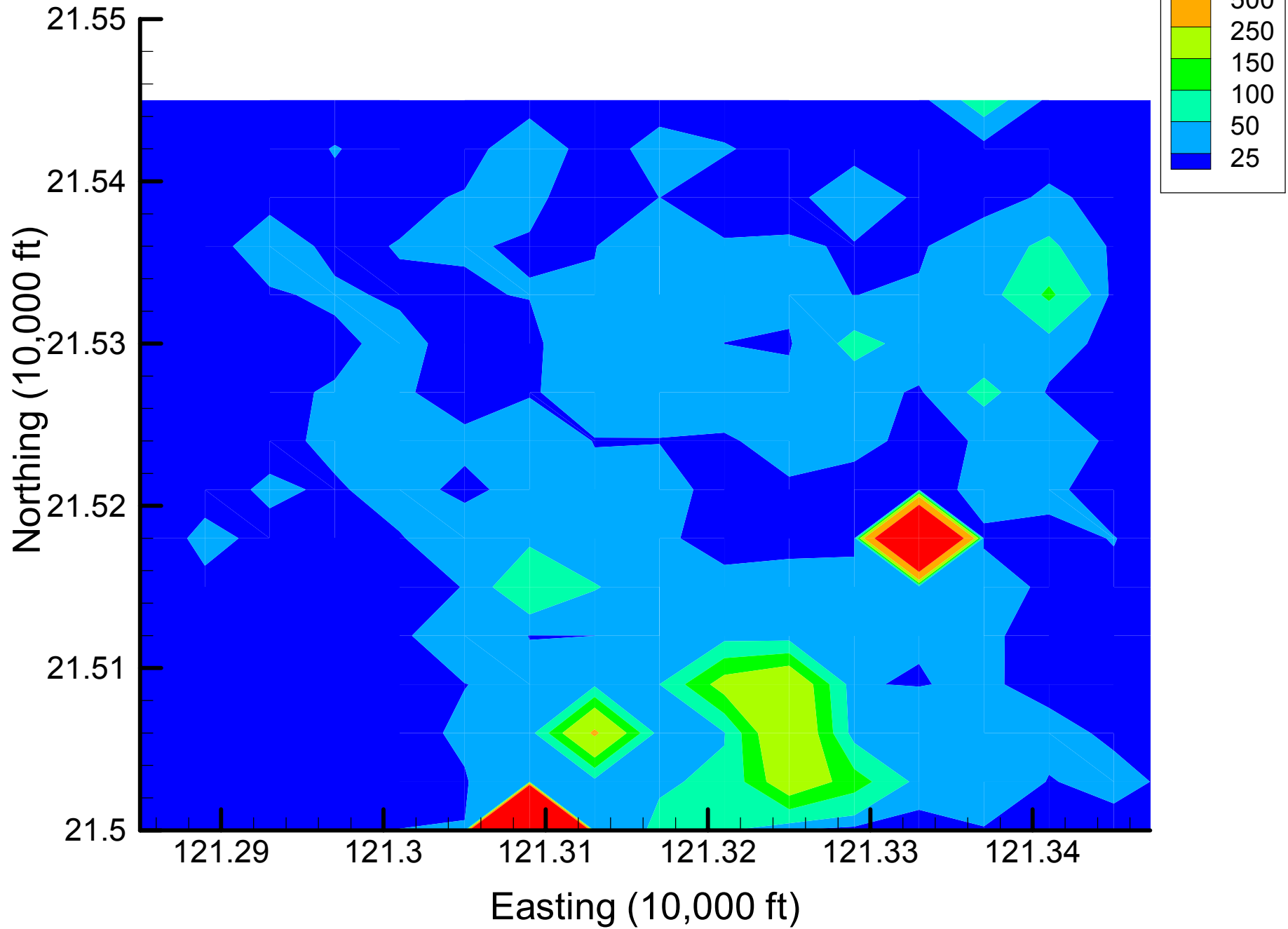
Site 49: DCA11 Local Variances, 2001, 50% Removal



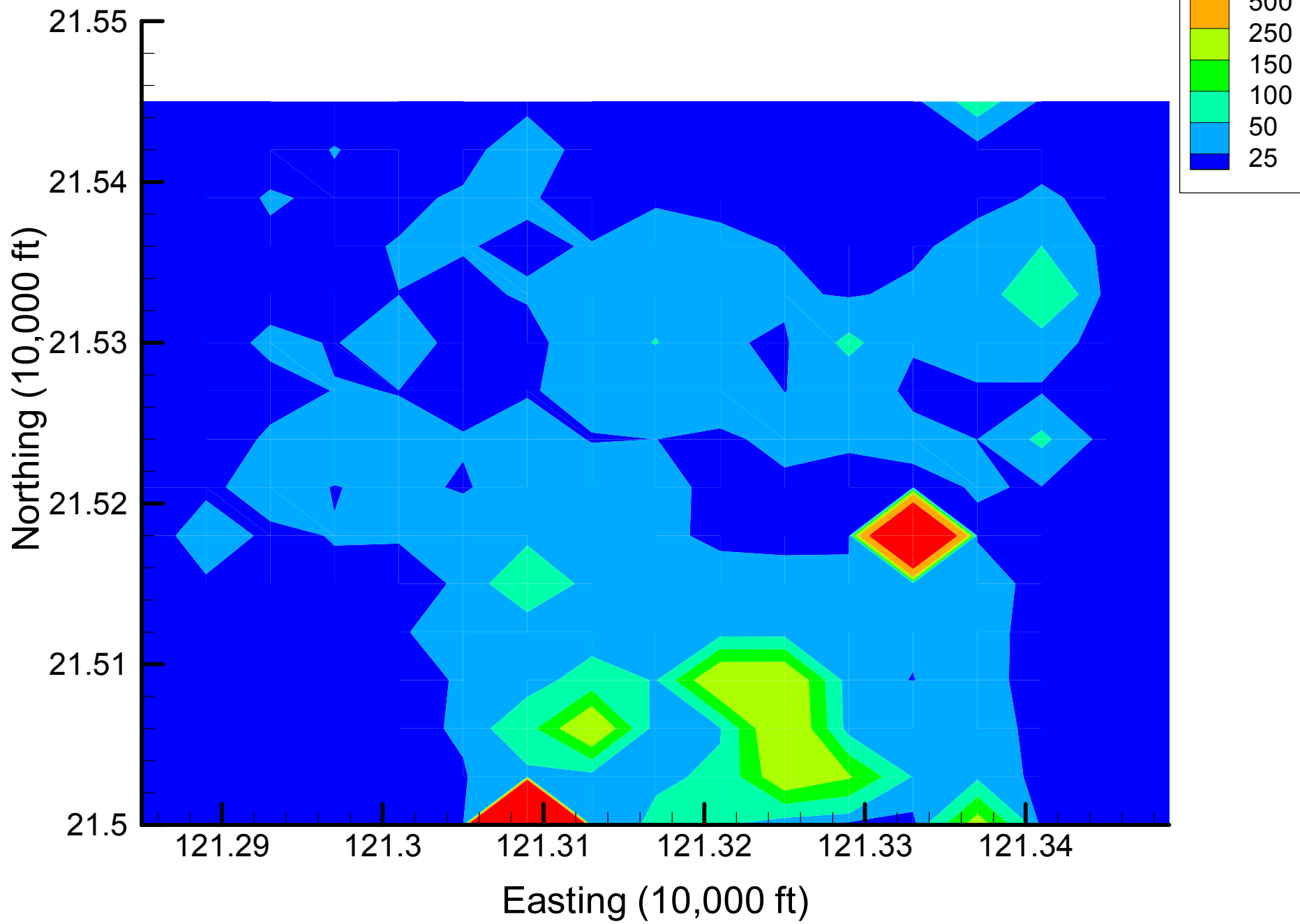
Site 49: DCA11 Local Variances, 2001, 55% Removal



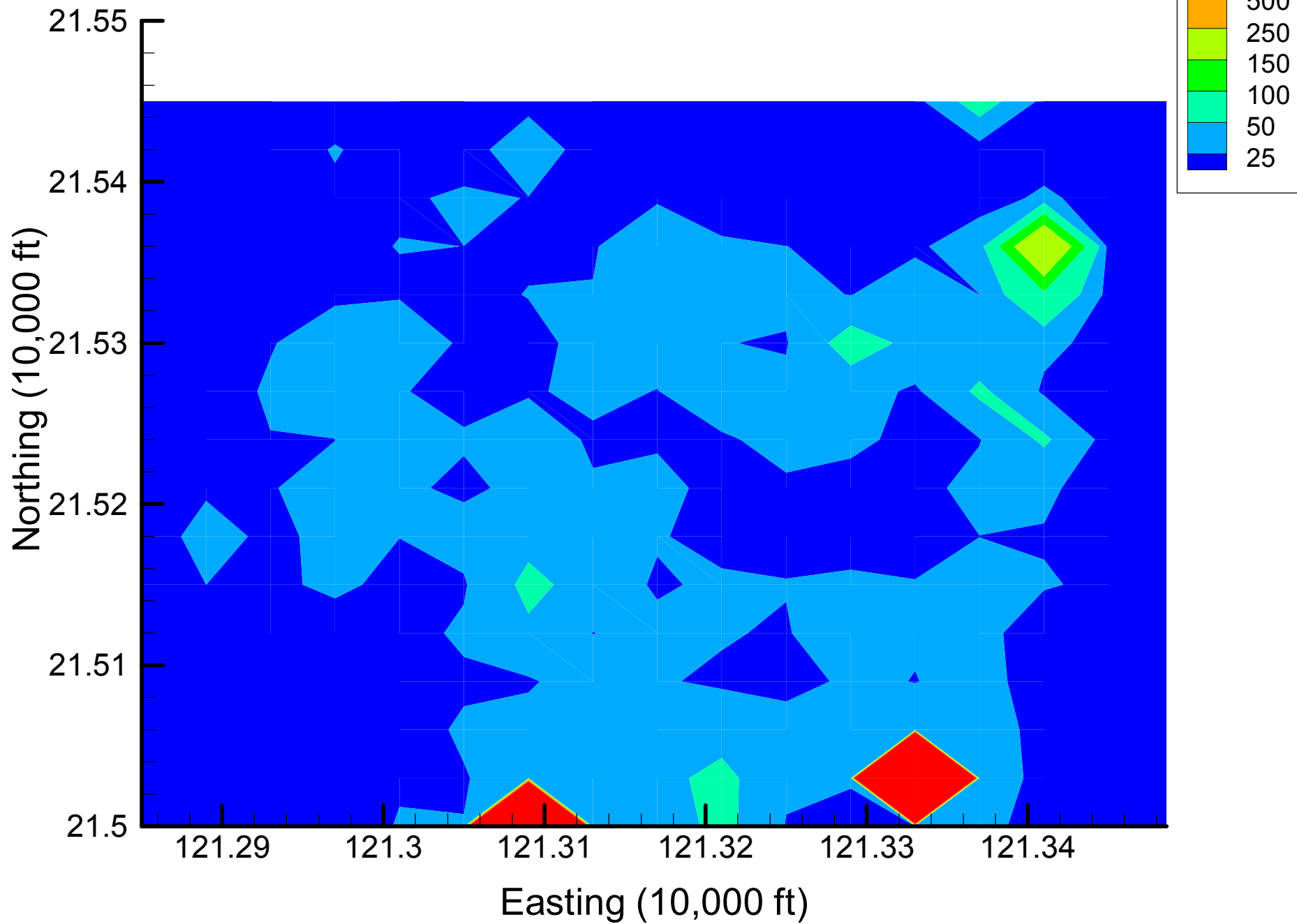
Site 49: DCA11 Local Variances, 2001, 60% Removal



Site 49: DCA11 Local Variances, 2001, 65% Removal

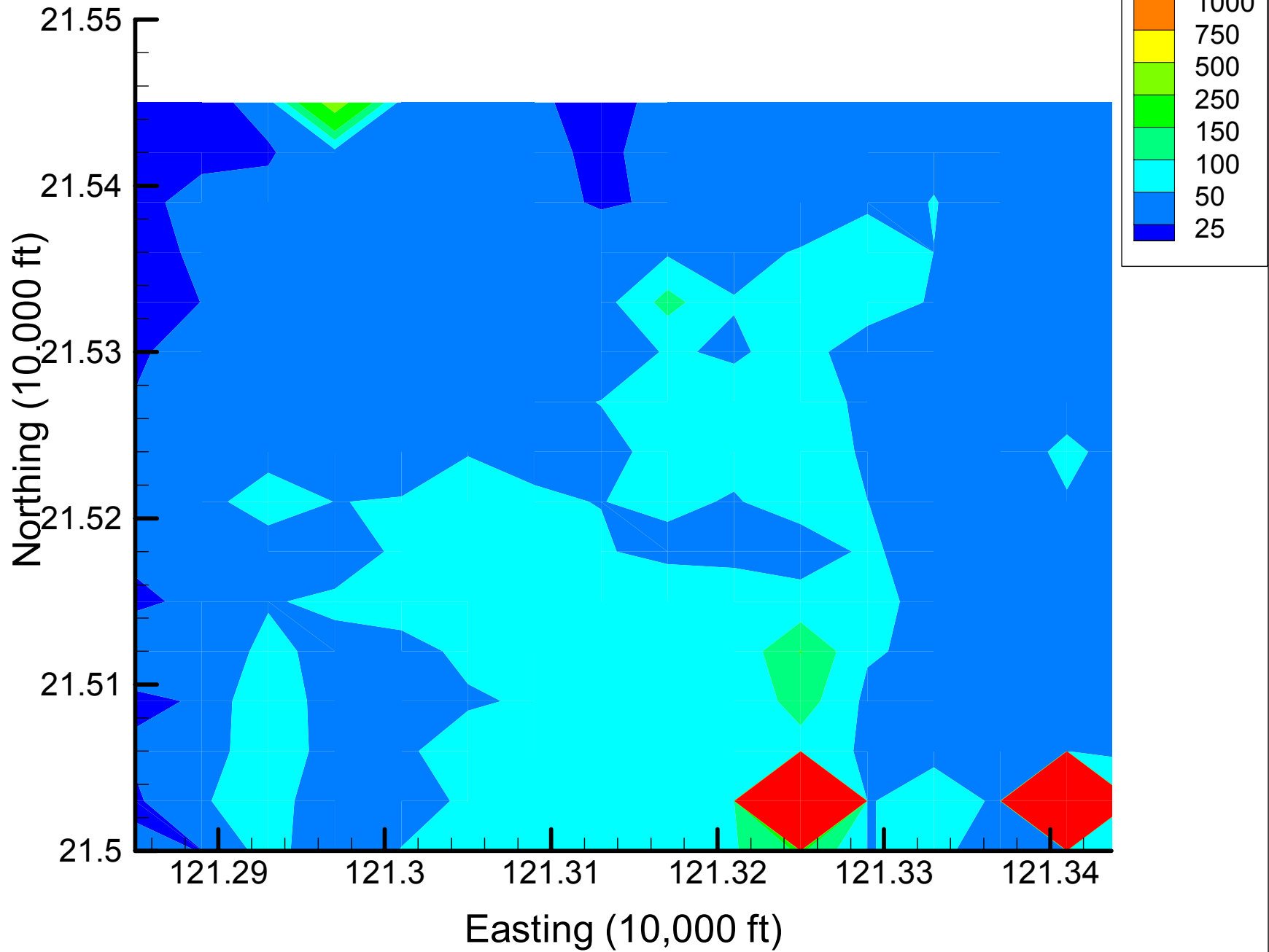


Site 49: DCA11 Local Variances, 2001, 70% Removal

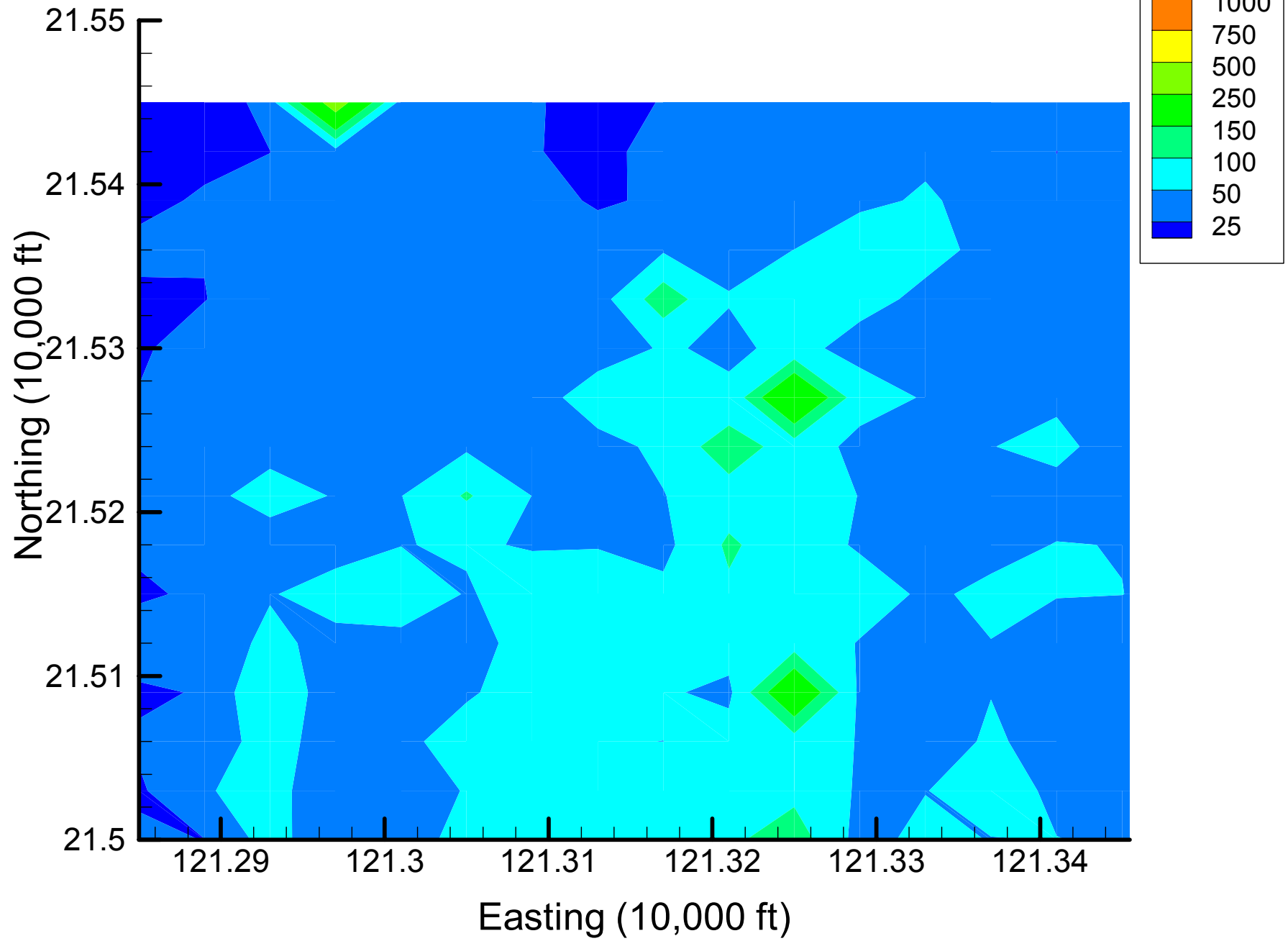


Appendix 4.3  
DCA11 Local Variance Maps  
Time Slice 2 — 2002

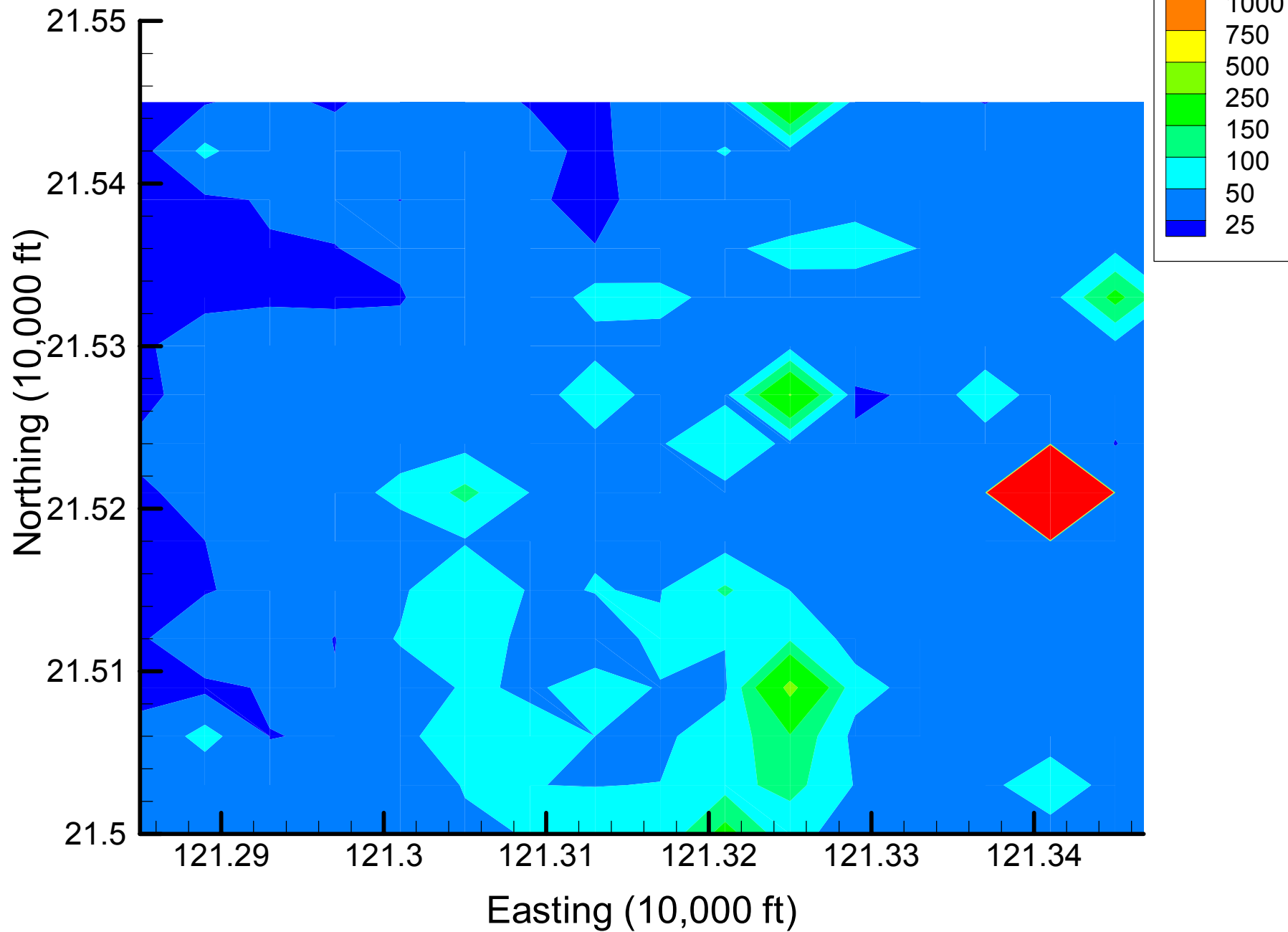
Site 49: DCA11 Local Variances, 2002, Base Map



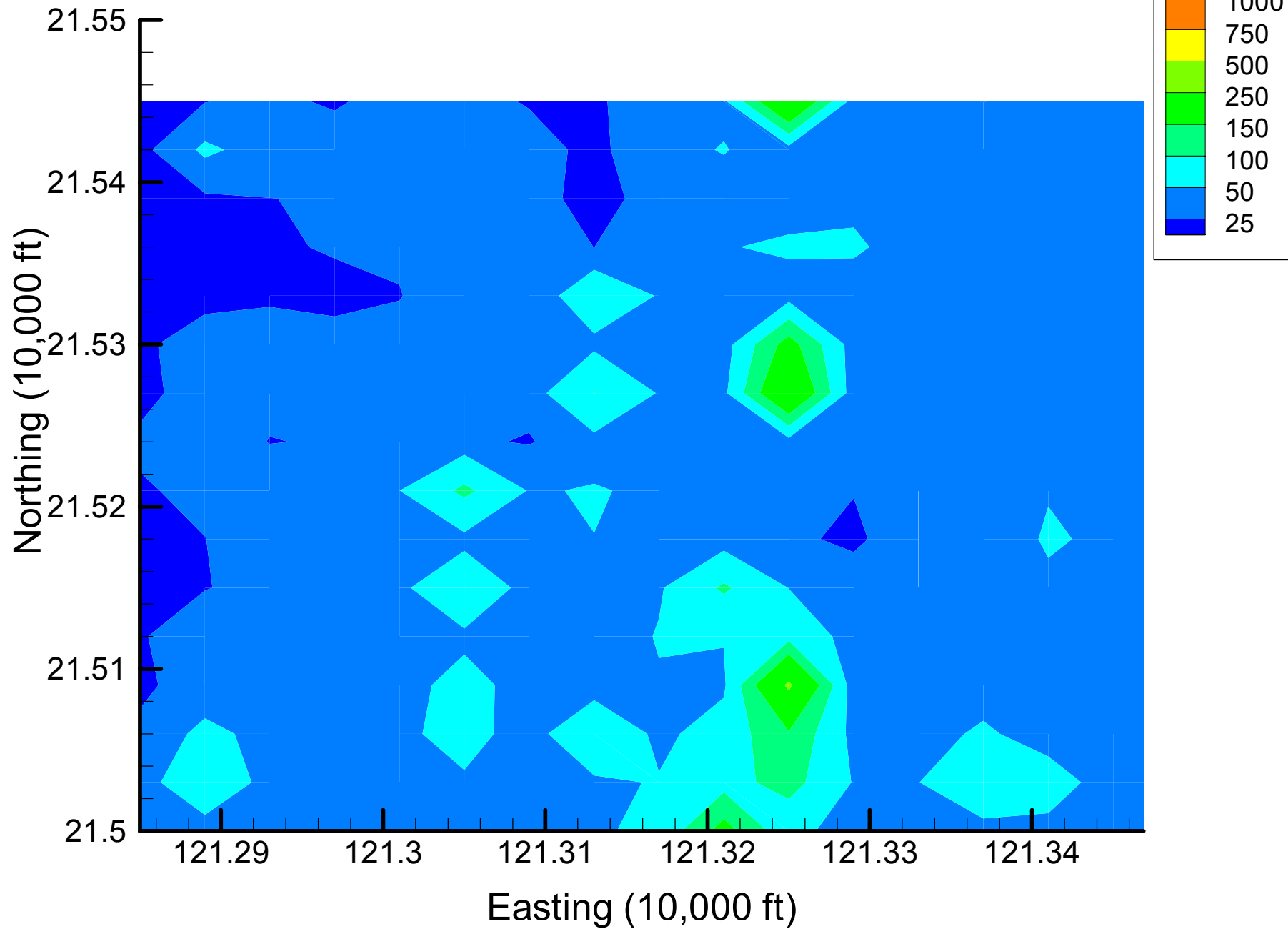
Site 49: DCA11 Local Variances, 2002, 5% Removal



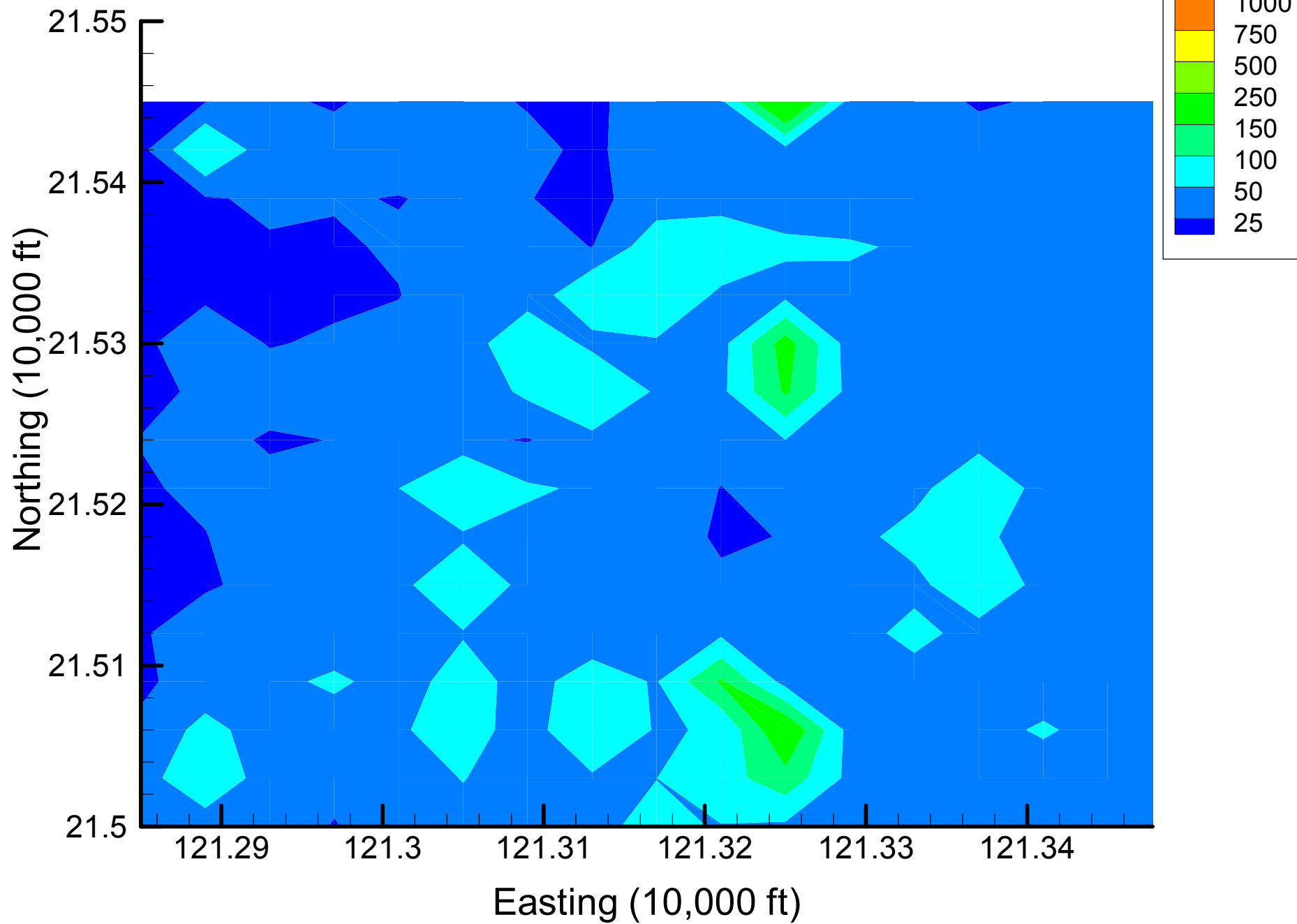
Site 49: DCA11 Local Variances, 2002, 10% Removal



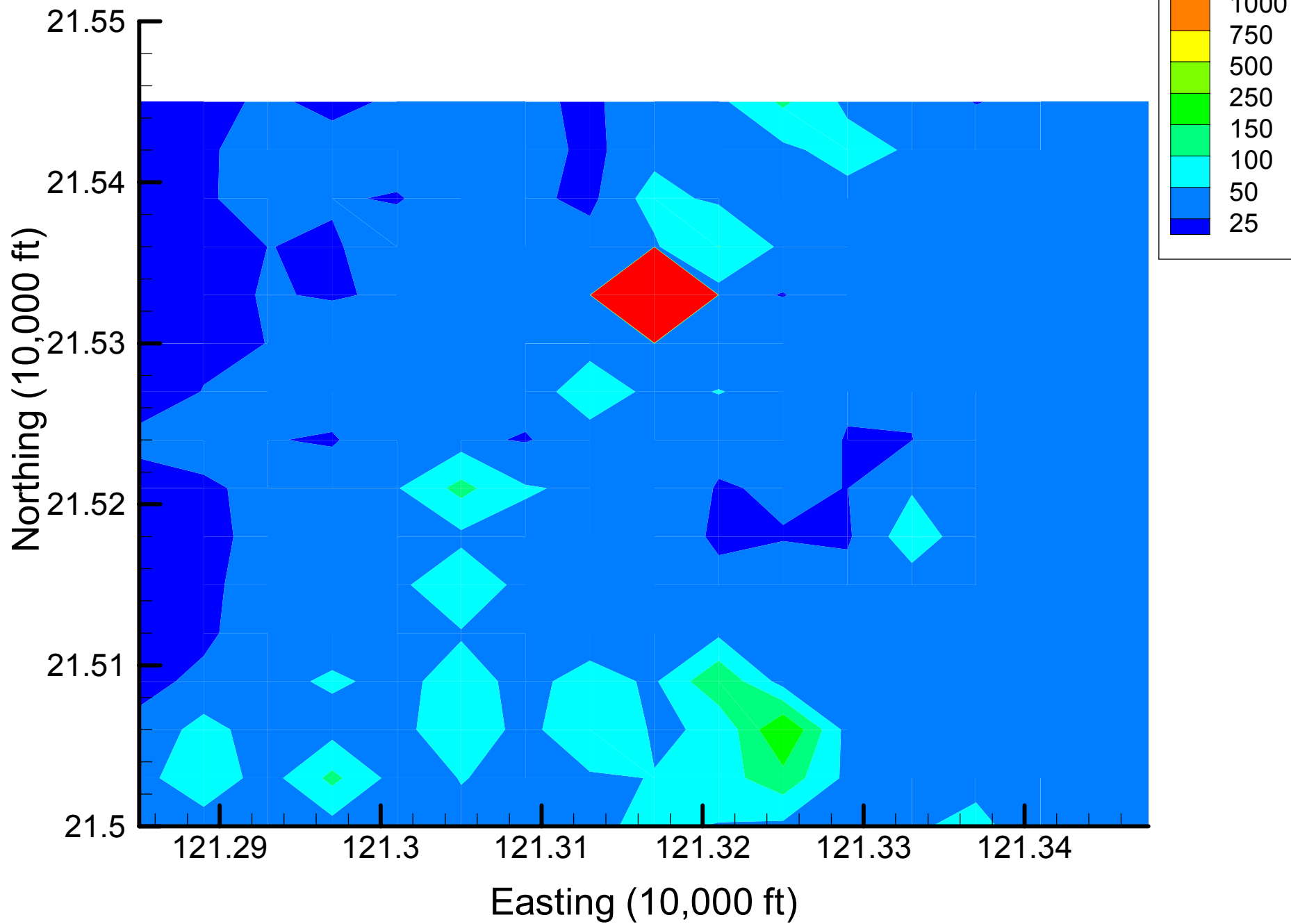
Site 49: DCA11 Local Variances, 2002, 15% Removal



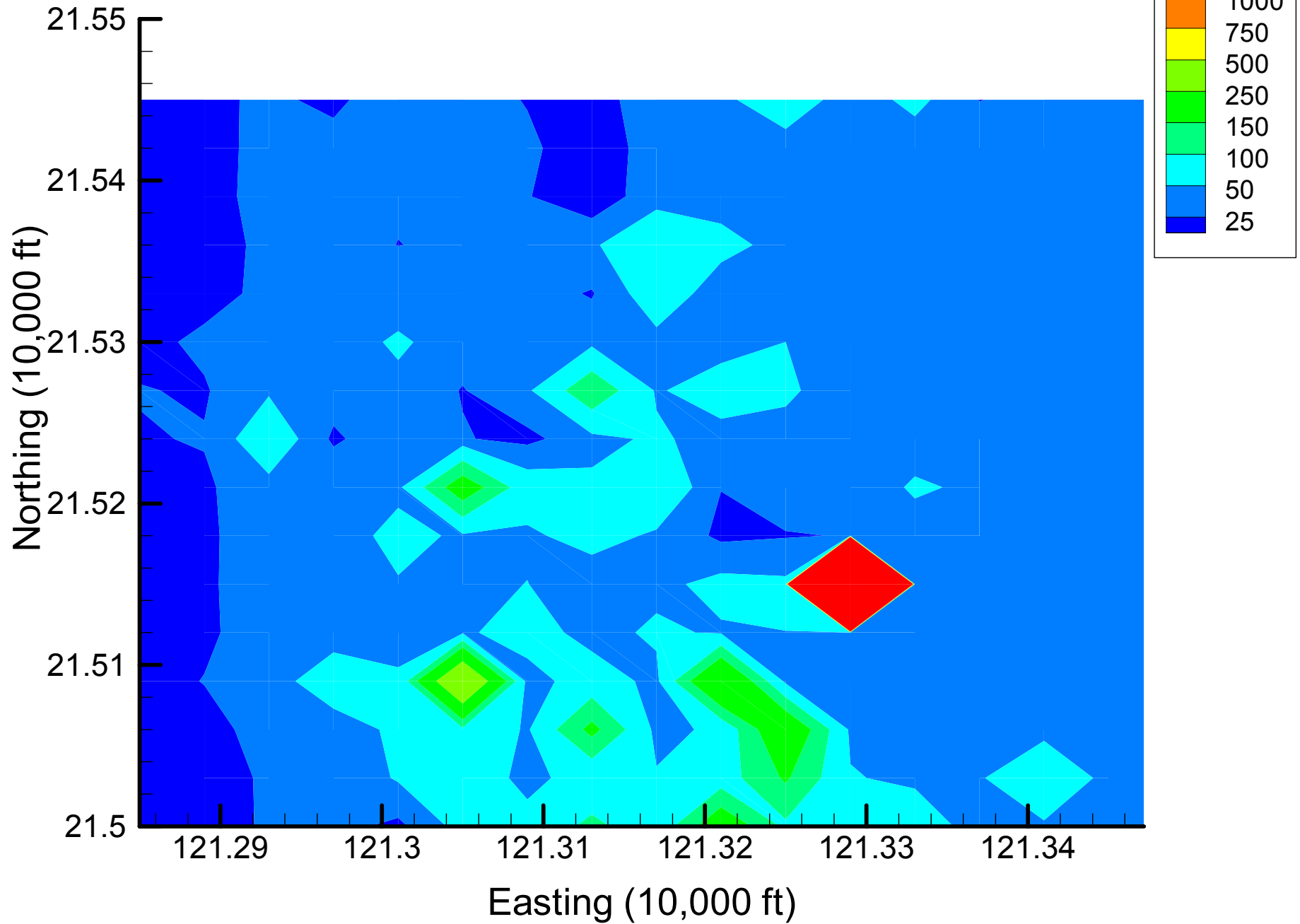
Site 49: DCA11 Local Variances, 2002, 20% Removal



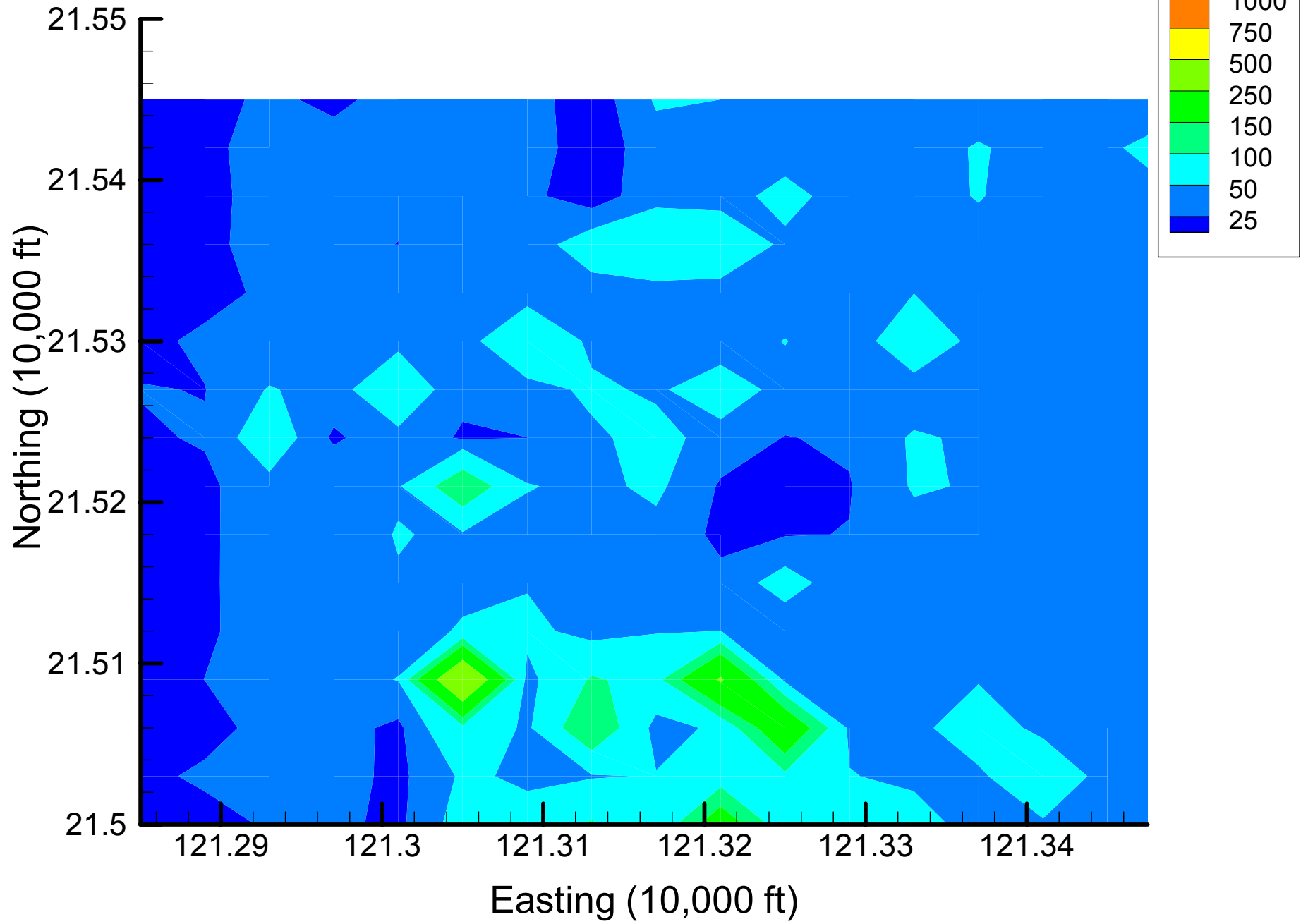
Site 49: DCA11 Local Variances, 2002, 25% Removal



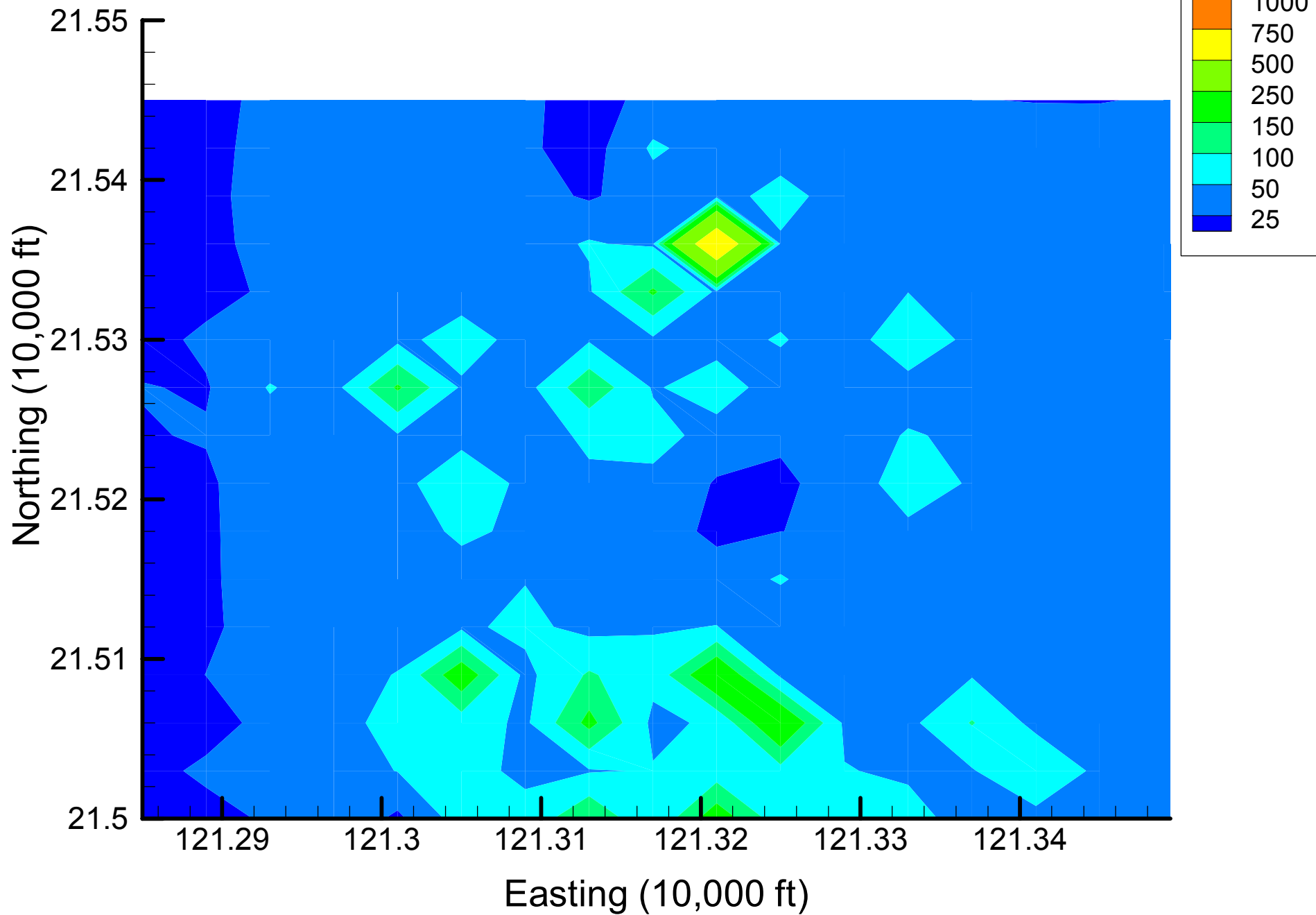
Site 49: DCA11 Local Variances, 2002, 30% Removal



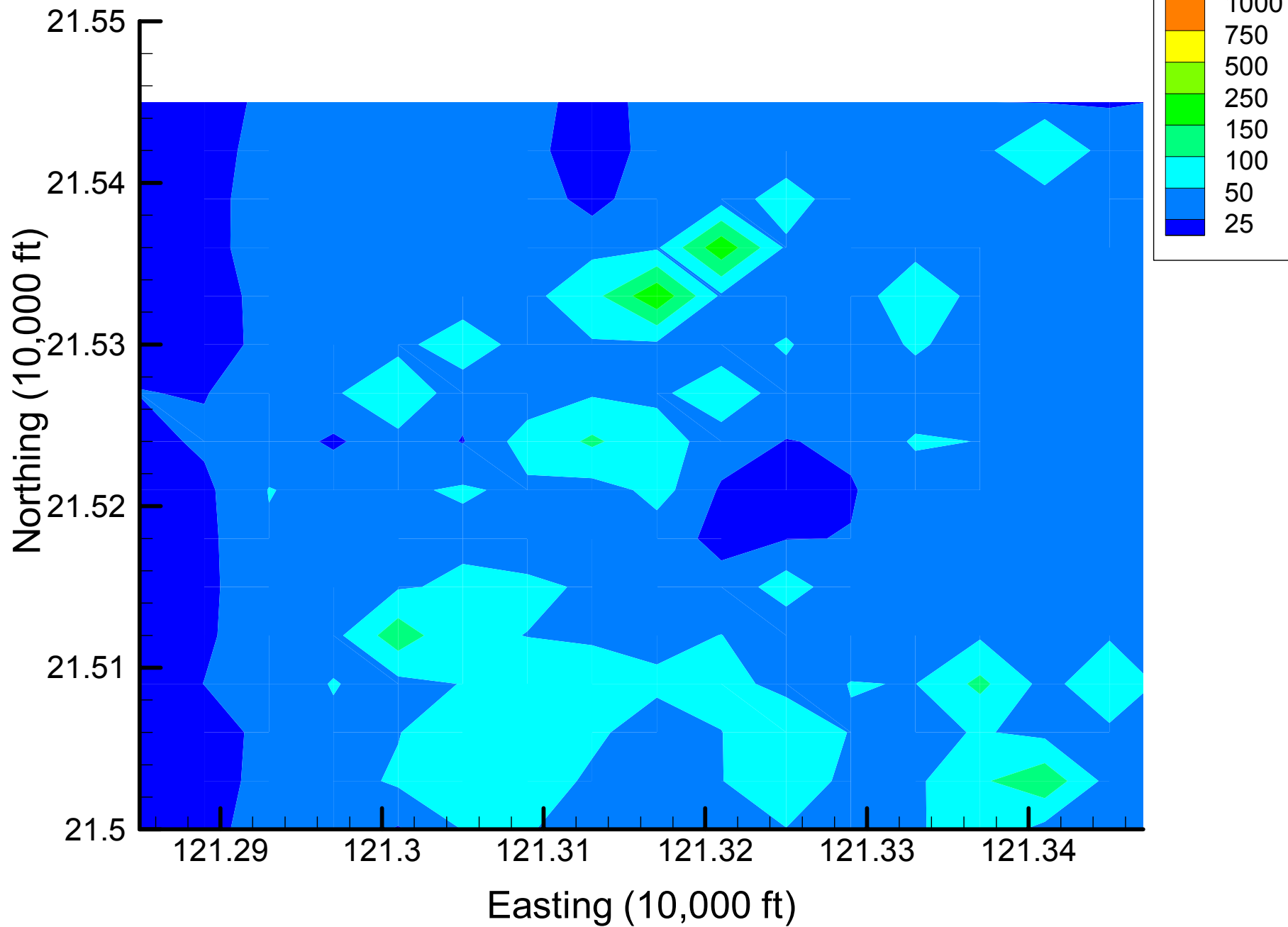
Site 49: DCA11 Local Variances, 2002, 35% Removal



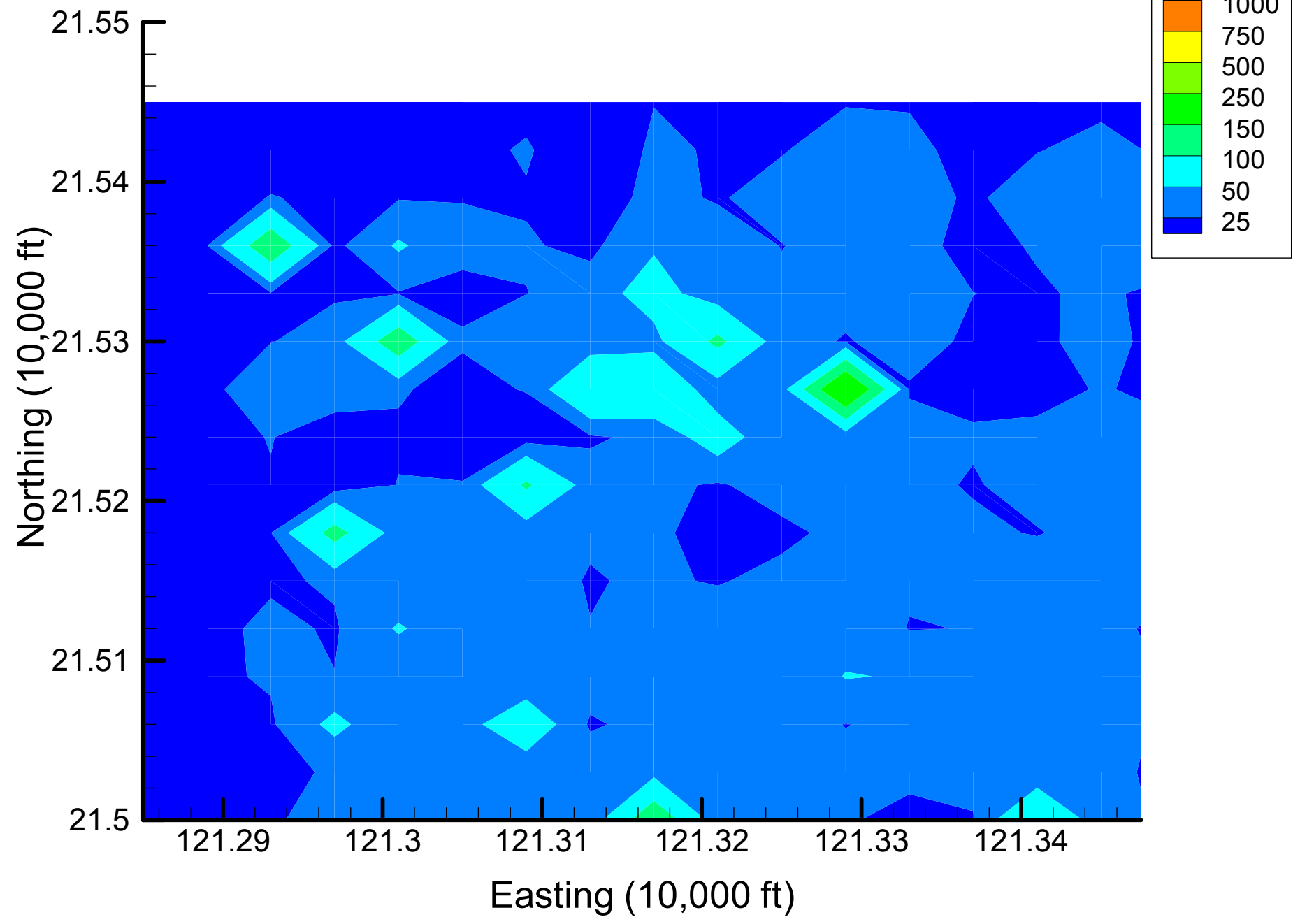
Site 49: DCA11 Local Variances, 2002, 40% Removal



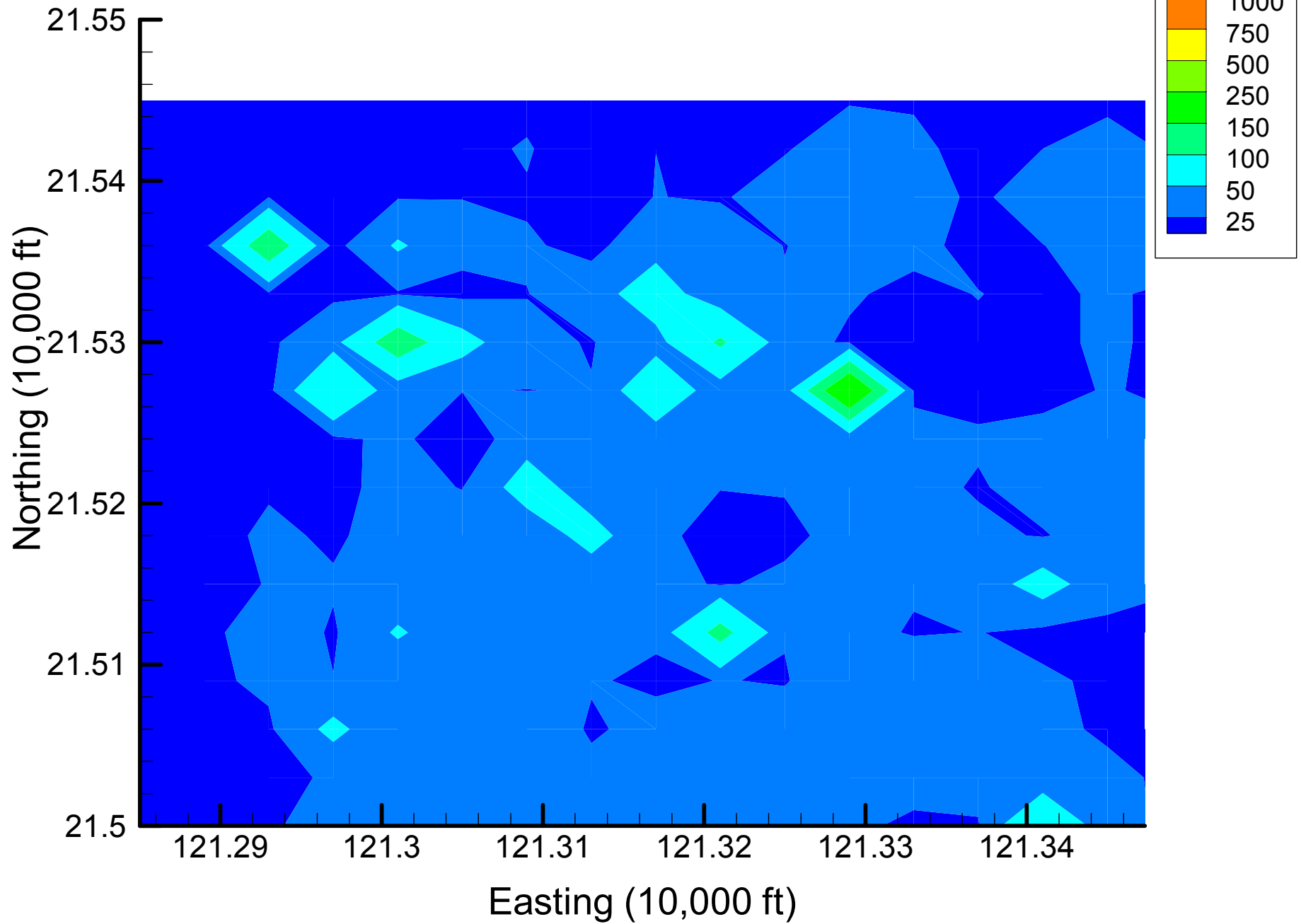
Site 49: DCA11 Local Variances, 2002, 45% Removal



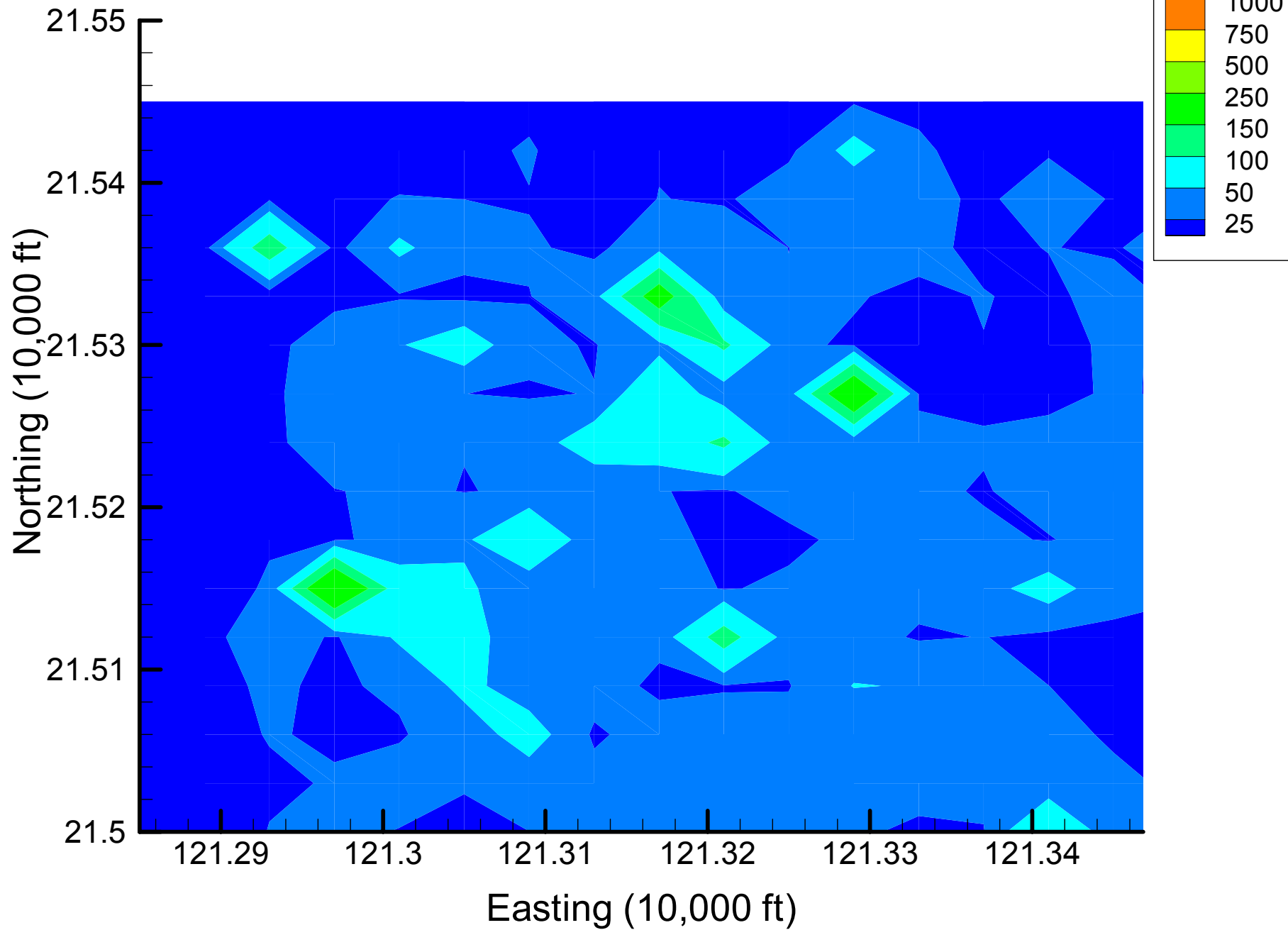
Site 49: DCA11 Local Variances, 2002, 50% Removal



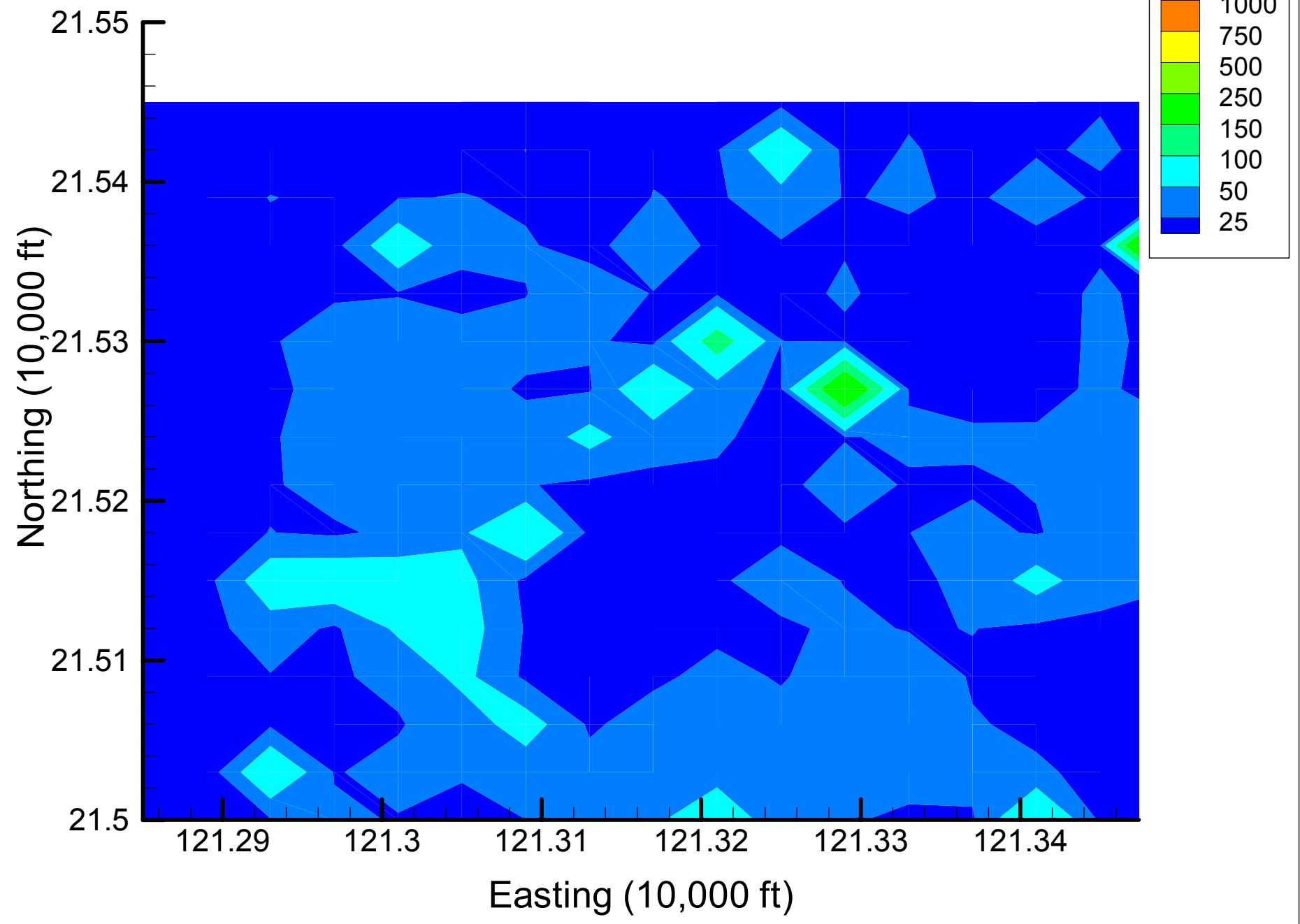
Site 49: DCA11 Local Variances, 2002, 55% Removal



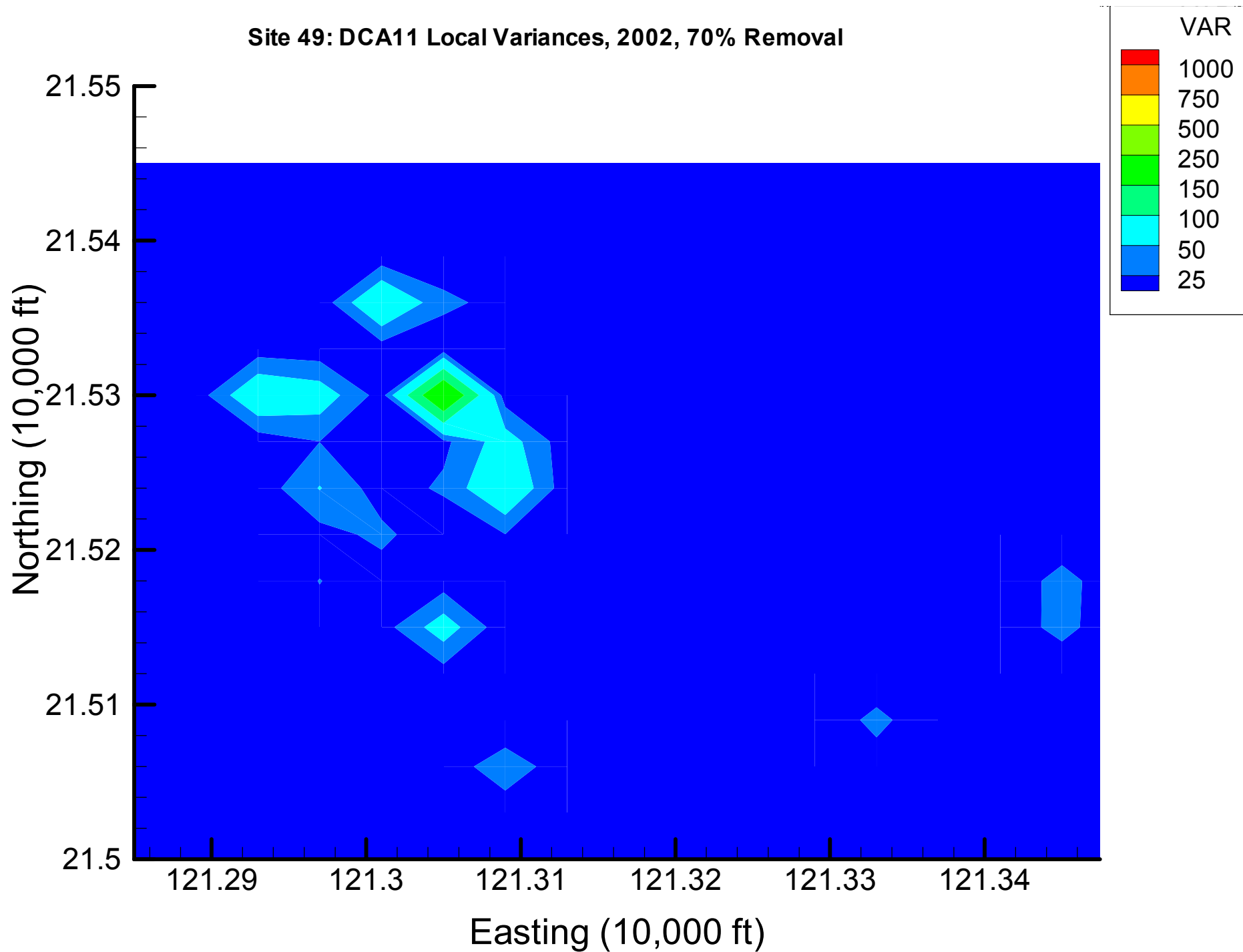
Site 49: DCA11 Local Variances, 2002, 60% Removal



Site 49: DCA11 Local Variances, 2002, 65% Removal

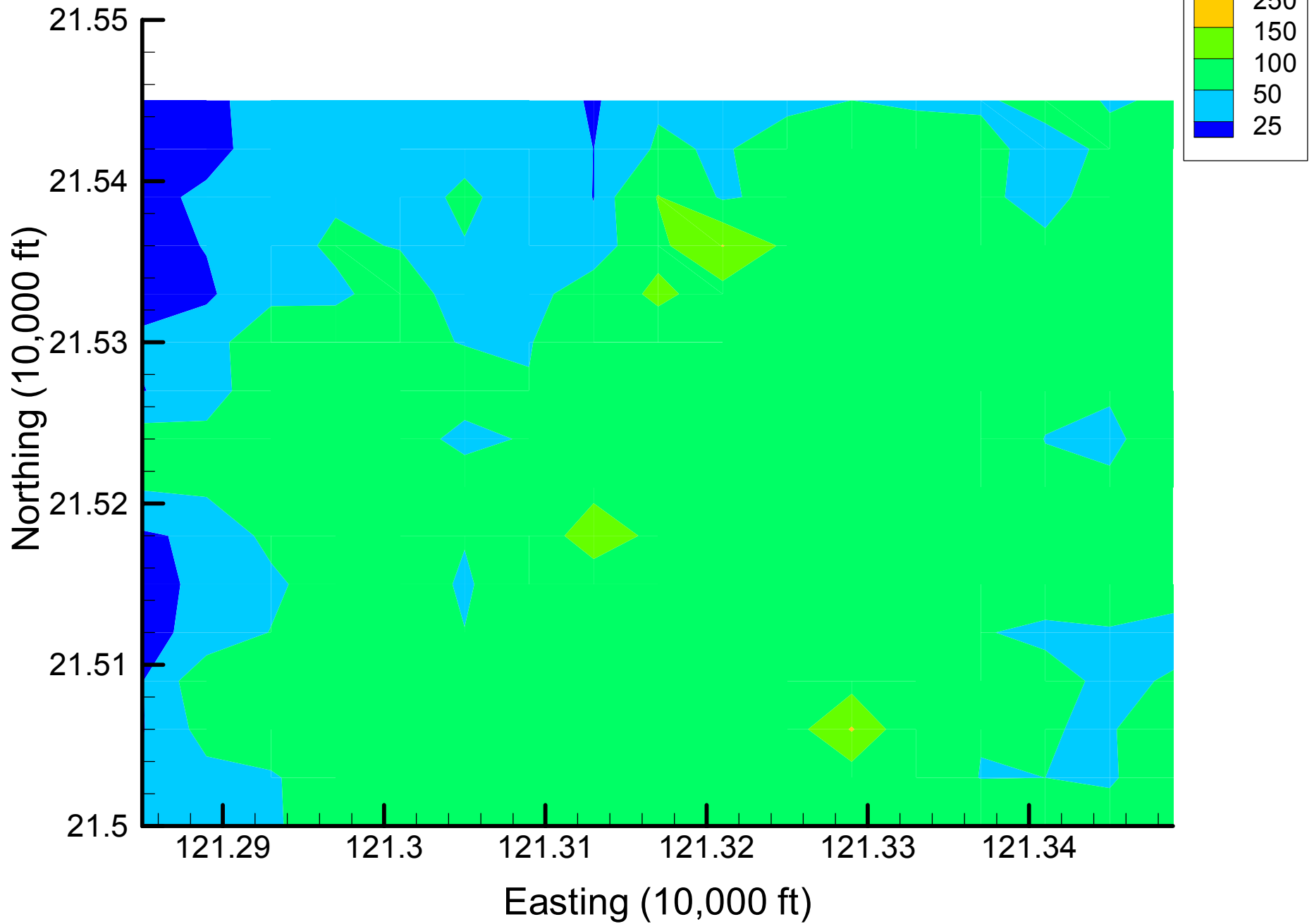


Site 49: DCA11 Local Variances, 2002, 70% Removal

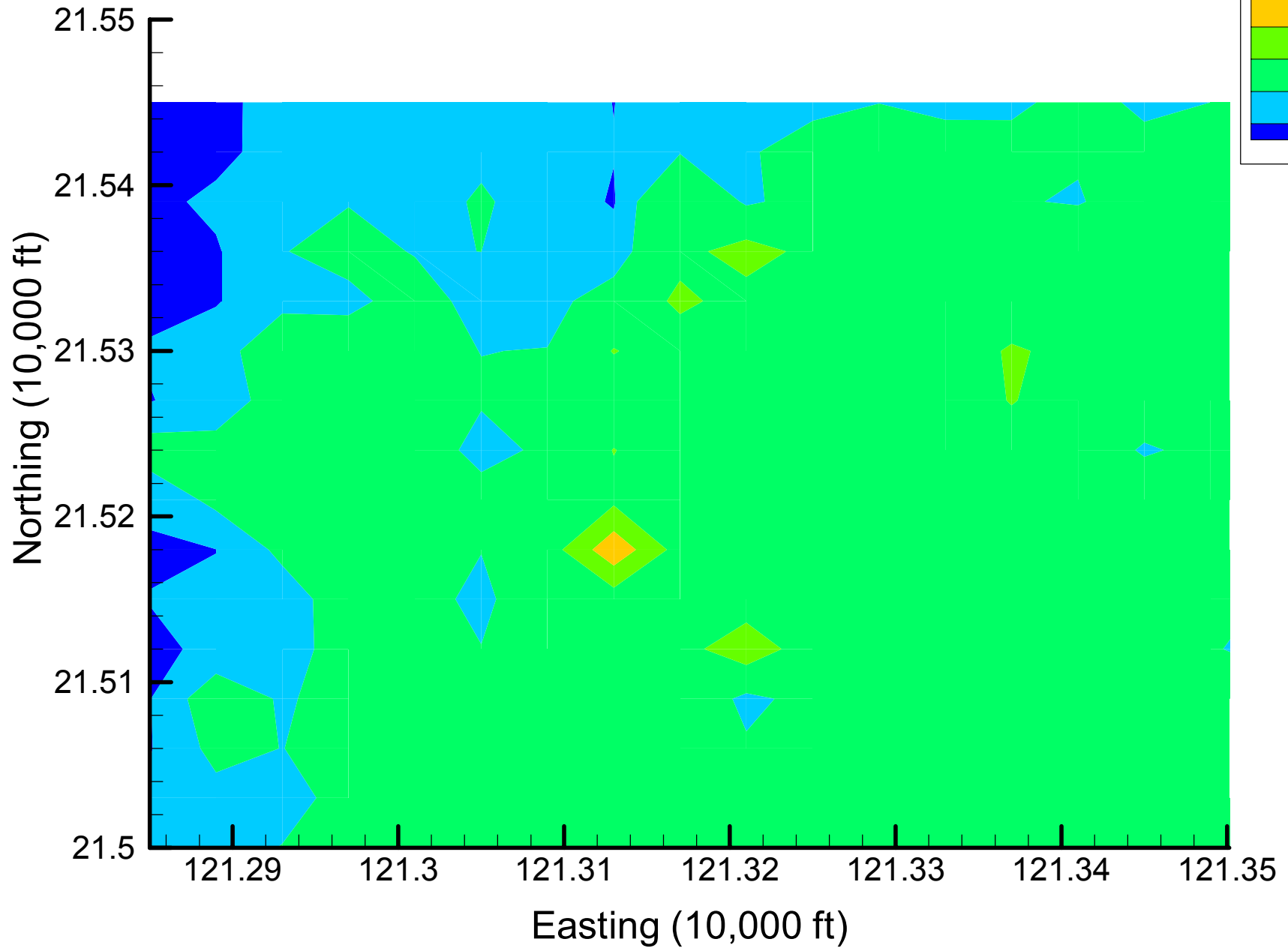


Appendix 4.3  
DCE12C Local Variance Maps  
Time Slice 1 — 2001

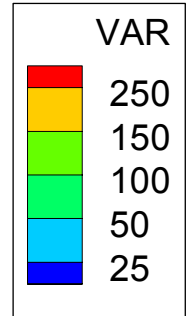
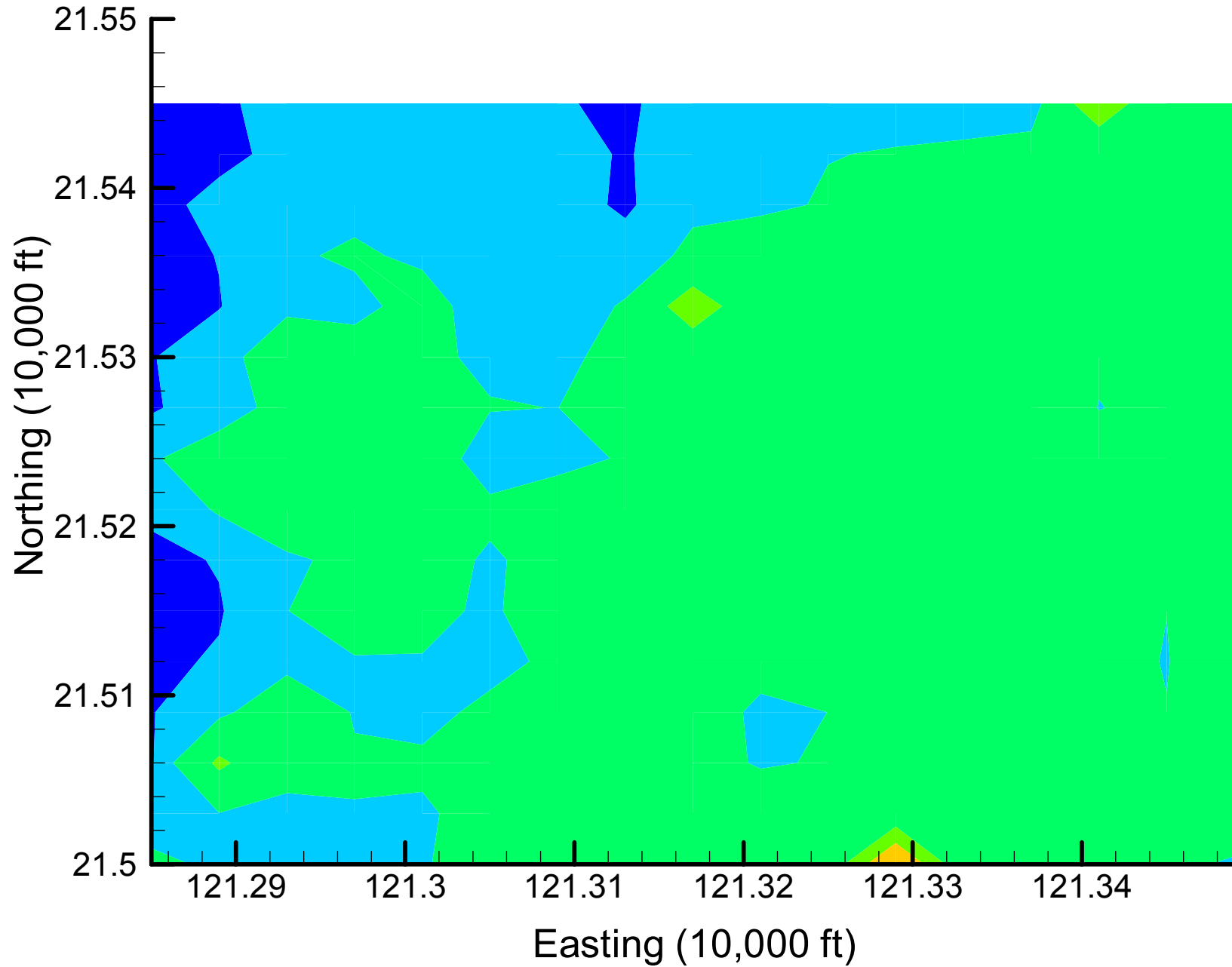
Site 49: DCE12C Local Variances, 2001, Base Map



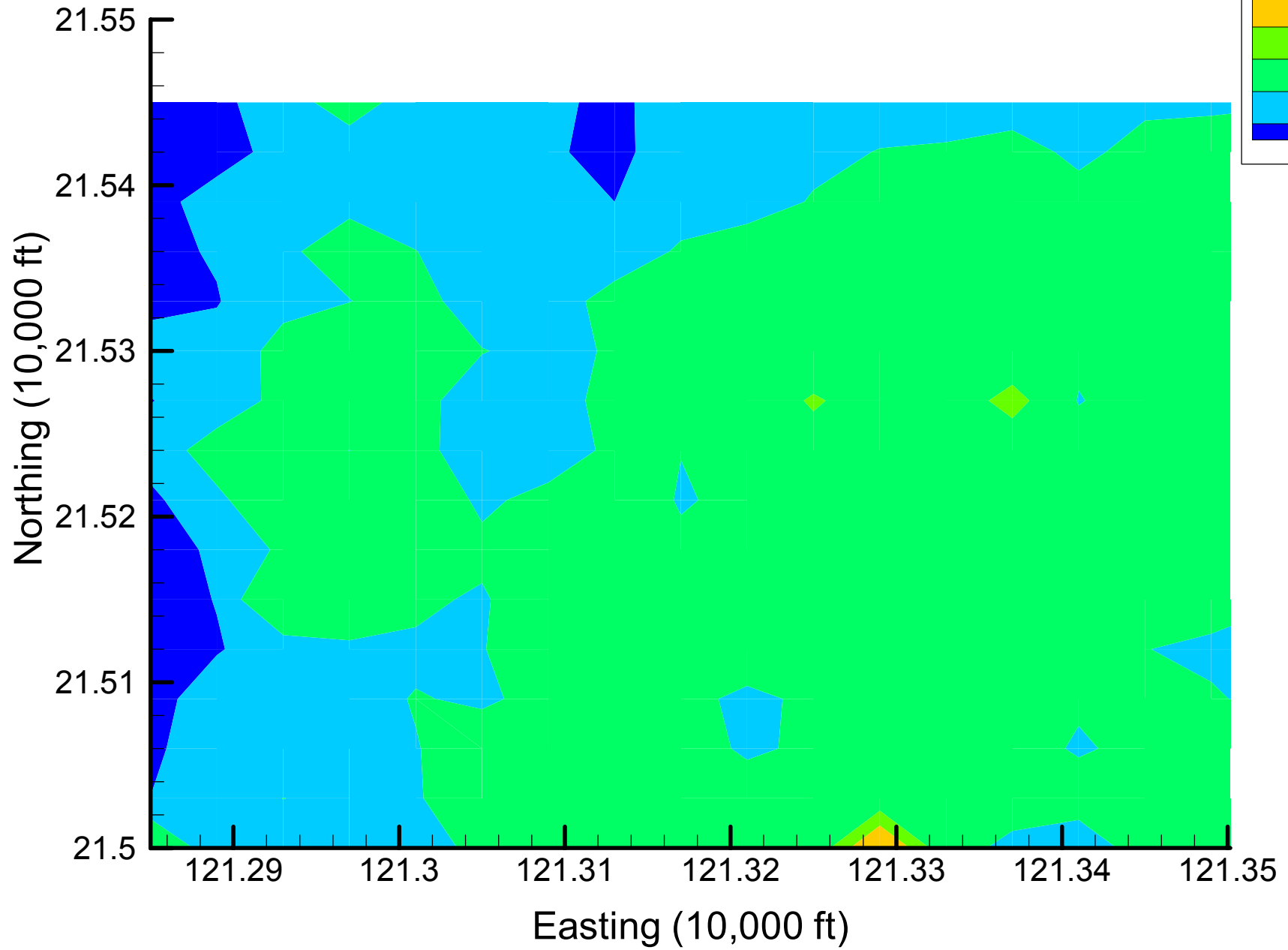
Site 49: DCE12C Local Variances, 2001, 5% Removal



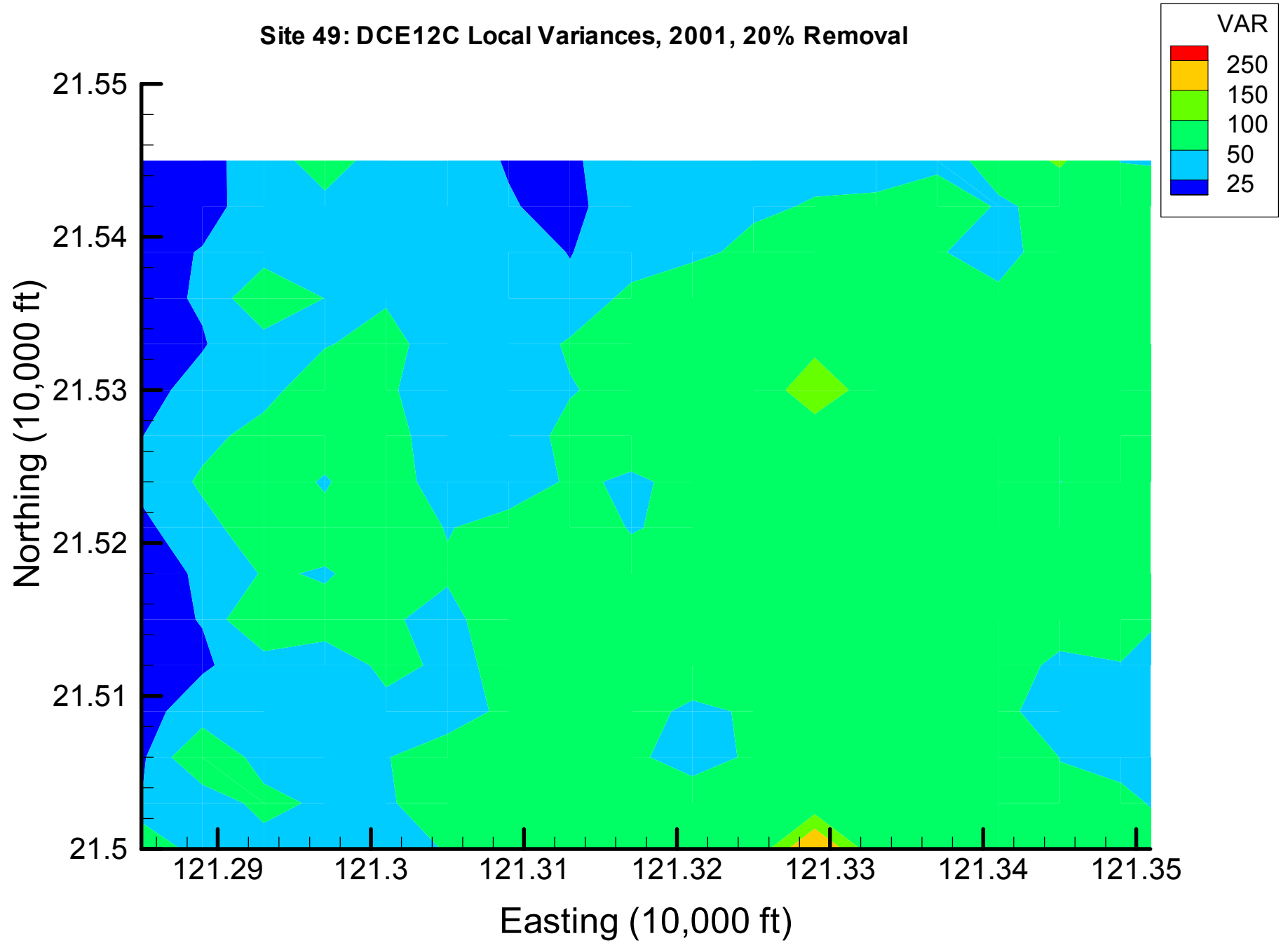
Site 49: DCE12C Local Variances, 2001, 10% Removal



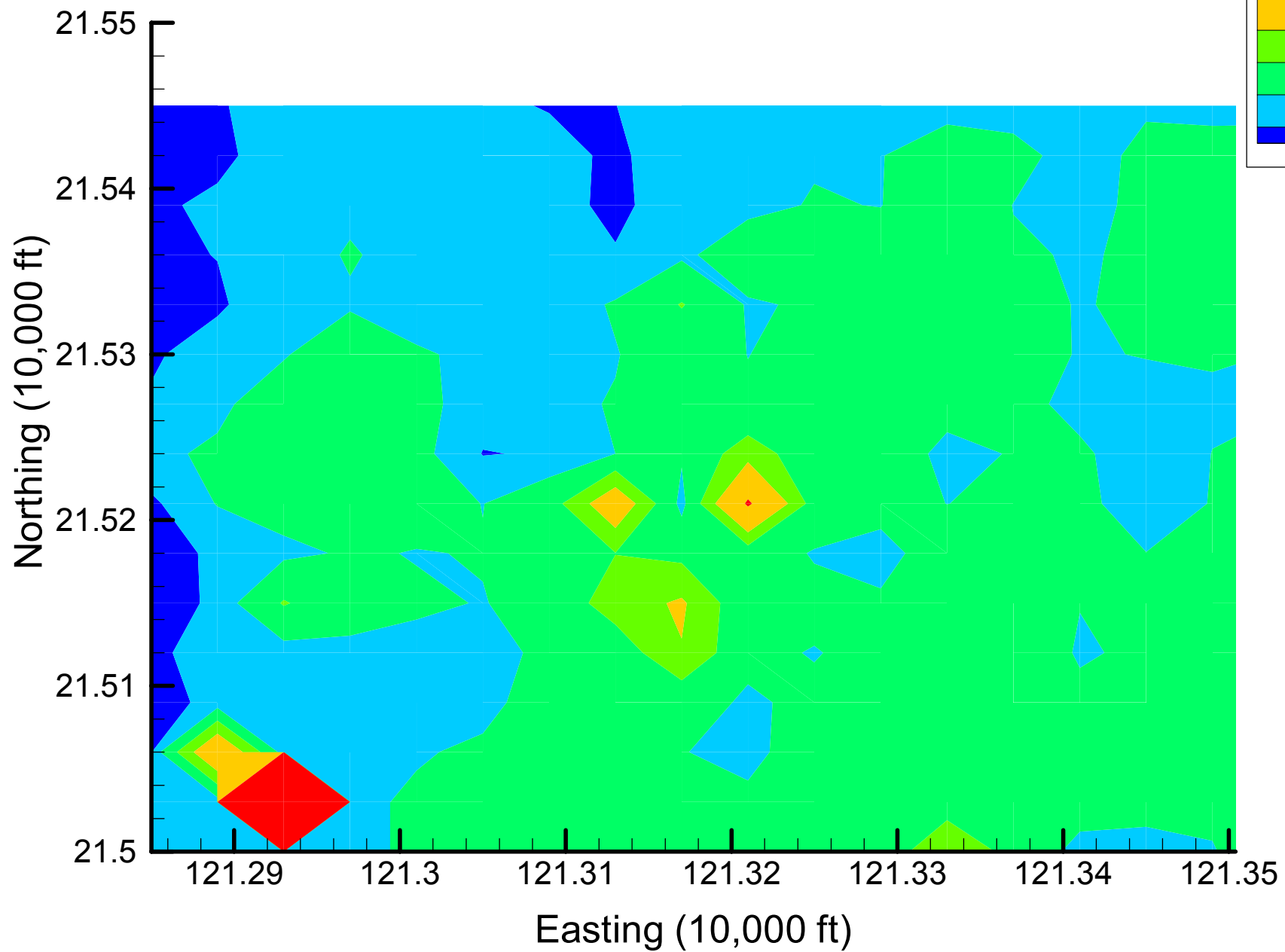
Site 49: DCE12C Local Variances, 2001, 15% Removal



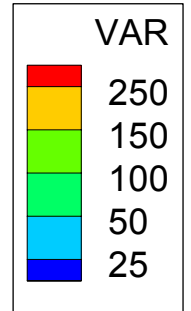
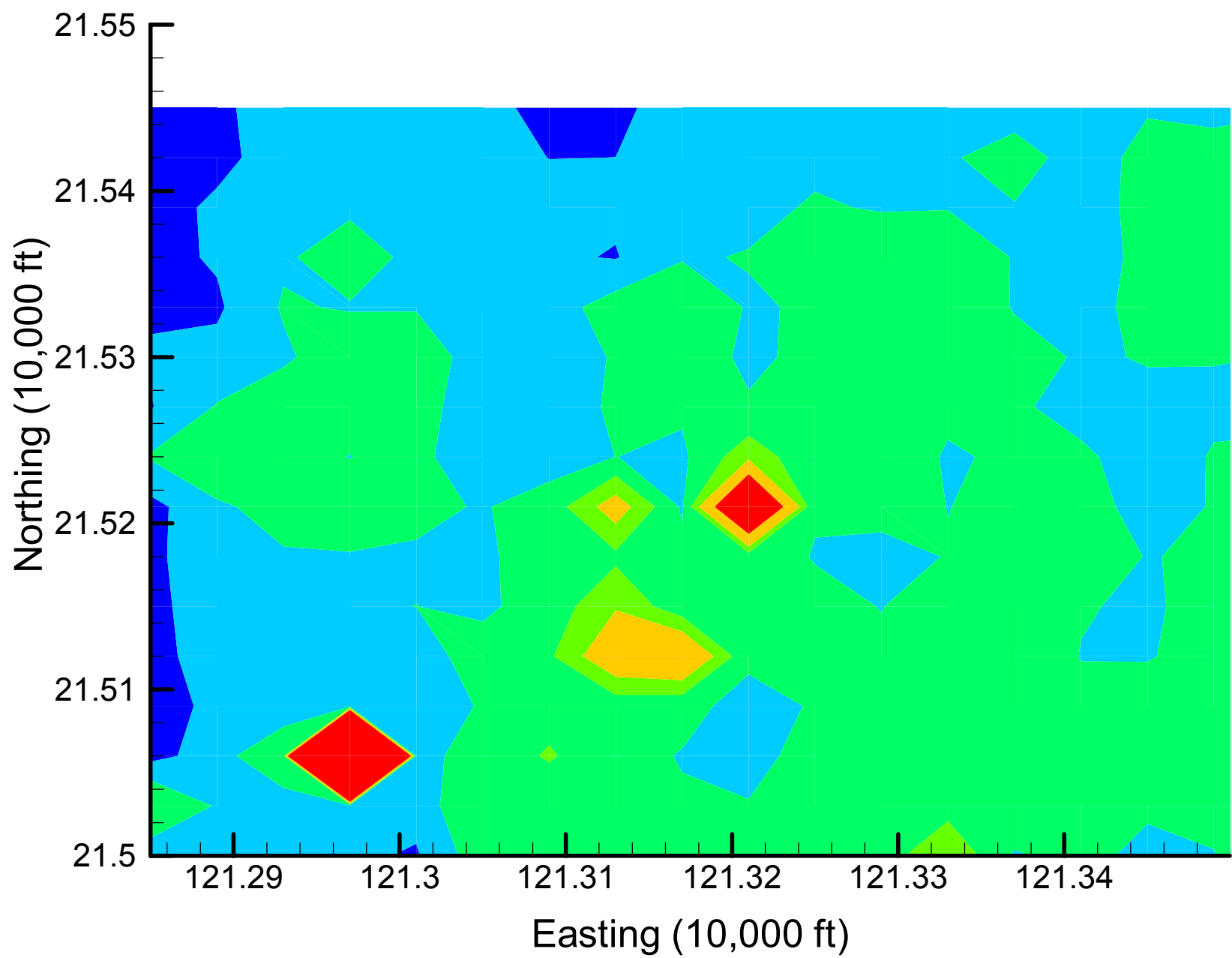
Site 49: DCE12C Local Variances, 2001, 20% Removal



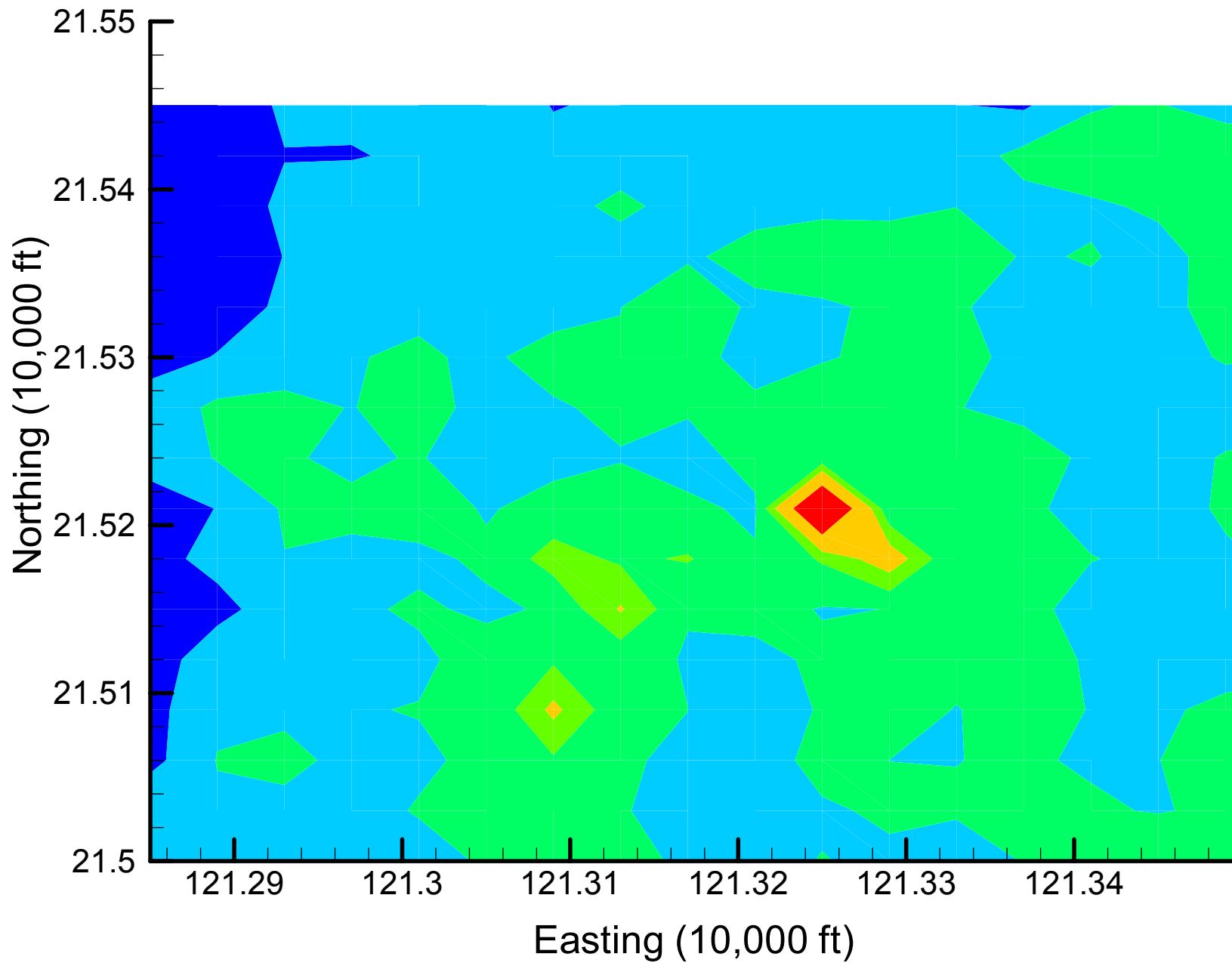
Site 49: DCE12C Local Variances, 2001, 25% Removal



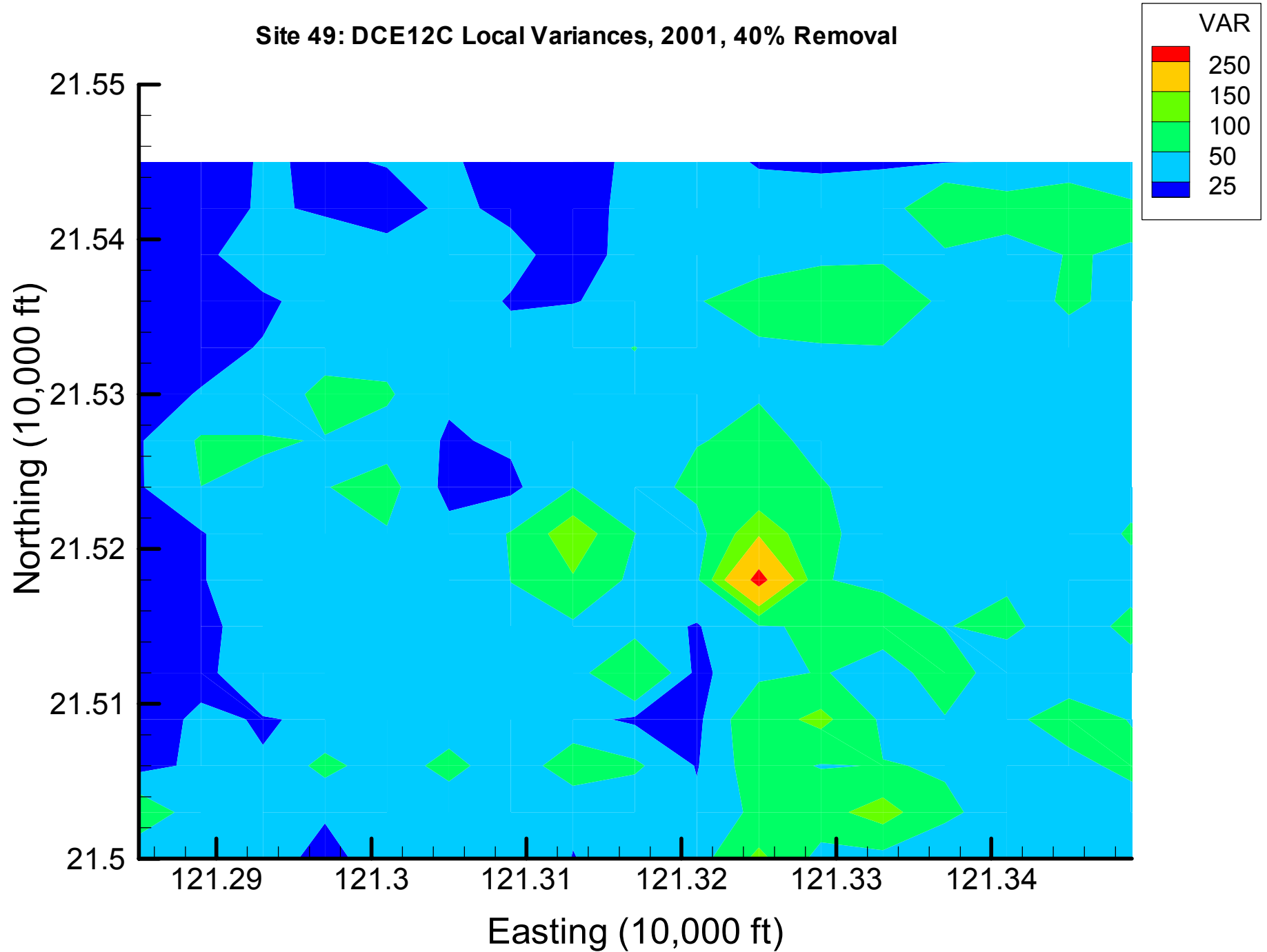
Site 49: DCE12C Local Variances, 2001, 30% Removal



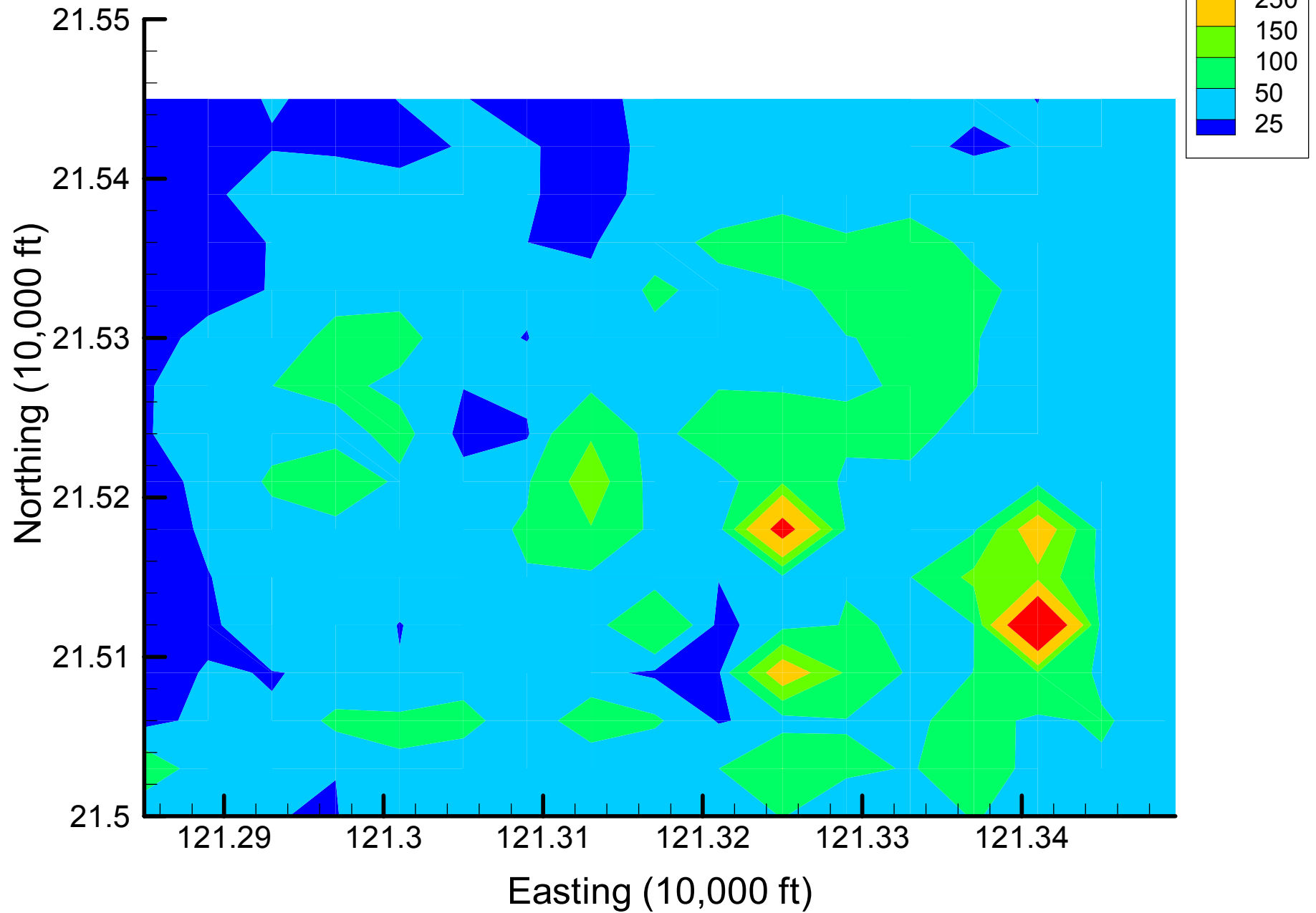
Site 49: DCE12C Local Variances, 2001, 35% Removal



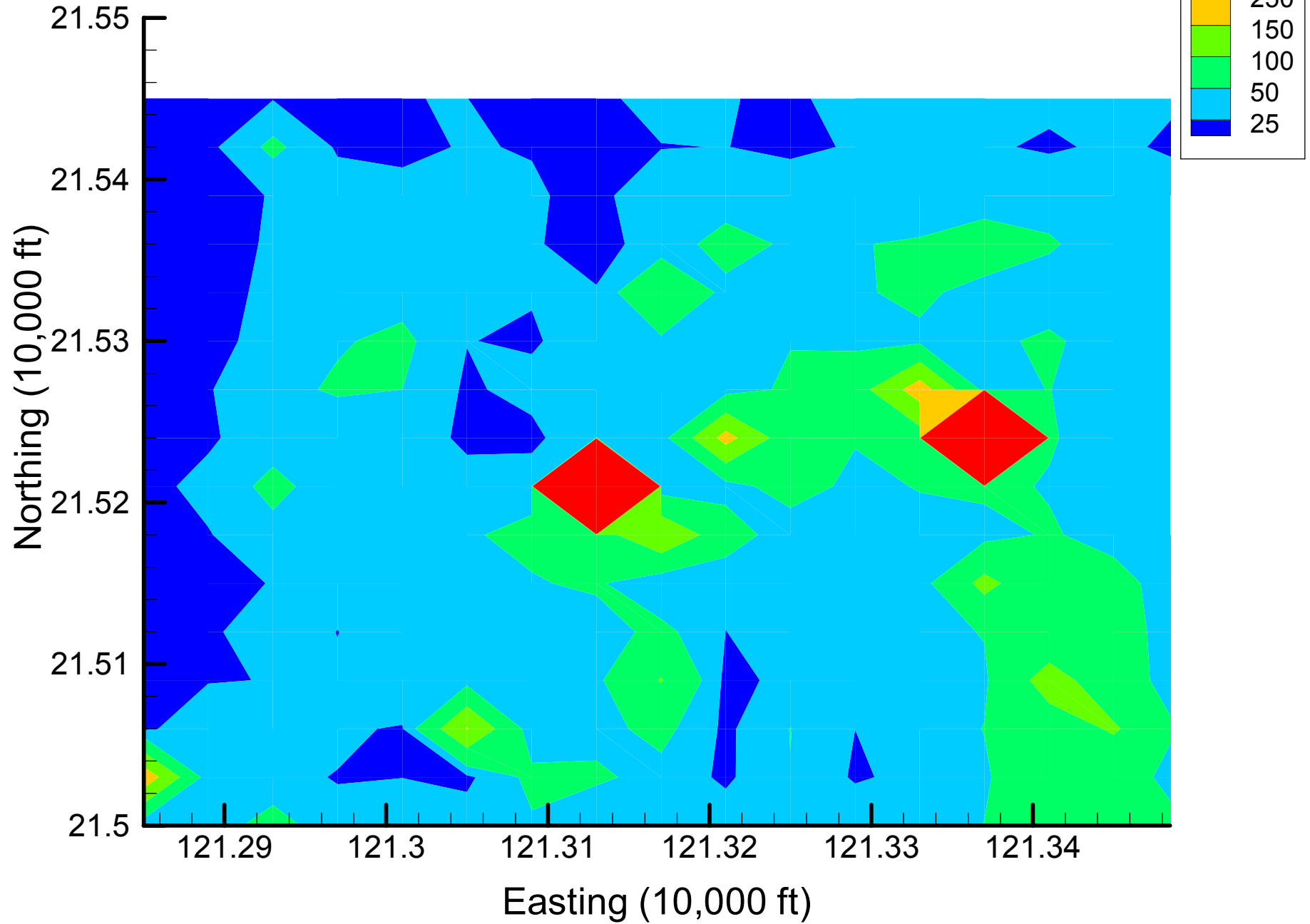
Site 49: DCE12C Local Variances, 2001, 40% Removal



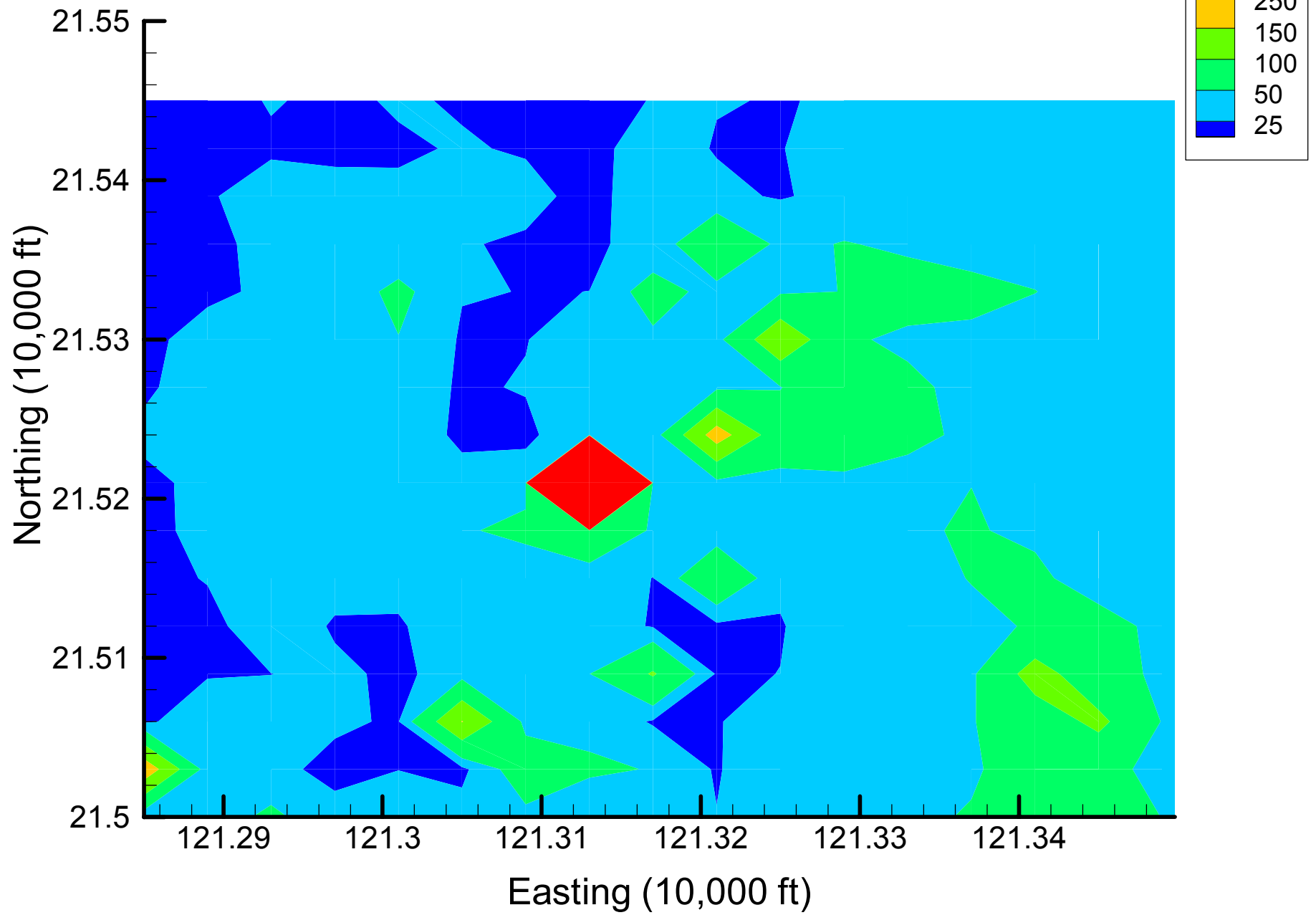
Site 49: DCE12C Local Variances, 2001, 45% Removal



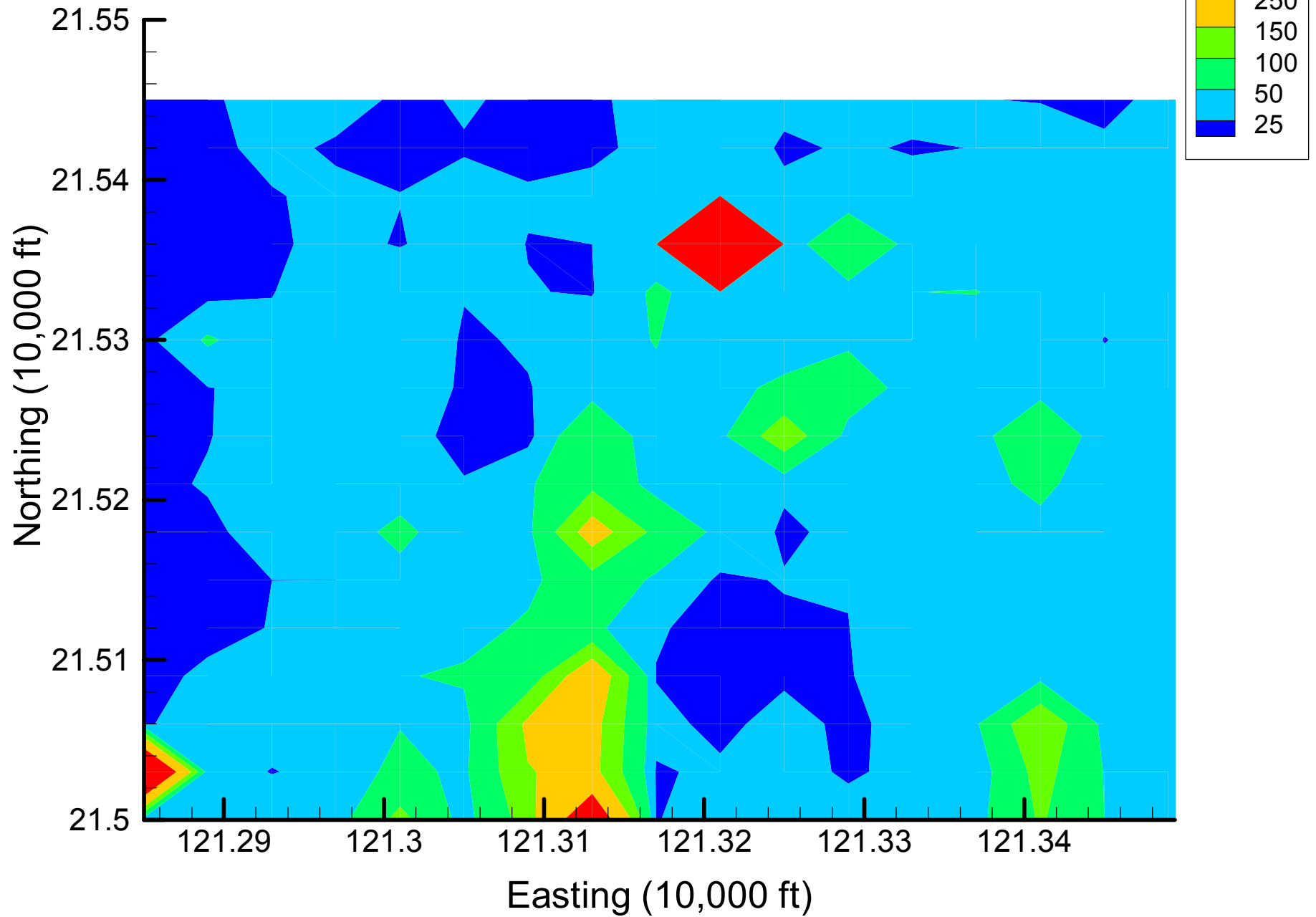
Site 49: DCE12C Local Variances, 2001, 50% Removal



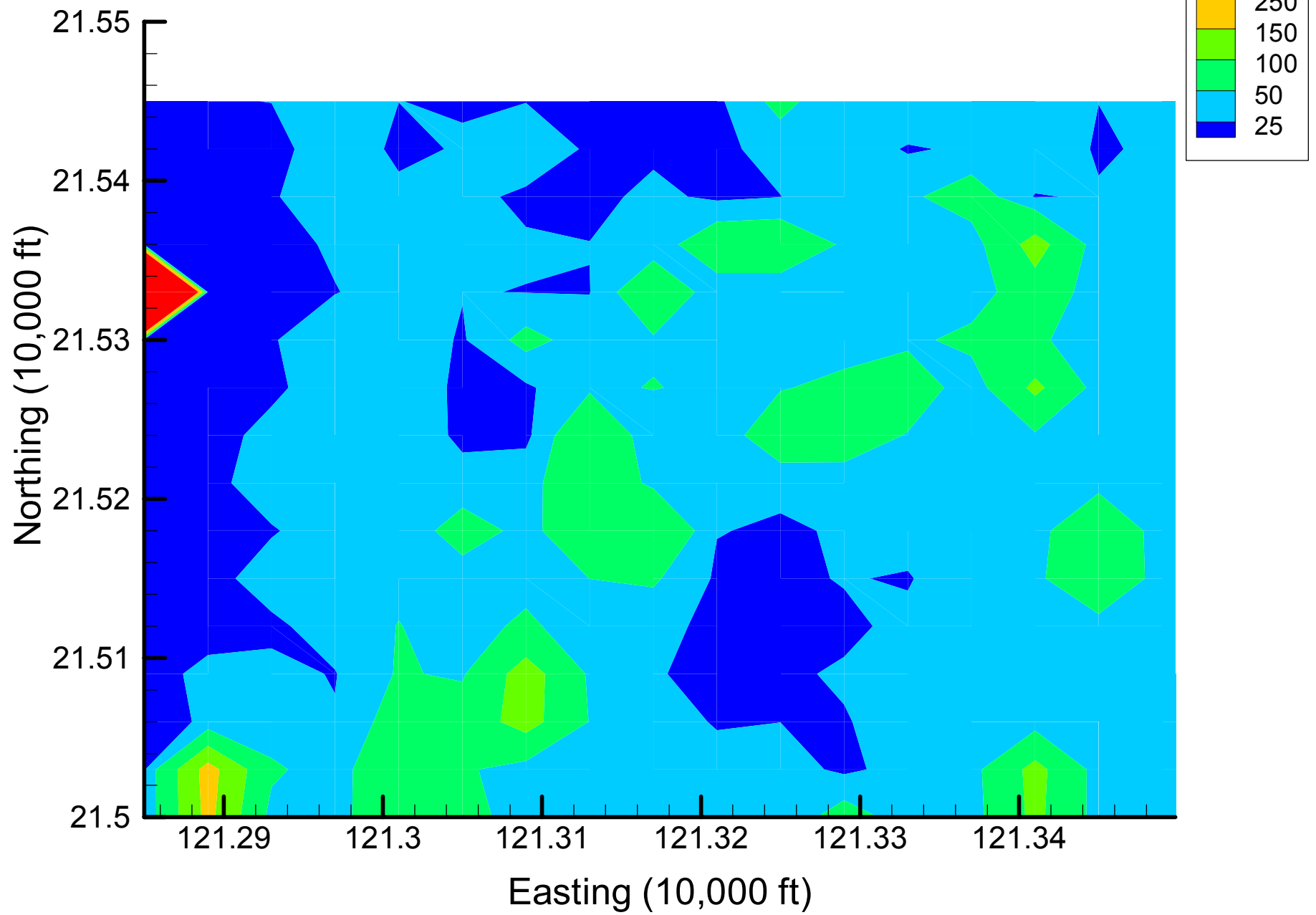
Site 49: DCE12C Local Variances, 2001, 55% Removal



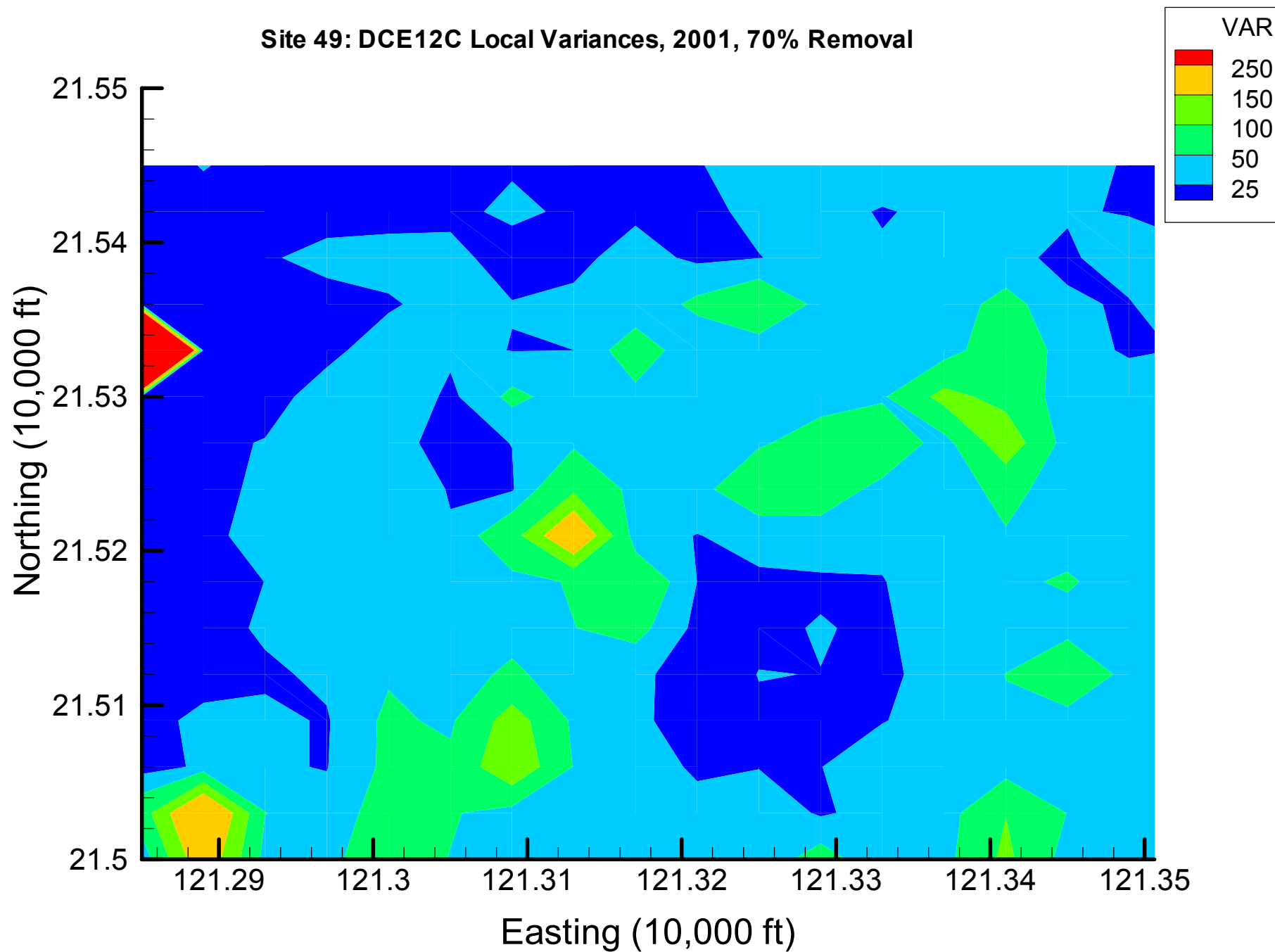
Site 49: DCE12C Local Variances, 2001, 60% Removal



Site 49: DCE12C Local Variances, 2001, 65% Removal

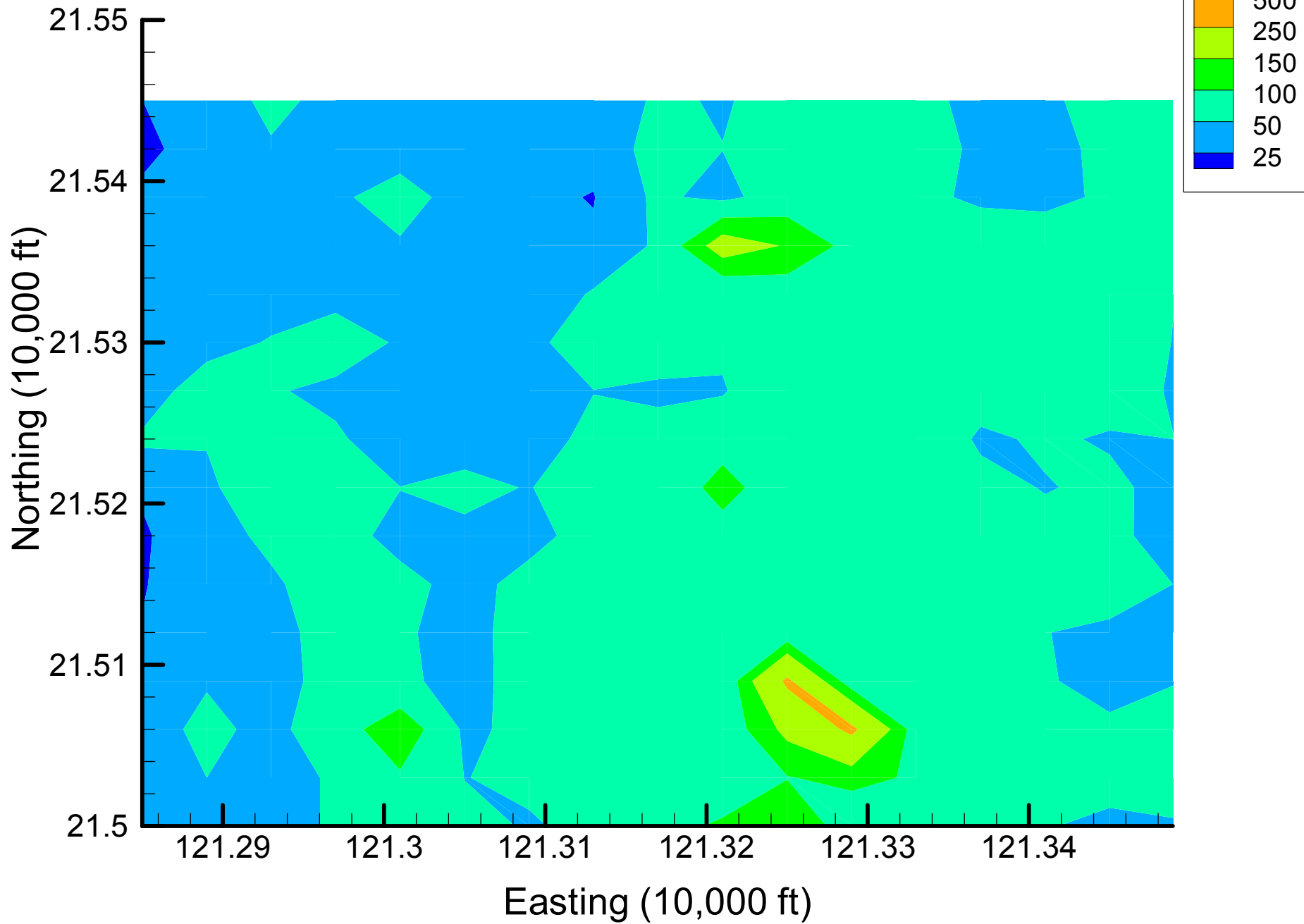


Site 49: DCE12C Local Variances, 2001, 70% Removal

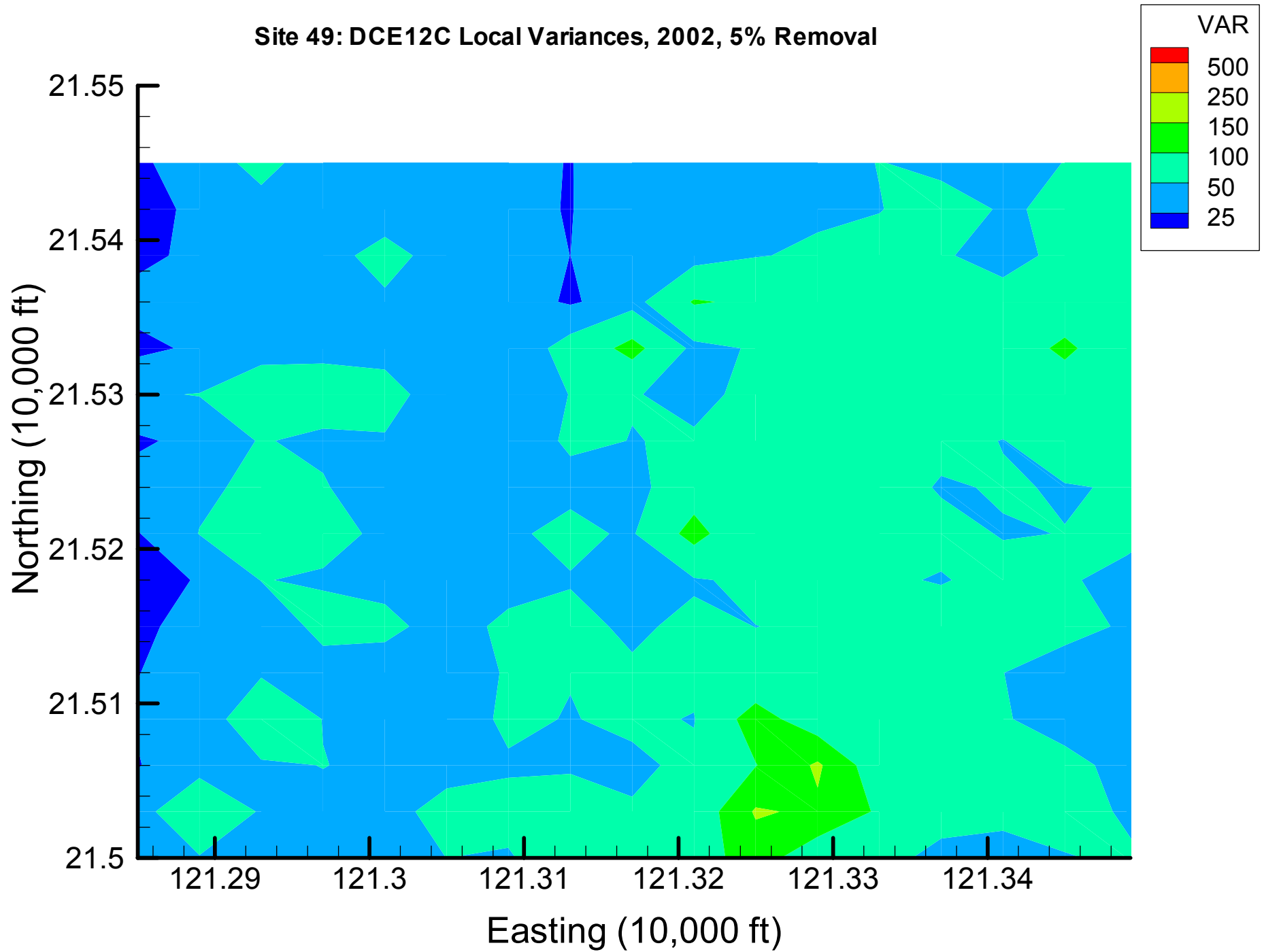


Appendix 4.3  
DCE12C Local Variance Maps  
Time Slice 2 — 2002

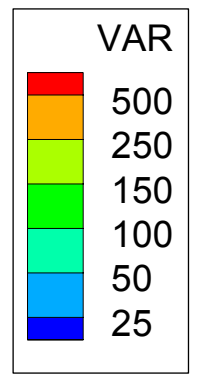
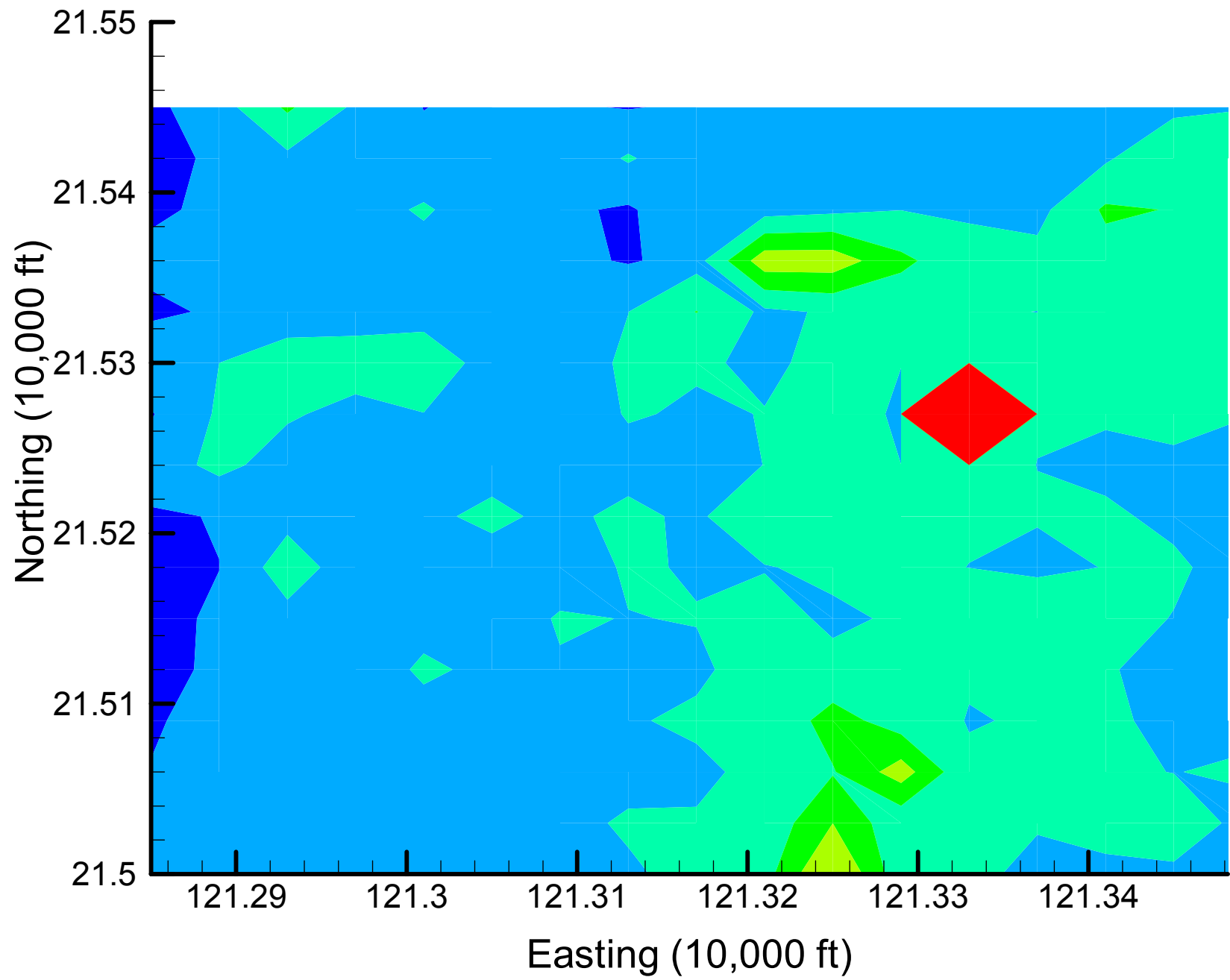
Site 49: DCE12C Local Variances, 2002, Base Map



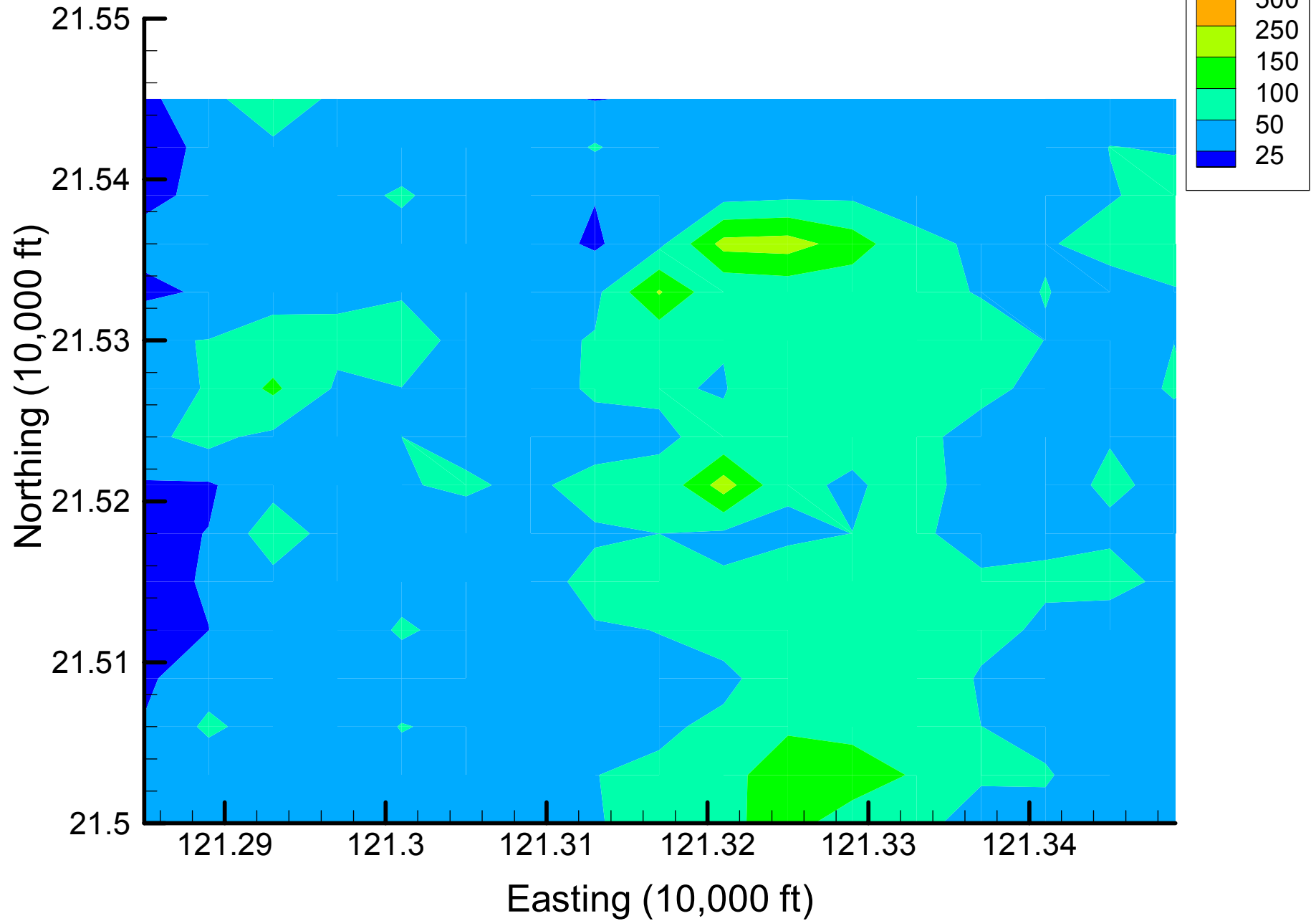
Site 49: DCE12C Local Variances, 2002, 5% Removal



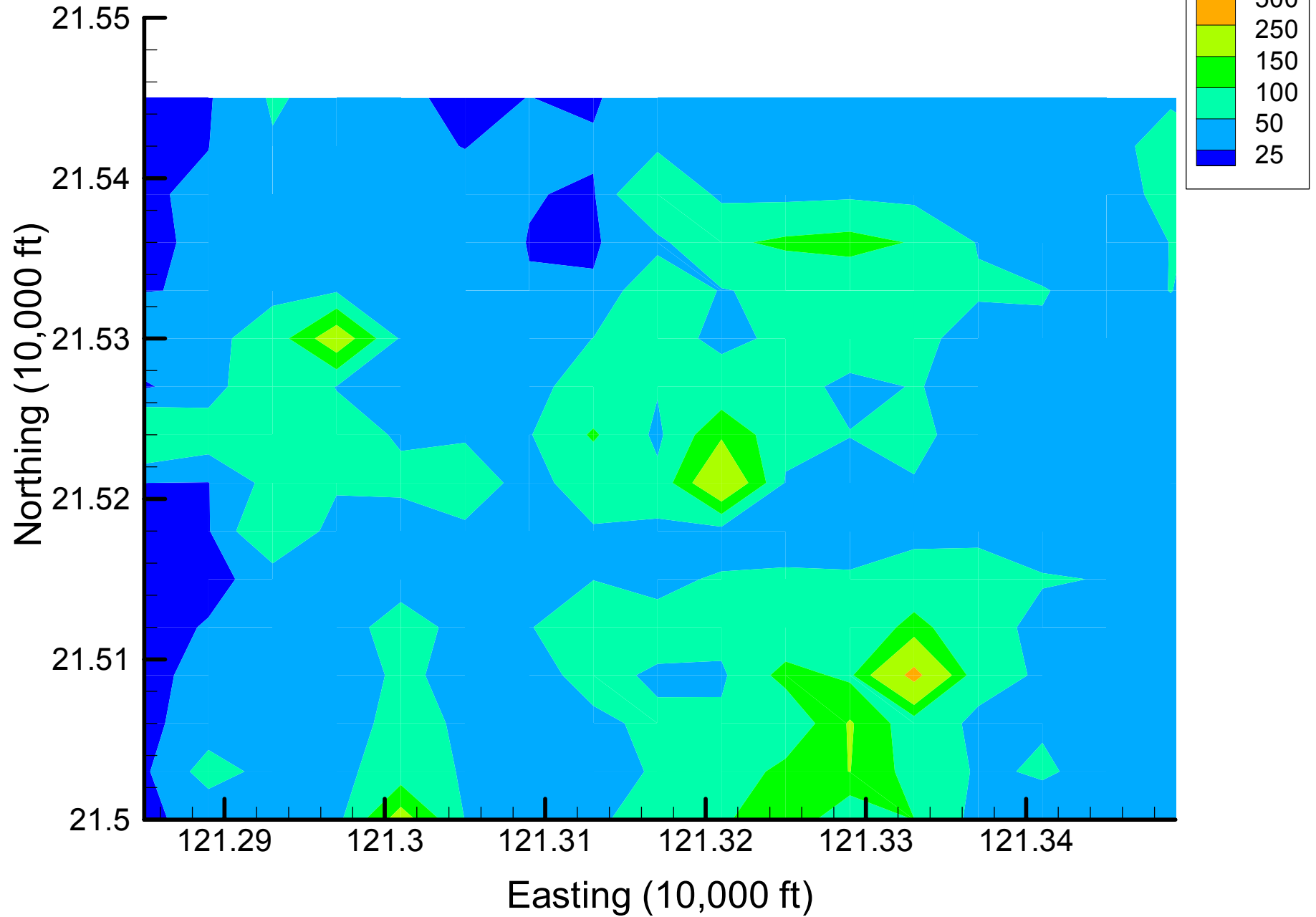
Site 49: DCE12C Local Variances, 2002, 10% Removal



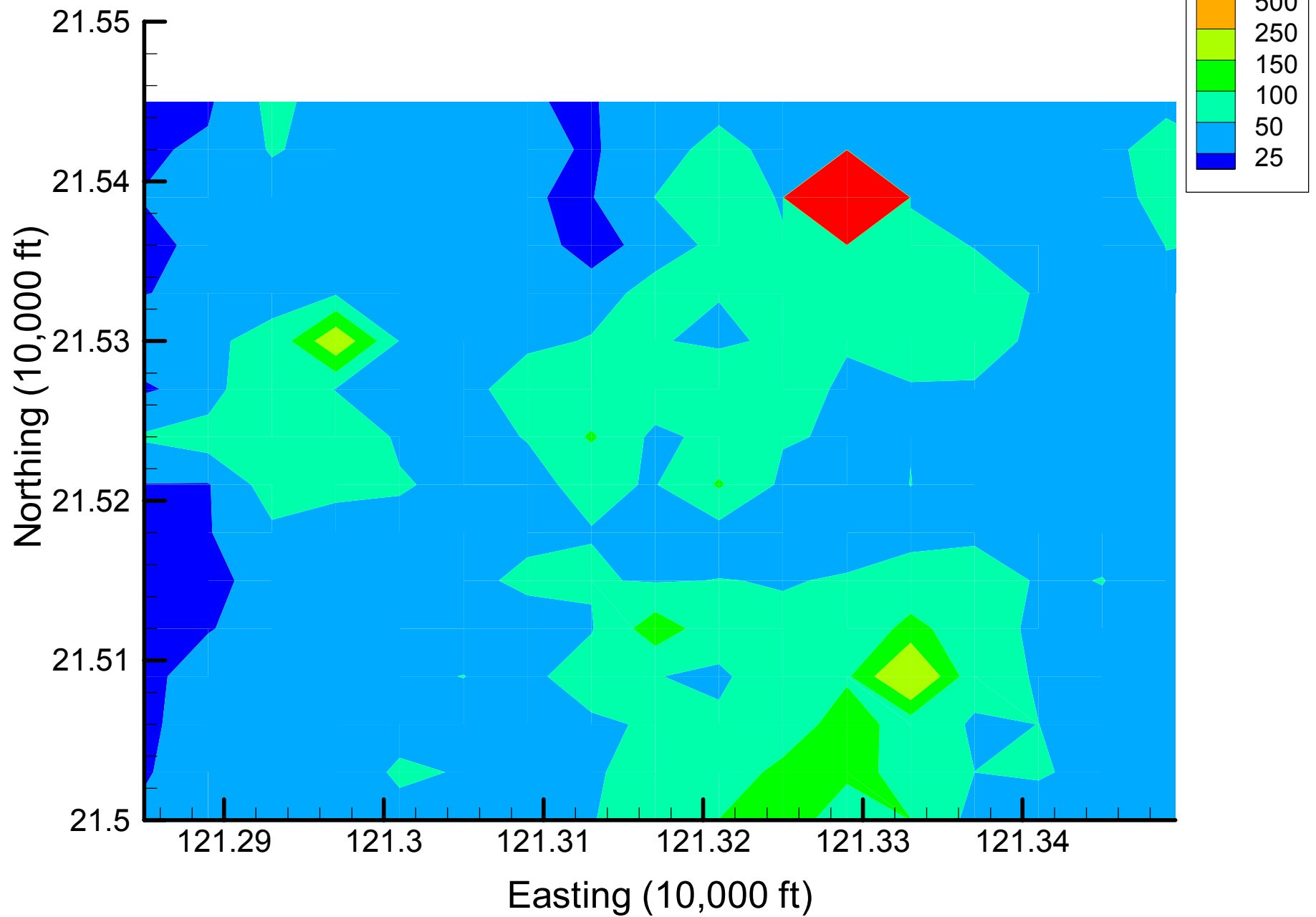
Site 49: DCE12C Local Variances, 2002, 15% Removal



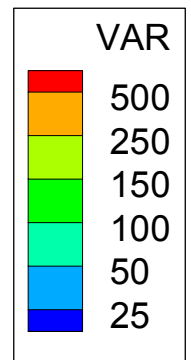
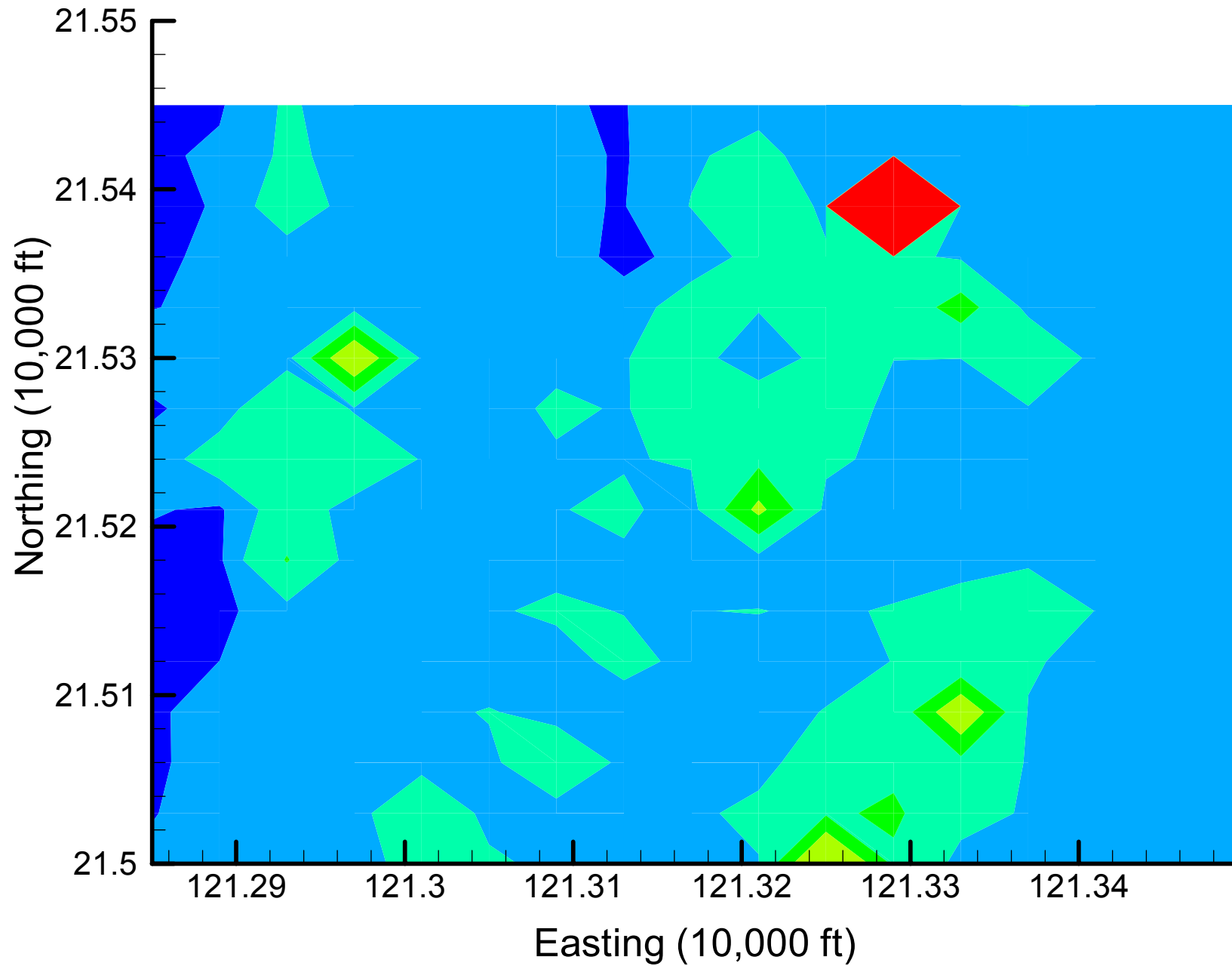
Site 49: DCE12C Local Variances, 2002, 20% Removal



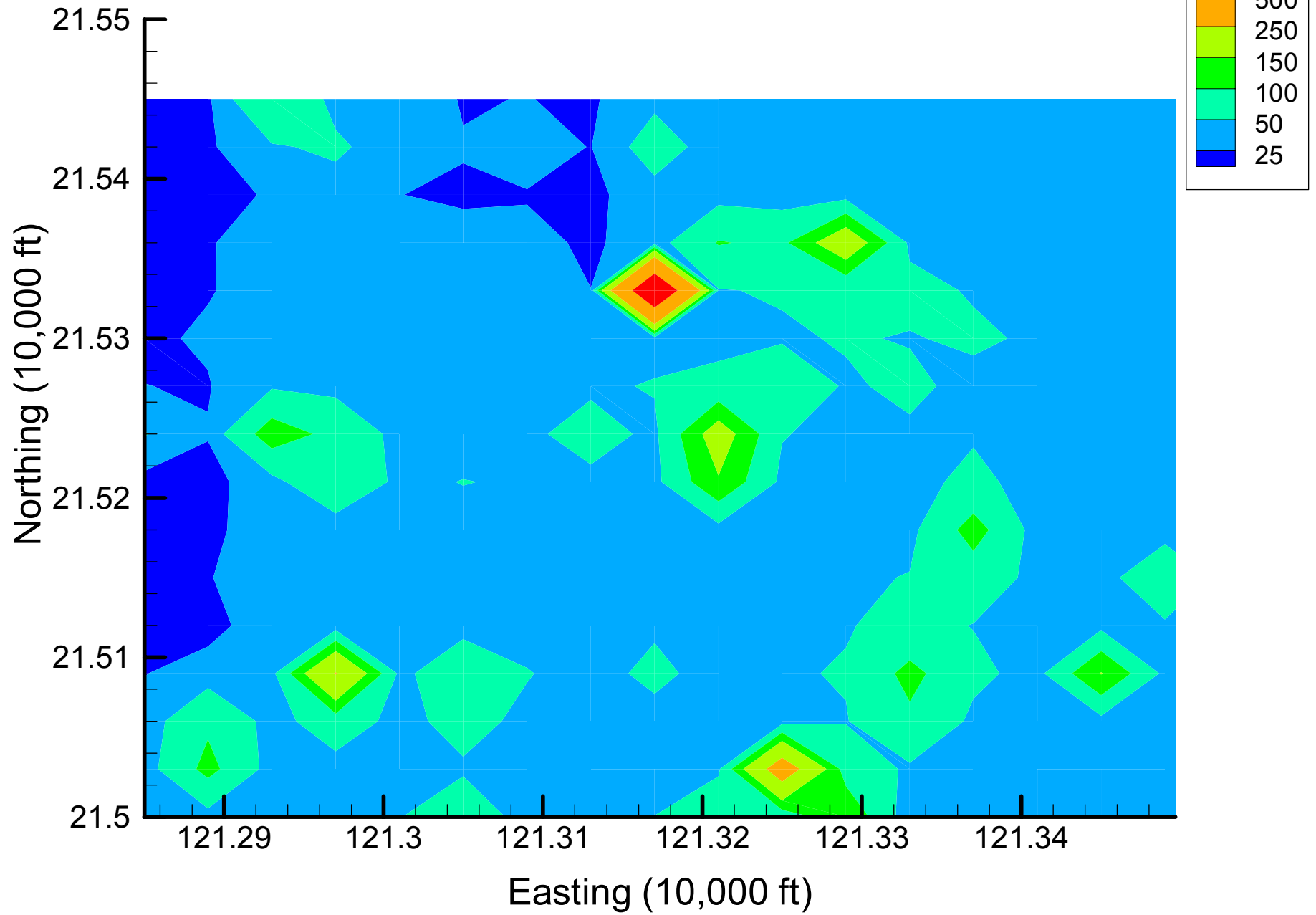
Site 49: DCE12C Local Variances, 2002, 25% Removal



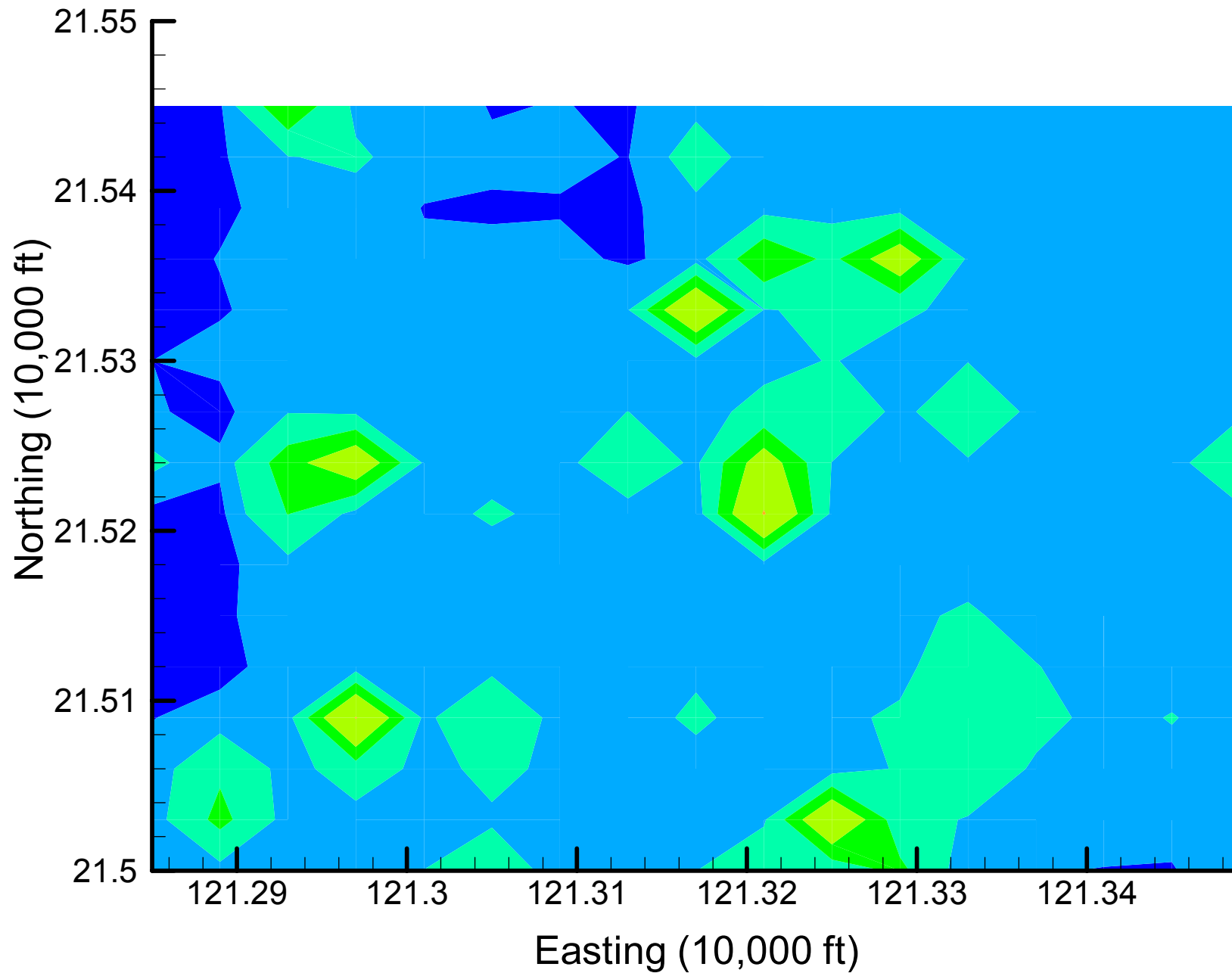
Site 49: DCE12C Local Variances, 2002, 30% Removal



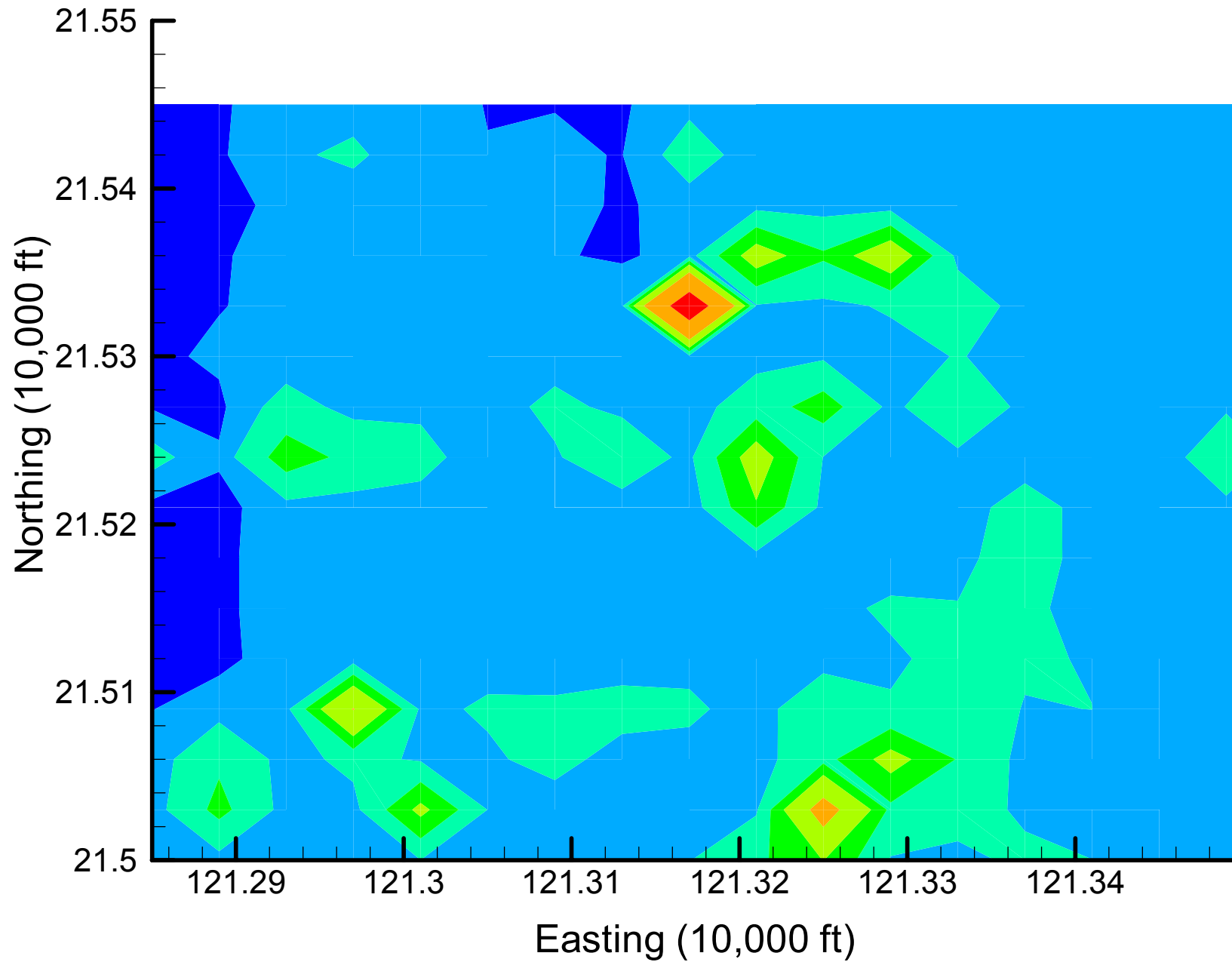
Site 49: DCE12C Local Variances, 2002, 35% Removal



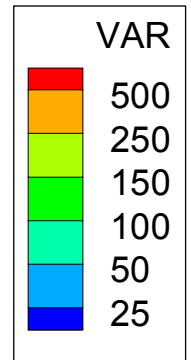
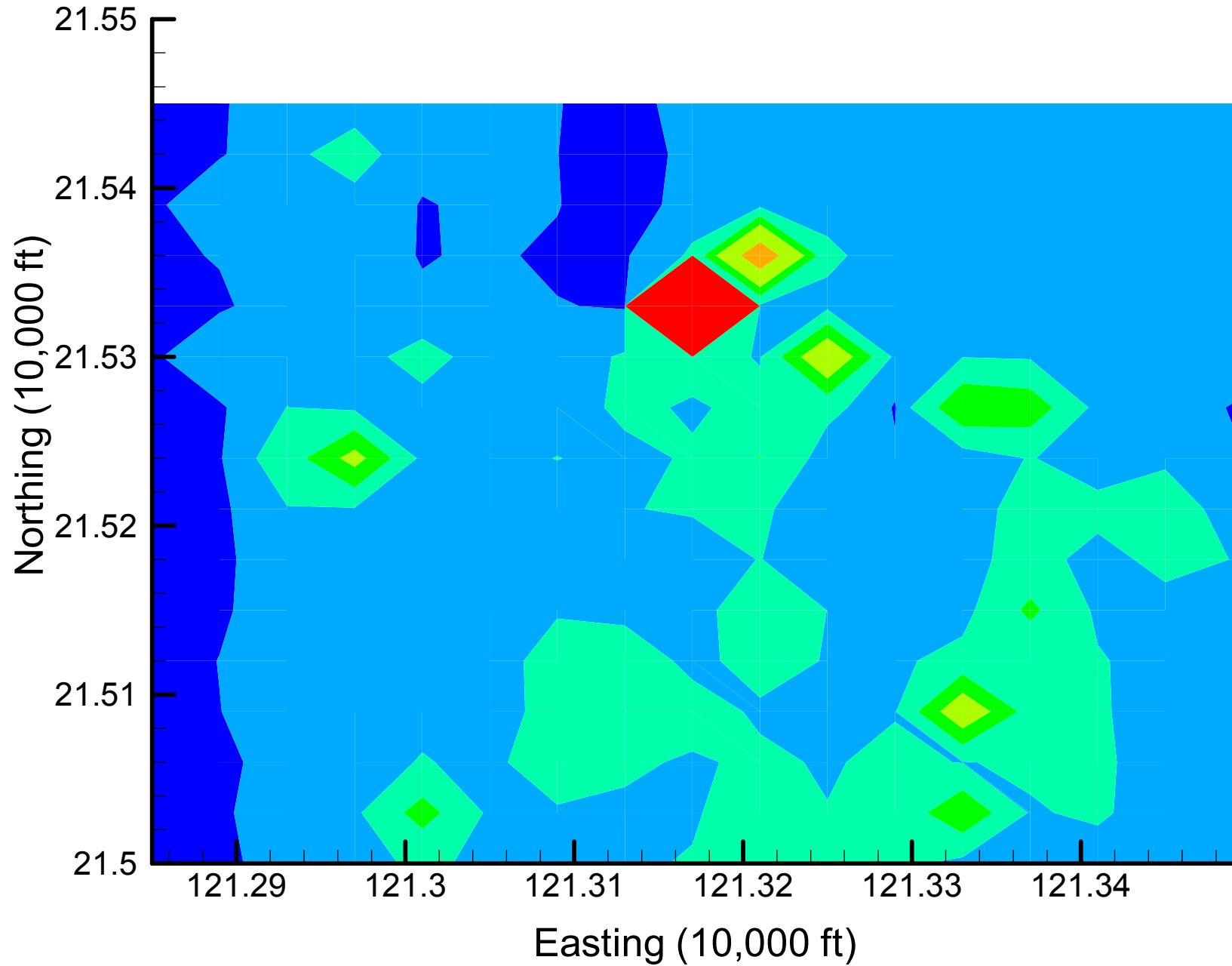
Site 49: DCE12C Local Variances, 2002, 40% Removal



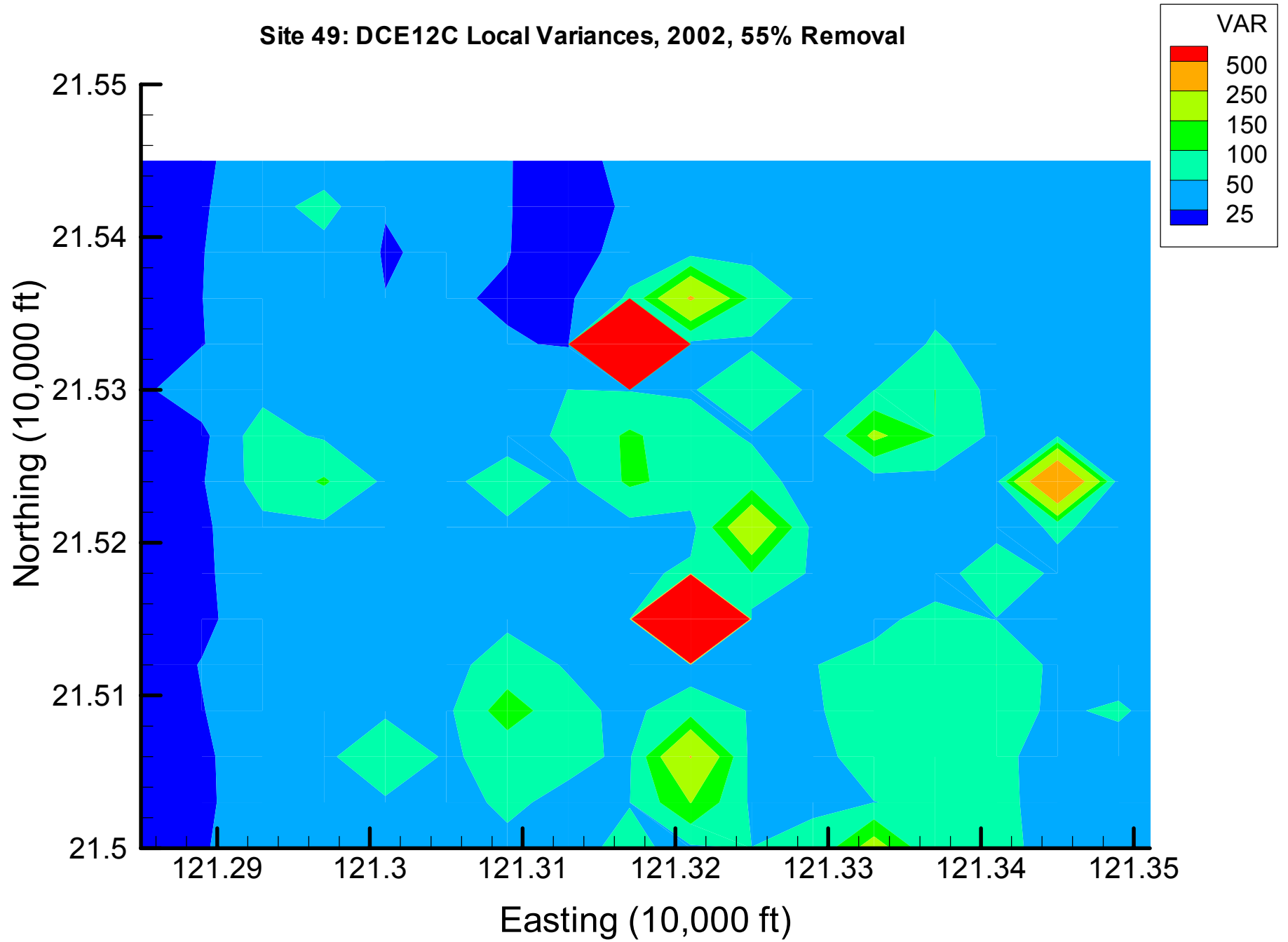
Site 49: DCE12C Local Variances, 2002, 45% Removal



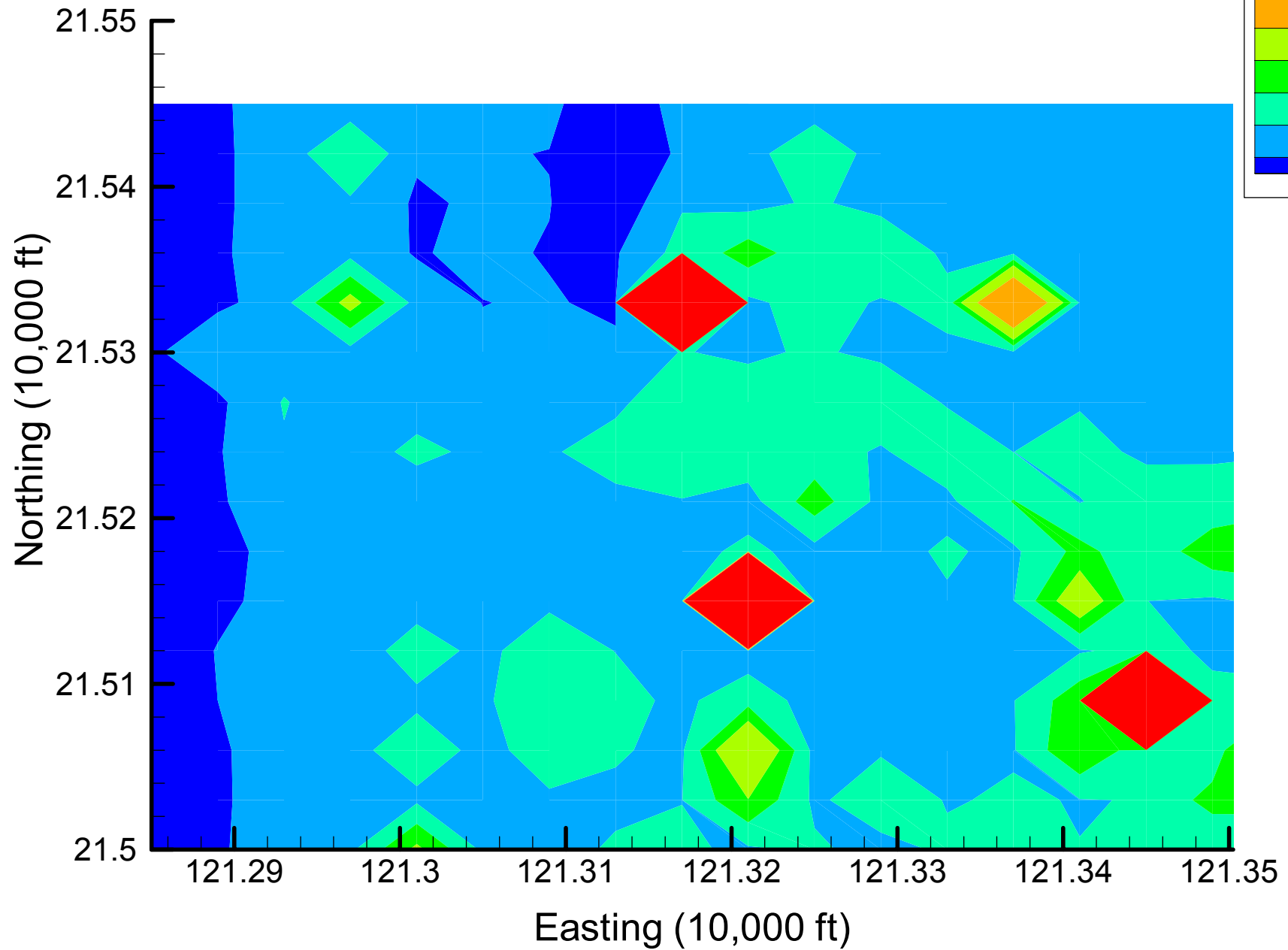
Site 49: DCE12C Local Variances, 2002, 50% Removal



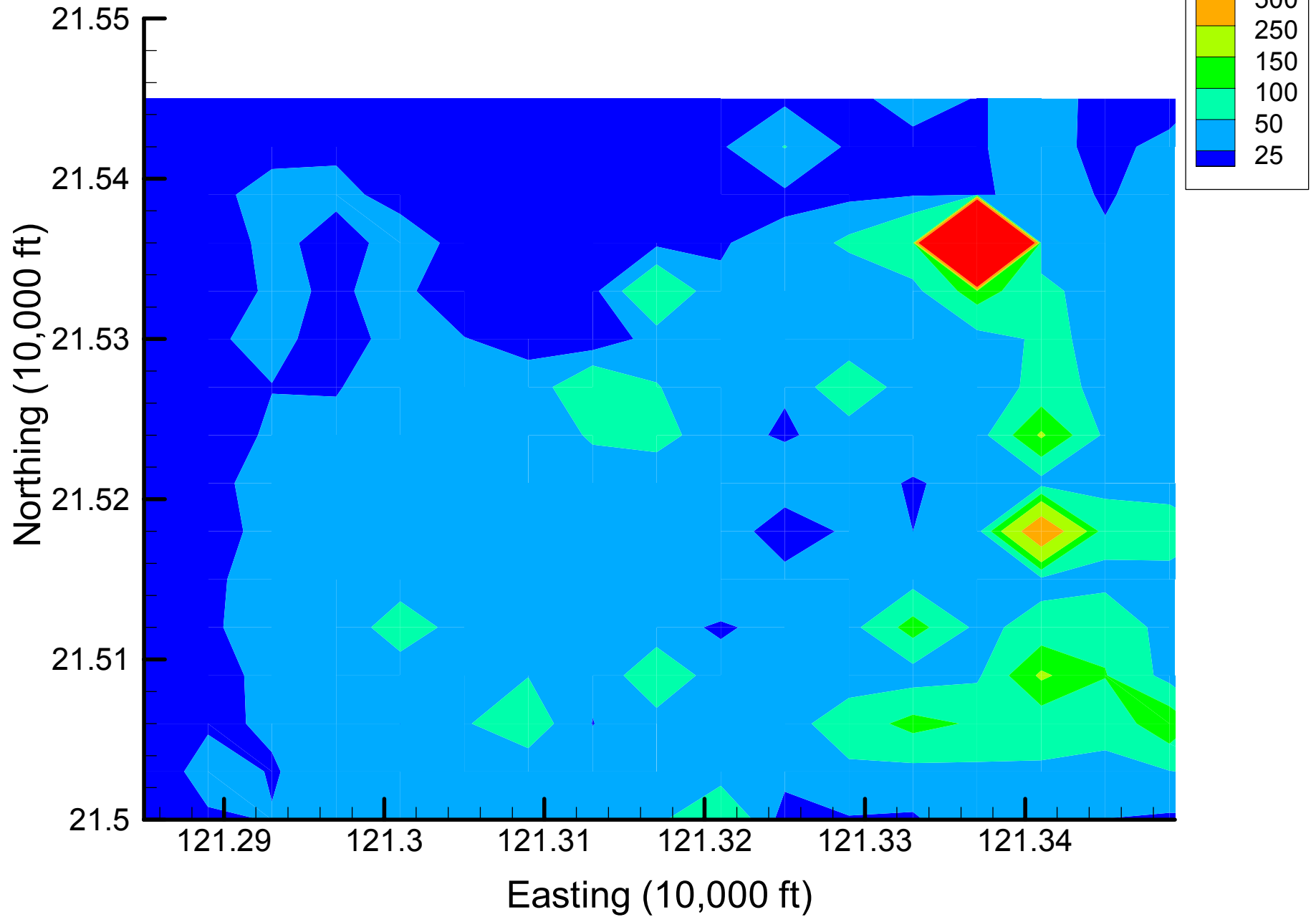
Site 49: DCE12C Local Variances, 2002, 55% Removal



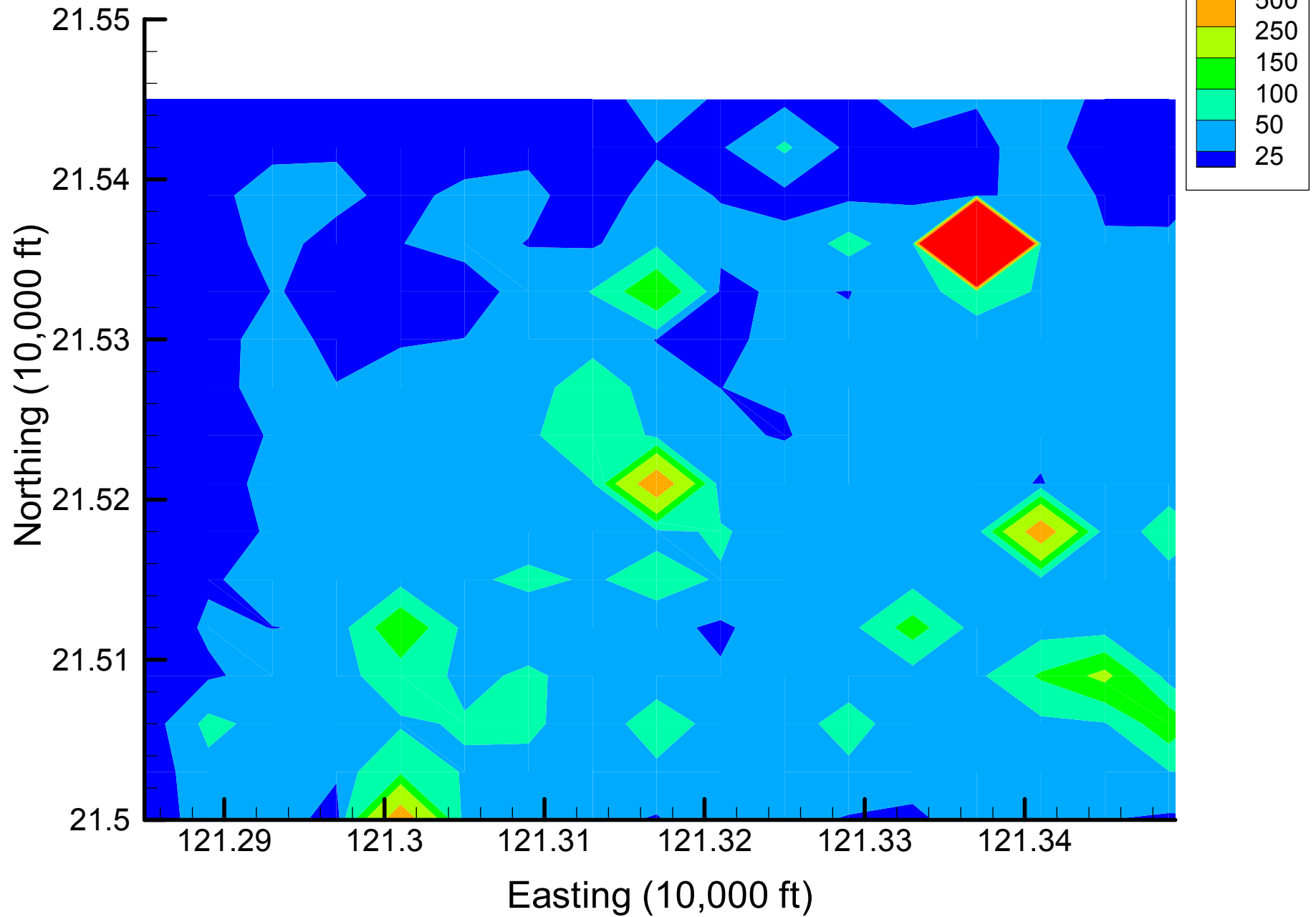
Site 49: DCE12C Local Variances, 2002, 60% Removal



Site 49: DCE12C Local Variances, 2002, 65% Removal

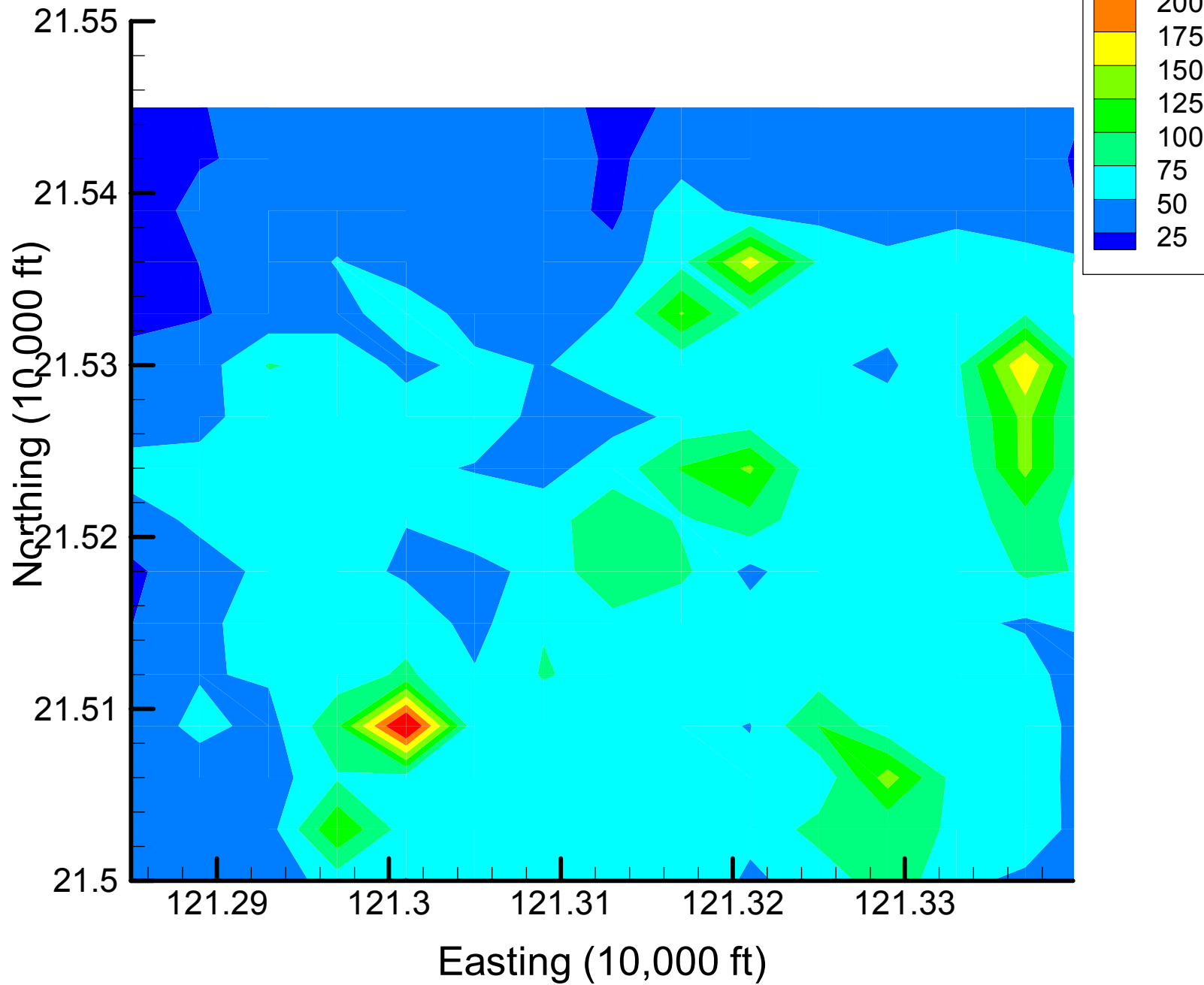


Site 49: DCE12C Local Variances, 2002, 70% Removal

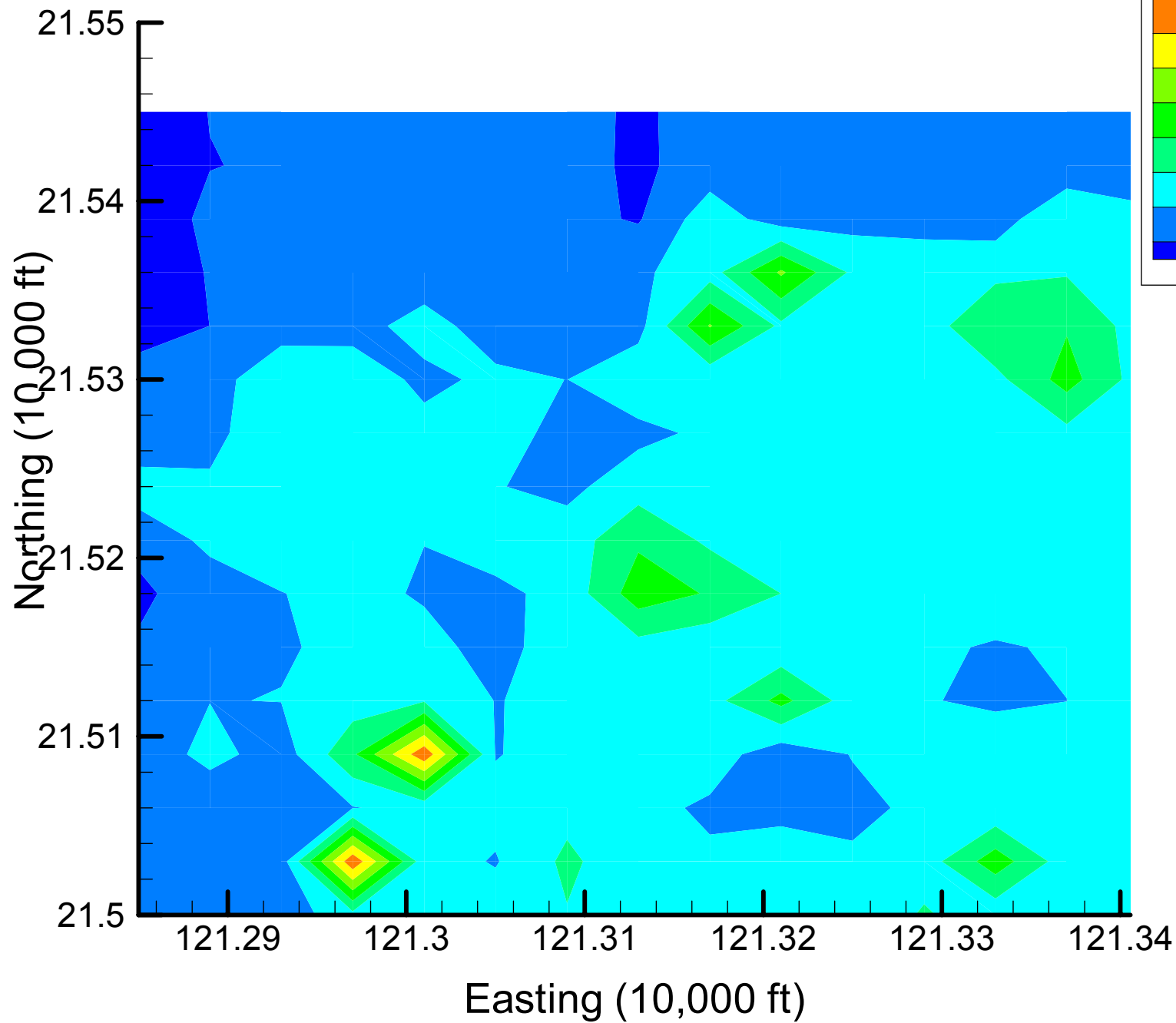


Appendix 4.3  
TCE Local Variance Maps  
Time Slice 1 — 2001

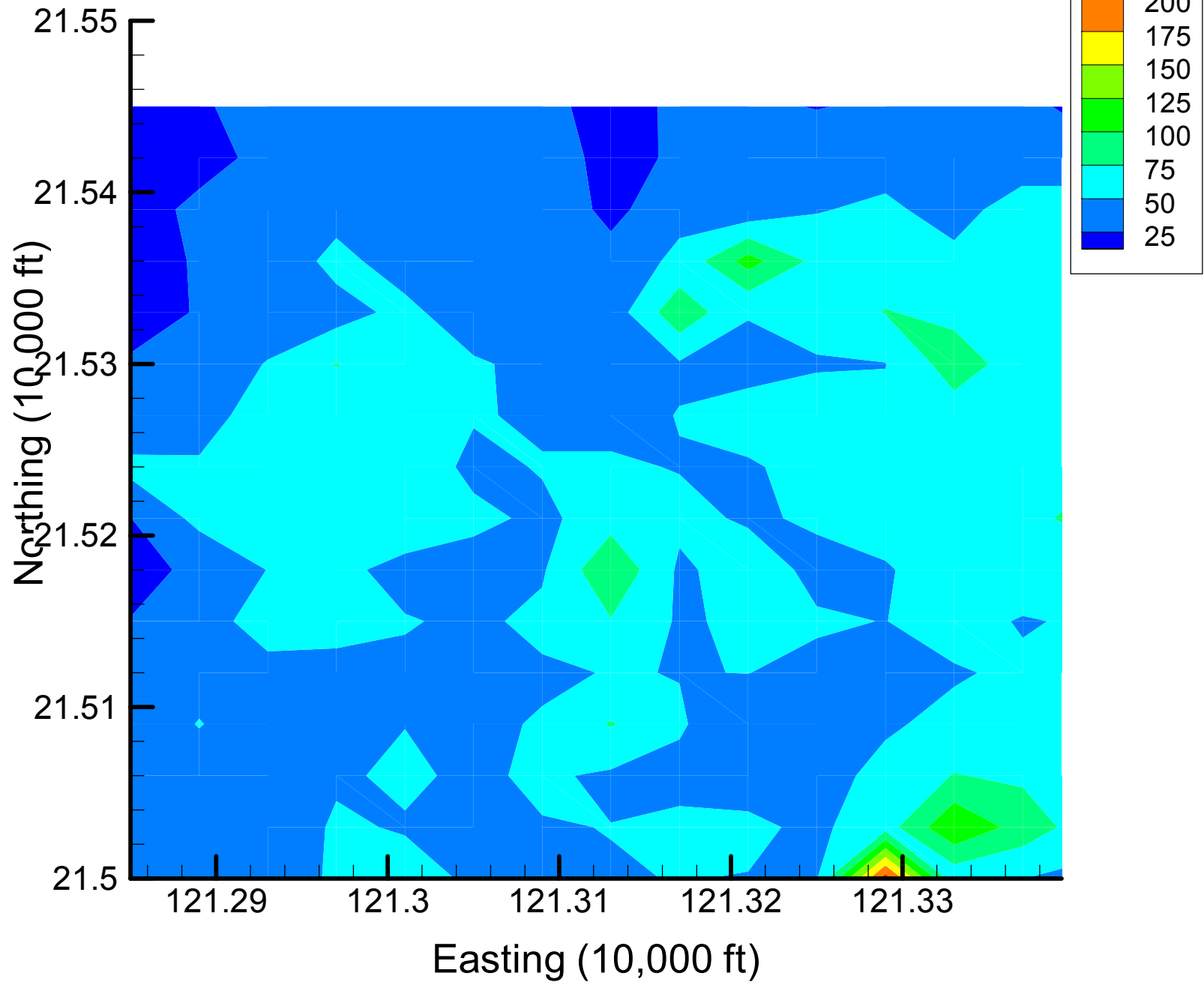
Site 49: TCE Local Variances, 2001, Base Map



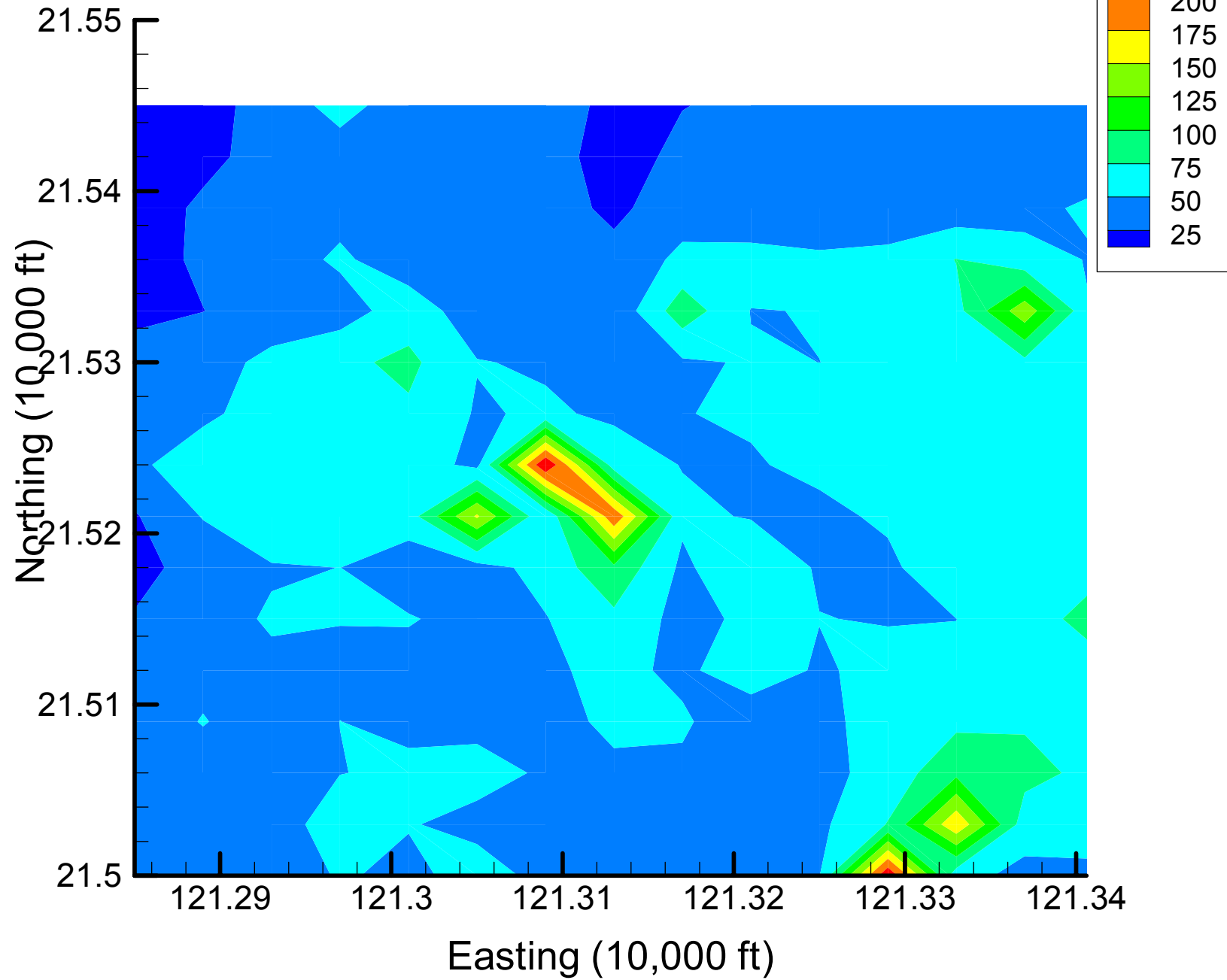
Site 49: TCE Local Variances, 2001, 5% Removal



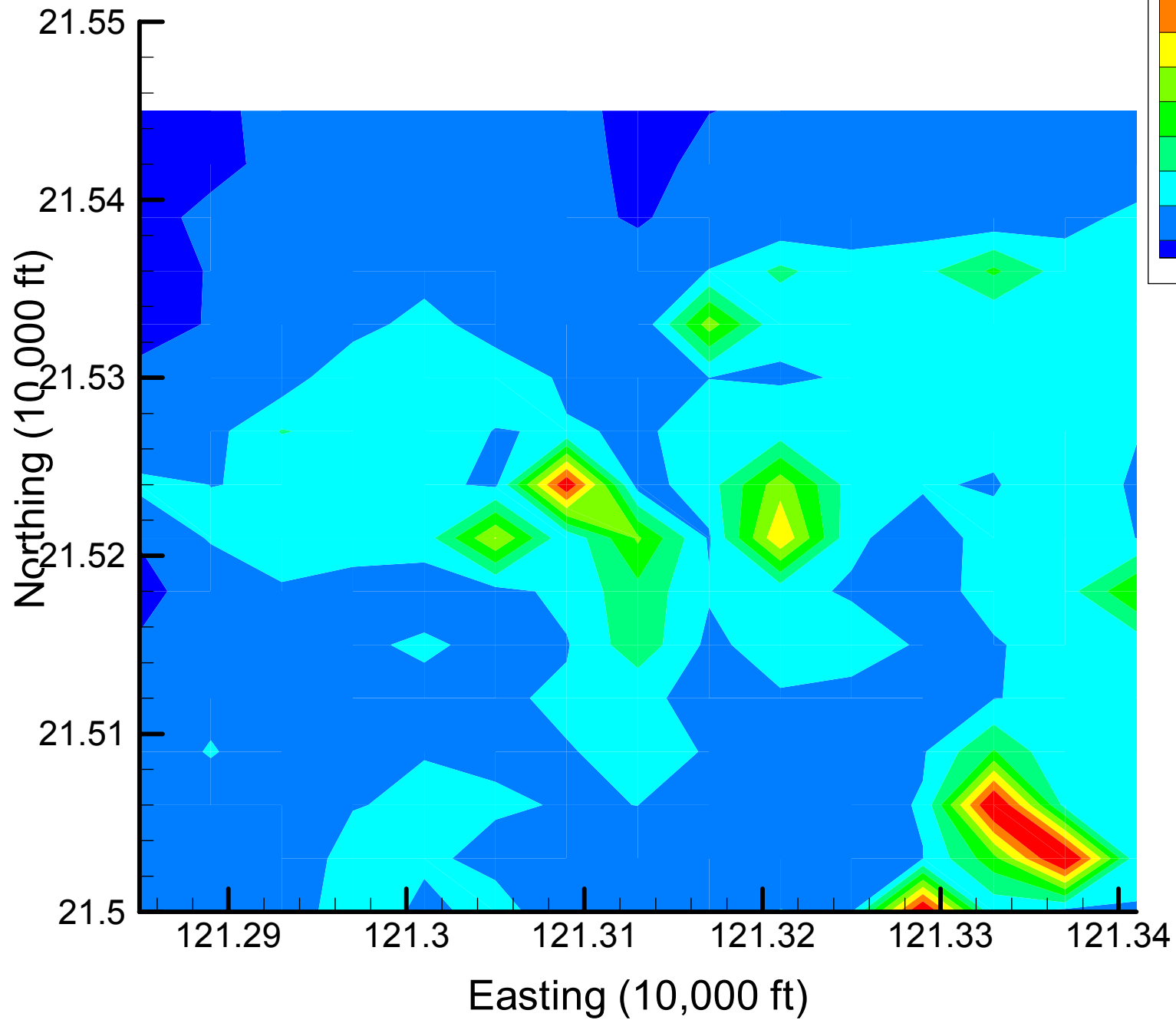
Site 49: TCE Local Variances, 2001, 10% Removal



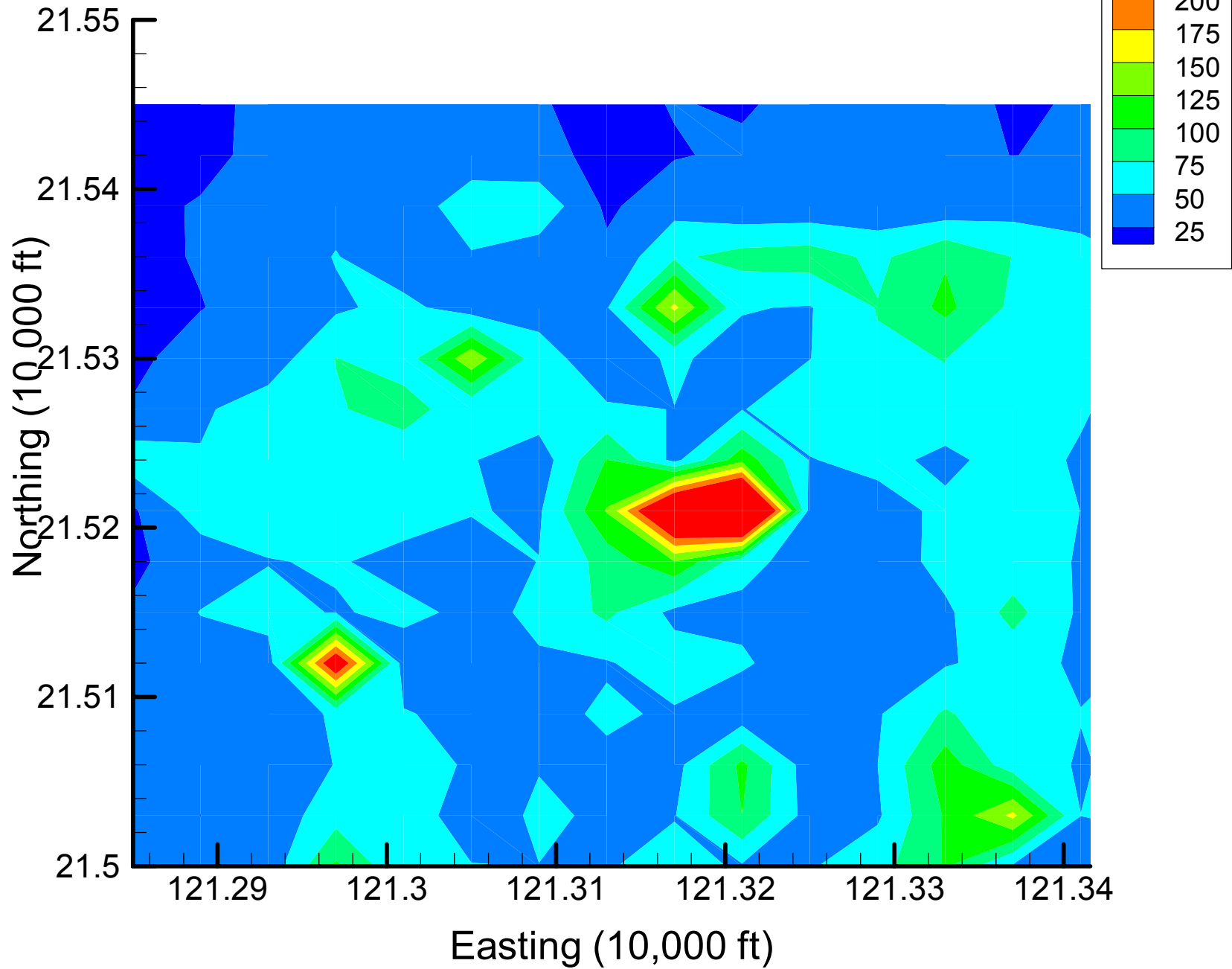
Site 49: TCE Local Variances, 2001, 15% Removal



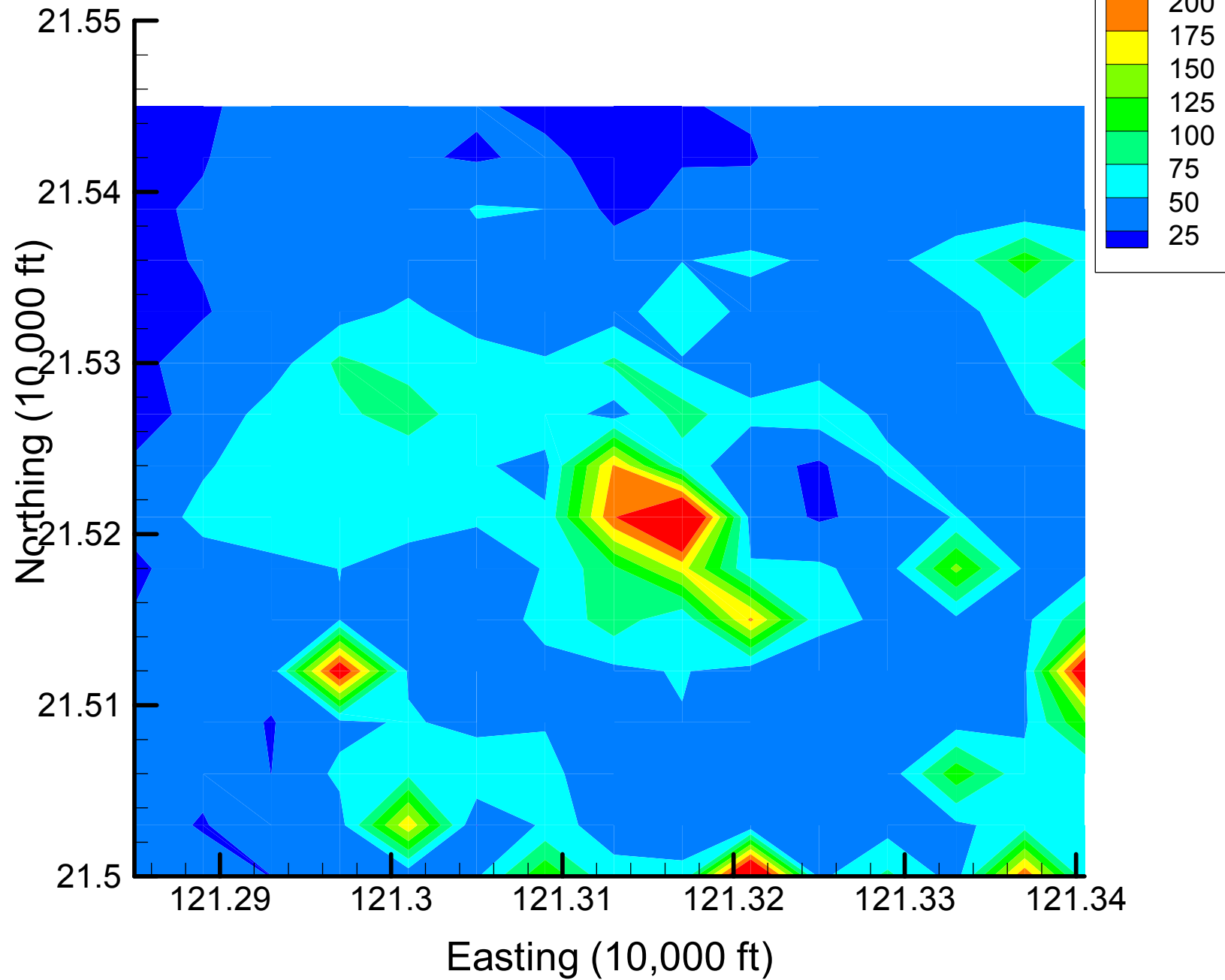
Site 49: TCE Local Variances, 2001, 20% Removal



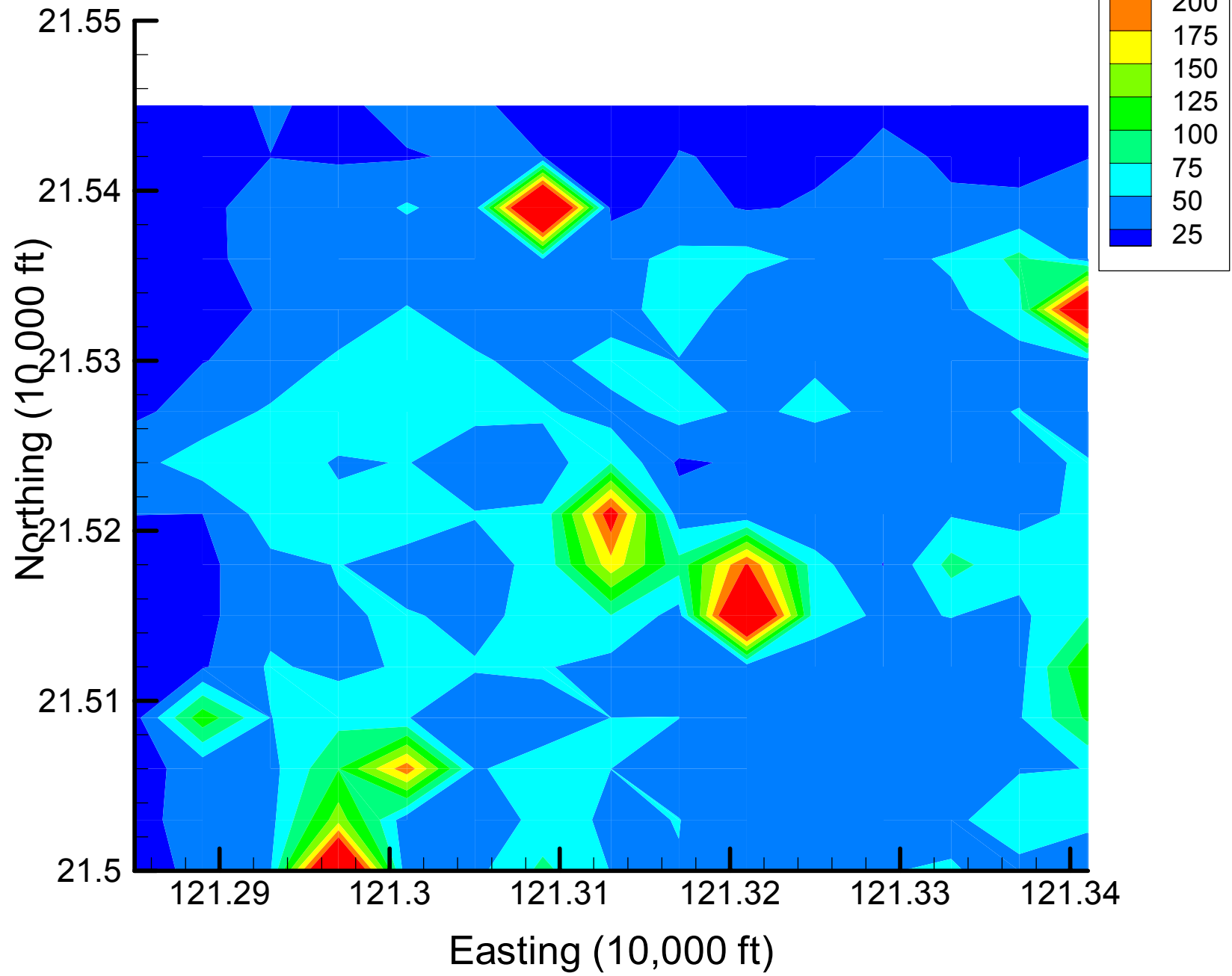
Site 49: TCE Local Variances, 2001, 25% Removal



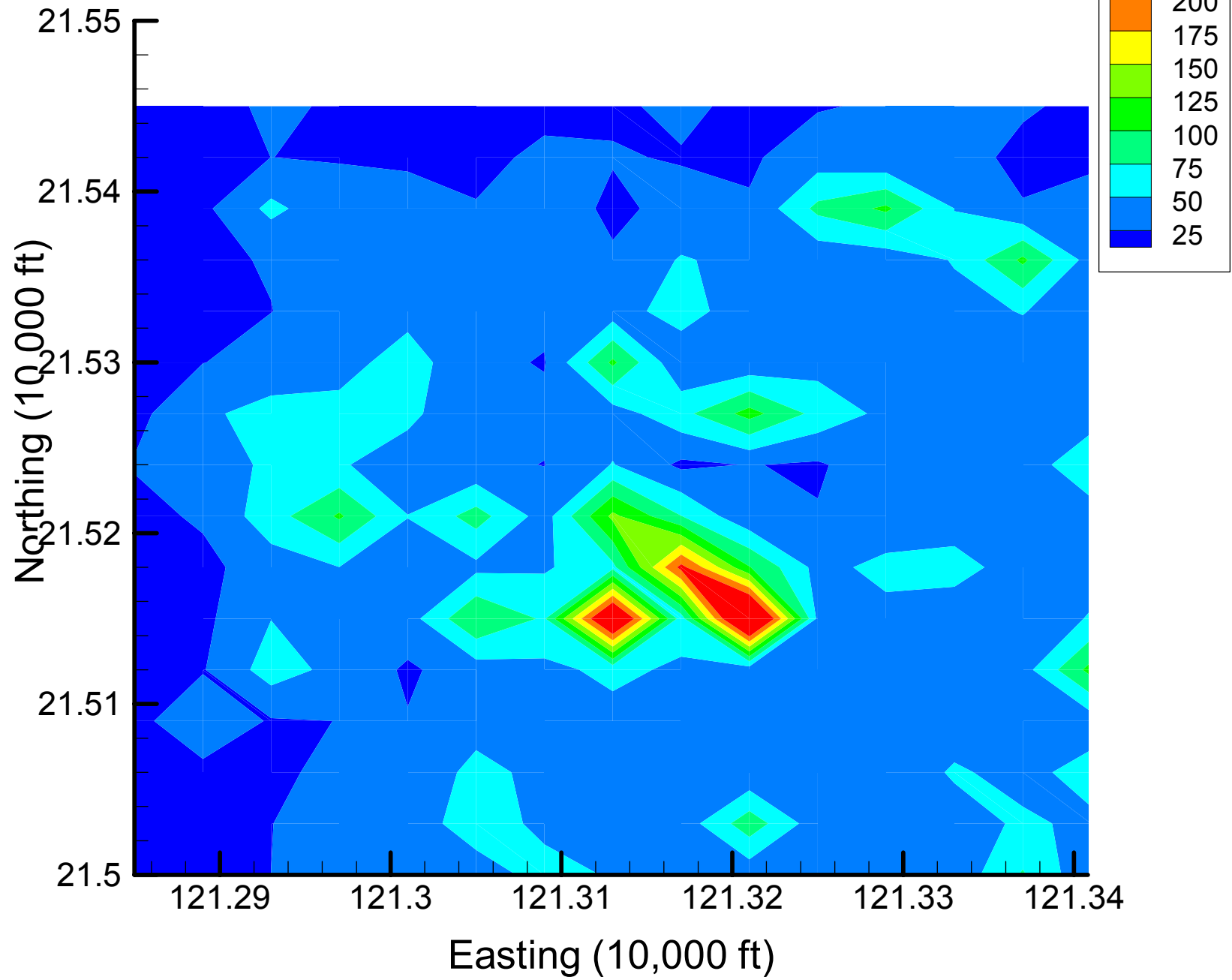
Site 49: TCE Local Variances, 2001, 30% Removal



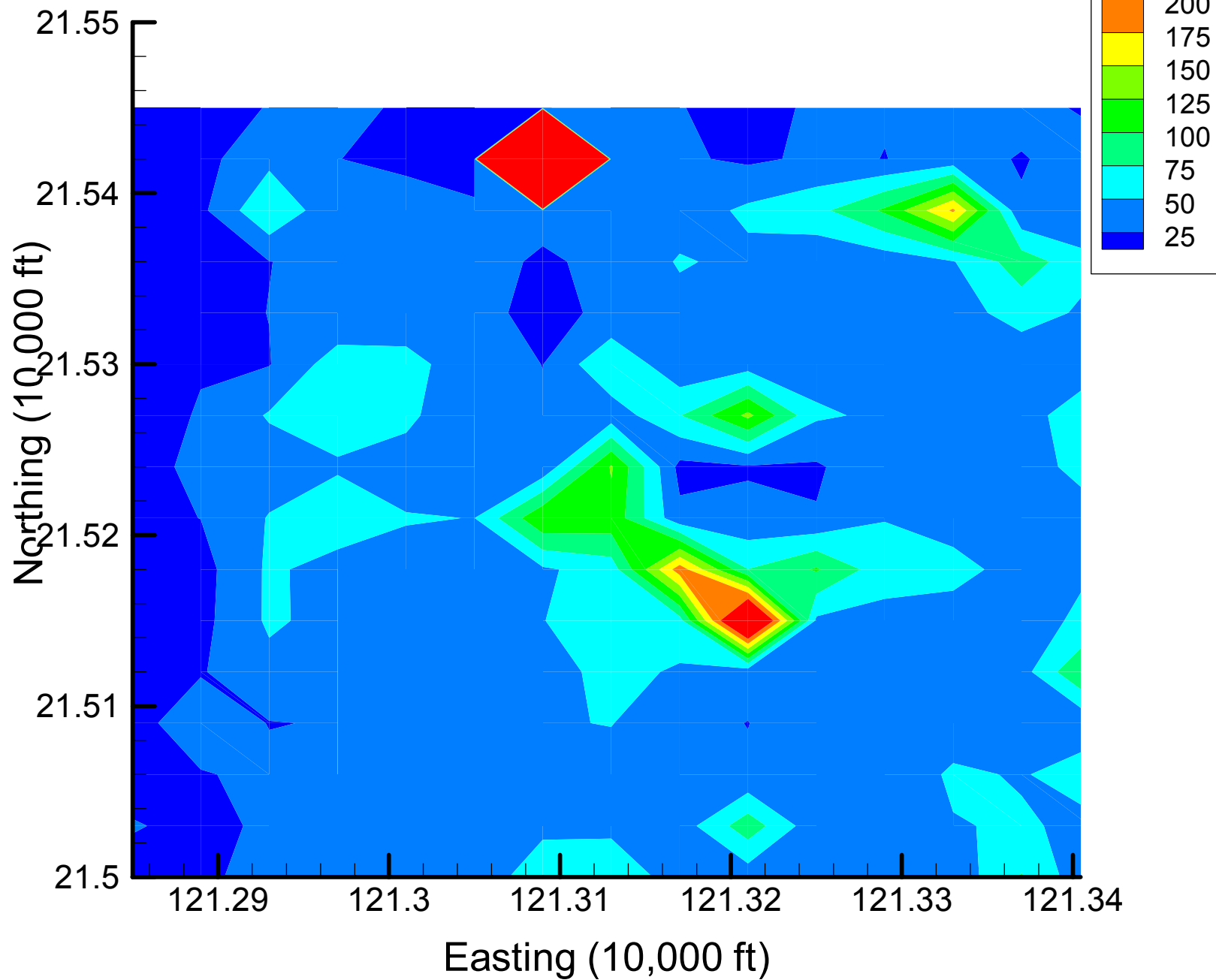
Site 49: TCE Local Variances, 2001, 35% Removal



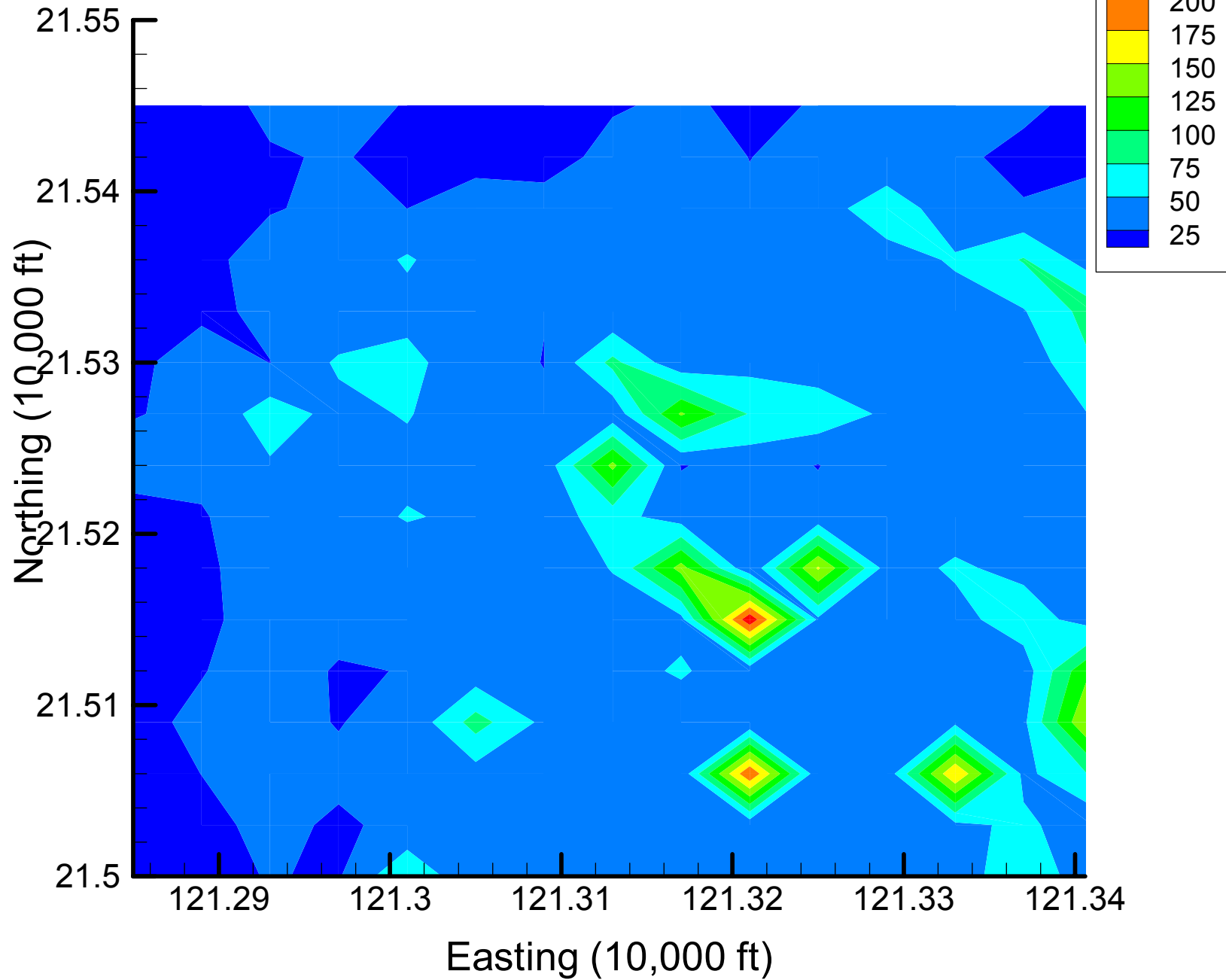
Site 49: TCE Local Variances, 2001, 40% Removal



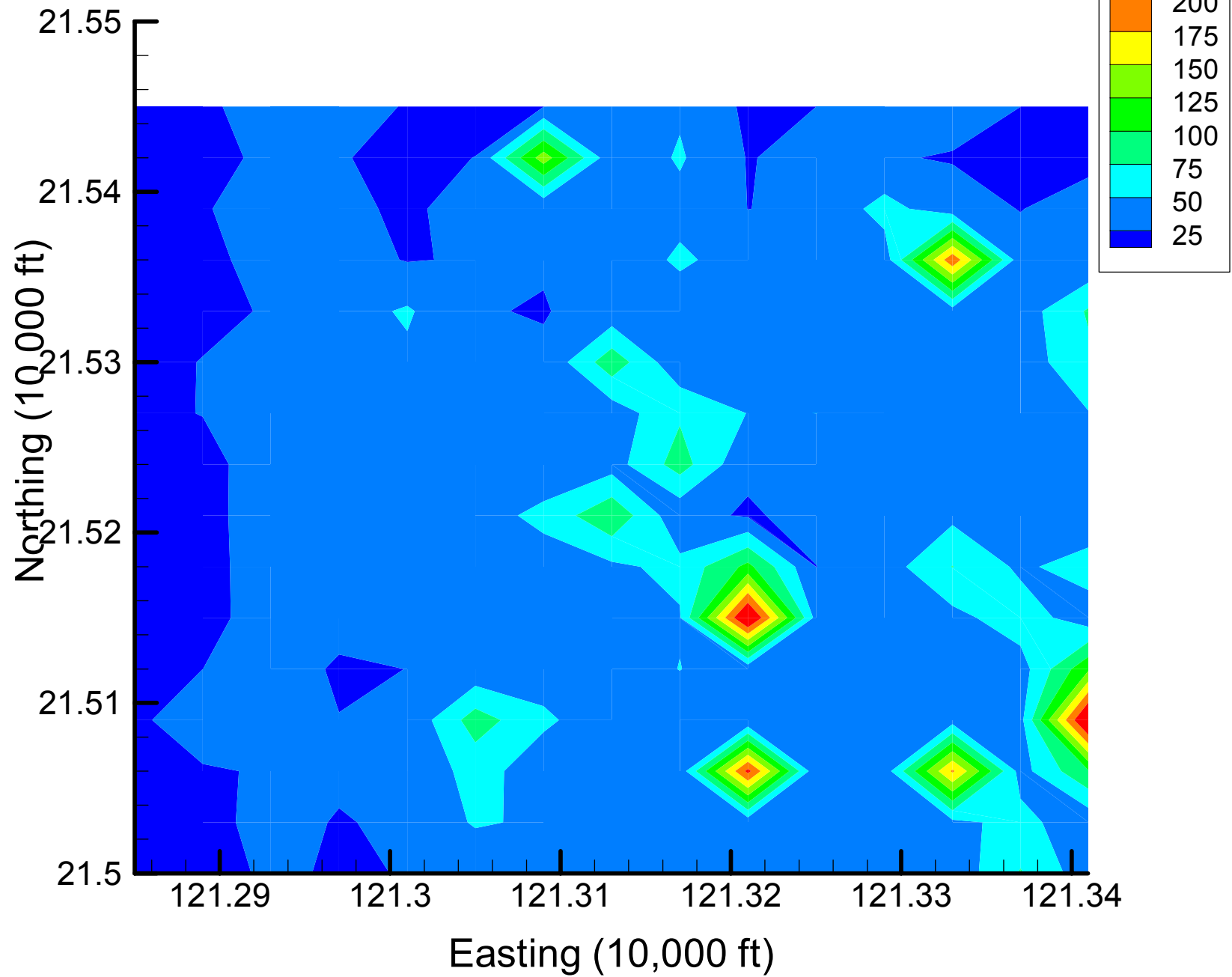
Site 49: TCE Local Variances, 2001, 45% Removal



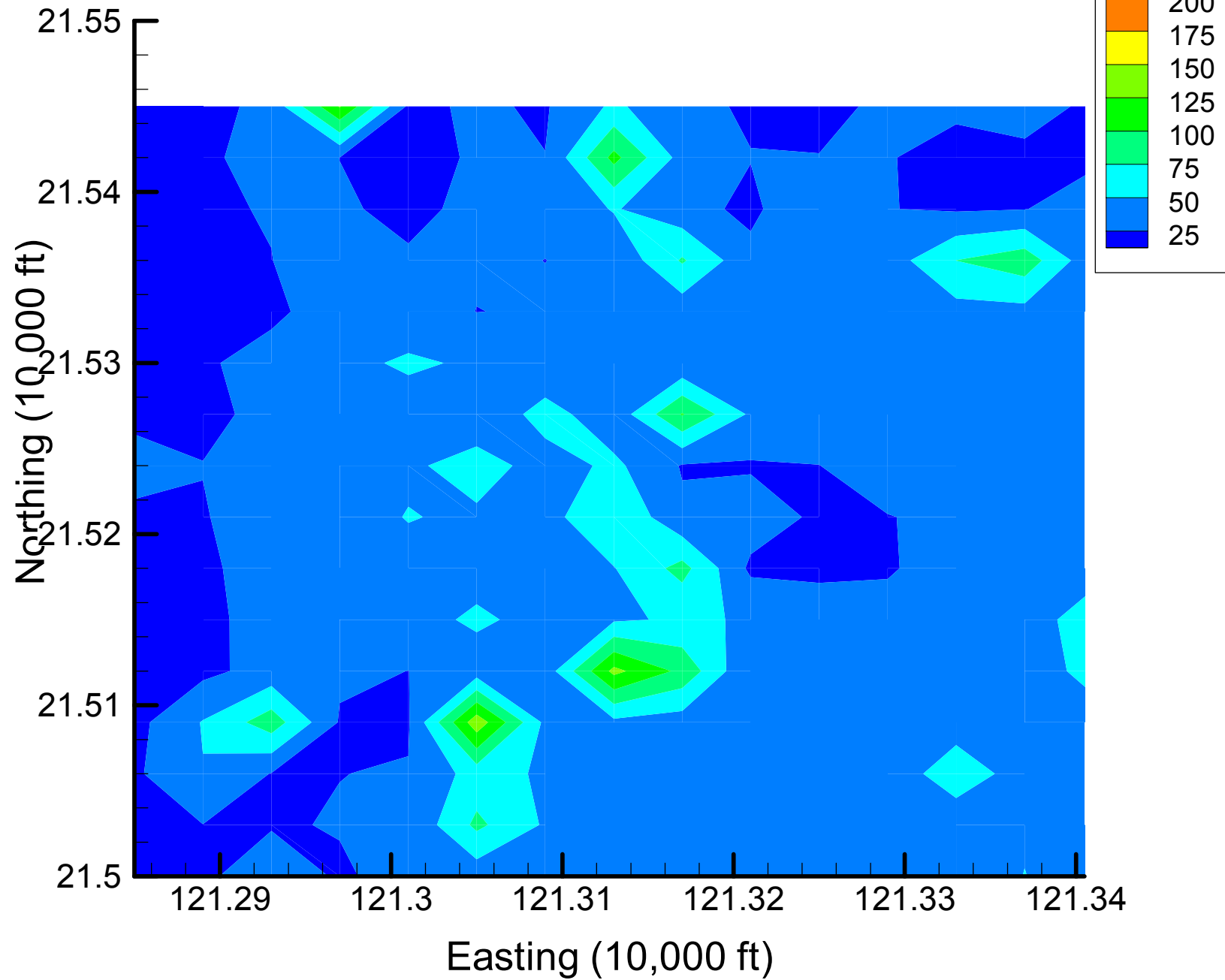
Site 49: TCE Local Variances, 2001, 50% Removal



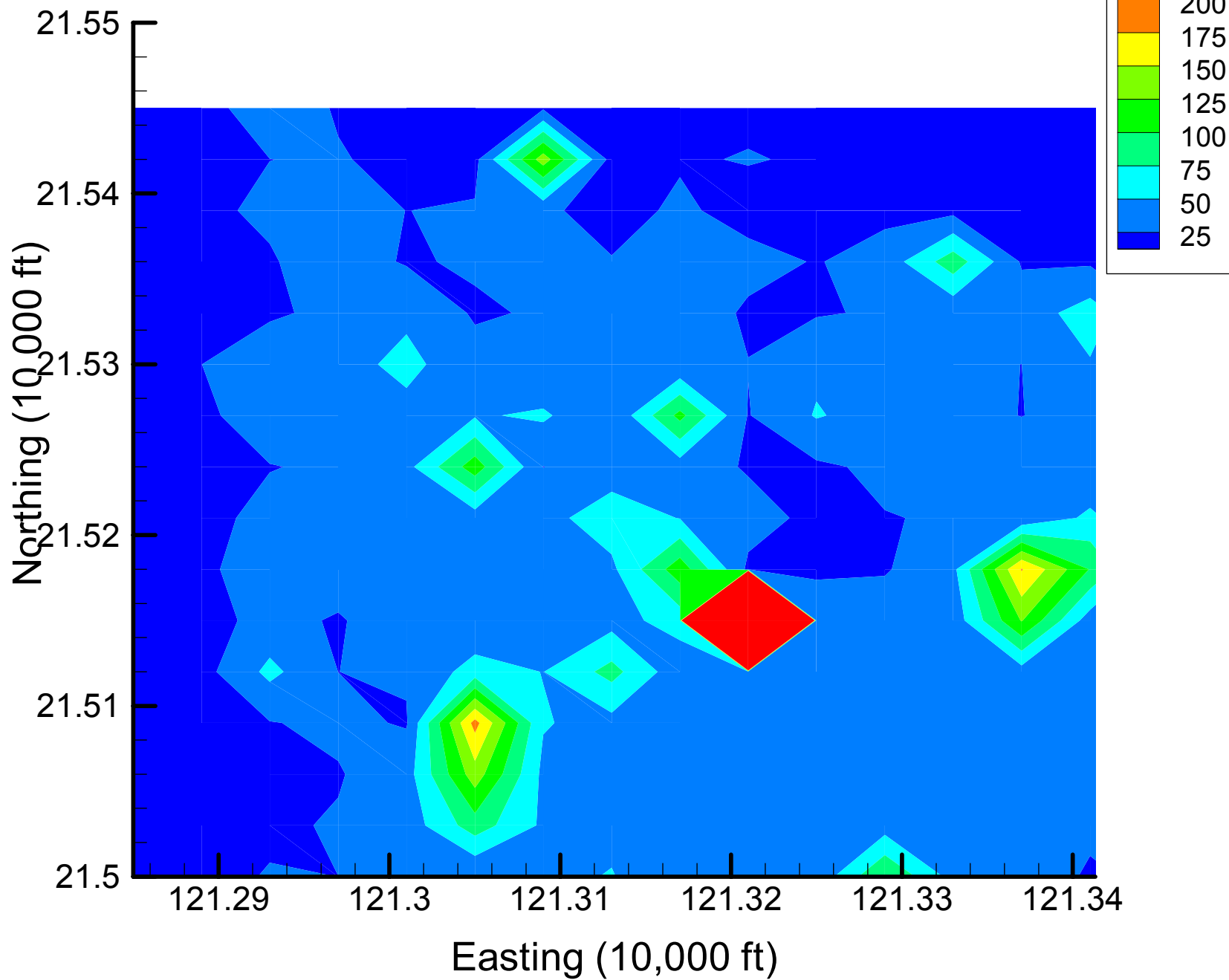
Site 49: TCE Local Variances, 2001, 55% Removal



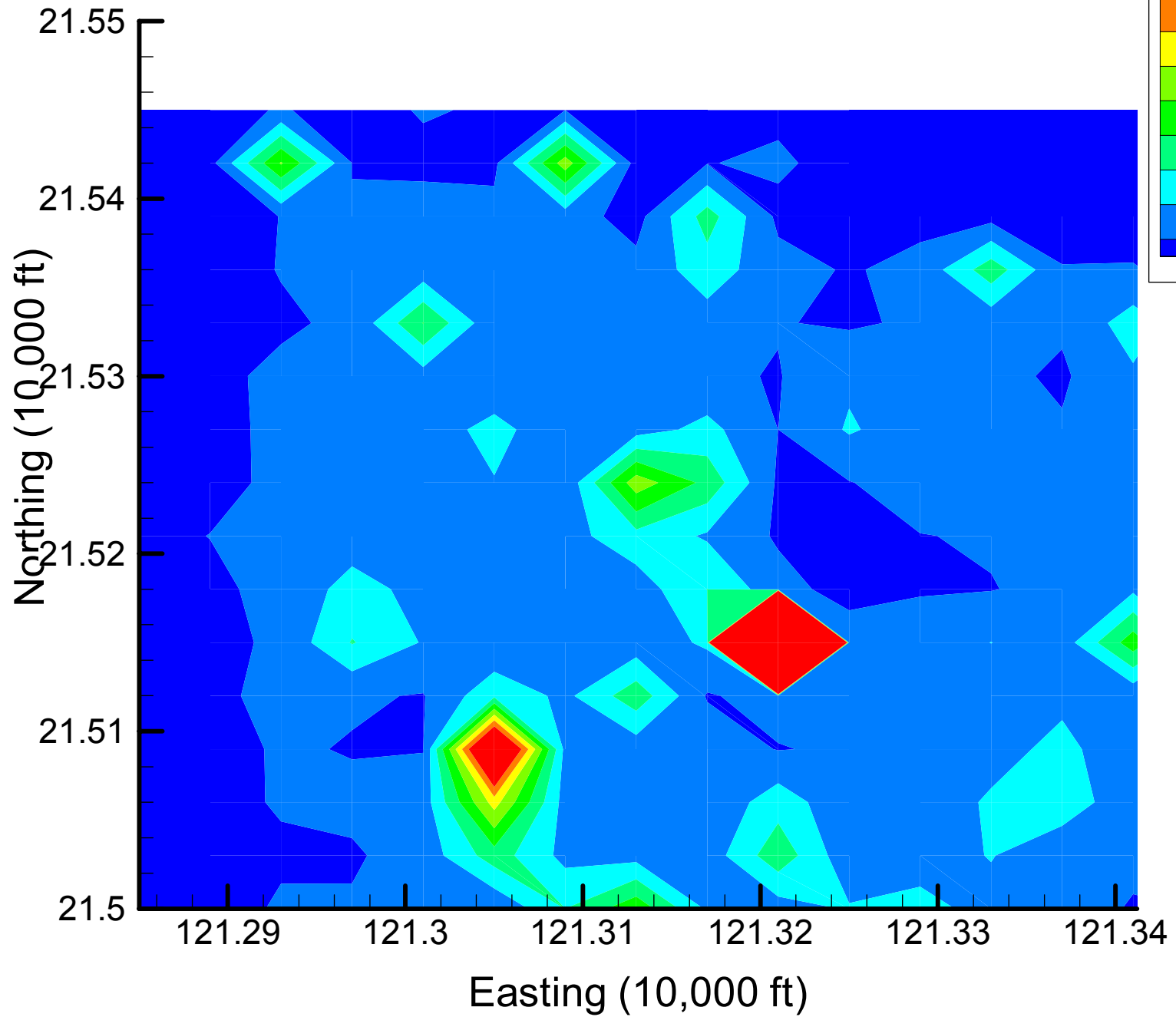
Site 49: TCE Local Variances, 2001, 60% Removal



Site 49: TCE Local Variances, 2001, 65% Removal

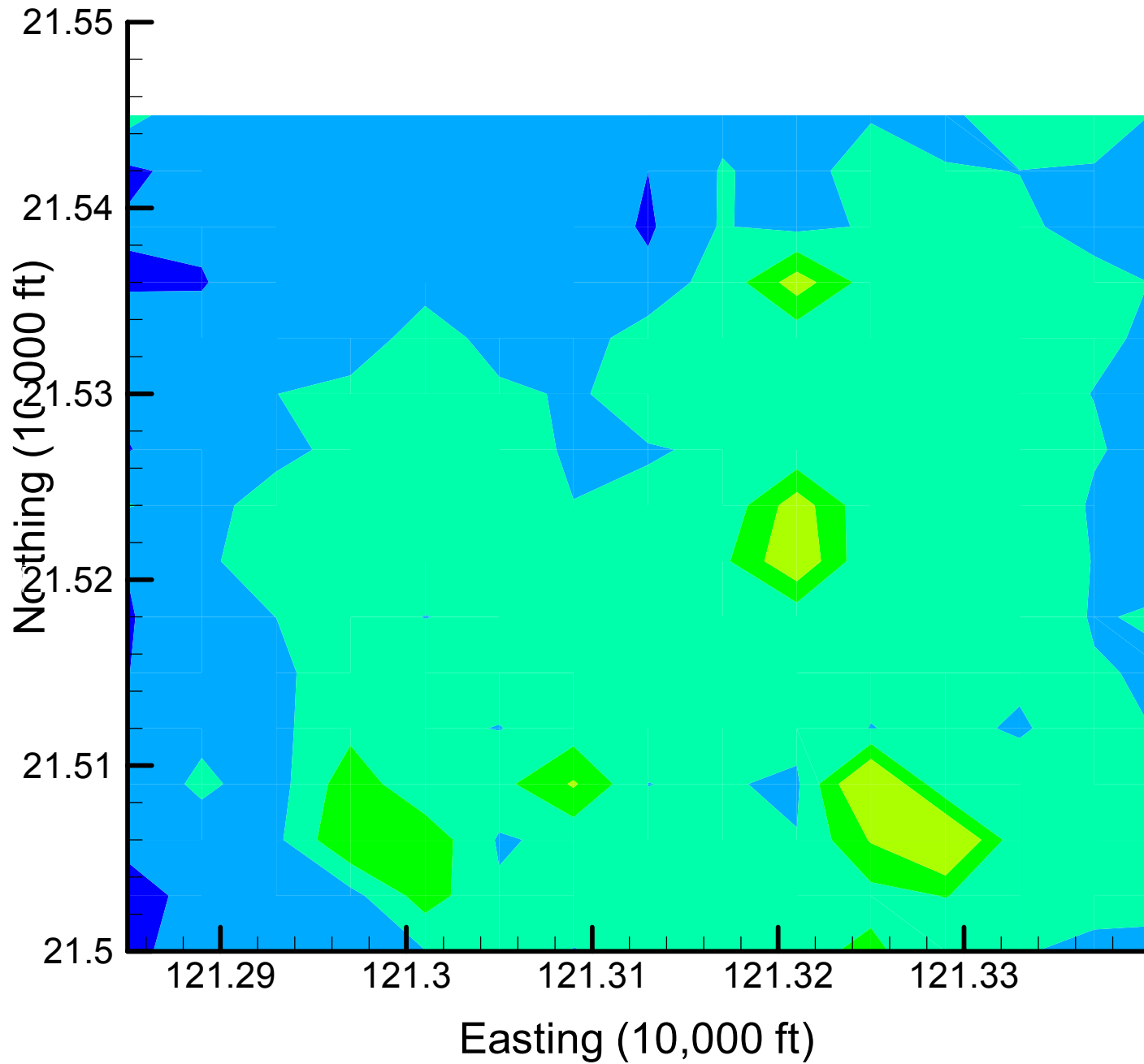


Site 49: TCE Local Variances, 2001, 70% Removal

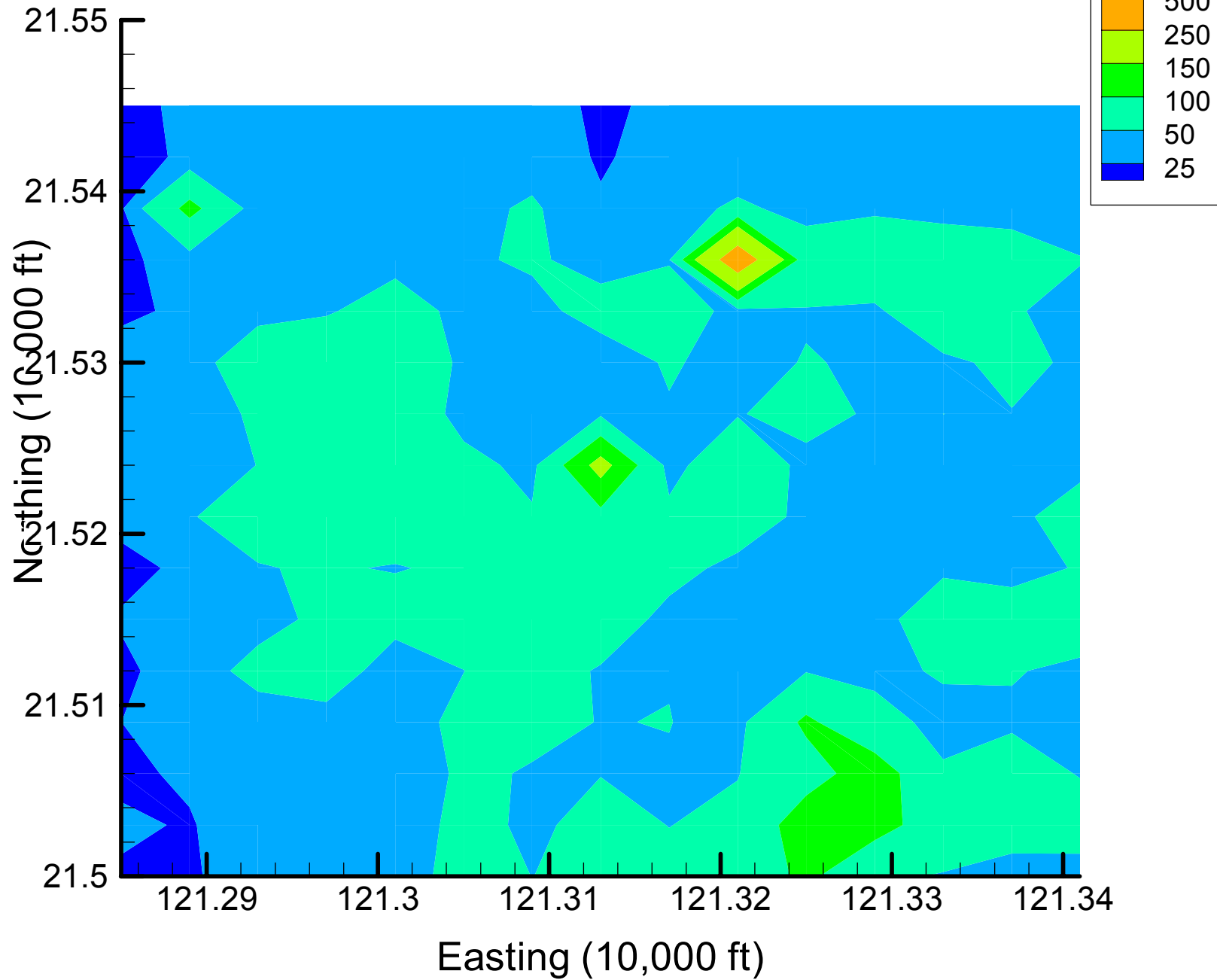


Appendix 4.3  
TCE Local Variance Maps  
Time Slice 2 — 2002

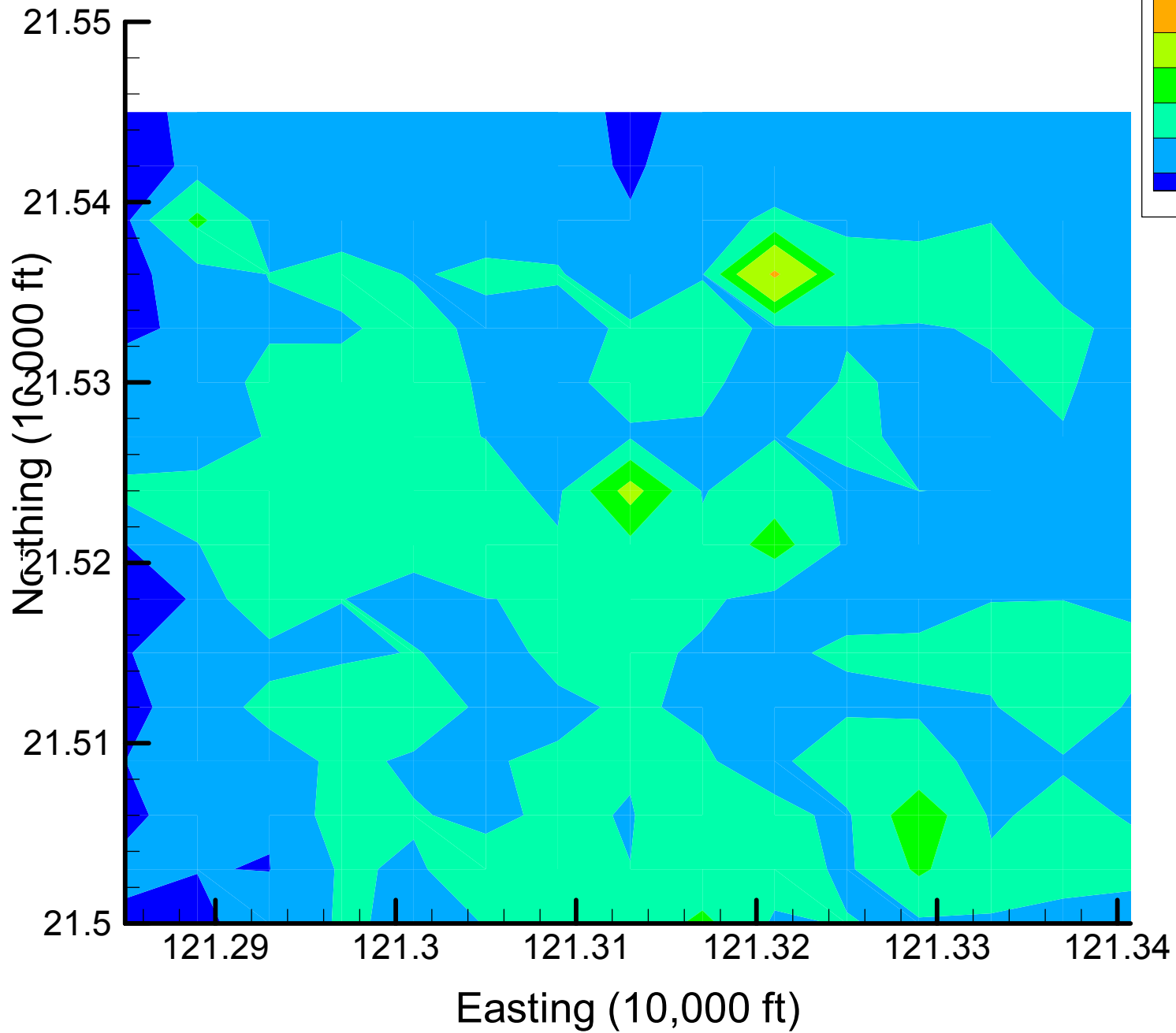
Site 49: TCE Local Variances, 2002, Base Map



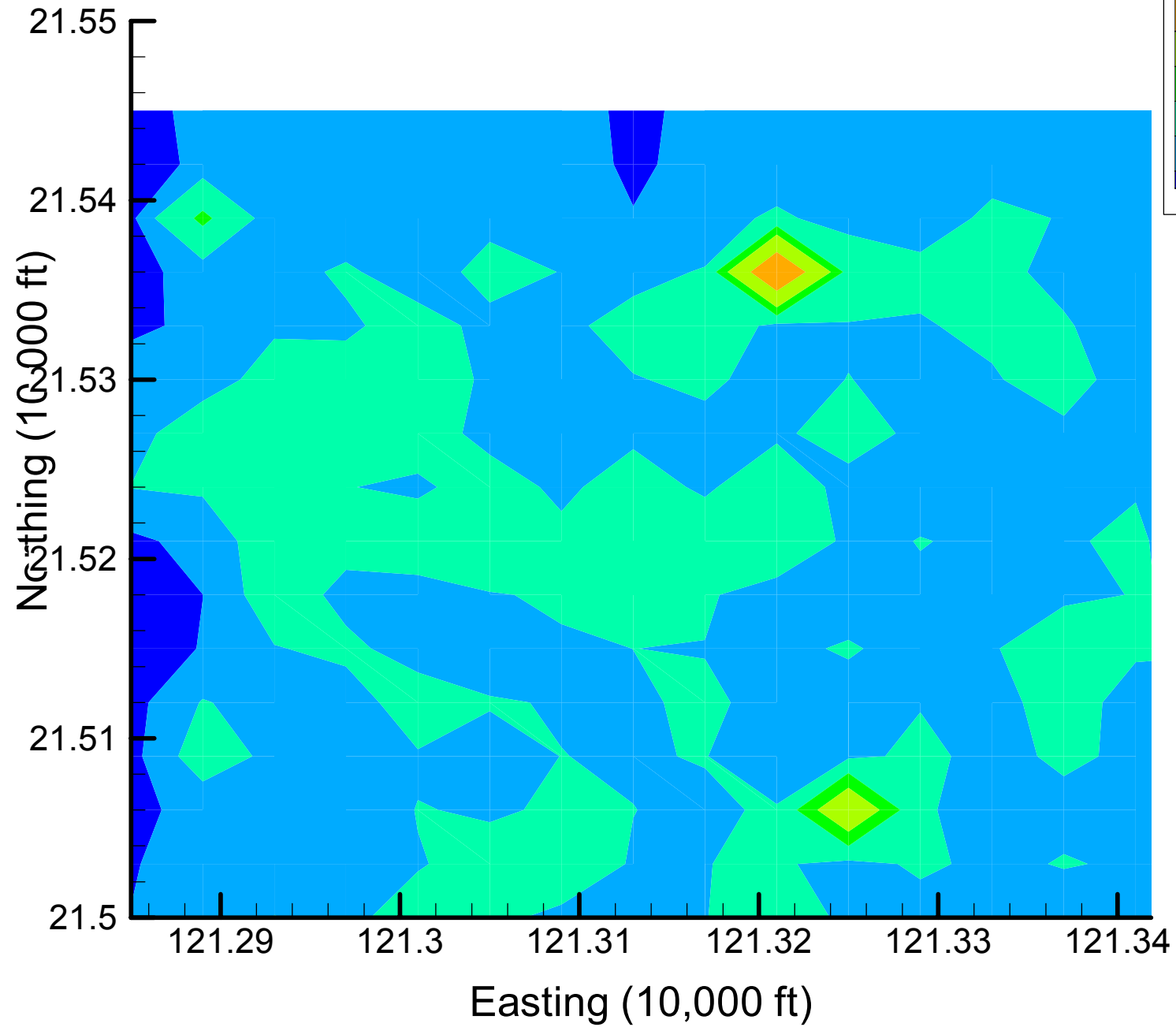
Site 49: TCE Local Variances, 2002, 5% Removal



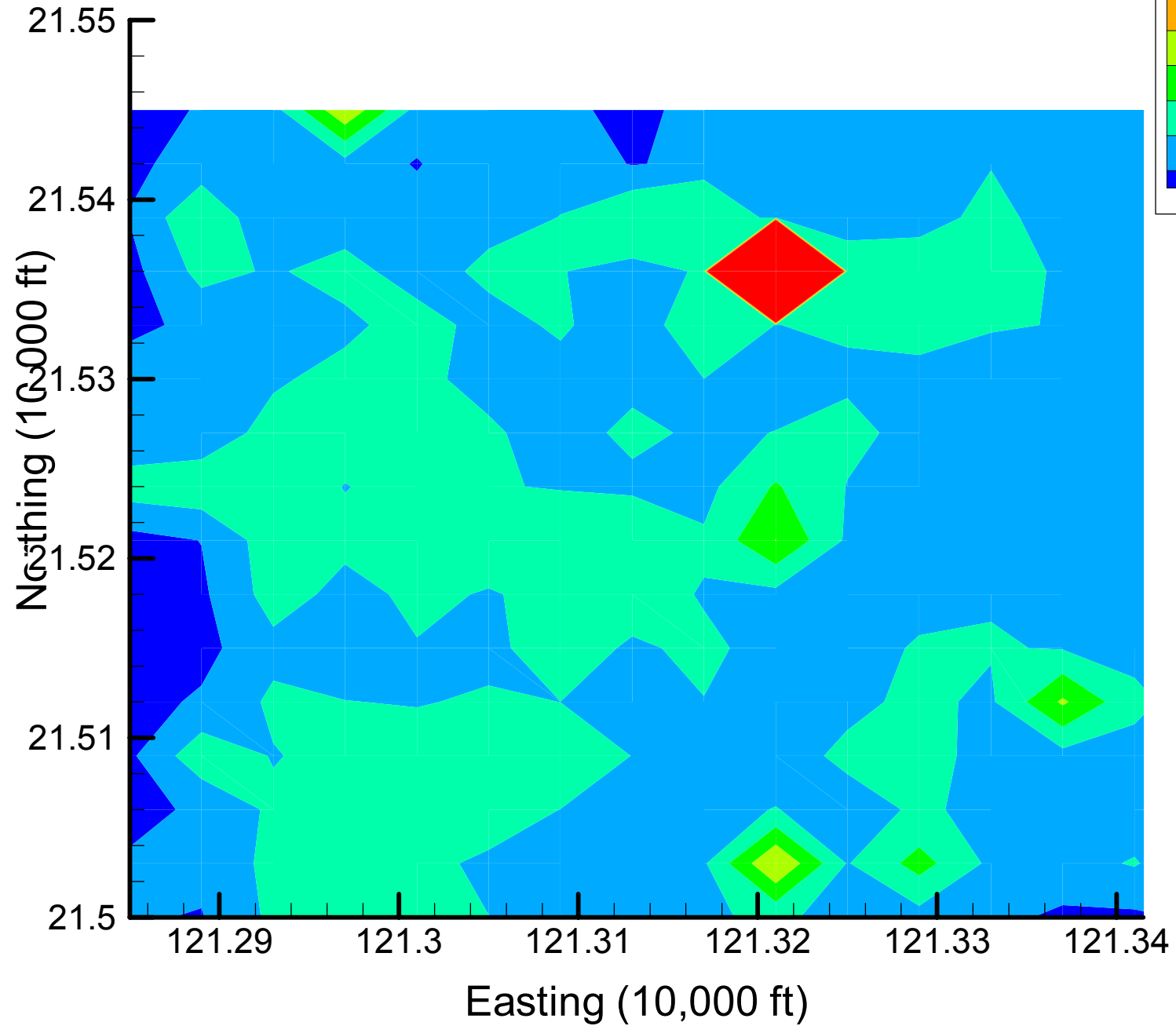
Site 49: TCE Local Variances, 2002, 10% Removal



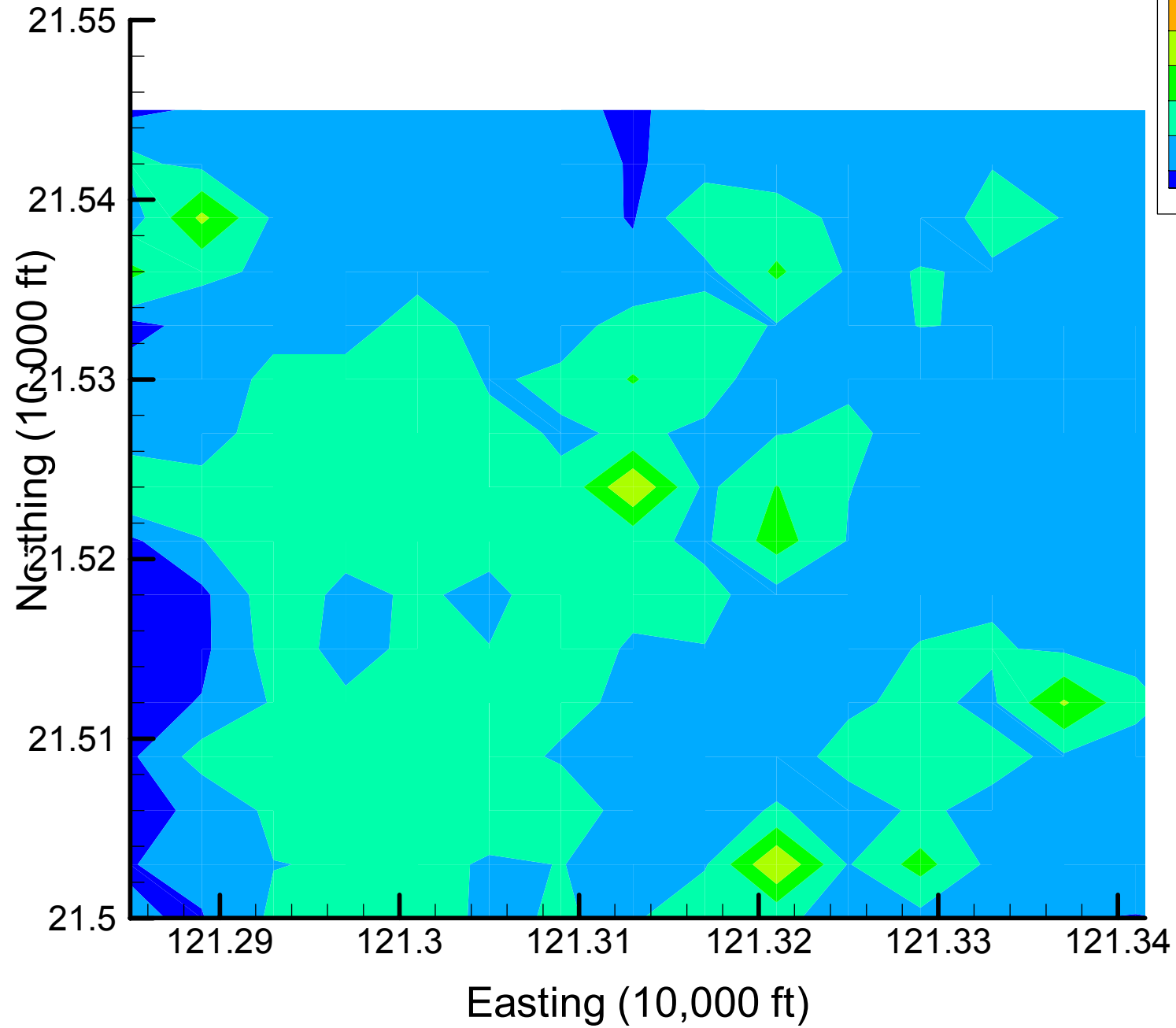
Site 49: TCE Local Variances, 2002, 15% Removal



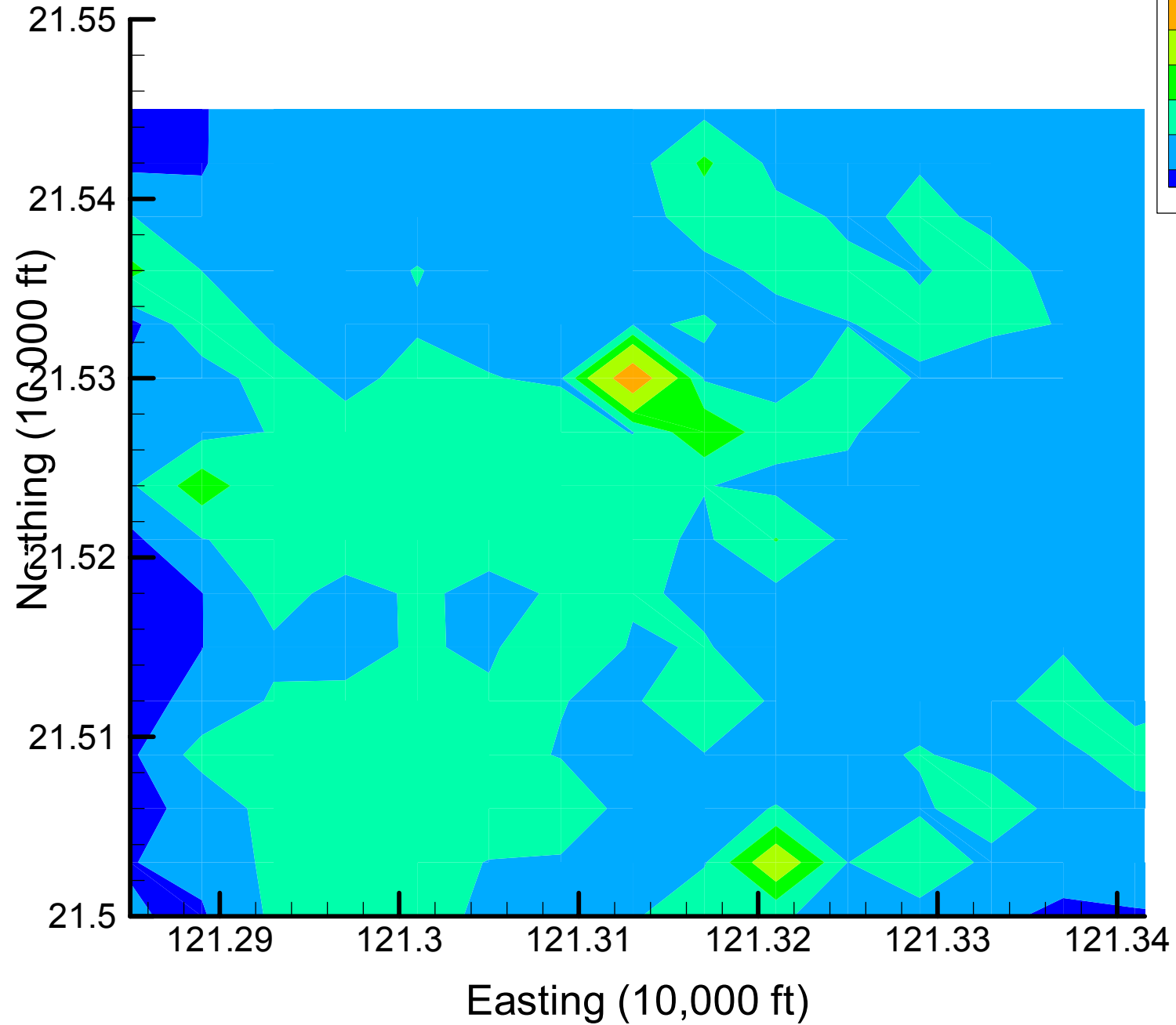
Site 49: TCE Local Variances, 2002, 20% Removal



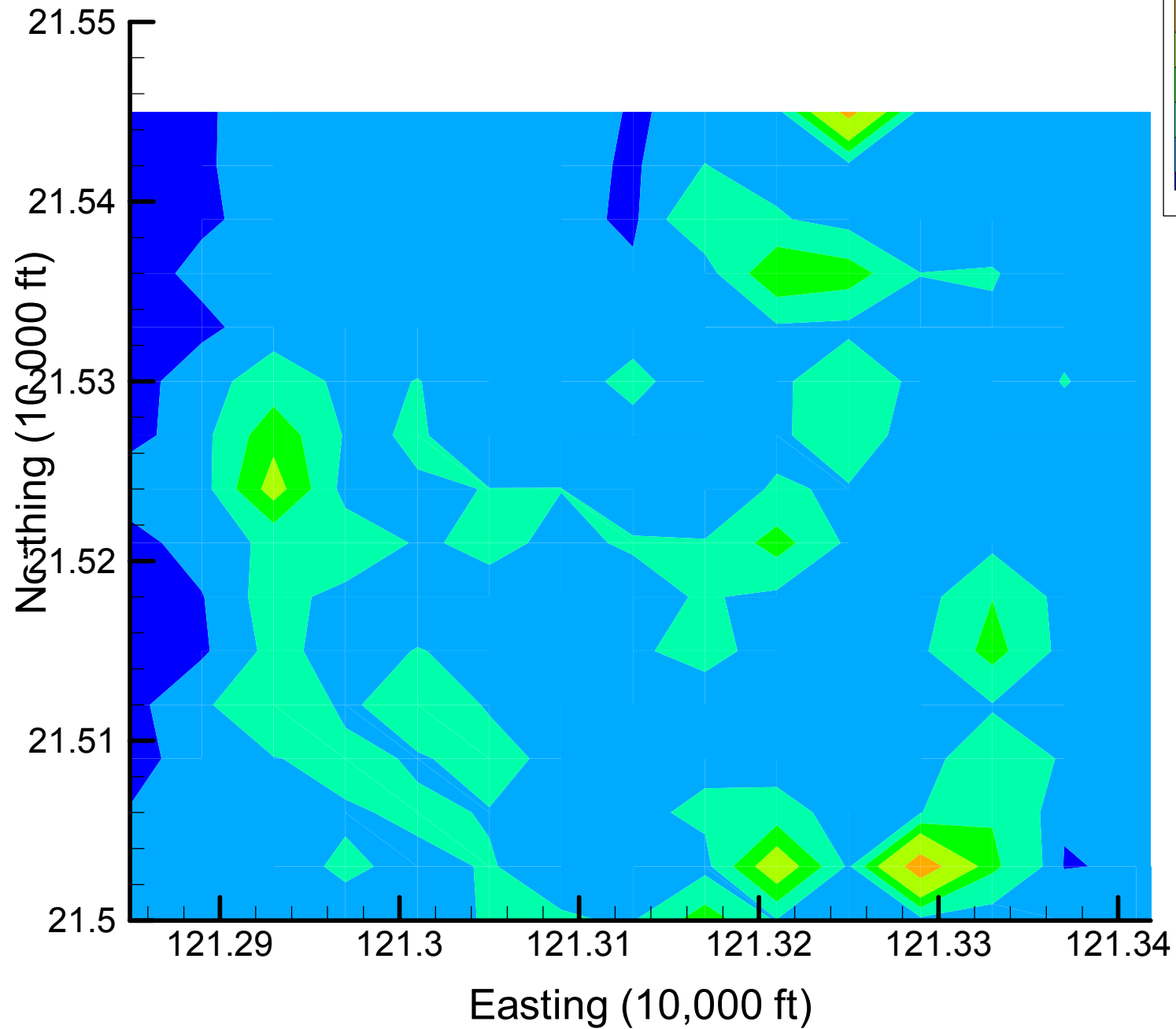
Site 49: TCE Local Variances, 2002, 25% Removal



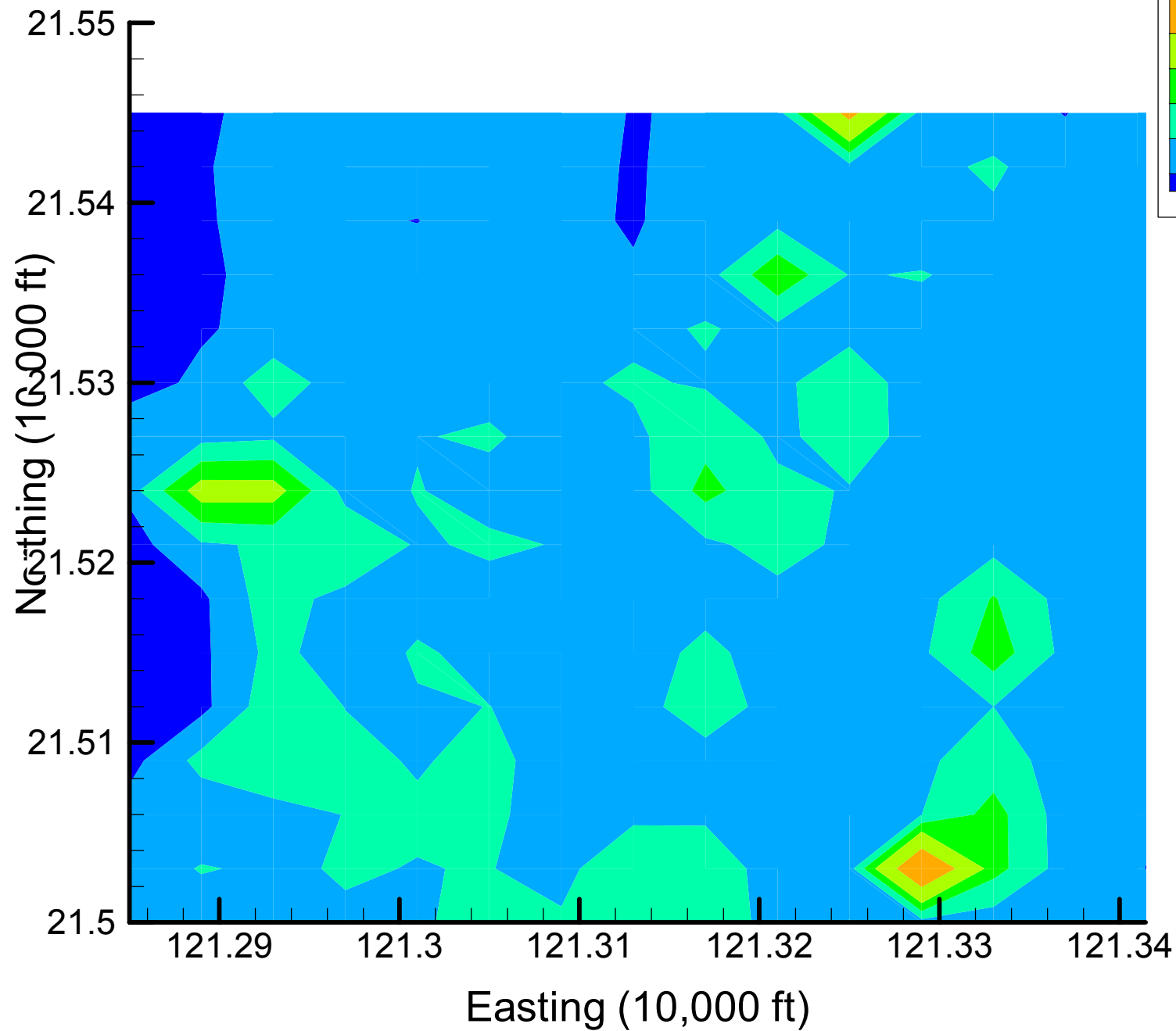
Site 49: TCE Local Variances, 2002, 30% Removal



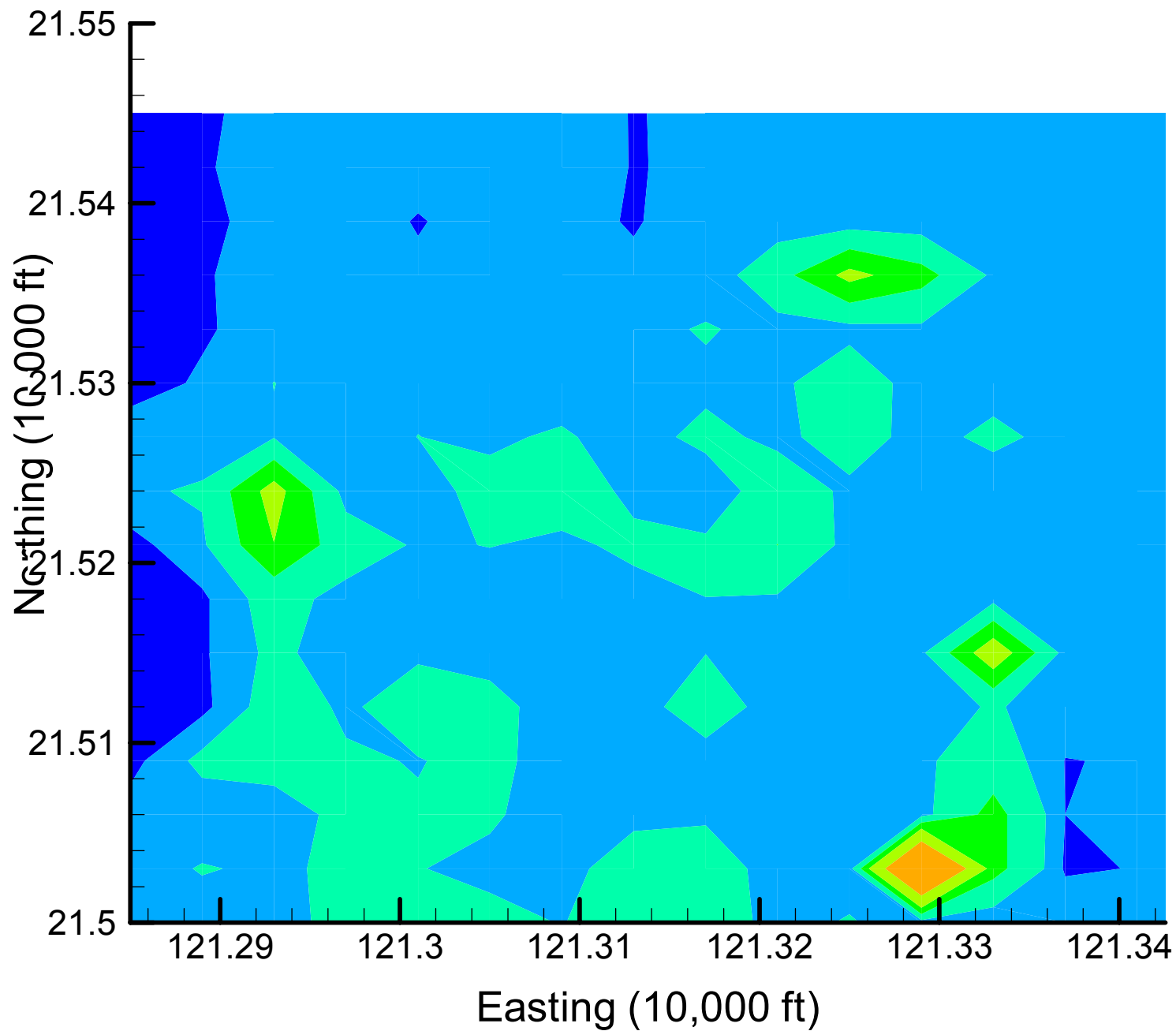
Site 49: TCE Local Variances, 2002, 35% Removal



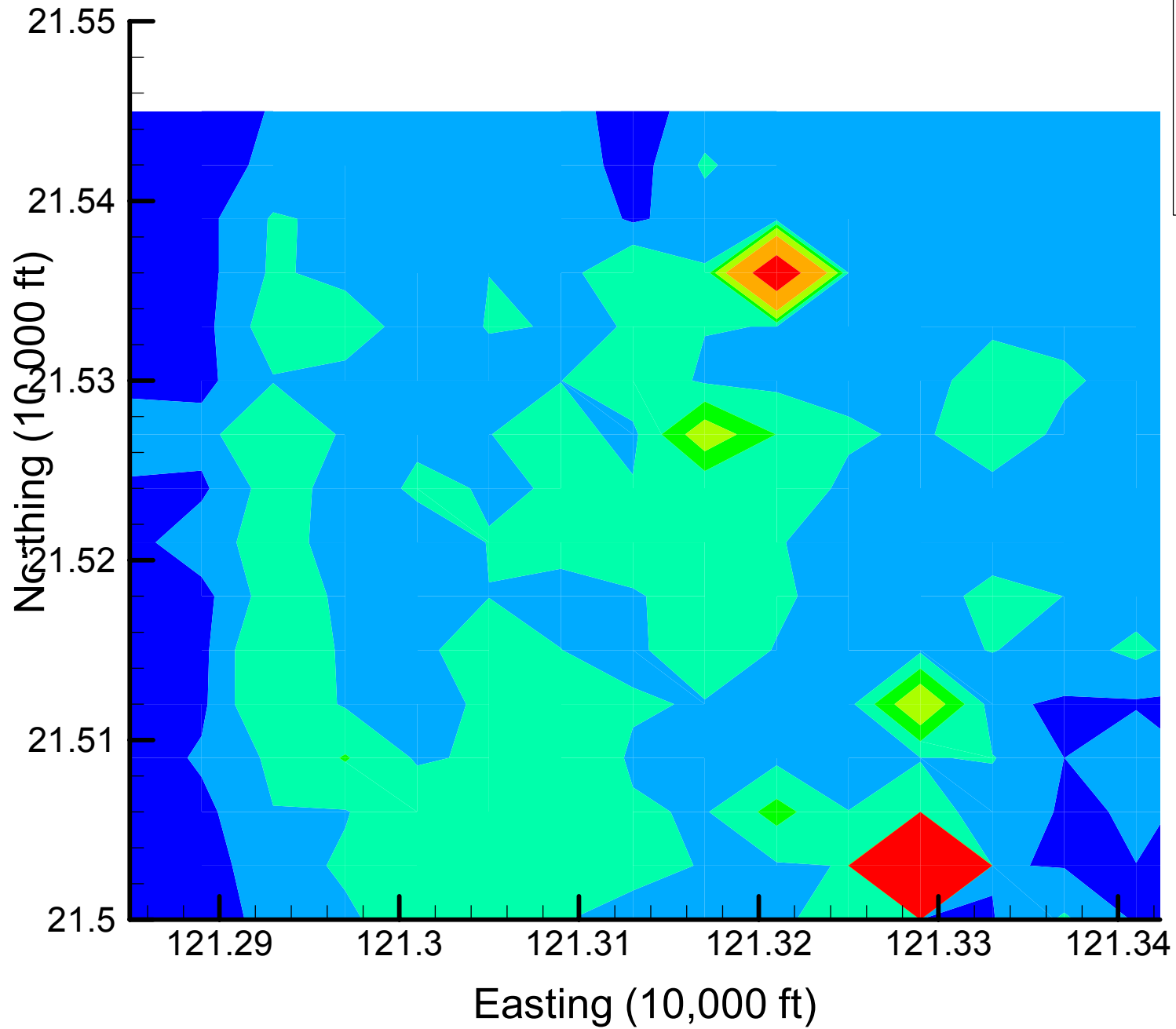
Site 49: TCE Local Variances, 2002, 40% Removal



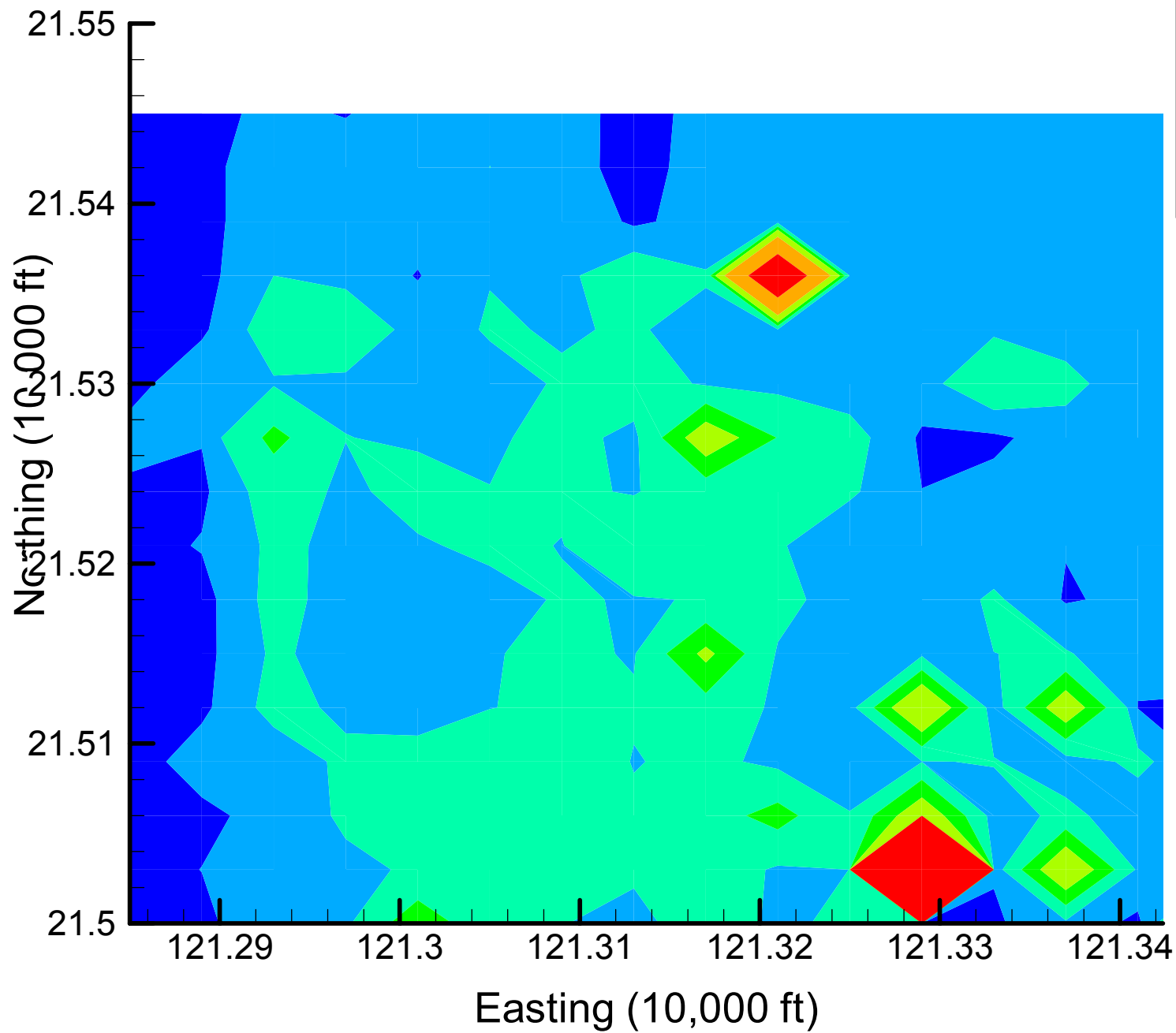
Site 49: TCE Local Variances, 2002, 45% Removal



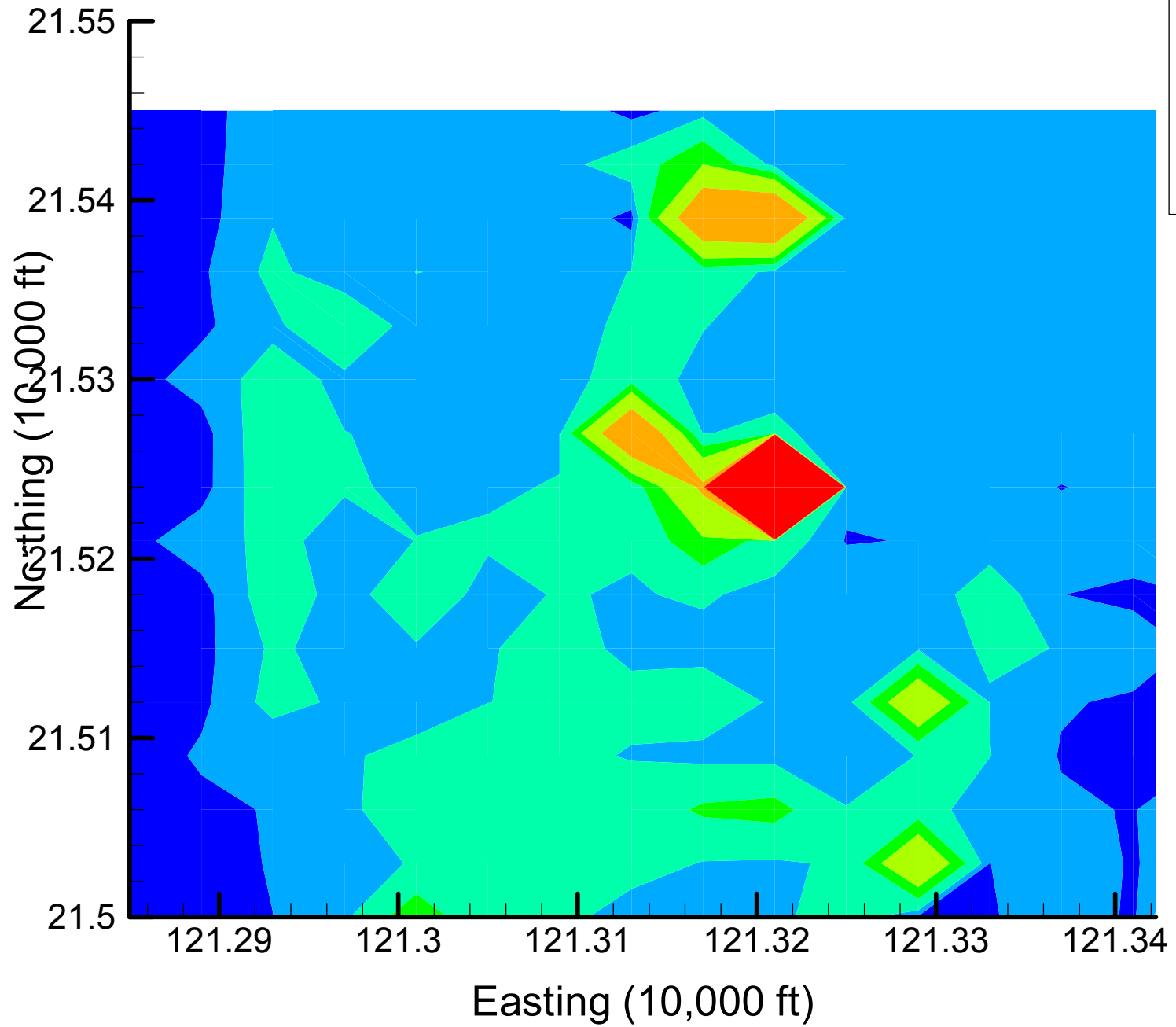
Site 49: TCE Local Variances, 2002, 50% Removal



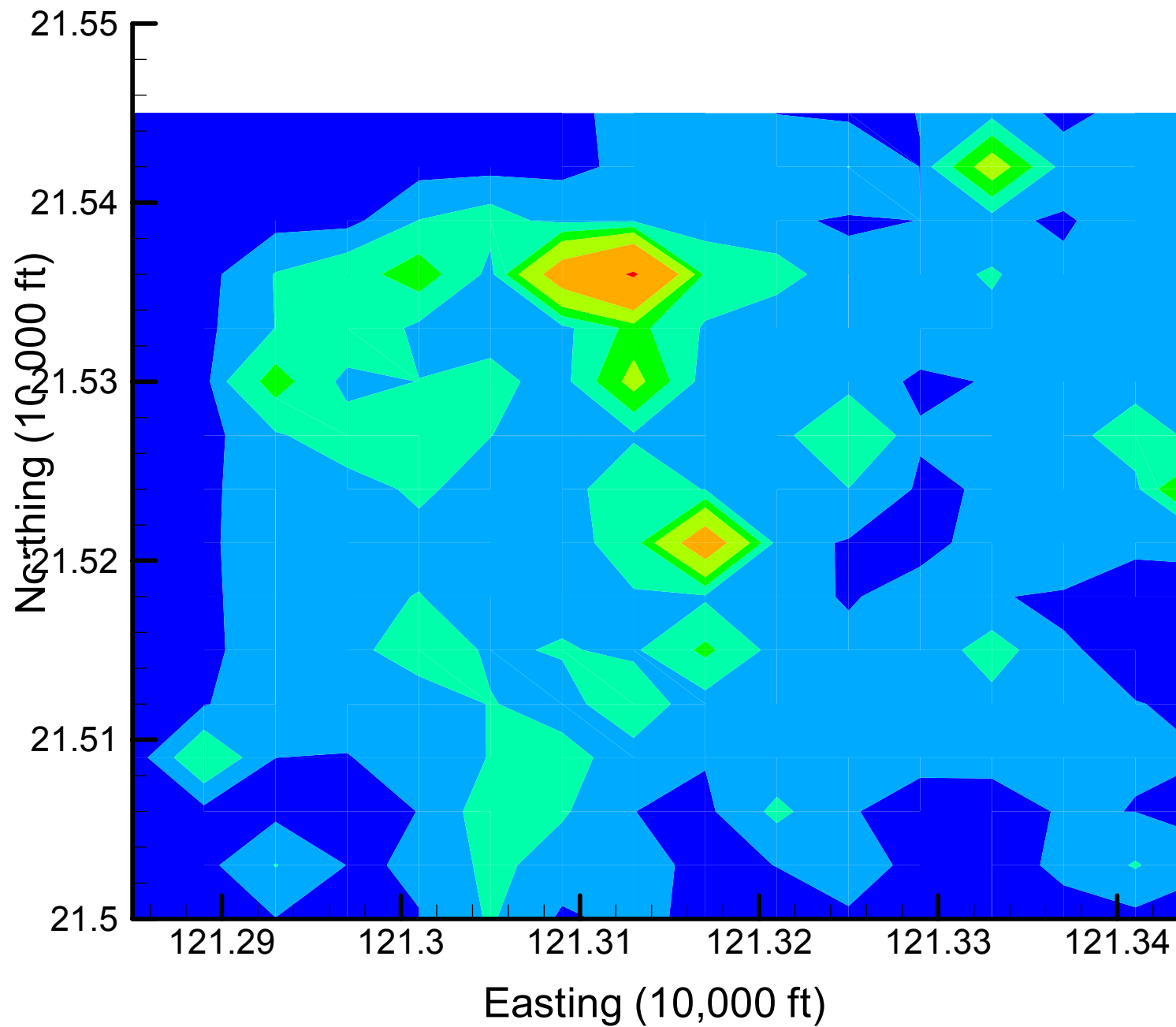
Site 49: TCE Local Variances, 2002, 55% Removal



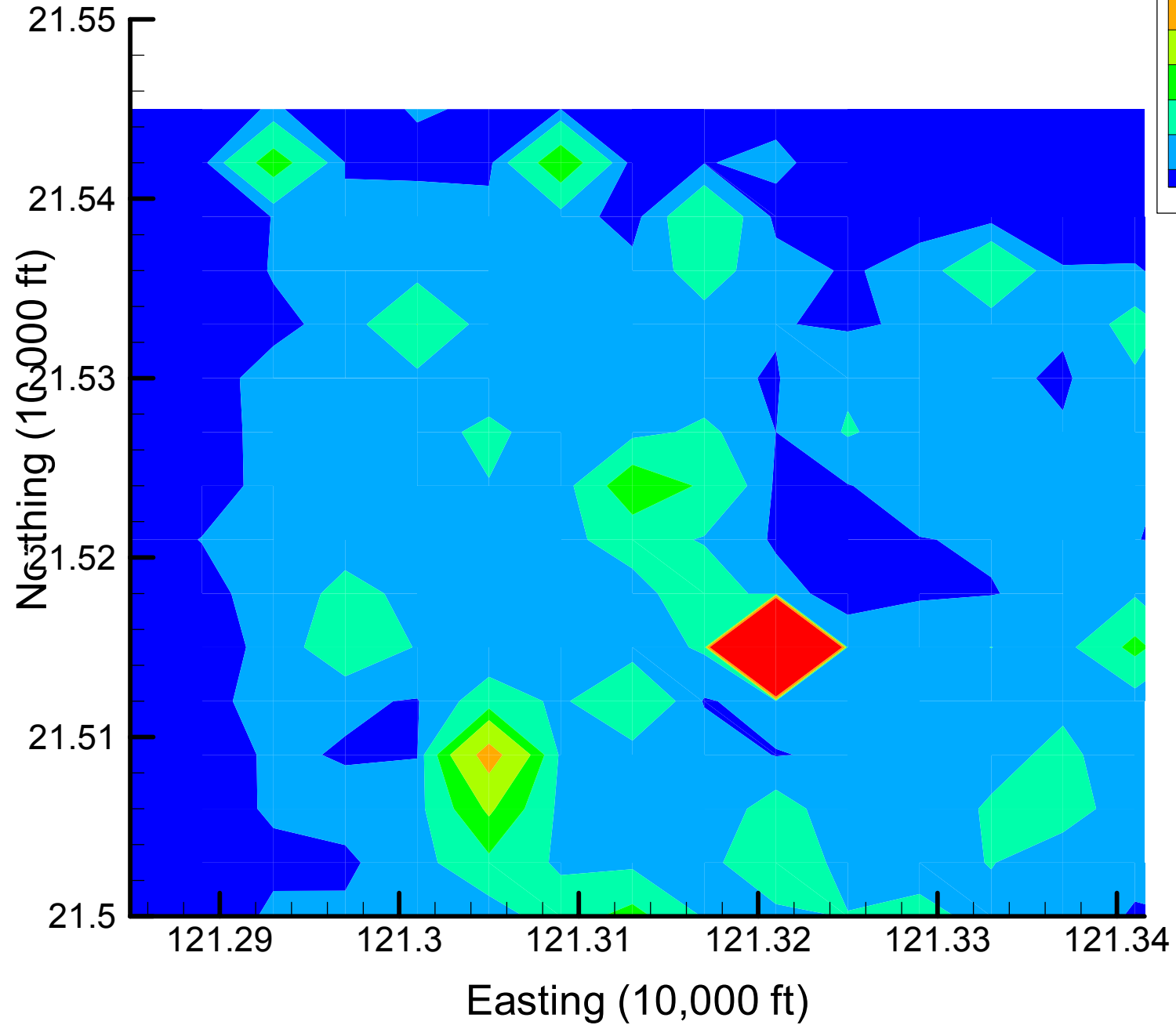
Site 49: TCE Local Variances, 2002, 60% Removal



### Site 49: TCE Local Variances, 2002, 65% Removal



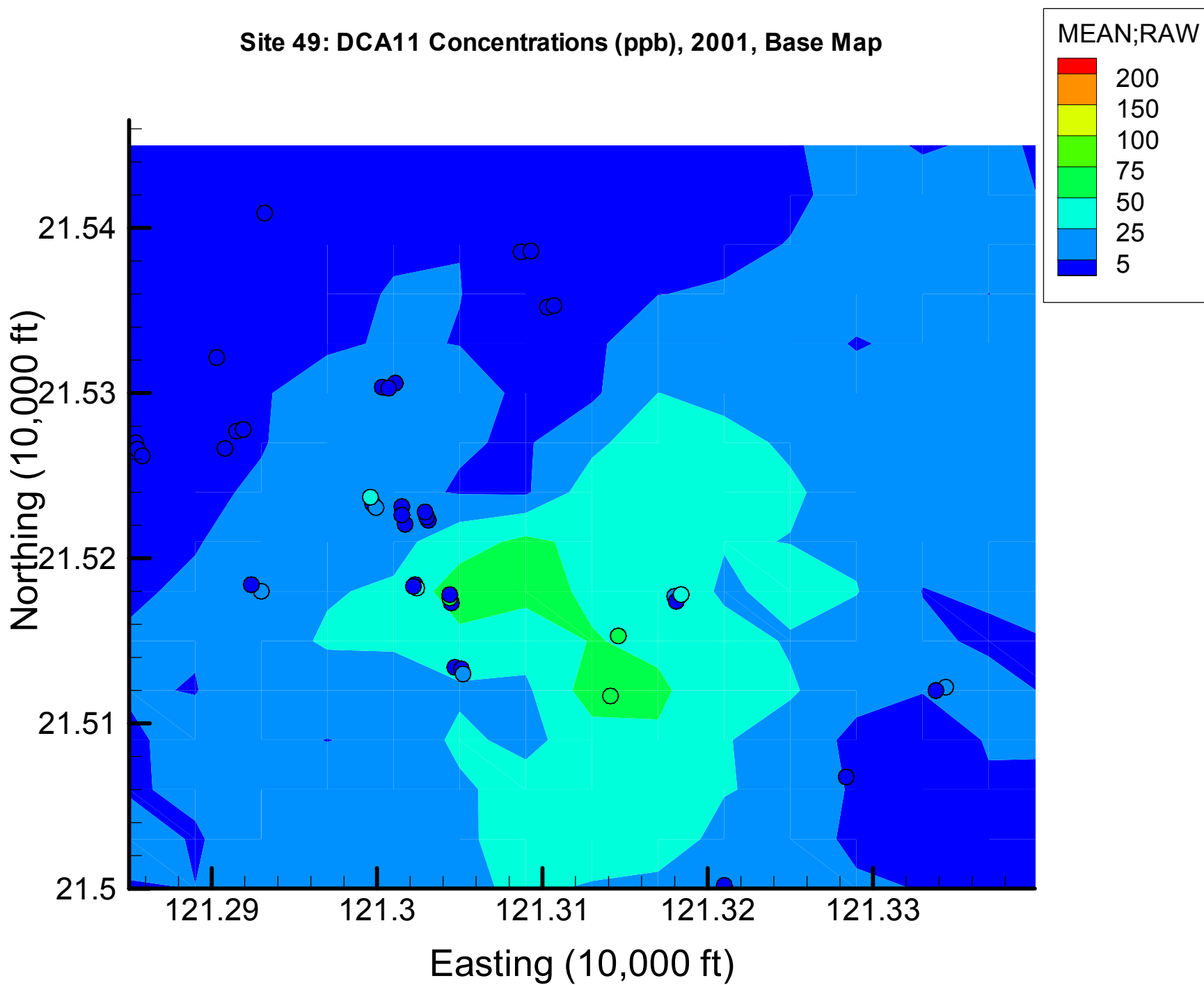
Site 49: TCE Local Variances, 2002, 70% Removal



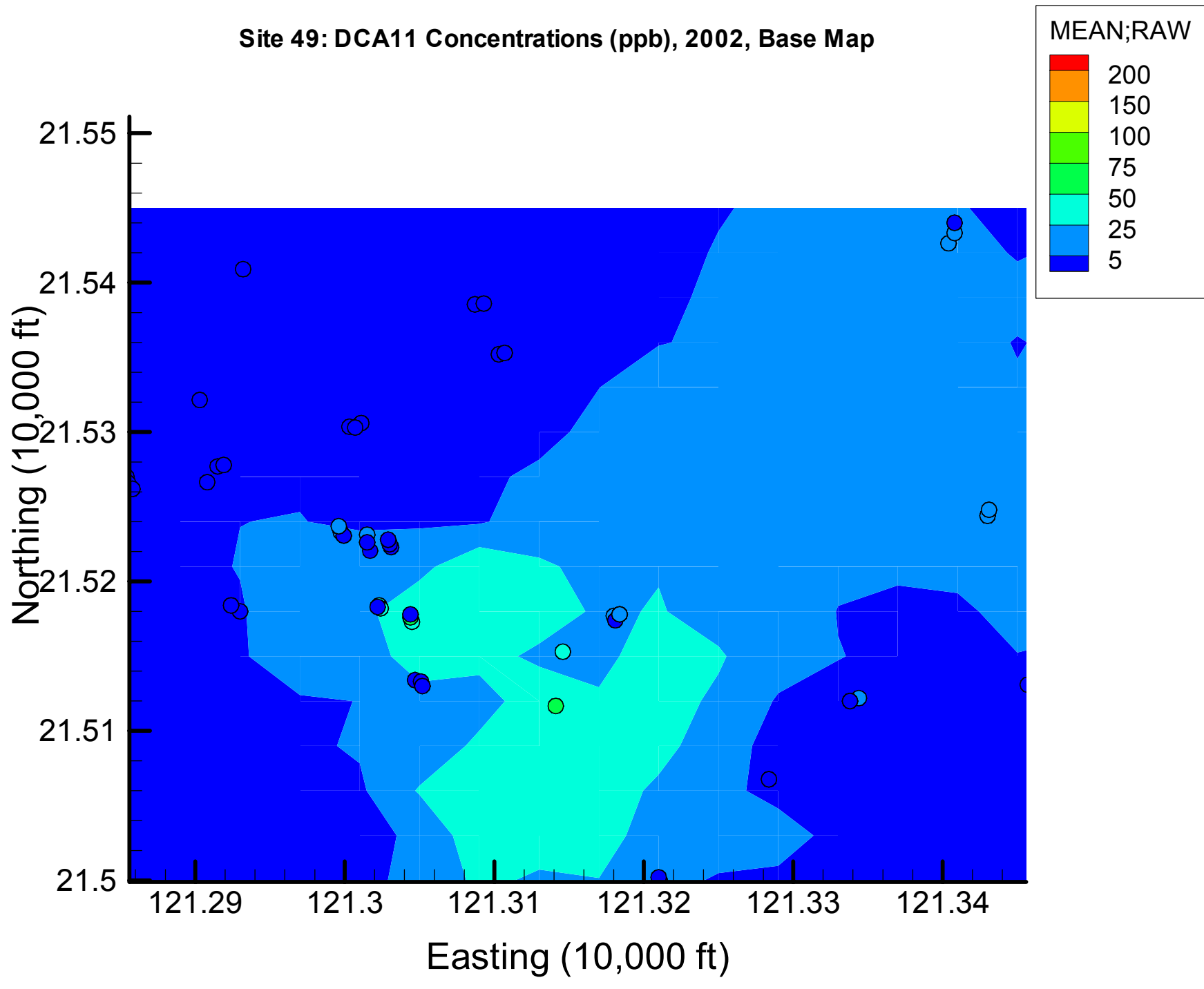
# Appendix 4.4

## DCA11 Base Concentration Maps

Site 49: DCA11 Concentrations (ppb), 2001, Base Map



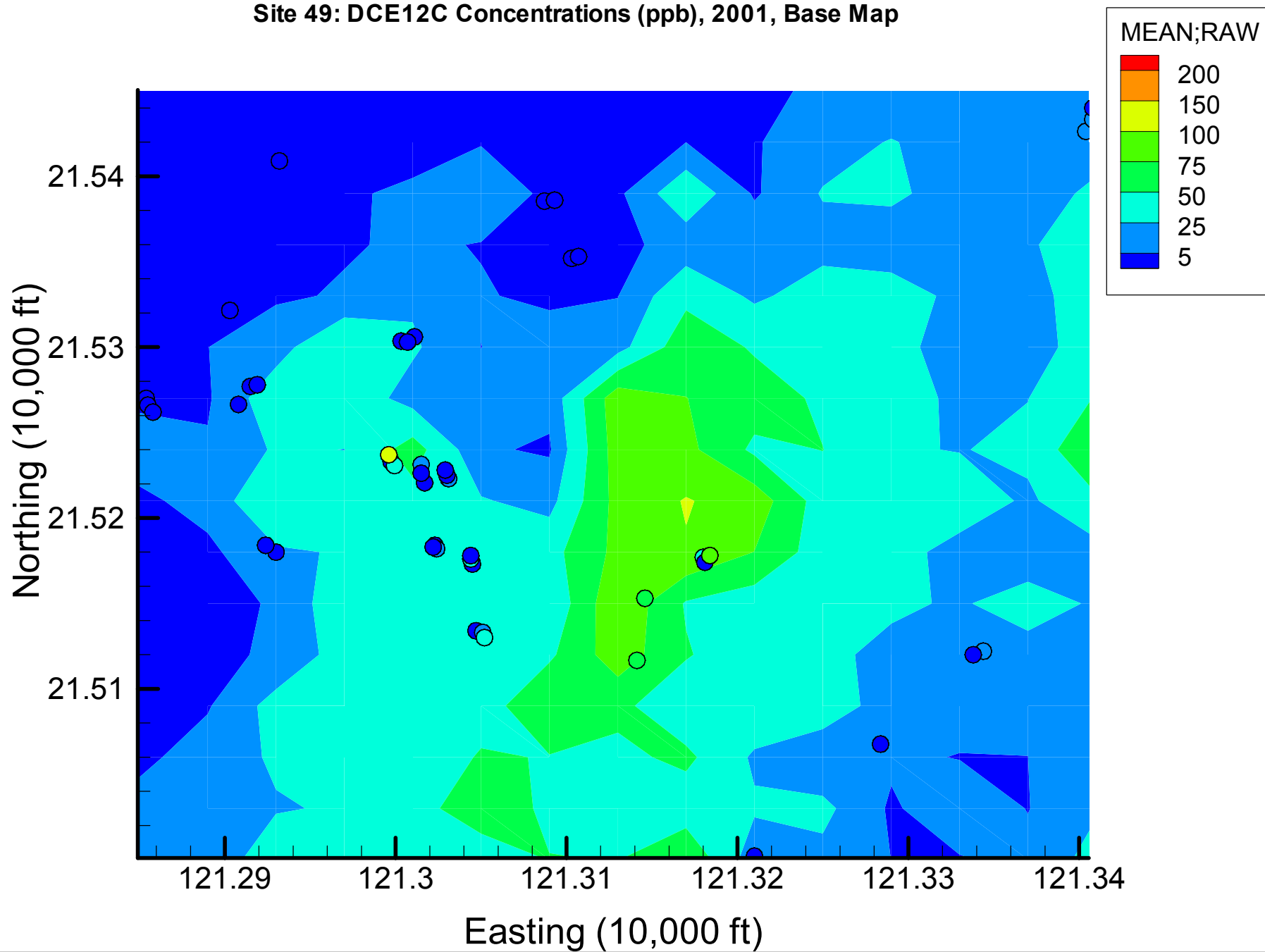
Site 49: DCA11 Concentrations (ppb), 2002, Base Map



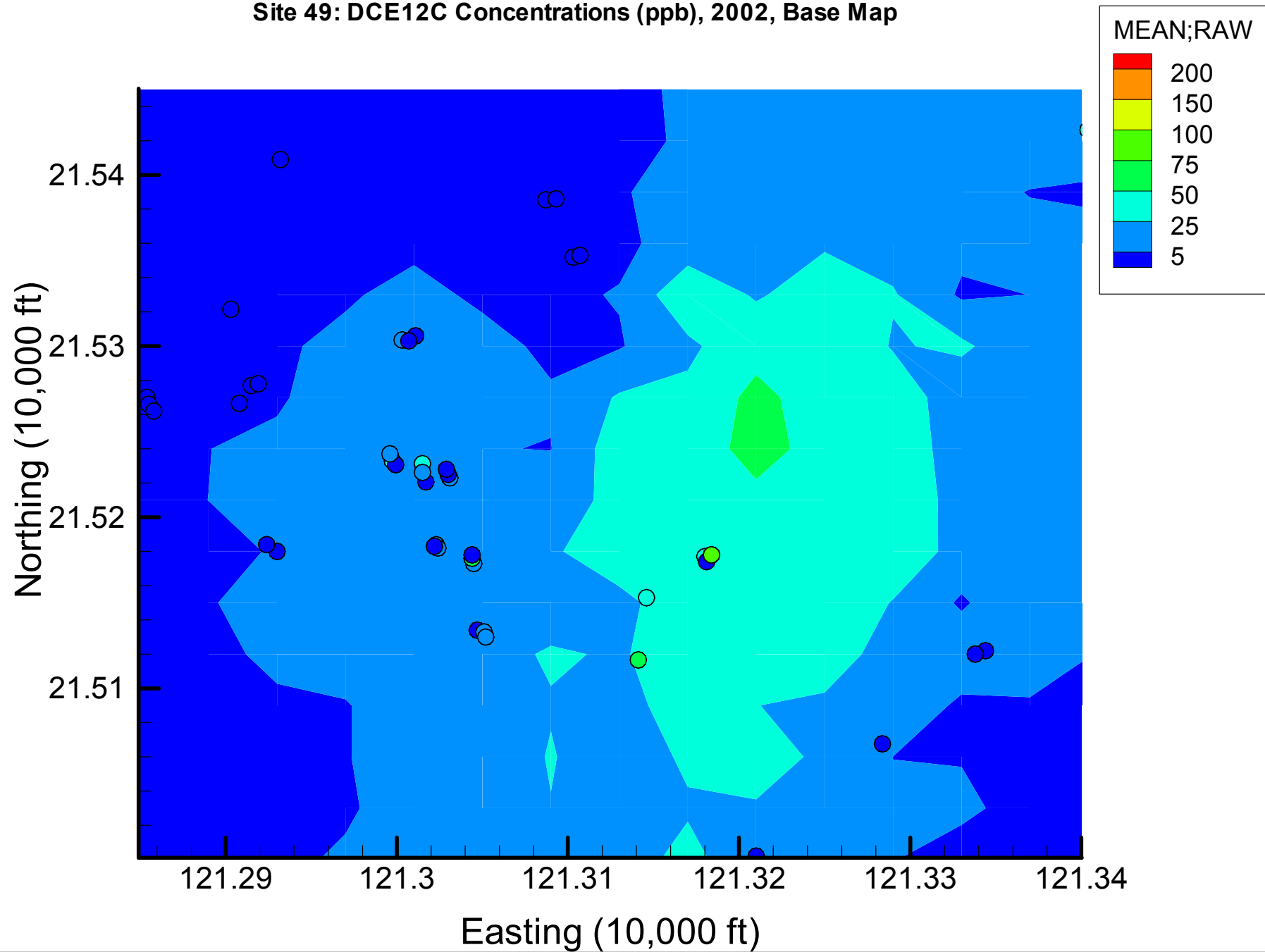
# Appendix 4.4

## DCE12C Base Concentration Maps

Site 49: DCE12C Concentrations (ppb), 2001, Base Map



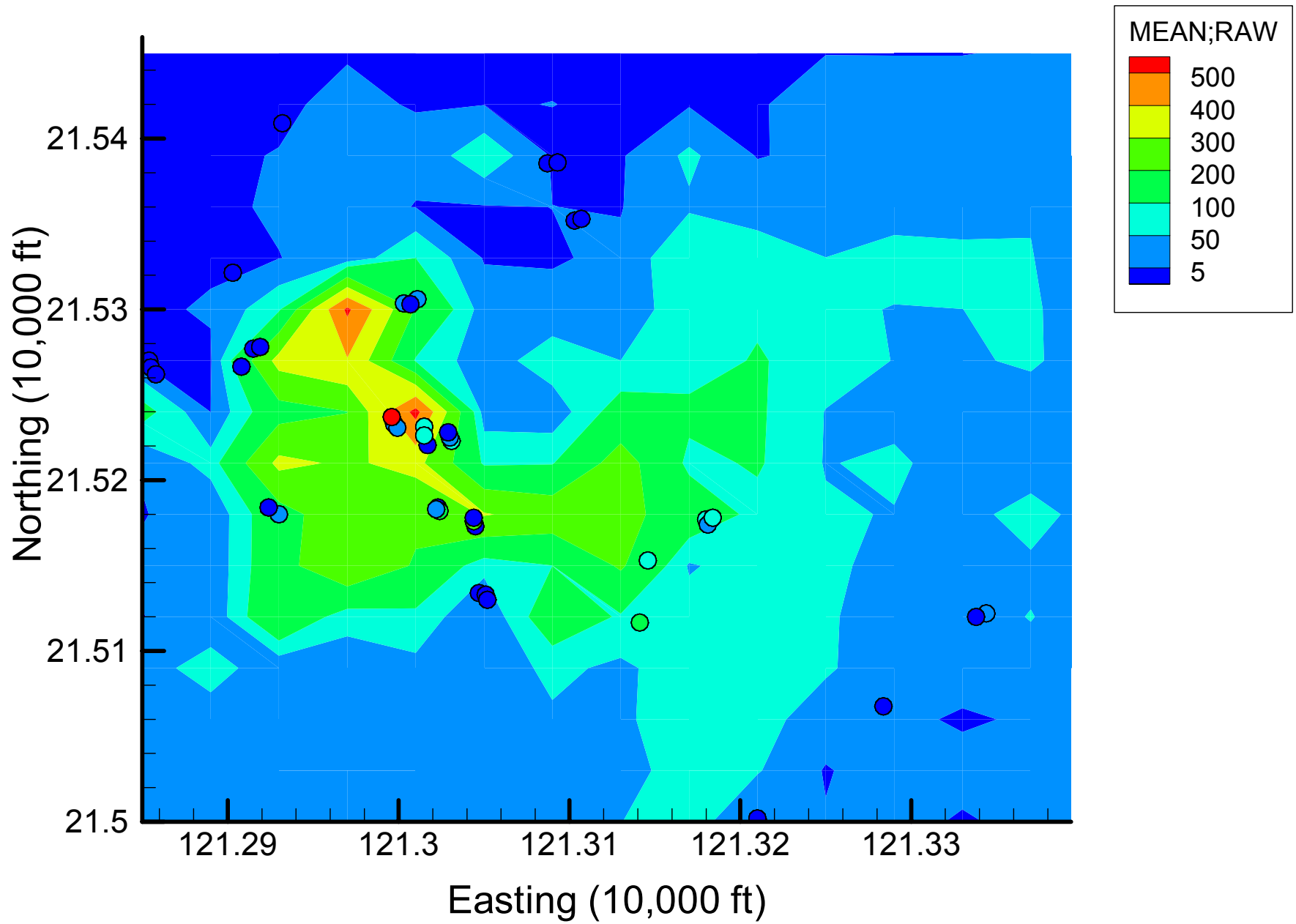
Site 49: DCE12C Concentrations (ppb), 2002, Base Map



# Appendix 4.4

## TCE Base Concentration Maps

Site 49: TCE Concentrations (ppb), 2001, Base Map



Site 49: TCE Concentrations (ppb), 2002, Base Map

